THESIS
S
7002

This is to certify that the

dissertation entitled

Self-Structuring Antennas

presented by

Christopher Mark Coleman

has been accepted towards fulfillment
of the requirements for

Ph.D. degree in Electrial Engineering

Edward J Rothwell
Major professor

Date 2/27/02

MSU is an Affirmative Action/Equal Opportunity Institution O-12771

LIBRARY
Michigan State
University

PLACE IN RETURN BOX to remove this checkout from your record.
TO AVOID FINES return on or before date due.
MAY BE RECALLED with earlier due date if requested.

DATE DUE	DATE DUE	DATE DUE
MAR 0 7 2007		

6/01 c:/CIRC/DateDue.p65-p.15

SELF-STRUCTURING ANTENNAS

VOLUME I

By

Christopher Mark Coleman

A DISSERTATION

Submitted to
Michigan State University
in partial fulfillment of the requirements
for the degree of

DOCTOR OF PHILOSOPHY

Department of Electrical and Computer Engineering

2002

ABSTRACT

SELF-STRUCTURING ANTENNAS

By

Christopher Mark Coleman

This dissertation presents a new class of antennas called 'self-structuring antennas' (SSAs). SSAs are capable of altering their electrical characteristics in response to their electromagnetic environment. These electrical characteristics are altered by controlling the states of electrical switches on the radiating structure that influence the current distribution on the antenna. Sensors evaluate the electromagnetic characteristics of the antenna for a configuration of switch states. The sensors send this information to an embedded microprocessor that makes decisions on the future configurations of switch states on the radiating structure.

When the possible switch state combinations become too numerous for the microprocessor to search exhaustively, binary search search algorithms are employed to reduce the total search time. The performance of random, simulated annealing (SA), Ant Colony Optimization (ACO), and genetic algorithms (GAs) are investigated.

Measurements of a prototype SSA system are discussed. Computer simulations are presented to gain an understanding of the characteristics of SSAs by building from simple to more complicated structures. Possible future research related to SSAs is presented.

Copyright by

Christopher Mark Coleman

2002

For my Grandparents

ACKNOWLEDGMENTS

Foremost, I thank my wife Johnna for her encouragement and support throughout this seemingly endless process.

Many thanks go to my thesis advisor, Dr. Edward Rothwell. He has been very encouraging throughout my graduate career and has become a good friend. I hope that I have learned from his creativity as well as his intelligence.

I also want to thank Dr. Nyquist, Dr. Kempel, and Dr. Drachman for their time and support as my thesis committee advisors.

Dr. John E. Ross, III and Dr. David Infante have been very encouraging throughout my graduate studies, and I want to thank them for their advice and support. I thank Brian Warner for helping me figure out how to keep focused on my research. I also want to thank Dave Story for his encouragement and help with statistics.

Along with everyone else at the MSU EM lab, I owe Jeff Meese a debt of gratitude for his help with computers. He helped me learn how to program, and helped with various other computer problems. I want to thank Dr. Mike Havrilla for his help with experimental measurements. Thanks go to Greg Charvat for his circuit and prototype advice. I thank Dr. Ahmet Kizilay for his help with LaTeX and his thesis style file.

I want to thank Dr. Lou Nagy and Dr. Mark Krage of Delphi Research Labs for their support throughout this research.

TABLE OF CONTENTS

LIST OF TABLES x

LIST OF FIGURES xii

KEY TO SYMBOLS AND ABBREVIATIONS xxvii

CHAPTER 1
Introduction 1

CHAPTER 2
Overview of Self-Structuring Antennas 3

2.1 Introduction 3

2.2 Concept 4

2.3 Self-Structuring Antenna Template 5

2.4 Receiver 7

2.5 Microprocessor 8

2.6 Search Algorithms 8

2.7 A Brief History of Self-Structuring Antennas 9

2.8 Literature Review 9

2.9 Conclusion 12

CHAPTER 3
Prototype Self-Structuring Antennas and Experimental Results 13

3.1 Self-Structuring Antenna Prototype 13
3.1.1 Template 14
3.1.2 Feed Structure 17
3.1.3 Receivers 18
3.1.4 Microprocessor 22

3.2 Measured Results 22
3.2.1 SWR Optimization 22
3.2.2 Received Signal Optimization 29

3.3 Conclusion 37

CHAPTER 4
Search Algorithms for Self-Structuring Antennas 39

4.1 Introduction 39

4.2 Overview of Binary Search Algorithms Used with SSAs 39

4.2.1 General Search 40
4.2.2 Exhaustive Search 40
4.2.3 Random Search 41
4.2.4 Simulated Annealing (SA) 42
4.2.5 Genetic Algorithm (GA) 45
4.2.6 Ant Colony Optimization (ACO) 50

4.3 Simulated SSA Experiment Using Binary Search Algorithms 57
4.3.1 SSA Template Studied 57
4.3.2 Numerical Electromagnetics Code 58
4.3.3 SSA Computer Program 60
4.3.4 Fitness Function 60

4.4 Simulation Experiment Results 62
4.4.1 Minimum SWR search at 400 MHz 64
4.4.2 Minimum SWR search at 100 MHz 72
4.4.3 Minimum SWR search at 40 MHz 78

4.5 Conclusion 84

CHAPTER 5
Simplicity Analysis of Self-Structuring Antennas 85

5.1 Overview 85

5.2 Geometries Studied 85

5.3 Simulation Results 90
5.3.1 Layer 1 SSA Template 93
5.3.1.1 Layer 1 Type I SSA Template 93
5.3.1.2 Layer 1 Type II SSA Template 109
5.3.2 Layer 1.5 SSA Template 122
5.3.2.1 Layer 1.5 Type I SSA Template 123
5.3.2.2 Layer 1.5 Type II SSA Template 140
5.3.3 Layer 2 SSA Template 154
5.3.3.1 Layer 2 Type I SSA Template 155
5.3.3.2 Layer 2 Type II SSA Template 171
5.3.4 Layer 2.5 SSA Template 191
5.3.4.1 Layer 2.5 Type I SSA Template 192
5.3.4.2 Layer 2.5 Type II SSA Template 210
5.3.5 Layer 3 SSA Template 231
5.3.6 Layer 4 SSA Template 260
5.3.7 Layer 5 SSA Template 274
5.3.8 Layer 6 SSA Template 281
5.3.9 Layer 7 SSA Template 288

5.4 Conclusion 318

CHAPTER 6
Conclusions and Future Work 321

6.1 Conclusions 321

6.2 Potential Future Work 322
6.2.1 Fractal Template Geometries 322
6.2.2 Search Algorithms 323
6.2.3 Simulation of Self-Structuring Antennas 323
6.2.4 Integrated Self-Structuring Antennas 324
6.2.5 Prototype Self-Structuring Antenna Investigations 324
6.2.6 Applications of Self-Structuring Antennas 324
6.2.7 Practical Self-Structuring Antenna Issues 326

APPENDIX A
Self-Structuring Antenna Computer Programs 328

A.1 Overview 328

A.2 Self-Structuring Antenna Simulation Programs 328
A.2.1 Self-Structuring Antenna Class 328
A.2.2 EM Environment Class 329
A.2.3 Fitness Class 329
A.2.4 Search Routine Classes 329
A.2.4.1 Exhaustive Search 330
A.2.4.2 Random Search 330
A.2.4.3 Genetic Algorithm 331
A.2.4.4 Simulated Annealing 331
A.2.4.5 Ant Colony Optimization 331
A.2.5 SSA Template Geometry Classes 331
A.2.5.1 Simple Template 331
A.2.5.2 Irregular Template 332
A.2.5.3 Original Prototype Template 332
A.2.5.4 Rectangles Template 332
A.2.6 NEC Manipulation Classes 332
A.2.6.1 NEC Card Class 332
A.2.6.2 NEC Input File Class 333
A.2.6.3 NEC Output File Class 334
A.2.7 Other Classes, Structures, and Functions 334
A.2.7.1 Wire Class 334
A.2.7.2 XYZ Coordinate Classes 334
A.2.7.3 General Switch Class 335
A.2.7.4 Template Section Class 337
A.2.7.5 File String Structure 338
A.2.7.6 Radiation Pattern Parameter Structure 338
A.2.7.7 Random Number Generating Function 338
A.2.7.8 String Locating Functions 339

A.3 Prototype SSA Computer Programs 339
A.3.1 Basic Stamp II Programs 340
A.3.1.1 LTC-1298 AD Converter Basic Stamp II Code 340

BIBLIOGRAPHY 342

LIST OF TABLES

Table 3.1 Simulated annealing (SA) parameters used for SWR optimization. 25

Table 3.2 Genetic algorithm (GA) parameters used for SWR optimization. . 25

Table 3.3 Simulated annealing (SA) parameters used for reception optimization at 300 MHz. 32

Table 3.4 Number of temperatures for the simulated annealing algorithm at each measurement angle. 33

Table 3.5 Simulated annealing (SA) parameters used for reception optimization at 275 MHz. 36

Table 4.1 Possible SSA configurations for a template with n switches. . . . 41

Table 4.2 Variables, terms, and parameters used with ACO. 55

Table 4.3 Dimensions of the SSA template used in the search algorithm studies. 59

Table 4.4 ACO parameter values for the simulated SSA experiment at 400 MHz. 68

Table 4.5 SA parameter values for the simulated SSA experiment at 400 MHz. 69

Table 4.6 GA parameter values for the simulated SSA experiment at 400 MHz. 69

Table 4.7 Lowest SWR and the iteration number where the lowest SWR first occurred for the random search at 400 MHz (1500 total iterations). 69

Table 4.8 Lowest SWR and the iteration number where the lowest SWR first occurred for the ACO search at 400 MHz (1500 total iterations). . 70

Table 4.9 Lowest SWR and the iteration number where the lowest SWR first occurred for the SA search at 400 MHz (1500 total iterations). . . 70

Table 4.10 Lowest SWR and the iteration number where the lowest SWR first occurred for the GA search at 400 MHz (1500 total iterations). . 71

Table 4.11 ACO parameter values for the simulated SSA experiment at 100 MHz. 75

Table 4.12 SA parameter values for the simulated SSA experiment at 100 MHz. 76

Table 4.13 GA parameter values for the simulated SSA experiment at 100 MHz. 76

Table 4.14 Lowest SWR and the iteration number where the lowest SWR first occurred for the random search at 100 MHz (1500 total iterations). 76

Table 4.15 Lowest SWR and the iteration number where the lowest SWR first occurred for the ACO search at 100 MHz (1500 total iterations). . 77

Table 4.16 Lowest SWR and the iteration number where the lowest SWR first occurred for the SA search at 100 MHz (1500 total iterations). . . 77

Table 4.17 Lowest SWR and the iteration number where the lowest SWR first occurred for the GA search at 100 MHz (1500 total iterations). . 78
Table 4.18 ACO parameter values for the simulated SSA experiment at 40 MHz. 81
Table 4.19 SA parameter values for the simulated SSA experiment at 40 MHz. 81
Table 4.20 GA parameter values for the simulated SSA experiment at 40 MHz. 81
Table 4.21 Lowest SWR and the iteration number where the lowest SWR first occurred for the random search at 40 MHz (1500 total iterations). 82
Table 4.22 Lowest SWR and the iteration number where the lowest SWR first occurred for the ACO search at 40 MHz (1500 total iterations). . 82
Table 4.23 Lowest SWR and the iteration number where the lowest SWR first occurred for the SA search at 40 MHz (1500 total iterations). . . 83
Table 4.24 Lowest SWR and the iteration number where the lowest SWR first occurred for the GA search at 40 MHz (1500 total iterations). . . 83
Table 5.1 Number of switches and possible SSA configurations for the SSA template layers in the simplicity study. 89
Table 5.2 Simulation parameters for the simplicity study. 91
Table 5.3 Dimensions of the layer 1 Type I SSA template. 93
Table 5.4 Dimensions of the layer 1 Type II SSA template. 93
Table 5.5 Dimensions of the layer 1.5 Type I SSA template. 123
Table 5.6 Dimensions of the layer 1.5 Type II SSA template. 124
Table 5.7 Dimensions of the layer 2 Type I SSA template. 156
Table 5.8 Dimensions of the layer 2 Type II SSA template. 156
Table 5.9 Dimensions of the layer 2.5 Type I SSA template. 193
Table 5.10 Dimensions of the layer 2.5 Type II SSA template. 193
Table 5.11 Dimensions of the layer 3 Type I SSA template. 234
Table 5.12 Dimensions of the layer 4 Type I SSA template. 262
Table 5.13 Dimensions of the layer 5 Type I SSA template. 276
Table 5.14 Dimensions of the layer 6 Type I SSA template. 283
Table 5.15 Dimensions of the layer 7 Type I and Type II SSA templates. . . 290

LIST OF FIGURES

Figure 2.1 Block diagram of a self-structuring antenna system. 5

Figure 2.2 Diagram of a generic self-structuring antenna template. 6

Figure 3.1 Photograph of the SSA prototype. 15

Figure 3.2 Photograph showing the wiring of the back of the SSA prototype. 16

Figure 3.3 Photograph showing the back of the SSA prototype and the connecting cables. 17

Figure 3.4 SWR optimization measurement setup. 19

Figure 3.5 Received signal optimization measurement setup. 21

Figure 3.6 Data acquisition circuit. 24

Figure 3.7 Switch configuration of prototype template used for SWR optimization. 26

Figure 3.8 Measured SWR of prototype SSA optimized at each frequency. 27

Figure 3.9 A closer look at the measured SWR of prototype optimized at each frequency. 28

Figure 3.10 Switch configuration of prototype template used for the first reception optimization study. 31

Figure 3.11 Illustration of the first SSA orientation for reception measurements (transmitting antenna is along the x-axis). 32

Figure 3.12 Normalized prototype reception at 300 MHz, optimized at each measurement angle. 35

Figure 3.13 Illustration of the second SSA orientation for reception measurements (transmitting antenna is along the x-axis). 36

Figure 3.14 Normalized prototype reception at 275 MHz, optimized at each measurement angle. 38

Figure 4.1 Block diagram of a genetic algorithm. 49

Figure 4.2 Diagram of ants foraging for food. 51

Figure 4.3 Diagram of paths through nodes for Ant Colony Optimization (ACO). 53

Figure 4.4 Diagram of the SSA template used in the search algorithm study. 58

Figure 4.5 Distribution of SWR values (relative to 50 Ω) for the SSA template at 400 MHz (500,000 random samples). Error bars show the 95% confidence intervals. 65

Figure 4.6 Detailed distribution of SWR values (relative to 50 Ω) for the SSA template at 400 MHz (500,000 random samples). Error bars show the 95% confidence intervals. 66

Figure 4.7 Distribution of SWR values (relative to 50 Ω) for the SSA template at 100 MHz (500,000 random samples). Error bars show the 95% confidence intervals. 73

Figure 4.8 Detailed distribution of SWR values (relative to 50 Ω) for the SSA template at 100 MHz (500,000 random samples). Error bars show the 95% confidence intervals. 74

Figure 4.9 Distribution of SWR values (relative to 50 Ω) for the SSA template at 40 MHz (500,000 random samples). Error bars show the 95% confidence intervals. 79

Figure 5.1 Diagram of the layer 1 SSA template. 87

Figure 5.2 Progression of template layers in the simplicity study. 88

Figure 5.3 Diagram of the Type I and Type II SSA templates based on three maximum layers. 97

Figure 5.4 SWR vs. frequency for the layer 1 Type I SSA template in free space. 98

Figure 5.5 SWR vs. frequency for the layer 1 Type I SSA template above ground. 99

Figure 5.6 Minimum SWR vs. frequency for the layer 1 Type I SSA template. 100

Figure 5.7 Proportion of configurations with SWRs less than 50.0 vs. frequency for the layer 1 Type I SSA template (linear scale). . . . 101

Figure 5.8 Smith chart for the layer 1 Type I SSA template in free space at 40 MHz. 102

Figure 5.9 Smith chart for the layer 1 Type I SSA template above ground at 40 MHz. 103

Figure 5.10 Smith chart for the layer 1 Type I SSA template in free space at 800 MHz. 104

Figure 5.11 Smith chart for the layer 1 Type I SSA template above ground at 800 MHz. 105

Figure 5.12 Proportion of configurations with minimum vertical gains in the horizontal plane above 0 dB vs. frequency for the layer 1 Type I SSA template (linear scale). 106

Figure 5.13 Proportion of configurations with maximum vertical gains in the horizontal plane above 3.0 dB vs. frequency for the layer 1 Type I SSA template (linear scale). 107

Figure 5.14 Proportion of configurations with SWRs less than 50.0 and minimum vertical gains in the horizontal plane above 0 dB vs. frequency for the layer 1 Type I SSA template (linear scale). . . . 108

Figure 5.15 Proportion of configurations with SWRs less than 50.0 and maximum vertical gains in the horizontal plane above 3.0 dB vs. frequency for the layer 1 Type I SSA template (linear scale). . . . 109

Figure 5.16 SWR vs. frequency for the layer 1 Type II SSA template in free space. 112

Figure 5.17 SWR vs. frequency for the layer 1 Type II SSA template above ground. 113

Figure 5.18 Minimum SWR vs. frequency for the layer 1 Type II SSA template. 114

Figure 5.19 Proportion of configurations with SWRs less than 3.0 vs. frequency for the layer 1 Type II SSA template (linear scale). . . . 115

Figure 5.20 Proportion of configurations with SWRs less than 2.0 vs. frequency for the layer 1 Type II SSA template (linear scale). . . . 116

Figure 5.21 Smith chart for the layer 1 Type II SSA template in free space at 800 MHz. 117

Figure 5.22 Smith chart for the layer 1 Type II SSA template above ground at 800 MHz. 118

Figure 5.23 Proportion of configurations with minimum vertical gains above 0 dB vs. frequency for the layer 1 Type II SSA template (linear scale). 119

Figure 5.24 Proportion of configurations with maximum vertical gains above 3 dB vs. frequency for the layer 1 Type II SSA template (linear scale). 120

Figure 5.25 Proportion of configurations with SWRs less than 2.0 and and minimum vertical gains in the horizontal plane above 0 dB vs. frequency for the layer 1 Type II SSA template (linear scale). 121

Figure 5.26 Proportion of configurations with SWRs less than 2.0 and and maximum vertical gains in the horizontal plane above 3.0 dB vs. frequency for the layer 1 Type II SSA template (linear scale). 122

Figure 5.27 Diagram of the layer 1.5 SSA template. 123

Figure 5.28 SWR vs. frequency for the layer 1.5 Type I SSA template in free space. 127

Figure 5.29 SWR vs. frequency for the layer 1.5 Type I SSA template above ground. 128

Figure 5.30 Minimum SWR vs. frequency for the layer 1.5 Type I SSA template. 129

Figure 5.31 Smith chart for the layer 1.5 Type I SSA template in free space at 40 MHz. 130
Figure 5.32 Smith chart for the layer 1.5 Type I SSA template above ground at 40 MHz. 131
Figure 5.33 Smith chart for the layer 1.5 Type I SSA template in free space at 800 MHz. 132
Figure 5.34 Smith chart for the layer 1.5 Type I SSA template above ground at 800 MHz. 133
Figure 5.35 Proportion of configurations with SWRs less than 4.0 vs. frequency for the layer 1.5 Type I SSA template (linear scale). . . 134
Figure 5.36 Proportion of configurations with SWRs less than 2.0 vs. frequency for the layer 1.5 Type I SSA template (linear scale). . . 135
Figure 5.37 Proportion of configurations with minimum vertical gains in the horizontal plane above -3.0 dB vs. frequency for the layer 1.5 Type I SSA template (linear scale). 136
Figure 5.38 Proportion of configurations with minimum vertical gains in the horizontal plane above 0 dB vs. frequency for the layer 1.5 Type I SSA template (linear scale). 137
Figure 5.39 Proportion of configurations with SWRs less than 4.0 and minimum vertical gains in the horizontal plane above -3.0 dB vs. frequency for the layer 1.5 Type I SSA template (linear scale). . . 138
Figure 5.40 Proportion of configurations with maximum vertical gains in the horizontal plane above 3.0 dB vs. frequency for the layer 1.5 Type I SSA template (linear scale). 139
Figure 5.41 Proportion of configurations with SWRs less than 4.0 and maximum vertical gains in the horizontal plane above 3.0 dB vs. frequency for the layer 1.5 Type I SSA template (linear scale). . . 140
Figure 5.42 SWR vs. frequency for the layer 1.5 Type II SSA template in free space. 143
Figure 5.43 SWR vs. frequency for the layer 1.5 Type II SSA template above ground. 144
Figure 5.44 Minimum SWR vs. frequency for the layer 1.5 Type II SSA template. 145
Figure 5.45 Smith chart for the layer 1.5 Type II SSA template in free space at 800 MHz. 146
Figure 5.46 Smith chart for the layer 1.5 Type II SSA template above ground at 800 MHz. 147

Figure 5.47 Proportion of configurations with SWRs less than 3.0 vs. frequency for the layer 1.5 Type II SSA template (linear scale). . . 148
Figure 5.48 Proportion of configurations with SWRs less than 2.0 vs. frequency for the layer 1.5 Type II SSA template (linear scale). . . 149
Figure 5.49 Proportion of configurations with minimum vertical gains in the horizontal plane above -3.0 dB vs. frequency for the layer 1.5 Type II SSA template (linear scale). 150
Figure 5.50 Proportion of configurations with minimum vertical gains in the horizontal plane above 0 dB vs. frequency for the layer 1.5 Type II SSA template (linear scale). 151
Figure 5.51 Proportion of configurations with SWRs less than 3.0 and minimum vertical gains in the horizontal plane above -3.0 dB vs. frequency for the layer 1.5 Type II SSA template (linear scale). . . 152
Figure 5.52 Proportion of configurations with maximum vertical gains in the horizontal plane above 3.0 dB vs. frequency for the layer 1.5 Type II SSA template (linear scale). 153
Figure 5.53 Proportion of configurations with SWRs less than 3.0 and maximum vertical gains in the horizontal plane above 3.0 dB vs. frequency for the layer 1.5 Type II SSA template (linear scale). . . 154
Figure 5.54 Diagram of the layer 2 SSA template. 155
Figure 5.55 SWR vs. frequency for the layer 2 Type I SSA template in free space. 158
Figure 5.56 SWR vs. frequency for the layer 2 Type I SSA template above ground. 159
Figure 5.57 Minimum SWR vs. frequency for the layer 2 Type I SSA template. 160
Figure 5.58 Smith chart for the layer 2 Type I SSA template in free space at 800 MHz. 161
Figure 5.59 Smith chart for the layer 2 Type I SSA template above ground at 800 MHz. 162
Figure 5.60 Proportion of configurations with SWRs less than 4.0 vs. frequency for the layer 2 Type I SSA template (linear scale). . . . 163
Figure 5.61 Proportion of configurations with SWRs less than 2.0 vs. frequency for the layer 2 Type I SSA template (linear scale). . . . 164
Figure 5.62 Proportion of configurations with SWRs less than 1.5 vs. frequency for the layer 2 Type I SSA template (linear scale). . . . 165
Figure 5.63 Proportion of configurations with minimum vertical gains in the horizontal plane above -3.0 dB vs. frequency for the layer 2 Type I SSA template (linear scale). 166

Figure 5.64 Proportion of configurations with minimum vertical gains in the horizontal plane above 0 dB vs. frequency for the layer 2 Type I SSA template (linear scale). 167
Figure 5.65 Proportion of configurations with SWRs less than 4.0 and minimum vertical gains above -3.0 dB vs. frequency for the layer 2 Type I SSA template (linear scale). 168
Figure 5.66 Proportion of configurations with SWRs less than 2.0 and minimum vertical gains in the horizontal plane above 0 dB vs. frequency for the layer 2 Type I SSA template (linear scale). . . . 169
Figure 5.67 Proportion of configurations with maximum vertical gains in the horizontal plane above 3.0 dB vs. frequency for the layer 2 Type I SSA template (linear scale). 170
Figure 5.68 Proportion of configurations with SWRs less than 2.0 and maximum vertical gains in the horizontal plane above 3.0 dB vs. frequency for the layer 2 Type I SSA template (linear scale). . . . 171
Figure 5.69 SWR vs. frequency for the layer 2 Type II SSA template in free space. 174
Figure 5.70 SWR vs. frequency for the layer 2 Type II SSA template above ground. 175
Figure 5.71 Minimum SWR vs. frequency for the layer 2 Type II SSA template. 176
Figure 5.72 Smith chart for the layer 2 Type II SSA template in free space at 500 MHz. 177
Figure 5.73 Smith chart for the layer 2 Type II SSA template above ground at 500 MHz. 178
Figure 5.74 Proportion of configurations with SWRs less than 4.0 vs. frequency for the layer 2 Type II SSA template (linear scale). . . . 179
Figure 5.75 Proportion of configurations with SWRs less than 2.0 vs. frequency for the layer 2 Type II SSA template (linear scale). . . . 180
Figure 5.76 Proportion of configurations with SWRs less than 1.5 vs. frequency for the layer 2 Type II SSA template (linear scale). . . . 181
Figure 5.77 Smith chart for the layer 2 Type II SSA template in free space at 780 MHz. 182
Figure 5.78 Smith chart for the layer 2 Type II SSA template above ground at 780 MHz. 183
Figure 5.79 Proportion of configurations with minimum vertical gains in the horizontal plane above -3.0 dB vs. frequency for the layer 2 Type II SSA template (linear scale). 184

Figure 5.80 Proportion of configurations with minimum vertical gains in the horizontal plane above 0 dB vs. frequency for the layer 2 Type II SSA template (linear scale). 185

Figure 5.81 Proportion of configurations with SWRs less than 2.0 and minimum vertical gains in the horizontal plane above 0 dB vs. frequency for the layer 2 Type II SSA template (linear scale). . . . 186

Figure 5.82 Proportion of configurations with SWRs less than 4.0 and minimum vertical gains in the horizontal plane above -3.0 dB vs. frequency for the layer 2 Type II SSA template (linear scale). . . . 187

Figure 5.83 Proportion of configurations with maximum vertical gains in the horizontal plane above 3.0 dB vs. frequency for the layer 2 Type II SSA template (linear scale). 188

Figure 5.84 Proportion of configurations with SWRs less than 2.0 and maximum vertical gains in the horizontal plane above 3.0 dB vs. frequency for the layer 2 Type II SSA template (linear scale). . . . 189

Figure 5.85 Proportion of configurations with maximum vertical gains in the horizontal plane above 6.0 dB vs. frequency for the layer 2 Type II SSA template (linear scale). 190

Figure 5.86 Proportion of configurations with SWRs less than 2.0 and maximum vertical gains in the horizontal plane above 6.0 dB vs. frequency for the layer 2 Type II SSA template (linear scale). . . . 191

Figure 5.87 Diagram of the layer 2.5 SSA template. 192

Figure 5.88 SWR vs. frequency for the layer 2.5 Type I SSA template in free space. 196

Figure 5.89 SWR vs. frequency for the layer 2.5 Type I SSA template above ground. 197

Figure 5.90 Minimum SWR vs. frequency for the layer 2.5 Type I SSA template. 198

Figure 5.91 Smith chart for the layer 2.5 Type I SSA template in free space at 800 MHz. 199

Figure 5.92 Smith chart for the layer 2.5 Type I SSA template above ground at 800 MHz. 200

Figure 5.93 Proportion of configurations with SWRs less than 4.0 vs. frequency for the layer 2.5 Type I SSA template (linear scale). . . 201

Figure 5.94 Proportion of configurations with SWRs less than 4.0 vs. frequency for the layer 2.5 Type I SSA template. 202

Figure 5.95 Proportion of configurations with SWRs less than 3.0 vs. frequency for the layer 2.5 Type I SSA template. 203

Figure 5.96 Proportion of configurations with SWRs less than 2.0 vs. frequency for the layer 2.5 Type I SSA template. 204
Figure 5.97 Proportion of configurations with SWRs less than 1.5 vs. frequency for the layer 2.5 Type I SSA template. 205
Figure 5.98 Proportion of configurations with SWRs less than 1.1 vs. frequency for the layer 2.5 Type I SSA template. 206
Figure 5.99 Proportion of configurations with minimum vertical gains in the horizontal plane above 0 dB vs. frequency for the layer 2.5 Type I SSA template. 207
Figure 5.100 Proportion of configurations with SWRs less than 2.0 and minimum vertical gains in the horizontal plane above 0 dB vs. frequency for the layer 2.5 Type I SSA template. 208
Figure 5.101 Proportion of configurations with maximum vertical gains in the horizontal plane above 3.0 dB vs. frequency for the layer 2.5 Type I SSA template. 209
Figure 5.102 Proportion of configurations with SWRs less than 2.0 and maximum vertical gains in the horizontal plane above 3.0 dB vs. frequency for the layer 2.5 Type I SSA template. 210
Figure 5.103 SWR vs. frequency for the layer 2.5 Type II SSA template in free space. 213
Figure 5.104 SWR vs. frequency for the layer 2.5 Type II SSA template above ground. 214
Figure 5.105 Minimum SWR vs. frequency for the layer 2.5 Type II SSA template. 215
Figure 5.106 Proportion of configurations with SWRs less than 4.0 vs. frequency for the layer 2.5 Type II SSA template. 216
Figure 5.107 Proportion of configurations with SWRs less than 2.0 vs. frequency for the layer 2.5 Type II SSA template. 217
Figure 5.108 Proportion of configurations with SWRs less than 1.5 vs. frequency for the layer 2.5 Type II SSA template. 218
Figure 5.109 Proportion of configurations with SWRs less than 2.0 vs. frequency for the layer 2.5 Type II SSA template (linear scale). . . 219
Figure 5.110 Smith chart for the layer 2.5 Type II SSA template in free space at 380 MHz. 220
Figure 5.111 Smith chart for the layer 2.5 Type II SSA template in free space at 400 MHz. 221
Figure 5.112 Smith chart for the layer 2.5 Type II SSA template in free space at 420 MHz. 222

Figure 5.113 Smith chart for the layer 2.5 Type II SSA template in free space at 440 MHz. 223
Figure 5.114 Smith chart for the layer 2.5 Type II SSA template in free space at 460 MHz. 224
Figure 5.115 Smith chart for the layer 2.5 Type II SSA template in free space at 480 MHz. 225
Figure 5.116 Smith chart for the layer 2.5 Type II SSA template in free space at 500 MHz. 226
Figure 5.117 Smith chart for the layer 2.5 Type II SSA template in free space at 520 MHz. 227
Figure 5.118 Proportion of configurations with minimum vertical gains in the horizontal plane above 0 dB vs. frequency for the layer 2.5 Type II SSA template. 228
Figure 5.119 Proportion of configurations with SWRs less than 2.0 and minimum vertical gains in the horizontal plane above 0 dB vs. frequency for the layer 2.5 Type II SSA template. 229
Figure 5.120 Proportion of configurations with maximum vertical gains in the horizontal plane above 3.0 dB vs. frequency for the layer 2.5 Type II SSA template. 230
Figure 5.121 Proportion of configurations with SWRs less than 2.0 and maximum vertical gains in the horizontal plane above 3.0 dB vs. frequency for the layer 2.5 Type II SSA template. 231
Figure 5.122 Diagram of the layer 3 SSA template. 233
Figure 5.123 SWR vs. frequency for the layer 3 Type I SSA template in free space (5000 random samples). 237
Figure 5.124 SWR vs. frequency for the layer 3 Type I SSA template above ground (5000 random samples). 238
Figure 5.125 Minimum SWR vs. frequency for the layer 3 Type I SSA template (5000 random samples). 239
Figure 5.126 Proportion of configurations with SWRs less than 4.0 vs. frequency for the layer 3 Type I SSA template in free space (5000 random samples). Error bars show the 95% confidence intervals. 240
Figure 5.127 Proportion of configurations with SWRs less than 4.0 vs. frequency for the layer 3 Type I SSA template over ground (5000 random samples). Error bars show the 95% confidence intervals. 241
Figure 5.128 Proportion of configurations with SWRs less than 4.0 vs. frequency for the layer 3 Type I SSA template (5000 random samples). 242

Figure 5.129 Proportion of configurations with SWRs less than 2.0 vs. frequency for the layer 3 Type I SSA template in free space (5000 random samples). Error bars show the 95% confidence intervals. 243

Figure 5.130 Proportion of configurations with SWRs less than 2.0 vs. frequency for the layer 3 Type I SSA template over ground (5000 random samples). Error bars show the 95% confidence intervals. 244

Figure 5.131 Proportion of configurations with SWRs less than 2.0 vs. frequency for the layer 3 Type I SSA template (5000 random samples). 245

Figure 5.132 Proportion of configurations with SWRs less than 1.5 vs. frequency for the layer 3 Type I SSA template in free space (5000 random samples). Error bars show the 95% confidence intervals. 246

Figure 5.133 Proportion of configurations with SWRs less than 1.5 vs. frequency for the layer 3 Type I SSA template over ground (5000 random samples). Error bars show the 95% confidence intervals. 247

Figure 5.134 Proportion of configurations with SWRs less than 1.5 vs. frequency for the layer 3 Type I SSA template (5000 random samples). 248

Figure 5.135 Proportion of configurations with minimum vertical gains in the horizontal plane above 0 dB vs. frequency for the layer 3 Type I SSA template in free space (5000 random samples). Error bars show the 95% confidence intervals. 249

Figure 5.136 Proportion of configurations with minimum vertical gains in the horizontal plane above 0 dB vs. frequency for the layer 3 Type I SSA template above ground (5000 random samples). Error bars show the 95% confidence intervals. 250

Figure 5.137 Proportion of configurations with minimum vertical gains in the horizontal plane above 0 dB vs. frequency for the layer 3 Type I SSA template (5000 random samples). 251

Figure 5.138 Proportion of configurations with SWRs less than 2.0 and minimum vertical gains in the horizontal plane above 0 dB vs. frequency for the layer 3 Type I SSA template in free space (5000 random samples). Error bars show the 95% confidence intervals. 252

Figure 5.139 Proportion of configurations with SWRs less than 2.0 and minimum vertical gains in the horizontal plane above 0 dB vs. frequency for the layer 3 Type I SSA template above ground (5000 random samples). Error bars show the 95% confidence intervals. 253

Figure 5.140 Proportion of configurations with SWRs less than 2.0 and minimum vertical gains in the horizontal plane above 0 dB vs. frequency for the layer 3 Type I SSA template (5000 random samples). 254

Figure 5.141 Proportion of configurations with maximum vertical gains in the horizontal plane above 3.0 dB vs. frequency for the layer 3 Type I SSA template in free space (5000 random samples). Error bars show the 95% confidence intervals. 255

Figure 5.142 Proportion of configurations with maximum vertical gains in the horizontal plane above 3.0 dB vs. frequency for the layer 3 Type I SSA template above ground (5000 random samples). Error bars show the 95% confidence intervals. 256

Figure 5.143 Proportion of configurations with maximum vertical gains in the horizontal plane above 3.0 dB vs. frequency for the layer 3 Type I SSA template (5000 random samples). 257

Figure 5.144 Proportion of configurations with SWRs less than 2.0 and maximum vertical gains in the horizontal plane above 3.0 dB vs. frequency for the layer 3 Type I SSA template in free space (5000 random samples). Error bars show the 95% confidence intervals. 258

Figure 5.145 Proportion of configurations with SWRs less than 2.0 and maximum vertical gains in the horizontal plane above 3.0 dB vs. frequency for the layer 3 Type I SSA template above ground (5000 random samples). Error bars show the 95% confidence intervals. 259

Figure 5.146 Proportion of configurations with SWRs less than 2.0 and maximum vertical gains in the horizontal plane above 3.0 dB vs. frequency for the layer 3 Type I SSA template (5000 random samples). 260

Figure 5.147 Diagram of the layer 4 SSA template. 261

Figure 5.148 SWR vs. frequency for the layer 4 Type I SSA template (5000 random samples). 264

Figure 5.149 Minimum SWR vs. frequency for the layer 4 Type I SSA template (5000 random samples). 265

Figure 5.150 Proportion of configurations with SWRs less than 4.0 vs. frequency for the layer 4 Type I SSA template (5000 random samples). Error bars show the 95% confidence intervals. 266

Figure 5.151 Proportion of configurations with SWRs less than 2.0 vs. frequency for the layer 4 Type I SSA template (5000 random samples). Error bars show the 95% confidence intervals. 267

Figure 5.152 Proportion of configurations with SWRs less than 1.5 vs. frequency for the layer 4 Type I SSA template (5000 random samples). Error bars show the 95% confidence intervals. 268

Figure 5.153 Proportion of configurations with SWRs less than 1.1 vs. frequency for the layer 4 Type I SSA template (5000 random samples). Error bars show the 95% confidence intervals. 269

Figure 5.154 Proportion of configurations with SWRs less than 1.05 vs. frequency for the layer 4 Type I SSA template (5000 random samples). Error bars show the 95% confidence intervals. 270

Figure 5.155 Proportion of configurations with minimum vertical gains in the horizontal plane above 0 dB vs. frequency for the layer 4 Type I SSA template (5000 random samples). Error bars show the 95% confidence intervals. 271

Figure 5.156 Proportion of configurations with SWRs less than 2.0 and minimum vertical gains in the horizontal plane above 0 dB vs. frequency for the layer 4 Type I SSA template (5000 random samples). Error bars show the 95% confidence intervals. 272

Figure 5.157 Proportion of configurations with maximum vertical gains in the horizontal plane above 3.0 dB vs. frequency for the layer 4 Type I SSA template (5000 random samples). Error bars show the 95% confidence intervals. 273

Figure 5.158 Proportion of configurations with SWRs less than 2.0 and maximum vertical gains in the horizontal plane above 3.0 dB vs. frequency for the layer 4 Type I SSA template (5000 random samples). Error bars show the 95% confidence intervals. 274

Figure 5.159 Diagram of the layer 5 SSA template. 275

Figure 5.160 SWR vs. frequency for the layer 5 Type I SSA template (5000 random samples). 277

Figure 5.161 Minimum SWR vs. frequency for the layer 5 Type I SSA template (5000 random samples). 278

Figure 5.162 Proportion of configurations with SWRs less than 2.0 vs. frequency for the layer 5 Type I SSA template (5000 random samples). Error bars show the 95% confidence intervals. 279

Figure 5.163 Proportion of configurations with SWRs less than 2.0 and maximum vertical gains in the horizontal plane above 3.0 dB vs. frequency for the layer 5 Type I SSA template (5000 random samples). Error bars show the 95% confidence intervals. 280

Figure 5.164 Proportion of configurations with SWRs less than 2.0 and minimum vertical gains in the horizontal plane above 0 dB vs. frequency for the layer 5 Type I SSA template (5000 random samples). Error bars show the 95% confidence intervals. 281

Figure 5.165 Diagram of the layer 6 SSA template. 282

Figure 5.166 SWR vs. frequency for the layer 6 Type I SSA template (5000 random samples). 284

Figure 5.167 Minimum SWR vs. frequency for the layer 6 Type I SSA template (5000 random samples). 285

Figure 5.168 Proportion of configurations with SWRs less than 2.0 vs. frequency for the layer 6 Type I SSA template (5000 random samples). Error bars show the 95% confidence intervals. 286

Figure 5.169 Proportion of configurations with SWRs less than 2.0 and maximum vertical gains in the horizontal plane above 3.0 dB vs. frequency for the layer 6 Type I SSA template (5000 random samples). Error bars show the 95% confidence intervals. 287

Figure 5.170 Proportion of configurations with SWRs less than 2.0 and minimum vertical gains in the horizontal plane above -3.0 dB vs. frequency for the layer 6 Type I SSA template (5000 random samples). Error bars show the 95% confidence intervals. 288

Figure 5.171 Diagram of the layer 7 SSA template. 289

Figure 5.172 SWR vs. frequency for the layer 7 SSA template in free space (5000 random samples). 292

Figure 5.173 SWR vs. frequency for the layer 7 SSA template above ground (5000 random samples). 293

Figure 5.174 Minimum SWR vs. frequency for the layer 7 SSA template (5000 random samples). 294

Figure 5.175 Proportion of configurations with SWRs less than 4.0 vs. frequency for the layer 7 SSA template in free space (5000 random samples). Error bars show the 95% confidence intervals. 295

Figure 5.176 Proportion of configurations with SWRs less than 4.0 vs. frequency for the layer 7 SSA template over ground (5000 random samples). Error bars show the 95% confidence intervals. 296

Figure 5.177 Proportion of configurations with SWRs less than 4.0 vs. frequency for the layer 7 SSA template (5000 random samples). . 297

Figure 5.178 Proportion of configurations with SWRs less than 2.0 vs. frequency for the layer 7 SSA template in free space (5000 random samples). Error bars show the 95% confidence intervals. 298

Figure 5.179 Proportion of configurations with SWRs less than 2.0 vs. frequency for the layer 7 SSA template over ground (5000 random samples). Error bars show the 95% confidence intervals. 299

Figure 5.180 Proportion of configurations with SWRs less than 2.0 vs. frequency for the layer 7 SSA template (5000 random samples). . 300

Figure 5.181 Proportion of configurations with SWRs less than 1.5 vs. frequency for the layer 7 SSA template in free space (5000 random samples). Error bars show the 95% confidence intervals. 301

Figure 5.182 Proportion of configurations with SWRs less than 1.5 vs. frequency for the layer 7 SSA template over ground (5000 random samples). Error bars show the 95% confidence intervals. 302

Figure 5.183 Proportion of configurations with SWRs less than 1.5 vs. frequency for the layer 7 SSA template (5000 random samples). . 303

Figure 5.184 Proportion of configurations with SWRs less than 1.1 vs. frequency for the layer 7 SSA template in free space (5000 random samples). Error bars show the 95% confidence intervals. 304

Figure 5.185 Proportion of configurations with SWRs less than 1.1 vs. frequency for the layer 7 SSA template over ground (5000 random samples). Error bars show the 95% confidence intervals. 305

Figure 5.186 Proportion of configurations with SWRs less than 1.1 vs. frequency for the layer 7 SSA template (5000 random samples). . 306

Figure 5.187 Proportion of configurations with minimum vertical gains in the horizontal plane above 0 dB vs. frequency for the layer 7 SSA template in free space (5000 random samples). Error bars show the 95% confidence intervals. 307

Figure 5.188 Proportion of configurations with minimum vertical gains in the horizontal plane above 0 dB vs. frequency for the layer 7 SSA template above ground (5000 random samples). Error bars show the 95% confidence intervals. 308

Figure 5.189 Proportion of configurations with minimum vertical gains in the horizontal plane above 0 dB vs. frequency for the layer 7 SSA template (5000 random samples). 309

Figure 5.190 Proportion of configurations with SWRs less than 4.0 and minimum vertical gains in the horizontal plane above 0 dB vs. frequency for the layer 7 SSA template in free space (5000 random samples). Error bars show the 95% confidence intervals. 310

Figure 5.191 Proportion of configurations with SWRs less than 4.0 and minimum vertical gains in the horizontal plane above 0 dB vs. frequency for the layer 7 SSA template above ground (5000 random samples). Error bars show the 95% confidence intervals. 311

Figure 5.192 Proportion of configurations with SWRs less than 4.0 and minimum vertical gains in the horizontal plane above 0 dB vs. frequency for the layer 7 SSA template (5000 random samples). . 312

Figure 5.193 Proportion of configurations with maximum vertical gains in the horizontal plane above 3.0 dB vs. frequency for the layer 7 SSA template in free space (5000 random samples). Error bars show the 95% confidence intervals. 313

Figure 5.194 Proportion of configurations with maximum vertical gains in the horizontal plane above 3.0 dB vs. frequency for the layer 7 SSA template above ground (5000 random samples). Error bars show the 95% confidence intervals. 314

Figure 5.195 Proportion of configurations with maximum vertical gains in the horizontal plane above 3.0 dB vs. frequency for the layer 7 SSA template (5000 random samples). 315

Figure 5.196 Proportion of configurations with SWRs less than 2.0 and maximum vertical gains in the horizontal plane above 3.0 dB vs. frequency for the layer 7 SSA template in free space (5000 random samples). Error bars show the 95% confidence intervals. 316

Figure 5.197 Proportion of configurations with SWRs less than 2.0 and maximum vertical gains in the horizontal plane above 3.0 dB vs. frequency for the layer 7 SSA template above ground (5000 random samples). Error bars show the 95% confidence intervals. 317

Figure 5.198 Proportion of configurations with SWRs less than 2.0 and maximum vertical gains in the horizontal plane above 3.0 dB vs. frequency for the layer 7 SSA template (5000 random samples). . 318

Figure A.1 Example SSA template generated using an object from the class `rectangles_template`. 333

Figure A.2 Diagram of the switch model `swLeverWire`. 337

KEY TO SYMBOLS AND ABBREVIATIONS

ACO: Ant Colony Optimization

GA: Genetic Algorithm

MEMS: Microelectromechanical systems

NEC: Numerical Electromagnetics Code

SA: Simulated Annealing

SSA: Self-Structuring Antenna

CHAPTER 1

INTRODUCTION

This dissertation investigates a new class of antennas called 'self-structuring antennas' (SSAs). SSAs are capable of altering their electrical characteristics in response to their electromagnetic environment. Although other types of adaptive antennas have been studied in the past, it is shown that SSAs are fundamentally different from these and other traditional antenna systems.

A basic description of SSAs and the concepts behind their operation are given in Chapter 2. A review of the literature is also given in this chapter to provide a perspective of how SSAs compare to existing antenna systems.

Chapter 3 presents a prototype SSA built at Michigan State University. This chapter includes experimental results that demonstrate the capabilities of SSAs.

SSAs are capable of being arranged into a large number of possible electromagnetic configurations. Searching through these possible configurations could take a substantial amount of time before a configuration with desirable characteristics is located. To reduce searching time, SSAs employ the use of modern algorithms. The application of Ant Colony Optimization (ACO), simulated annealing (SA), and genetic algorithms (GAs) to SSAs is presented in Chapter 4. Results are presented that compare these algorithms with random searches of simulated SSAs.

To gain a better understanding of the capabilities of SSAs and to understand the role of the number of switches on SSA performance, a study of simple SSAs is presented in Chapter 5. In this study, numerical simulations are performed that model SSAs with a small number of switches so that exhaustive searches are possible. The number of switches is then increased until random searches are required.

A conclusion to this dissertation is given in Chapter 6. Original contributions are

identified in this chapter. Conclusions are drawn from the research detailed in the dissertation. Possible future work in the area of self-structuring antennas is discussed. Finally, Appendix A provides a description of the computer programs that are used to simulate SSAs.

CHAPTER 2

OVERVIEW OF SELF-STRUCTURING ANTENNAS

2.1 Introduction

Traditional antennas typically have fixed geometrical configurations and are generally designed to operate under specific electrical and environmental conditions [1]. Considerable engineering is performed to assure that an antenna will have acceptable electrical characteristics (gain, bandwidth, input impedance, etc.) prior to deployment in a particular environment such as in a handheld communications device or aboard an aircraft or automobile. Coupling with other objects in the vicinity of traditional antennas can strongly affect performance and must be accounted for prior to deployment. Unfortunately, these effects are generally difficult to predict and mitigate using analytical or numerical methods. The result is that many antennas are still designed using costly and time consuming measurements along with cut and try engineering. When put in place, these antennas are not able to respond to changes in the environment for which they were designed. For example, an automotive antenna cannot respond to either the rapid changes in the car's motion or to changes to the car from the addition of aftermarket items (speakers, roof racks, etc.). Similarly, a cellular phone antenna cannot compensate for being held against different users' heads.

Given these difficulties, a new type of antenna has been developed that is capable of adapting to new situations and environments without the need for extensive engineering and design prior to deployment. The term 'Self-Structuring Antenna' (SSA) has been coined to describe this new class of antennas. An SSA can alter its electrical shape in response to changes in its environment or application.

An SSA consists of a number of wires, patches, or other conducting bodies in-

terconnected by controllable switches. The electrical characteristics of the antenna are adjusted by selectively opening or closing switches using a microprocessor-based controller. The SSA performance is evaluated by a receiver that can measure signal strength, input impedance, or any other appropriate available measure. By using many switches, the SSA is capable of arranging itself into any one of a very large number of discrete electrical configurations. In contrast to traditional antennas, the electrical characteristics of SSAs are generally unknown at the onset of operation. Efficient binary algorithms are used to quickly search through the possible configurations.

This chapter provides an overview of self-structuring antennas. The basic concepts behind SSAs and their operation are given in Section 2.2. Section 2.2 also defines some of the requirements of SSA systems. A brief historical background on SSAs is given in Section 2.7. This is followed by a review of the literature to explain where SSA research fits into existing antenna technology.

2.2 Concept

A basic overview of the self-structuring antenna concept is presented here. A block diagram of a general self-structuring antenna system is shown in Figure 2.1. This diagram shows the major components of an SSA: a template, a receiver, and a microprocessor. A self-structuring antenna template has the capability of realizing a large number of different antenna configurations. A receiver measures the performance or quality of a specific configuration. The receiver then provides a feedback signal to a microprocessor, which uses this information along with an efficient binary search routine to make decisions about the future configurations of the antenna system. The microprocessor then controls the template to set a new configuration. These SSA components will now be explained in further detail in the following subsections.

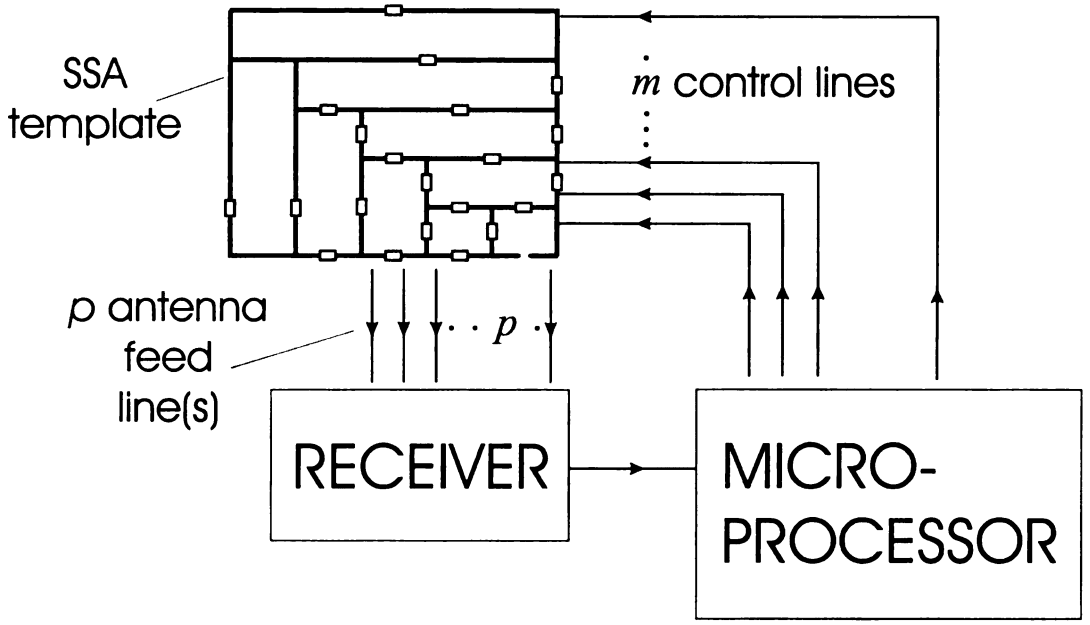


Figure 2.1. Block diagram of a self-structuring antenna system.

2.3 Self-Structuring Antenna Template

A self-structuring antenna 'template' is the primary intended radiator and receiver of electromagnetic energy for a self-structuring antenna system. Templates are also called the 'skeletons' or 'radiating structures' of the SSA. A template is simply a collection of wire sections, patches, or other conductors interconnected by controllable switches. A typical template comprised of wire sections is shown in Figure 2.2. The white rectangles denote the switches on the template.

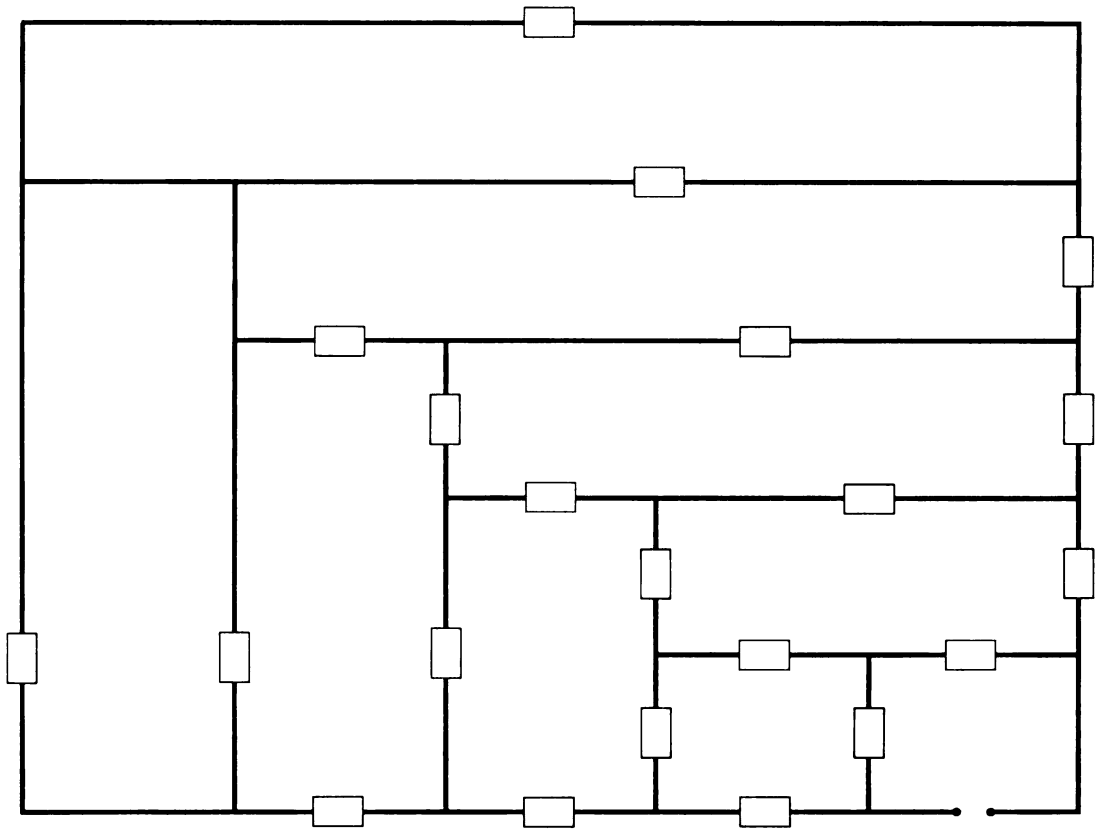


Figure 2.2. Diagram of a generic self-structuring antenna template.

A template can be arranged into a large number of different possible configurations or electrical shapes. This is achieved by setting the states of the switches on the antenna template. The term *configuration* refers to the combination of 'on' or 'off' states of the SSA template switches. The switches alter the current on the template and nearby conductors and therefore influence the electrical characteristics of the self-structuring antenna system.

The template illustrated in Figure 2.2 shows an asymmetric topology. This asymmetry is exploited to maximize the 'diversity' of the antenna system by minimizing the repeated states of the antenna. A template using n switches is capable of being arranged into 2^n possible configurations. With an asymmetric topology, changing the

state of any one of these switches guarantees a new and unique configuration of the template. For each configuration of a template using a symmetric topology, there may be several other configurations that are geometrically equivalent, thus reducing the number of unique configurations.

The performance of a traditional antenna is often impaired by the presence of nearby objects. These effects are difficult if not impossible to predict prior to the antenna's deployment. In contrast, an SSA can adjust its characteristics to compensate for the nearby objects. In some cases, coupling to other objects can actually enhance the performance of an SSA. Experimental results shown in Chapter 3 demonstrate that an SSA can make effective use of coupling between the template and control lines, power supply lines, and support structures, to enhance the performance of the antenna system.

2.4 Receiver

A critical component of a self-structuring antenna system is the receiver used to measure and quantify the performance of an antenna configuration. Depending on the intended application and needs of the antenna system, the receiver could measure input impedance or SWR, frequency characteristics and bandwidth, received signal strength, antenna pattern, adjacent channel interference, or other quantities. The receiver then sends information to a microprocessor regarding the measurement of one or more of these quantities for an antenna configuration.

The term 'sensor' is sometimes used to identify the receiver of an SSA. This is usually done to clear up any ambiguity about the purpose of the receiver. An SSA can be used as a transmitting antenna, but the SSA system will still use a receiver to obtain the characteristics of the SSA such as input impedance, SWR, radiated signal strength, etc.

2.5 Microprocessor

Another essential component of a self-structuring antenna system is a microprocessor. The microprocessor controls the configuration of the antenna system by setting the states of the switches on the antenna template. The microprocessor acquires the performance information of the antenna system's measured configurations sent by the receiver. This information helps the microprocessor make a decision on which switches to set on the antenna template to achieve a configuration that performs well.

2.6 Search Algorithms

In order to find a configuration that best meets the desired performance criteria, the microprocessor must search through the set of possible configurations. As mentioned previously, an antenna system using a template with n switches has 2^n possible configurations. As n grows large, it quickly becomes unfeasible to exhaustively search through all of the possible configurations to find the one with the best performance characteristics, especially if the antenna system is to be adapted in real-time. A random search of the possible configurations may be employed to find a suitable configuration, but this may take an acceptable amount of time. For these reasons, a critical component of an SSA with an appreciable number of switches is an efficient binary search routine. This search routine is run by the microprocessor of the SSA.

Genetic algorithms (GAs), simulated annealing (SA), and Ant Colony Optimization (ACO) have been investigated as binary search routines for SSAs. Chapter 4 describes the implementation of these algorithms with SSAs. Random and exhaustive searches performed for SSAs with small numbers of switches are presented in Chapter 5.

2.7 A Brief History of Self-Structuring Antennas

Self-structuring antennas were invented by Dr. Edward J. Rothwell at Michigan State University. Dr. Rothwell conceived of the SSA concept in 1997, and he built the first several prototypes in the same year. After experimental evidence indicated that the SSA had promising characteristics, Dr. Rothwell filed for a U.S. patent with the help of Michigan State University.

SSA research began to accelerate in 1998-1999 as Dr. John Ross began intensive numerical simulations. As Dr. Rothwell's graduate student, the author became involved with SSA research in the summer of 1999 at the beginning of his Ph.D. program. Delphi Research Labs got involved in the project in 2000 and began funding in 2001. The first conference papers on SSAs were presented in the summer of 2000 at the AP-S / URSI conference in Salt Lake City, Utah [2], [3].

SSA research is continuing at Michigan State University, John Ross and Associates, and Delphi Research Labs. U.S. patent number 6,175,723 was issued in January 2001 to Michigan State University that covers the self-structuring antenna concept.

2.8 Literature Review

SSAs constitute a nascent technology where little has been published to this date. The Electromagnetics Research Group at Michigan State University has been the primary researcher in the area and has helped author the only known literature on the subject [2]–[6]. Although little literature exists that deals with SSAs, there are many types of antenna concepts and technologies that appear to have common ideas with those used by SSAs. This section will contrast existing technologies and techniques with those employed by SSAs.

Phased array systems have been investigated thoroughly in antenna research [7]. While at first glance the SSA may appear to resemble a phased array system, an SSA

can be implemented with a single feed point and without complicated and expensive phase shifters used by phased array systems. An SSA uses simple 'on' or 'off' switches to alter its electrical characteristics.

Adaptive phased array systems have been studied extensively in the literature. Introduced in the early- to mid-1960s [7]–[26], these systems are characterized by sophisticated feedback systems that alter the amplitudes and phases of the signals received or transmitted by the array elements [27]–[98]. Many antenna systems such as retrodirective arrays, self-cohering arrays, self-focusing arrays, self-phasing arrays, Antennafier arrays, correlating arrays, and others have names that describe their specific application, but still fall under the more general category of adaptive phased arrays. While most adaptive phased arrays have the capability to alter their electromagnetic characteristics, they differ from SSA systems in that they still require expensive and complicated phase shifters for array elements needed in normal phased arrays. The electrical sizes of the SSAs in this dissertation will typically be much smaller than those of a corresponding phased array or adaptive phased array.

Direction finding is an important area of electromagnetics research that has been studied in the literature [99], [100]. Most direction finding antenna systems use phased array systems or other antenna systems that fundamentally differ from SSAs.

Due to the proliferation of cellular and mobile communications, a great deal of research on wireless communications is surfacing that is related to both handset and base station technology as well as propagation characteristics [101]–[130]. Smart antennas have been investigated for use with mobile communications [131]–[136]. While many base station smart antenna systems are capable of adapting to interference using sophisticated signal processing techniques, most smart antennas are array based and are very similar to adaptive phased arrays [131]. There also has been increased interest in novel electrically small antennas due to the size restrictions on wireless handsets. Although there are inherent physical limitations of electrically small an-

tennas [137], [138], several areas of research have surfaced to investigate new types of physically and electrically small antennas. These include fractal antennas [139]–[146], planar inverted F antennas (PIFAs) [147]–[150], and other electrically small antennas [151].

Automobiles operate in a tough electromagnetic environment that is constantly changing. Antenna systems for automotive applications have been investigated [152], but these systems do not employ the concepts used by SSAs.

There are several types of adaptive antennas that use switches or other devices to select different discrete configurations. These include reconfigurable-aperture (RECAP) antennas [153], switchable antennas [154]–[157], diversity antennas [158]–[161], and other adaptive antennas [135]. These differ from SSAs because the number of possible electromagnetic configurations of these adaptive antennas is small enough to search through exhaustively, and a real-time modern search algorithm is not utilized. It is also important to emphasize that at the onset of operation of an SSA, it is possible that none of the electromagnetic characteristics of any of the configurations is known. This is fundamentally different from most other adaptive antennas, where the system selects between a few states with known properties.

In recent years, many optimization problems have been simplified by using genetic algorithms (GAs) [162]–[166]. As will be discussed in Chapter 4, GAs attempt to mimic the natural non-linear optimization methods inherent in biological systems. GAs have been applied to a wide range of electromagnetic problems [167]–[177], including antenna design [145], [178]–[186], arrays [187]–[190], and adaptive phased arrays [191], [192].

Another optimization method that attempts to mimic nature is simulated annealing (SA) [193]. Simulated annealing models the cooling process of a solid and attempts to locate the lowest energy state. An advantage of SA is that it is usually easier to implement than a GA. SA has been applied to some electromagnetics

problems [194]–[196], but it has not enjoyed the same success that GAs have had.

A group of evolutionary algorithms that have gained considerable interest in recent years are Ant Colony Optimization (ACO) algorithms [197]–[207]. These algorithms mimic the collective foraging behavior of ants. A conference paper that used ACO with SSAs was presented at the Boston AP-S / URSI conference in the summer of 2001 [4]. Although applications of these algorithms are growing in number, applications to electromagnetics other than the SSA have not surfaced.

This section discusses many antenna technologies and search algorithms that appear in literature. Although these topics are only a sample of all possible technologies, the purpose here is to show that SSAs belong to a new body of knowledge that needs to be researched.

2.9 Conclusion

This chapter provides an overview of self-structuring antennas. The SSA concept is discussed in Section 2.2. The fundamental components of an SSA, including the template, receiver, microprocessor, and search algorithms, are detailed in Sections 2.3-2.6. A brief history of SSAs in Section 2.7 is then followed by a review of the literature in Section 2.8 that shows how SSA technology compares to existing technologies.

The next chapter presents a prototype SSA built at Michigan State University. Measured results demonstrate some of the capabilities of SSAs.

CHAPTER 3

PROTOTYPE SELF-STRUCTURING ANTENNAS AND EXPERIMENTAL RESULTS

To gain a better understanding of the properties and capabilities of self-structuring antennas, a prototype SSA was constructed and tested at Michigan State University. This chapter discusses the details of this prototype antenna system and presents experimental results.

Section 3.1 describes the self-structuring antenna prototype. The components of this SSA system such as its template, feed point, receivers, and microprocessor are discussed in Section 3.1.1 through Section 3.1.4. The measured results for the SSA prototype are discussed in Section 3.2. Measurements investigating standing wave ratio (SWR) optimization as well as reception optimization are presented.

3.1 Self-Structuring Antenna Prototype

The first SSA prototypes were constructed at Michigan State University by Dr. Edward J. Rothwell, the inventor of the self-structuring antenna. The first few prototypes did not perform well because they only utilized a few switches and their template topologies were highly symmetric, resulting an a low number of unique antenna configurations for each prototype. For instance, one prototype utilized eight switches to create 256 possible antenna configurations. Many of these configurations were repeated because of the symmetry of the template, thus reducing the number of unique configurations. When measured, the prototype performed poorly because none of the possible antenna configurations had an acceptable input impedance.

A successful prototype was created when Dr. Rothwell increased the number of switches to 23 and used an asymmetric template topology. Input impedance mea-

surements of this prototype improved dramatically. This section presents the details of this prototype. The measured results are presented in Section 3.2.

3.1.1 Template

A photograph of the prototype SSA is shown in Figure 3.1. The prototype uses 23 controllable switches to provide the antenna system with 2^{23} or 8,388,608 possible configurations. An asymmetric topology is used to ensure that each configuration is unique to enhance the capabilities of the antenna system.

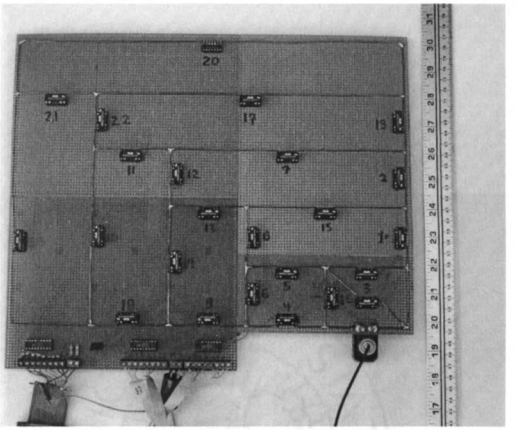


Figure 3.1. Photograph of the SSA prototype.

The template dimensions are 34.8 cm by 26.2 cm. The template wires and switches are mounted on plastic perforated boards. The power lines and control lines that connect to each switch are wired on the back of the perforated boards, as shown in Figure 3.2 and Figure 3.3. These wires influence the electrical characteristics of the prototype antenna system.

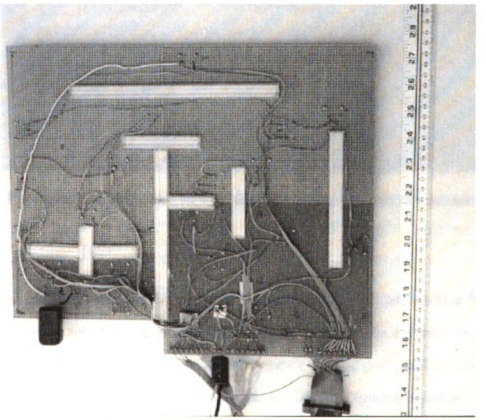


Figure 3.2. Photograph showing the wiring of the back of the SSA prototype.

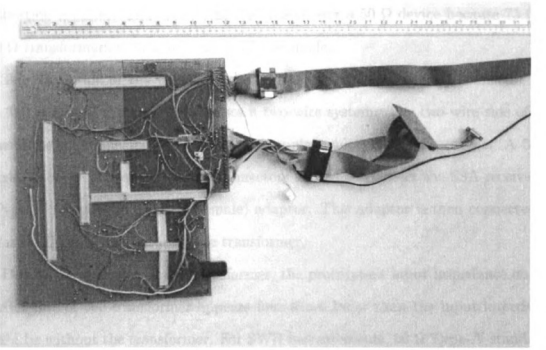


Figure 3.3. Photograph showing the back of the SSA prototype and the connecting cables.

A personal computer decides the states of the 23 switches with information from a receiver, and then sets the states of these switches. Eight of the switches on the prototype's template are controlled from the computer's parallel port, and the fifteen remaining switches are controlled from a Basic Stamp II (BS2) microcontroller. This Basic Stamp II receives its instructions from the personal computer over a serial port [208].

3.1.2 Feed Structure

A single feed point is used for the prototype template. The feed point is shown in the lower right hand corner of the prototype in Figure 3.1. A 75 Ω to 300 Ω transformer is used at the feed point of the prototype's template to balance the currents on the network analyzer's test port cable to ensure accurate measurements.

This transformer fixture simplifies the connection to the coaxial input cable such that calibration is easier. This transformer is chosen over a 50 Ω device because 75 Ω to 300 Ω transformers are cheap and readily available.

The 75 Ω side of the transformer uses a Type-*F* (male) coaxial connector and the 300 Ω side of the transformer uses a two-wire system. The two-wire side of the transformer is connected directly to the template wires of the prototype. A 50 Ω coaxial cable with Type-*N* (male) connectors is used to connect the SSA receiver to a Type-*N* (female) to Type-*F* (female) adaptor. This adaptor is then connected to the male Type-*F* connector on the transformer.

Due to the presence of the transformer, the prototype's input impedance on the coaxial side of the transformer appears four times lower than the input impedance would be without the transformer. For SWR measurements, 50 Ω Type-*N* standards are used to establish a calibration plane at the end of the coaxial cable leading to the receiver (at the Type-*N* to Type-*F* adaptor). A measured SWR value of 1.0 relative to the 50 Ω calibration standards therefore corresponds to a 200 Ω prototype input impedance on the 300 Ω side of the transformer. This assumes that the transformer and adaptors can be modeled as lumped elements at the frequencies studied.

3.1.3 Receivers

Different devices are used as the receiver of the prototype SSA depending on the type of feedback signal that the system is trying to optimize. Standing wave ratio (SWR) and received signal strength are feedback signals that have been investigated. For SWR optimization, a Hewlett Packard 8510C Network Analyzer is used to measure the SWR for each antenna configuration. Information is transferred to the PC using the Hewlett Packard Interface Bus (HPIB). A diagram of the prototype antenna system using the HP 8510C is shown in Figure 3.4.

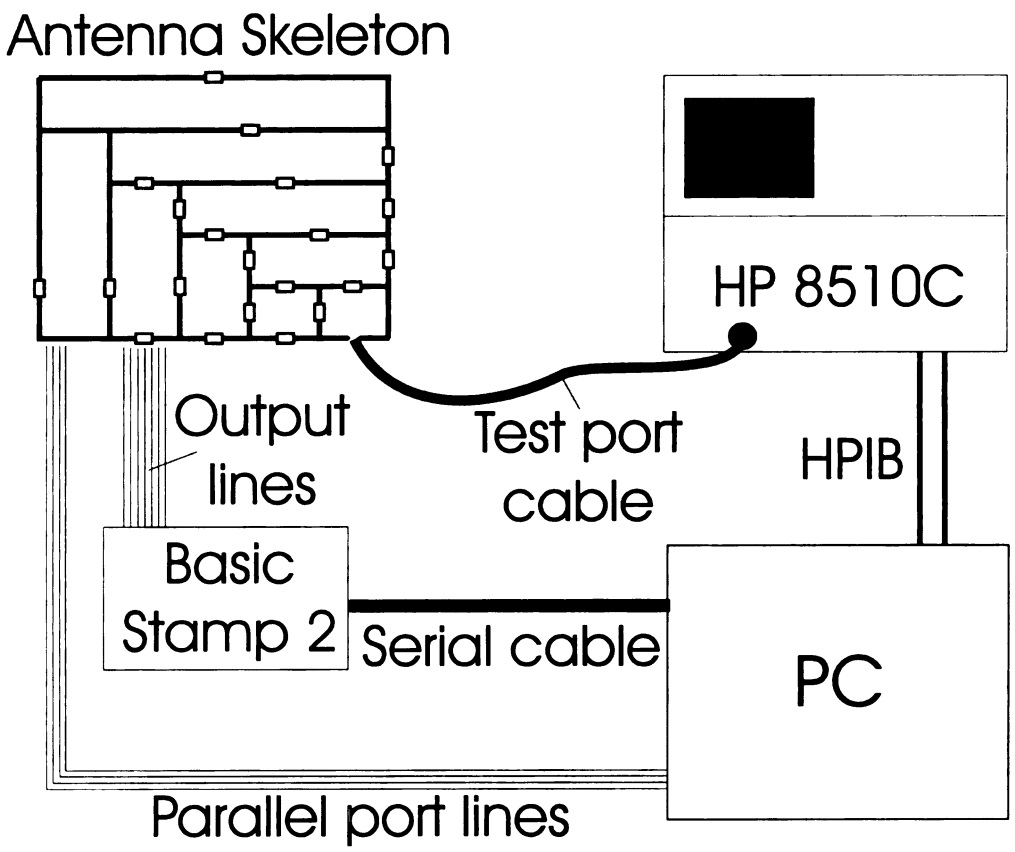


Figure 3.4. SWR optimization measurement setup.

For reception optimization, a different receiver system is used as shown in Figure 3.5. An HP 8551B Spectrum Analyzer measures the strength of the signal that is received by the prototype's template for each antenna configuration. An external circuit was constructed to measure the vertical deflection of the spectrum analyzer's CRT and convert the result into a digital representation. A schematic diagram of this circuit is shown in Figure 3.6. An LTC 1298 analog to digital converter is used to digitize the signal conditioned by the circuit. The circuit uses the horizontal deflection of the spectrum analyzer's CRT to synchronize each analog to digital conversion. A secondary BS2 is used to control the LTC 1298 and to return the digital result to the

PC. The BS2 controls the LTC 1298 through the $\overline{CS}$ and CLK pins on the analog to digital converter chip.

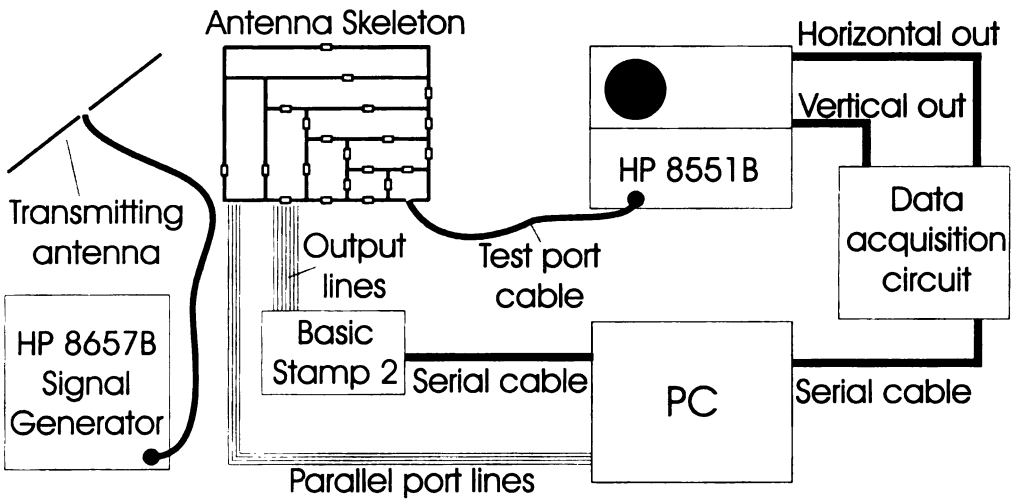


Figure 3.5. Received signal optimization measurement setup.

3.1.4 Microprocessor

A Dell Pentium 133 MHz personal computer is used as the microprocessor for the prototype SSA system. The computer acquires information about the quality of each SSA configuration of the antenna from the receiver. The personal computer uses a program written in BASIC to control the SSA and run the search algorithms. This program is described in Appendix A. Exhaustive searches are unfeasible because the computer requires between 0.5 to 1.0 seconds to acquire an SWR measurement and 0.05 to 0.5 seconds to acquire a received signal measurement. Therefore simulated annealing (SA) and genetic algorithms (GAs) are used to search for optimal SSA configurations. A thorough explanation of the application of these algorithms to SSAs is given in Chapter 4. Only the parameters of the algorithms used for measurements are presented in this chapter.

3.2 Measured Results

As discussed in the introduction to this chapter, measurements were performed to investigate the capabilities of the prototype SSA. Section 3.2.1 discusses the standing wave ratio optimization measurements and Section 3.2.2 discusses the received signal optimization measurements of the prototype SSA system.

3.2.1 SWR Optimization

A study was performed to investigate the tunable bandwidth of the prototype SSA system. This was done by searching for SSA configurations with low standing wave ratios (SWRs) at individual fixed frequencies within a chosen band.

As described in Section 3.1.3, an HP 8510C network analyzer was used as the receiver for the prototype SSA system for SWR optimization studies. The experimental arrangement for SWR optimization studies is shown in Figure 3.4.

The prototype template was placed inside an anechoic chamber to separate the template from nearby objects, but it is important to note that the absorber on the

chamber walls is not effective at frequencies lower than 500 MHz.

50 Ω standards were used to establish a calibration plane on the coaxial side of the template feed structure. This feed structure is described in Section 3.1.2. The switch numbering on the template for this investigation is shown in Figure 3.7. A permanent open circuit exists at the top of the template because only 23 control lines are available using the experimental arrangements described in this chapter.

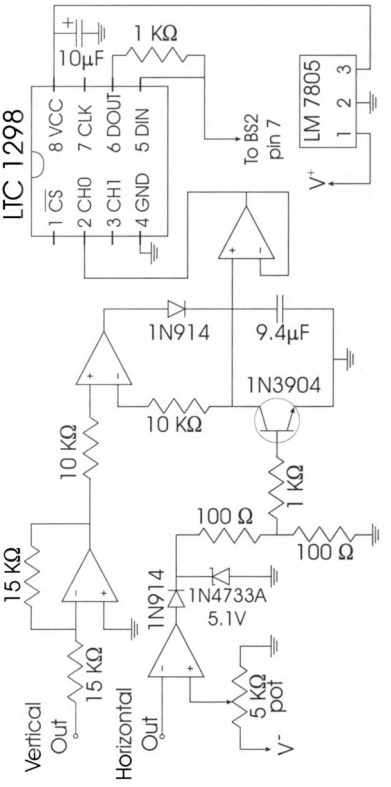


Figure 3.6. Data acquisition circuit.

Table 3.1. Simulated annealing (SA) parameters used for SWR optimization.

Initial temperature, T_0	3.0 K
Temperature fraction, T_f	0.966
Number of temperatures, N_{gen}	200
Number of iterations at each temperature, N_{pop}	20

Table 3.2. Genetic algorithm (GA) parameters used for SWR optimization.

Probability of crossover, p_{cross}	0.5
Probability of mutation, p_{mut}	0.01
Number of generations, N_{gen}	400
Population number, N_{pop}	100

Measurements were performed from 50 MHz to 750 MHz at 25 MHz intervals. Measurements were also performed at 45 MHz, which is the lowest operating frequency of the HP 8510C network analyzer. SSA configurations with low standing wave ratios relative to 50 Ω were sought using simulated annealing (SA) and genetic algorithms (GAs). The parameters used for the simulated annealing algorithm are shown in Table 3.1, and the parameters used for the genetic algorithm are shown in Table 3.2. These search algorithm parameters are explained in Chapter 4.

The measured results are shown in Figure 3.8. The prototype SSA is able to achieve an acceptable SWR over a large band of frequencies by re-optimizing at each studied frequency. The minimum standing wave ratio rises above 2.0 at 725 MHz, but stays below 2.0 at the studied frequencies lower than 700 MHz.

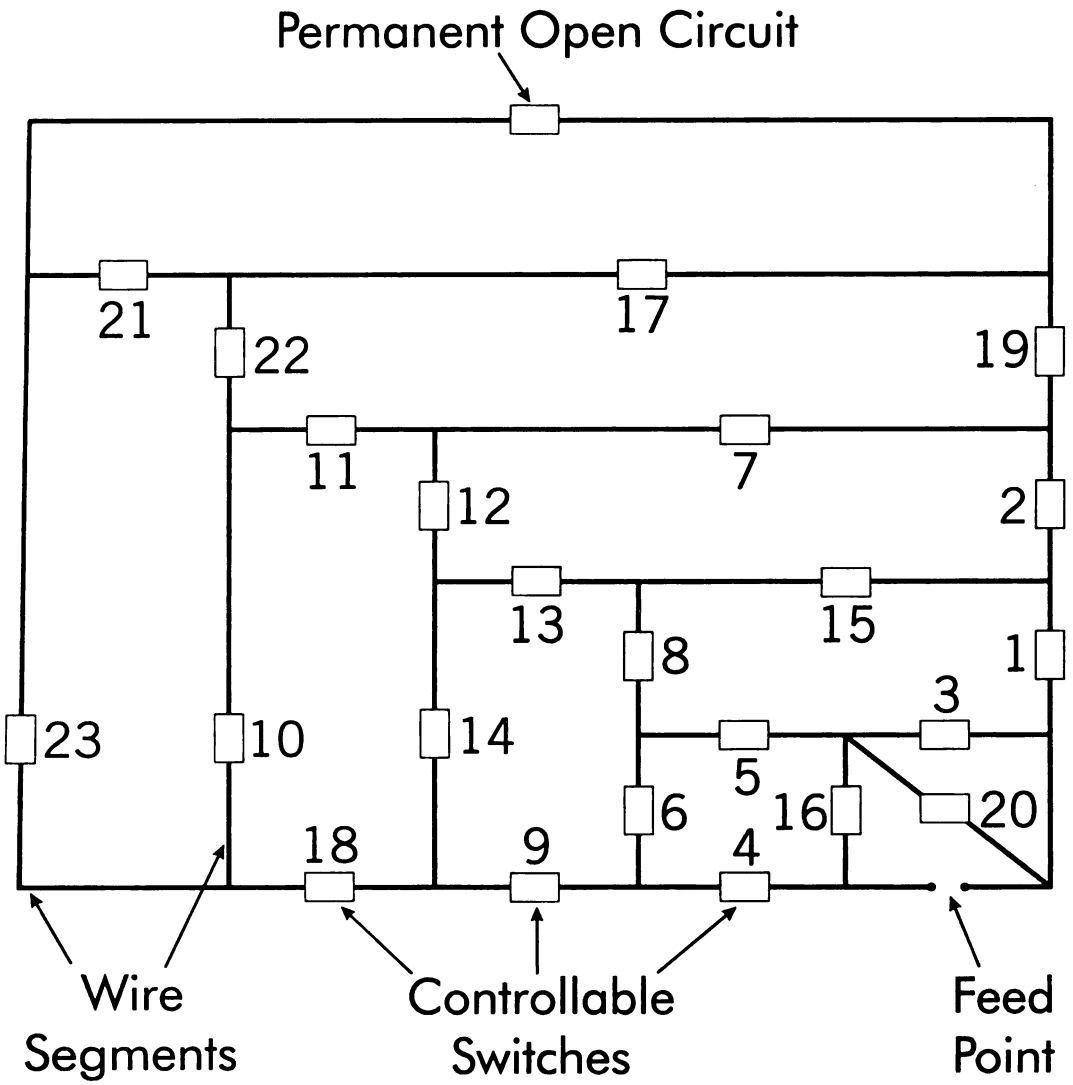


Figure 3.7. Switch configuration of prototype template used for SWR optimization.

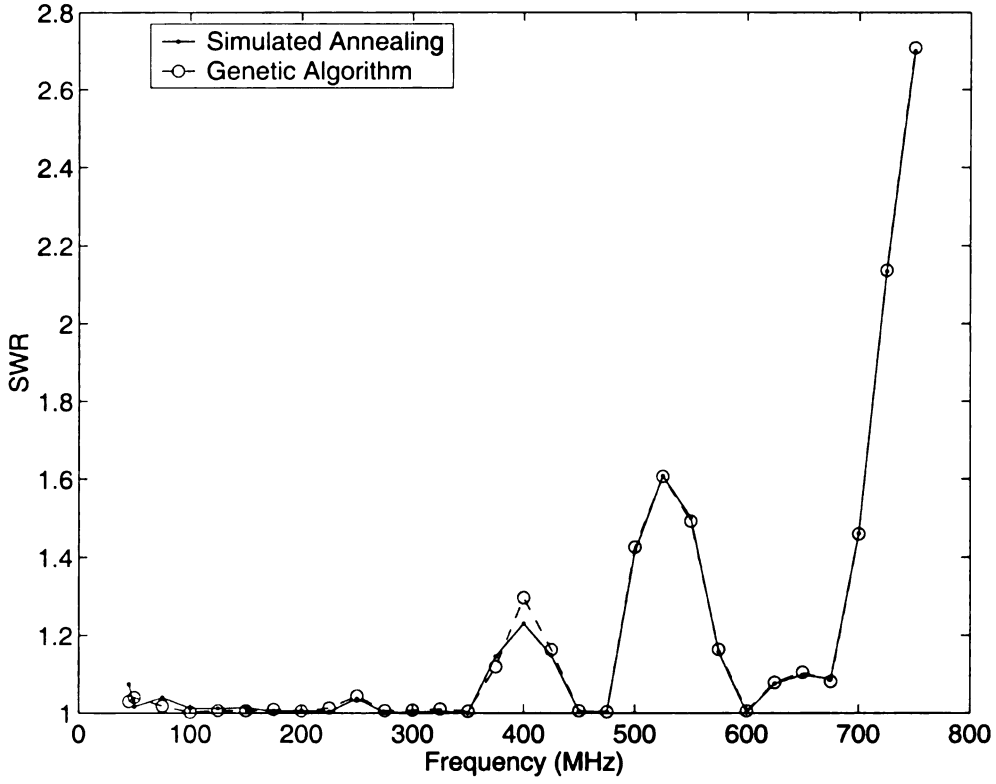


Figure 3.8. Measured SWR of prototype SSA optimized at each frequency.

A more detailed SWR plot over the ten to one frequency range from 45 MHz to 450 MHz is shown in Figure 3.9. The SWR of the prototype antenna system is below 1.1 at nearly every frequency in this range. The poorest performing SSA configurations in this range were found at 400 MHz, where the simulated annealing and genetic algorithms found SSA configurations with SWRs of 1.26 and 1.3, respectively.

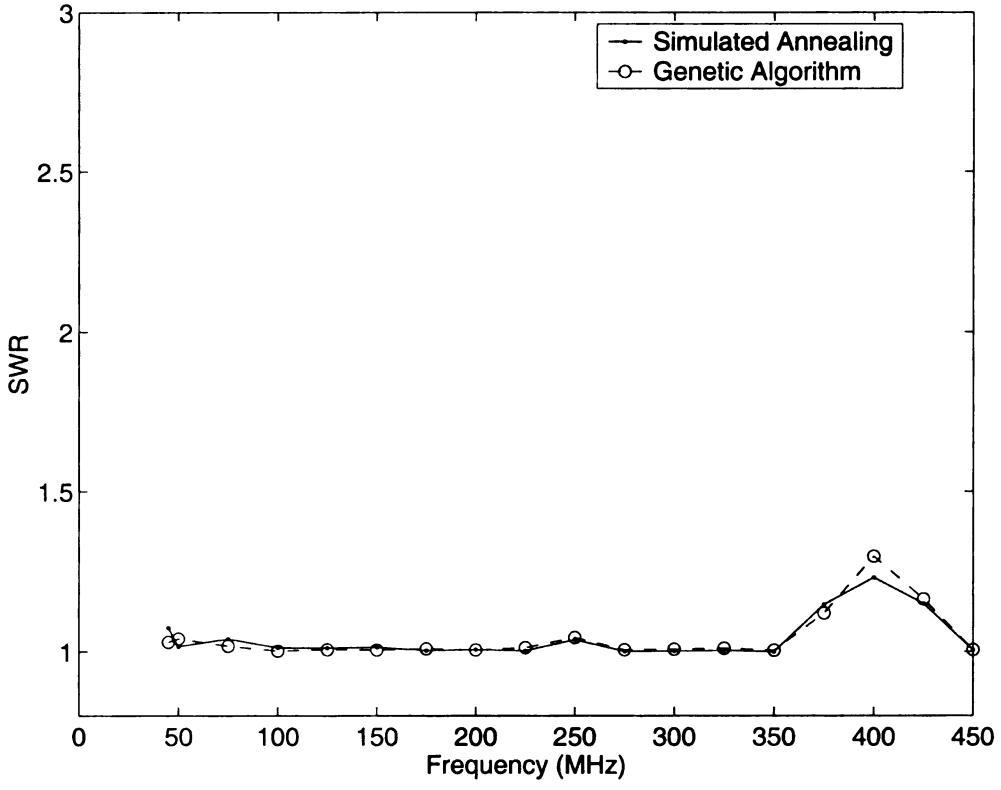


Figure 3.9. A closer look at the measured SWR of prototype optimized at each frequency.

Notice that at frequencies below 100 MHz where the prototype's template is electrically small, SSA configurations are found that exhibit extremely low SWR values. It needs to be mentioned that for the SWR measurements presented here, the coupling of current to the power lines, data lines, or the wires on the back of the template was not suppressed. Thus, electromagnetic energy was permitted to couple to these lines and radiate, allowing for the possibility of lower SWR values. The template is therefore not the only radiating element, and the additional conductors shown in Figure 3.2 and Figure 3.3 are part of the prototype self-structuring antenna system.

The ability to adapt to nearby conductors is one of the benefits of using an

SSA system. A conventional antenna system is designed for specific conditions and geometries, and any change in these conditions or unforeseen nearby conductors will possibly degrade the desired performance of the antenna. An SSA takes into account all of the surrounding conditions and nearby conductors when the system is optimized, so performance degradation is minimized. In the case of the SWR measurements presented here, the nearby conductors possibly enhanced the performance of the prototype antenna system by increasing the electrical length of the antenna system over the electrically small prototype template.

3.2.2 Received Signal Optimization

Investigations into reception optimization were also performed on the prototype SSA. In these measurements, the prototype SSA attempted to maximize the received signal from a transmitting antenna.

A diagram of the reception optimization measurement setup is shown in Figure 3.5. As discussed in Section 3.1.3, an HP 8551B Spectrum Analyzer is used as the receiver for the SSA system during reception optimization. The transmitting antennas used were horizontally polarized dipole and horn antennas. The measurements were performed in an anechoic chamber.

The prototype template and switch numbering is slightly different for this study. This is shown in Figure 3.10, where there is no switch across the diagonal near the feed point. The diagonal switch shown in Figure 3.7 was inserted to see if performance would improve at higher frequencies, and this was done after measurements were performed using the switch arrangement shown in Figure 3.10. No direct comparison between the two switch arrangements was performed for the sake of time.

The first reception optimization measurements were performed at 300 MHz. The antenna was rotated through the angle θ between 0° and 90° as shown in Figure 3.11. A total of seven orientations were investigated. A horizontally polarized horn antenna was used as the transmitting antenna. The received signal was optimized at each ori-

entation using simulated annealing. The simulated annealing parameters used for this optimization are shown in Table 3.3. The total number of temperatures used by the SA algorithm was varied with the measurement angle as shown in Table 3.4 to obtain acceptable results. The results from this investigation are shown in Figure 3.12. Over the angles studied, the SSA can be reoptimized to find a configuration with a suitable received signal strength. The variation in received signal strength versus orientation angle is quite small (3.7 dB maximum to minimum ratio).

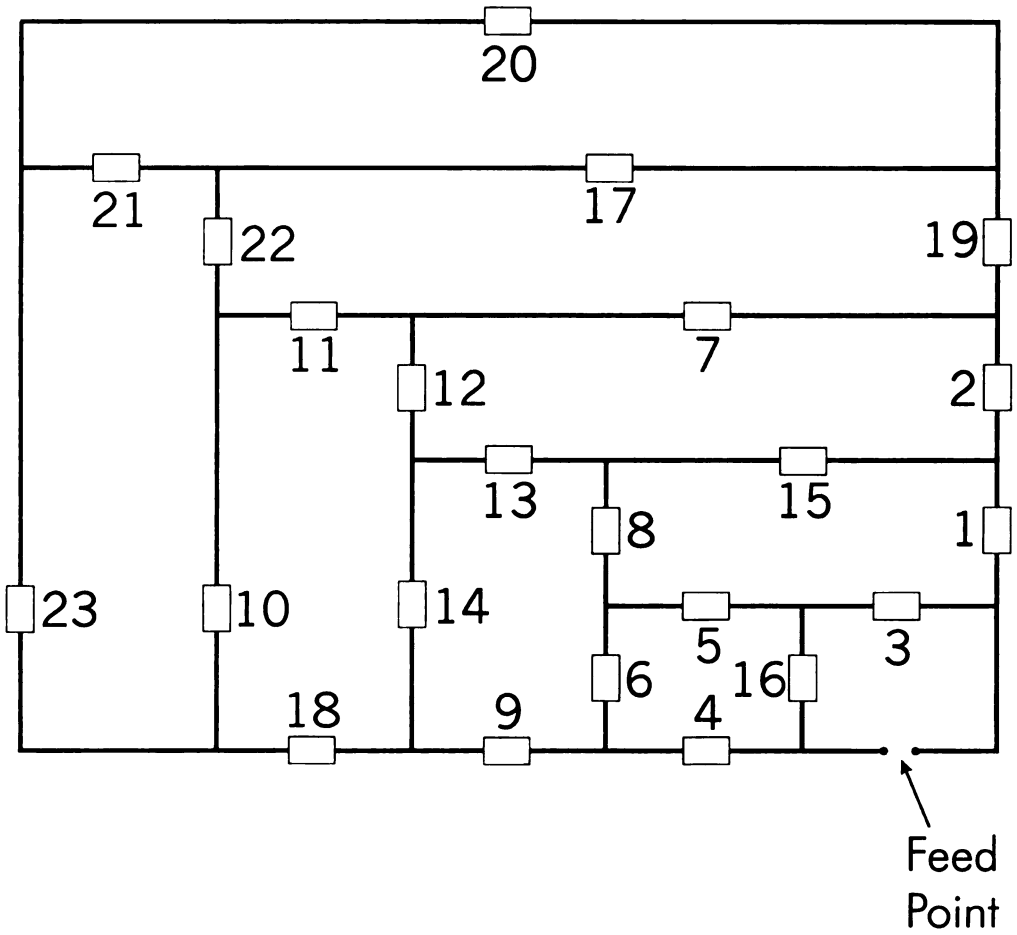


Figure 3.10. Switch configuration of prototype template used for the first reception optimization study.

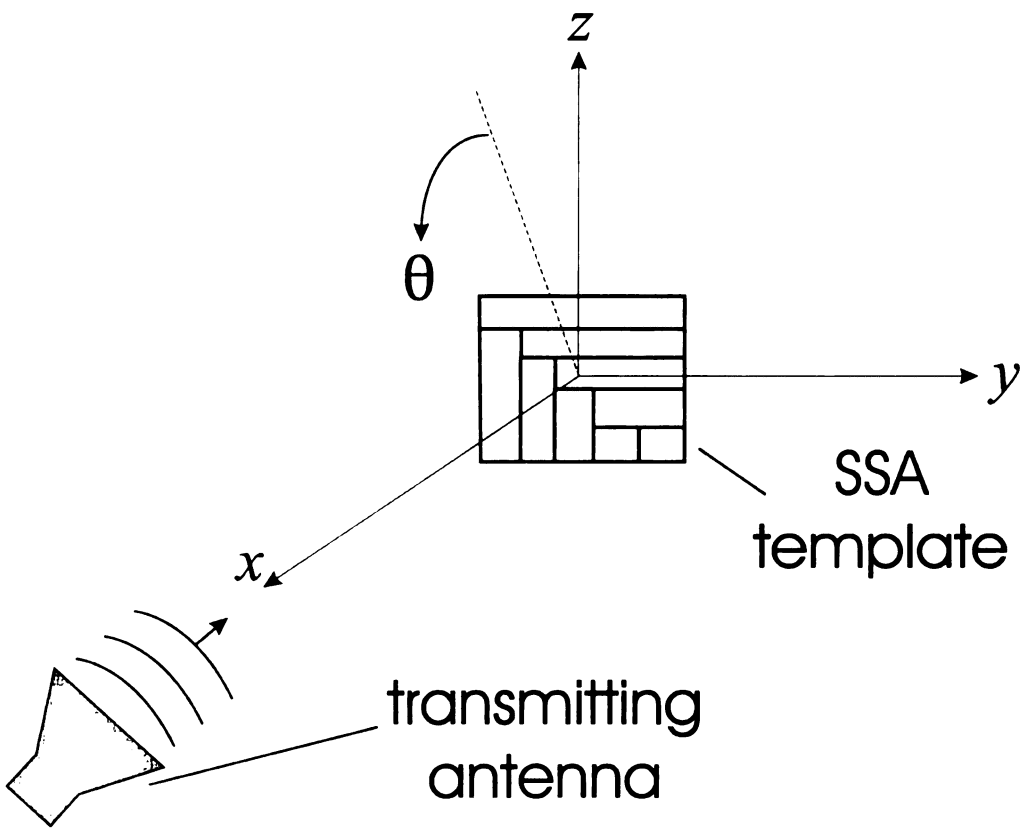


Figure 3.11. Illustration of the first SSA orientation for reception measurements (transmitting antenna is along the x-axis).

Table 3.3. Simulated annealing (SA) parameters used for reception optimization at 300 MHz.

Initial temperature, T_0	0.5 K
Temperature fraction, T_f	0.95
Number of iterations at each temperature, N_{pop}	10

Table 3.4. Number of temperatures for the simulated annealing algorithm at each measurement angle.

Measurement angle, θ	Number of temperatures, N_{gen}
0°	100
20°	100
40°	130
60°	130
70°	130
80°	140
90°	200

A second study of the reception optimization capabilities of the prototype SSA was performed at 275 MHz. A horizontally polarized dipole antenna was used as the transmitting antenna, and the SSA prototype was oriented as shown in Figure 3.13. To reduce the coupling to nearby conductors, ferrite blocks were placed around the switch control lines and the switch power lines connected to the template of the prototype. The switch numbering and template layout is shown in Figure 3.7, which is the same for the SWR optimization study.

Using simulated annealing, the SSA was optimized for the best received signal at 10° increments between $\phi = 0°$ and 350°. The simulated annealing parameters used for this optimization are found in Table 3.5. As shown in Figure 3.14, the SSA found a configuration that resulted in a strong received signal at every orientation, with a maximum to minimum ratio of 5.3 dB.

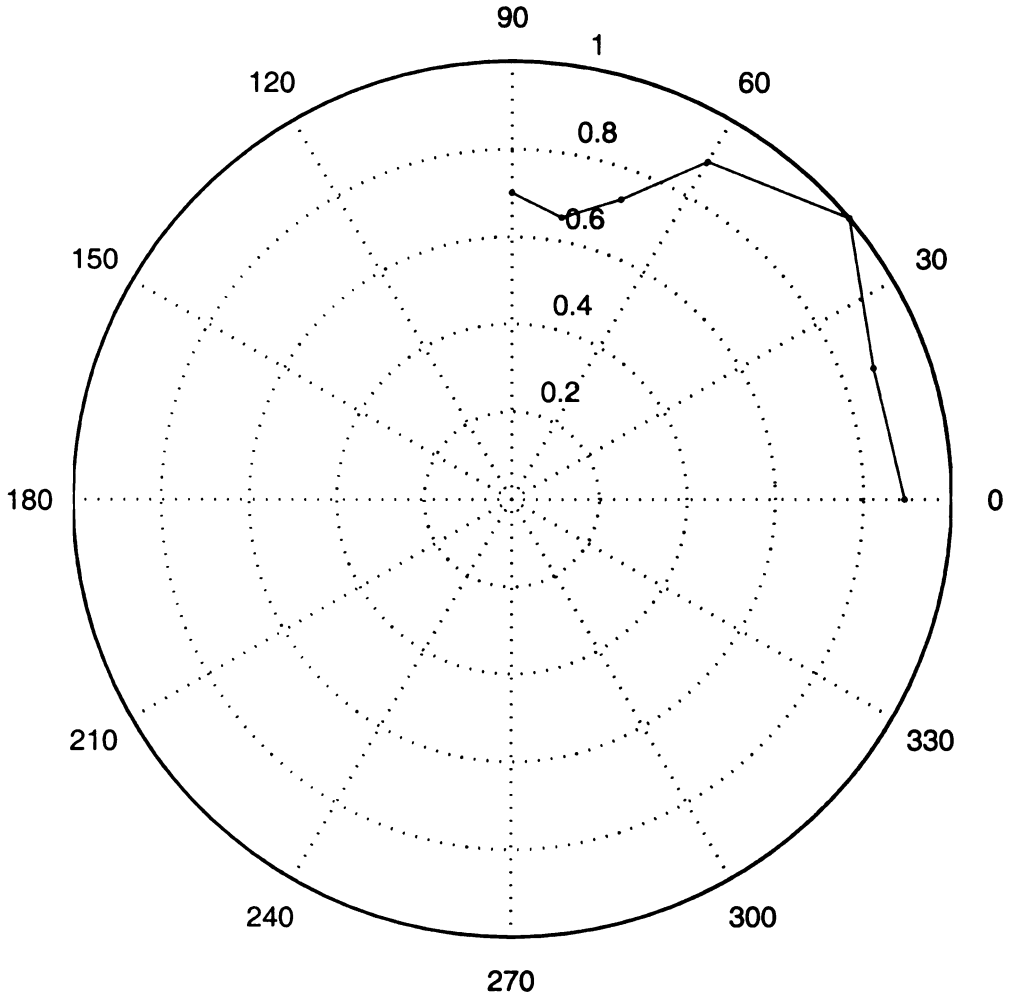


Figure 3.12. Normalized prototype reception at 300 MHz, optimized at each measurement angle.

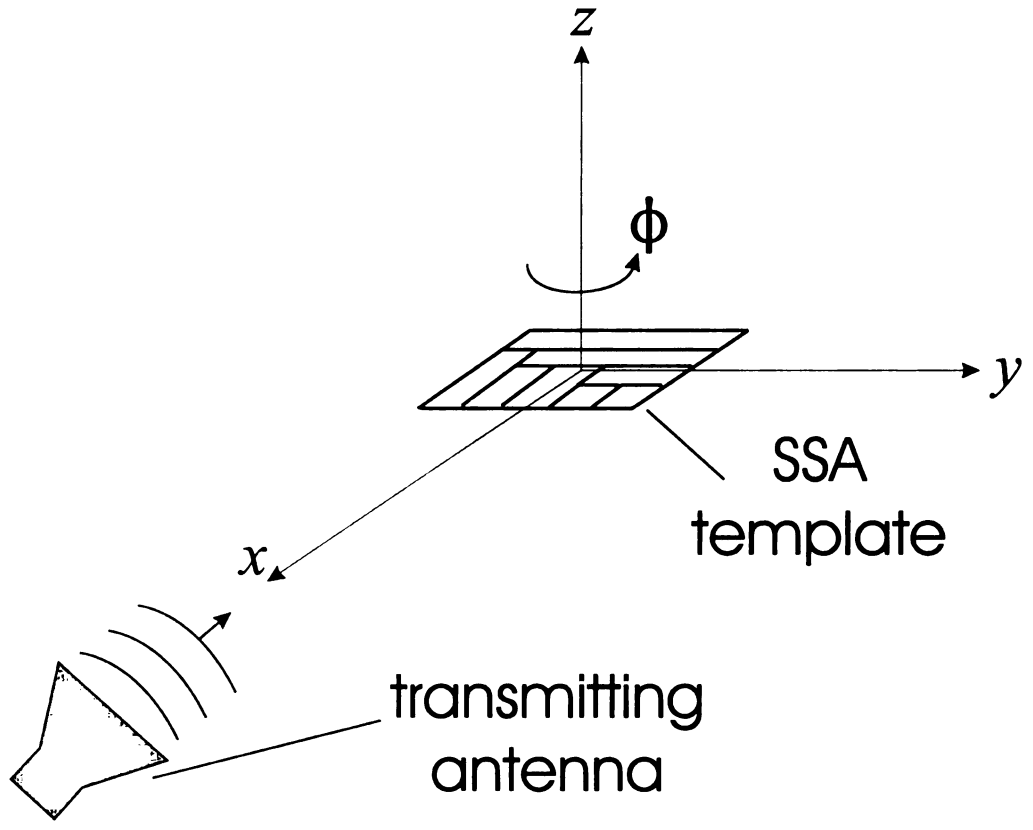


Figure 3.13. Illustration of the second SSA orientation for reception measurements (transmitting antenna is along the x-axis).

Table 3.5. Simulated annealing (SA) parameters used for reception optimization at 275 MHz.

Initial temperature, T_0	3.0 K
Temperature fraction, T_f	0.966
Number of temperatures, N_{gen}	200
Number of iterations at each temperature, N_{pop}	20

3.3 Conclusion

This chapter presents a prototype SSA constructed at Michigan State University. Measured results demonstrate that the prototype can be optimized to provide a low SWR over a large range of frequencies. A uniform pattern can be achieved when the SSA is reconfigured at several angles. The next chapter investigates several search algorithms used with SSAs, including simulated annealing, genetic algorithms, and Ant Colony Optimization.

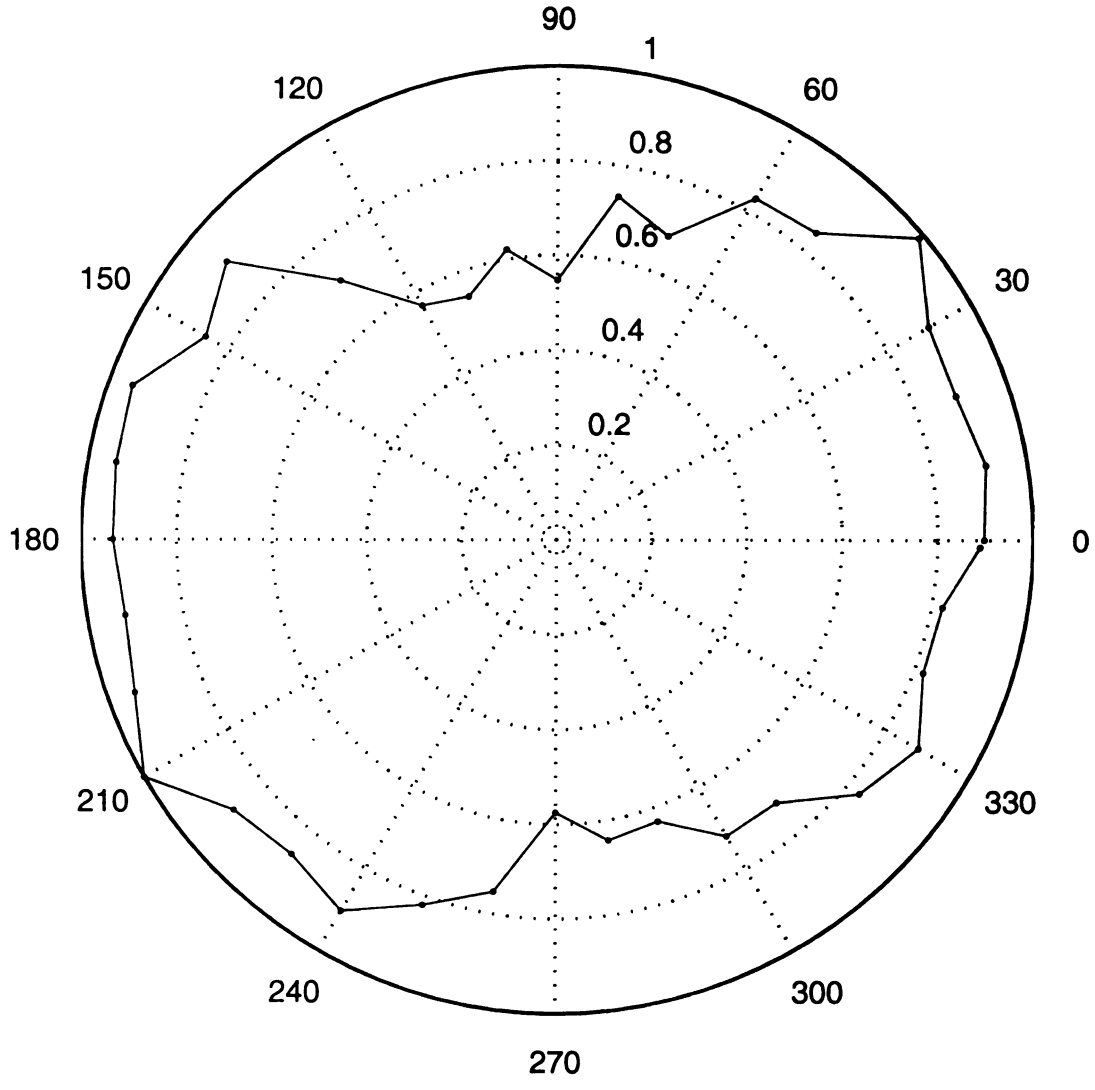


Figure 3.14. Normalized prototype reception at 275 MHz, optimized at each measurement angle.

CHAPTER 4

SEARCH ALGORITHMS FOR SELF-STRUCTURING ANTENNAS

4.1 Introduction

As discussed in Chapter 2, an important component of a self-structuring antenna system is an efficient search algorithm that is used to reduce the time needed to locate acceptable SSA configurations. Due to the simple 'on' or 'off' nature of the switch states on an SSA, a modern binary search algorithm is suitable for SSA applications. Chapter 3 presents measured results of prototype SSAs that use both simulated annealing (SA) and genetic algorithms (GAs) to locate SSA configurations with minimal standing wave ratio (SWR) values. This chapter provides descriptions of SA and GAs, as well as another evolutionary algorithm, Ant Colony Optimization (ACO).

An overview of the different binary search algorithms used with SSAs is given in Section 4.2. A simulated SSA experiment performed to determine the effectiveness of these algorithms is described in Section 4.3, and results are presented in Section 4.4.

4.2 Overview of Binary Search Algorithms Used with SSAs

This section gives an overview of the binary search algorithms that are used to locate SSA configurations with acceptable characteristics. Section 4.2.1 provides an explanation of how a general algorithm searches through the SSA configurations. Sections 4.2.2 and 4.2.3 discuss exhaustive and random searches, respectively. These search methods are primitive and generally inefficient for SSA templates with many switches. Sections 4.2.4 and 4.2.5 discuss simulated annealing and genetic algorithms, respectively. These two methods are popular search algorithms that have been used for several years in many areas of engineering. Section 4.2.6 introduces Ant Colony

Optimization (ACO).

4.2.1 General Search

As described in Chapter 2, the current on an SSA and nearby conductors or objects is influenced by the states of the switches on the SSA template. This means that the electromagnetic characteristics potentially differ for each unique combination of switch states. The search algorithms discussed in this chapter attempt to locate configurations with acceptable characteristics by selecting the states of the switches on the template using a rule or set of rules. The algorithms use a measure of the characteristics of each configuration called a 'fitness' or 'objective' function.

Search algorithms generally attempt to maximize or minimize the fitness function, depending on how the function is defined for each specific algorithm. For instance, if the fitness is defined as the reciprocal of SWR, the search algorithms look for SSA configurations with maximum fitness values. Assuming passive antennas, these values would be between 0.0 and 1.0.

Each SSA configuration is cataloged by a string of '0's or '1's that correspond to the 'open' or 'closed' nature of a switch on the SSA template, respectively. Each switch number is mapped to a single bit in the string. The search algorithms generate these strings during operation.

The term 'chromosome' is also used in this dissertation to describe the string of '0's or '1's that represent an SSA configuration. This comes from the application of the genetic algorithm to the SSA discussed in Subsection 4.2.5. Although the term chromosome comes from genetic algorithms, this term is often used with the other search algorithms discussed in this dissertation to describe the string of switch states.

4.2.2 Exhaustive Search

An exhaustive search is the simplest type of search algorithm that is employed by an SSA. An exhaustive search is simply a test of every possible SSA configuration.

Table 4.1. Possible SSA configurations for a template with n switches.

Number of Switches, n	Possible Configurations, 2^n
1	2
2	4
3	8
4	16
5	32
6	64
7	128
8	256
9	512
10	1024
⋮	⋮
22	4,194,304
23	8,388,608
24	16,777,216
⋮	⋮
32	4,294,967,296
⋮	⋮
50	1.259×10^{15}

This requires 2^n tests of SSA configurations for an SSA with n switches. Table 4.1 illustrates the unfeasible nature of using an exhaustive search for SSA templates with many switches. The total time required to exhaustively search the possible SSA configurations grows exponentially assuming a finite amount of time is needed to evaluate each SSA configuration. Exhaustive searches of SSA templates with few switches are presented in Chapter 5.

4.2.3 Random Search

A random search is a sample of the possible SSA configurations. A random search applied to an SSA proceeds as follows. A random number R ($0 < R < 1$) is tested against a threshold value, R_T, usually chosen to be equal to 0.5. If the random number is less than R_T, a state of '0' is chosen for a particular switch. Otherwise, a

state of '1' is chosen. This process is repeated until all of the bits of a configuration are chosen. The configuration is set on the SSA template switches, and the SSA is evaluated. This process proceeds until a certain number of configurations have been tested, or when performance criteria have been met.

There are variations of this method. The value of R_T ($0 < R_T < 1$) can be varied. If the threshold level is altered from $R_T = 0.5$, there are unequal probabilities of choosing a '0' or a '1'. This alters the average percentage of switches in the 'on' or 'off' state. The results presented in this dissertation use $R_T = 0.5$.

Although random searches are generally quicker than exhaustive searches, they are far from ideal. The number of iterations that are required to find an acceptable configuration may be unacceptably large. There is no information that is passed from one iteration to the next. This means that if there is a promising configuration with a relatively high fitness value, there is no local or intelligent search to test configurations that have some of the same switch states.

Random searches are performed to estimate the characteristics of a population of configurations. This is presented in Section 4.3.

4.2.4 Simulated Annealing (SA)

Simulated annealing (SA) techniques were among the first evolutionary or nature-based search algorithms [209]. SA attempts to search large solution spaces by modeling the behavior of a metal in the cooling process. SA is often called the 'Metropolis algorithm,' since the first numerical simulations of the annealing process were performed by Nick Metropolis and his coworkers in 1953 [209].

Molecules of a metal in liquid form have little organization, and move freely. As the substance cools near the metal's freezing point, bonds between molecules begin to form. This cooling process is called annealing. If the metal cools slowly, the molecules are able to form bonds such that the metal becomes crystalline and the substance achieves its least energy state. If the metal cools too quickly, the molecules

are unable to form bonds with one another in a way that leads to a crystalline form. The molecules are bound together in a form that has many local low energy regions, but that is not ordered at all levels. This type of metal is polycrystalline and weak.

The simulation of this annealing process is an effective nonlinear search method. The objective function of an SSA is used to represent the 'energy' of a fictitious metal. Here the objective function is defined such that the optimal SSA configuration yields an objective function of zero, and sub-optimal configurations yield higher values. The SA algorithm starts with an initial SSA configuration, changes the state of a single switch or a few switches, and monitors the change in energy of the SSA system by using the objective function. The new configuration is kept based on a probability P related to the Boltzmann probability distribution:

$$P(E) = e^{-E/kT} \tag{4.1}$$

where E is the change in energy between configurations, T is the current temperature, and k is Boltzmann's constant. If the energy is lower in a new configuration, the new configuration is always accepted. If the energy is higher, implying the new configuration is worse, the new configuration is accepted with probability P. This ensures that local minima do not dominate the search. Sub-optimal configurations have a finite probability to be chosen, which is important because optimal configurations are often found by investigating poorly performing configurations with similar switch configurations.

A critical part of the SA algorithm is the 'annealing schedule,' which is the initial temperature, T_0, and the rate that T decreases. As mentioned above, if the cooling rate is too fast, the final configuration is likely weak and therefore suboptimal. If the rate is too slow, the algorithm will need too many iterations to settle on a strong configuration, which may negate the purpose of using the complicated search tech-

nique. The annealing schedule implemented for the SA algorithms presented in this dissertation is

$$T_n = \alpha^n \cdot T_0 \ , \tag{4.2}$$

where T_n is the nth temperature, T_0 is the initial temperature, and α is a parameter that determines the cooling rate. The temperature fraction, α, ranges in value from 0.0 to 1.0, and is often denoted T_f in this dissertation. At the nth temperature, N_{pop} iterations of the SA algorithm are performed. Thus, for N_{gen} total temperatures, $N_{total} = N_{gen} \cdot N_{pop}$ total iterations are performed. The terms N_{pop} and N_{gen} originate from the population and generation totals used by the genetic algorithms discussed in Section 4.2.5.

The schedule shown in Equation 4.2 is often called the *geometric* annealing schedule [210]. Other annealing schedules exist for SA. For instance, the optimal *logarithmic* annealing schedule shows promising results for traveling salesman problems (TSPs):

$$T_n = \frac{c}{\log(n + n_0)} \tag{4.3}$$

where c is a constant, and n_0 is greater than 1 [210]. The geometric annealing schedule shown in Equation 4.2 is the only annealing schedule presented in this dissertation. Future research on SSAs could involve implementing the logarithmic annealing schedule shown in 4.3.

Since random numbers are needed to perform SA, it is often misunderstood that SA is simply a random search. The fundamental concept that needs to be understood is that while random numbers are utilized, SA is a *directed random search.* SA has performed remarkably well for many difficult problems that require nonlinear searches, most notably the traveling salesman problem (TSP) [166], [204], [209]–[211].

Directed random events can lead to emergent behavior, as shown by the generation of the Sierpinski Gasket fractal using random numbers [212]. SA and the

other evolutionary algorithms discussed in this dissertation attempt to create environments where optimal configurations emerge from solution sets using directed random searches.

4.2.5 Genetic Algorithm (GA)

The genetic algorithm (GA) is possibly the most widely used evolutionary or nature-based algorithm. GAs are used in many academic, research, and industry areas. GAs model the optimization method described by the 'survival of the fittest' evolutionary theory. GAs were developed by John Holland in the 1960s and 1970s at the University of Michigan [162], [213]. The name 'evolutionary algorithm' is used to describe GAs, SA, Ant Colony Optimization (ACO), and other novel optimization methods, but the term 'evolutionary' came from the GA's model of natural selection. The other optimization methods just mentioned are commonly called 'evolutionary algorithms' because some of the concepts are parallel to those used in GAs, but the term 'nature-based algorithms' is also used to identify these search methods, including GAs.

As discussed in Section 2.8, GAs have been applied to many electromagnetics optimization problems during the past ten years. Since a tremendous amount of literature already exists for GAs, only a brief description is given here.

Recall that an SSA configuration is simply a string of '0's or '1's that represents the states of the switches on an SSA template. In other words, this string contains the information needed to set the states of the switches in a particular manner. This is similar to biological chromosomes that contain the information needed to create a being's physical structure and the instructions that are needed for it to function. Thus, the binary string used to represent an SSA configuration is viewed as a 'chromosome' that contains genetic information.

In biology, individuals from the same species with different sets of chromosomes have different characteristics. From natural selection theory, an individual with a set of chromosomes that result in characteristics that have a high 'fitness' relative to other

individuals has a higher probability of surviving longer and producing more offspring than an individual with a lower relative fitness value. Assuming the population of this species remains constant from one generation to the next, the genetic material of subsequent populations contains more information from ancestors with high relative fitness values. Similarly, the GA applied to SSAs creates populations that have genetic material from ancestor chromosomes that performed well.

A block diagram showing the steps involved in a genetic algorithm is shown in Figure 4.1. The steps identified in this figure are as follows:

Encode Parameters: The parameters that will be searched by the GA need to be encoded onto a chromosome. As discussed, this is simply the values of the switch states.

Initialize Population: An initial population is created by generating random chromosomes. More complicated GAs use other methods of generating initial populations such as starting with existing populations from previous runs.

Evaluate Fitness: The chromosome of each individual in the population is decoded to set the switch states of each SSA configuration. Evaluations of the individuals are performed and the fitness of each individual is calculated.

Perform Selection: The *parents* of the individuals in the next generation are chosen in the selection process. Parents are individuals that will pass genetic information to the next generation. There are many methods that have been studied that perform selection; the GAs presented in this dissertation employ a roulette wheel selection scheme. The roulette wheel method chooses an individual with a probability proportional to the individual's fitness relative to the total fitness of the population. In this method, individuals with higher fitness values have higher probabilities of passing their genetic material to the next generation, but individuals with low fitness values may also be chosen with lower probabilities.

Perform Crossover: After selection, the parents are paired, and genetic crossovers are performed with probability p_{cross}. If a genetic crossover is performed, random crossover points are selected, and children are created by switching the parent at the crossover points during genetic transcription. For instance, consider two parents P_1 and P_2 with the following chromosomes:

$$P_1 = x_0x_1x_2x_3x_4x_5x_6\ldots x_n \tag{4.4}$$

$$P_2 = y_0y_1y_2y_3y_4y_5y_6\ldots y_n \ . \tag{4.5}$$

If a single crossover is performed with a crossover point between positions 3 and 4, the resulting children C_1 and C_2 have the following chromosomes:

$$C_1 = x_0x_1x_2x_3y_4y_5y_6\ldots y_n \tag{4.6}$$

$$C_2 = y_0y_1y_2y_3x_4x_5x_6\ldots x_n \ . \tag{4.7}$$

If a crossover is not performed, the genetic material for the parents is copied directly into children's genes for the next generation:

$$C_1 = x_0x_1x_2x_3x_4x_5x_6\ldots x_n \tag{4.8}$$

$$C_2 = y_0y_1y_2y_3y_4y_5y_6\ldots y_n \ . \tag{4.9}$$

Perform Mutation: Before the next population is finalized, random mutations are performed. The value of each bit of each chromosome is negated with probability p_{mut}.

Fill Next Population: After mutations are performed, the genetic material for the next population is complete. This population then becomes the current population, and its fitness is then evaluated.

Test Termination Criteria: If the total number of generations desired has been tested, the algorithm stops. There can also be a termination of the algorithm if an individual is found with a fitness better than some threshold value. If termination criteria are not met, the algorithm continues with the new population.

The study of GAs is so widespread that it has its own research area. There are many tricks and novel ideas that involve improving an application of a GA. These are too numerous to discuss here and are not the focus of this dissertation. The GAs used for the research presented in this dissertation use the simple, standard concepts discussed in this subsection. The specific methods and parameters used for each application of a GA in this dissertation are included in the sections where GA results are presented.

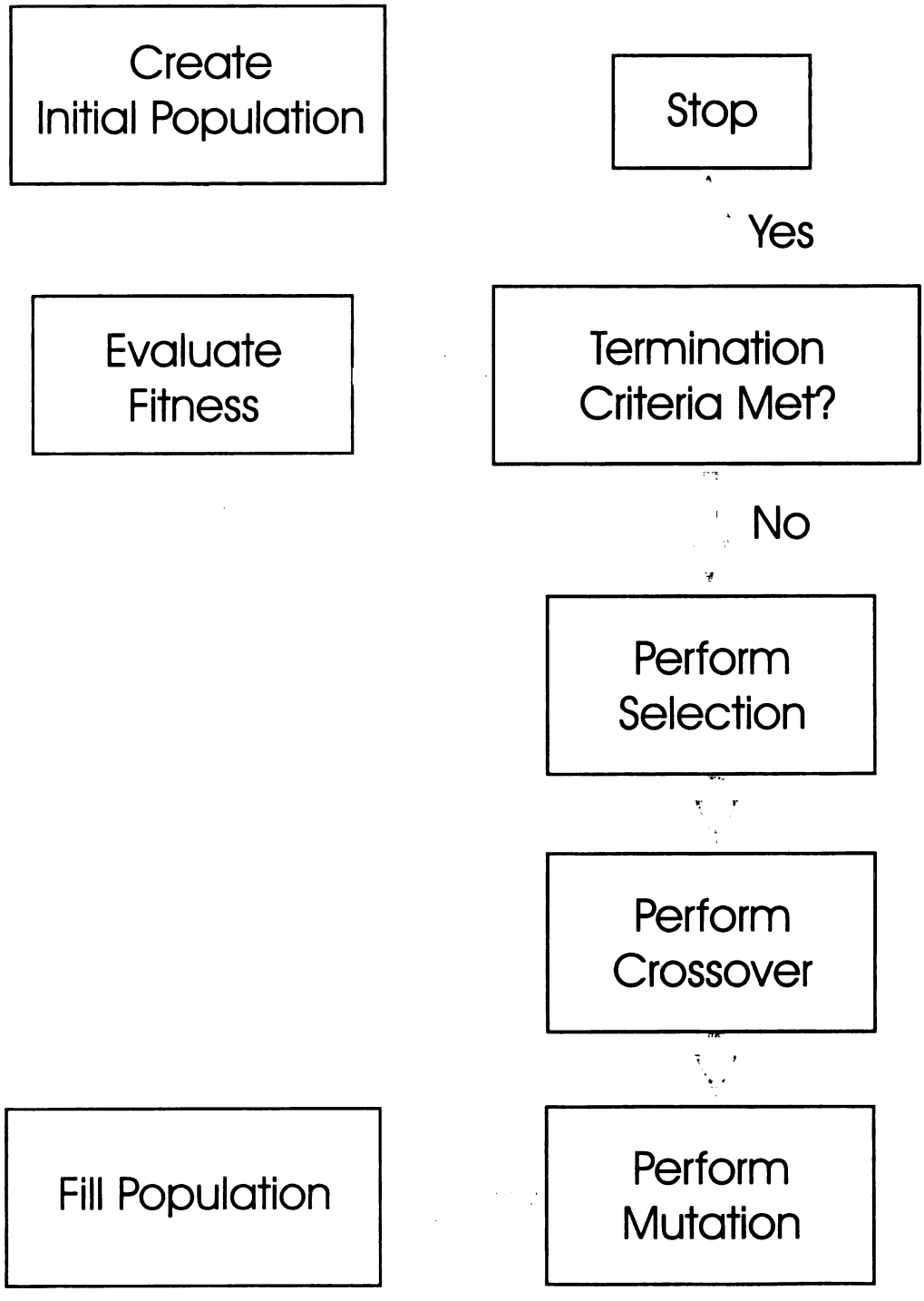


Figure 4.1. Block diagram of a genetic algorithm.

4.2.6 Ant Colony Optimization (ACO)

A group of evolutionary algorithms that have gained considerable interest in recent years are Ant Colony Optimization (ACO) algorithms [197]–[207]. These algorithms mimic the collective foraging behavior of ants. A conference paper involving ACO of SSAs was presented at the 2001 AP-S / URSI conference in Boston [4]. Although applications to these algorithms are growing in number, other applications of ACO to electromagnetics have not surfaced.

An ant is a relatively simple creature with few complicated functions. The typical activities of a single ant often appear to be random, disorganized, and unmotivated. The collective behavior of a colony of ants, however, is highly organized and efficient. This is evident from the food foraging behavior of ant colonies, where ants collect food and bring it back to their nest quickly. It is this efficiency that ACO algorithms try to exploit in simulated ant colonies. The collective and individual behavior of ants is complicated, and is greatly simplified for the discussion presented here and for the ACO algorithms implemented for this dissertation.

Central to the complex behavior of ants is their use of *pheromone*. As ants travel, they deposit a pheromone trail that is detectable by other ants. This pheromone trail influences the routes that other ants choose. The use of pheromone is a primary method of communication for ants.

A simple diagram of ants foraging for food is shown in Figure 4.2. Two ants leave their nest in different directions at the same time to search for food to bring back to the nest. Assuming that no initial pheromone exists outside of the nest, the routes that they choose are generally random. Both ants deposit pheromone along the routes that they take. Assume that **Ant 1** finds **Food Source 1** at the same time that **Ant 2** is still wandering aimlessly with no food in sight. **Ant 1** picks up some of the food from **Food Source 1** and returns to the nest by following the pheromone trail that it left on its way to the food. As it follows its pheromone trail

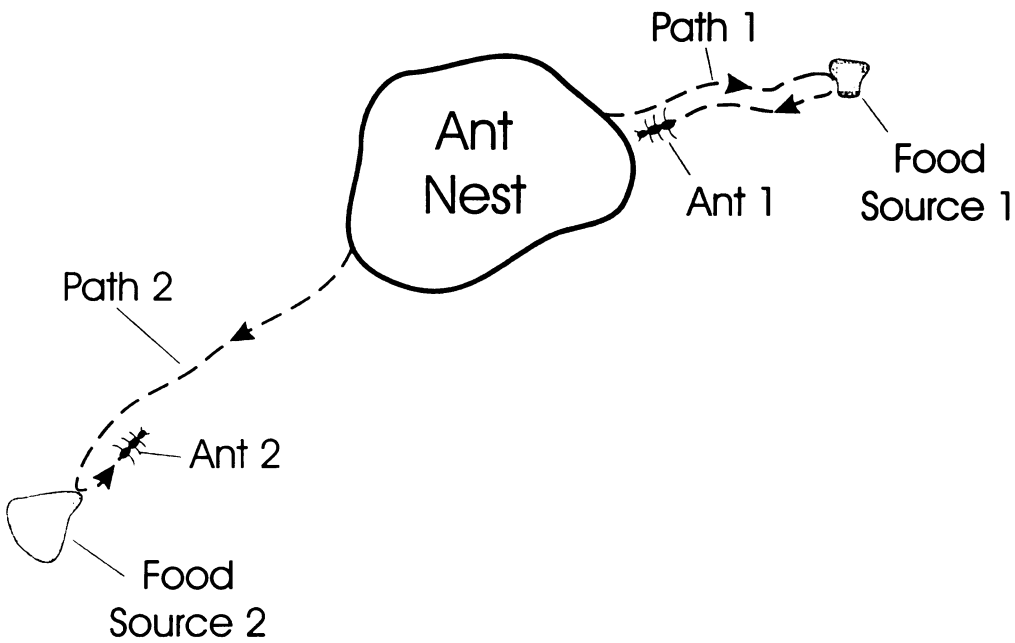


Figure 4.2. Diagram of ants foraging for food.

back, it lays additional pheromone along the path. **Ant 1** completes its journey near the same time that **Ant 2** finds **Food Source 2**.

When the next set of ants leaves the nest to search for food, the ants detect twice as much pheromone along the trail to **Food Source 1** as they do for **Food Source 2**, neglecting any evaporation of the pheromone. The probability is greater that these ants will choose to take the path to **Food Source 1** due to the higher pheromone concentration. These ants also deposit pheromone as they travel, which further strengthens the probability that future ants will choose the path to **Food Source 1**. Thus, **Food Source 1** is brought back to the nest by many ants in an efficient manner.

When the supply at **Food Source 1** is exhausted, many ants turn around and follow the pheromone trail back to the nest without food. Some ants, however, will continue into uncharted territory beyond the empty food source, and some will

randomly break off of the trail to or from **Food Source 1**. These sporadic events help the ant colony find additional food sources, including the remains at **Food Source 2**. The evaporation of pheromone is also an important part of this complex process, and this helps deemphasize older trails leading to exhausted food sources.

In this simplified example, ants efficiently collect food from two sources and bring it back to the nest. ACO algorithms attempt to exploit the efficiency of ants by creating an abstract environment of possible paths, and simulating ants traveling through these paths.

ACO algorithms simulate the passage of time, t, in discrete steps. A total of $m = N_{pop}$ ants are simulated per time step, and N_{gen} time cycles are performed for a complete search. Thus, $N_{pop} \cdot N_{gen}$ total evaluations are performed.

ACO algorithms usually define a certain number of nodes that simulated ants visit and the local paths or edges between these nodes. For the application of ACO to SSAs presented here, the nodes are the switches on the SSA template. Ants visit each switch on the template in sequential order exactly once per cycle. There are four possible paths between each node, as shown in Figure 4.3. The partial trail between node l and node $l+1$ along path ij is denoted edge lij. The nodes wrap around such that node n looks forward to node 0 for an SSA with n switches.

If an ant occupies the '0' state of node l, the ant can move to the '0' state of node $l+1$ using path 00 or to the '1' state of node $l+1$ using path 01. Similarly, if an ant occupies the '1' state of node l, the ant can move to the '0' state of node $l+1$ using path 10 or to the '1' state of node $l+1$ using path 11. Thus, although four possible paths exist between two nodes, only two are available for each state of a node. The paths that an ant chooses determine the states of the nodes that it visits through a single cycle, and these states correspond to the states of the switches on the SSA template.

The partial length of the trail along edge lij is denoted d_{lij}. Since the length of

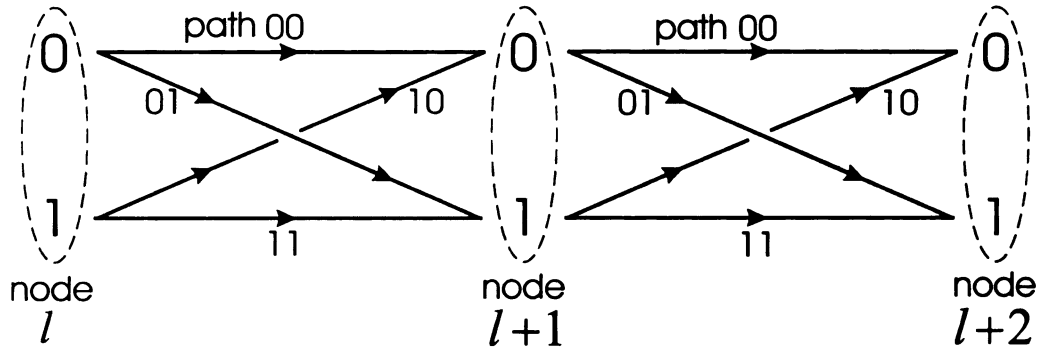


Figure 4.3. Diagram of paths through nodes for Ant Colony Optimization (ACO).

a complete cycle taken by ant k is the sum of all lengths of the edges chosen by ant k, the total cycle length, L_k can be expressed as

$$L_k = \sum_{\text{edges } lij \text{ taken}} d_{lij} \quad . \tag{4.10}$$

L_k is determined by evaluating the fitness function, f_k, for the SSA configuration corresponding to the kth ant. The greater the fitness, the shorter the length. The results presented in this chapter use $L_k = 1/f_k$.

The pheromone intensity, τ, along edge lij as a function of time can be expressed as

$$\tau_{lij}(t+1) = \rho \cdot \tau_{lij}(t) + \Delta\tau_{lij} \; . \tag{4.11}$$

Here $\Delta\tau_{lij}$ is the change in pheromone concentration between time steps, and ρ is a parameter that describes the evaporation of the pheromone trail. The quantity $(1-\rho)$ is the evaporation of the trail between time steps.

The change in pheromone concentration between time steps, $\Delta\tau_{lij}$, is

$$\Delta\tau_{lij} = \sum_{k=1}^{m} \Delta\tau_{lij}^{k} \tag{4.12}$$

where $\Delta\tau_{lij}^k$ is the additional pheromone laid by the kth ant on the edge lij between time t and $t+1$. $\Delta\tau_{lij}^k$ is given by

$$\Delta\tau_{lij}^k = \begin{cases} \frac{Q}{L_k} & \cdots \quad \text{if ant } k \text{ uses the edge } lij \text{ during its cycle} \\ 0 & \cdots \quad \text{otherwise} \end{cases} \tag{4.13}$$

where Q is a parameter called the *pheromone constant.*

The probability that the kth ant will choose edge lij at time t is expressed as

$$p_{lij}^k(t) = \frac{[\tau_{lij}(t)]^\alpha \cdot [\eta_{lij}]^\beta}{\sum_{k \in k_a} [\tau_{lik}(t)]^\alpha \cdot [\eta_{lik}]^\beta} \tag{4.14}$$

if the edge lij is allowable. Here k_a represents the set of k such that the edge lik is allowable, and α and β are constant parameters.

The variable η_{lij} in Equation 4.14 represents the *vision* of an ant, and is related to the local increase or decrease in length associated with the ant choosing edge lij. Many implementations of ACO use vision to avoid stagnation of the algorithm [201]. It is difficult to formulate an implementation of vision for the ACO algorithms applied to SSAs, and such implementations would require more evaluations of antenna structures for each search. Thus, the ACO algorithms presented in this dissertation use 'blind' ants by setting $\beta = 1.0$ and $\eta_{lij} = 1.0$ for all lij. Equation 4.14 then simplifies to

$$p_{lij}^k(t) = \frac{[\tau_{lij}(t)]^\alpha}{\sum_{k \in k_a} [\tau_{lik}(t)]^\alpha} \tag{4.15}$$

To help prevent early stagnant behavior of the ACO algorithm, a minimum probability, p_{min}, is defined for each allowable edge. If $p_{lij}^k(t)$ is less than p_{min} using Equation 4.15, $p_{lij}^k(t)$ is set equal to p_{min}. The probabilities for the other allowable paths from i are adjusted so that the sum of the allowable probabilities is equal to 1. p_{min} is usually set to a small value such as 0.05. This provides non-zero probabilities

Table 4.2. Variables, terms, and parameters used with ACO.

$p_{lij}^{k}(t)$	Probability that ant k will choose edge lij at time t
$\tau_{lij}(t)$	Pheromone trail intensity at time t along edge lij
$\Delta\tau_{lij}$	Change in pheromone trail intensity along edge lij
$\Delta\tau_{lij}^{k}$	Change in pheromone trail intensity along edge lij due to the kth ant
τ_0	Initial pheromone trail intensity
ρ	Parameter related to pheromone evaporation
η_{lij}	'Vision' of an ant at node l looking along path ij
α	Constant parameter
β	Constant parameter used to weight the ants' vision
Q	Pheromone constant

for ants to try new paths, and stagnate behavior is minimized.

A list of the variables involved with ACO is given in Table 4.2. The steps in the ACO algorithm are summarized as follows:

Initialize pheromone intensity: The pheromone intensity, τ_{lij}, is initialized to the value τ_0 along all edges.

Calculate transition probabilities: The probabilities for every possible transition along edge lij are calculated using Equation 4.15. Since the initial pheromone intensity is evenly distributed, all edges have equal probabilities.

Simulate the cycles of $m = N_{pop}$ ants: m SSA configurations are chosen using m ants to travel through the n nodes representing the switches. The ants choose the switch states by selecting edges with probabilities based on Equation 4.15.

Evaluate the lengths of the ant cycles: The electromagnetic characteristics of the m SSA configurations are evaluated, and the fitness function is calculated. The total length of the cycle, L_k, is calculated from the inverse of the fitness.

Calculate the change in pheromone: Pheromone is added to the edges chosen by the kth ant based on the L_k using Equations 4.12 and 4.13.

Calculate the pheromone intensity for time $t+1$: $\tau_{lij}(t+1)$ is calculated using Equation 4.11. The time is then advanced by a single step: $t = t + 1$.

Update probabilities: The transition probabilities, $p^k_{lij}(t)$, are recalculated for the new pheromone intensities using Equation 4.15.

Continue time steps: A new set of m ants is run through the nodes. This process repeats for N_{gen} time steps.

The ACO algorithm described here is able to find SSA configurations with desirable characteristics. This is shown by the search algorithm study presented in Sections 4.3 and 4.4.

4.3 Simulated SSA Experiment Using Binary Search Algorithms

Experiments were performed on a simulated SSA template to evaluate the effectiveness of the binary search algorithms. The SSA template, electromagnetics solver, computer program, and fitness function used in the experiments are presented in the following subsections. The results from the experiments are presented in Section 4.4.

The purpose of this study is to determine if random searches of SSAs are acceptable, or if sophisticated algorithms such as SA, GA, or ACO are necessary to locate acceptable configurations. It is important to understand, however, that direct comparisons of the performance of the SA, GA, and ACO algorithms are not complete based on the results from this study. This is because the algorithms were altered, modified, and tweaked only to the point where acceptable SSA configurations are consistently found by the algorithms. Since this study does not implement state-of-the-art versions of the SA, GA, and ACO algorithms, it would be unfair to try to directly compare the performance of these modern algorithms.

4.3.1 SSA Template Studied

Due to the enormous number of possible configurations in an SSA, it is almost impossible to conceive of the best SSA template geometry for any given application. Therefore, an SSA template was designed with an asymmetric arrangement of wire segments. The asymmetry was chosen to reduce the possibility of multiple SSA configurations with equivalent electromagnetic characteristics. The SSA template is shown in Figure 4.4. This template is very similar to the layer 7 SSA template presented in Chapter 5. The physical dimensions of the template are shown in Table 4.3.

A large number of possible SSA configurations is desired for the studies of search algorithms presented here. The SSA template shown in Figure 4.4 uses 39 switches and has 549,755,813,888 possible SSA configurations. It is not feasible to search through these configurations exhaustively in a reasonable length of time. Thus, the

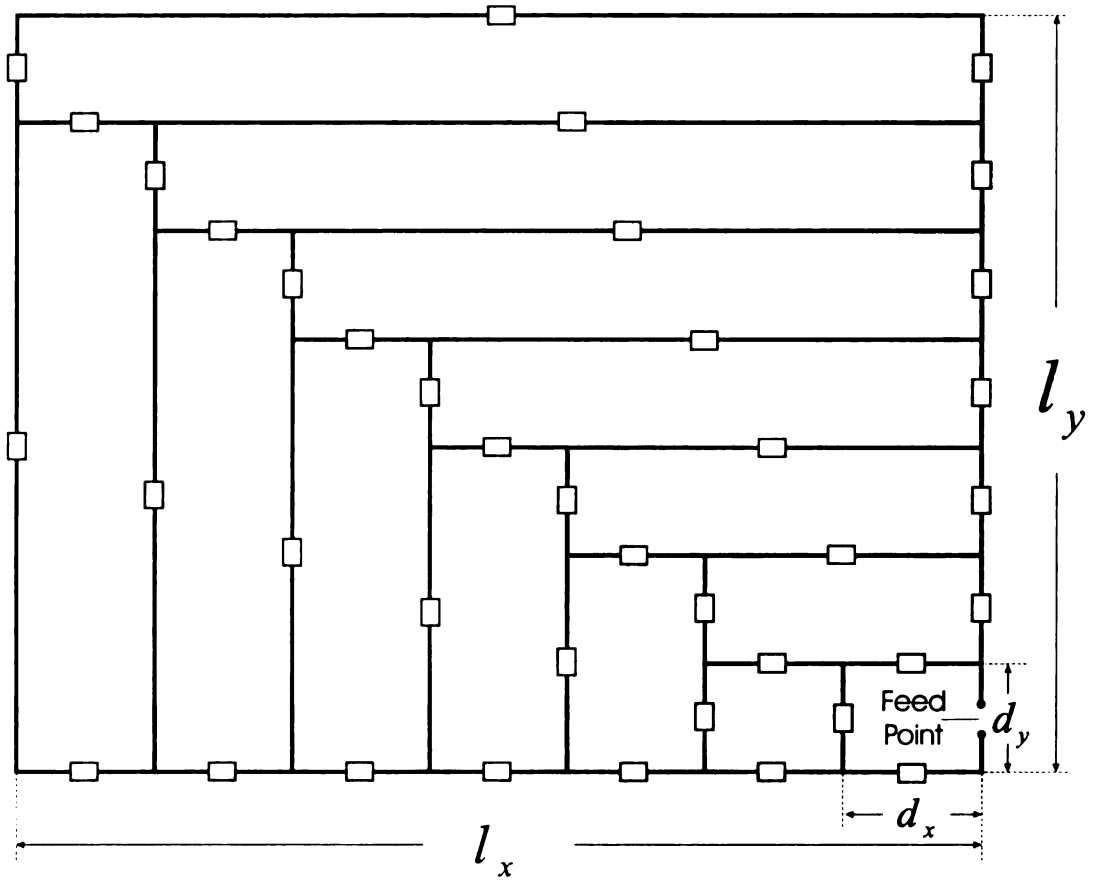


Figure 4.4. Diagram of the SSA template used in the search algorithm study.

random, SA, GA, and ACO search algorithms are used to locate configurations.

4.3.2 Numerical Electromagnetics Code

The solution for the currents in an antenna system is a traditional electromagnetics research problem. For the research on simulated SSAs presented in this dissertation, the Numerical Electromagnetics Code (NEC) ([214], [215]) is used to solve for the unknown antenna currents. NEC is chosen because it is widely used by the EM research community, it models wire antennas very well, and it has simple input and output text files that can be manipulated by other computer programs.

NEC is based on the Method of Moments (MoM) solution of electric field integral equations (EFIEs) and magnetic field integral equations (MFIEs) derived from

Table 4.3. Dimensions of the SSA template used in the search algorithm studies.

l_x	60.0 cm
d_x	8.57 cm
l_y	60.0 cm
d_y	8.57 cm
Outer electrical dimensions at 40 MHz	$0.0800\lambda \times 0.0800\lambda$
Outer electrical dimensions at 100 MHz	$0.200\lambda \times 0.200\lambda$
Outer electrical dimensions at 400 MHz	$0.800\lambda \times 0.800\lambda$

Maxwell's equations and appropriate boundary conditions. The version used for the research in this dissertation was NEC-4. A single-precision compilation of NEC-4 was used.

The radii of the template wires are 2.0 mm for all wires in this study. The switches on the SSA template are modeled using the **swLeverWire** switch model described in Section A.2.7.3 in the appendix. A diagram of the switch model is shown in Figure A.2 on page 337. The switch levers are opened a small distance ($h_1 = 9.06$ mm) to simulate an open circuit.

Each segment of a wire modeled in NEC is no longer than $\lambda/10.0$ for all of the simulations presented in this dissertation. Wires are placed such that radii do not overlap.

The purpose of the simulation research presented in this dissertation is to investigate SSAs and search algorithms, and not to design specific practical antennas. General NEC guidelines are followed so that realistic results are obtained. Accurate and precise antenna models of each SSA configuration, however, are not the focus of this research. If a practical wire antenna is constructed using the geometry specification in the NEC input file for an SSA configuration, the measured input impedance of the practical structure will potentially differ from the simulated input impedance. The NEC simulations indicate the distribution of possible impedances and test the

ability of search algorithms to locate configurations with desirable standing wave ratios.

4.3.3 SSA Computer Program

A computer program was written in C++ to simulate the SSAs presented in this dissertation. The program generates the geometrical specifications of the SSA template, solves for the unknown currents by calling NEC, and runs the binary search algorithms discussed in this chapter. This computer program is discussed in Appendix A.

4.3.4 Fitness Function

As discussed in Section 4.2.1, a fitness or objective function is necessary for the search algorithms discussed in this chapter. The simulated SSA experiment presented in this chapter searches for SSA configurations with minimal SWR values. The SWR is computed assuming a characteristic impedance of $Z_0 = 50\ \Omega$. The general fitness function used for the search results presented here is

$$f = \begin{cases} \dfrac{1}{\mathtt{SWR}^{\gamma}} & \cdots \text{ if } \mathtt{SWR} <= \mathtt{SWR}_{\mathrm{Threshold}} \\ \\ \dfrac{1}{\mathtt{SWR}^{\gamma}} \cdot \dfrac{1}{\delta} & \cdots \text{ if } \mathtt{SWR} > \mathtt{SWR}_{\mathrm{Threshold}} \end{cases} \tag{4.16}$$

where SWR is the standing wave ratio of the configuration under evaluation, and γ, δ, and $\mathtt{SWR}_{\mathrm{Threshold}}$ are constant parameters. The search algorithms seek to maximize this fitness function. The additional scaling by $1/\delta$ is done so that configurations with SWRs greater than a threshold value are assessed a penalty. This allows for more effective search algorithms.

In the results presented in this chapter, $\mathtt{SWR}_{\mathrm{Threshold}} = 2.0$. The parameter δ is set to 1.15 unless otherwise noted. The parameter γ is set equal to 2.0 for the results presented in this chapter. These parameters were selected by trial and error.

If an SSA configuration has an SWR value of 1.0, the fitness f reaches a maximum

value of 1.0. For SWR values of ∞, f approaches 0. Thus the fitness values range from $0 < f \leq 1$ where $f = 1$ corresponds to an optimal SSA configuration.

Note that the fitness function for the simulated annealing algorithm is altered from f in Equation 4.16. Since the simulated annealing algorithm seeks to minimize the fitness function, the fitness is scaled in the SA algorithm as follows:

$$f_{SA} = \frac{1}{f} \, . \tag{4.17}$$

Thus the fitness values for the SA algorithm range from $0 < f_{SA} \leq 1$ where $f_{SA} = 0$ corresponds to an optimal SSA configuration.

4.4 Simulation Experiment Results

The results for the search algorithm experiment are presented in the following subsections. Results are presented for random, SA, GA, and ACO searches for SSA configurations with minimal SWR values for the SSA template discussed in Section 4.3.1. Recall that the SWR values are computed relative to 50 Ω. Searches were performed at 400 MHz, 100 MHz, and 40 MHz.

Knowledge of the characteristics of every possible SSA configuration at each studied frequency would be invaluable in evaluating the performance of the SA, GA, and ACO search algorithms. The exact proportion of total configurations that meet performance criteria would be known, and the probability of finding one of these configurations randomly could be calculated. As discussed, however, it is not feasible to obtain exhaustive search data for the 2^{39} configurations of the SSA template shown in Figure 4.4. Therefore, a large random sample of the configuration space is taken for each of the frequencies studied, and parameters of the configuration space are estimated.

For the studies presented in this chapter, the proportions of configurations below given SWR values are the parameters that are estimated by the random samples. A single trial of the sample yields a 'success' if the trial configuration has an SWR value below a given threshold value, $\mathtt{SWR}_{\mathrm{Max}}$. If y total successes occur in a sample of n trials, an estimate of the proportion of the possible configurations with SWR values below $\mathtt{SWR}_{\mathrm{Max}}$, $\hat{p}$, is

$$\hat{p} = \frac{y}{n} . \tag{4.18}$$

Confidence intervals around the population estimate are established by using

$$\hat{p} \pm z_{\alpha/2} \sqrt{\frac{\hat{p}(1-\hat{p})}{n}} \tag{4.19}$$

where $z_{\alpha/2}$ is a tabulated parameter defined in most statistics texts [216]. For 95% confidence intervals, $z_{\alpha/2} = 1.96$ is used. The intervals are valid only if $n\hat{p} > 5$ and $n(1-\hat{p}) > 5$. If these conditions are not met, the interval estimation is ignored. For sampled data plots in this chapter, parameter estimates are only displayed at frequencies where enough data exist to estimate confidence intervals.

The parameter estimates presented in this study use a sample size of 500,000 trials. This sample size was chosen based on computation time. About 24 hours are needed to evaluate a sample of this size using a 1.8 GHz Pentium 4 computer. For each trial, the SWR value is evaluated for the SSA configuration chosen randomly. Since at least six successes are needed to make valid parameter interval estimates,

$$\hat{p} = \frac{6}{500,000} = 1.2 \times 10^{-5} \tag{4.20}$$

is the smallest estimate possible, and 95% confidence intervals for this estimate are

$$2.40 \times 10^{-6} < \hat{p} < 2.16 \times 10^{-5} \, . \tag{4.21}$$

Although $\hat{p}$ is small for this case, the total number of configurations that meet the test criterion is

$$2^{39} \cdot \hat{p} = 6.60 \times 10^{6} \tag{4.22}$$

where 2^{39} is the total number of possible configurations for the 39 switch SSA template shown in Figure 4.4. 95% confidence intervals estimate this number between

$$1.32 \times 10^{6} < 2^{39} \cdot \hat{p} < 1.19 \times 10^{7} \, . \tag{4.23}$$

Thus, although it may take many iterations of a random search to locate configurations with a probability of 1.2×10^{-5}, there are millions of total possible configurations

within this proportion, and the SA, GA, and ACO algorithms may have greater success in locating some of these configurations.

4.4.1 Minimum SWR search at 400 MHz

500,000 random configurations of the SSA template shown in Figure 4.4 were evaluated at 400 MHz, and the SWR value of each configuration was calculated. Using this data, the proportion of total configurations with SWR values less than x is shown in Figure 4.5 where x corresponds to the SWR values on the x-axis of the plot. An additional parameter estimate plot is found in Figure 4.6, where more detail is shown for lower SWR values. 95% confidence intervals are used for the parameter estimates. Notice that nearly 3% of the possible configurations have SWRs less than 2.0, and over 1% have SWRs less than 1.5. This means that there is a high probability that at least one configuration with an SWR of 1.5 or less would be found in a random search using only a few hundred iterations.

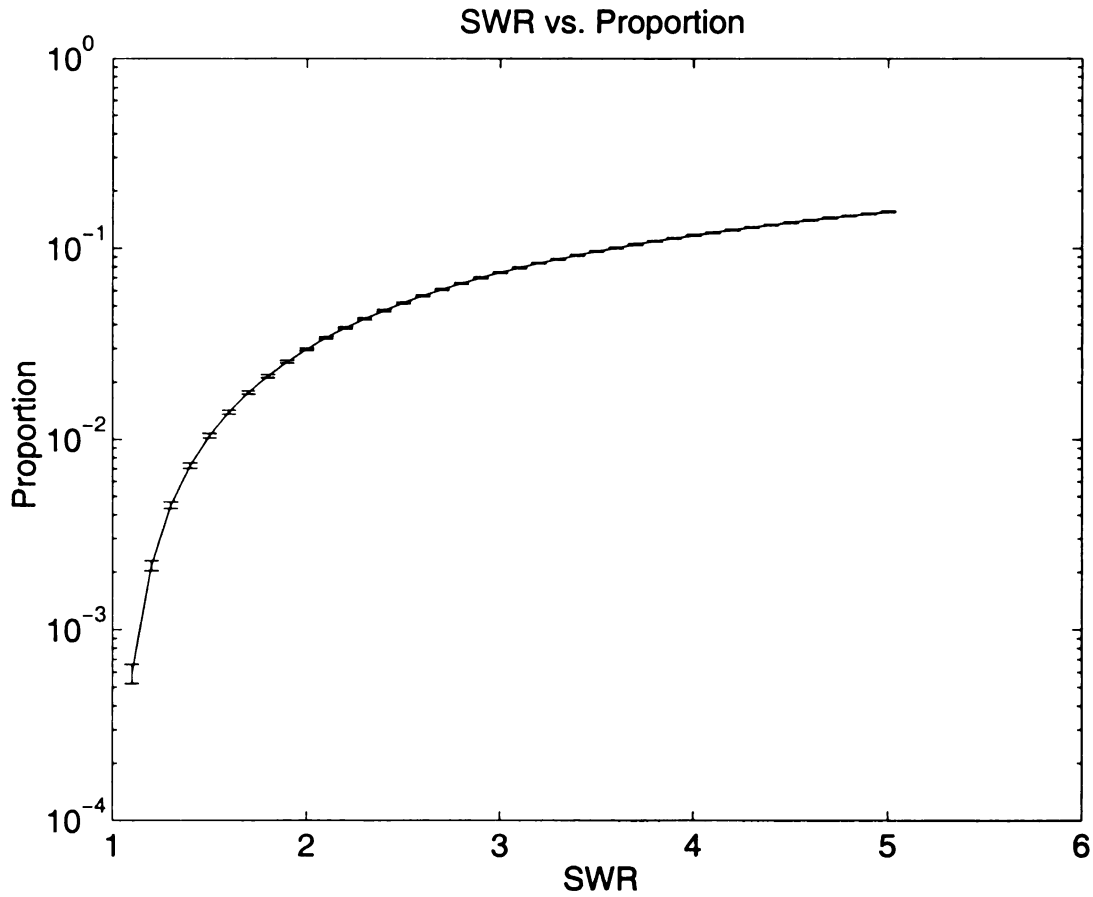


Figure 4.5. Distribution of SWR values (relative to 50 Ω) for the SSA template at 400 MHz (500,000 random samples). Error bars show the 95% confidence intervals.

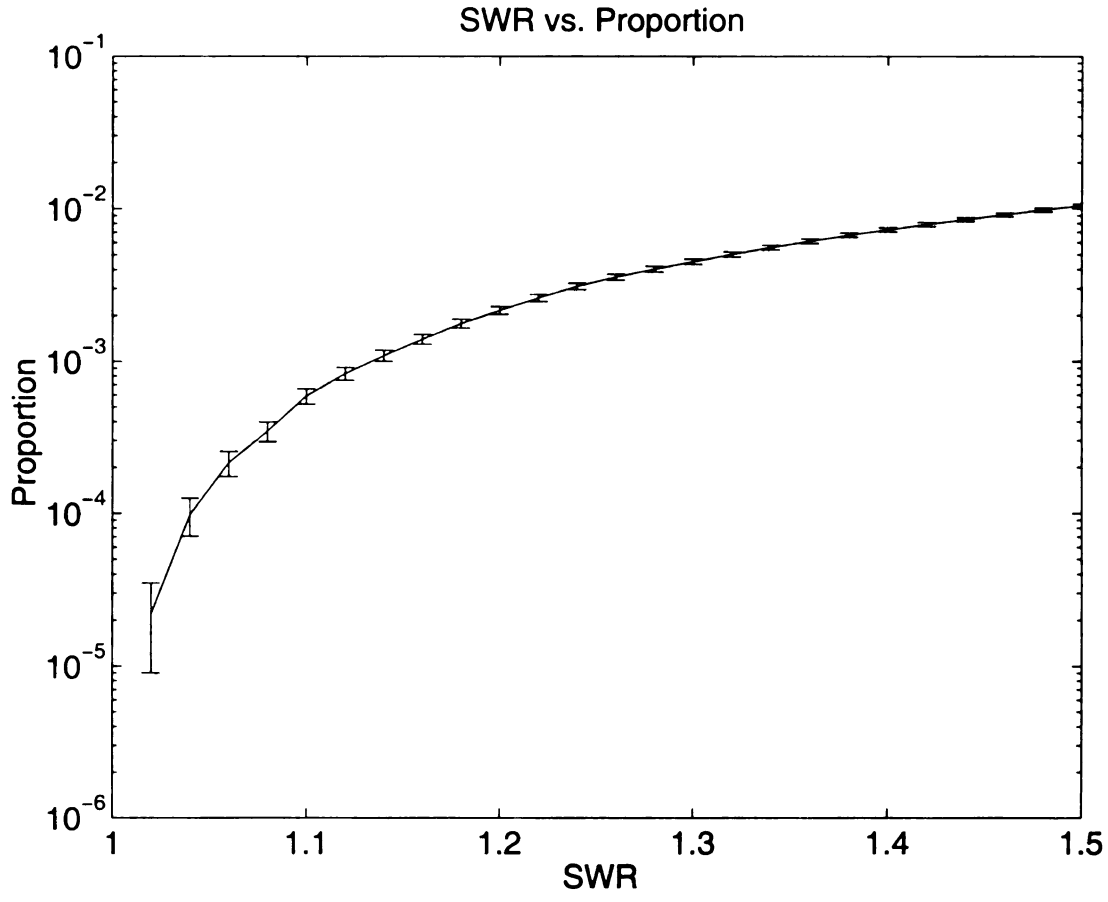


Figure 4.6. Detailed distribution of SWR values (relative to 50 Ω) for the SSA template at 400 MHz (500,000 random samples). Error bars show the 95% confidence intervals.

ACO, SA, and GA routines are used to search for configurations of this SSA template with minimal SWRs at 400 MHz. 1500 total iterations are performed for each algorithm. As a comparison, a search for the minimum SWR of 1500 random configurations is performed. Ten trials of each of these searches is performed.

The fitness function used for the SA, GA, and ACO searches is shown in Equation 4.16, where $\gamma = 2.0$, $\mathtt{SWR}_{\mathrm{Threshold}} = 2.0$, and $\delta = 1.15$. Recall that the SA algorithm adjusts this fitness using Equation 4.17.

The ACO, SA, and GA algorithm parameters are shown in Table 4.4, Table 4.5, and Table 4.6, respectively. Note that the ACO algorithm uses 39 ants in 39 runs,

implying that 1521 iterations are used. The algorithm is stopped, however, after 1500 iterations to remain consistent with the SA, GA, and random searches presented here. Ten separate trials of each algorithm are run. The parameters for the algorithms presented in this chapter were selected using rules of thumb found in the literature and by trial and error.

The random, ACO, SA, and GA search results are shown in Table 4.7–Table 4.10. The lowest SWR value found during each trial as well as the first iteration number where this value is found are tabulated. The mean and standard deviation, σ, are included in the tables. Note that the iteration numbers displayed in the tables in this chapter are indexed from 0 to 1499.

The ACO, SA, and GA searches all found minimum SWR values that are lower on average than those found by the random search. The average minimum SWRs for the ten trials are 1.0204, 1.0251, and 1.0086 for the ACO, SA, and GA searches, respectively. An average minimum SWR of 1.0891 is found by the random search.

Although the modern algorithms perform better than the random search, the important point shown here is that random searches are adequate under certain conditions. If a random search can find an SWR of 1.10 or better in 1500 iterations, the added complexity of the modern search algorithms is not worth an incremental improvement in SWR. The population estimates found in Figure 4.5 and Figure 4.6 show that between 1 in 1500 and 1 in 1900 configurations have SWRs less than 1.10, so it is not improbable that random searches with sample sizes of 1500 can find minimum SWR values near 1.10.

The lowest SWR value found from the 500,000 random samples for the population estimate at 400 MHz is 1.0059. It is interesting to note that several of the trials for the modern algorithms found SWR values below 1.0059. Recall that 1500 iterations are performed for each trial. The ACO searches found minimum SWR values of 1.0046 and 1.0049, the SA searches found minimum SWR values of 1.0014, 1.0019,

Table 4.4. ACO parameter values for the simulated SSA experiment at 400 MHz.

Q	2.0×10^{-4}
τ_0	5.0×10^{-4}
ρ	0.8
α	1.0
β	1.0
Minimum transition probability, p_{min}	0.05
Number of ants, $m = N_{pop}$	39
Number of runs, N_{gen} (Algorithm is stopped when $N_{TotalIts}$ iterations are complete)	39
Total number of iterations, $N_{TotalIts}$	1500

1.0028, and 1.0029, and the GA searches found minimum SWR values of 1.0041 and 1.0056. Since only 1500 iterations are performed for each of these trials and eight of the thirty trials beat the 500,000 random sample, it is an extremely improbable that the ACO, SA, and GA algorithms are simply random searches. The minimum SWR found in any of the trials for the 1500 iteration random search is 1.0251.

The results at 400 MHz show that although the ACO, SA, and GA algorithms are able to locate minimum SWR values that are lower than those found by random searches, the random searches are still capable of finding acceptable configurations. As shown in Table 4.3, the SSA template under study has outer electrical dimensions of $0.80\lambda \times 0.80\lambda$ at 400 MHz. Another good test of the algorithms is to study their ability to locate minimal SWR configurations for SSA templates that are smaller in electrical size. Thus, Sections 4.4.2 and 4.4.3 study these algorithms using the same SSA template at 100 MHz and 40 MHz, respectively. The electrical dimensions of the SSA template shown in Figure 4.4 are $0.20\lambda \times 0.20\lambda$ at 100 MHz and $0.080\lambda \times 0.080\lambda$ at 40 MHz.

Table 4.5. SA parameter values for the simulated SSA experiment at 400 MHz.

Initial temperature, T_0	1.0 K
Temperature fraction, T_f	0.980
Number of temperatures, N_{gen}	150
Number of iterations at each temperature, N_{pop}	10
Total number of iterations, $N_{TotalIts}$	1500

Table 4.6. GA parameter values for the simulated SSA experiment at 400 MHz.

Probability of crossover, p_{cross}	0.7
Maximum number of crossovers per mating operation, $N_{MaxCross}$	3
Probability of mutation, p_{mut}	0.075
Number of generations, N_{gen}	15
Population number, N_{pop}	100
Total number of iterations, $N_{TotalIts}$	1500
Number of elite chromosomes per population, N_{elites}	2

Table 4.7. Lowest SWR and the iteration number where the lowest SWR first occurred for the random search at 400 MHz (1500 total iterations).

	Lowest SWR	Iteration
Trial 1	1.1157	1274
Trial 2	1.0509	748
Trial 3	1.0847	1086
Trial 4	1.0251	265
Trial 5	1.1516	1111
Trial 6	1.0936	113
Trial 7	1.1020	361
Trial 8	1.0649	592
Trial 9	1.1206	61
Trial 10	1.0816	702
mean	1.0891	631.30
σ	0.0365	430.92

Table 4.8. Lowest SWR and the iteration number where the lowest SWR first occurred for the ACO search at 400 MHz (1500 total iterations).

	Lowest SWR	Iteration
Trial 1	1.0471	1398
Trial 2	1.0123	381
Trial 3	1.0173	1287
Trial 4	1.0049	1485
Trial 5	1.0316	1127
Trial 6	1.0075	891
Trial 7	1.0314	867
Trial 8	1.0366	1339
Trial 9	1.0046	1081
Trial 10	1.0106	855
mean	1.0204	1071.1
σ	0.0151	332.80

Table 4.9. Lowest SWR and the iteration number where the lowest SWR first occurred for the SA search at 400 MHz (1500 total iterations).

	Lowest SWR	Iteration
Trial 1	1.1687	585
Trial 2	1.0203	847
Trial 3	1.0108	1166
Trial 4	1.0028	1012
Trial 5	1.0019	982
Trial 6	1.0071	1449
Trial 7	1.0014	1188
Trial 8	1.0105	1496
Trial 9	1.0029	1290
Trial 10	1.0246	1483
mean	1.0251	1149.8
σ	0.0511	298.1

Table 4.10. Lowest SWR and the iteration number where the lowest SWR first occurred for the GA search at 400 MHz (1500 total iterations).

	Lowest SWR	Iteration
Trial 1	1.0096	867
Trial 2	1.0092	1212
Trial 3	1.0096	1372
Trial 4	1.0057	1492
Trial 5	1.0086	1176
Trial 6	1.0180	1242
Trial 7	1.0041	1259
Trial 8	1.0126	1459
Trial 9	1.0056	1259
Trial 10	1.0032	1227
mean	1.0086	1256.5
σ	0.0044	173.53

4.4.2 Minimum SWR search at 100 MHz

The ACO, SA, and GA searches are studied at 100 MHz to search for minimal SWR configurations of the SSA template shown in Figure 4.4. The results are presented in this section.

500,000 random samples of the possible SSA configurations were evaluated at 100 MHz to estimate the properties of the population of configurations. 95% confidence intervals are used for the parameter estimates. The proportion of total configurations with SWR values less than x is shown in Figure 4.7. An additional parameter estimate plot with more detail near low SWR values is found in Figure 4.8.

Notice that the proportion of configurations with SWRs less than 2.0 at 100 MHz has been significantly reduced from the proportion found at 400 MHz. Less than 0.1% meet this criterion at 100 MHz compared to nearly 3% at 400 MHz. Configurations with SWRs less than 1.10 are rare at 100 MHz, as shown in Figure 4.8 where only six of the 500,000 samples have SWRs less than 1.10.

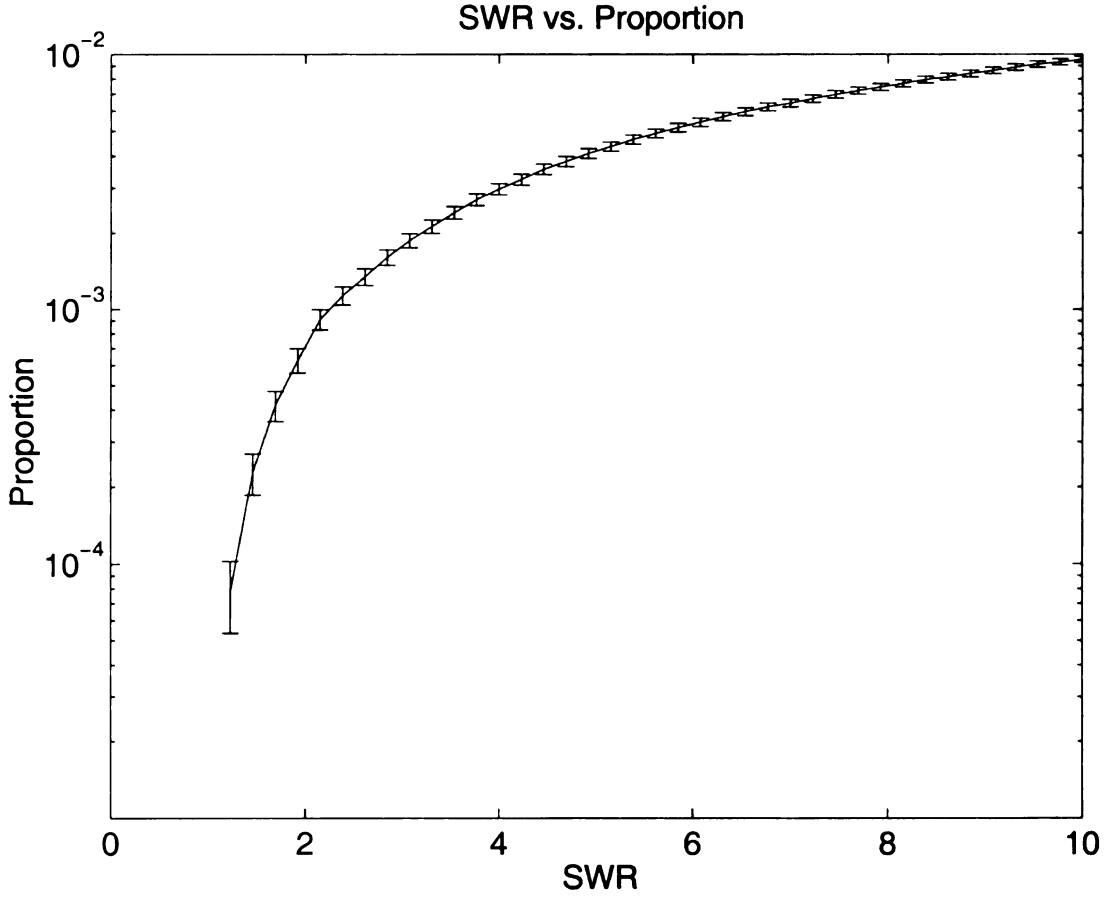


Figure 4.7. Distribution of SWR values (relative to 50 Ω) for the SSA template at 100 MHz (500,000 random samples). Error bars show the 95% confidence intervals.

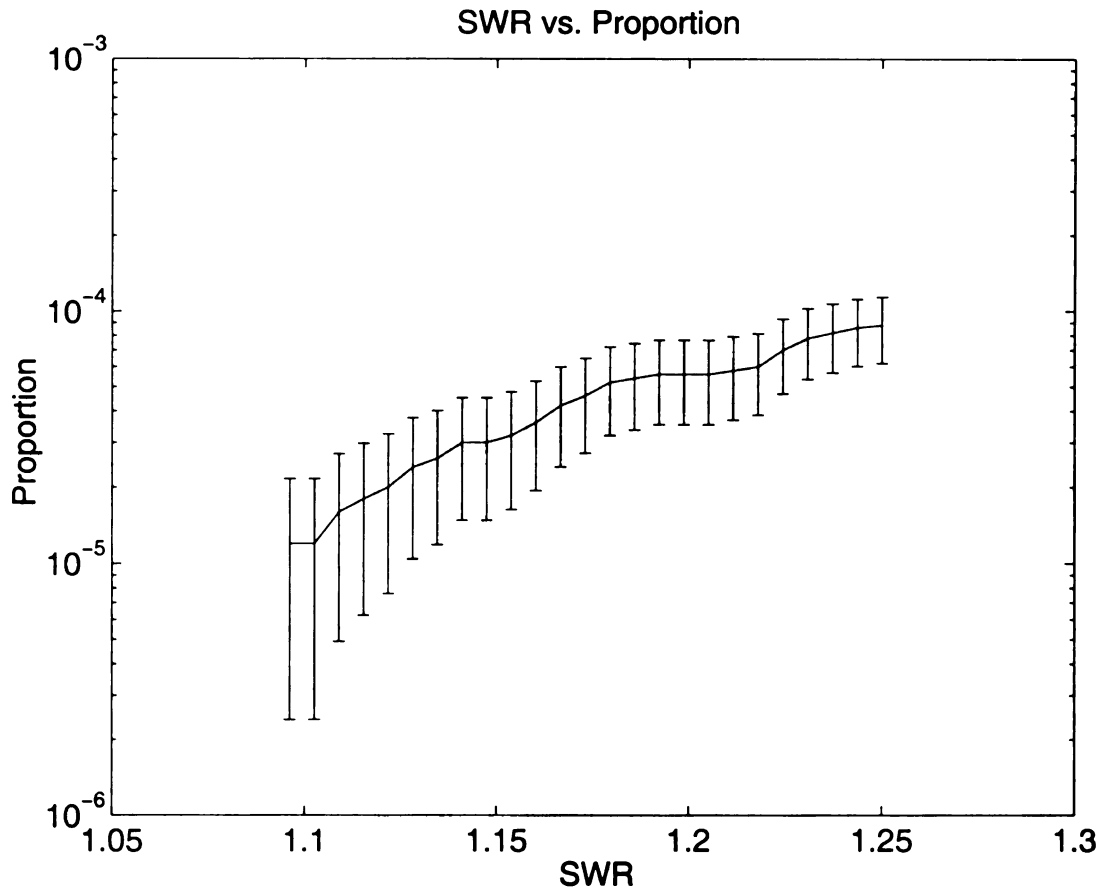


Figure 4.8. Detailed distribution of SWR values (relative to 50 Ω) for the SSA template at 100 MHz (500,000 random samples). Error bars show the 95% confidence intervals.

ACO, SA, and GA routines are used to search for configurations of this SSA template with minimal SWRs at 100 MHz. 1500 total iterations are performed for each algorithm. As a comparison, a search for the minimum SWR of 1500 random configurations is performed. Ten trials of each of these searches is performed.

The fitness function used for the SA, GA, and ACO searches is shown in Equation 4.16, where $\gamma = 2.0$, $\mathtt{SWR}_{\text{Threshold}} = 2.0$, and $\delta = 1.15$. Recall that the SA algorithm adjusts this fitness using Equation 4.17.

The ACO, SA, and GA algorithm parameters are shown in Table 4.11, Table 4.12, and Table 4.13, respectively. Note that the ACO algorithm uses 39 ants in 39 runs,

Table 4.11. ACO parameter values for the simulated SSA experiment at 100 MHz.

Q	2.0×10^{-4}
τ_0	5.0×10^{-4}
ρ	0.8
α	1.0
β	1.0
Minimum transition probability, p_{min}	0.05
Number of ants, $m = N_{pop}$	39
Number of runs, N_{gen} (Algorithm is stopped when $N_{TotalIts}$ iterations are complete)	39
Total number of iterations, $N_{TotalIts}$	1500

implying that 1521 iterations are used. The algorithm is stopped, however, after 1500 iterations to remain consistent with the SA, GA, and random searches presented here. The random, ACO, SA, and GA search results are shown in Table 4.14–Table 4.17.

It is evident from the results presented here that the ACO, SA, and GA search algorithms perform far better than the 1500 iteration random searches at 100 MHz. The ACO, SA, and GA searches found average minimum SWR values of 1.1039, 1.1176, and 1.0780, respectively, and the random searches of 1500 iterations found an average minimum SWR value of 1.9765. A minimum SWR as high as 2.0 may warrant the added complexity needed to implement the modern algorithms in exchange for lower possible SWR values.

The lowest SWR value found by the 500,000 random samples taken for the population estimate at 100 MHz is 1.0317. The ACO trials produced one SWR below this value, and the SA trials produced two SWRs below this value. This further shows the ability of these algorithms to perform better than random searches.

Table 4.12. SA parameter values for the simulated SSA experiment at 100 MHz.

Initial temperature, T_0	1.0 K
Temperature fraction, T_f	0.980
Number of temperatures, N_{gen}	150
Number of iterations at each temperature, N_{pop}	10
Total number of iterations, $N_{TotalIts}$	1500

Table 4.13. GA parameter values for the simulated SSA experiment at 100 MHz.

Probability of crossover, p_{cross}	0.7
Maximum number of crossovers per mating operation, $N_{MaxCross}$	3
Probability of mutation, p_{mut}	0.075
Number of generations, N_{gen}	15
Population number, N_{pop}	100
Total number of iterations, $N_{TotalIts}$	1500
Number of elite chromosomes per population, N_{elites}	2

Table 4.14. Lowest SWR and the iteration number where the lowest SWR first occurred for the random search at 100 MHz (1500 total iterations).

	Lowest SWR	Iteration
Trial 1	2.5939	1456
Trial 2	2.5277	884
Trial 3	1.3926	978
Trial 4	1.4578	1087
Trial 5	2.9019	695
Trial 6	1.3708	1439
Trial 7	1.5983	1054
Trial 8	1.3312	1356
Trial 9	2.6590	498
Trial 10	1.9016	1163
mean	1.9765	1061.0
σ	0.6317	313.80

Table 4.15. Lowest SWR and the iteration number where the lowest SWR first occurred for the ACO search at 100 MHz (1500 total iterations).

	Lowest SWR	Iteration
Trial 1	1.0246	1378
Trial 2	1.0371	1180
Trial 3	1.0418	942
Trial 4	1.0363	1056
Trial 5	1.1012	773
Trial 6	1.1692	903
Trial 7	1.1049	1213
Trial 8	1.2319	1150
Trial 9	1.1065	1262
Trial 10	1.1854	1078
mean	1.1039	1078
σ	0.0719	181.93

Table 4.16. Lowest SWR and the iteration number where the lowest SWR first occurred for the SA search at 100 MHz (1500 total iterations).

	Lowest SWR	Iteration
Trial 1	1.1516	189
Trial 2	1.0225	806
Trial 3	1.0644	388
Trial 4	1.1539	74
Trial 5	1.2632	992
Trial 6	1.1619	1481
Trial 7	1.0465	1360
Trial 8	1.1120	1147
Trial 9	1.1734	581
Trial 10	1.0263	1375
mean	1.1176	839.30
σ	0.0775	512.94

Table 4.17. Lowest SWR and the iteration number where the lowest SWR first occurred for the GA search at 100 MHz (1500 total iterations).

	Lowest SWR	Iteration
Trial 1	1.1212	1343
Trial 2	1.0909	1386
Trial 3	1.0778	1312
Trial 4	1.0414	736
Trial 5	1.0482	1254
Trial 6	1.0764	1075
Trial 7	1.0694	1178
Trial 8	1.0873	676
Trial 9	1.0942	581
Trial 10	1.0735	940
mean	1.0780	1107.0
σ	0.0229	249.11

4.4.3 Minimum SWR search at 40 MHz

The ACO, SA, and GA searches are studied at 40 MHz to search for minimal SWR configurations of the SSA template shown in Figure 4.4. The results are presented in this section.

Recall that the SSA template is only $0.080\lambda \times 0.080\lambda$ in electrical size at 40 MHz. This makes it very difficult for the template to provide configurations with low SWR values.

The sample size for the population estimates performed at 40 MHz is 500,000. The proportion of total configurations with SWR values less than x is shown in Figure 4.9. 95% confidence intervals are used for the parameter estimates.

The SSA template performs poorly at 40 MHz. Only six of the 500,000 random samples for the population estimate have SWRs less than 5.0. It can be said with 95% confidence that the proportion of configurations with an SWR less than 20.0 lies between 3.9×10^{-5} and 8.2×10^{-5}.

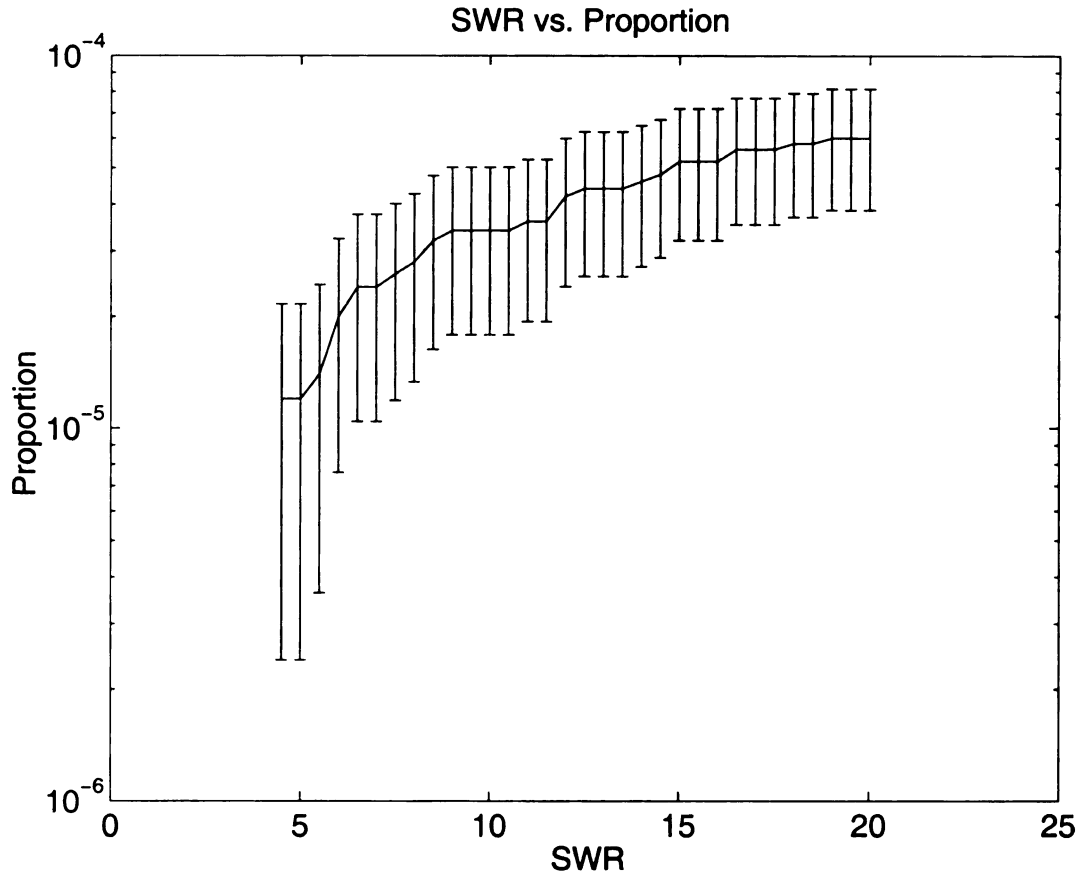


Figure 4.9. Distribution of SWR values (relative to 50 Ω) for the SSA template at 40 MHz (500,000 random samples). Error bars show the 95% confidence intervals.

ACO, SA, and GA routines are used to search for configurations of this SSA template with minimal SWRs at 40 MHz. 1500 total iterations are performed for each algorithm. As a comparison, a search for the minimum SWR of 1500 random configurations is performed. Ten trials of each of these searches is performed.

The fitness function used for the SA, GA, and ACO searches is shown in Equation 4.16, where $\gamma = 2.0$, $\texttt{SWR}_{\text{Threshold}} = 2.0$, and $\delta = 1.10$. Recall that the SA algorithm adjusts this fitness using Equation 4.17.

The ACO, SA, and GA algorithm parameters are shown in Table 4.18, Table 4.19, and Table 4.20, respectively. Note that the ACO algorithm uses 39 ants in 39 runs,

implying that 1521 iterations are used. The algorithm is stopped, however, after 1500 iterations to remain consistent with the SA, GA, and random searches presented here. The random, ACO, SA, and GA search results are shown in Table 4.21–Table 4.24.

Although the population estimates and the 1500 iteration random searches show that the SSA template performs poorly at 40 MHz, the ACO, SA, and GA searches often found configurations with acceptable SWR values. The ACO searches found seven SWRs below 3.0 and three SWRs below 2.0. The SA searches found four SWRs below 2.0. The GA searches found nine SWRs below 3.0 and six SWRs below 2.0. Compare this to the lowest SWR of 28.340 found in the ten trials of 1500 iteration random searches. The next lowest SWR found in these trials is 98.042. The lowest SWR found in the 500,000 random samples taken for the population estimates is 2.4851. Sixteen of the 30 trials of ACO, SA, and GA searches found minimum SWRs below 2.4851.

A configuration with an SWR above 28 is useless for most applications. The results presented here show that as the electromagnetic environment becomes more difficult through a change in operating frequency modern search algorithms can locate acceptable SSA configurations that are difficult to find using a random search.

Table 4.18. ACO parameter values for the simulated SSA experiment at 40 MHz.

Q	2.0×10^{-4}
τ_0	5.0×10^{-4}
ρ	0.8
α	1.0
β	1.0
Minimum transition probability, p_{min}	0.05
Number of ants, $m = N_{pop}$	39
Number of runs, N_{gen} (Algorithm is stopped when $N_{TotalIts}$ iterations are complete)	39
Total number of iterations, $N_{TotalIts}$	1500

Table 4.19. SA parameter values for the simulated SSA experiment at 40 MHz.

Initial temperature, T_0	1.0 K
Temperature fraction, T_f	0.980
Number of temperatures, N_{gen}	150
Number of iterations at each temperature, N_{pop}	10
Total number of iterations, $N_{TotalIts}$	1500

Table 4.20. GA parameter values for the simulated SSA experiment at 40 MHz.

Probability of crossover, p_{cross}	0.7
Maximum number of crossovers per mating operation, $N_{MaxCross}$	3
Probability of mutation, p_{mut}	0.075
Number of generations, N_{gen}	15
Population number, N_{pop}	100
Total number of iterations, $N_{TotalIts}$	1500
Number of elite chromosomes per population, N_{elites}	2

Table 4.21. Lowest SWR and the iteration number where the lowest SWR first occurred for the random search at 40 MHz (1500 total iterations).

	Lowest SWR	Iteration
Trial 1	365.4	391
Trial 2	958.7	1030
Trial 3	281.0	920
Trial 4	2274.8	135
Trial 5	1276.7	1438
Trial 6	222.7	110
Trial 7	28.340	578
Trial 8	98.042	1228
Trial 9	1306.8	184
Trial 10	133.40	1181
mean	694.59	719.50
σ	737.66	500.25

Table 4.22. Lowest SWR and the iteration number where the lowest SWR first occurred for the ACO search at 40 MHz (1500 total iterations).

	Lowest SWR	Iteration
Trial 1	2.1052	1313
Trial 2	2.6384	1387
Trial 3	1.2983	1437
Trial 4	2.6466	1433
Trial 5	12.392	1390
Trial 6	2.6620	1410
Trial 7	1.7787	1401
Trial 8	1.3721	1487
Trial 9	9.9923	718
Trial 10	6.9844	1277
mean	4.3870	1325.3
σ	3.9714	221.72

Table 4.23. Lowest SWR and the iteration number where the lowest SWR first occurred for the SA search at 40 MHz (1500 total iterations).

	Lowest SWR	Iteration
Trial 1	3.0731	762
Trial 2	1.4967	325
Trial 3	18.143	1486
Trial 4	3.2275	1209
Trial 5	1.6679	741
Trial 6	1.6165	598
Trial 7	1.1154	865
Trial 8	8.3711	570
Trial 9	4.2047	552
Trial 10	4.5326	1115
mean	4.7449	822.30
σ	5.1755	353.10

Table 4.24. Lowest SWR and the iteration number where the lowest SWR first occurred for the GA search at 40 MHz (1500 total iterations).

	Lowest SWR	Iteration
Trial 1	1.0864	369
Trial 2	2.8490	1422
Trial 3	2.2738	569
Trial 4	1.4017	539
Trial 5	2.3839	1082
Trial 6	1.9164	1498
Trial 7	1.2298	1323
Trial 8	1.7648	1441
Trial 9	1.7939	1095
Trial 10	4.9056	1153
mean	2.1605	1049.1
σ	1.1065	413.17

4.5 Conclusion

This chapter presents several binary search algorithms that are implemented in SSA applications. Simulated annealing, genetic algorithms, and Ant Colony Optimization (ACO) are described. The implementation of ACO is new to electromagnetics applications.

A simulated SSA experiment was performed to evaluate the effectiveness of these three algorithms compared to random searches. Studies of an SSA template are presented at 400 MHz, 100 MHz, and 40 MHz. The results at 400 MHz show that under some circumstances, random searches for configurations with minimal SWR values are acceptable. As the frequency decreases, however, configurations with low SWR are rarer, and the use of ACO, SA, or GA routines is advantageous. The results at 40 MHz show that random searches are infeasible for SSA templates in difficult electromagnetic environments, and modern search algorithms such as ACO, SA, or GA routines are not only advantageous, but necessary, for locating acceptable configurations.

CHAPTER 5

SIMPLICITY ANALYSIS OF SELF-STRUCTURING ANTENNAS

5.1 Overview

It is often difficult to resist viewing SSAs as conventional antenna systems. SSAs, however, are unique and complicated systems that require study from a different perspective. There exist too many unknowns and possible configurations to be able to use most conventional antenna evaluation methods on SSAs.

This chapter tries to gain an understanding of SSA characteristics by simulating simple SSA templates with relatively few switches. The number of possible SSA configurations is reduced, allowing for exhaustive studies of the possible antenna configurations. More complicated templates are generated by adding switches and wires to the simple templates. As the templates become more complicated, exhaustive searches become unfeasible, and random searches are performed to characterize the SSA templates.

The template geometries used in this study are explained in Section 5.2. The simulation results are presented in Section 5.3. Conclusions from this study are drawn in Section 5.4.

5.2 Geometries Studied

It is difficult to determine by intuition or rules of thumb the best type of geometry to use for the SSA templates in this simplicity study. Due to its asymmetric topology, a template geometry similar to the prototype template discussed in Chapter 3 is used. The template geometry used in this study is created by progressively adding *layers* to a simple starting template. This starting template is called the *layer 1* SSA template and is shown in Figure 5.1. Partial or complete layers are added to the

layer 1 template to create the layer 1.5 template, layer 2 template, layer 2.5 template, and so on. A diagram of the progression of layers from layer 1 to layer 3 is shown in Figure 5.2. The small white rectangles denote the switch locations on the template. Note that each of the studied SSA templates uses a single feed point.

The quantities l_x and l_y are the outer dimensions of the template, and d_x and d_y are the dimensions of the first layer within the template. As shown in Figure 5.1, $l_x = d_x$ and $l_y = d_y$ for the layer 1 template. For integer numbered layered templates (layer n templates), $l_x = n \cdot d_x$ and $l_y = n \cdot d_y$. For templates numbered $n.5$ (where n is an integer), $l_x = (n+1) \cdot d_x$ and $l_y = n \cdot d_y$. These quantities are clearer for the higher template layers shown in the diagrams throughout Section 5.3.

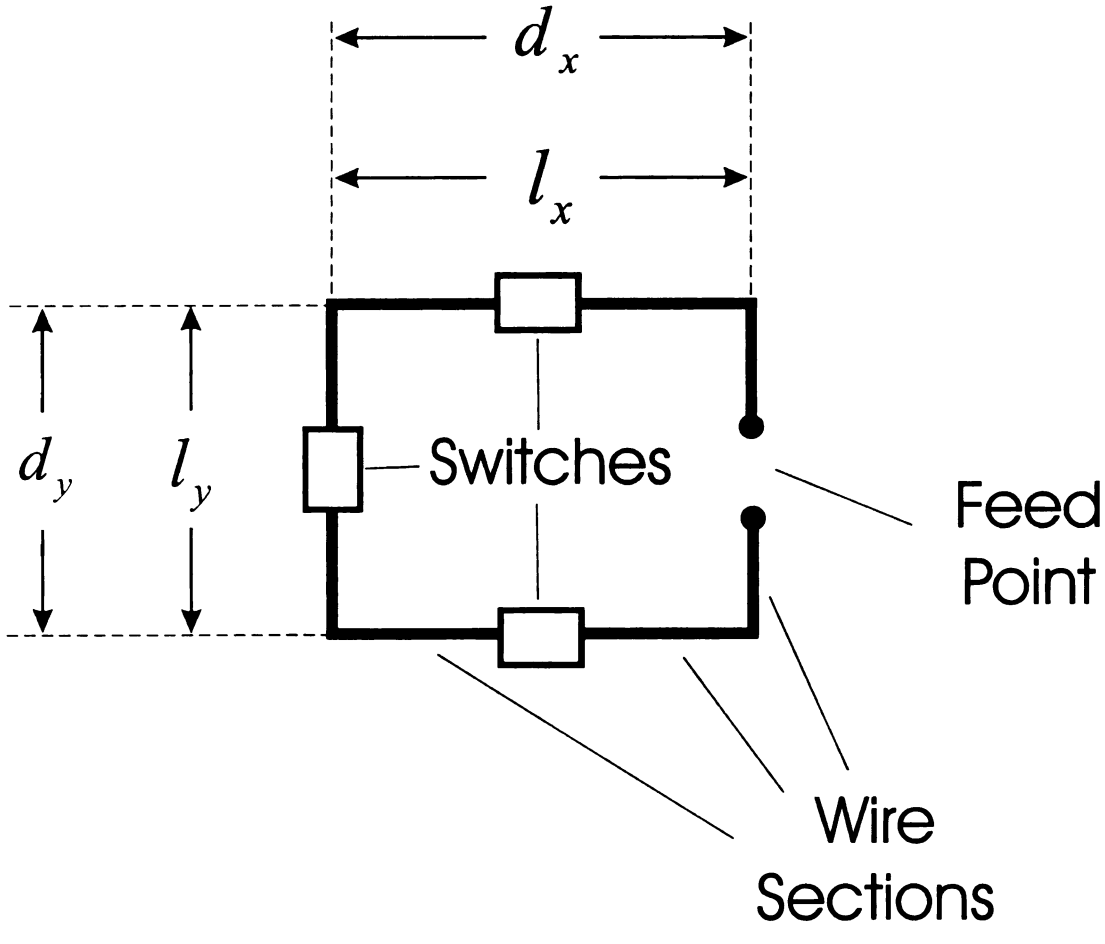


Figure 5.1. Diagram of the layer 1 SSA template.

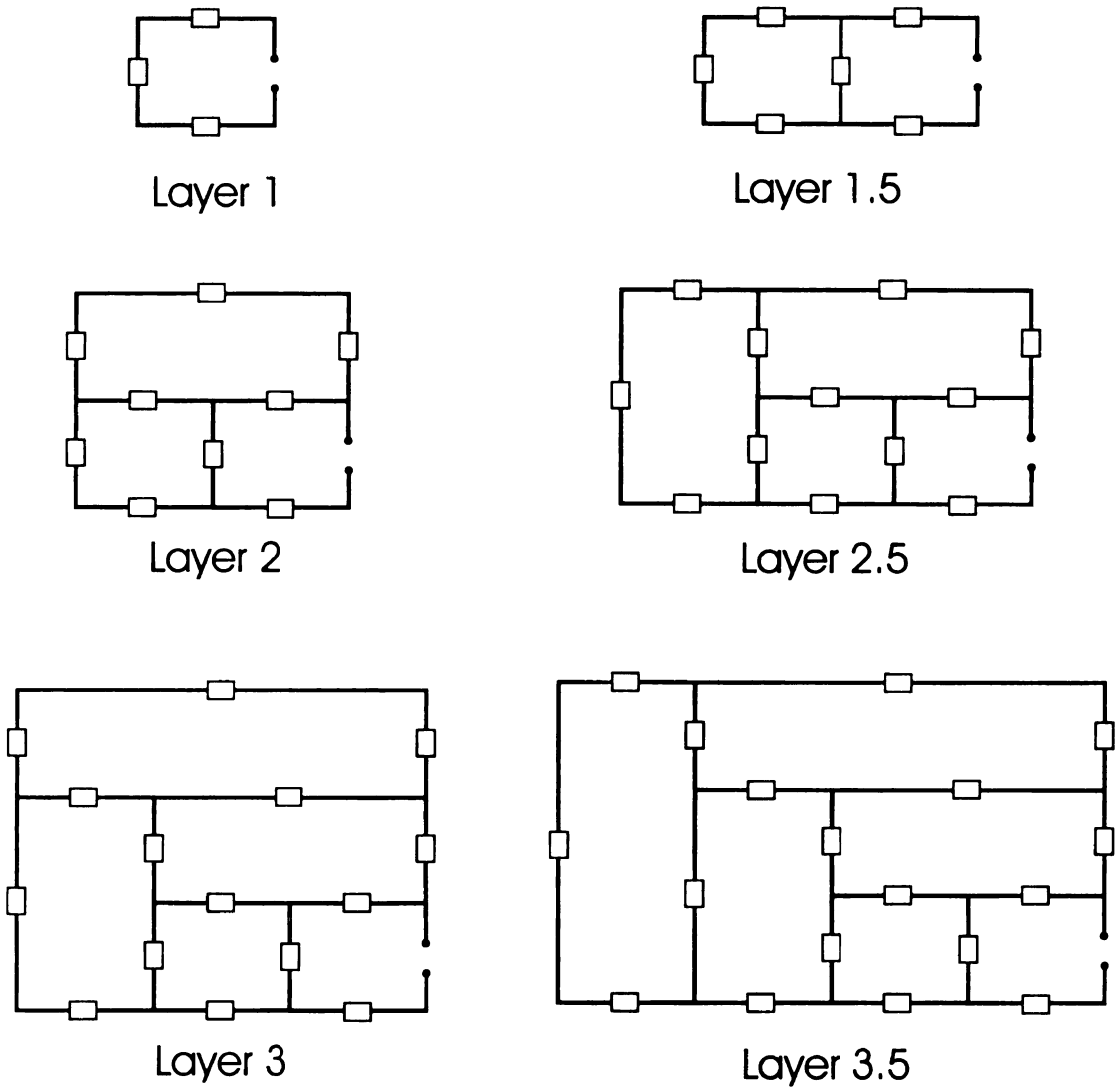


Figure 5.2. Progression of template layers in the simplicity study.

The layer 1 SSA template uses only three switches resulting in eight possible SSA configurations. As layers are added, more switches are used, resulting in a drastic increase in the number of possible SSA configurations. This exponential growth of the possible configurations is shown in Table 5.1. Note that not every layer in the table is presented in this chapter.

Table 5.1. Number of switches and possible SSA configurations for the SSA template layers in the simplicity study.

Layer	Switches	SSA Configurations
1	3	8
1.5	6	64
2	9	512
2.5	12	4,096
3	15	32,768
3.5	18	262,144
4	21	2,097,152
4.5	24	16,777,216
5	27	134,217,728
5.5	30	1,073,741,824
6	33	8,589,934,592
6.5	36	68,719,476,736
7	39	549,755,813,888

There are two types of templates used in this study. *Type I* templates grow in physical and electrical dimensions as layers are added. *Type II* templates use fixed outer dimensions and add wires and switches to the interior of the outer boundaries as layers are added. The two template types are illustrated in Figure 5.3 using three maximum layers as an example. Only the layers 1, 2, and 3 are shown for each template type for the sake of brevity. The Type I layer 1 template has outer dimensions of $w/3 \times h/3$. The Type I layer 2 template is larger, having outer dimensions of $2w/3 \times 2h/3$. The Type I layer 3 template is the maximum layer for this example, and its outer dimensions are $w \times h$. The outer dimensions for the Type II templates are $w \times h$ for all three layers. Notice that the Type I and Type II layer 3 templates are identical because three maximum layers are used for this example. Seven maximum layers are used for the study presented in this chapter. Thus, the results for the layer 7 Type I and Type II templates are the same.

5.3 Simulation Results

Simulations using the Numerical Electromagnetics Code were performed to determine the characteristics of the SSA templates for this simplicity study. The parameters of the study are summarized in Table 5.2. The SSA templates are studied from 40 MHz to 800 MHz at every 20 MHz step. Input impedance and pattern information is stored in a separate file for each studied SSA configuration. Standing wave ratios and Smith charts ([217], [218]) presented in this study assume a 200 Ω characteristic impedance.

The computer program used to simulate SSAs is explained in Appendix A. A Dell 1.8 GHz Pentium 4 personal computer was used to run the simulations. The results from this study are presented in Section 5.3.1 through Section 5.3.9.

The radiation pattern is computed in the horizontal (x-y) plane ($\theta = 90°$) for 360 observation angles in 1° increments. The results presented in this chapter include

Table 5.2. Simulation parameters for the simplicity study.

Frequency range studied	40 – 800 MHz
Number of frequencies	39
Frequency step	20 MHz
Number of angles studied in the x-y plane for pattern characteristics	360
Angle of rotation between the SSA template and the x-y plane	90°
Distance from the x-y plane at $z = 0$ and the bottom of the SSA template	0.1 m
Characteristic impedance, Z_0	200 Ω

information gathered from the gain at these observation angles. The gain is defined as a ratio of powers that are required to produce the same field strength in a given direction. The ratio is the power at the input of a loss free isotropic radiator to the power at the input of the SSA. Since there are no conductive losses modeled, the gain and the directive gain are the same. The gain is expressed in dB unless noted otherwise.

Gain is dependent on polarization, and only the vertical polarization (z-directed) information is presented in this dissertation. The quantities that are presented include the maximum vertical gain in the horizontal ($\theta = 90°$) plane and the minimum vertical gain in the horizontal plane. Comparing the maximum and minimum vertical gains to 0 dB relates an antenna's performance to a vertically polarized isotropic radiator. This is important to many automotive applications, where minimum vertical gains in the horizontal plane are required to ensure that signals are not lost due to changes in orientation. The maximum vertical gain is the highest value of vertical gain over the studied angles. The vertical gain at other angles is equal or less than this value.

The radii of the template wires are 2.0 mm for all wires in this study. The switches on the SSA template are modeled using the `swLeverWire` switch model

described in Section A.2.7.3 in the appendix. A diagram of the switch model is shown in Figure A.2 on page 337. The switch levers are opened a small distance ($h_1 = 9.06$ mm) to simulate an open circuit.

The templates are planar and are oriented vertically in the x-z plane. The wire segment containing the feed point is aligned in the z-direction. An applied voltage source is used at the feed point to excite the system.

The bottoms of the SSA templates lie at $z = 0.1$ m. This is done so that a ground can be included at the $z = 0$ plane. SSA templates in free space and the above ground are studied for most of the template layers presented here. Only the random searches of the layer 4, 5, and 6 templates do not include results above a ground plane.

Exhaustive searches are presented for layers 1, 1.5, 2, and 2.5 for the Type I and Type II templates. Random searches are presented for layers 3, 4, 5, 6, and 7 for Type I templates. Recall that the Type I and Type II layer 7 templates are the same.

Table 5.3. Dimensions of the layer 1 Type I SSA template.

l_x	8.57 cm
d_x	8.57 cm
l_y	8.57 cm
d_y	8.57 cm
Outer electrical dimensions at 40 MHz	$0.0114\lambda \times 0.0114\lambda$
Outer electrical dimensions at 800 MHz	$0.229\lambda \times 0.229\lambda$

Table 5.4. Dimensions of the layer 1 Type II SSA template.

l_x	60.0 cm
d_x	60.0 cm
l_y	60.0 cm
d_y	60.0 cm
Outer electrical dimensions at 40 MHz	$0.0800\lambda \times 0.0800\lambda$
Outer electrical dimensions at 800 MHz	$1.60\lambda \times 1.60\lambda$

5.3.1 Layer 1 SSA Template

A diagram of the layer 1 template is shown in Figure 5.1. Three switches are used for eight possible SSA configurations. The dimensions of the layer 1 Type I and Type II SSA templates are shown in Table 5.3 and Table 5.4, respectively.

5.3.1.1 Layer 1 Type I SSA Template

The SWR of each SSA configuration of the layer 1 Type I template in the absence of ground (free space) is shown in Figure 5.4. The SWR values are plotted as individual points at the discrete frequencies studied. Notice that over nearly the entire band of studied frequencies, none of the eight possible SSA configurations provide an SWR value less than 2.0. This is also shown in Figure 5.6, where the minimum SWR is plotted at each frequency on a linear scale from 1.0 to 10.0. Notice that no SSA configurations exhibit an SWR less than 10.0 for frequencies less than 560 MHz. The

lowest SWR at any frequency is found at 800 MHz, and this value is above 3.5.

The presence of a ground plane 0.1 m below the bottom of the layer 1 Type I SSA template does not significantly improve the poor SWR performance of this template. This is shown in a plot of the SWR values for the eight possible configurations of the layer 1 Type I template above ground found in Figure 5.5. Figure 5.6 shows that the presence of the ground plane allows for minimum SWR values less than 10.0 to be possible at 440 MHz and above. Recall that this occurs at 560 MHz in free space.

Notice in Figure 5.4 that although eight SSA configurations are possible for the layer 1 template, only six distinct SWR values are distinguishable at most frequencies. This is because the layer 1 template is nearly symmetrical, as shown in Figure 5.1. However, the lever switch on the top of the template faces one direction, and the lever switch on the bottom faces the other direction, creating a slight asymmetry in the template. This is more visible in the results shown for the template above ground in Figure 5.5, where eight distinct SWR values are distinguishable at 340 MHz. All template symmetry is lost for layers higher than layer 1.

An SWR greater than 50.0 is unacceptable for most practical antenna systems, but to illustrate the difficulty that the layer 1 Type I template has matching to 200 Ω, the proportion of SSA configurations with SWR values less than 50.0 is plotted in Figure 5.7. Notice the large step discontinuities across frequencies due to the low number of possible configurations. Below 340 MHz, no SSA configurations exhibit SWRs less than 50.0 for the template in free space. For the template above ground, no SSA configurations exhibit SWRs less than 50.0 at frequencies below 320 MHz.

If a system requires an antenna with an SWR of 2.0 or better, the layer 1 Type I template in free space or above ground is unacceptable for use over the studied frequency band. Only eight SSA configurations are possible, and the template is electrically small across the band. The layer 1.5 Type I SSA templates have more possible configurations and are electrically larger than the layer 1 Type I templates.

The layer 1.5 templates are presented in Section 5.3.2.

The poor low frequency impedance characteristics are also shown in a Smith chart of the input impedances of the possible configurations at 40 MHz found in Figure 5.8 for the layer 1 Type I template in free space. Each '×' denotes the input impedance of an SSA configuration. Seven of eight configurations exhibit near open-circuit impedances, and one configuration exhibits a near short-circuit impedance. This is the configuration with all three switches shorted ('111'). The seven other configurations have at least one open-circuited switch. The Smith chart for the layer 1 Type I template above ground found in Figure 5.9 shows similar behavior at 40 MHz.

At 800 MHz, the layer 1 Type I templates exhibit some radiation as shown in Figure 5.10 and Figure 5.11 for the templates in free space and above ground, respectively. Although no configurations provide a good match to 200 Ω, the impedances have migrated inside the Smith chart due to radiation.

Gain performance of the layer 1 Type I SSA template is slightly better than its impedance characteristics. The proportion of configurations with minimum vertical gains above 0 dB in the horizontal plane ($\theta = 90°$) is shown in Figure 5.12. An antenna with a minimum vertical gain above 0 dB has at least the same vertical field strength as an isotropic radiator at every studied angle in the horizontal plane. The induced current in the ground plane allows for higher gain values, as shown by the greater proportion of configurations above the 0 dB threshold for the template above ground. This is also shown in Figure 5.13, where the proportion of configurations with maximum vertical gains in the horizontal plane above 3.0 dB is plotted for the templates in free space and above ground. Recall that the maximum gain is the highest value of gain over the studied angles. Thus, if a configuration has a vertical gain above 3.0 dB only at a single angle, the configuration is counted into the proportion shown in Figure 5.13. There are more configurations with maximum

vertical gains above the 3.0 dB threshold for the template above ground across the studied frequency band.

Combining impedance and gain criteria for the proportion plots produces enlightening results. This is especially true for the higher layers in this study. The proportion of configurations with SWRs less than 50.0 and minimum vertical gains above 0 dB is shown in Figure 5.14 for the layer 1 Type I SSA templates in free space and above ground. Although the ground plane does not greatly affect the proportion of SWRs below 50.0 as shown in Figure 5.7, the additional minimum gain requirement shapes the proportion of successful configurations shown in Figure 5.14. Figure 5.15 also demonstrates that combining the SWR requirements with maximum vertical gain requirements shapes the proportion of acceptable configurations.

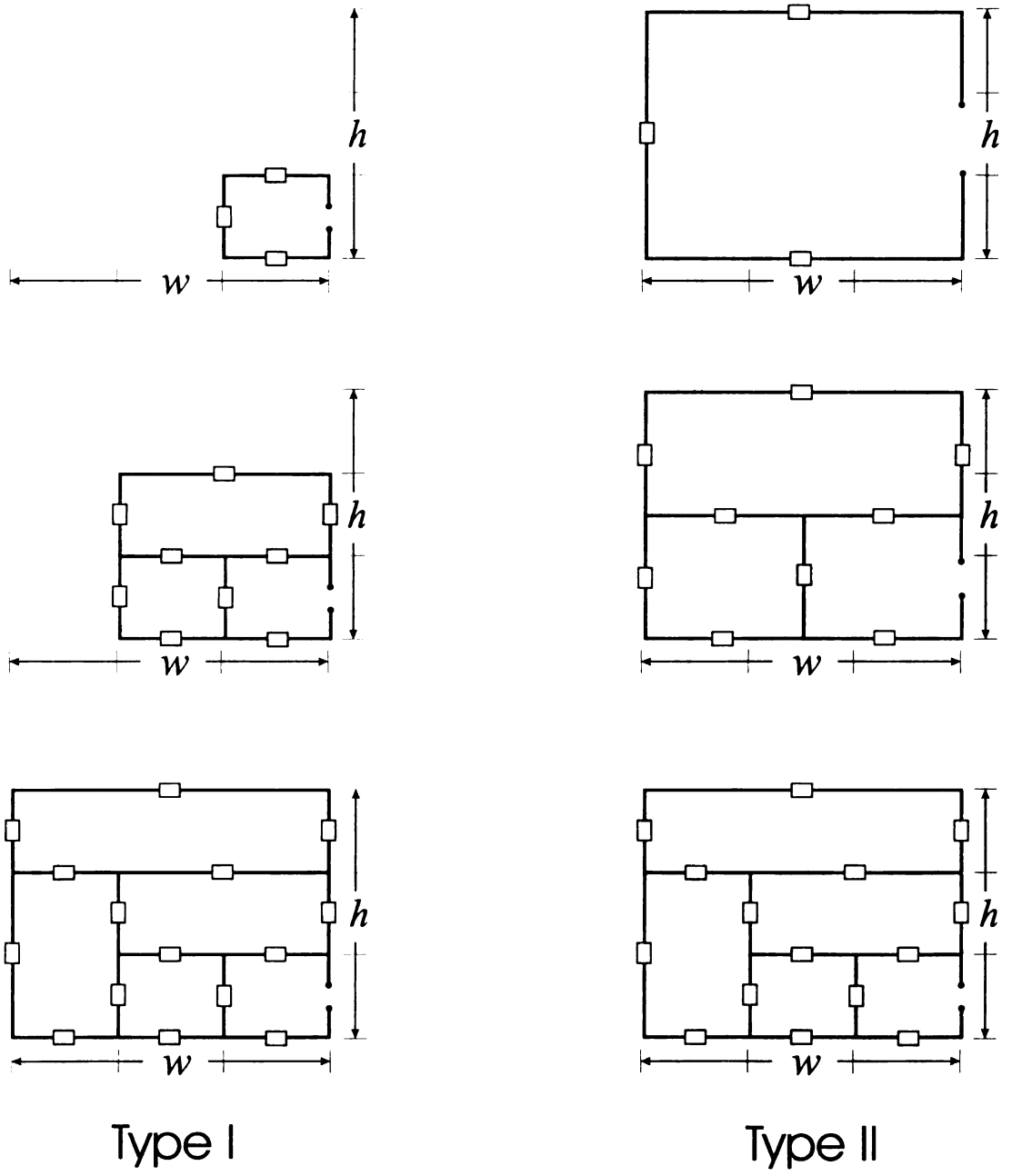


Figure 5.3. Diagram of the Type I and Type II SSA templates based on three maximum layers.

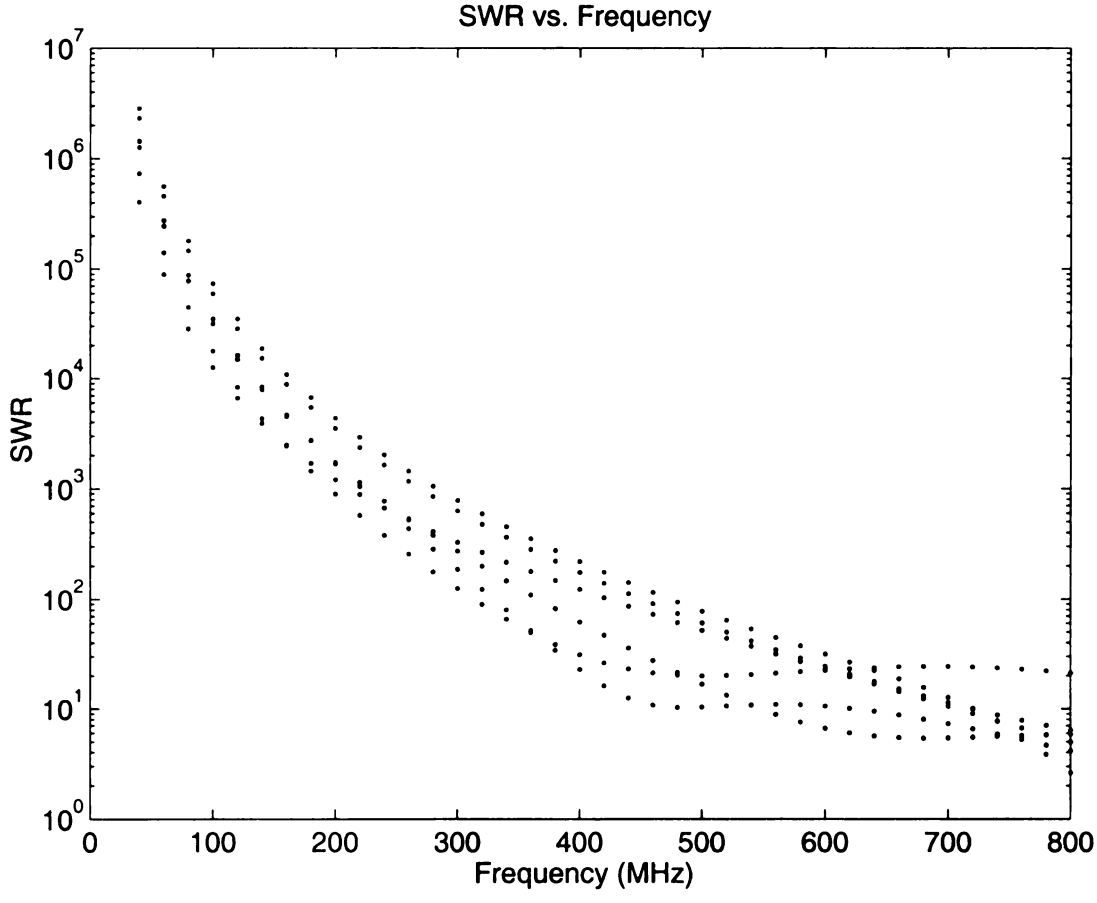


Figure 5.4. SWR vs. frequency for the layer 1 Type I SSA template in free space.

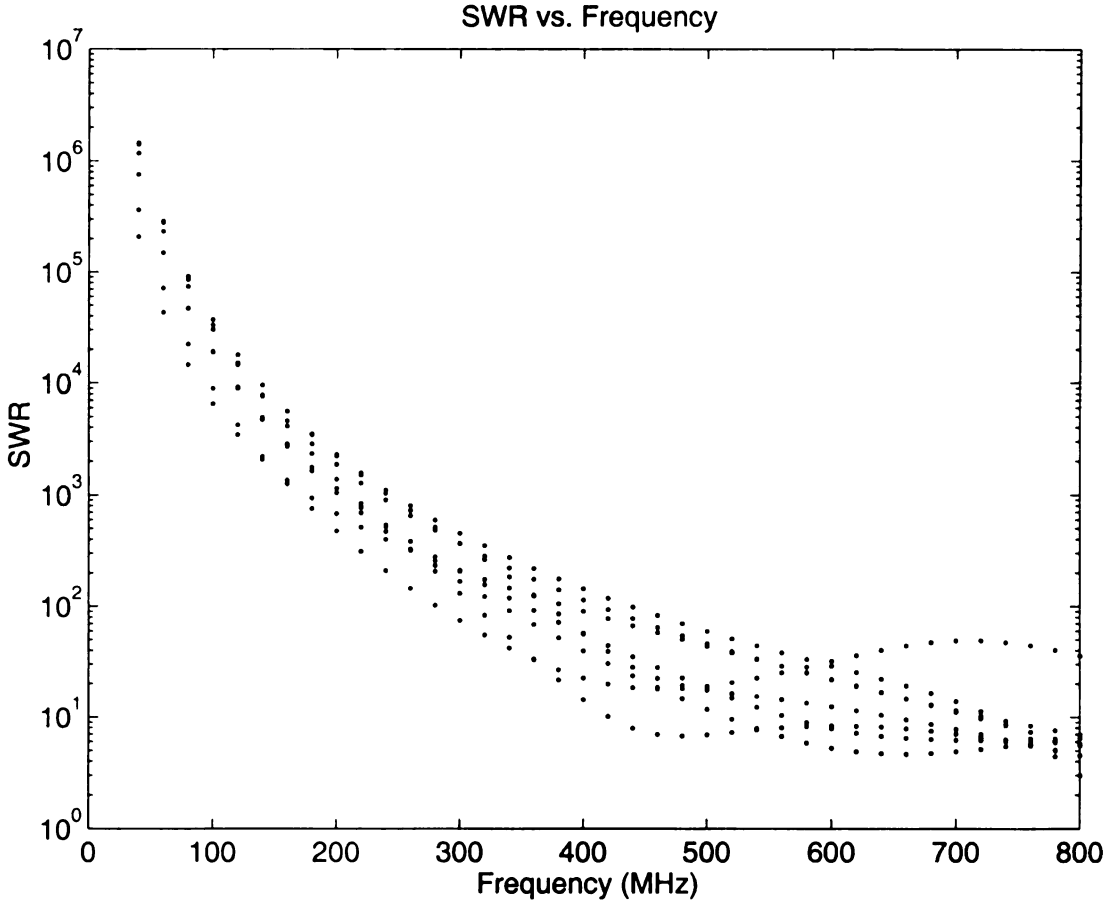


Figure 5.5. SWR vs. frequency for the layer 1 Type I SSA template above ground.

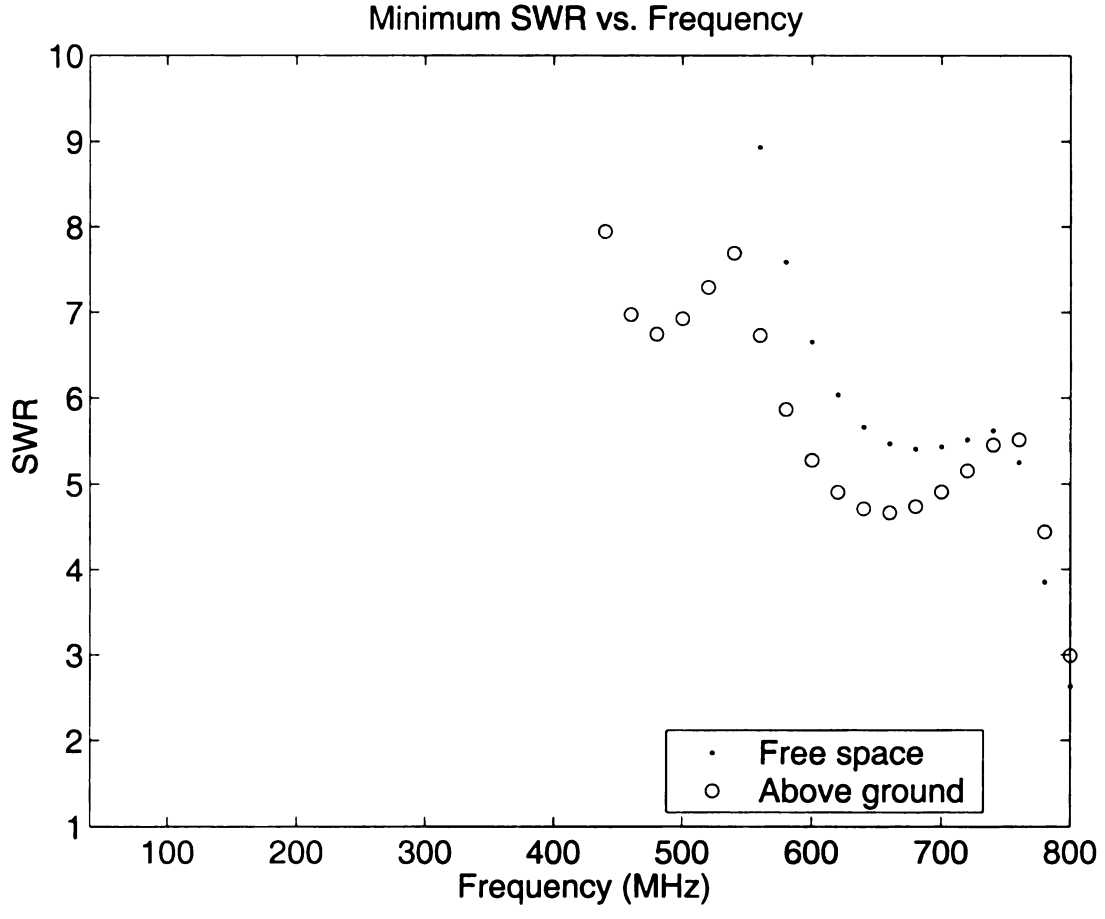


Figure 5.6. Minimum SWR vs. frequency for the layer 1 Type I SSA template.

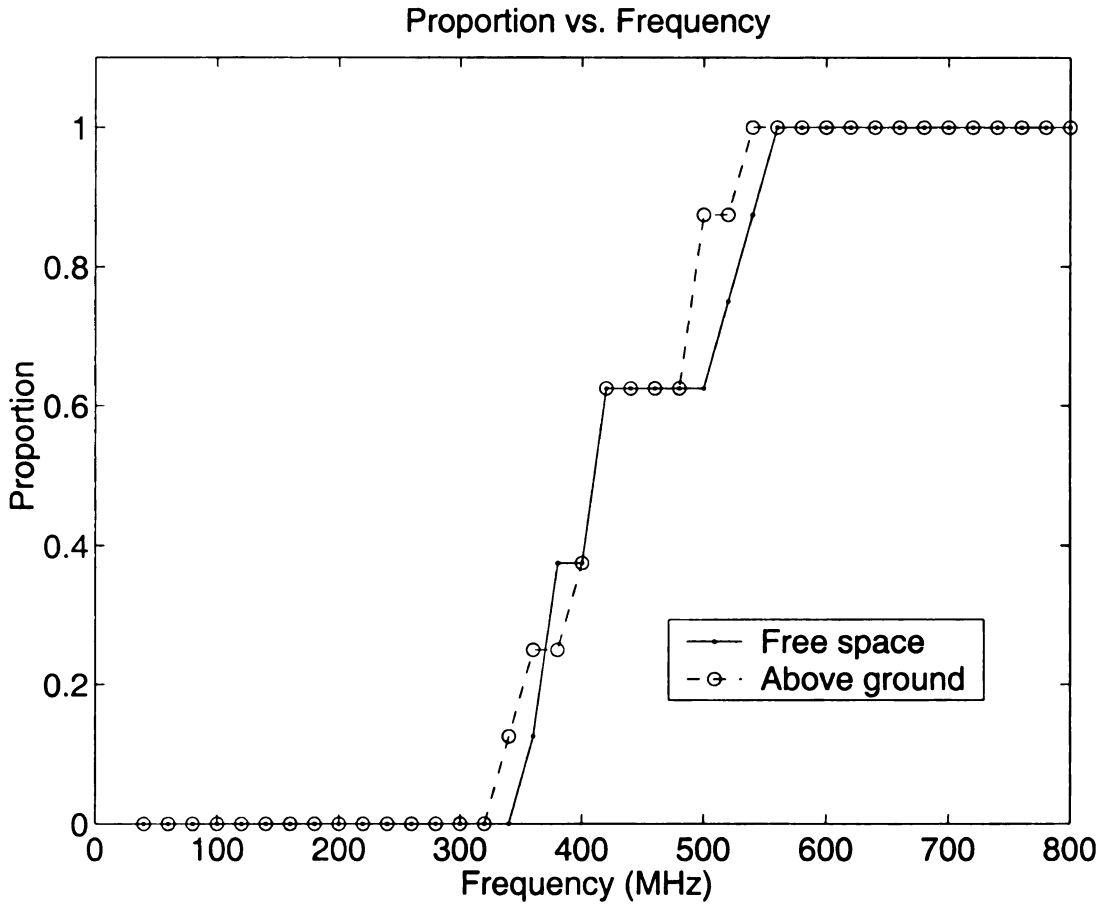


Figure 5.7. Proportion of configurations with SWRs less than 50.0 vs. frequency for the layer 1 Type I SSA template (linear scale).

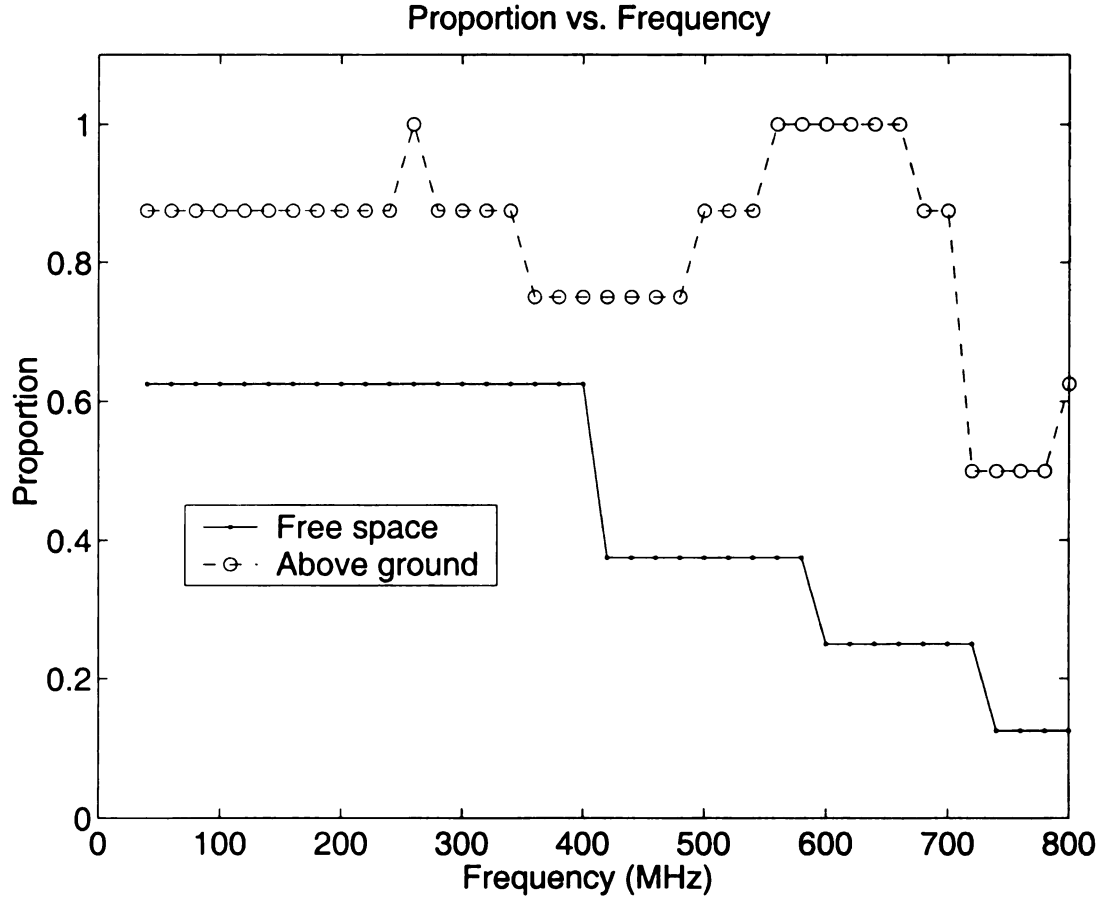


Figure 5.12. Proportion of configurations with minimum vertical gains in the horizontal plane above 0 dB vs. frequency for the layer 1 Type I SSA template (linear scale).

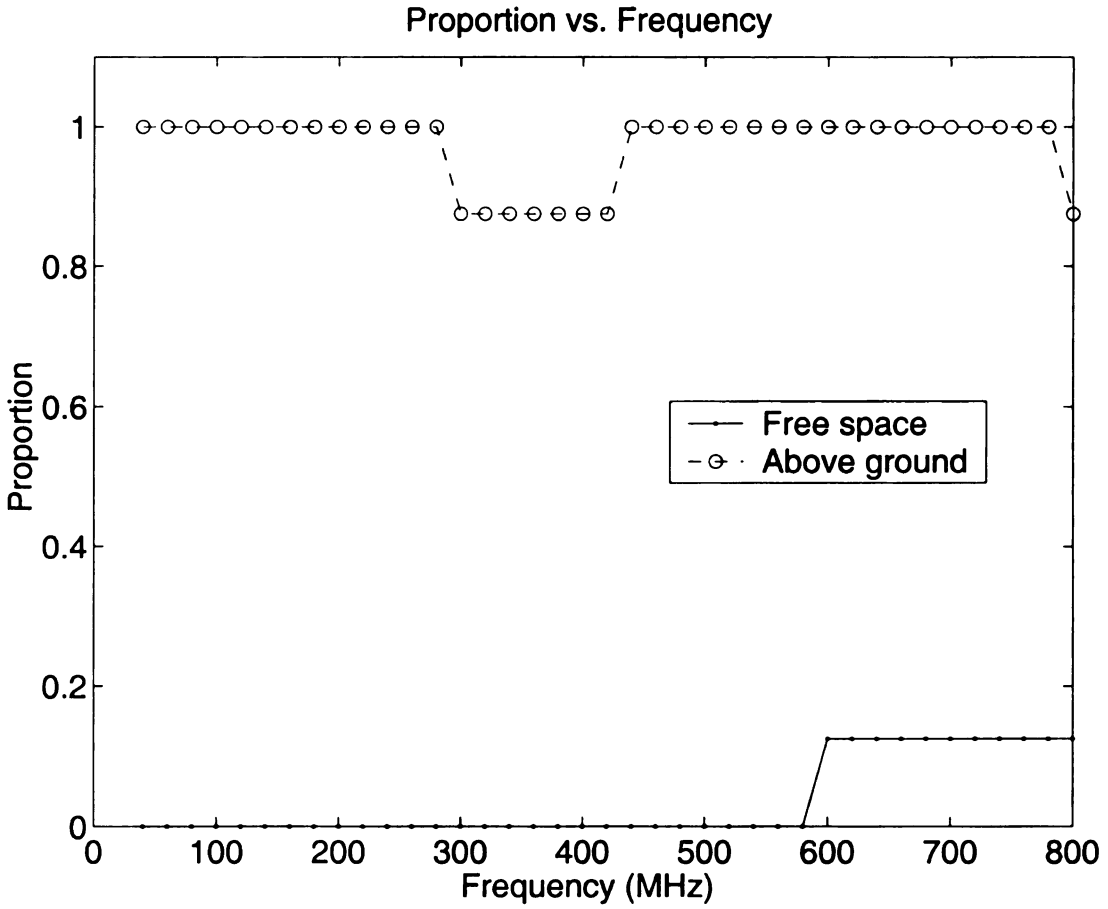


Figure 5.13. Proportion of configurations with maximum vertical gains in the horizontal plane above 3.0 dB vs. frequency for the layer 1 Type I SSA template (linear scale).

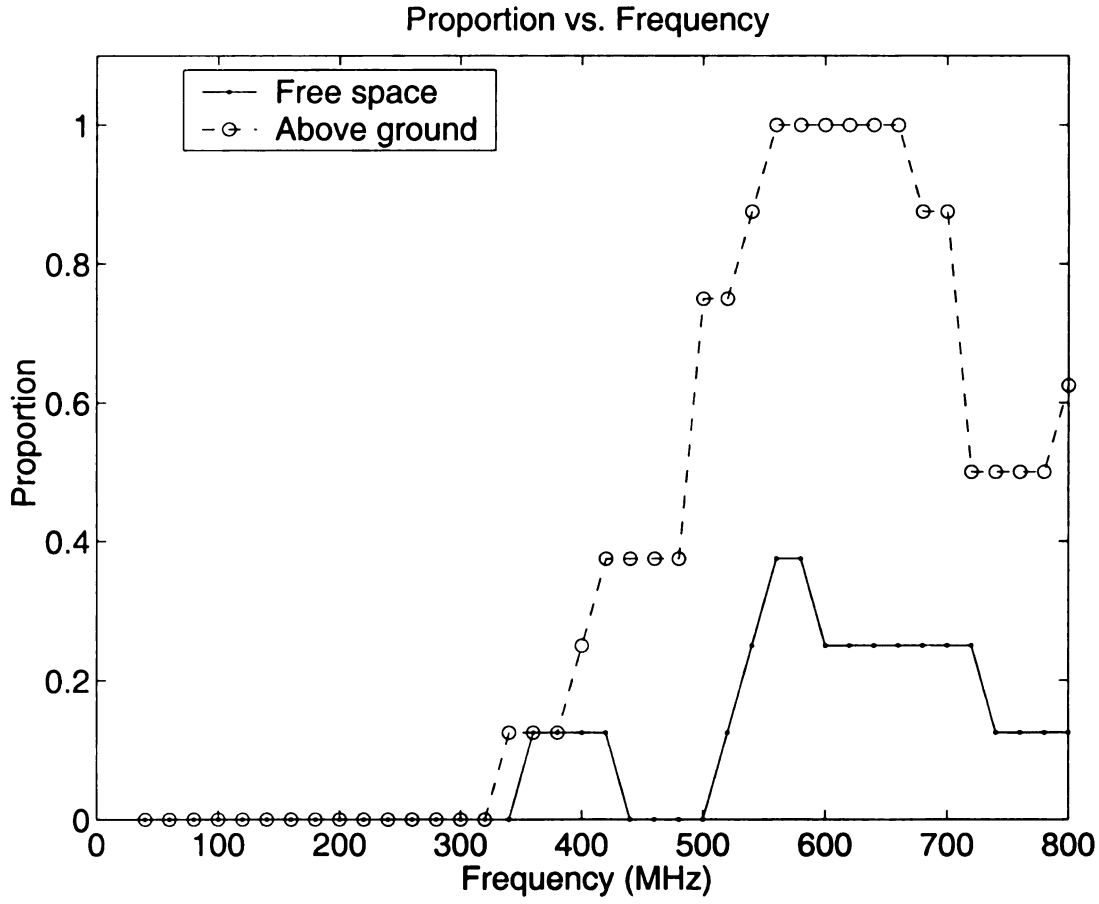


Figure 5.14. Proportion of configurations with SWRs less than 50.0 and minimum vertical gains in the horizontal plane above 0 dB vs. frequency for the layer 1 Type I SSA template (linear scale).

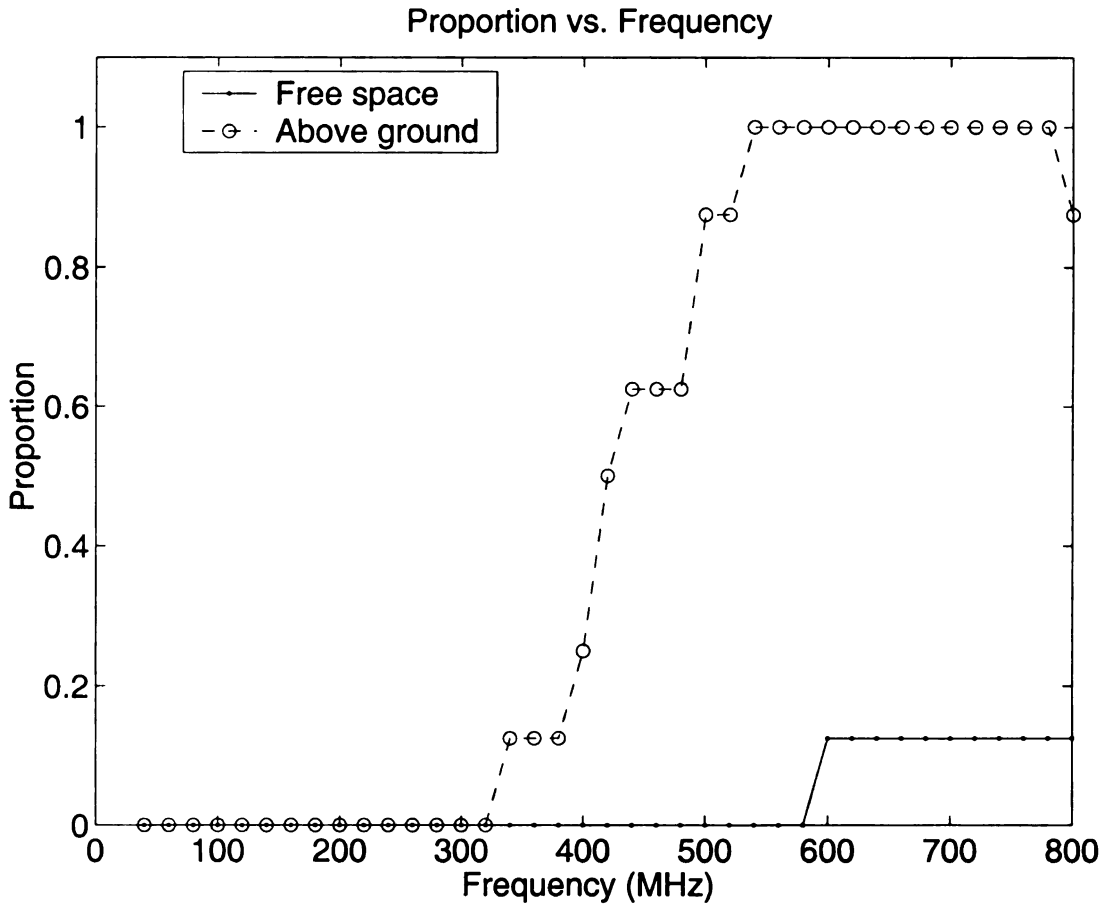


Figure 5.15. Proportion of configurations with SWRs less than 50.0 and maximum vertical gains in the horizontal plane above 3.0 dB vs. frequency for the layer 1 Type I SSA template (linear scale).

5.3.1.2 Layer 1 Type II SSA Template

The layer 1 Type II template is seven times larger on each side in electrical length than the layer 1 Type I template, and 49 times larger in electrical area. The dimensions of the layer 1 Type II template are shown in Table 5.4. However, the number of possible SSA configurations has not increased from eight.

The possible SWR values of the eight configurations at each frequency for the layer 1 Type II template in free space are shown in Figure 5.16. The increase in electrical length over the Type I template has allowed for more radiation and better

SWRs across the studied frequency band. Many SWRs less than 10.0 exist across the studied band. This is also true for the template above ground, as shown in Figure 5.17.

The minimum SWR achievable at each frequency is shown in Figure 5.18. For the template in free space, values are below 3.0 at all studied frequencies above 120 MHz except at 220 MHz, where the minimum SWR is above 4.5. For the template above ground, minimum SWR values below 3.0 are possible above 120 MHz except at 220 MHz.

Figure 5.19 shows that an appreciable proportion of the possible configurations exhibit SWRs less than 3.0, and that all of the configurations have SWRs less than 3.0 from 600 MHz to 700 MHz for the templates in free space and above ground. Figure 5.20 shows that many of the possible configurations have SWRs less than 2.0 across the studied band for the templates in free space and above ground.

Although the minimum SWR values for the layer 1 Type II templates in free space or above ground are much improved over those for the layer 1 Type I templates due to an increase in electrical size, the low number of possible configurations could make the layer 1 Type II templates unacceptable for many applications. Notice in Figure 5.16 and Figure 5.17 that above 400 MHz, the SWR values do not differ greatly for the different configurations. If a receiver requires an input impedance other than 200 Ω or if additional nearby conductors alter the template's impedance, the system may not be capable of providing a different configuration with acceptable characteristics. Smith charts at 800 MHz found in Figure 5.21 and Figure 5.22 show how close that all of the configurations' impedances are for the templates in free space and above ground, respectively.

The proportion of configurations with minimum vertical gains in the horizontal plane ($\theta = 90°$) above 0 dB is shown in Figure 5.23 for the layer 1 Type II SSA templates in free space and above ground. As is the case for the layer 1 Type I SSA

templates, the presence of the ground plane improves the minimum vertical gain. The presence of the ground plane also increases the proportion of configurations with maximum vertical gains above 3.0 dB, as shown in Figure 5.24.

The proportion of configurations with minimum gains above 0 dB and SWRs less than 2.0 is shown in Figure 5.25. No configurations meet these criteria for the template in free space, and there are few frequencies where configurations exist that meet these criteria for the template above ground. Figure 5.26 shows that from 540 MHz to 760 MHz, the template above ground has at least one configuration with an SWR less than 2.0 and a maximum vertical gain of 3.0 dB.

The results presented here for the layer 1 Type II template show that few, if any, SSA configurations meet impedance and gain requirements for many practical applications. The differences in the proportions of configurations meeting gain requirements due to the presence or absence of a ground plane indicate that this template will have a difficult time adapting to a changing electromagnetic environment. Both the Type I and Type II layer 1 templates exhibit these poor characteristics. Since the layer 1 Type I and Type II templates vary in electrical size but use the same number of switches, templates with more switches and wires are presented in this study.

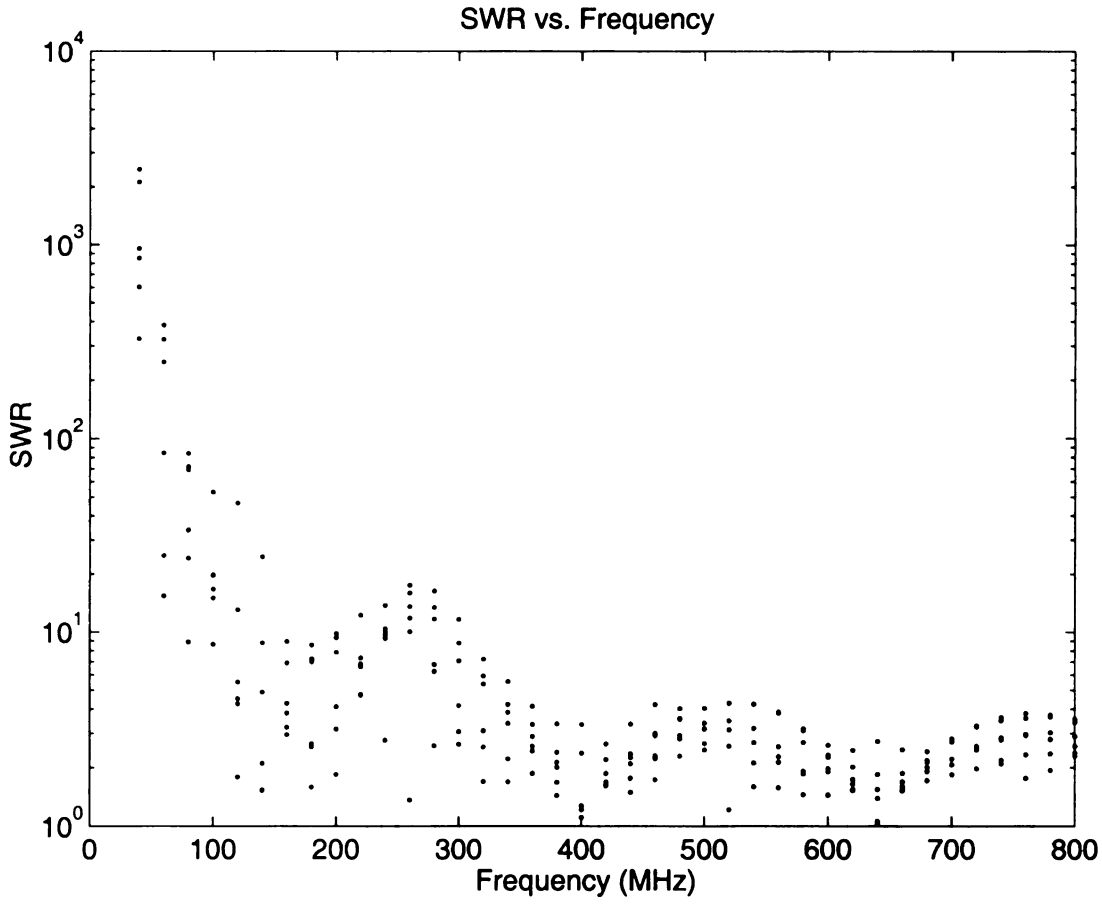


Figure 5.16. SWR vs. frequency for the layer 1 Type II SSA template in free space.

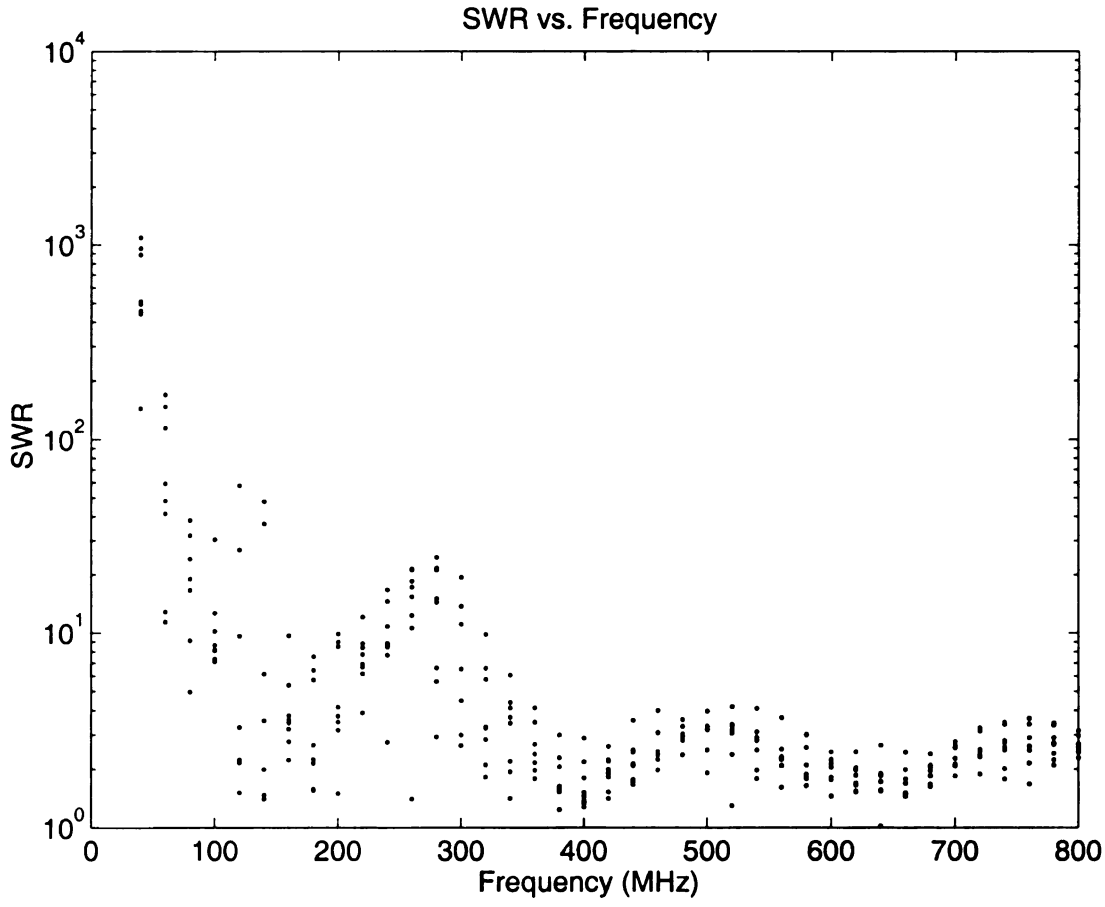


Figure 5.17. SWR vs. frequency for the layer 1 Type II SSA template above ground.

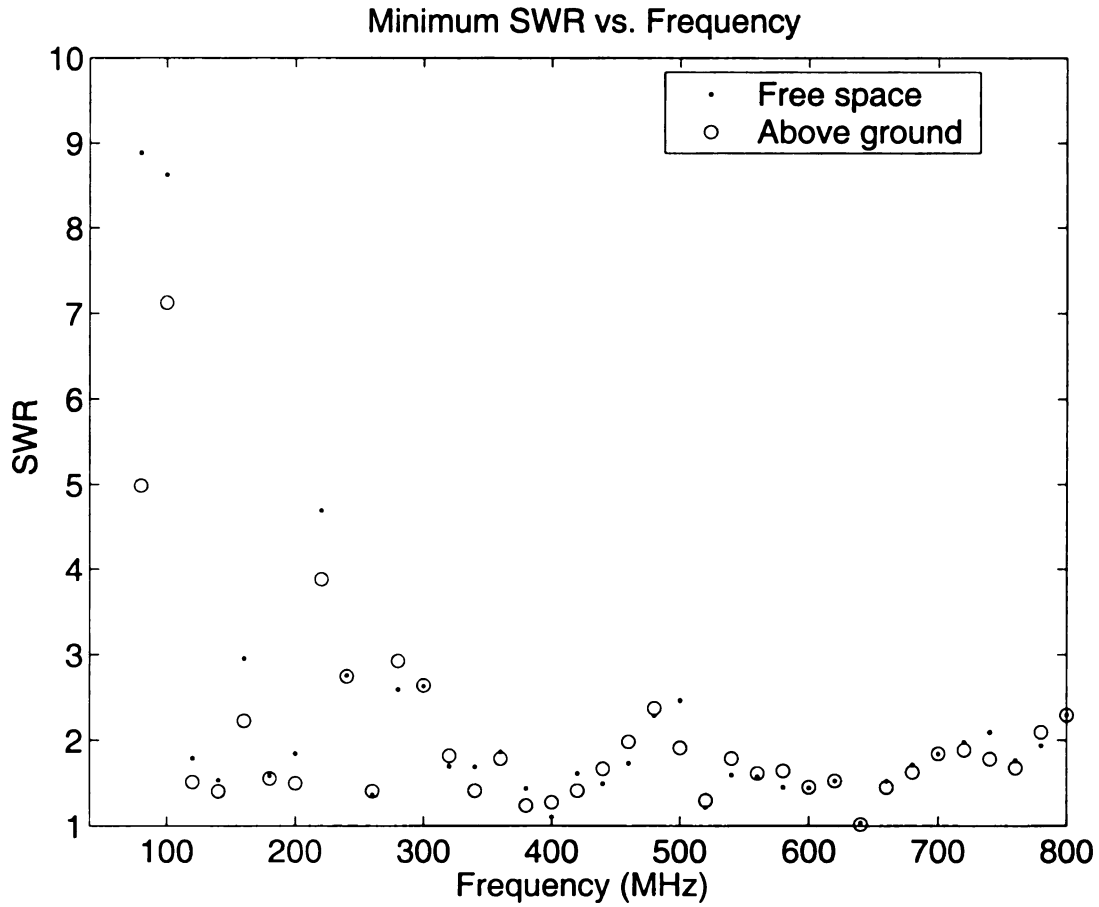


Figure 5.18. Minimum SWR vs. frequency for the layer 1 Type II SSA template.

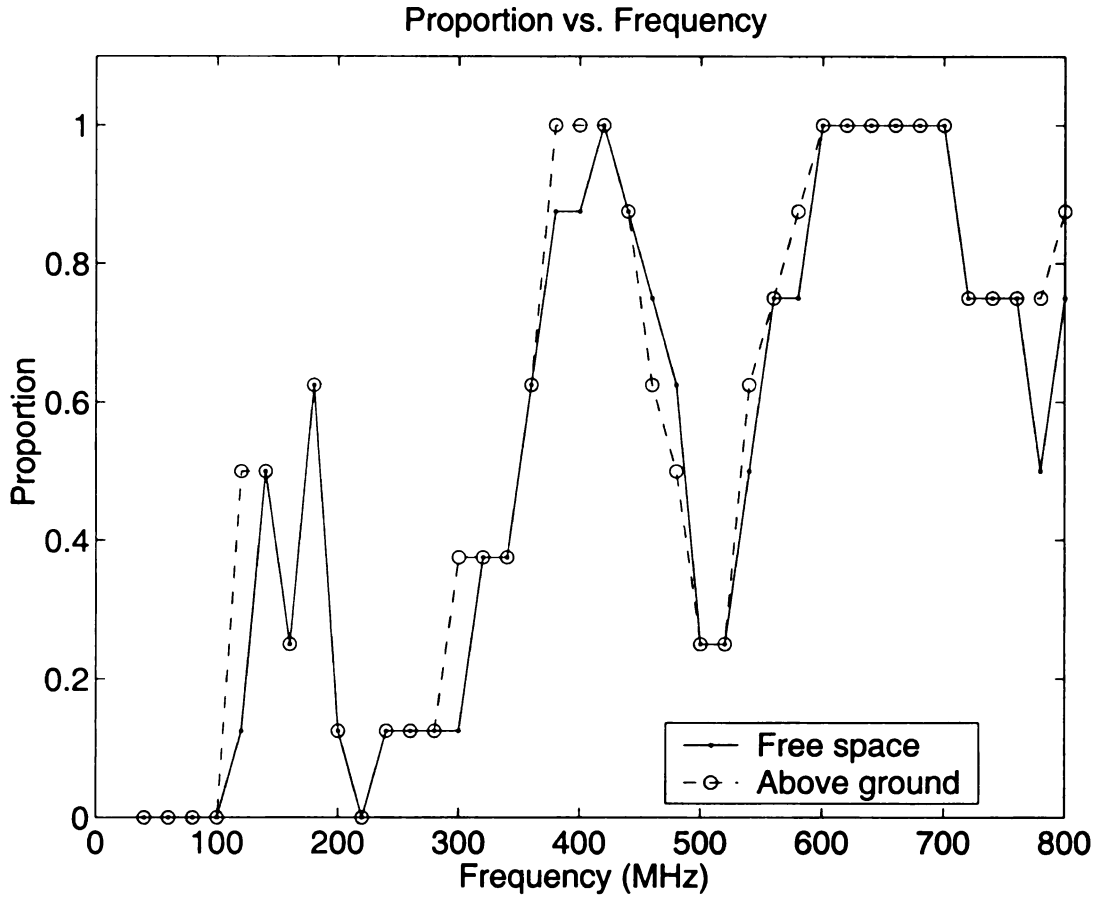


Figure 5.19. Proportion of configurations with SWRs less than 3.0 vs. frequency for the layer 1 Type II SSA template (linear scale).

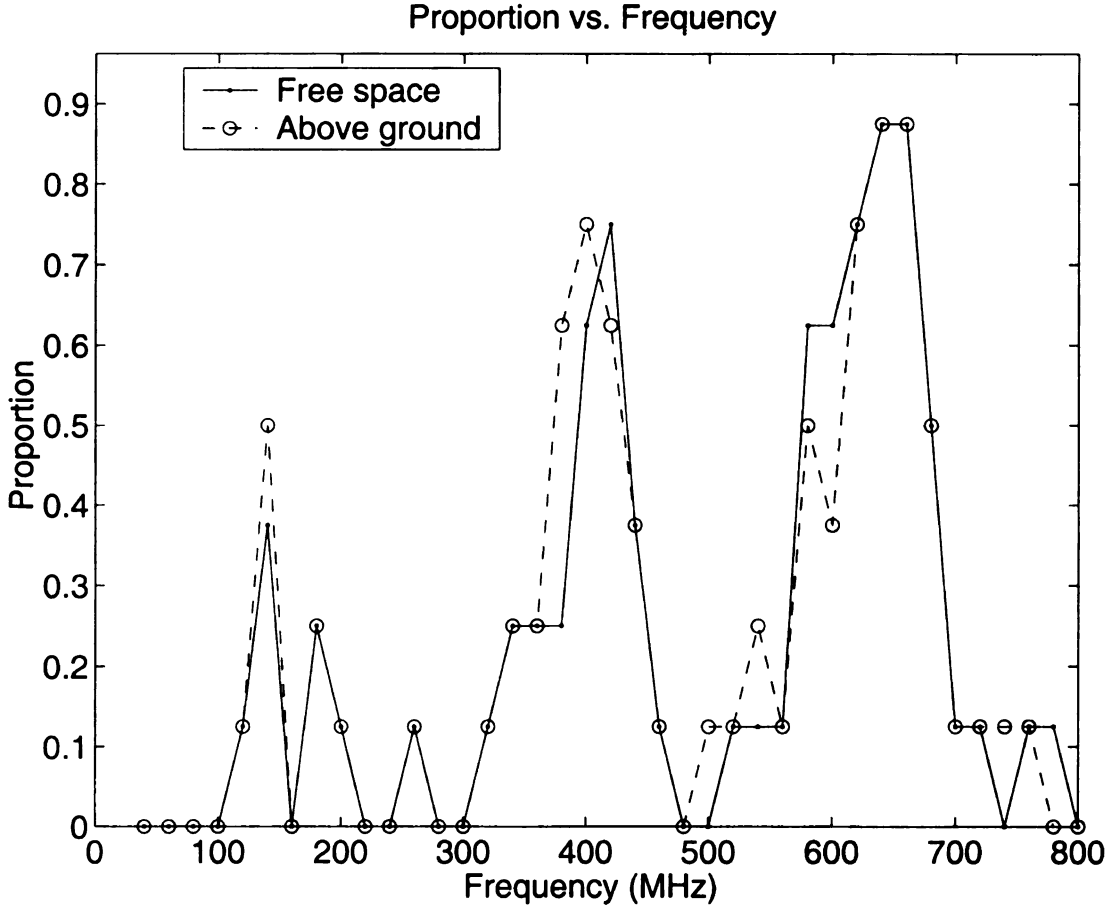


Figure 5.20. Proportion of configurations with SWRs less than 2.0 vs. frequency for the layer 1 Type II SSA template (linear scale).

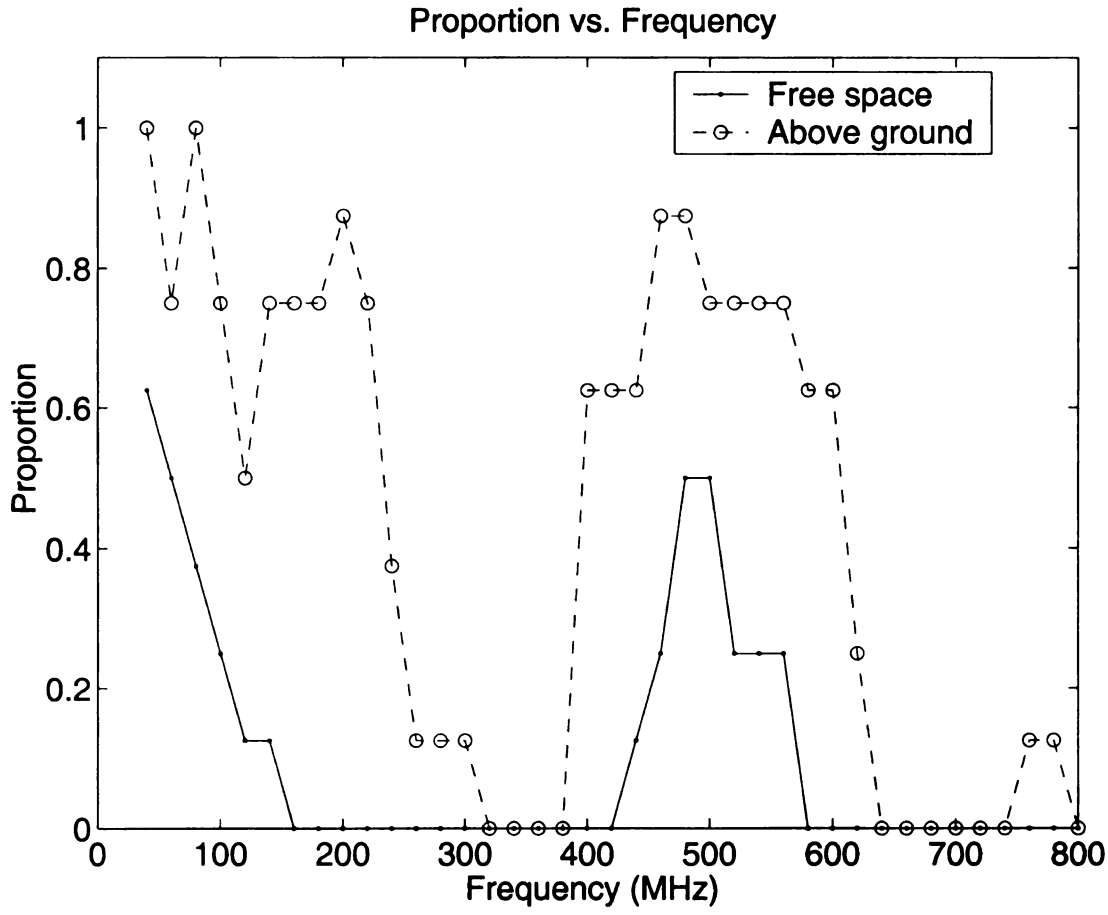


Figure 5.23. Proportion of configurations with minimum vertical gains above 0 dB vs. frequency for the layer 1 Type II SSA template (linear scale).

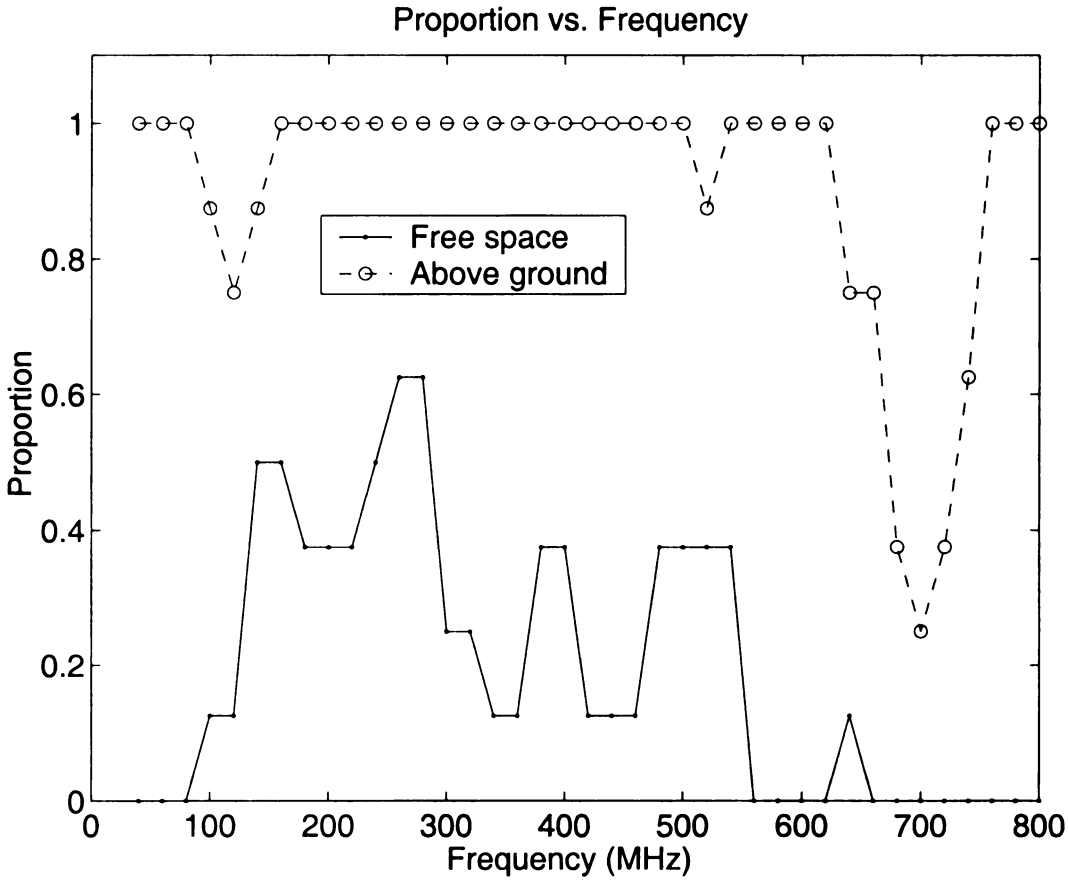


Figure 5.24. Proportion of configurations with maximum vertical gains above 3 dB vs. frequency for the layer 1 Type II SSA template (linear scale).

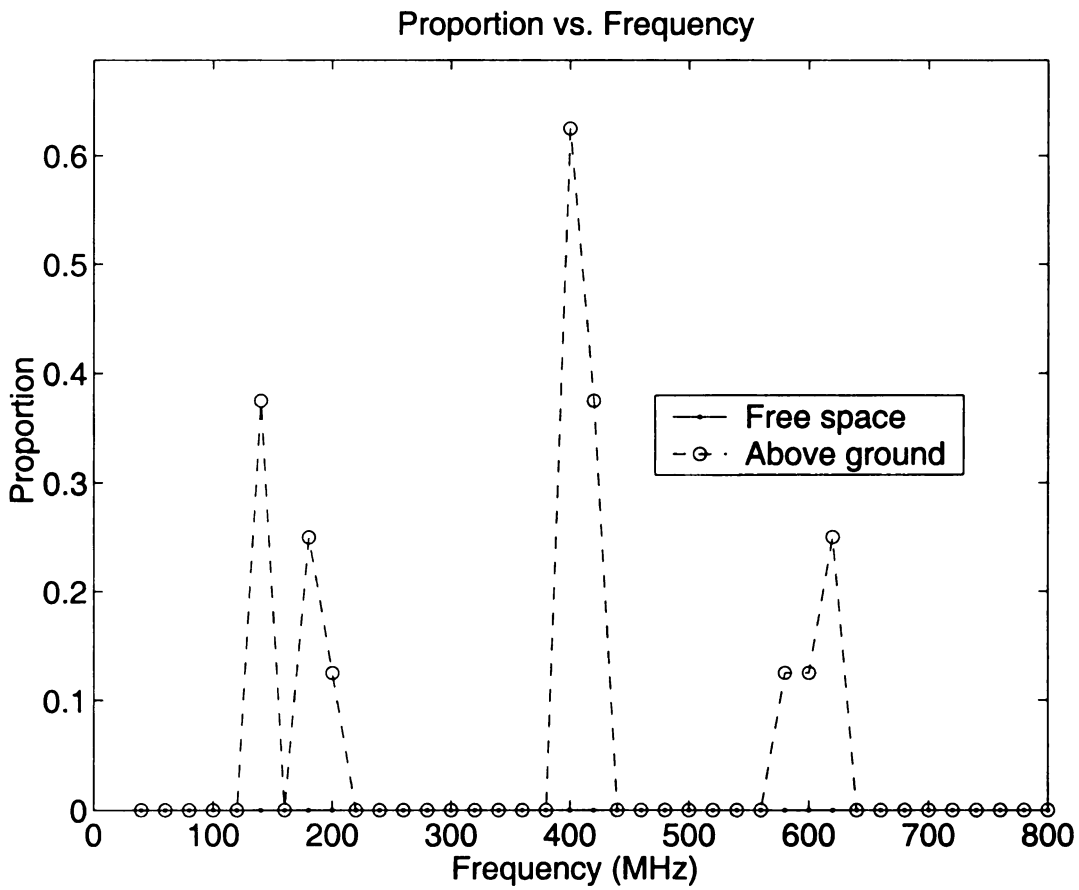


Figure 5.25. Proportion of configurations with SWRs less than 2.0 and and minimum vertical gains in the horizontal plane above 0 dB vs. frequency for the layer 1 Type II SSA template (linear scale).

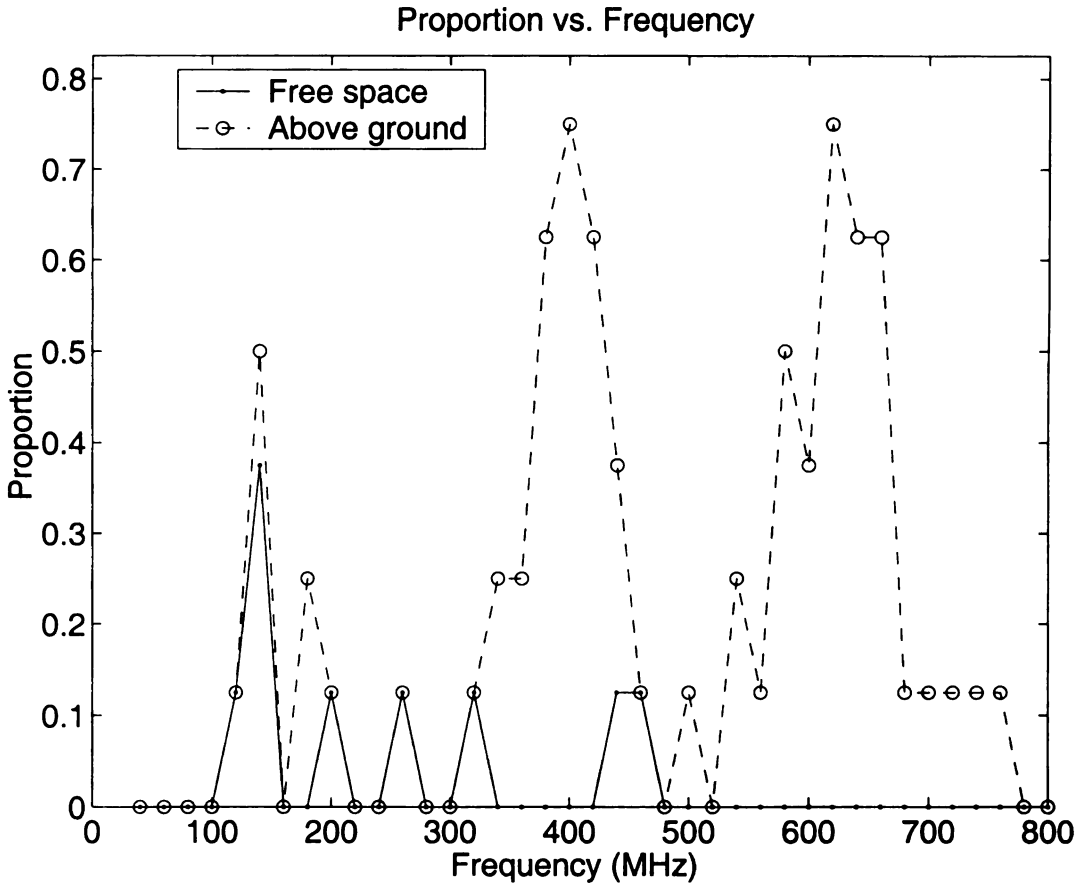


Figure 5.26. Proportion of configurations with SWRs less than 2.0 and and maximum vertical gains in the horizontal plane above 3.0 dB vs. frequency for the layer 1 Type II SSA template (linear scale).

5.3.2 Layer 1.5 SSA Template

As discussed in Section 5.2, the layer 1.5 SSA template is created by adding three switches and more wire segments to the layer 1 template. A diagram of the layer 1.5 template is shown in Figure 5.27. Six switches are used for 64 possible SSA configurations. Exhaustive studies of the possible configurations for the Type I and Type II layer 1.5 templates have been performed and are presented in this section.

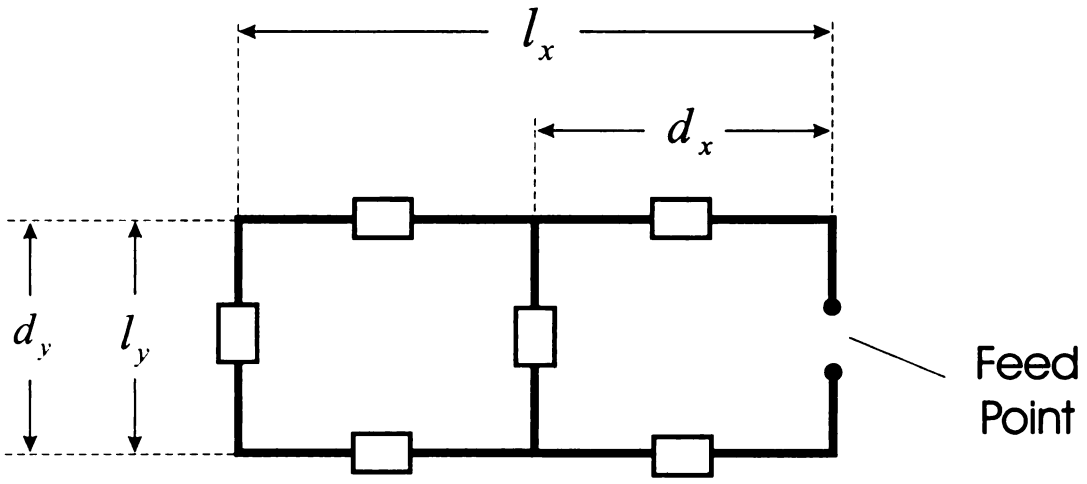


Figure 5.27. Diagram of the layer 1.5 SSA template.

Table 5.5. Dimensions of the layer 1.5 Type I SSA template.

l_x	17.1 cm
d_x	8.57 cm
l_y	8.57 cm
d_y	8.57 cm
Outer electrical dimensions at 40 MHz	$0.0229\lambda \times 0.0114\lambda$
Outer electrical dimensions at 800 MHz	$0.457\lambda \times 0.229\lambda$

The dimensions of the layer 1.5 Type I and Type II SSA templates are shown in Table 5.5 and Table 5.6, respectively. Layer 1.5 Type I templates are twice the size of layer 1 Type I templates.

5.3.2.1 Layer 1.5 Type I SSA Template

A plot of the SWRs of the 64 SSA configurations at each frequency is shown in Figure 5.28 for the layer 1.5 Type I template in free space. The addition of three switches and the increase in electrical size over the layer 1 template has significantly improved the possible SWR values for the layer 1.5 template over the studied fre-

Table 5.6. Dimensions of the layer 1.5 Type II SSA template.

l_x	60.0 cm
d_x	30.0 cm
l_y	60.0 cm
d_y	60.0 cm
Outer electrical dimensions at 40 MHz	$0.0800\lambda \times 0.0800\lambda$
Outer electrical dimensions at 800 MHz	$1.60\lambda \times 1.60\lambda$

quencies. Notice that the some SWR values extend below 10.0 above 260 MHz. A similar distribution exists for the layer 1.5 Type I SSA template above ground, as shown in Figure 5.29. Recall that configurations with SWR values less than 10.0 do not exist for the layer 1 Type I template below 560 MHz.

The minimum SWR value found at each frequency is plotted in Figure 5.30 for the layer 1.5 Type I templates in free space and above ground. A configuration with an SWR less than 2.0 is found at 380 MHz and at 360 MHz for the templates in free space and above ground, respectively. At 520 MHz and above, the minimum achievable SWR value is below 2.0 at every studied frequency. It is important to understand that the minimum SWR values are not necessarily from the same SSA configuration.

Smith charts at 40 MHz are shown in Figure 5.31 and Figure 5.32 for the layer 1.5 Type I templates in free space and above ground, respectively. Similarly to the layer 1 Type I templates, the layer 1.5 Type I templates have no configurations with enough radiation for low SWRs at 40 MHz. Smith charts at 800 MHz are shown in Figure 5.33 and Figure 5.34 for the layer 1.5 Type I templates in free space and above ground, respectively. At 800 MHz, the 64 configurations show a wide range of possible impedance values.

Figure 5.30 shows the minimum achievable SWR, but it does not quantify the number of configurations with SWR values below a given threshold. This is done

in Figure 5.35, where the proportion of configurations with SWR values below 4.0 is plotted over the studied frequencies for the layer 1.5 Type I templates in free space and above ground. Above 440 MHz, nearly 10% or more of the 64 possible SSA configurations for the layer 1.5 template in free space exhibit SWRs less than 4.0. This is also true for the template above ground for frequencies above 540 MHz. At 800 MHz, over 55% and 45% of the possible configurations meet the threshold criterion for the template in free space and above ground, respectively. Thus, if an electronic system is designed using a receiver with a 200 Ω input impedance and requires a maximum SWR of 4.0, the layer 1.5 Type I template could provide acceptable impedance values above 540 MHz through reconfiguration.

Figure 5.36 shows the proportion of configurations with SWRs less than 2.0 for the layer 1.5 Type I templates in free space and above ground. Above 500 MHz, at least three percent of the 64 possible configurations have SWRs lower than 2.0 for the templates in free space and above ground.

The proportion of configurations with minimum gains above -3.0 dB is shown in Figure 5.37 for the layer 1.5 Type I templates. Notice that the ground plane allows for a higher proportion of configurations that meet the minimum gain requirement. This is more pronounced in Figure 5.38, which shows the proportion of configurations with minimum gains above 0 dB. Figure 5.39 shows that there are few configurations with SWRs less than 4.0 and minimum vertical gains above -3.0 dB for the layer 1.5 Type I templates.

Figure 5.40 shows the proportion of configurations with maximum vertical gains in the horizontal plane above 3.0 dB for the layer 1.5 Type I templates in free space and above ground. There is a large difference between the proportions due to the presence of ground, especially at the lower frequencies. The template above ground has more configurations with higher vertical gains than the template in free space. Figure 5.41 shows that above 520 MHz, over 5% of the configurations for the template

above ground have SWRs less than 4.0 and maximum vertical gains above 3.0 dB. These criteria are met for the template in free space above 680 MHz.

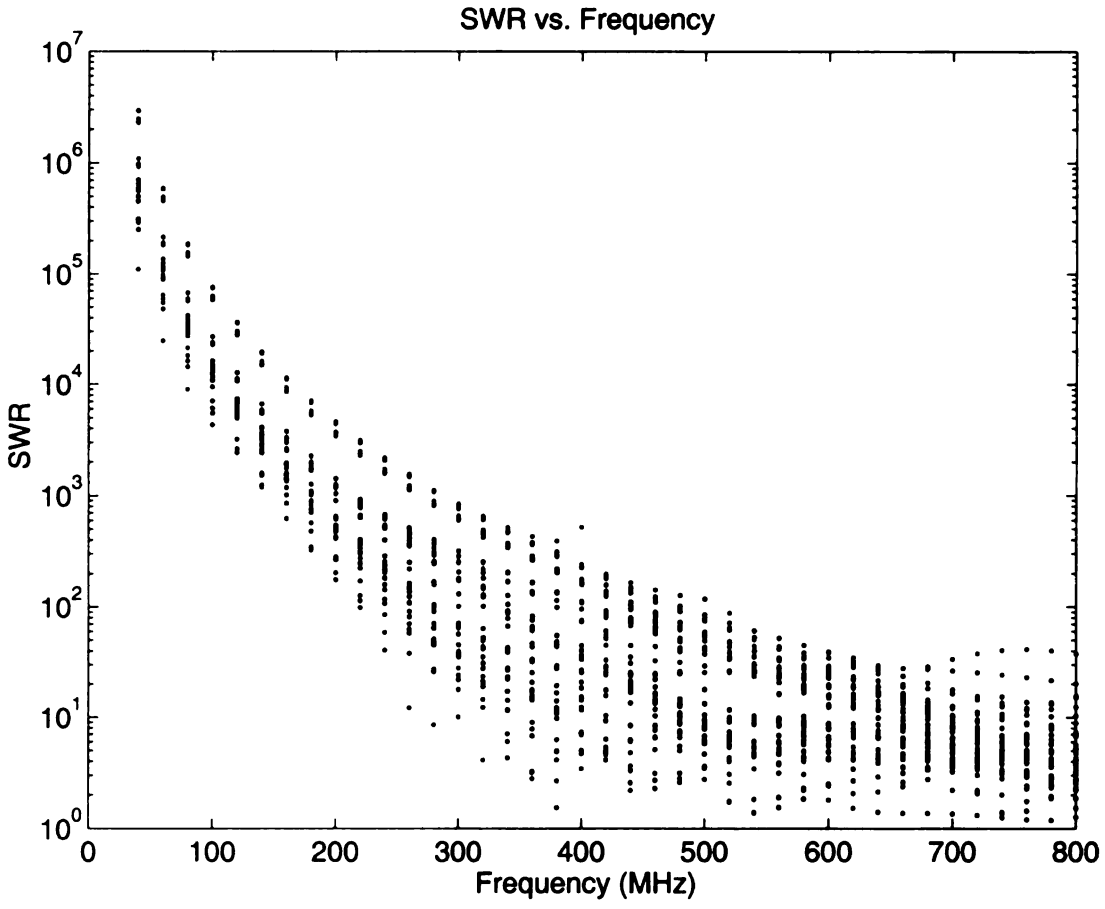


Figure 5.28. SWR vs. frequency for the layer 1.5 Type I SSA template in free space.

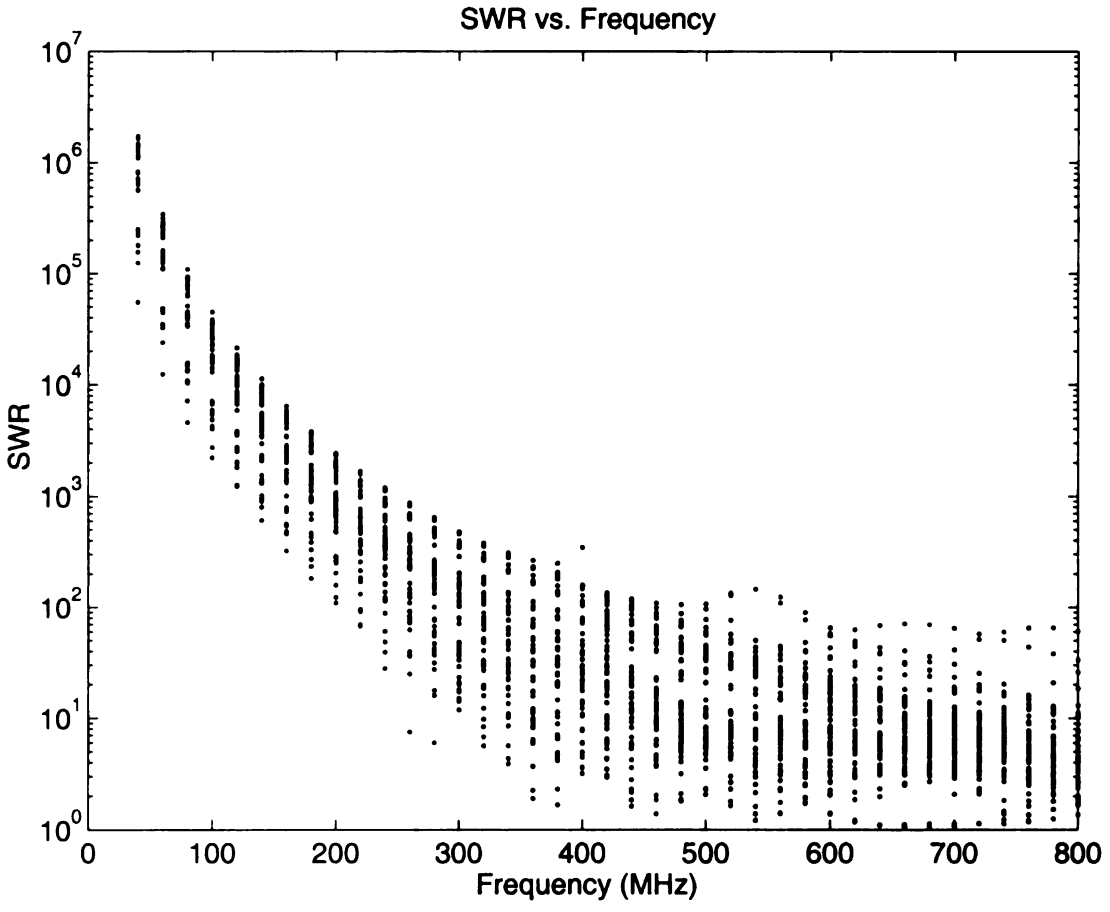


Figure 5.29. SWR vs. frequency for the layer 1.5 Type I SSA template above ground.

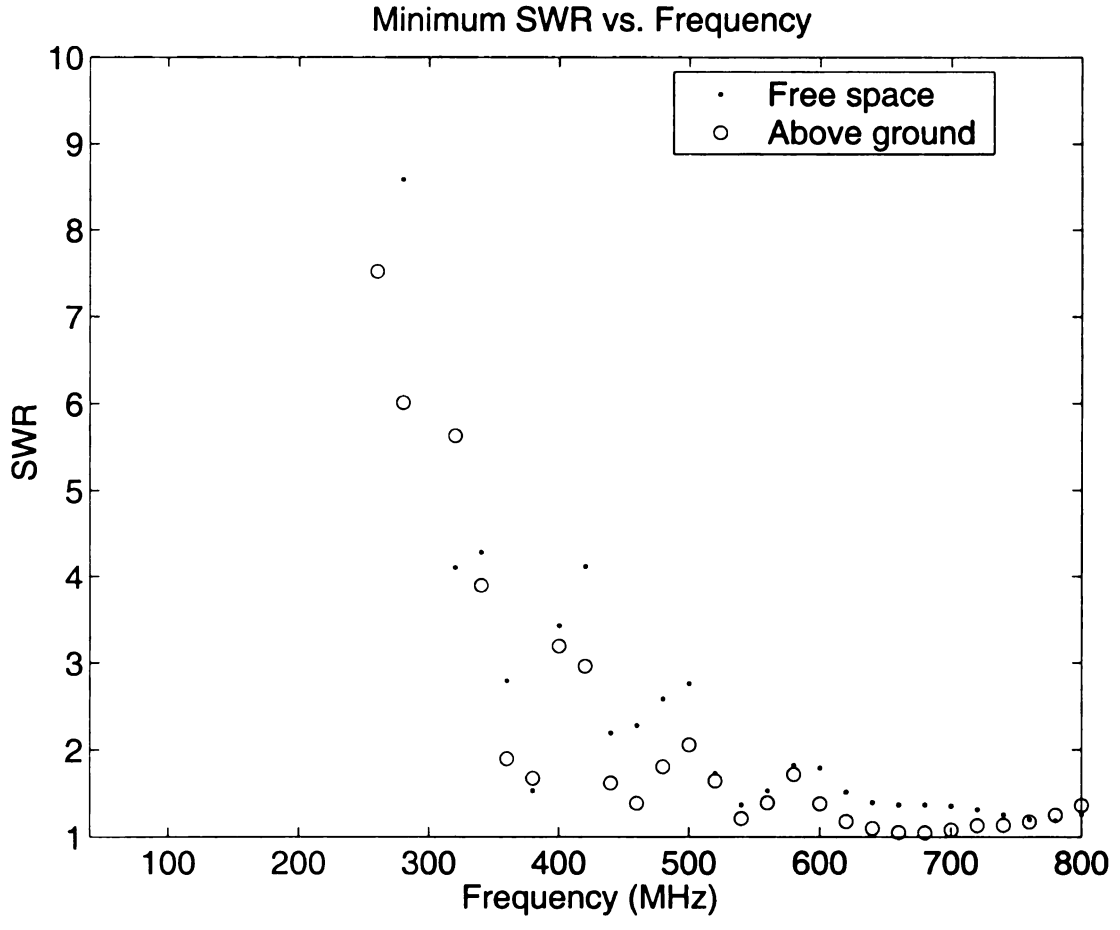


Figure 5.30. Minimum SWR vs. frequency for the layer 1.5 Type I SSA template.

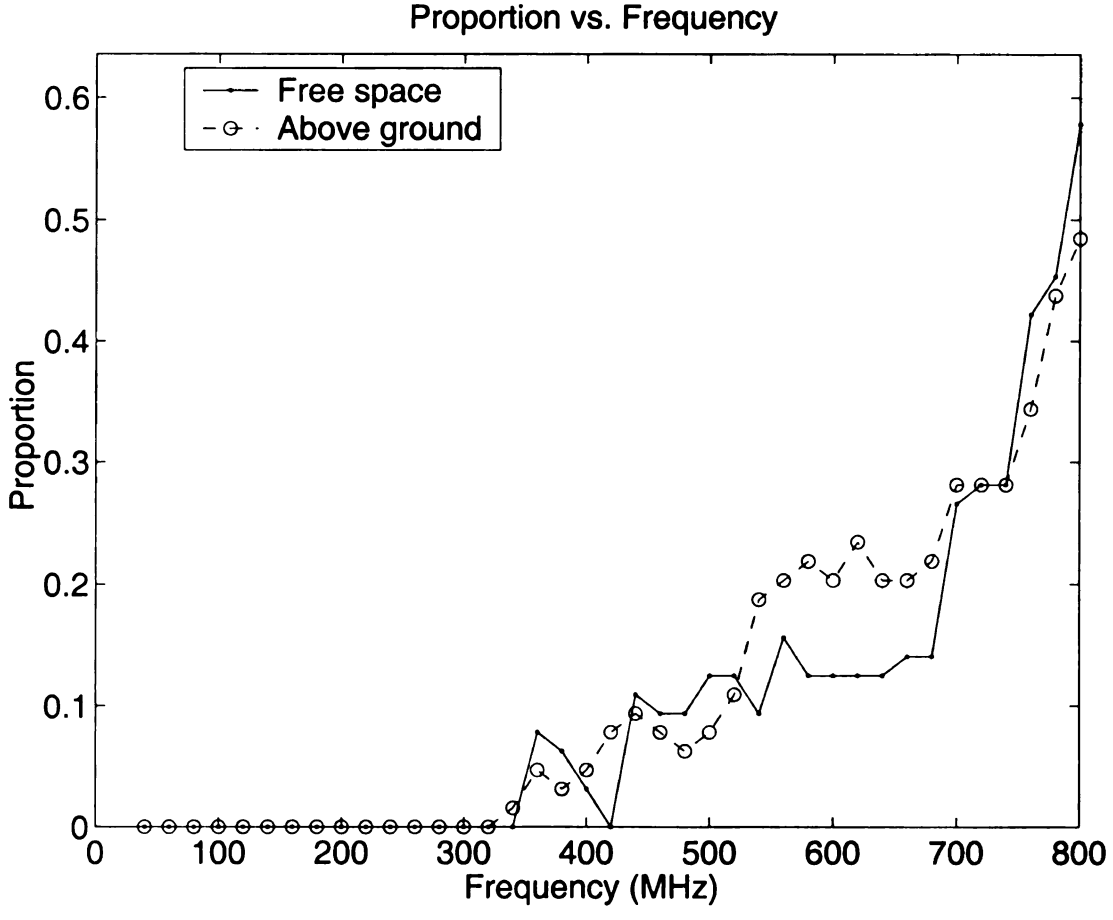


Figure 5.35. Proportion of configurations with SWRs less than 4.0 vs. frequency for the layer 1.5 Type I SSA template (linear scale).

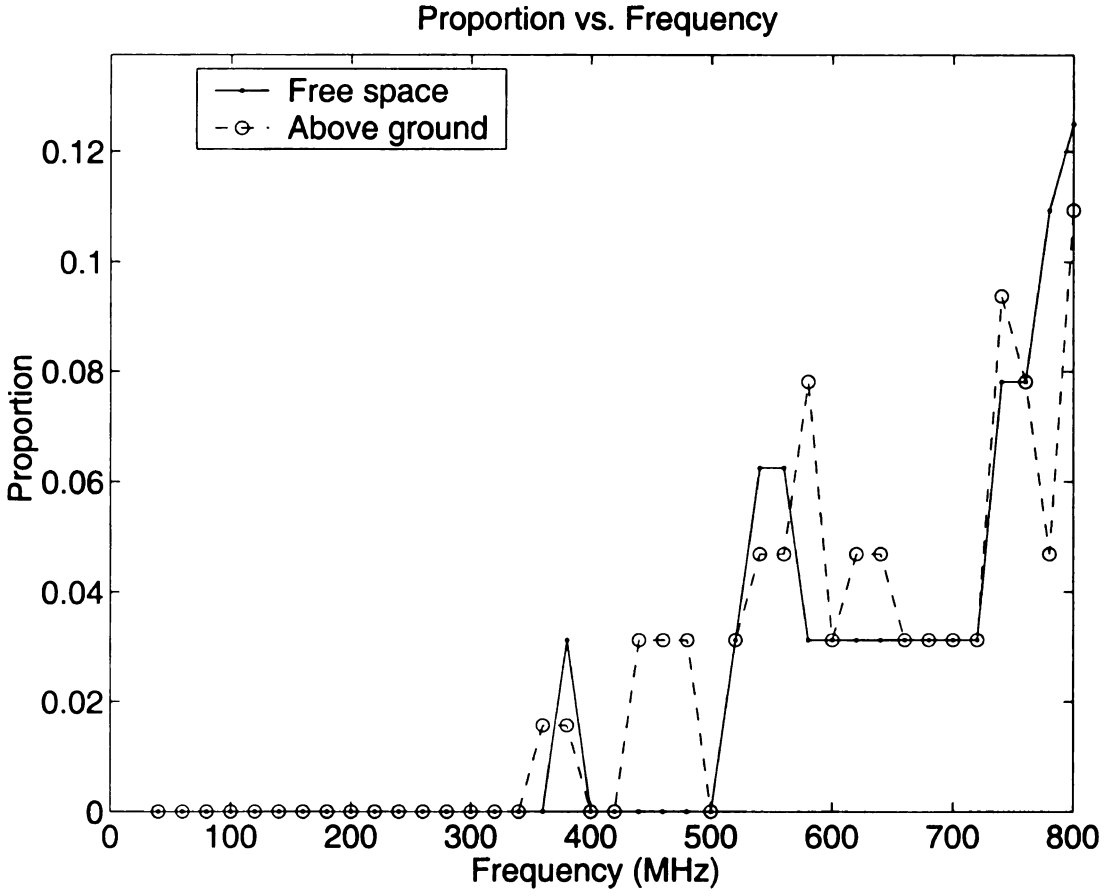


Figure 5.36. Proportion of configurations with SWRs less than 2.0 vs. frequency for the layer 1.5 Type I SSA template (linear scale).

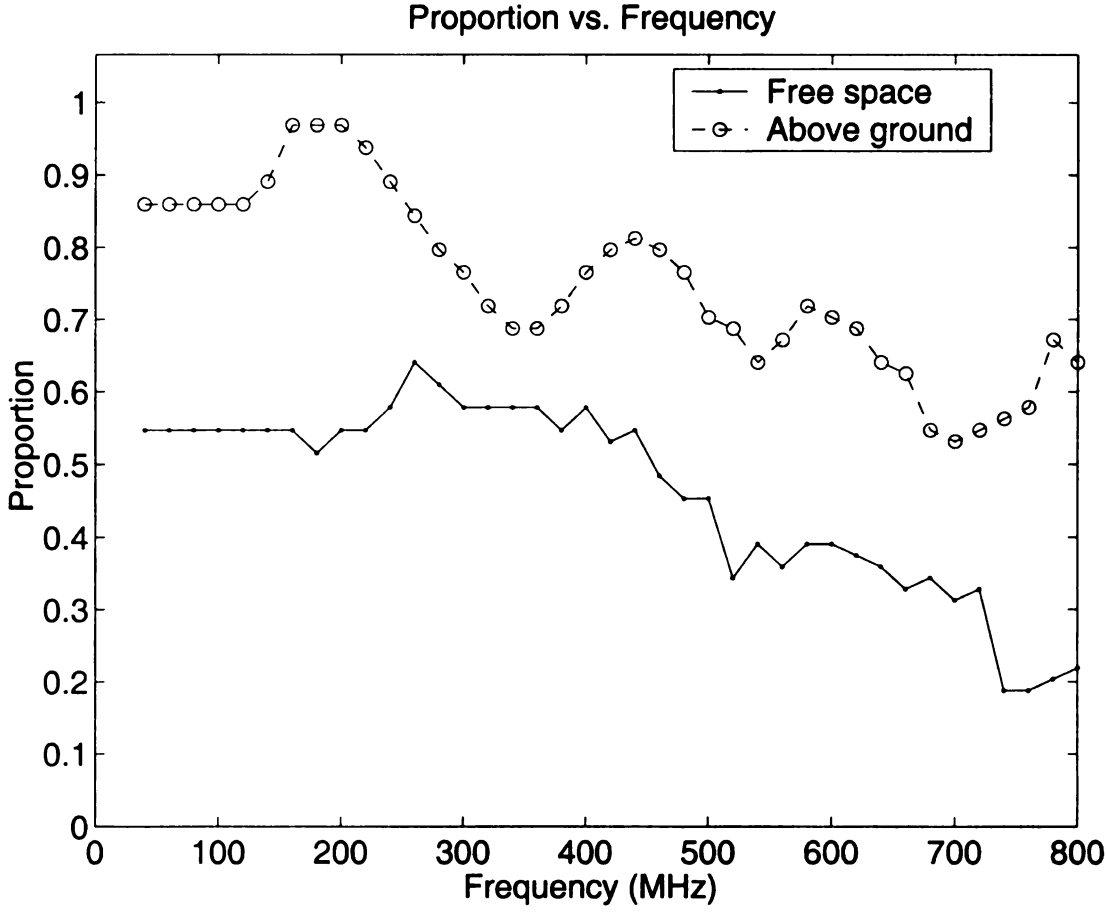


Figure 5.37. Proportion of configurations with minimum vertical gains in the horizontal plane above -3.0 dB vs. frequency for the layer 1.5 Type I SSA template (linear scale).

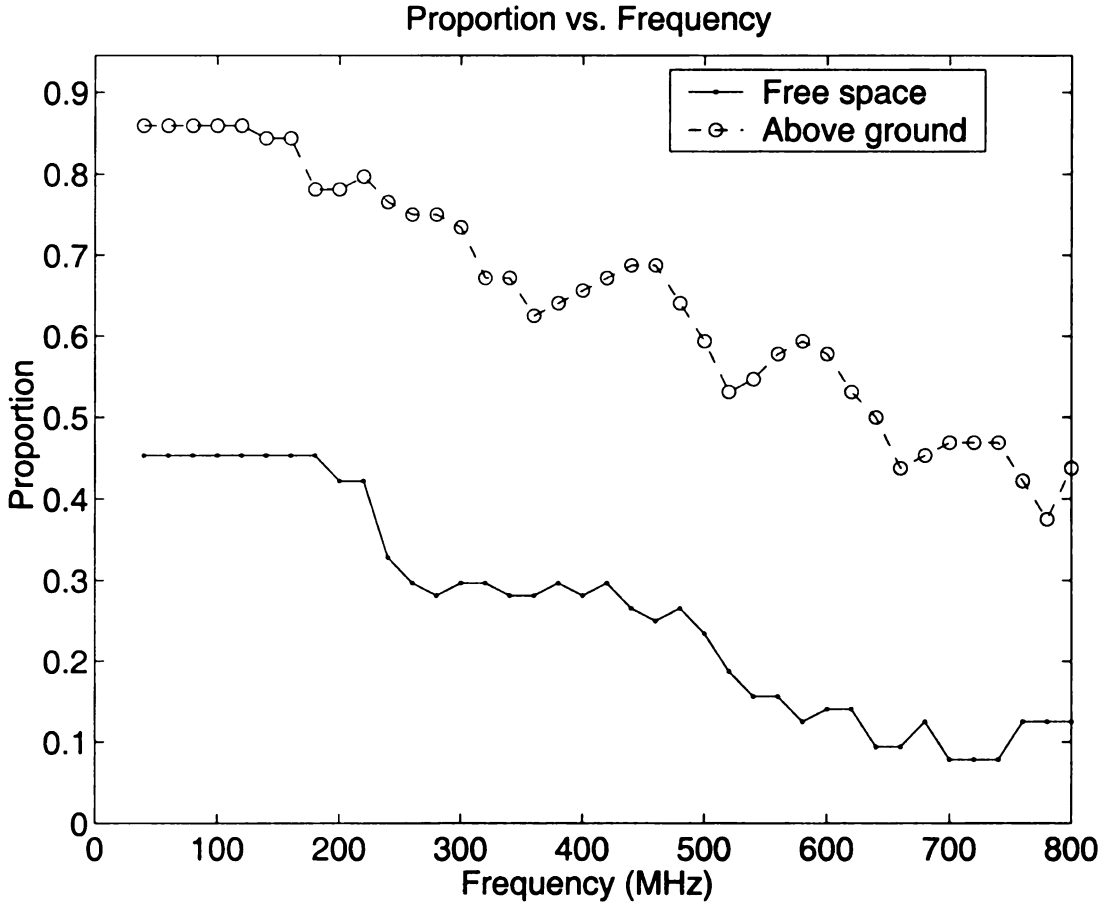


Figure 5.38. Proportion of configurations with minimum vertical gains in the horizontal plane above 0 dB vs. frequency for the layer 1.5 Type I SSA template (linear scale).

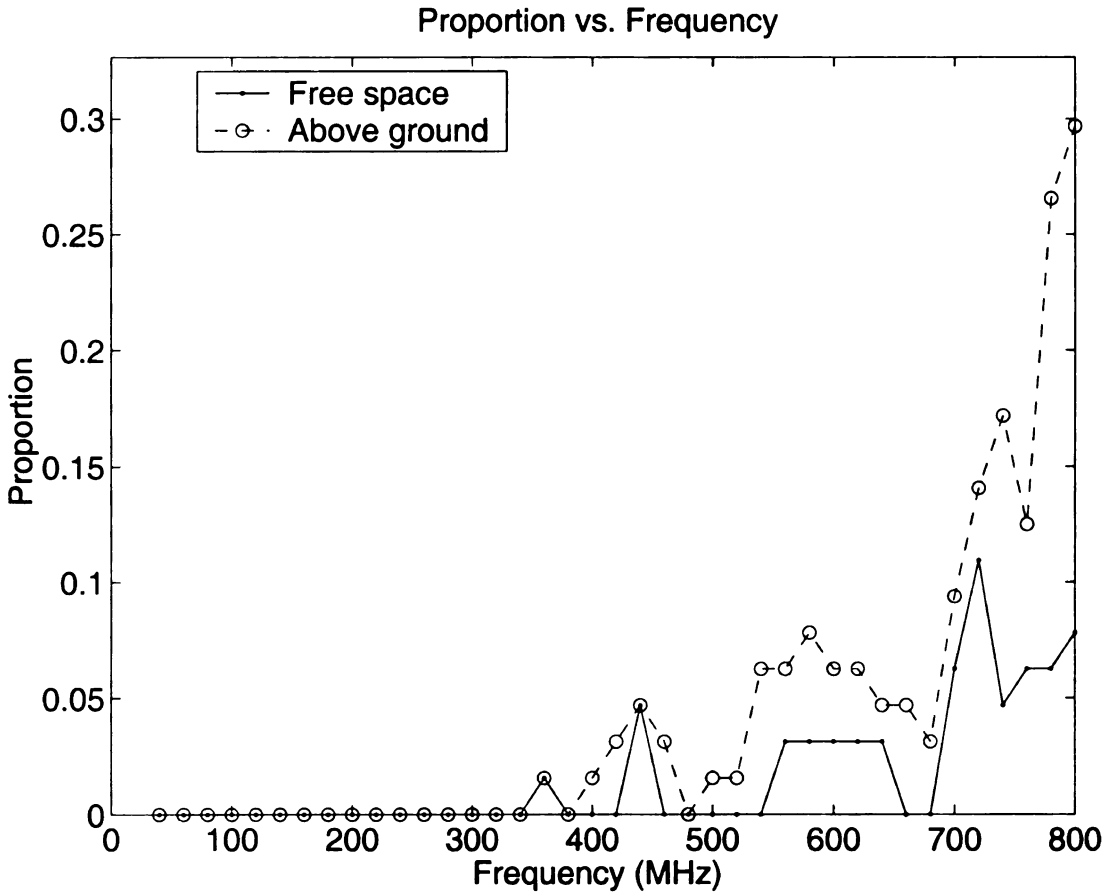


Figure 5.39. Proportion of configurations with SWRs less than 4.0 and minimum vertical gains in the horizontal plane above -3.0 dB vs. frequency for the layer 1.5 Type I SSA template (linear scale).

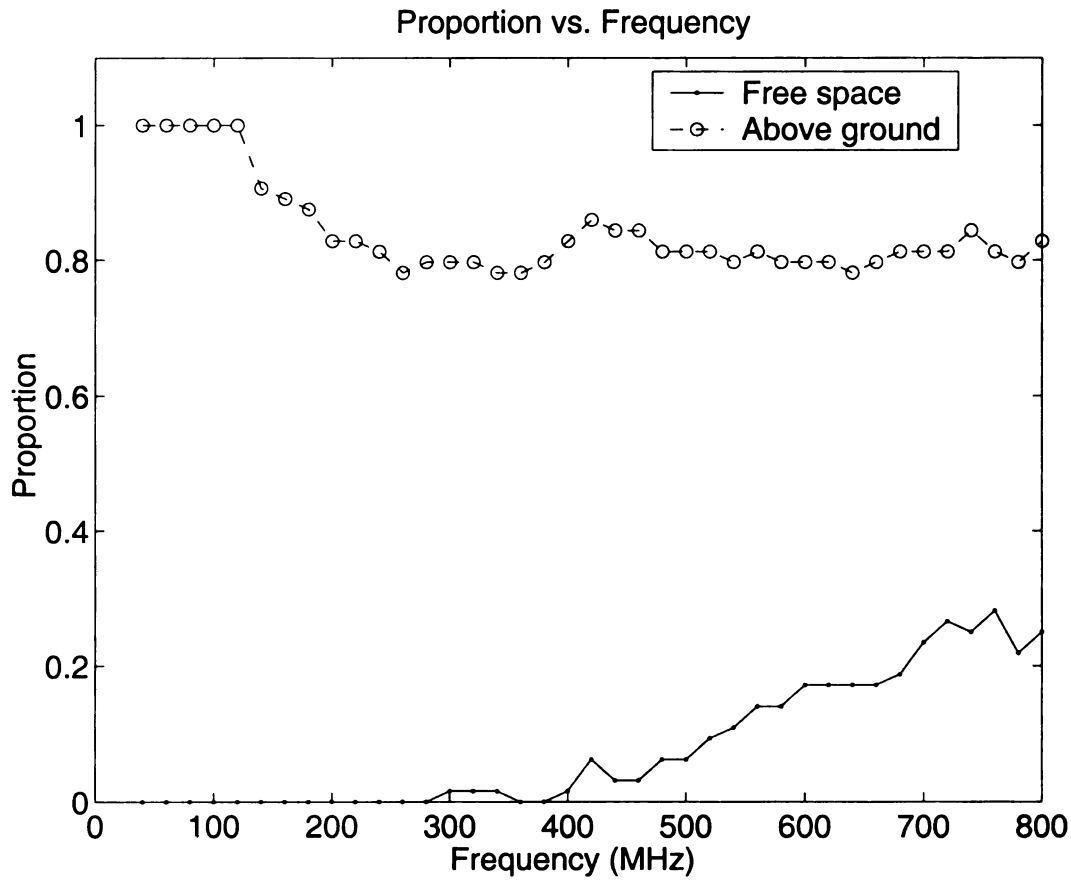


Figure 5.40. Proportion of configurations with maximum vertical gains in the horizontal plane above 3.0 dB vs. frequency for the layer 1.5 Type I SSA template (linear scale).

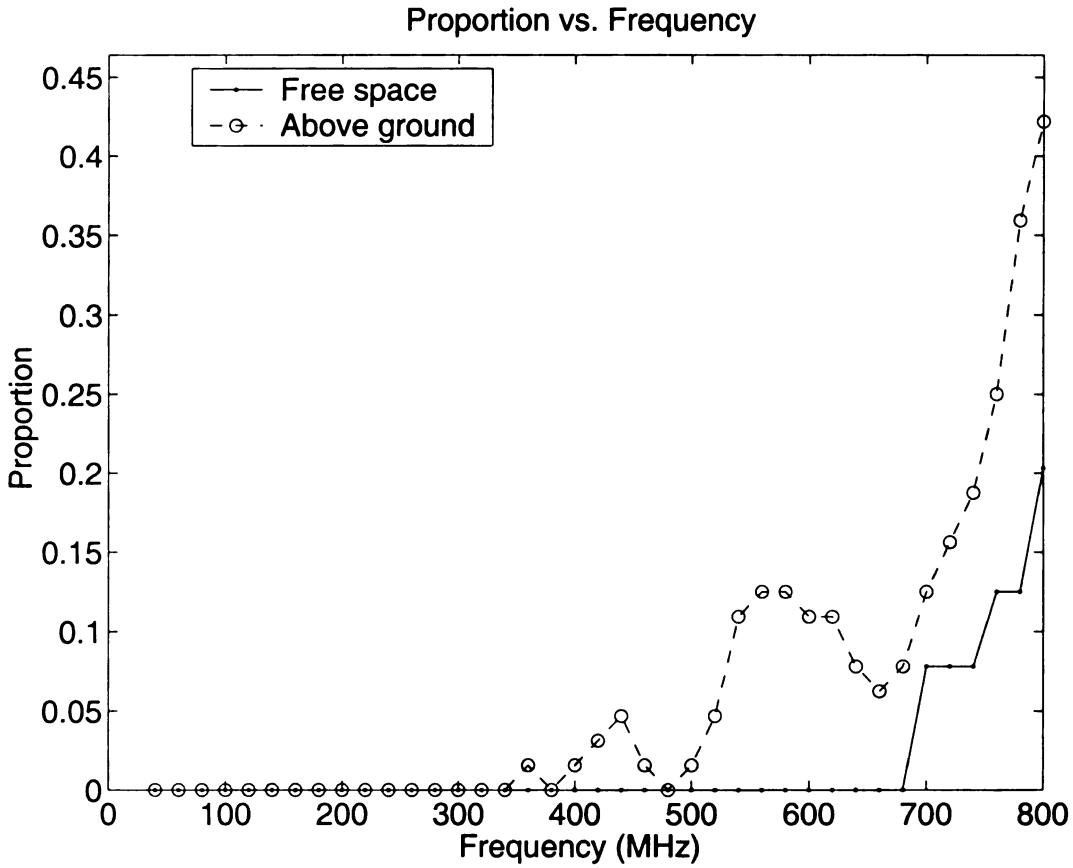


Figure 5.41. Proportion of configurations with SWRs less than 4.0 and maximum vertical gains in the horizontal plane above 3.0 dB vs. frequency for the layer 1.5 Type I SSA template (linear scale).

5.3.2.2 Layer 1.5 Type II SSA Template

Recall that the layer 1.5 Type II template is electrically larger than the layer 1.5 Type I template. The outer dimensions of the layer 1.5 Type I and Type II templates are shown in Table 5.5 and Table 5.6, respectively.

The SWRs of the 64 possible configurations of the layer 1.5 Type II template in free space are shown in Figure 5.42 at each studied frequency. The SWR distribution for the template above ground is shown in Figure 5.43. Similarly to the layer 1 Type II template, the layer 1.5 Type II template has configurations that exhibit relatively

low SWR values at the lower studied frequencies. For instance, from 200 MHz to 260 MHz, minimum SWR values are found below 1.3 for the templates in free space and above ground, as shown in Figure 5.44.

Figure 5.42 and Figure 5.43 show tight groupings of SWRs at higher frequencies, which may be undesirable. A Smith chart at 800 MHz found in Figure 5.45 shows two tight groupings of impedances for the layer 1.5 Type II template in free space. This also occurs for the template above ground, as shown in Figure 5.46. Although there are 64 possible configurations, the states of the switches do not greatly alter the induced current at the template's feed point at the higher frequencies. This effect is not as pronounced for the layer 1.5 Type I templates because they are electrically smaller.

Due to the tight groupings near low SWR values, Figure 5.47 and Figure 5.48 show that many of the 64 possible configurations for the layer 1.5 Type II template in free space and above ground exhibit SWRs less than 3.0 and 2.0, respectively, near 500 MHz-600 MHz and near 800 MHz.

The proportion of configurations with minimum vertical gains above -3.0 dB is shown in Figure 5.49 for the layer 1.5 Type II templates in free space and above ground. The vertical gain drops below the threshold for almost all configurations from 500 MHz to 540 MHz for the template in free space and above ground. At other frequencies, the template above ground again exhibits higher gains. This is also shown in Figure 5.50, where the minimum gain threshold is increased to 0 dB. Figure 5.51 shows that the proportion of configurations with SWRs below 3.0 and minimum vertical gains above -3.0 dB varies greatly over the studied frequency band.

Figure 5.52 shows the proportion of configurations with maximum vertical gains in the horizontal plane above 3.0 dB for the layer 1.5 Type II templates in free space and above ground. Again, the proportion is much greater for the template above ground over the frequency band. Figure 5.53 shows the proportion of configurations

with SWRs less than 3.0 and maximum vertical gains above 3.0 dB. The proportion varies greatly across the band, and the proportion for the template above ground is generally greater than the proportion for the template in free space.

The study of the layer 1.5 Type I and Type II SSA templates presented here have shown that six switches for 64 possible configurations may not provide suitable characteristics for many applications. Therefore, more complicated SSA templates are studied.

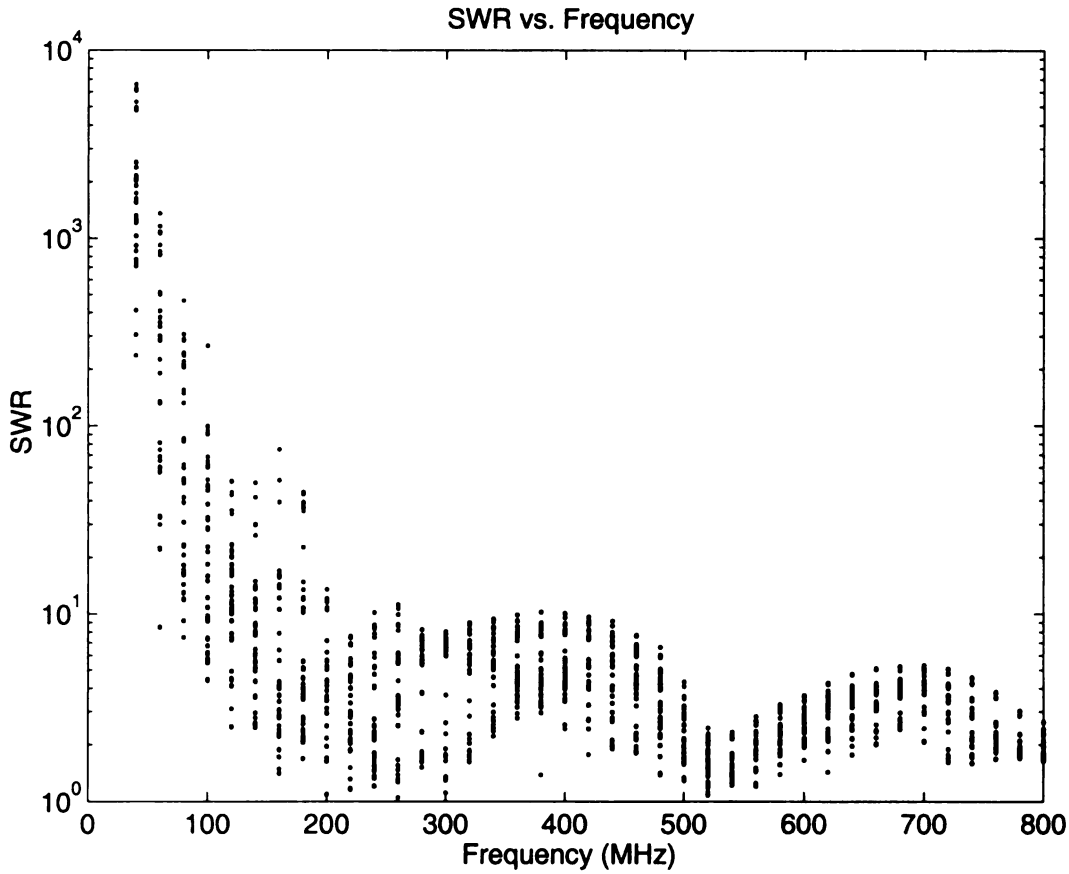


Figure 5.42. SWR vs. frequency for the layer 1.5 Type II SSA template in free space.

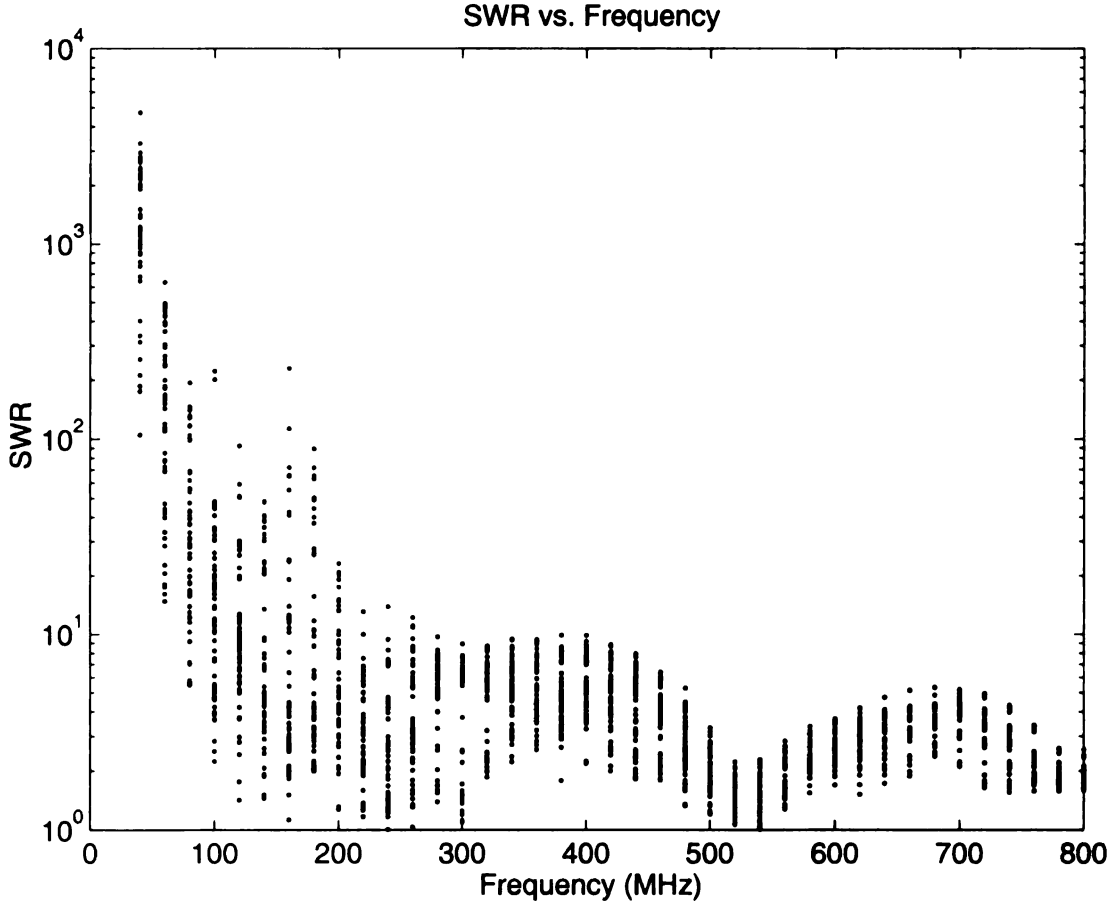


Figure 5.43. SWR vs. frequency for the layer 1.5 Type II SSA template above ground.

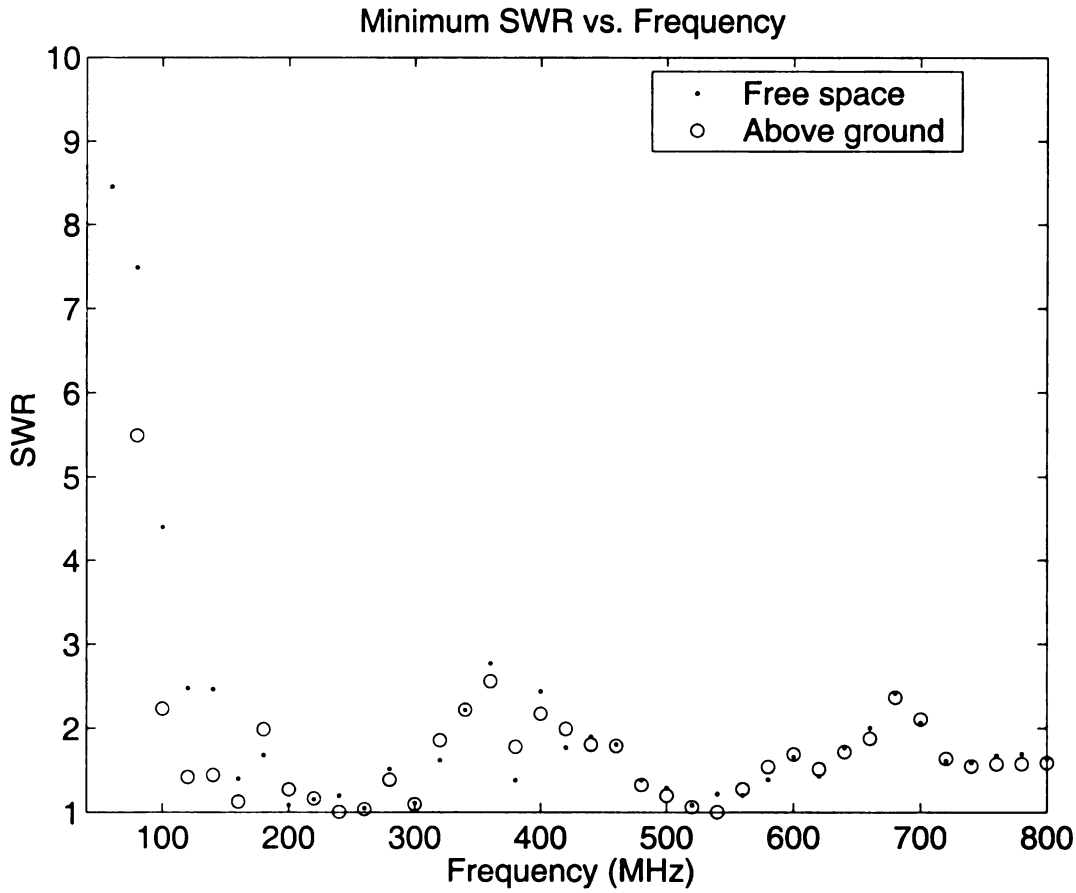


Figure 5.44. Minimum SWR vs. frequency for the layer 1.5 Type II SSA template.

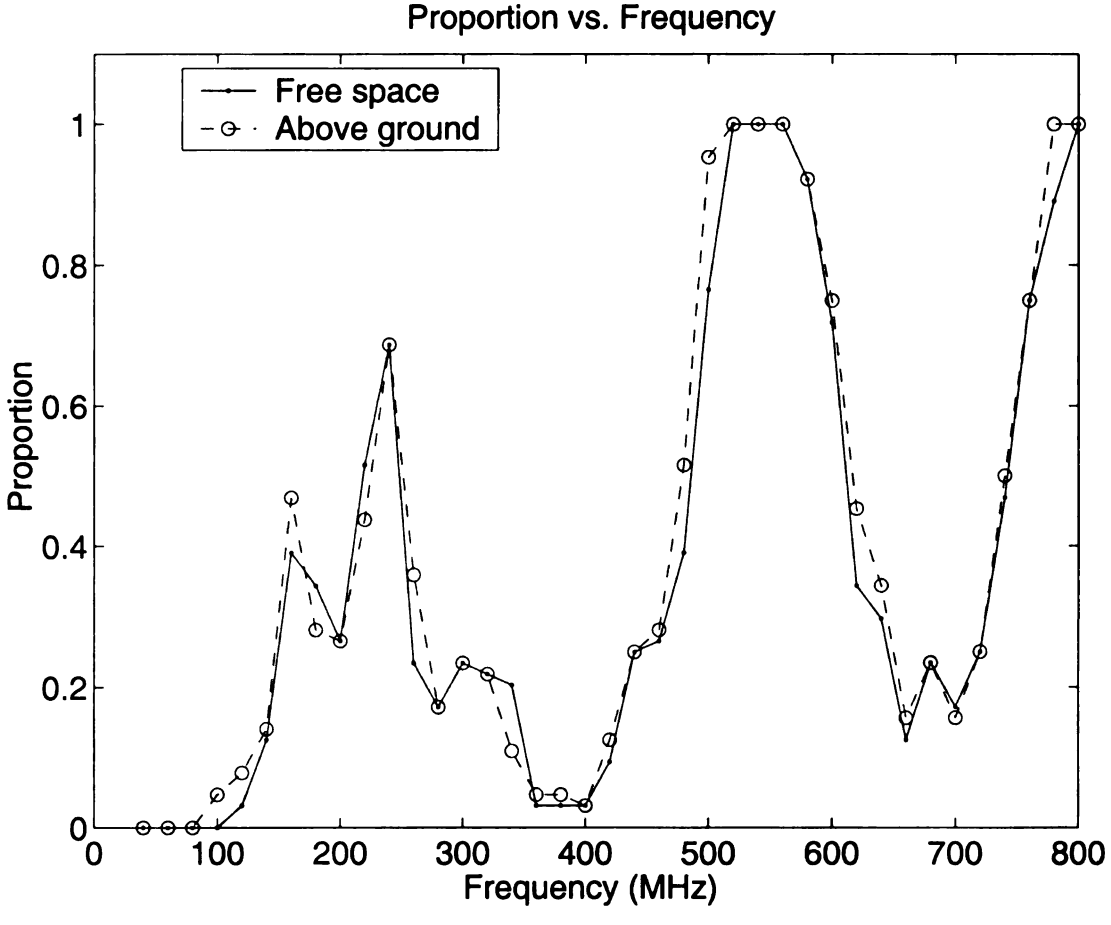


Figure 5.47. Proportion of configurations with SWRs less than 3.0 vs. frequency for the layer 1.5 Type II SSA template (linear scale).

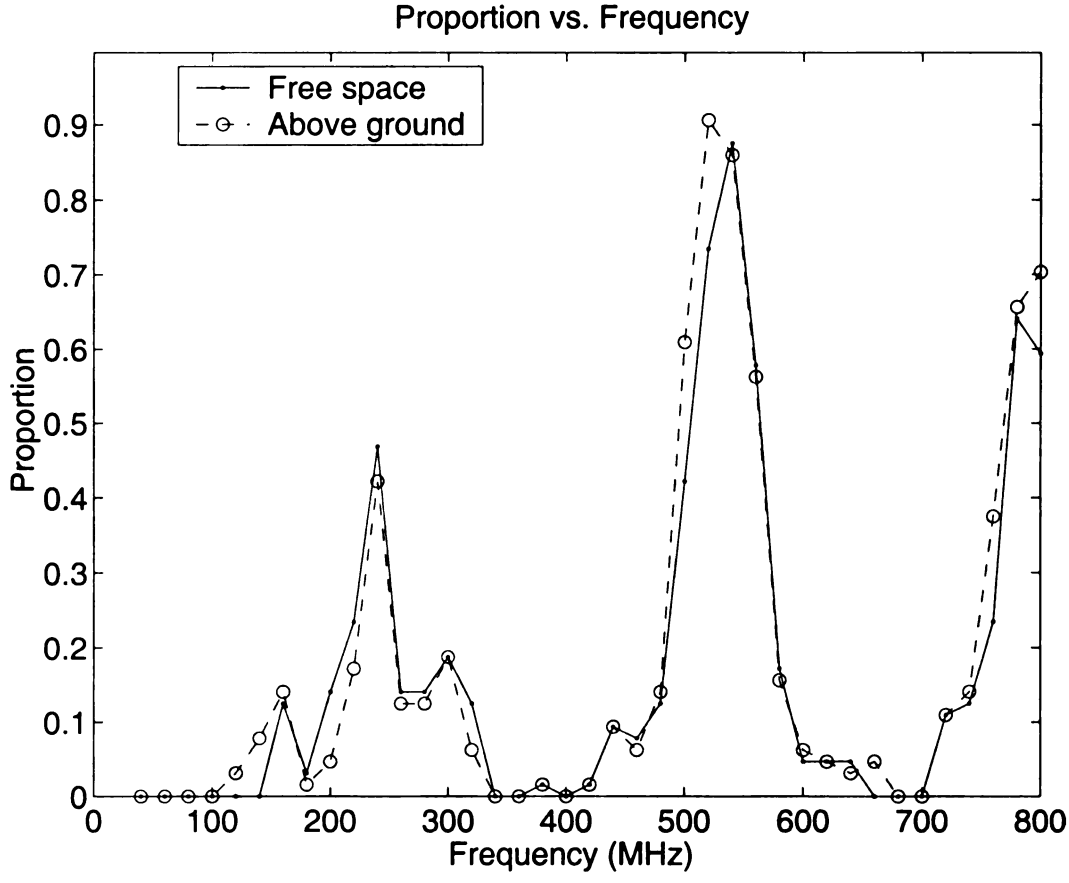


Figure 5.48. Proportion of configurations with SWRs less than 2.0 vs. frequency for the layer 1.5 Type II SSA template (linear scale).

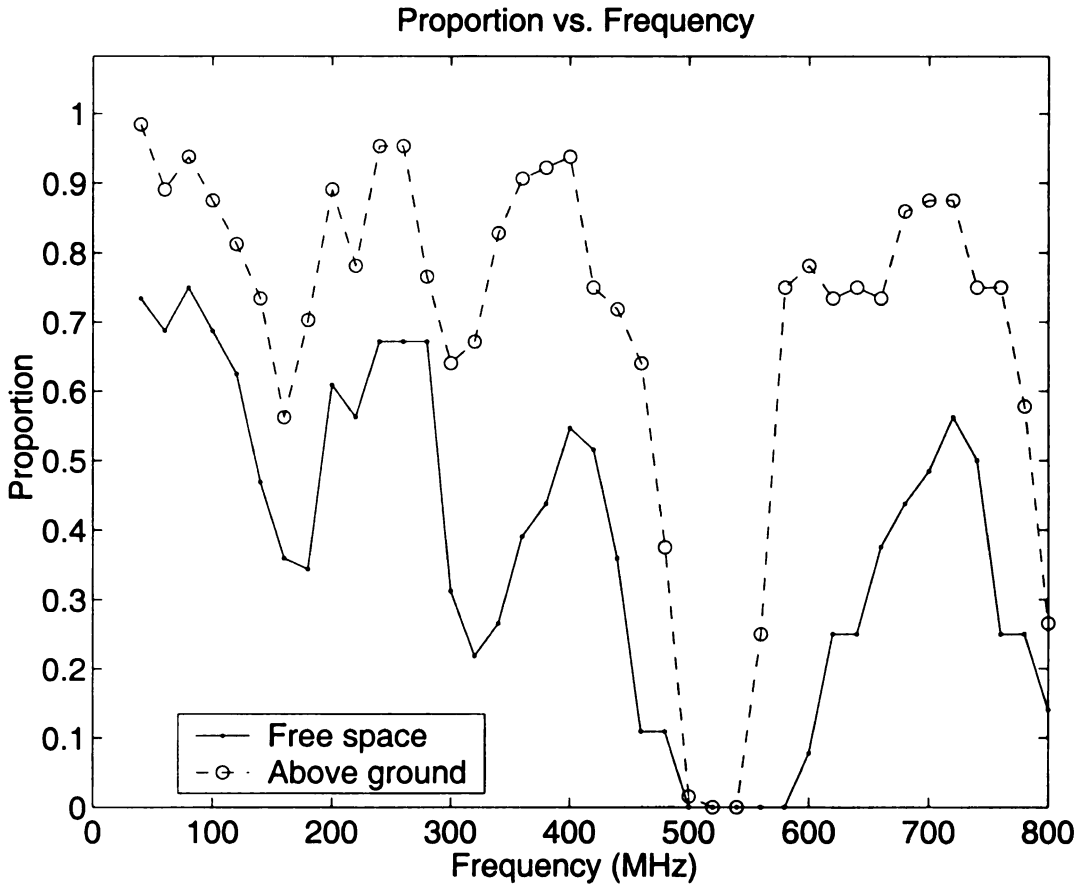


Figure 5.49. Proportion of configurations with minimum vertical gains in the horizontal plane above -3.0 dB vs. frequency for the layer 1.5 Type II SSA template (linear scale).

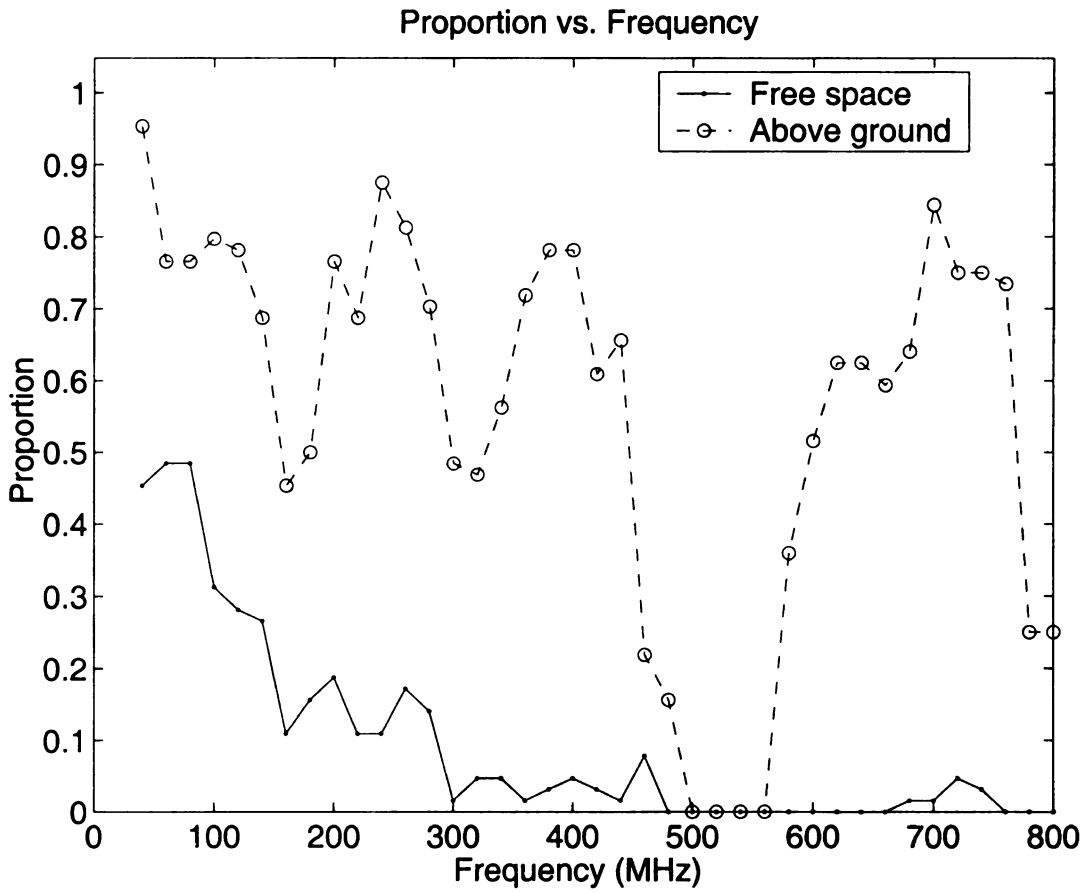


Figure 5.50. Proportion of configurations with minimum vertical gains in the horizontal plane above 0 dB vs. frequency for the layer 1.5 Type II SSA template (linear scale).

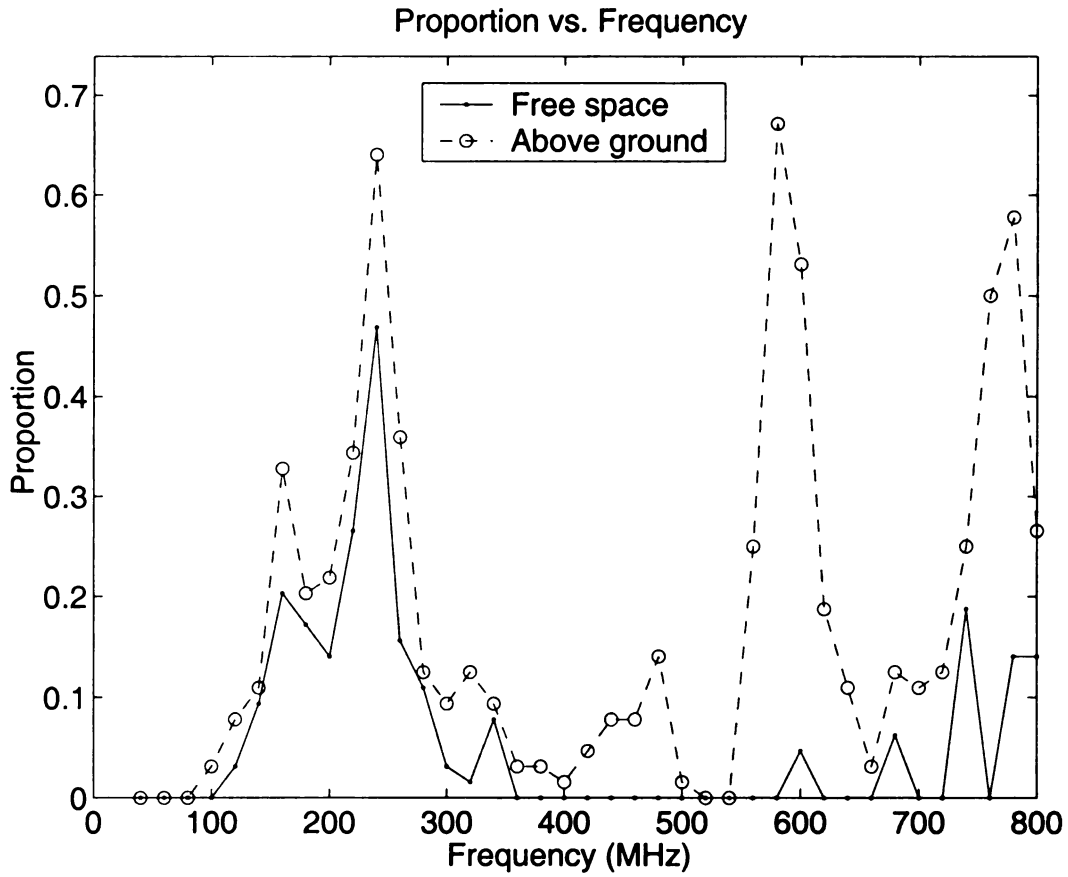


Figure 5.51. Proportion of configurations with SWRs less than 3.0 and minimum vertical gains in the horizontal plane above -3.0 dB vs. frequency for the layer 1.5 Type II SSA template (linear scale).

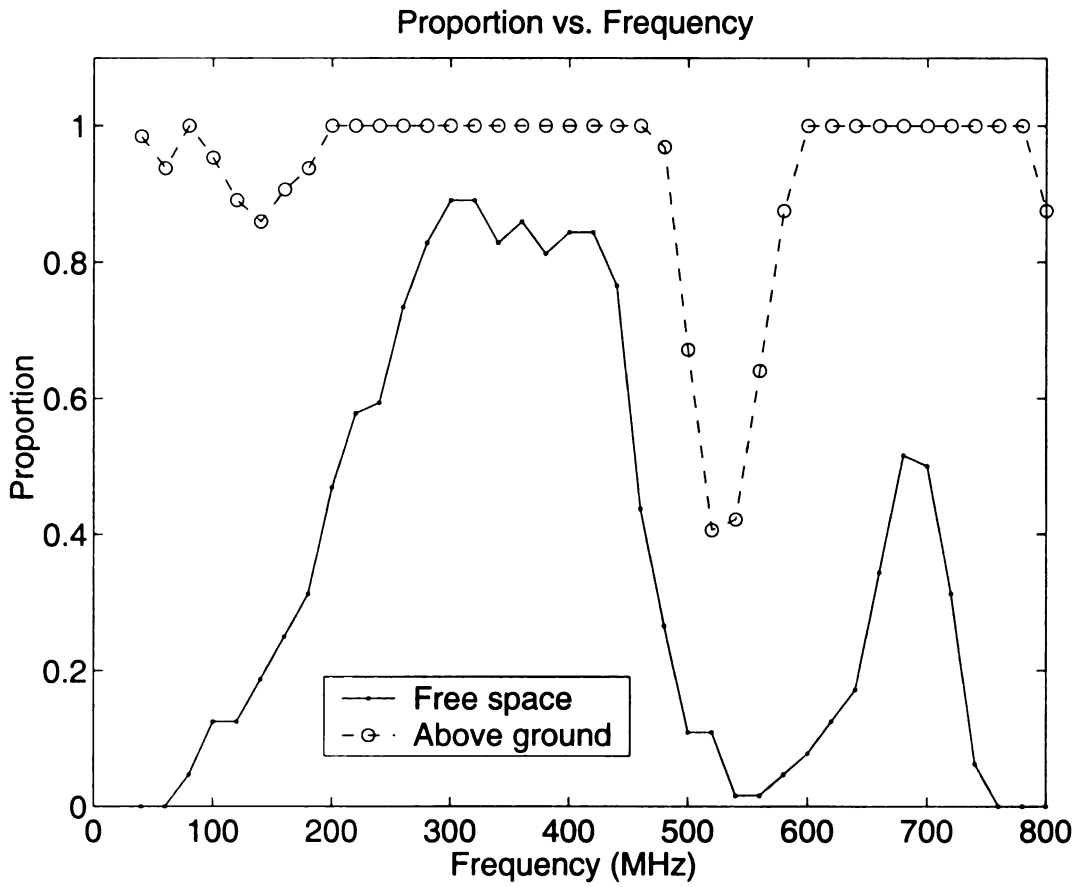


Figure 5.52. Proportion of configurations with maximum vertical gains in the horizontal plane above 3.0 dB vs. frequency for the layer 1.5 Type II SSA template (linear scale).

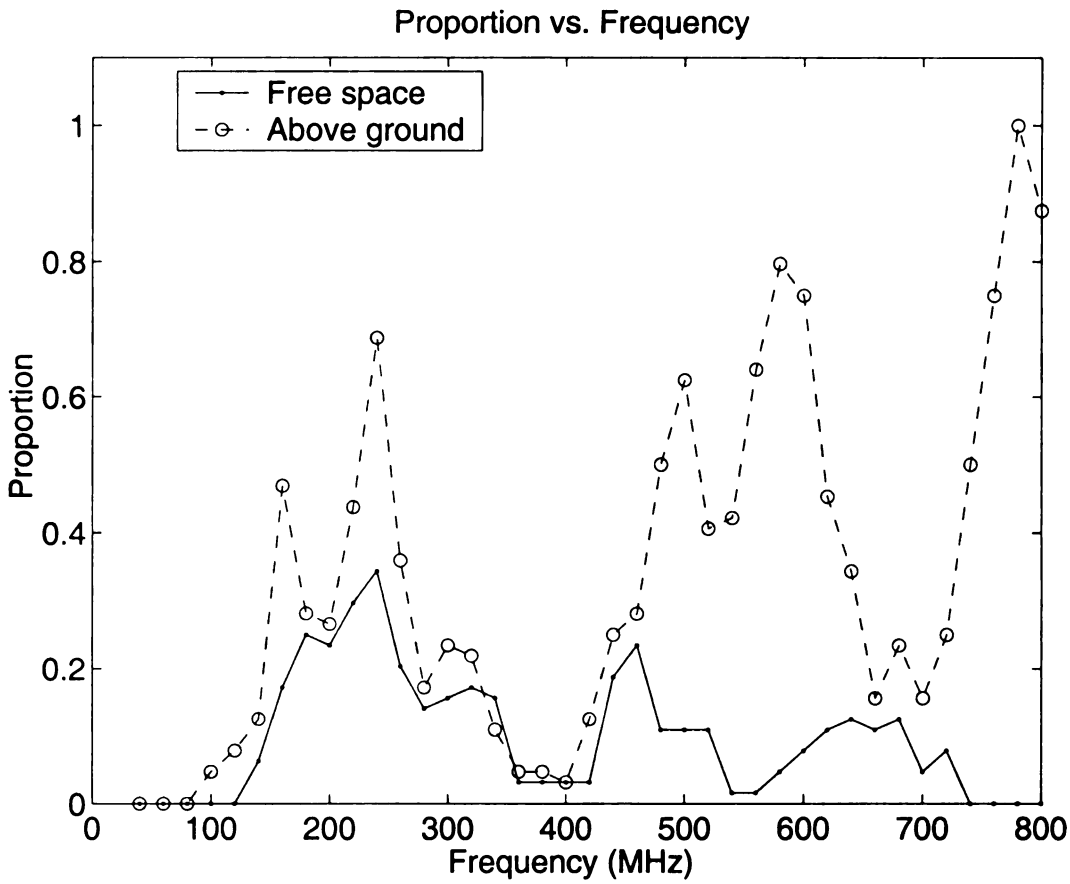


Figure 5.53. Proportion of configurations with SWRs less than 3.0 and maximum vertical gains in the horizontal plane above 3.0 dB vs. frequency for the layer 1.5 Type II SSA template (linear scale).

5.3.3 Layer 2 SSA Template

The layer 2 SSA template, shown in Figure 5.54, uses nine switches for 512 possible SSA configurations. The dimensions of the layer 2 Type I and Type II SSA templates are shown in Table 5.7 and Table 5.8, respectively. The characteristics of these configurations were evaluated exhaustively, and the results are presented in this section.

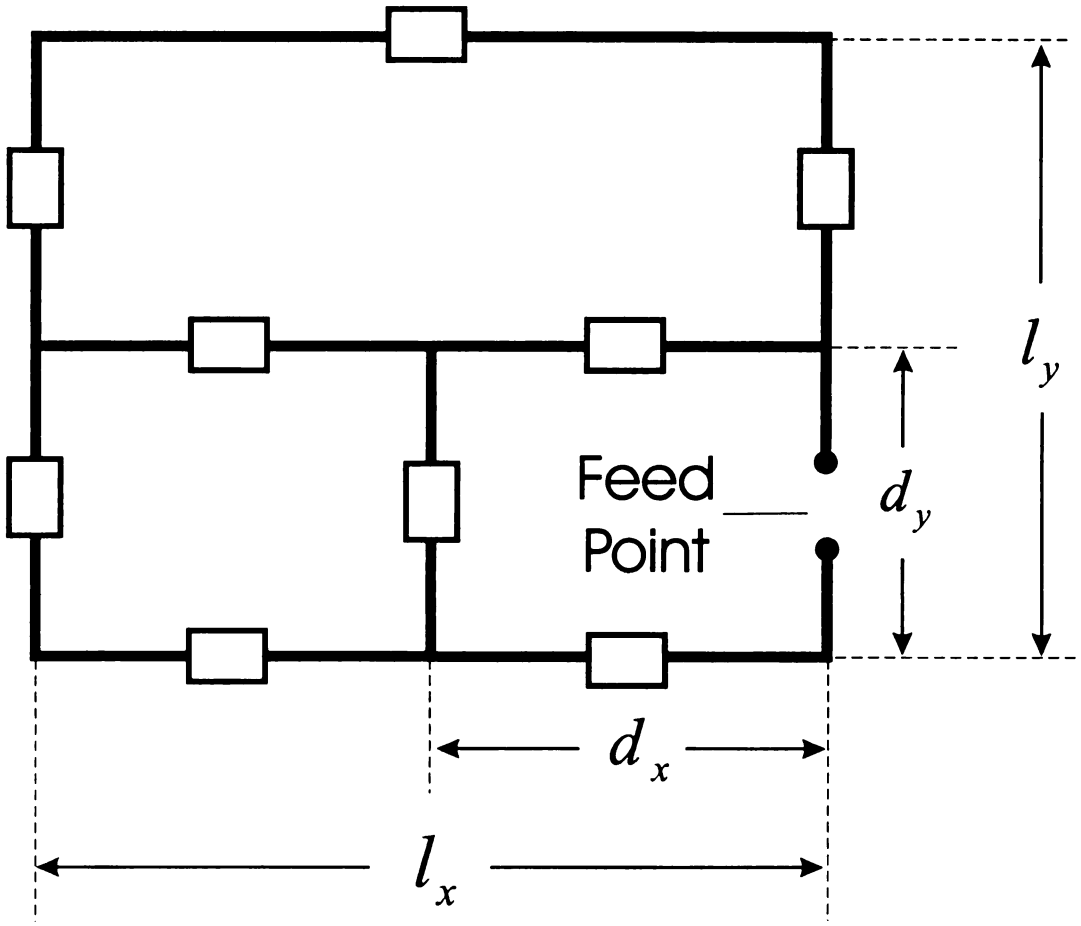


Figure 5.54. Diagram of the layer 2 SSA template.

5.3.3.1 Layer 2 Type I SSA Template

A plot of the SWRs of the 512 SSA configurations at each frequency is shown in Figure 5.55 for the layer 2 Type I template in free space. The distribution of SWRs for the template above ground is shown in Figure 5.56. Bands of nearly continuous possible SWR values exist at each studied frequency. Above 400 MHz, configurations exhibit many SWR values between 1.0 and 10.0 at most frequencies. The Smith charts shown in Figure 5.58 and Figure 5.59 show a uniform distribution over possible impedances at 800 MHz for the templates in free space and above ground, respectively. This diverse distribution may be important for an adaptive or a recon-

Table 5.7. Dimensions of the layer 2 Type I SSA template.

l_x	17.1 cm
d_x	8.57 cm
l_y	17.1 cm
d_y	8.57 cm
Outer electrical dimensions at 40 MHz	$0.0229\lambda \times 0.0229\lambda$
Outer electrical dimensions at 800 MHz	$0.457\lambda \times 0.457\lambda$

Table 5.8. Dimensions of the layer 2 Type II SSA template.

l_x	60.0 cm
d_x	30.0 cm
l_y	60.0 cm
d_y	30.0 cm
Outer electrical dimensions at 40 MHz	$0.0800\lambda \times 0.0800\lambda$
Outer electrical dimensions at 800 MHz	$1.60\lambda \times 1.60\lambda$

figurable antenna system, because changes in the electromagnetic environment could alter the impedances of all configurations. If the impedance distribution is diverse, suitable configurations may remain.

Figure 5.57 shows the minimum achievable SWR at each frequency for the layer 2 Type I templates in free space and above ground. An SWR of 2.0 or less is possible at most frequencies above 220 MHz for the template in free space and above ground. This is a dramatic improvement over the layer 1.5 Type I template, which has minimum SWR values less than 2.0 above 520 MHz.

The proportion of configurations with SWR values less than 4.0 at each frequency is shown in Figure 5.60 for the layer 2 Type I templates in free space and above ground. As shown in Figure 5.61 and Figure 5.62, the proportion drops as the threshold SWR is changed to 2.0 and 1.5, respectively. Above 440 MHz, at least 5% of the 512 configurations have SWR values less than 2.0. This percentage tops 25%

at 800 MHz for the template in free space, and is over 20% for the template above ground.

The proportion of configurations with minimum vertical gains in the horizontal plane above -3.0 dB is shown in Figure 5.63 for the layer 2 Type I templates in free space and above ground. As is the case for the layer 1 and layer 1.5 templates, the proportion of configurations that meet the gain threshold is greater for the template above ground than for the template in free space. This is further shown in Figure 5.64, where the minimum gain threshold is 0 dB.

Figure 5.65 shows the proportion of configurations with SWRs less than 4.0 and minimum gains above -3.0 dB for the layer 2 Type I template in free space and above ground. The proportion is nearly 45% at 800 MHz for the template above ground, and is over 15% for the template in free space. Figure 5.66 shows that there are few configurations with SWRs less than 2.0 and minimum gains above 0 dB for the template in free space. Some configurations meet these requirements for the template above ground at the higher studied frequencies.

The proportion of configurations with maximum gains in the horizontal plane above 3.0 dB is shown in Figure 5.67. Again, the presence of the ground plane allows for higher maximum gain values. Figure 5.68 shows the proportion of configurations with SWRs less than 2.0 and maximum gains above 3.0 dB. Over 20% of the configurations meet these requirements for the template above ground at 800 MHz.

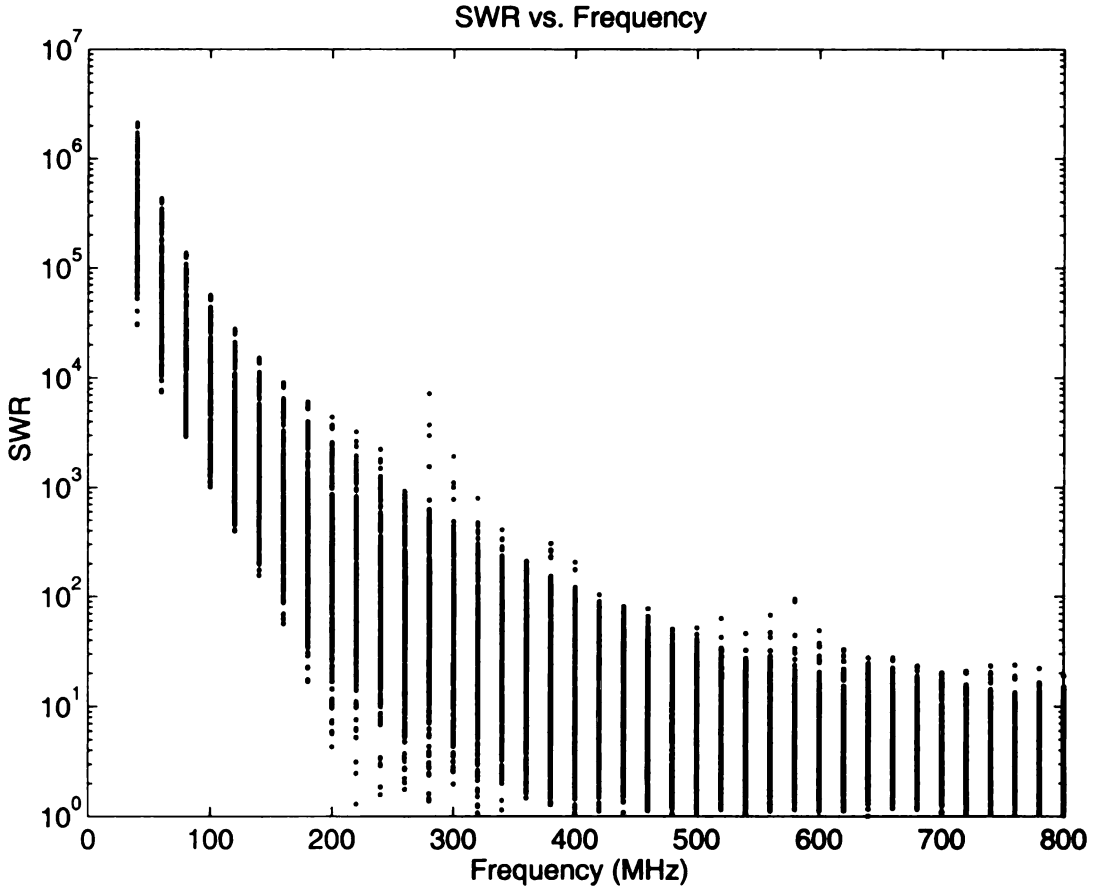


Figure 5.55. SWR vs. frequency for the layer 2 Type I SSA template in free space.

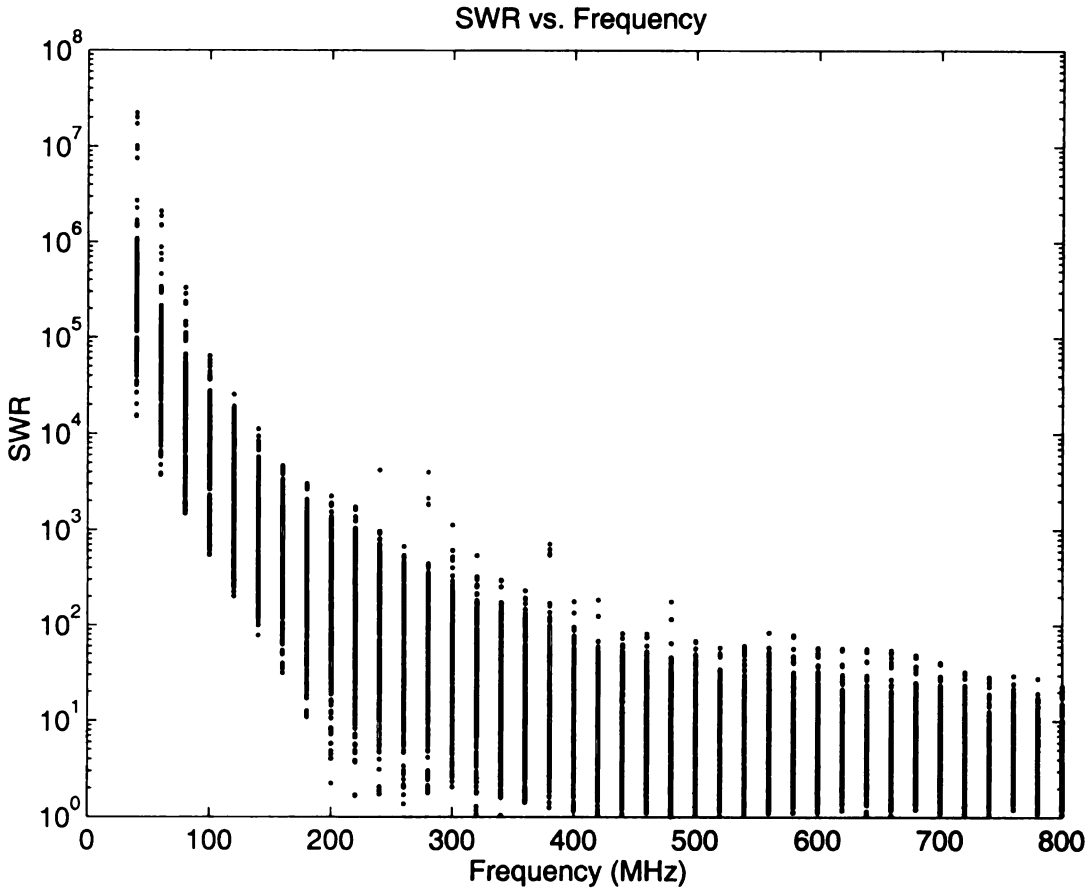


Figure 5.56. SWR vs. frequency for the layer 2 Type I SSA template above ground.

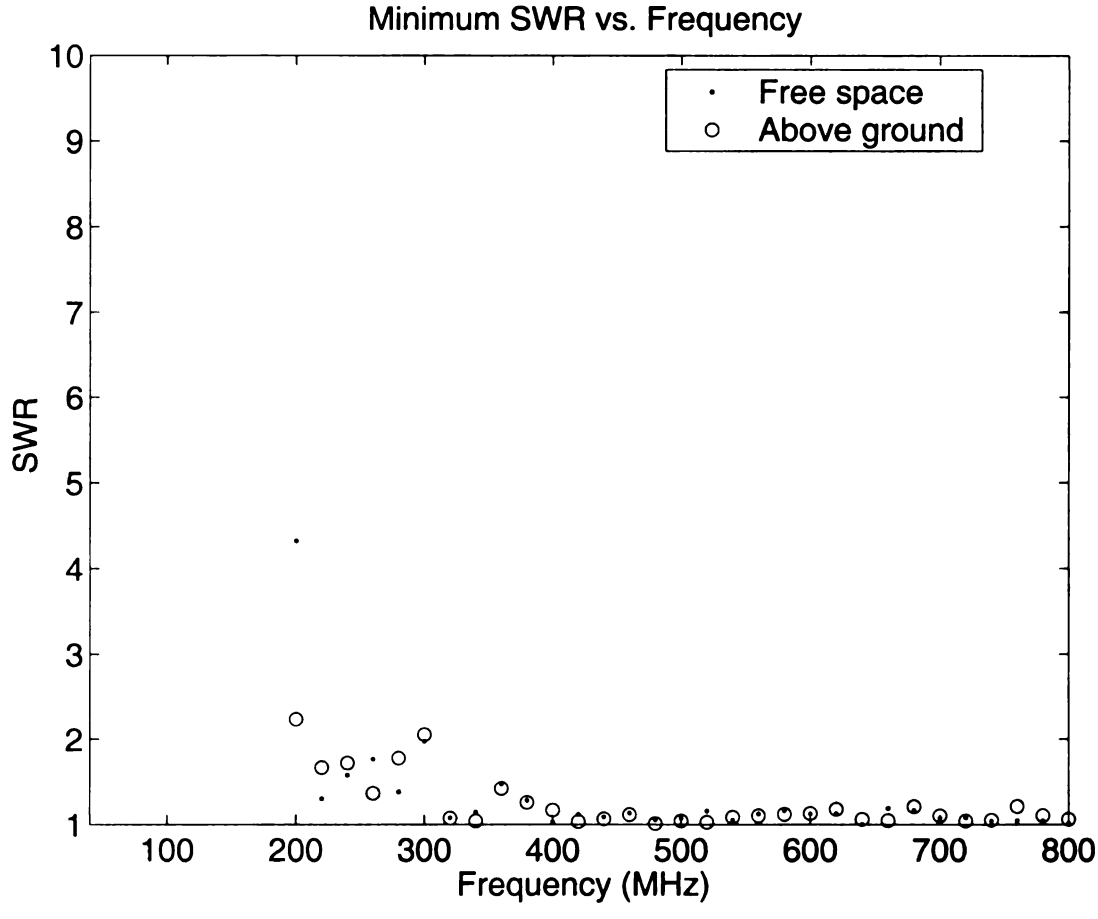


Figure 5.57. Minimum SWR vs. frequency for the layer 2 Type I SSA template.

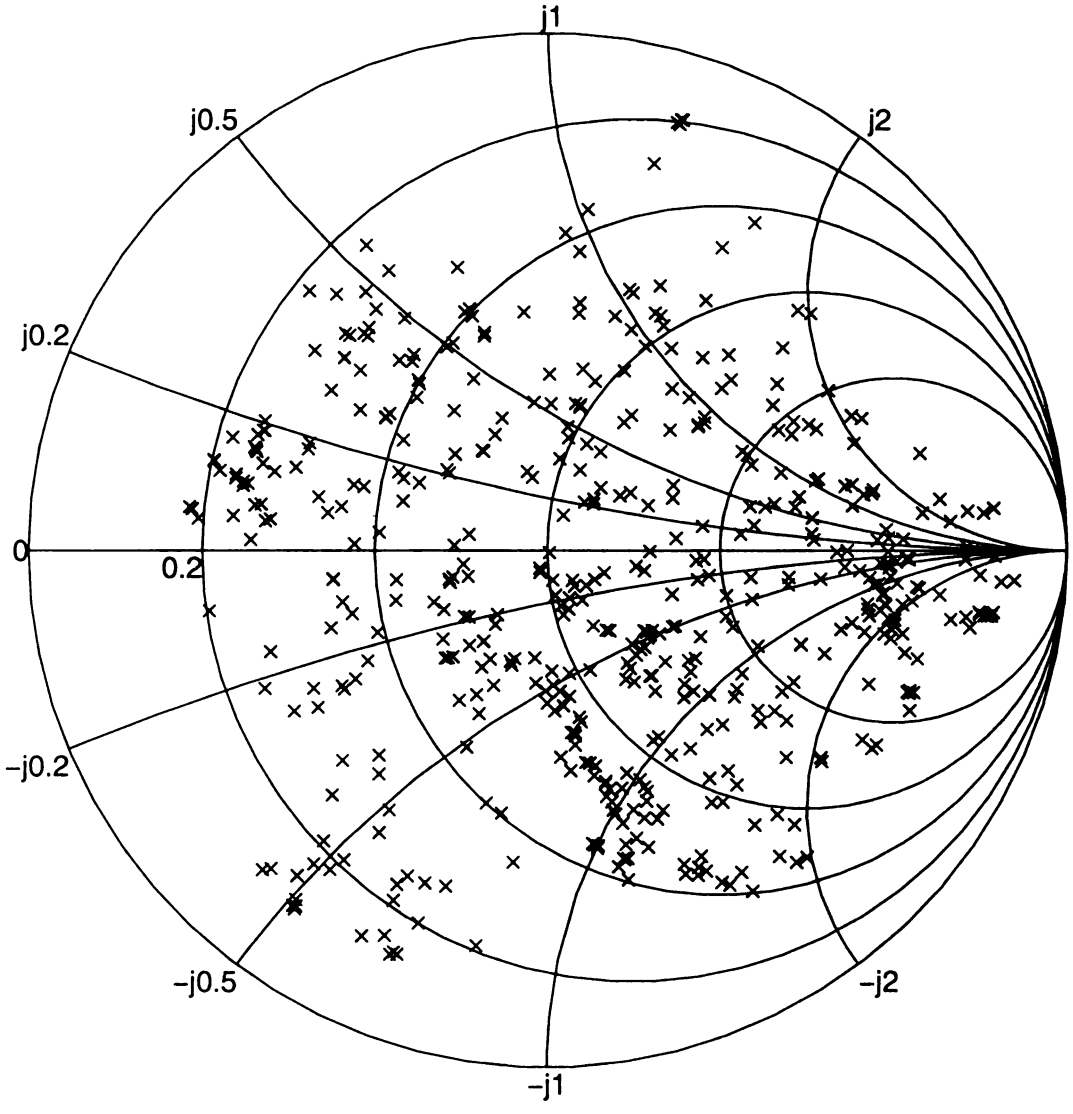


Figure 5.58. Smith chart for the layer 2 Type I SSA template in free space at 800 MHz.

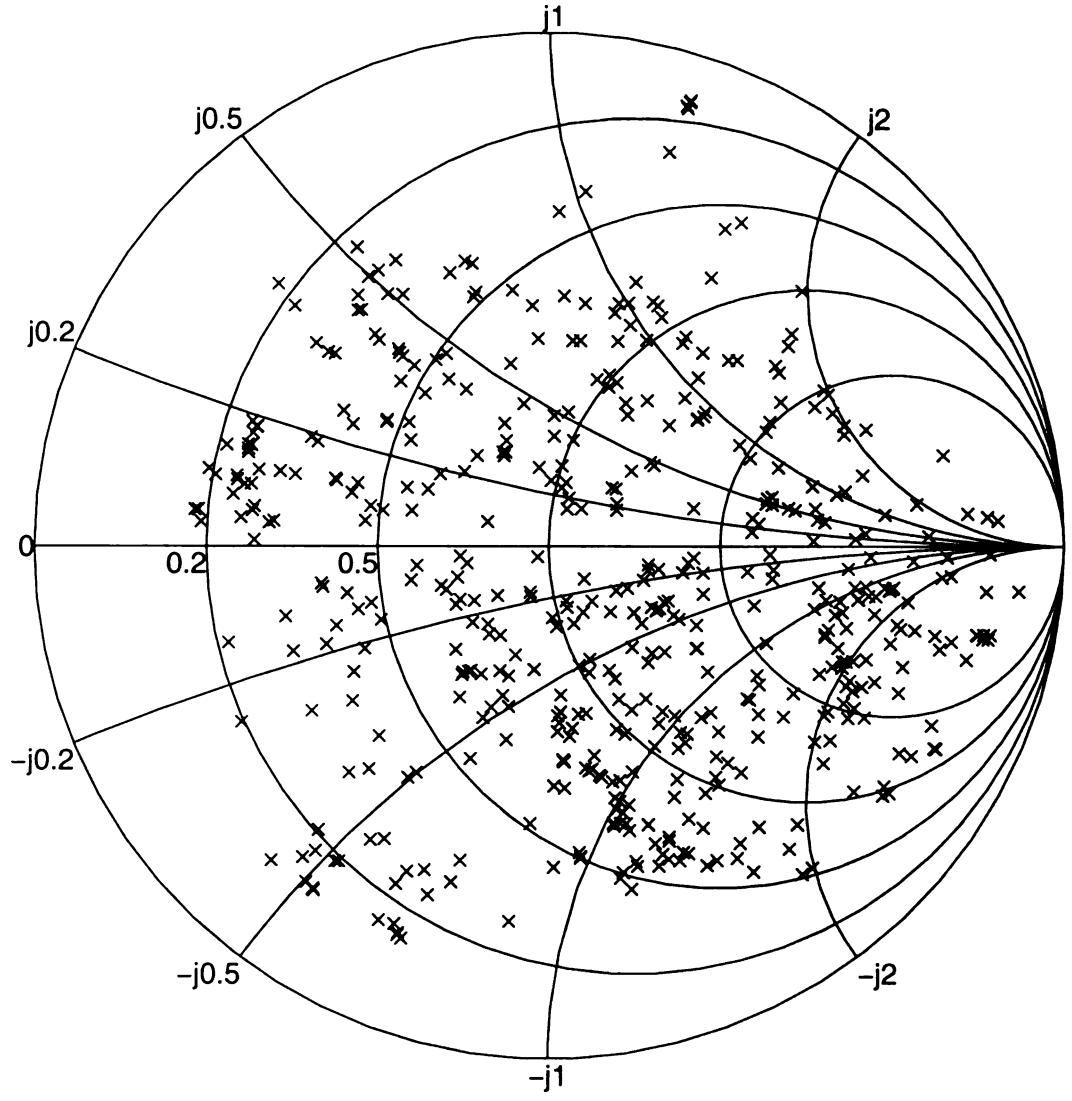


Figure 5.59. Smith chart for the layer 2 Type I SSA template above ground at 800 MHz.

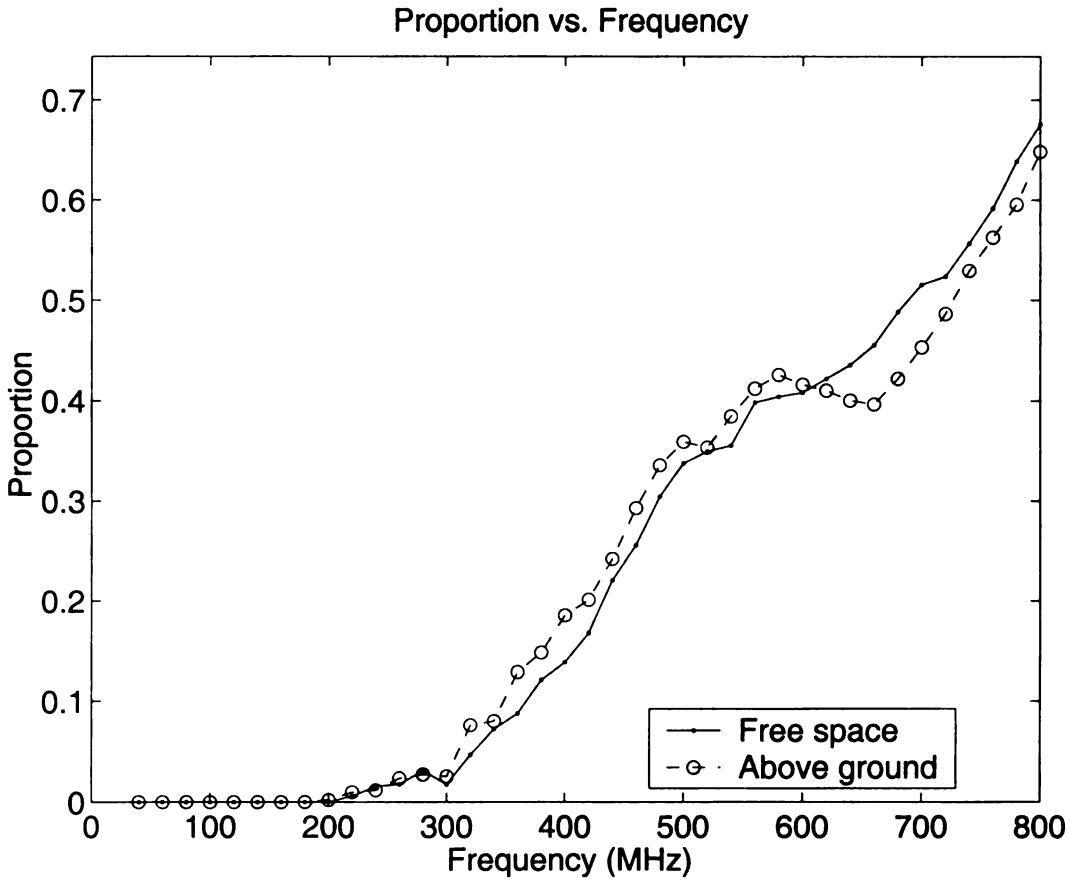


Figure 5.60. Proportion of configurations with SWRs less than 4.0 vs. frequency for the layer 2 Type I SSA template (linear scale).

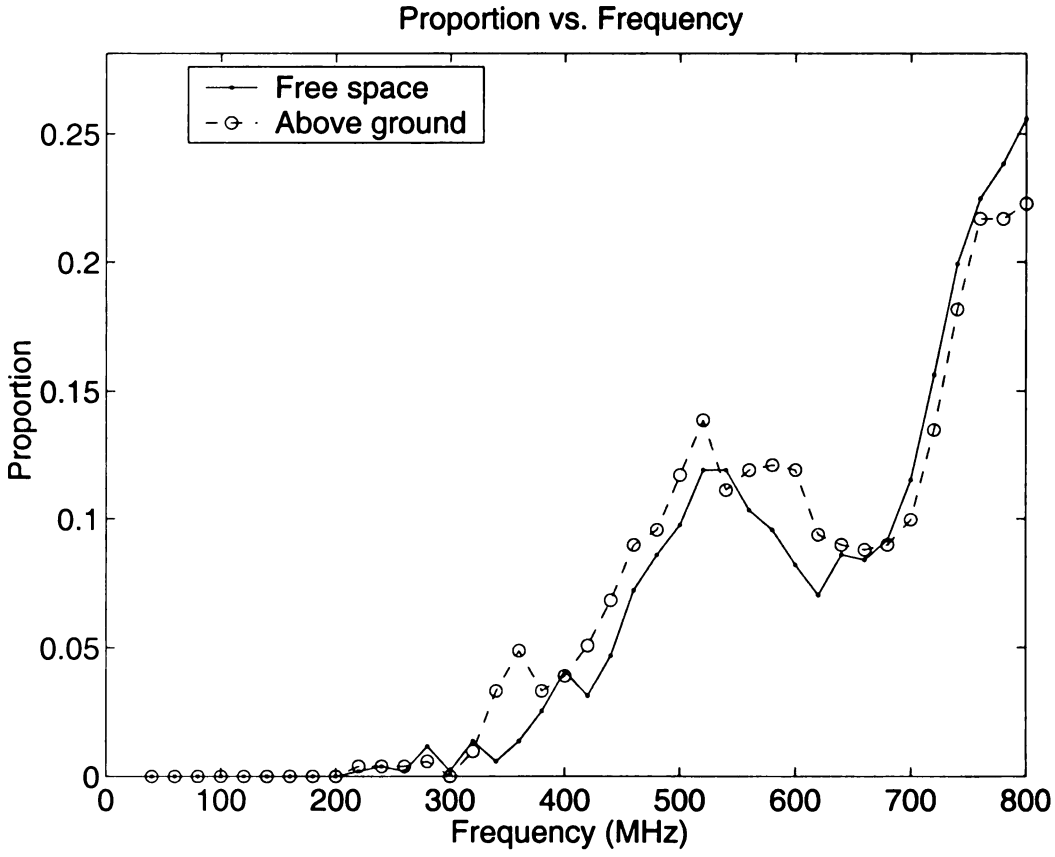


Figure 5.61. Proportion of configurations with SWRs less than 2.0 vs. frequency for the layer 2 Type I SSA template (linear scale).

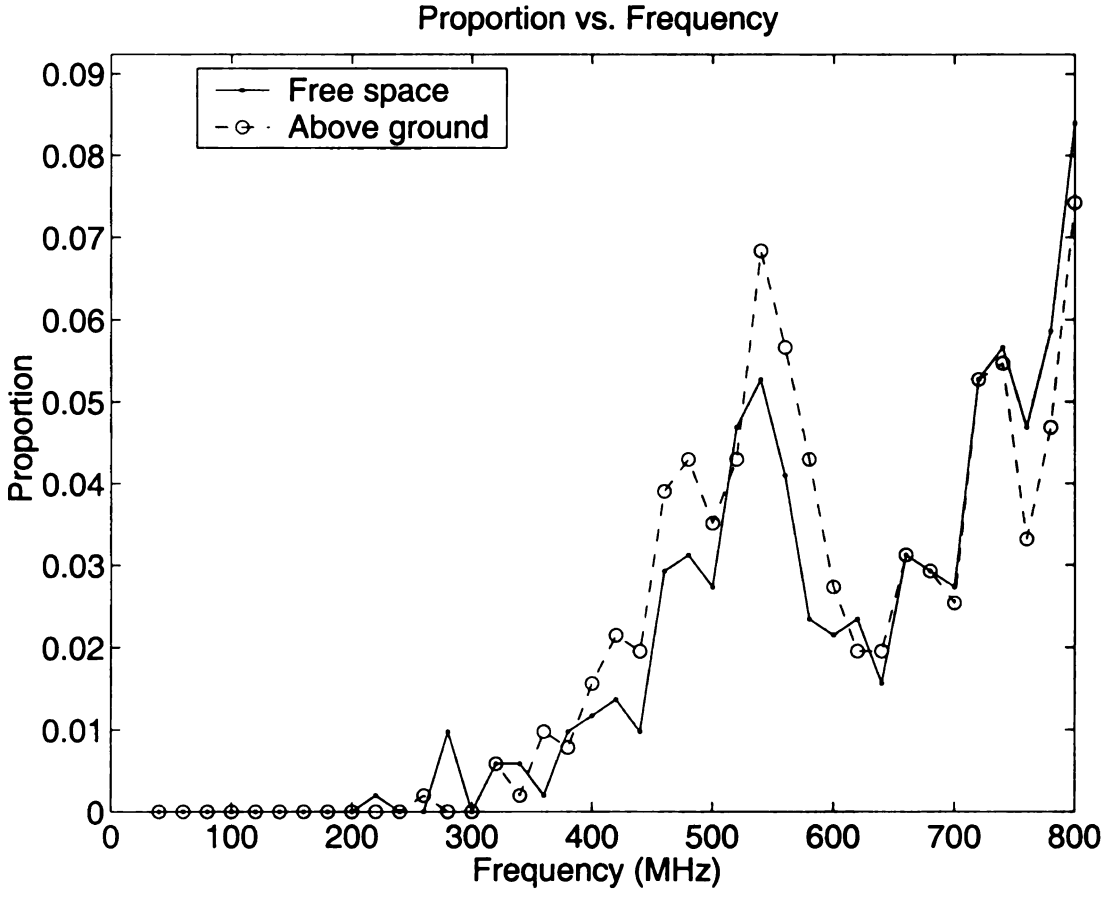


Figure 5.62. Proportion of configurations with SWRs less than 1.5 vs. frequency for the layer 2 Type I SSA template (linear scale).

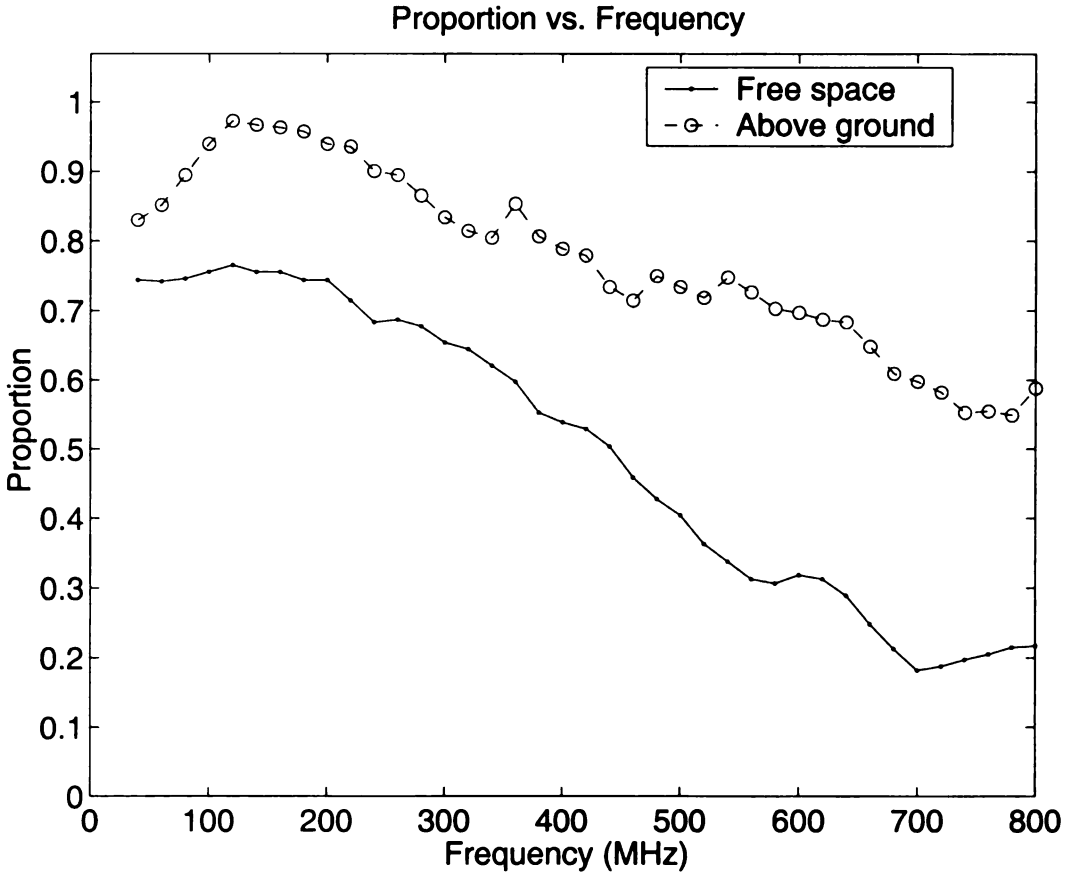


Figure 5.63. Proportion of configurations with minimum vertical gains in the horizontal plane above -3.0 dB vs. frequency for the layer 2 Type I SSA template (linear scale).

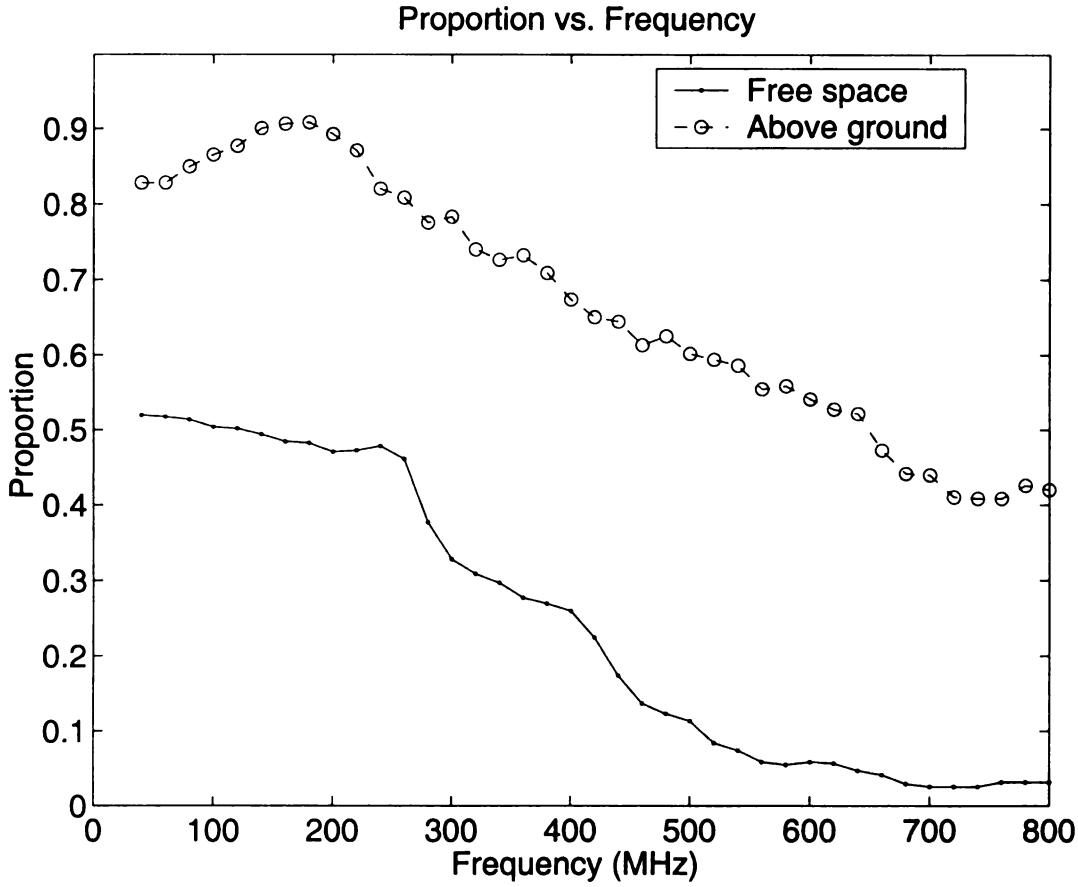


Figure 5.64. Proportion of configurations with minimum vertical gains in the horizontal plane above 0 dB vs. frequency for the layer 2 Type I SSA template (linear scale).

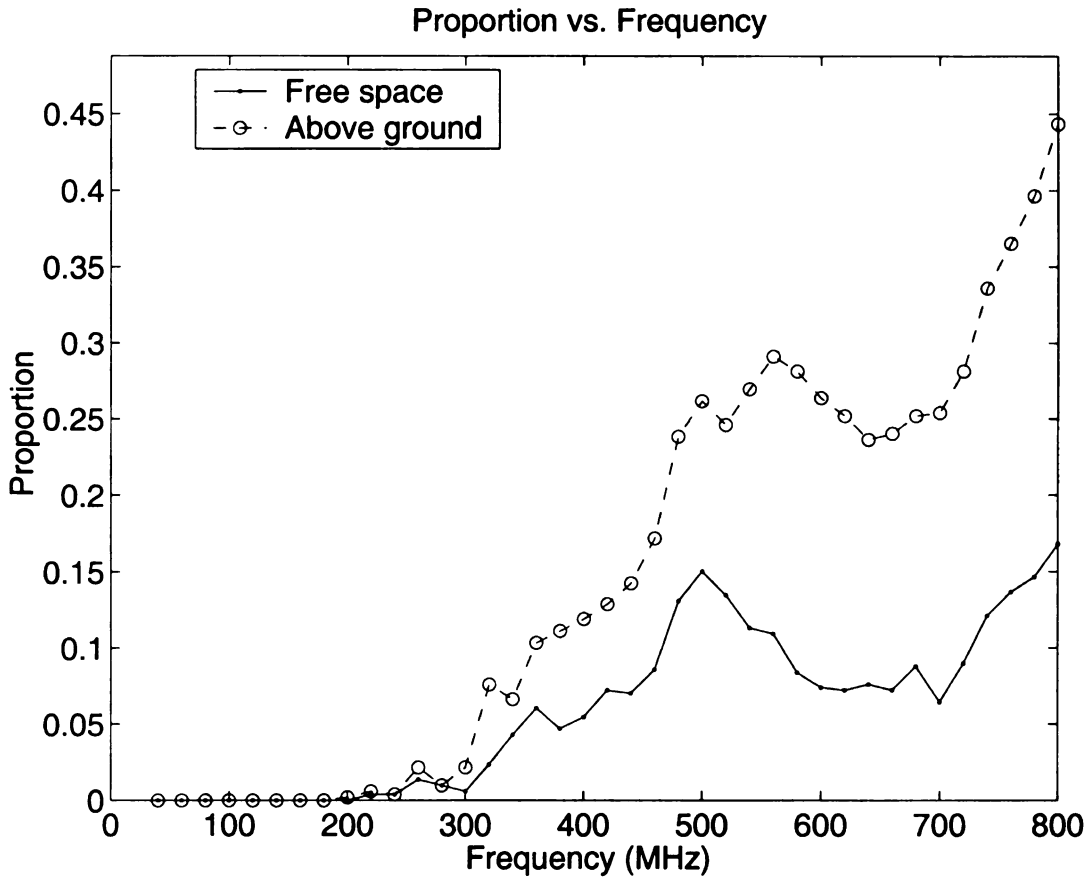


Figure 5.65. Proportion of configurations with SWRs less than 4.0 and minimum vertical gains above -3.0 dB vs. frequency for the layer 2 Type I SSA template (linear scale).

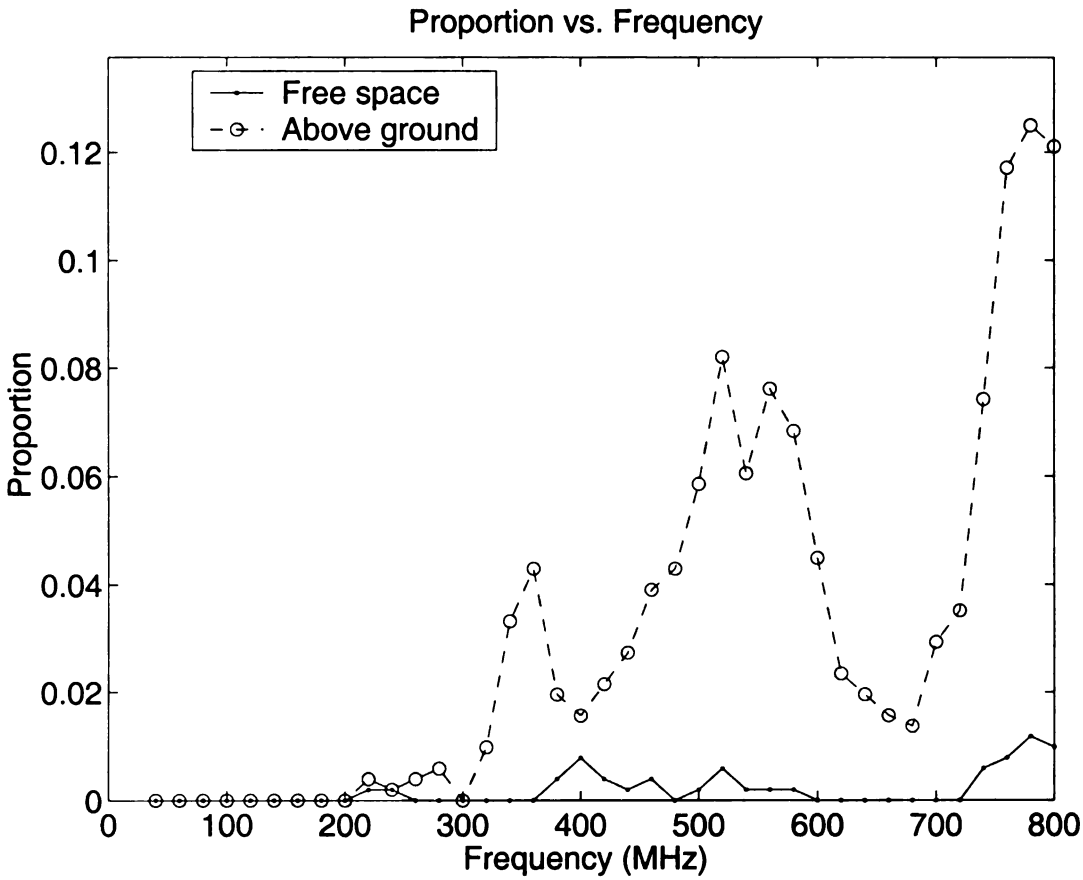


Figure 5.66. Proportion of configurations with SWRs less than 2.0 and minimum vertical gains in the horizontal plane above 0 dB vs. frequency for the layer 2 Type I SSA template (linear scale).

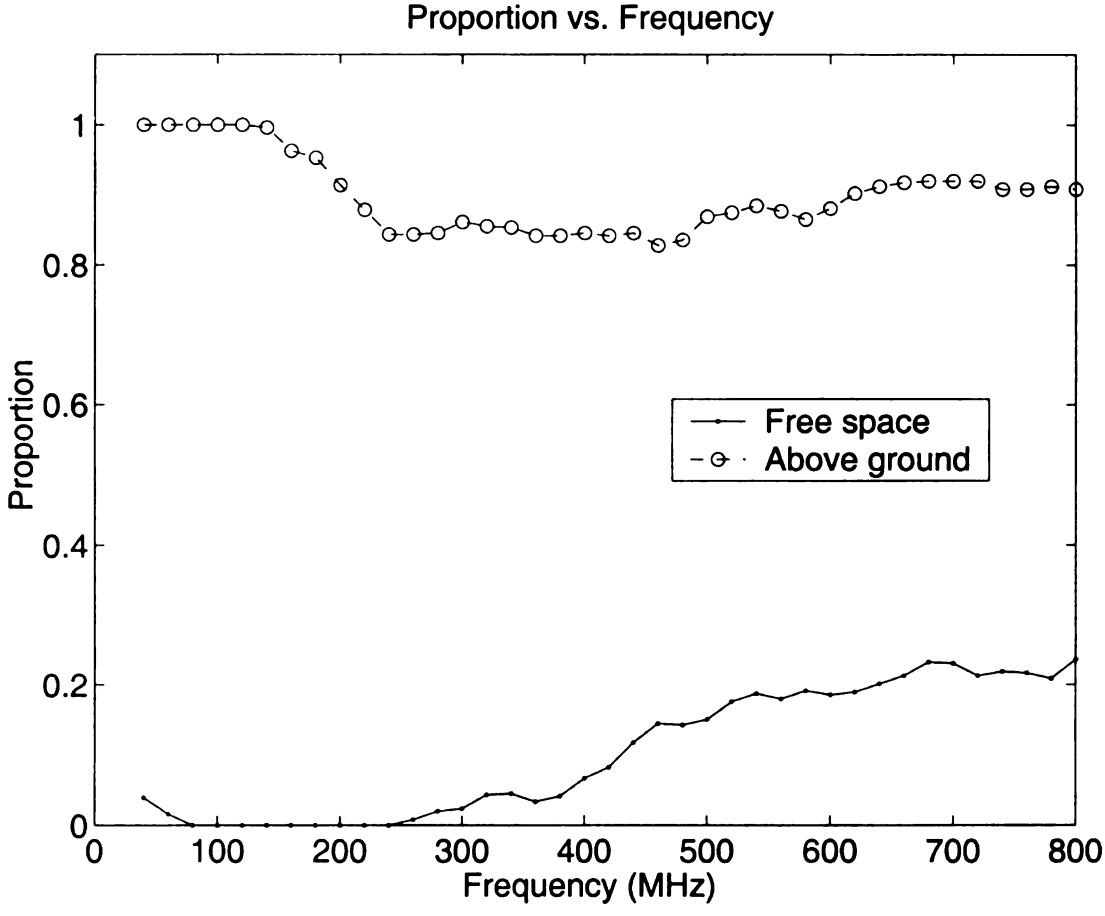


Figure 5.67. Proportion of configurations with maximum vertical gains in the horizontal plane above 3.0 dB vs. frequency for the layer 2 Type I SSA template (linear scale).

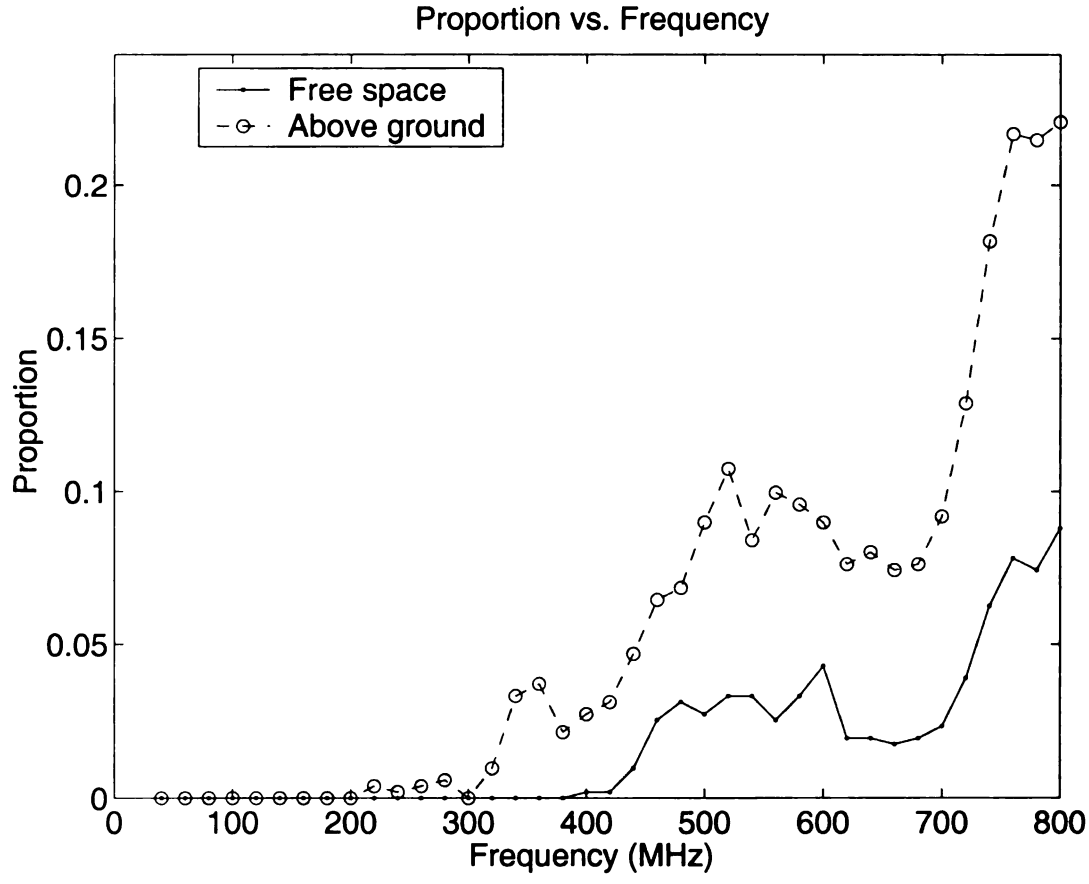


Figure 5.68. Proportion of configurations with SWRs less than 2.0 and maximum vertical gains in the horizontal plane above 3.0 dB vs. frequency for the layer 2 Type I SSA template (linear scale).

5.3.3.2 Layer 2 Type II SSA Template

The layer 2 Type II SSA template is electrically larger than the layer 2 Type I template. The dimensions of the layer 2 Type II template are shown in Table 5.8.

Plots of the possible SWRs at each frequency are shown in Figure 5.69 and Figure 5.70 for the layer 2 Type II templates in free space and above ground, respectively. As is the case with the layer 2 Type I template, bands of nearly continuous possible SWR values exist at each frequency. However, the Type II template does not provide any configurations with low SWRs at several frequencies. For instance, at 500 MHz

there are no configurations with SWRs less than about 5.0 for the template in free space, and most configurations have SWR values between 7.0 and 15. This is also shown by the Smith charts at 500 MHz found in Figure 5.72 and Figure 5.73 for the templates in free space and above ground, respectively. The impedances of most configurations are clumped in a tight group away from the 200 Ω center of the chart.

This clumping hurts the layer 2 Type II templates' ability to provide configurations with low SWRs at many frequencies, as shown in Figure 5.71 for the templates in free space and above ground. The minimum SWR at 500 MHz is nearly 5.0 for the template in free space, and is over 4.0 for the template above ground. The percentage of configurations with SWR values less than 4.0 falls close to zero from 480 MHz to 540 MHz, as shown in Figure 5.74 for the templates in free space and above ground. As shown in Figure 5.75, the percentage of configurations with SWR values less than 2.0 is close to zero over a wider range, from 460 MHz to 640 MHz, for the templates in free space and above ground. The band of frequencies for low proportions of configurations grows larger when the SWR threshold is reduced to 1.5, as shown in Figure 5.76.

Clumping can occur in groups of good impedance values at some frequencies, as shown by the Smith charts at 780 MHz in Figure 5.77 and Figure 5.78 for the templates in free space and above ground, respectively. Nearly 65% of the 512 configurations of the layer 2 Type II template have SWR values less than 2.0 at this frequency for the template in free space, and over 70% of the configurations have SWRs less than 2.0 for the template above ground.

The proportions of configurations with minimum vertical gains in the horizontal plane above -3.0 dB and 0 dB are shown in Figure 5.79 and Figure 5.80, respectively, for the templates in free space and above ground. Again, the presence of the ground plane helps the template produce more configurations with higher minimum vertical gains. Below 580 MHz, over 20% of the configurations have minimum vertical gains

above 0 dB for the template above ground. Above 400 MHz, however, there are almost no configurations with SWRs less than 2.0 and minimum vertical gains above 0 dB, as shown in Figure 5.81. The proportion of configurations with SWRs less than 4.0 and minimum gains above -3.0 dB is also very low above 500 MHz, as shown in Figure 5.82.

The proportion of configurations with maximum vertical gains in the horizontal plane above 3.0 dB are shown in Figure 5.83 for the templates in free space and above ground. This shows that many configurations have high maximum gain values for the template above ground, and that nearly 90% of the configurations for the template in free space have maximum gains above 3.0 dB at 520 MHz. Recall, however that no configurations have SWRs less than 2.0 at this frequency for the template in free space. This is also shown in Figure 5.84, where the SWR and gain criteria are combined. Figure 5.85 shows that many configurations exist with maximum vertical gains above 6.0 dB for the template above ground, but Figure 5.86 shows that the template above ground is unacceptable for use from 480 MHz to 640 MHz if SWRs less than 2.0 as well as maximum gains above 6.0 dB are required for an application. No configurations exist with SWRs less than 2.0 and maximum gains above 6.0 dB for the template in free space across the studied frequency band.

The poor characteristics of the layer 2 Type II template near 500 MHz suggest that relatively large templates with few switches and wires may not perform well at large ranges of frequencies. The smaller Type I templates seem to provide a greater range of possible characteristics that is advantageous for a reconfigurable system.

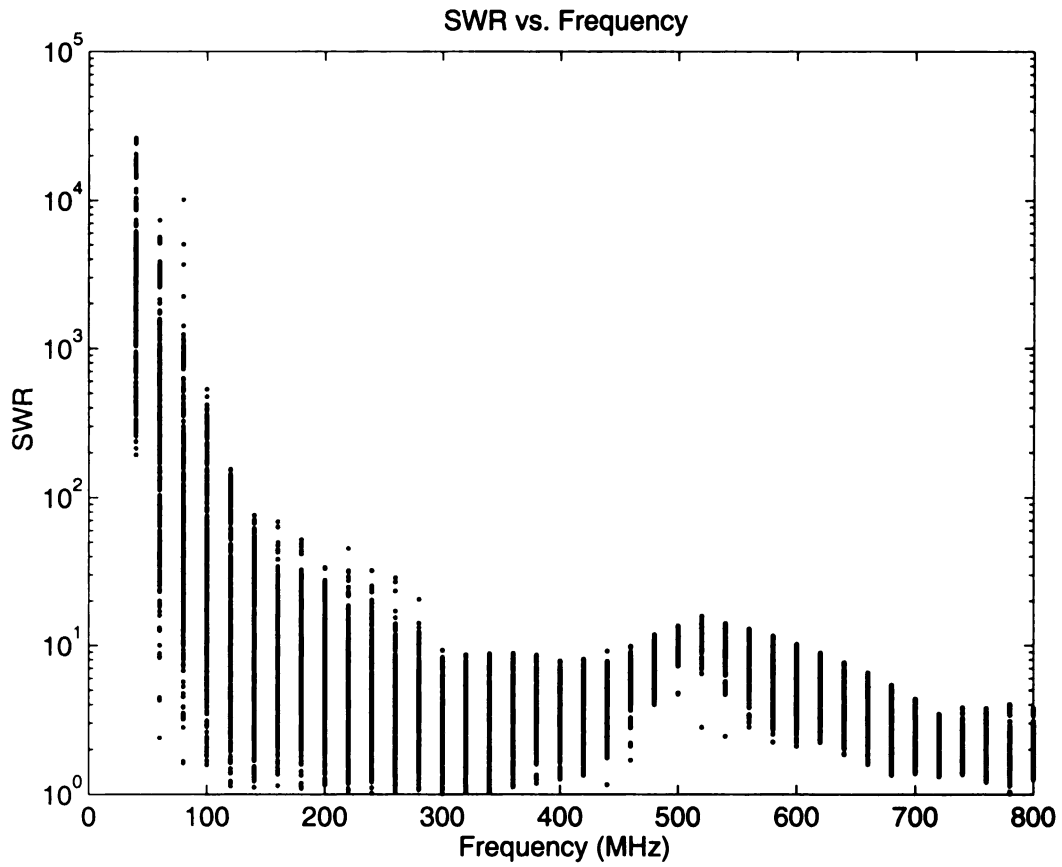


Figure 5.69. SWR vs. frequency for the layer 2 Type II SSA template in free space.

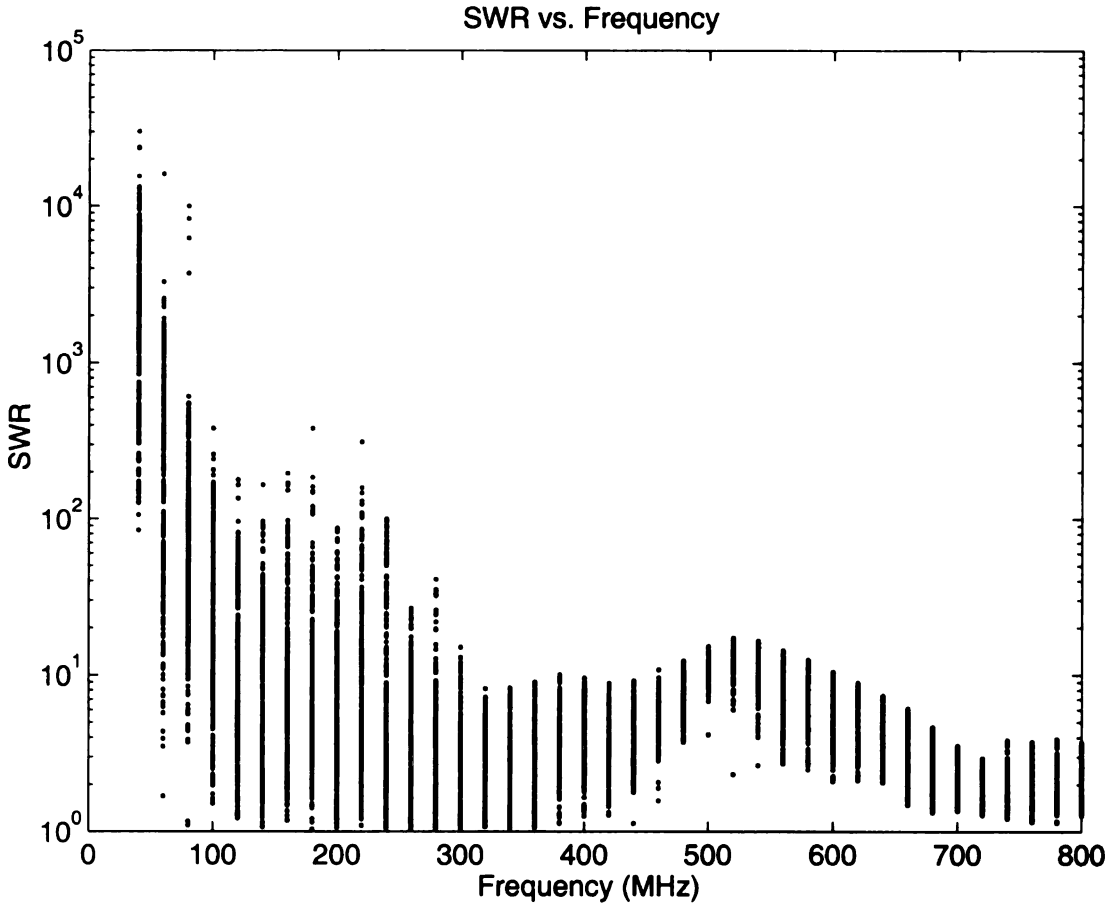


Figure 5.70. SWR vs. frequency for the layer 2 Type II SSA template above ground.

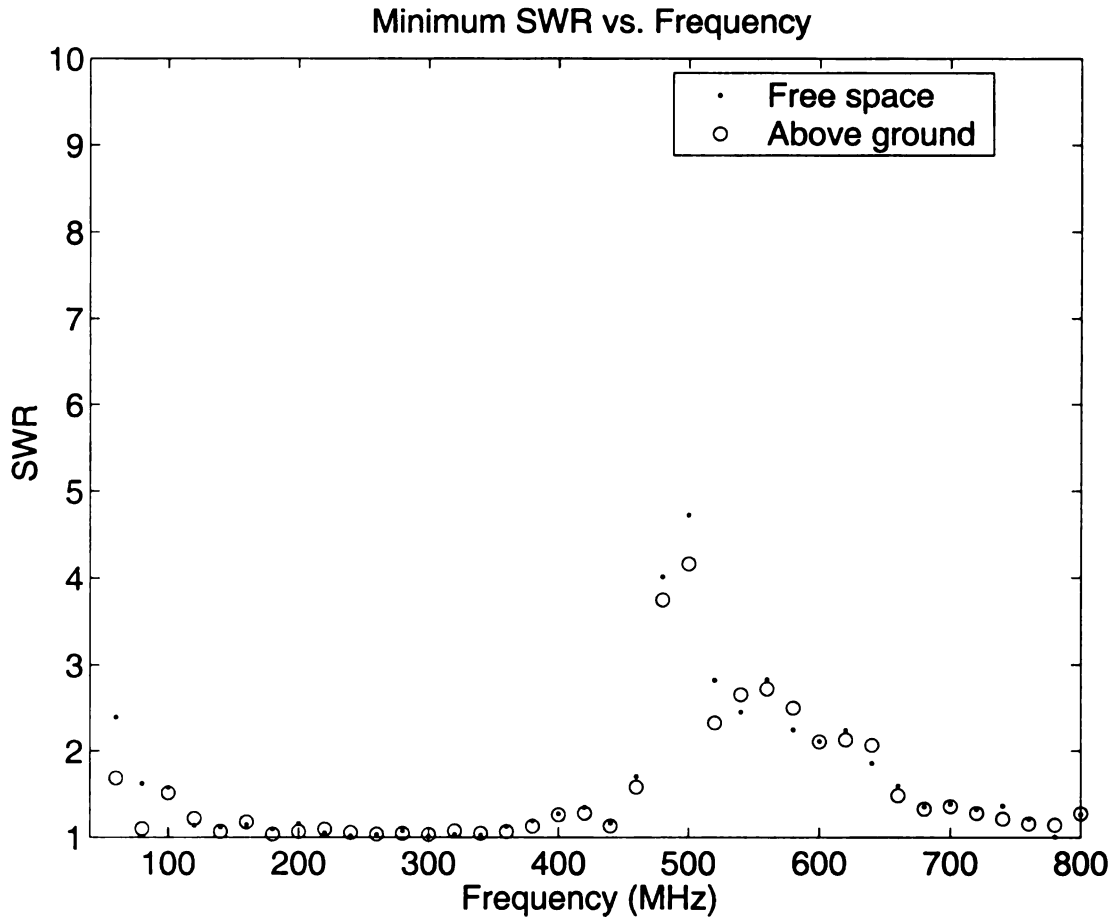


Figure 5.71. Minimum SWR vs. frequency for the layer 2 Type II SSA template.

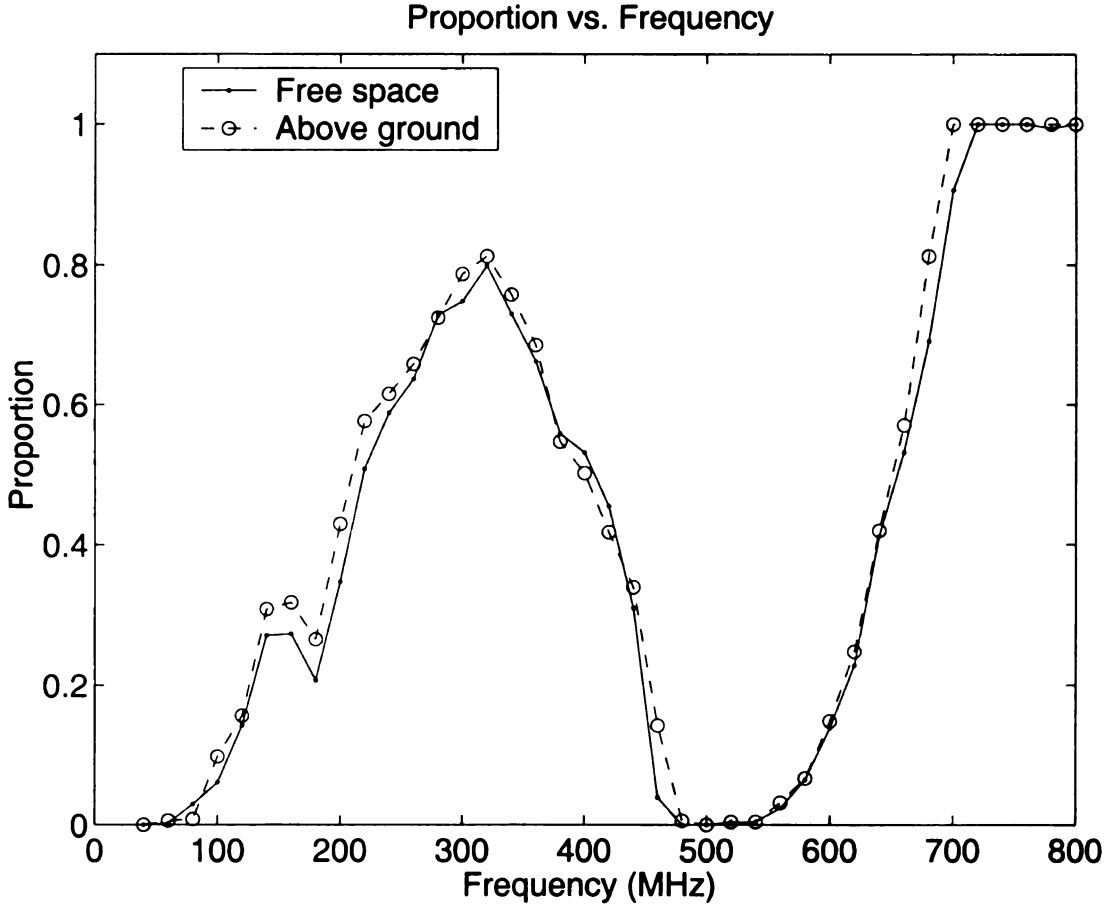


Figure 5.74. Proportion of configurations with SWRs less than 4.0 vs. frequency for the layer 2 Type II SSA template (linear scale).

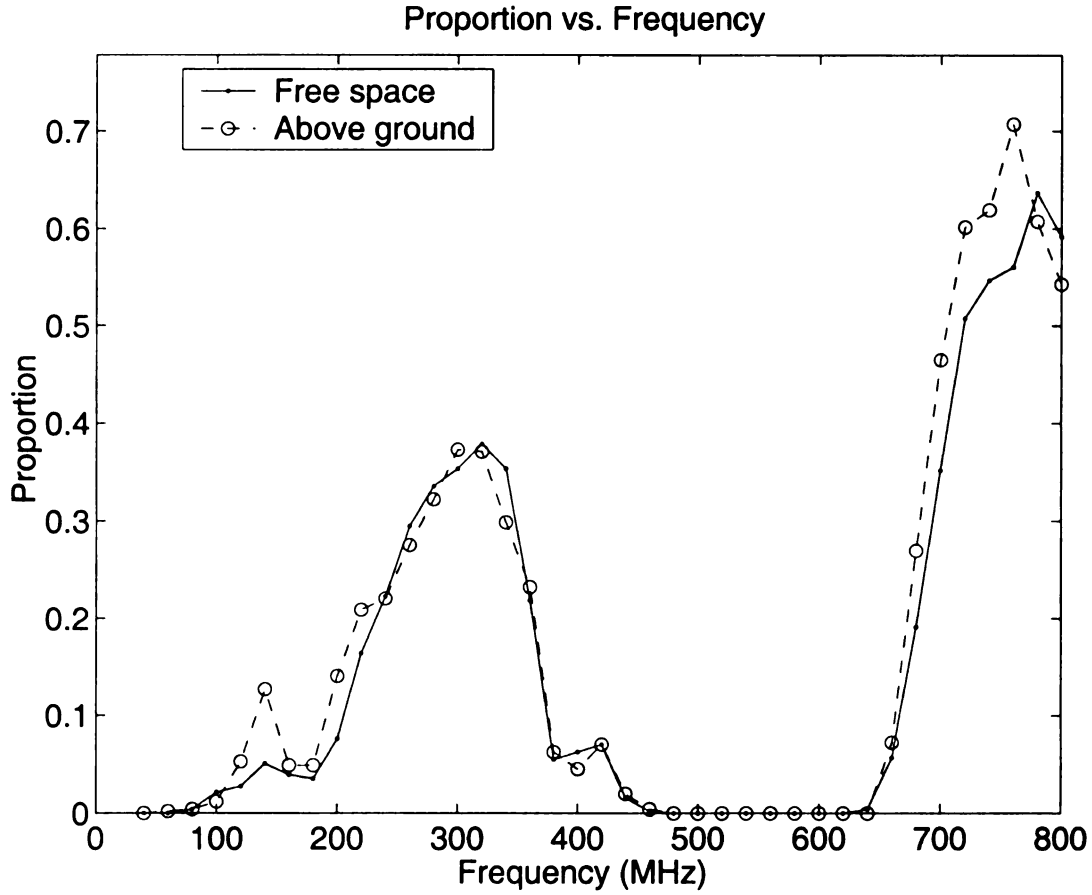


Figure 5.75. Proportion of configurations with SWRs less than 2.0 vs. frequency for the layer 2 Type II SSA template (linear scale).

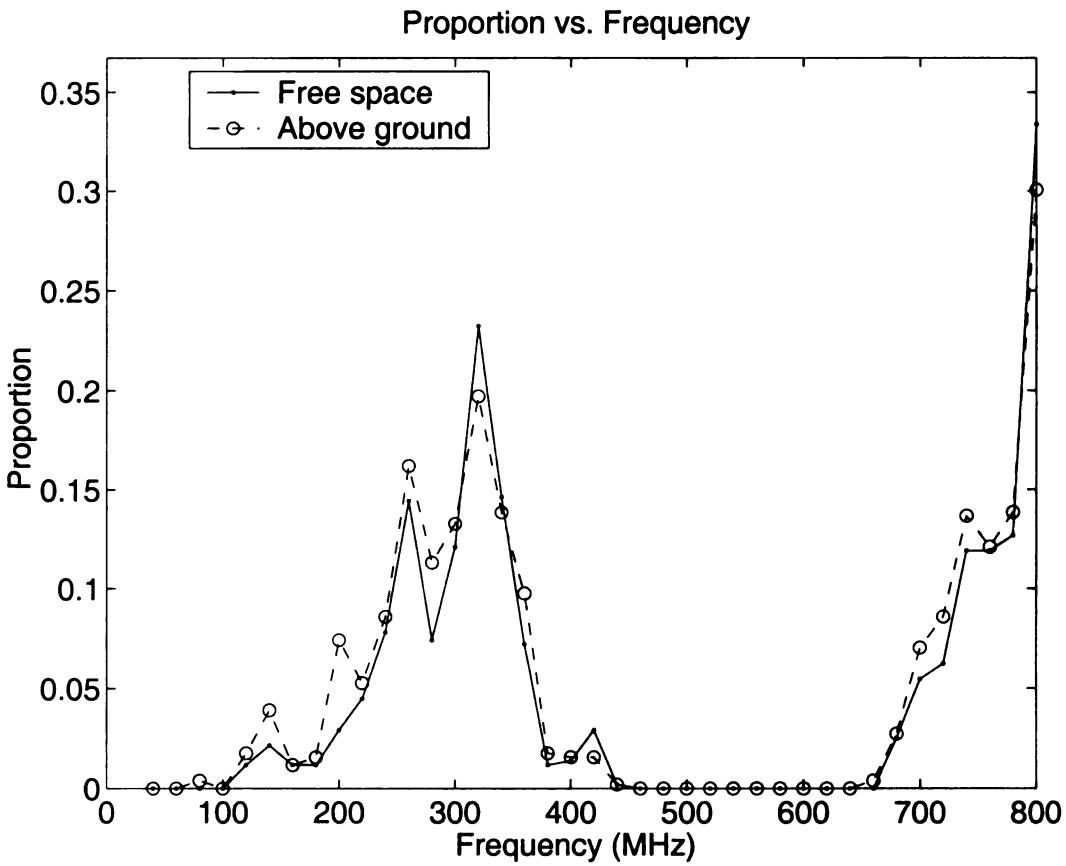


Figure 5.76. Proportion of configurations with SWRs less than 1.5 vs. frequency for the layer 2 Type II SSA template (linear scale).

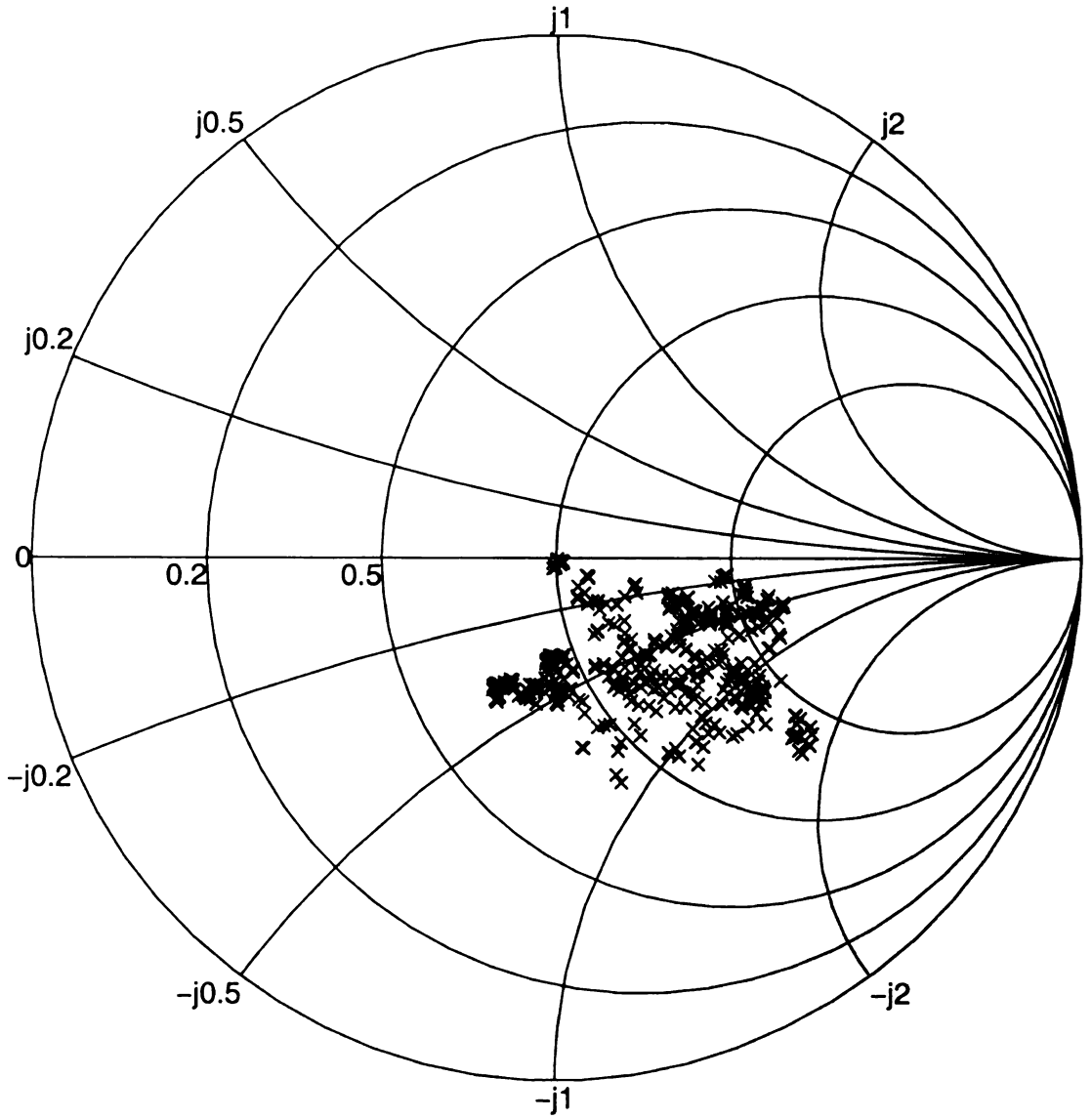


Figure 5.77. Smith chart for the layer 2 Type II SSA template in free space at 780 MHz.

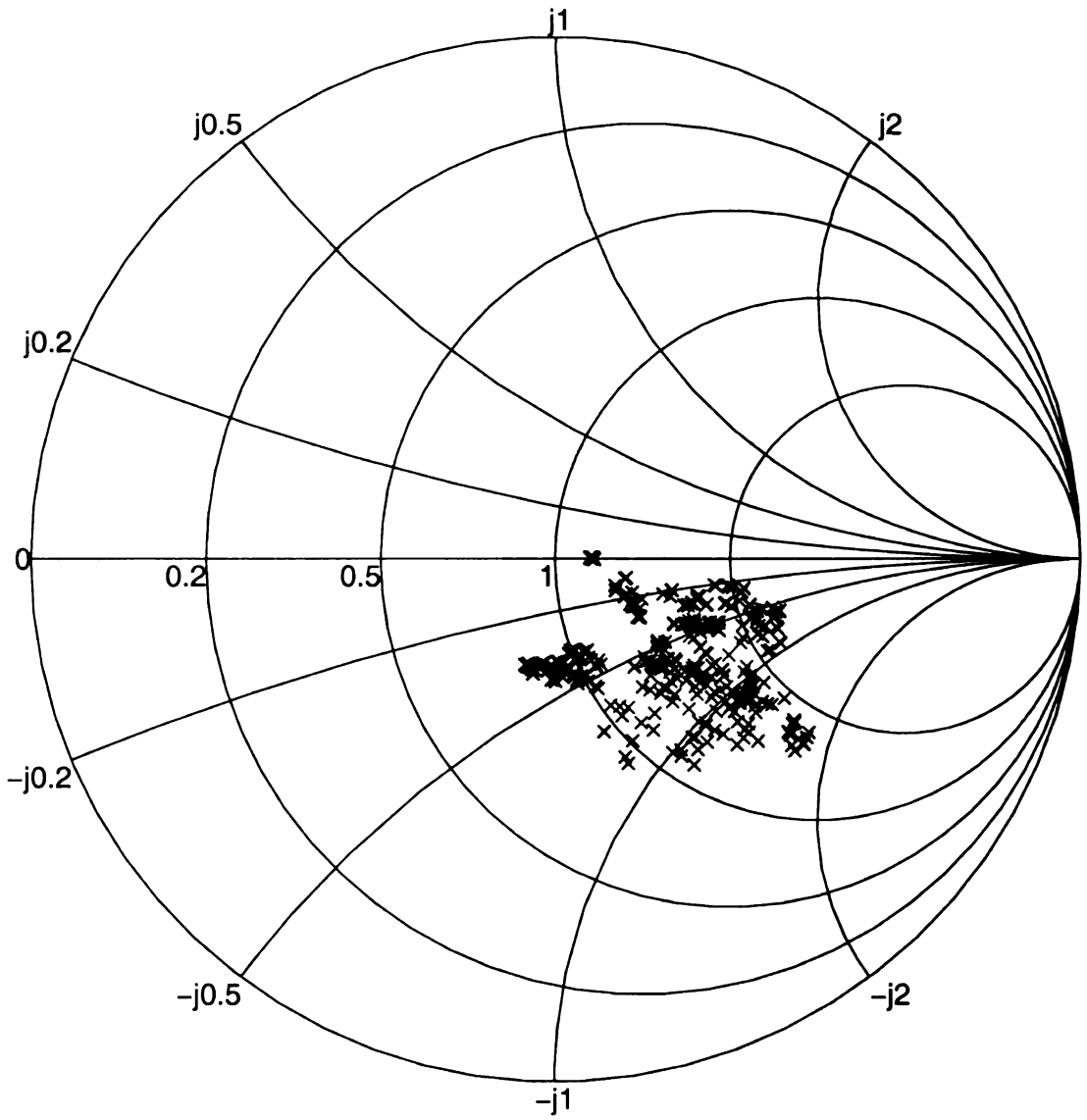


Figure 5.78. Smith chart for the layer 2 Type II SSA template above ground at 780 MHz.

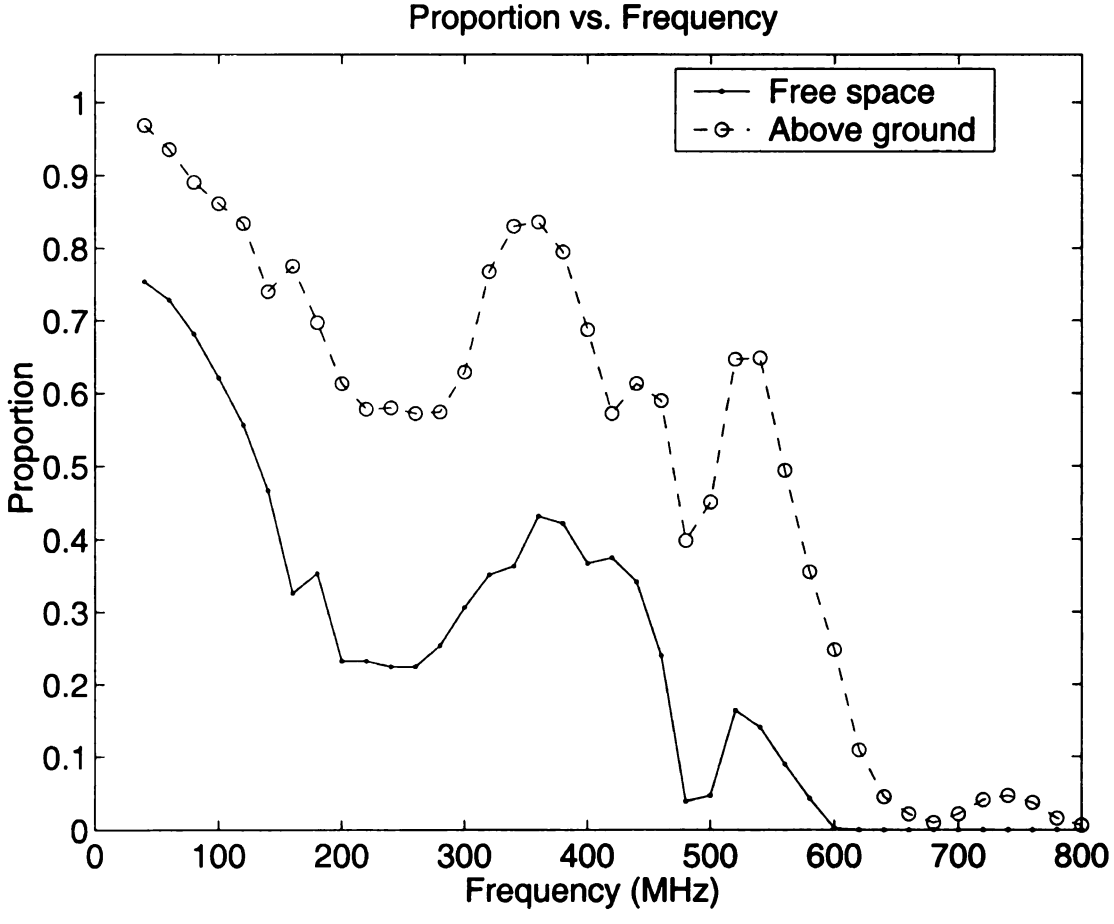


Figure 5.79. Proportion of configurations with minimum vertical gains in the horizontal plane above -3.0 dB vs. frequency for the layer 2 Type II SSA template (linear scale).

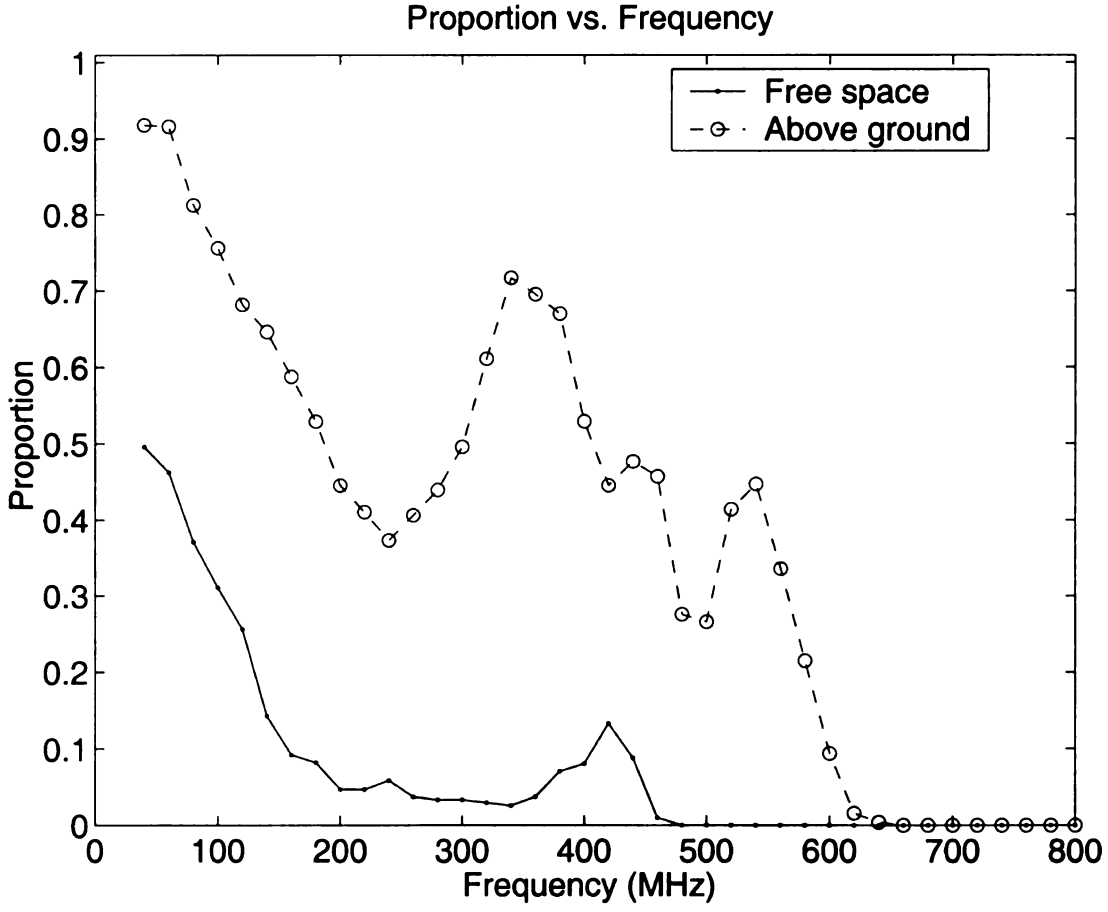


Figure 5.80. Proportion of configurations with minimum vertical gains in the horizontal plane above 0 dB vs. frequency for the layer 2 Type II SSA template (linear scale).

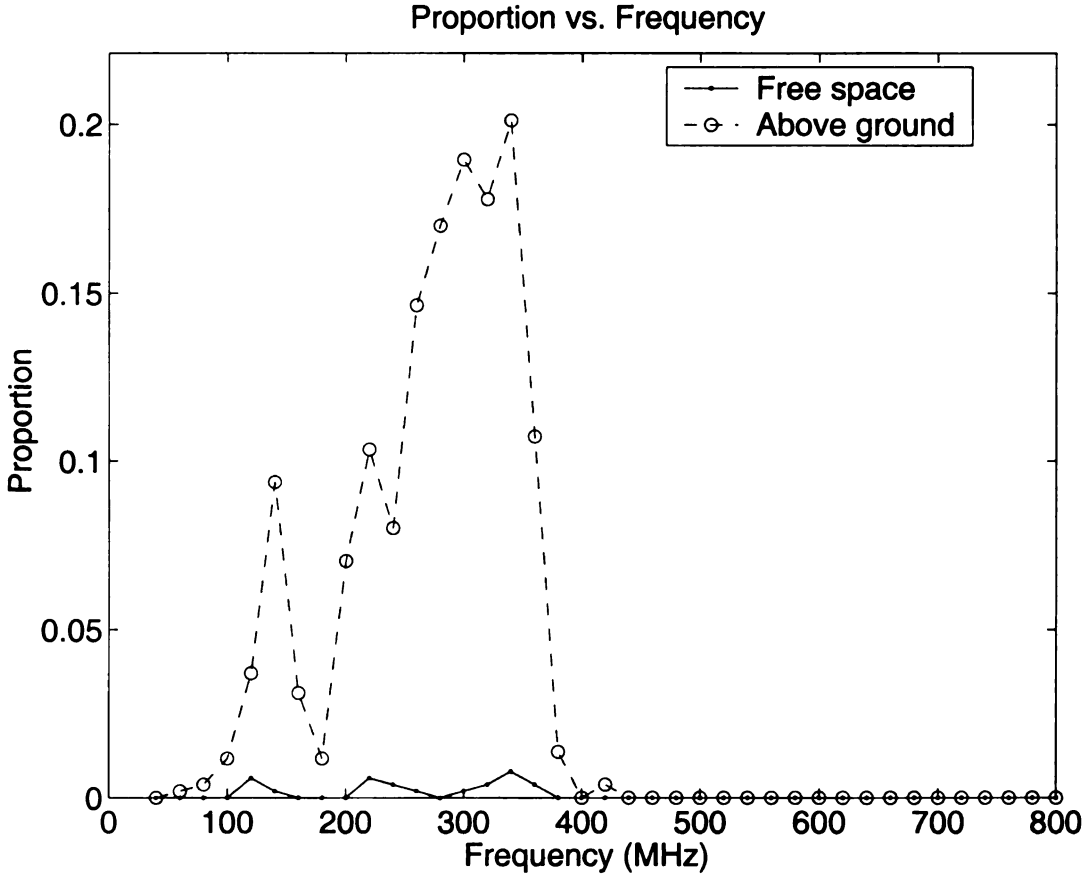


Figure 5.81. Proportion of configurations with SWRs less than 2.0 and minimum vertical gains in the horizontal plane above 0 dB vs. frequency for the layer 2 Type II SSA template (linear scale).

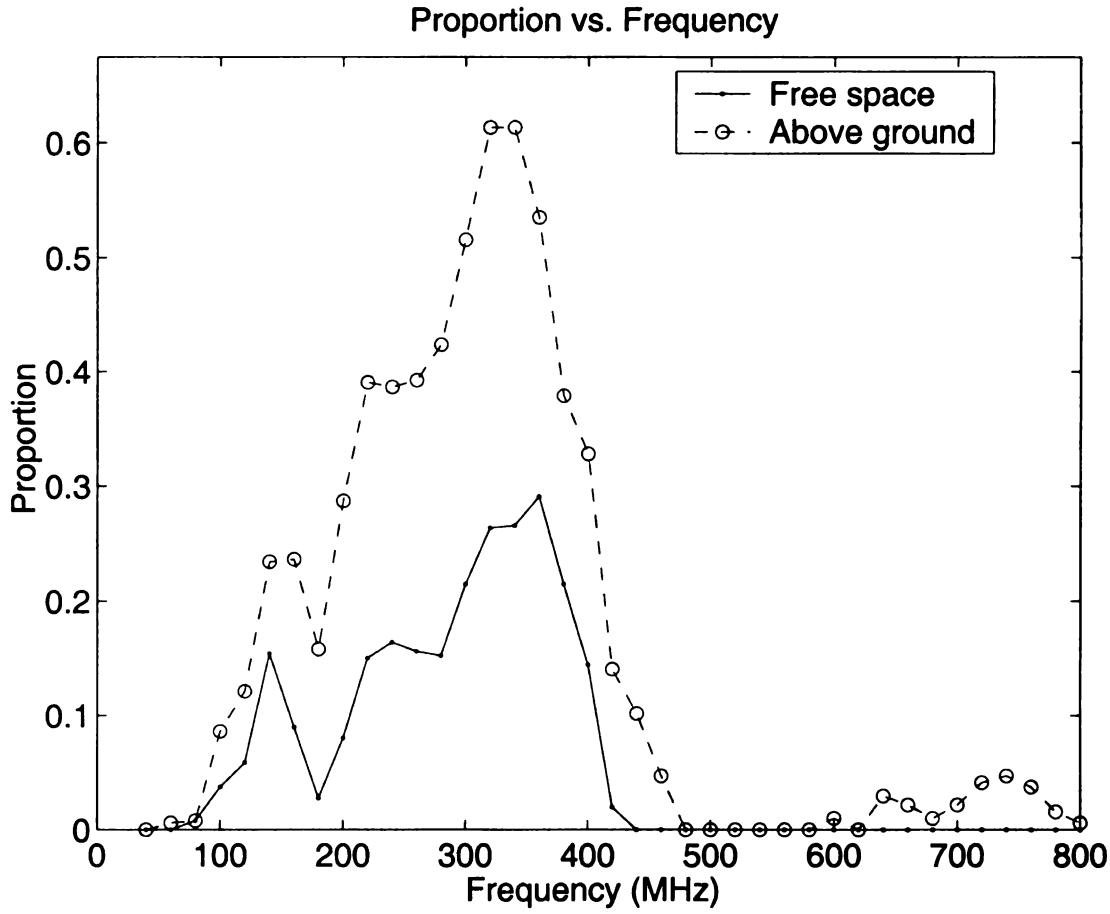


Figure 5.82. Proportion of configurations with SWRs less than 4.0 and minimum vertical gains in the horizontal plane above -3.0 dB vs. frequency for the layer 2 Type II SSA template (linear scale).

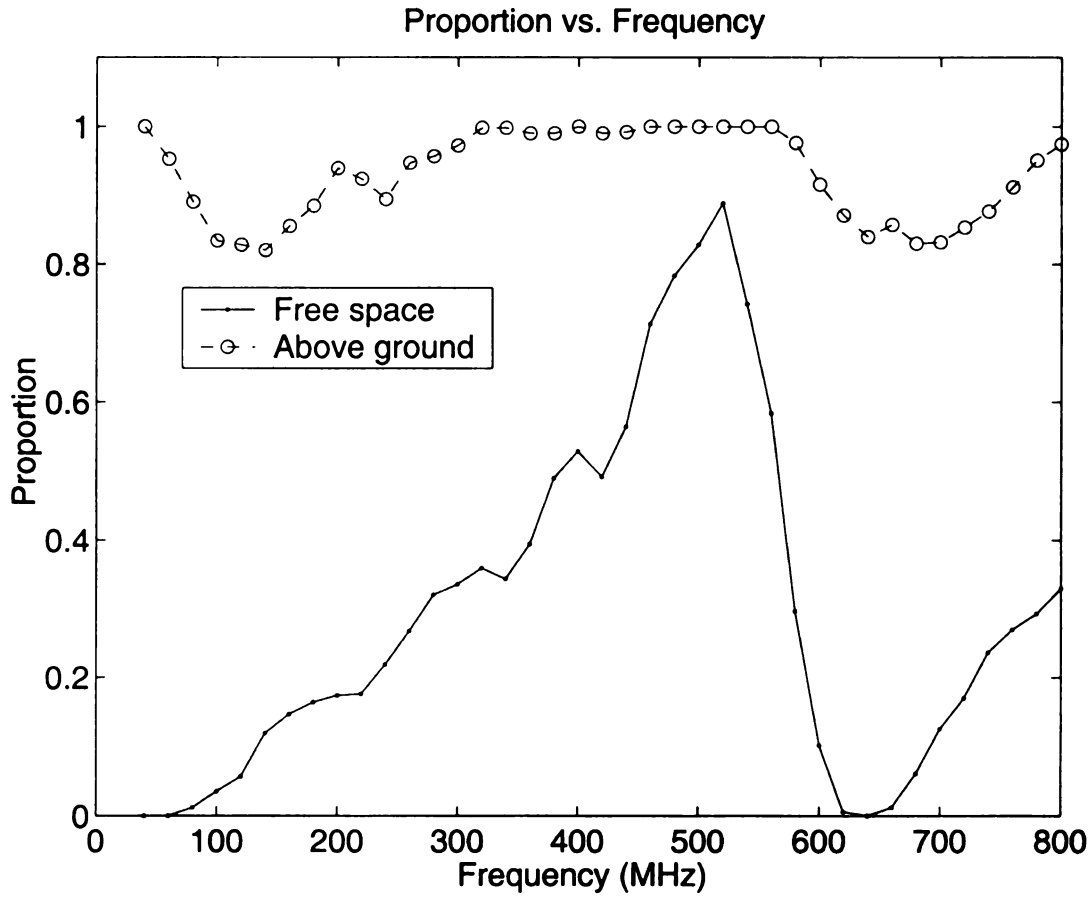


Figure 5.83. Proportion of configurations with maximum vertical gains in the horizontal plane above 3.0 dB vs. frequency for the layer 2 Type II SSA template (linear scale).

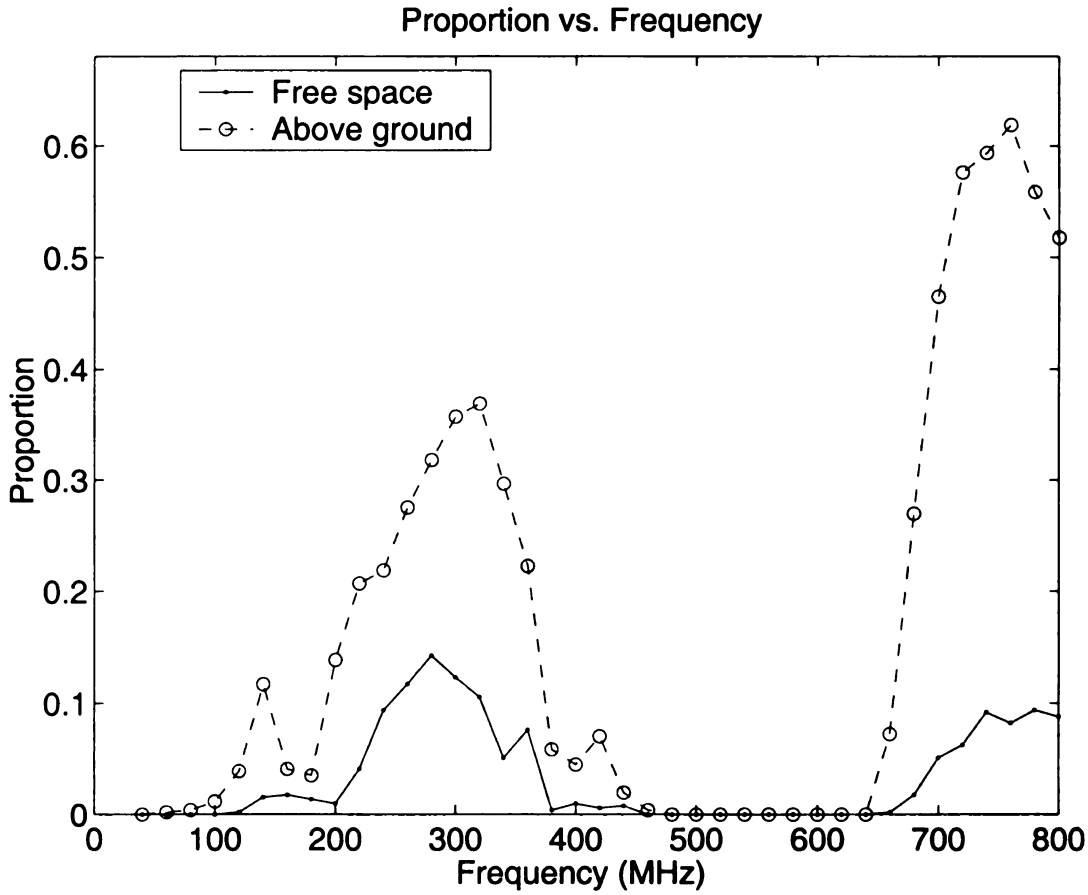


Figure 5.84. Proportion of configurations with SWRs less than 2.0 and maximum vertical gains in the horizontal plane above 3.0 dB vs. frequency for the layer 2 Type II SSA template (linear scale).

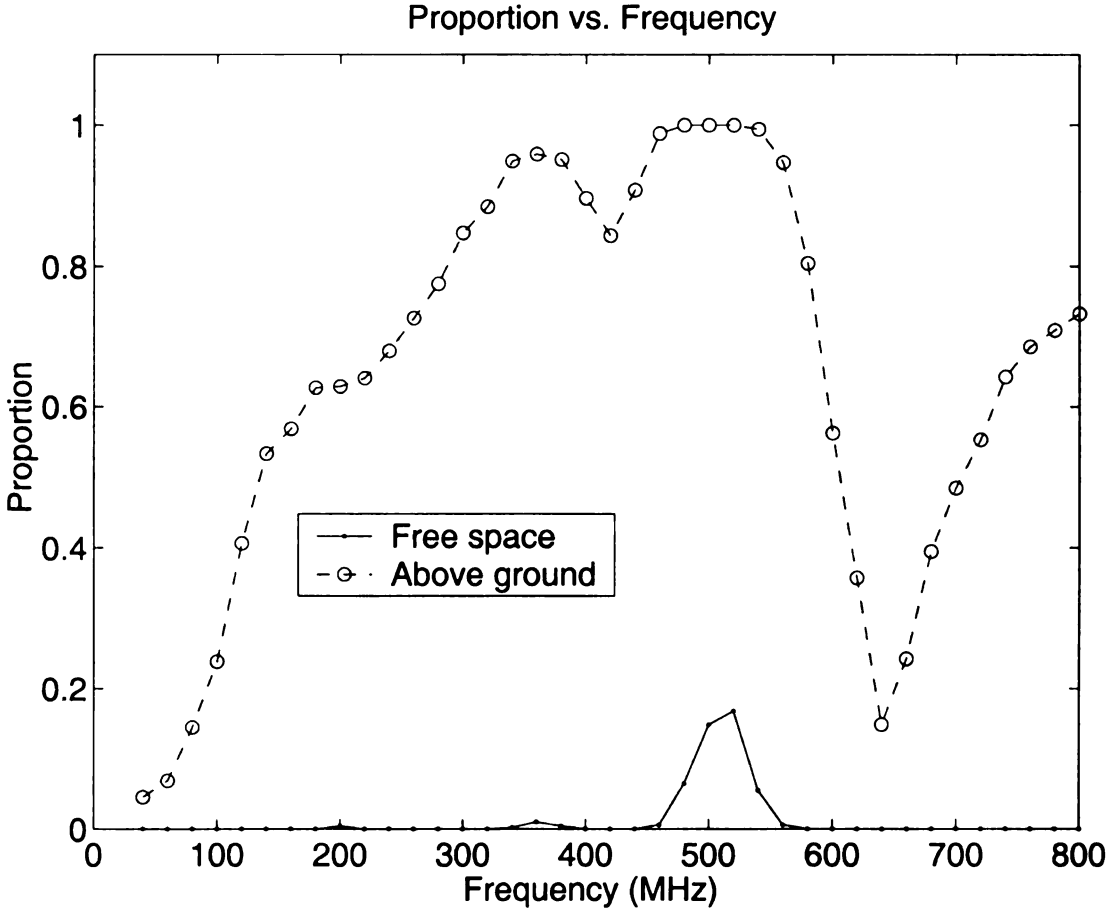


Figure 5.85. Proportion of configurations with maximum vertical gains in the horizontal plane above 6.0 dB vs. frequency for the layer 2 Type II SSA template (linear scale).

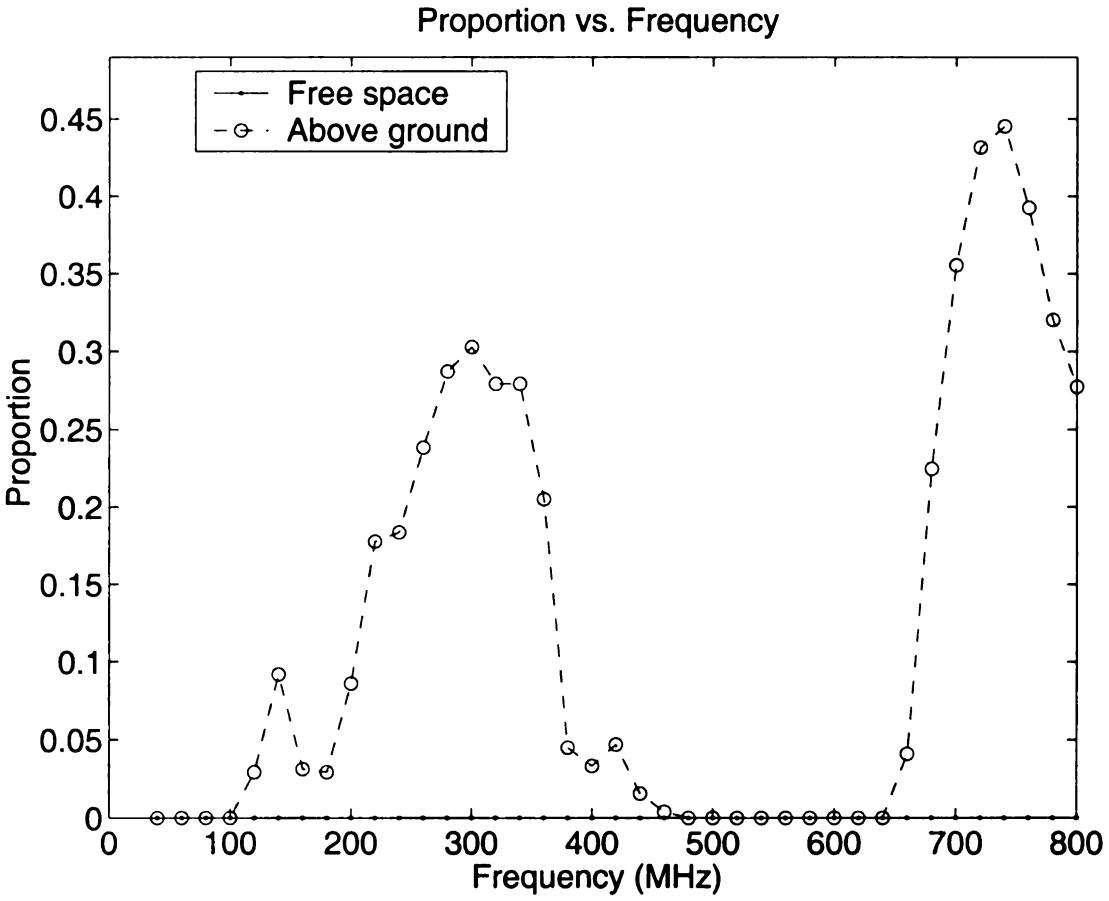


Figure 5.86. Proportion of configurations with SWRs less than 2.0 and maximum vertical gains in the horizontal plane above 6.0 dB vs. frequency for the layer 2 Type II SSA template (linear scale).

5.3.4 Layer 2.5 SSA Template

The layer 2.5 SSA template, shown in Figure 5.87, uses twelve switches for 4,096 possible configurations. The dimensions of the layer 2.5 Type I and Type II SSA templates are shown in Table 5.9 and Table 5.10, respectively. This is the highest layer that is searched exhaustively.



THESIS
S
2002

LIBRARY
Michigan State
University

PLACE IN RETURN BOX to remove this checkout from your record.
TO AVOID FINES return on or before date due.
MAY BE RECALLED with earlier due date if requested.

DATE DUE	DATE DUE	DATE DUE
03307 MAR 07 2007		

6/01 c:/CIRC/DateDue.p65-p.15

SELF-STRUCTURING ANTENNAS

VOLUME II

By

Christopher Mark Coleman

A DISSERTATION

Submitted to
Michigan State University
in partial fulfillment of the requirements
for the degree of

DOCTOR OF PHILOSOPHY

Department of Electrical and Computer Engineering

2002

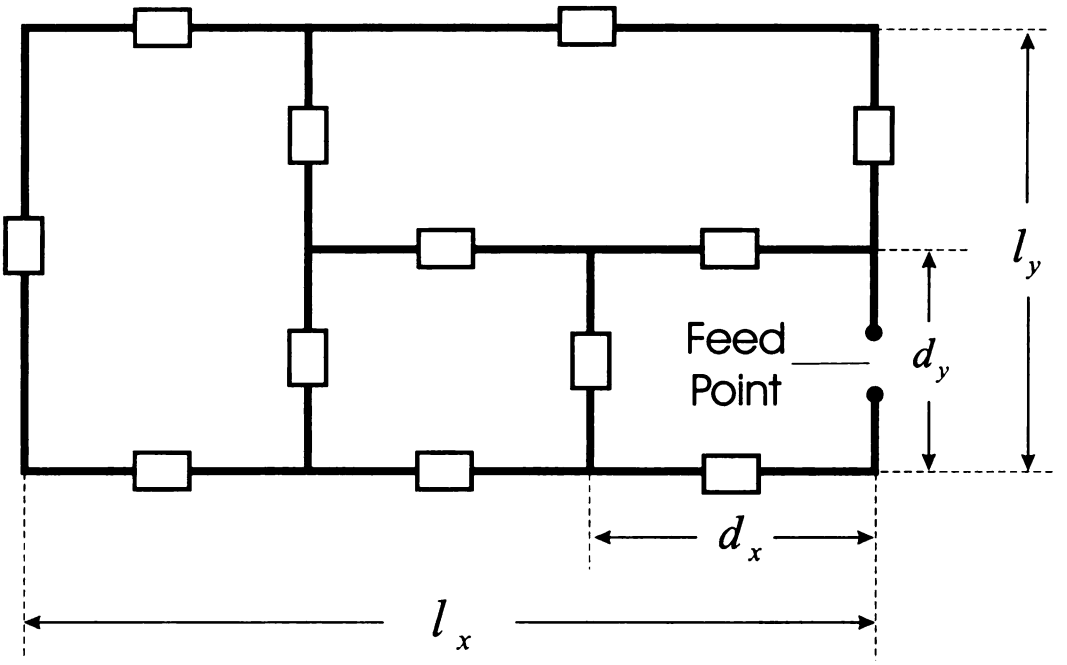


Figure 5.87. Diagram of the layer 2.5 SSA template.

5.3.4.1 Layer 2.5 Type I SSA Template

Plots of the SWRs of the 4096 SSA configurations at each frequency are shown in Figure 5.88 and Figure 5.89 for the layer 2.5 Type I templates in free space and above ground, respectively. As is the case for the layer 2 Type I template, nearly continuous bands of possible SWR values exist at each studied frequency. Above 200 MHz, configurations exhibit many SWR values close to 1.0. The wide range of possible impedance values at 800 MHz is illustrated in the Smith charts shown in Figure 5.91 and Figure 5.92 for the templates in free space and above ground, respectively. The minimum SWR at each frequency is shown in Figure 5.90 for the templates in free space and above ground.

Figure 5.93 shows the proportion of configurations with SWRs less than 4.0 for the layer 2.5 Type I templates in free space and above ground. This figure uses a linear scale on the vertical axis, as is done with the proportion plots for layers 2

Table 5.9. Dimensions of the layer 2.5 Type I SSA template.

l_x	25.7 cm
d_x	8.57 cm
l_y	17.1 cm
d_y	8.57 cm
Outer electrical dimensions at 40 MHz	$0.0343\lambda \times 0.0229\lambda$
Outer electrical dimensions at 800 MHz	$0.686\lambda \times 0.457\lambda$

Table 5.10. Dimensions of the layer 2.5 Type II SSA template.

l_x	60.0 cm
d_x	20.0 cm
l_y	60.0 cm
d_y	30.0 cm
Outer electrical dimensions at 40 MHz	$0.0800\lambda \times 0.0800\lambda$
Outer electrical dimensions at 800 MHz	$1.60\lambda \times 1.60\lambda$

and less. Figure captions indicate the use of linear vertical scales for the proportion plots presented in this chapter. Layers 2.5 and higher have many possible configurations, and logarithmic proportion plots are also instructive because large variations in proportion can be better viewed in the same figure. This is seen in a plot of the proportion of configurations with SWRs less than 4.0 found in Figure 5.94 using a logarithmic scale. Data is only plotted on the logarithmic plots for frequencies at which non-zero proportions exist. Notice that below 300 MHz, it is easier to view the proportions in Figure 5.94 than it is in Figure 5.93. These small proportions may be important because there are many total configurations for the higher layer SSA templates.

Figure 5.95 shows the proportion of configurations with SWRs less than 3.0 for the layer 2.5 Type I templates in free space and above ground. With 4096 total possible configurations, proportions higher than 10^{-3} correspond to four or more

configurations, proportions higher than 10^{-2} correspond to 40 or more configurations, and proportions higher than 10^{-1} correspond to 400 or more configurations. Therefore, four or more configurations have SWRs less than 3.0 above 180 MHz, 40 or more above 220 MHz, and 400 or more above 400 MHz. Figure 5.96 shows that 400 to 800 of the possible configurations (10% to 20%) have SWRs less than 2.0 above 500 MHz. Figure 5.97 shows that 40 or more configurations have SWRs less than 1.5 above 400 MHz. The total number of successful configurations grows for higher layers for an equal proportion of successful configurations.

Figure 5.98 shows the proportion of configurations with SWRs less than 1.1. Few configurations meet this requirement across the band, and this is seen in the discrete jumps in proportion between frequencies. The proportion of a single configuration to the total possible configurations is roughly $1/4096 \simeq 2.44 \times 10^{-4}$. Discrete jumps occur that are close to this value.

The proportion of configurations with minimum vertical gains in the horizontal plane above 0 dB is shown in Figure 5.99 for the layer 2.5 Type I template in free space and above ground. More than 10% of the configurations meet the 0 dB gain criterion below 400 MHz for the template in free space. The template above ground exhibits higher proportions at every studied frequency. Figure 5.100 shows that above 200 MHz, there are configurations of the template above ground at every frequency that have SWRs less than 2.0 and minimum vertical gains above 0 dB. However, there are many frequencies above 200 MHz where no configurations meet these SWR and gain criteria for the template in free space.

Figure 5.101 shows the proportion of configurations with maximum vertical gains in the horizontal plane above 3.0 dB. Again, the template above ground has much higher proportions at every frequency than does the template in free space. However, as shown in Figure 5.102, less than three times as many configurations for the template above ground have SWRs less than 2.0 and maximum gains above 3.0 dB than

those for the template in free space above 540 MHz. Over 120 of the 4096 possible configurations meet these criteria for the template in free space above 540 MHz.

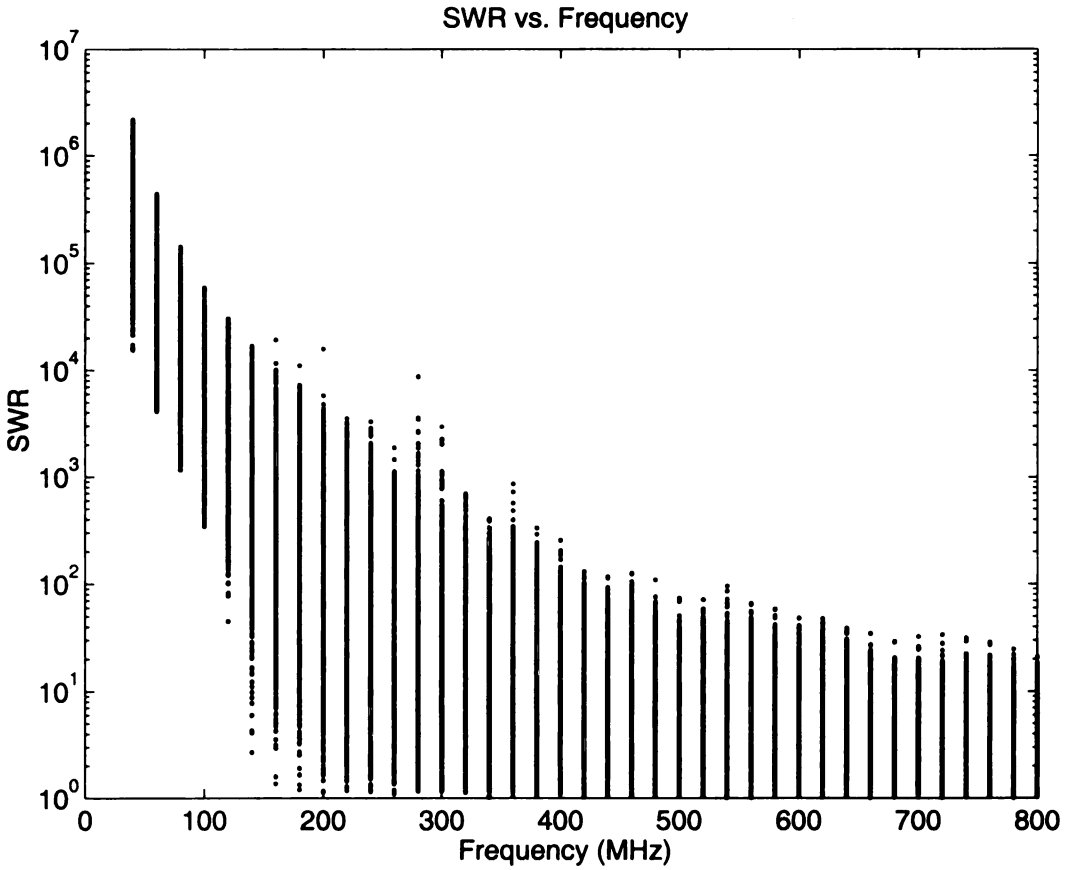


Figure 5.88. SWR vs. frequency for the layer 2.5 Type I SSA template in free space.

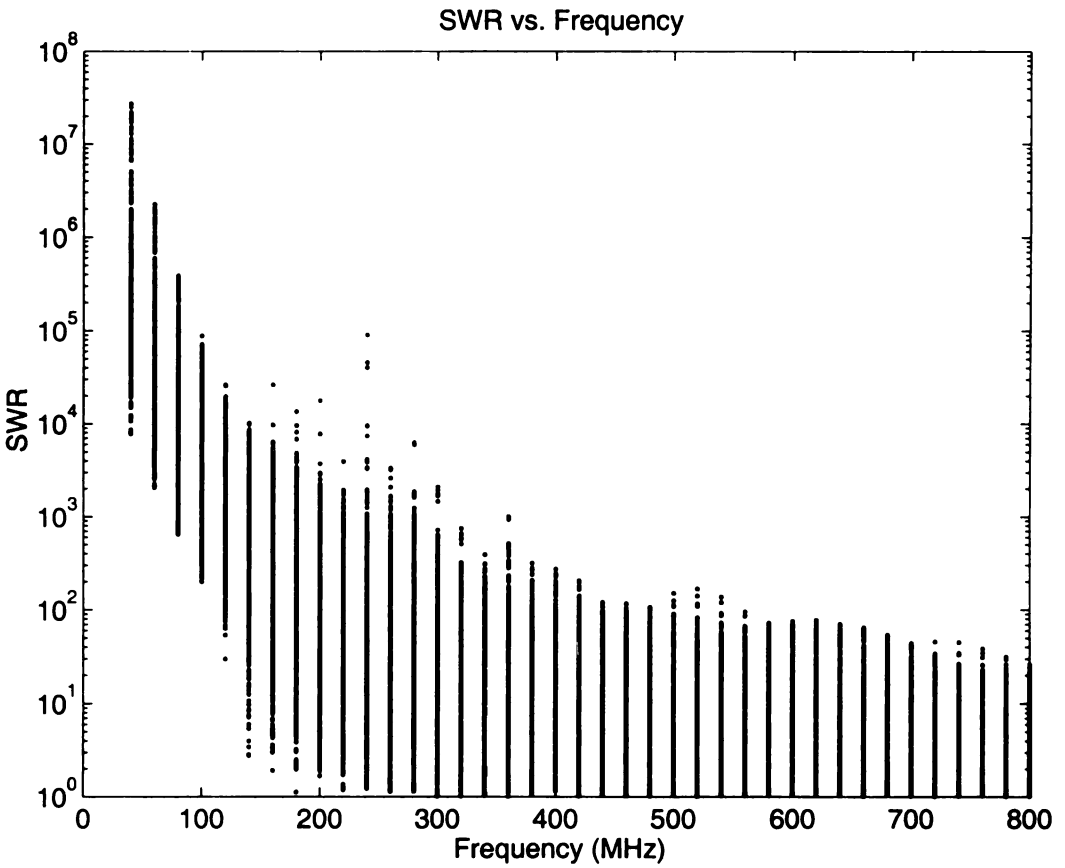


Figure 5.89. SWR vs. frequency for the layer 2.5 Type I SSA template above ground.

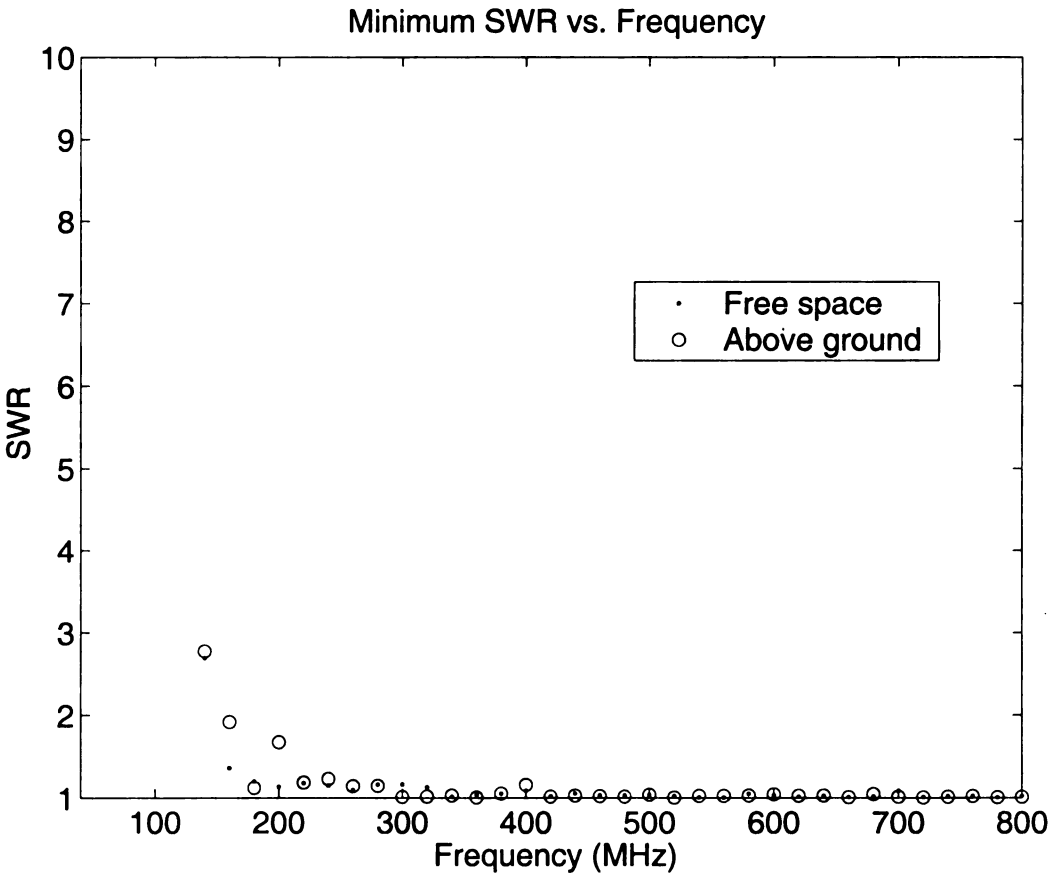


Figure 5.90. Minimum SWR vs. frequency for the layer 2.5 Type I SSA template.

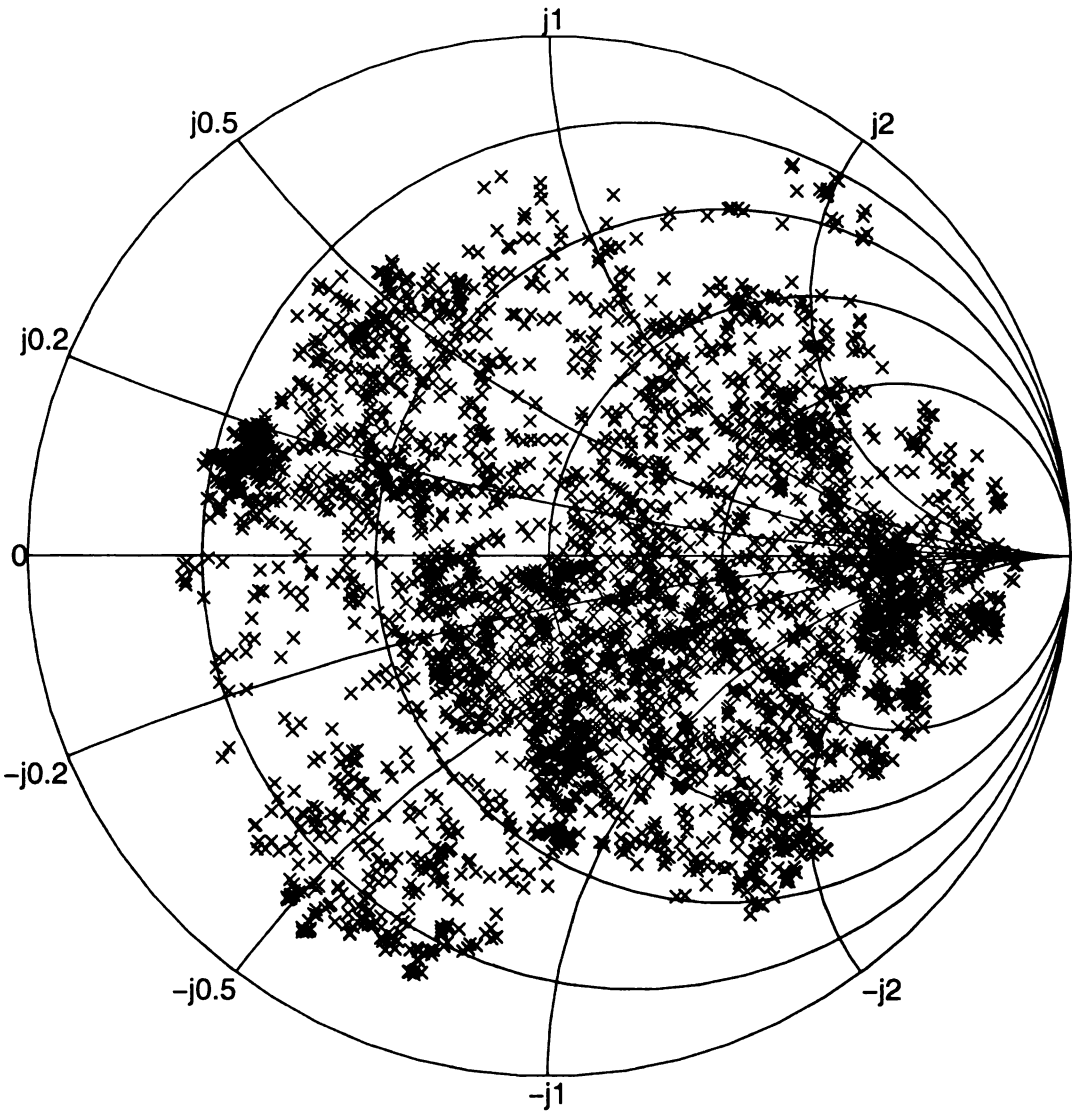


Figure 5.91. Smith chart for the layer 2.5 Type I SSA template in free space at 800 MHz.

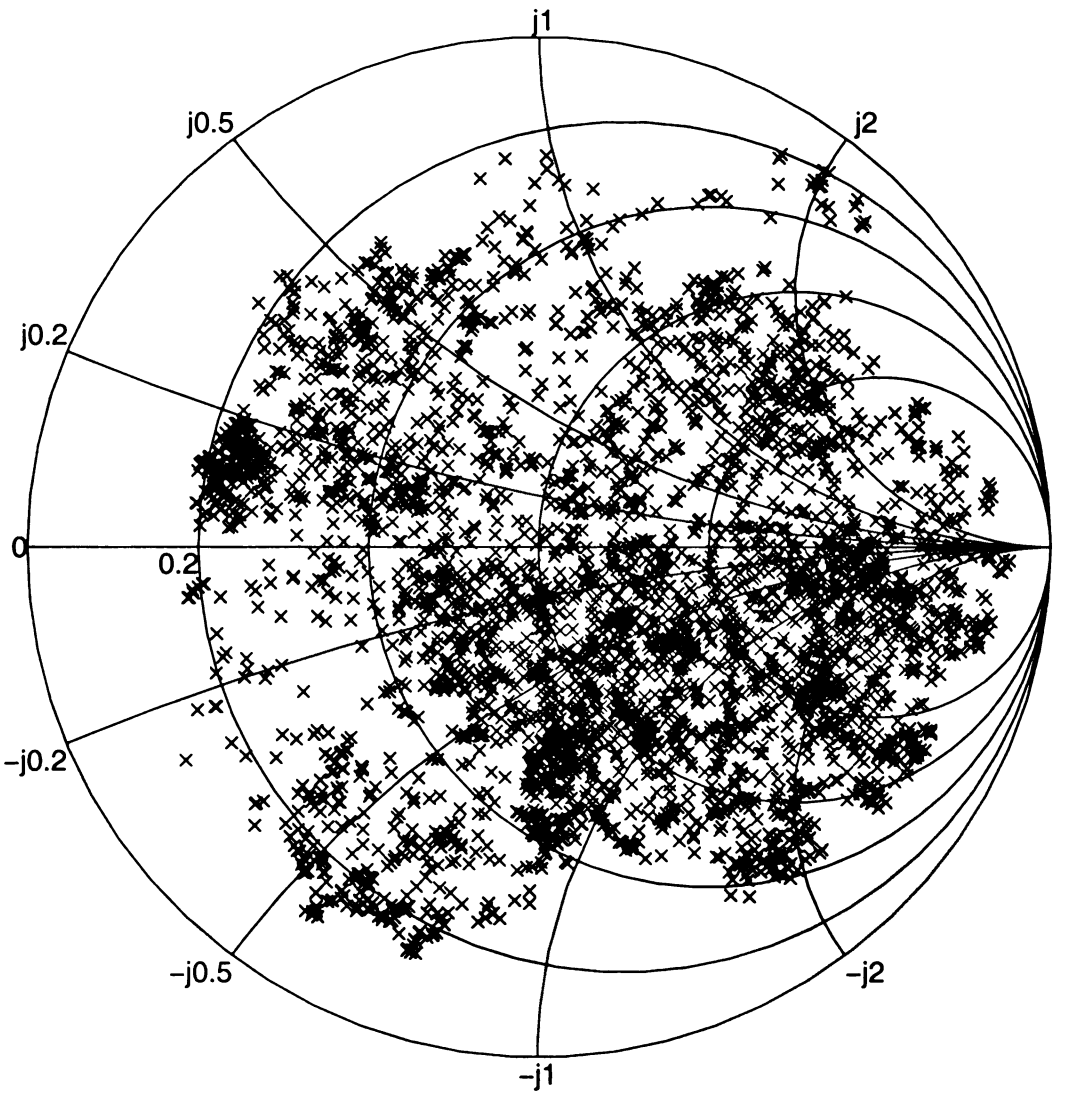


Figure 5.92. Smith chart for the layer 2.5 Type I SSA template above ground at 800 MHz.

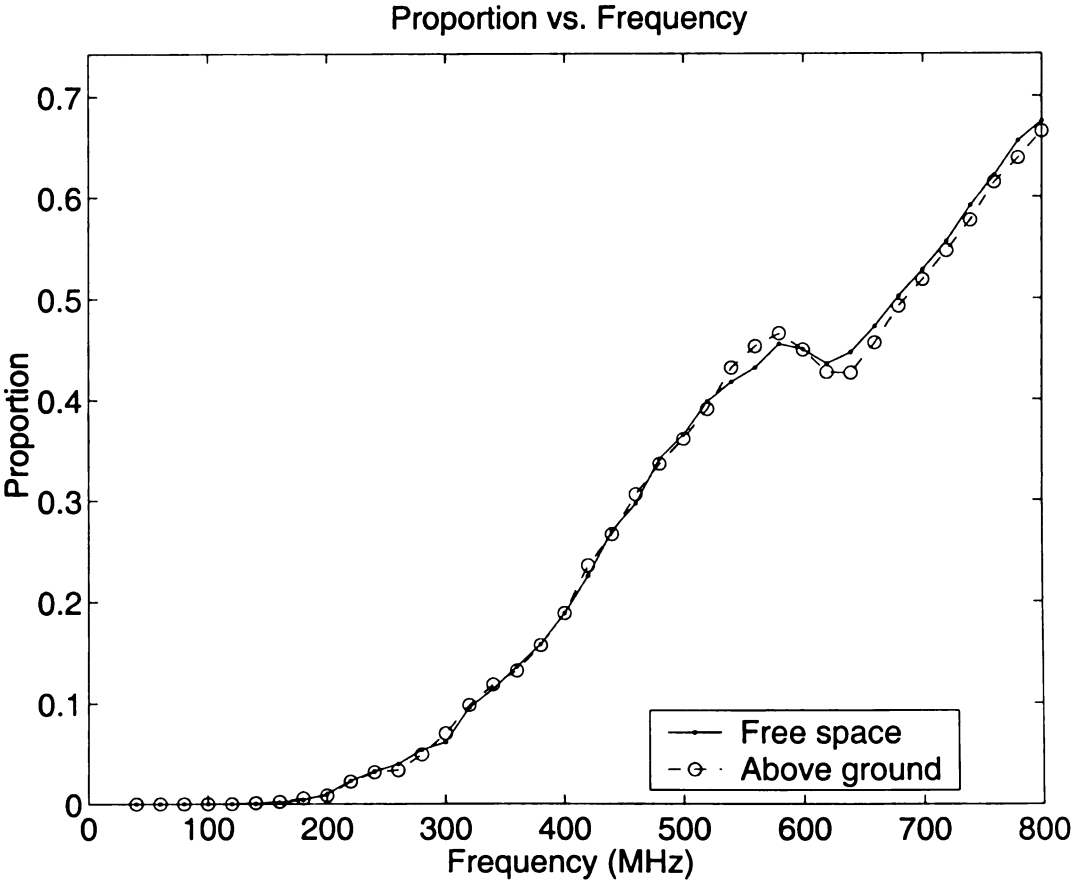


Figure 5.93. Proportion of configurations with SWRs less than 4.0 vs. frequency for the layer 2.5 Type I SSA template (linear scale).

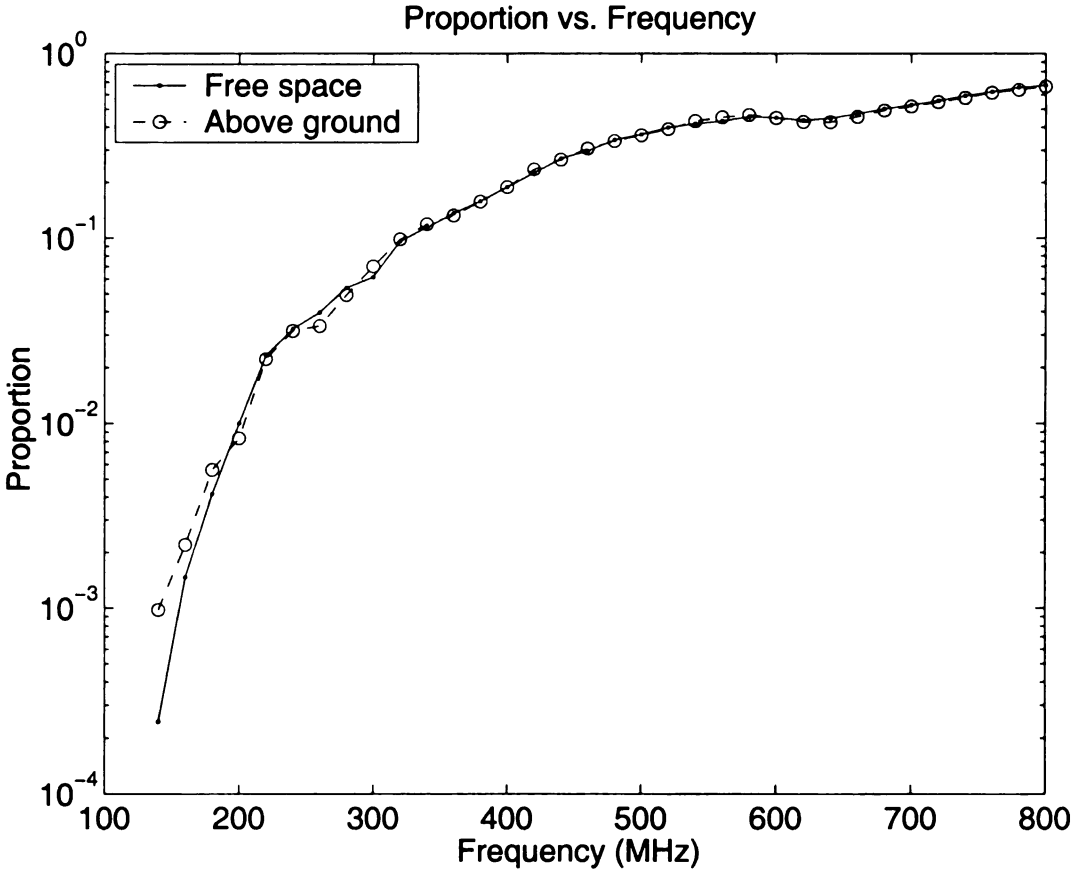


Figure 5.94. Proportion of configurations with SWRs less than 4.0 vs. frequency for the layer 2.5 Type I SSA template.

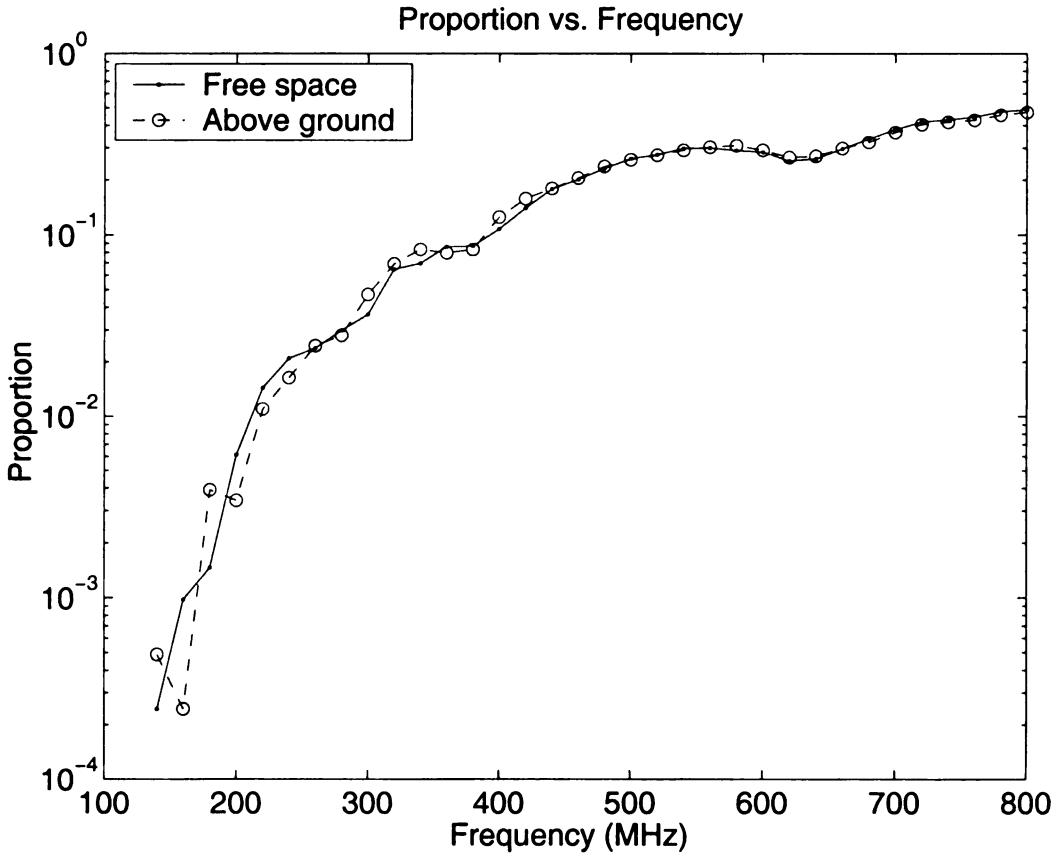


Figure 5.95. Proportion of configurations with SWRs less than 3.0 vs. frequency for the layer 2.5 Type I SSA template.

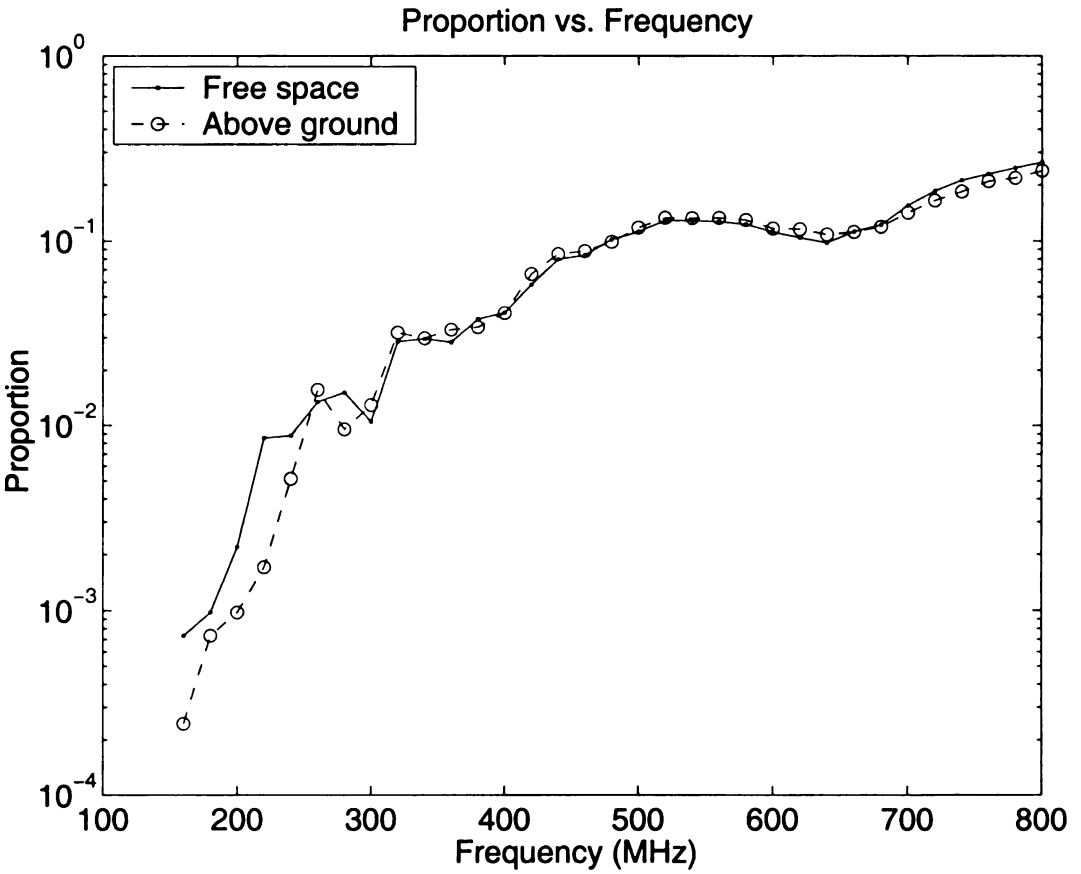


Figure 5.96. Proportion of configurations with SWRs less than 2.0 vs. frequency for the layer 2.5 Type I SSA template.

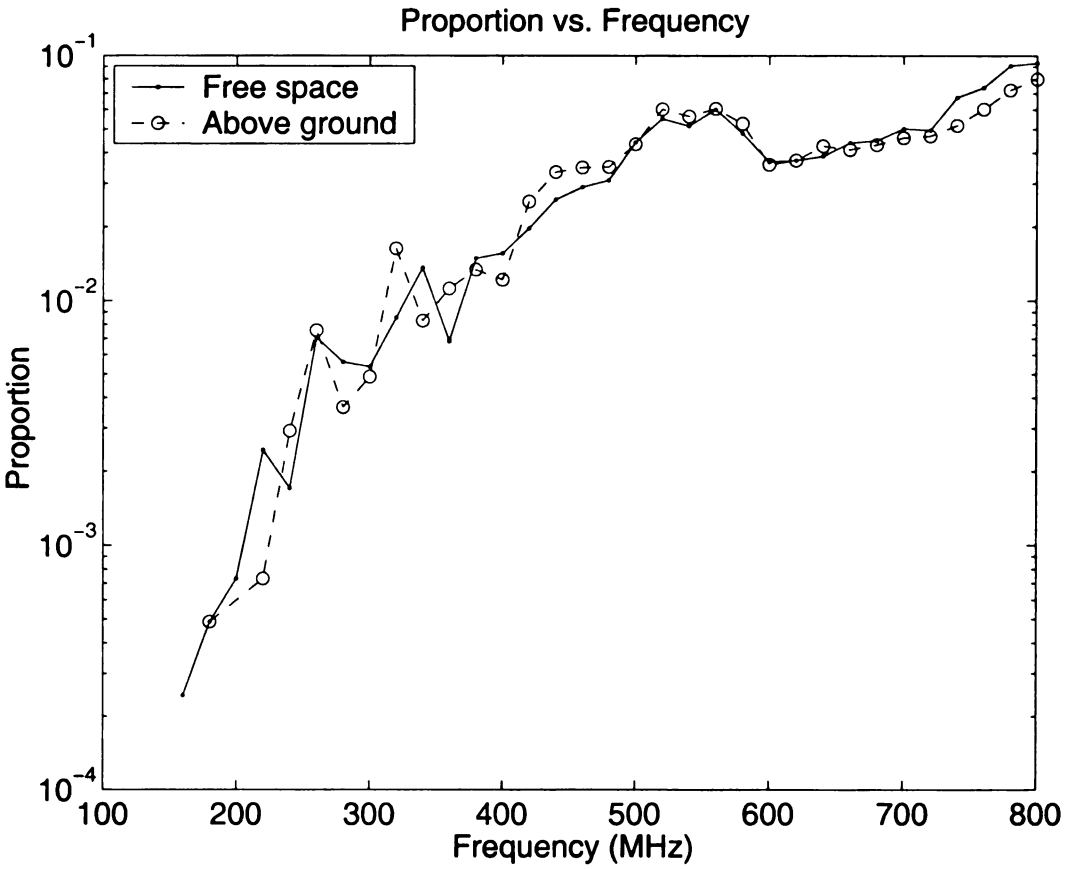


Figure 5.97. Proportion of configurations with SWRs less than 1.5 vs. frequency for the layer 2.5 Type I SSA template.

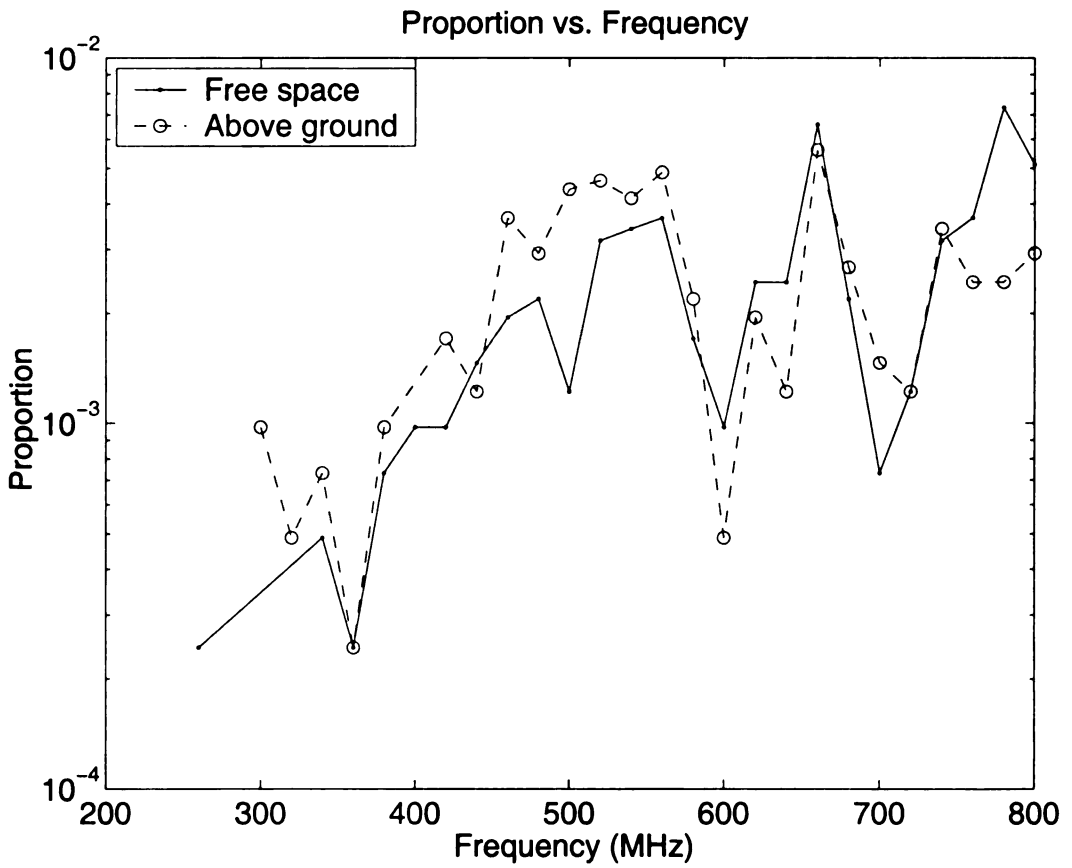


Figure 5.98. Proportion of configurations with SWRs less than 1.1 vs. frequency for the layer 2.5 Type I SSA template.

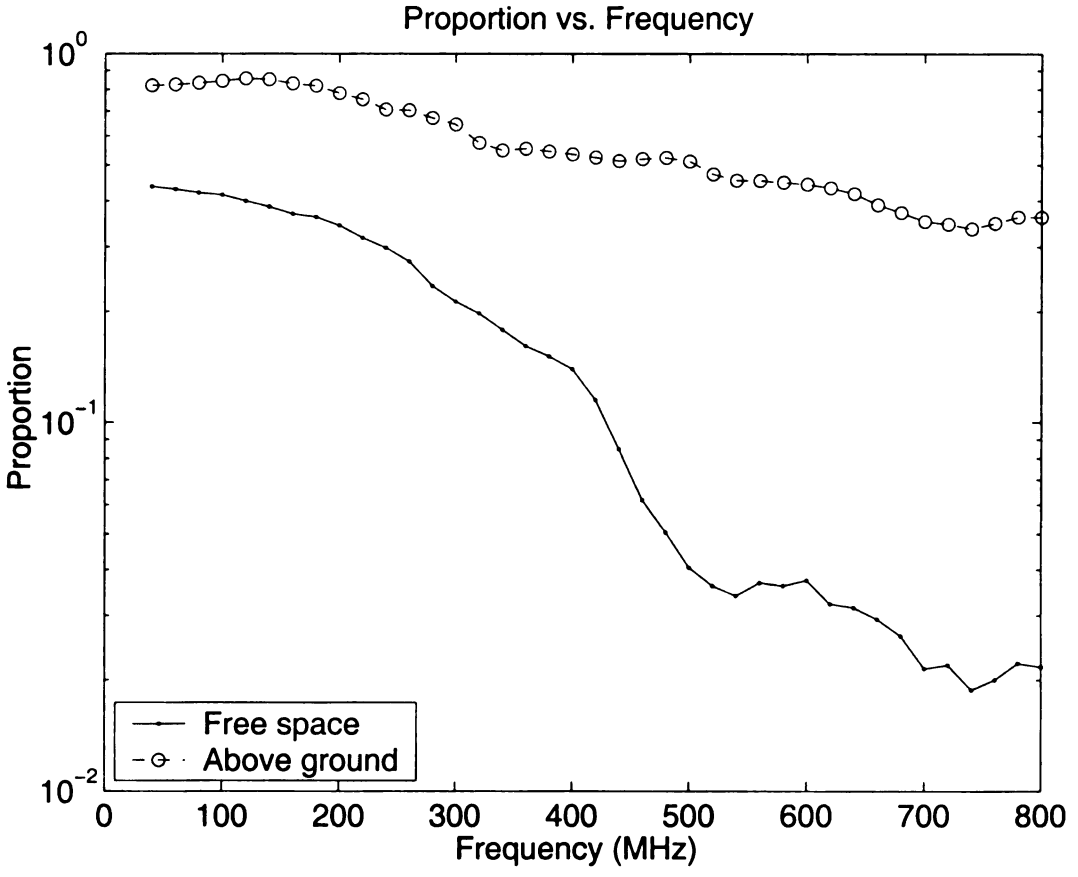


Figure 5.99. Proportion of configurations with minimum vertical gains in the horizontal plane above 0 dB vs. frequency for the layer 2.5 Type I SSA template.

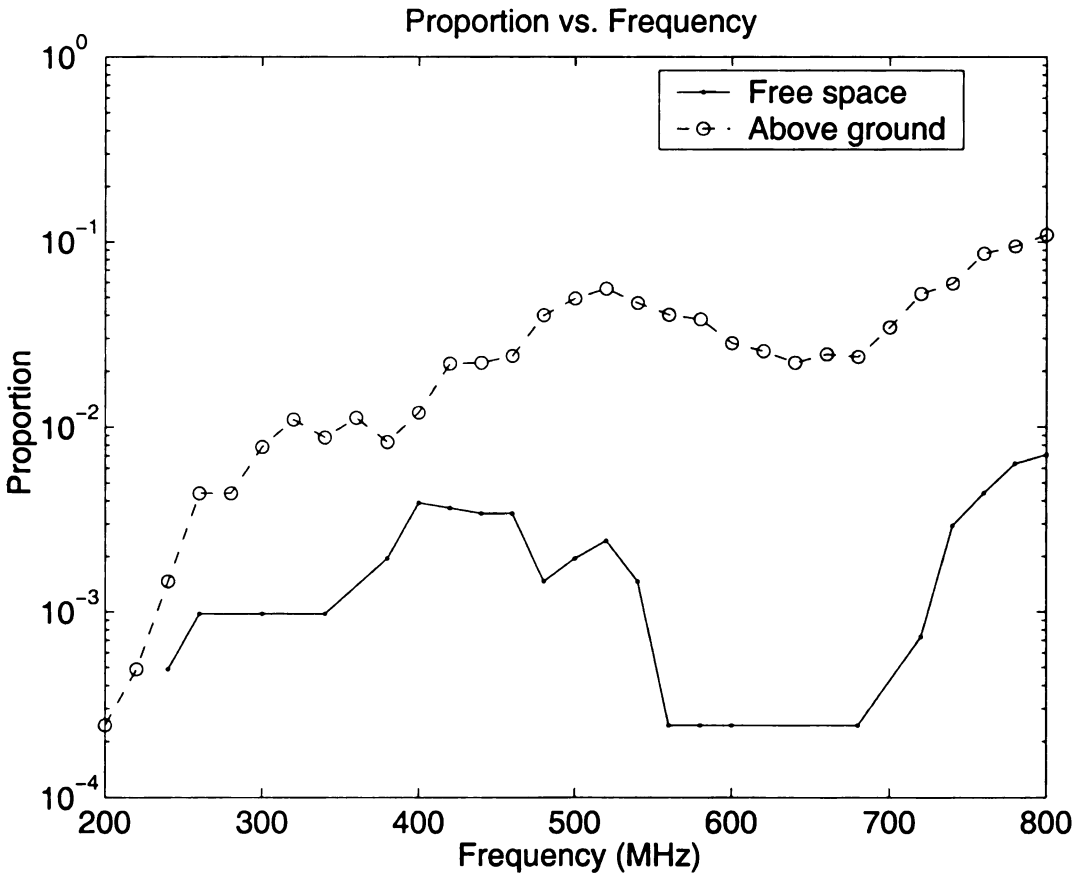


Figure 5.100. Proportion of configurations with SWRs less than 2.0 and minimum vertical gains in the horizontal plane above 0 dB vs. frequency for the layer 2.5 Type I SSA template.

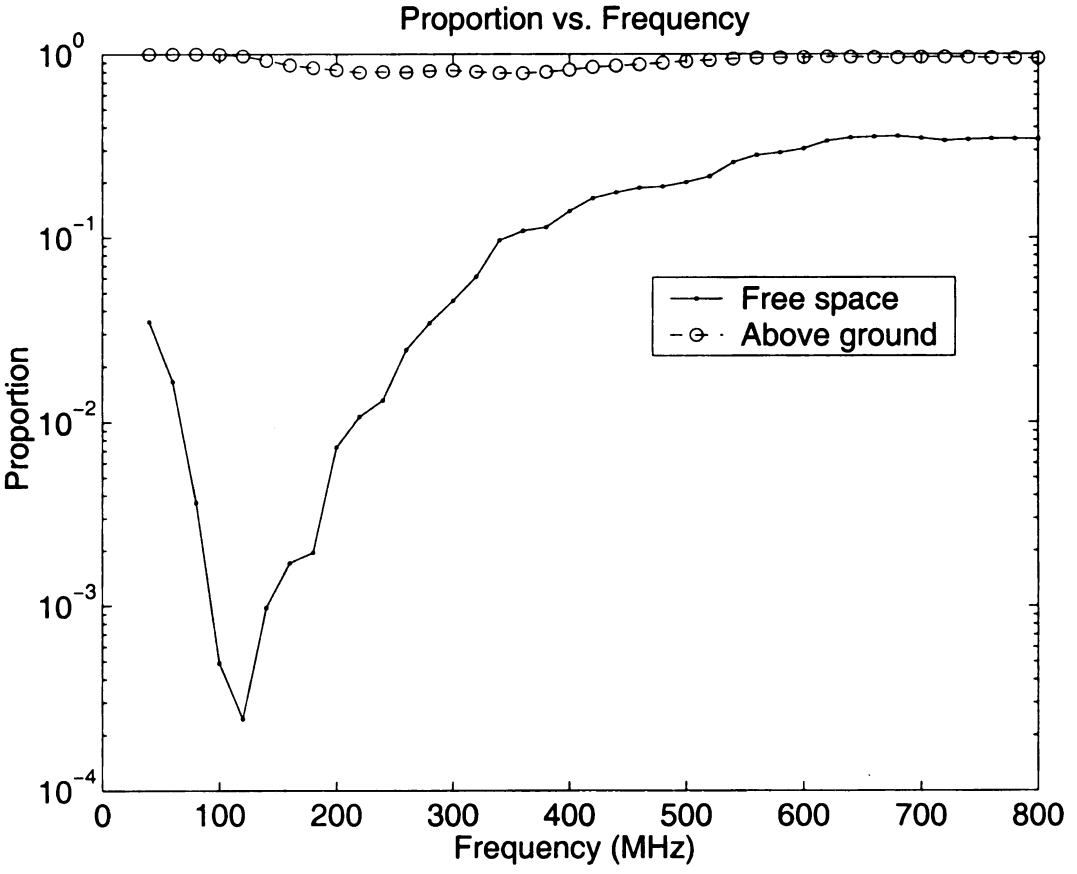


Figure 5.101. Proportion of configurations with maximum vertical gains in the horizontal plane above 3.0 dB vs. frequency for the layer 2.5 Type I SSA template.

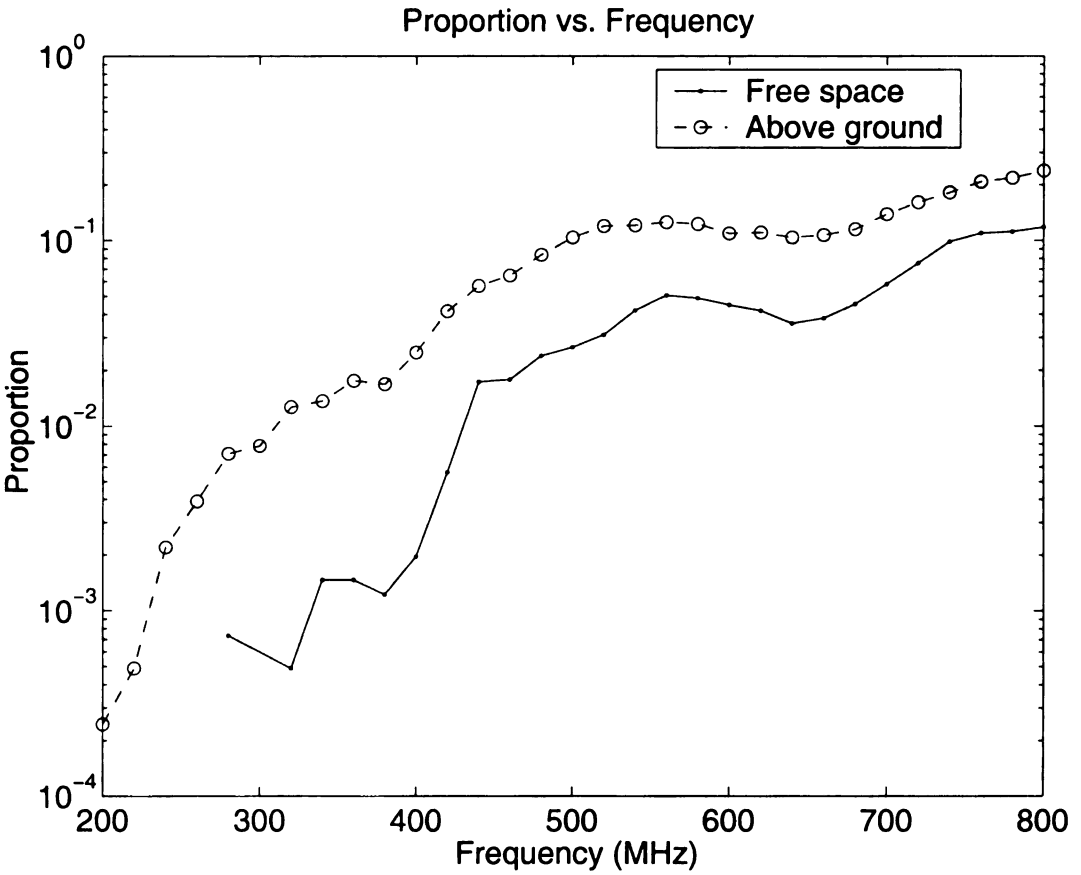


Figure 5.102. Proportion of configurations with SWRs less than 2.0 and maximum vertical gains in the horizontal plane above 3.0 dB vs. frequency for the layer 2.5 Type I SSA template.

5.3.4.2 Layer 2.5 Type II SSA Template

The outer dimensions of the Type II templates are shown in Table 5.10. Recall than the outer dimensions of all Type II template layers are equal.

Plots of the 4096 SWRs at each frequency are shown in Figure 5.103 and Figure 5.104 for the layer 2.5 Type II SSA templates in free space and above ground, respectively. Similarly to the layer 2 Type II templates, there is a band of frequencies where configurations with SWRs close to 1.0 do not exist for the layer 2.5 Type II templates. This is also shown in Figure 5.105, where the minimum achievable SWR

is plotted at each frequency. From 460 MHz to 800 MHz, extremely low SWRs are not possible at most frequencies.

The proportions of configurations with SWRs below 4.0, 2.0, and 1.5 are plotted in Figure 5.106 through Figure 5.108 for the layer 2.5 Type II SSA templates in free space and above ground. Notice a sharp drop in the proportion around 460 MHz. This is more pronounced in the proportion of configurations with SWRs below 2.0 plotted using a linear scale in Figure 5.109. The proportion drops from over 30% to below 5% as the frequency changes from 400 MHz to 460 MHz. A sequence of Smith charts from 380 MHz to 520 MHz shown in Figure 5.110 through Figure 5.117 for the template in free space illustrates the migration of impedances from low SWR regions of the Smith chart to higher regions and then back to low regions. At 460 MHz and 480 MHz, few of the configurations lie below SWRs of 2.0. The template above ground exhibits similar characteristics, so the Smith charts from 380 MHz to 520 MHz have been omitted for the sake of brevity.

Figure 5.118 shows the proportion of configurations with minimum vertical gains in the horizontal plane above 0 dB for the layer 2.5 Type II templates in free space and above ground. The proportions drop considerably near 450 MHz and 750 MHz for the template in free space and the template above ground, respectively. The proportion of configurations with SWRs less than 2.0 and minimum gains above 0 dB is shown in Figure 5.119. Above 400 MHz, no configurations meet the criteria for the template in free space, and few meet the criteria for the template above ground.

Figure 5.120 shows the proportion of configurations with maximum vertical gains above 3.0 dB for the layer 2.5 Type II SSA templates in free space and above ground. Almost all of the configurations for the template above ground meet the gain criterion, as do many configurations for the template in free space across most of the frequency band. However, an additional criterion requiring SWRs to be less than 2.0 greatly reduces the proportion of acceptable configurations at many frequencies, as shown in

Figure 5.121.

The study of the layer 2.5 Type I and Type II templates shows that the use of more switches for large numbers of possible configurations can increase the probability that configurations exist that meet performance criteria. Studies of higher layer templates are desirable, but they are difficult to perform exhaustively. Therefore, the layer 2.5 templates are the highest layer templates that are searched exhaustively, and random searches are performed for the higher layers.

Studies of the Type II templates are presented for layers 1, 1.5, 2, and 2.5. These templates perform poorly over large bands within the studied frequency range. For this reason and for the sake of brevity, results for Type II templates for layers higher than 2.5 (except layer 7, where the Type I and Type II templates are identical) are not presented in this dissertation.

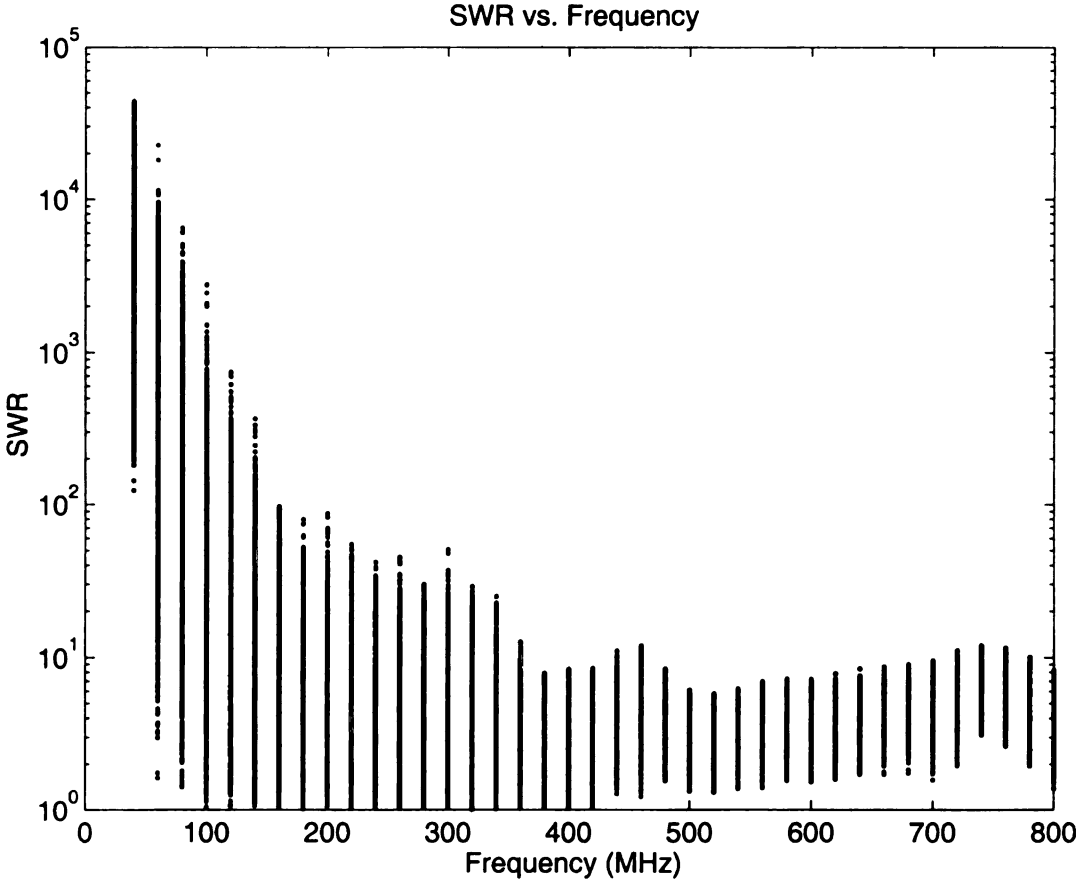


Figure 5.103. SWR vs. frequency for the layer 2.5 Type II SSA template in free space.

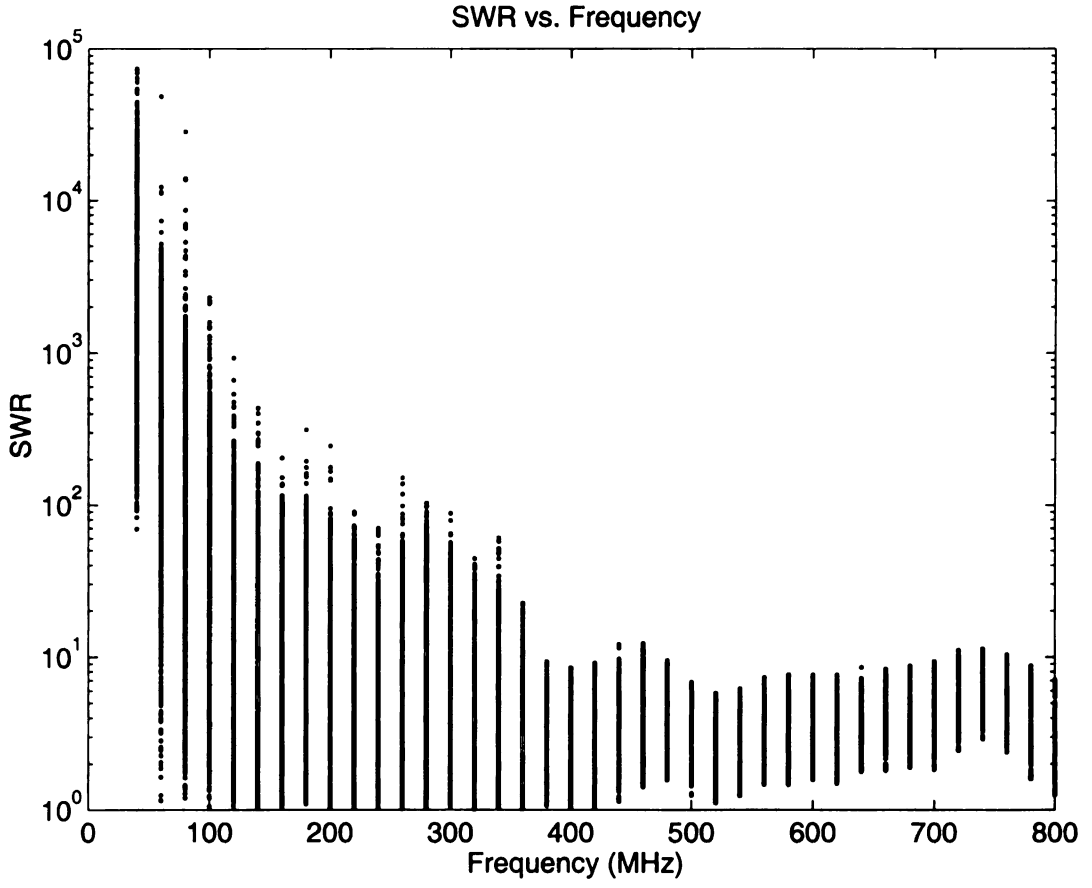


Figure 5.104. SWR vs. frequency for the layer 2.5 Type II SSA template above ground.

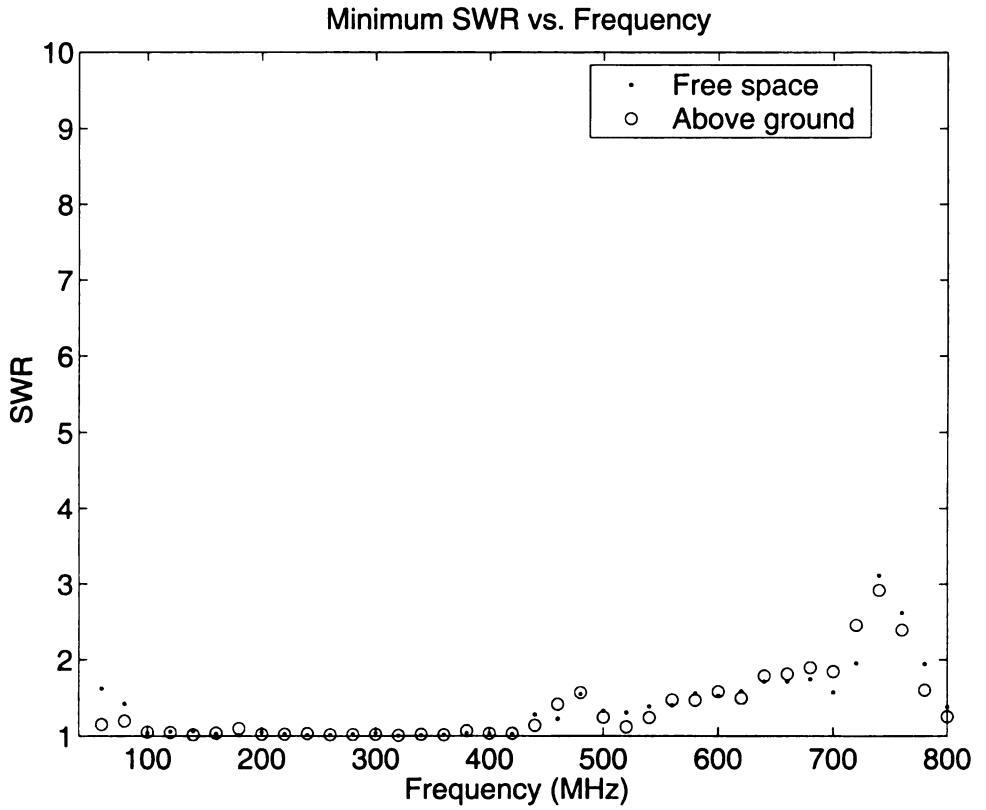


Figure 5.105. Minimum SWR vs. frequency for the layer 2.5 Type II SSA template.

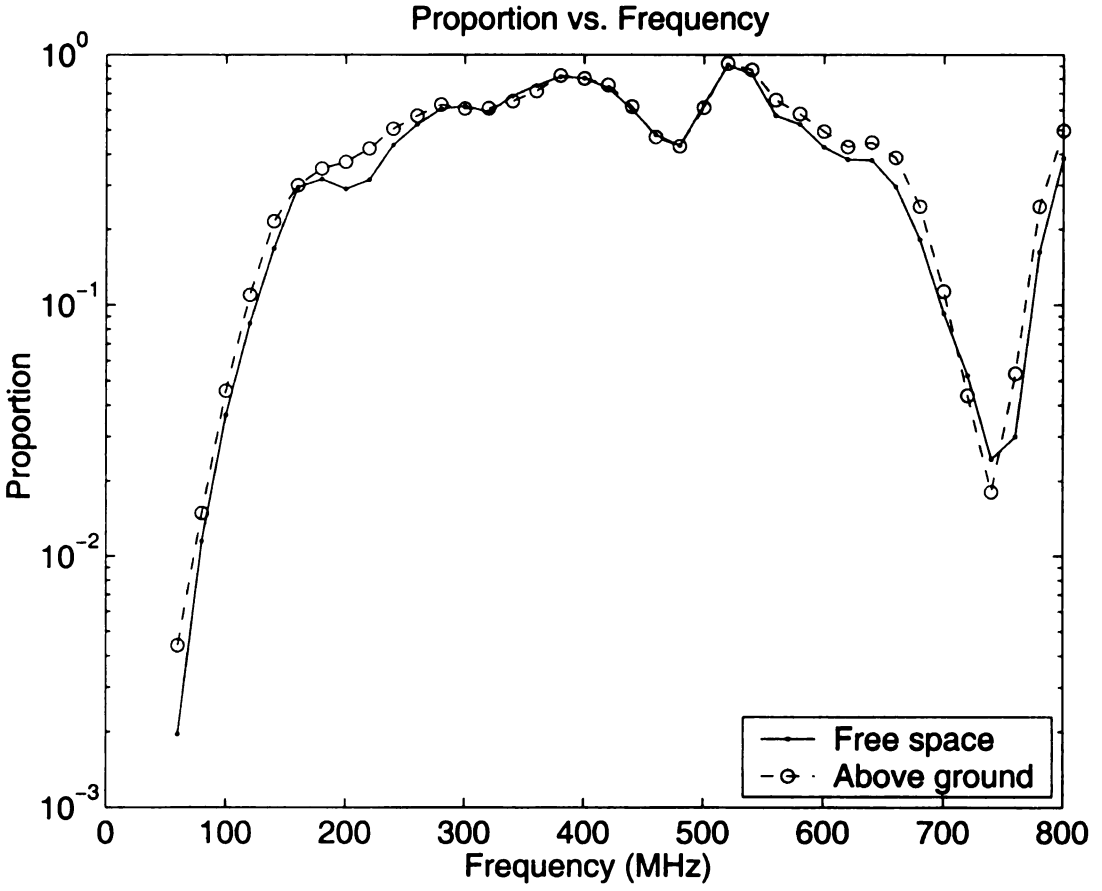


Figure 5.106. Proportion of configurations with SWRs less than 4.0 vs. frequency for the layer 2.5 Type II SSA template.

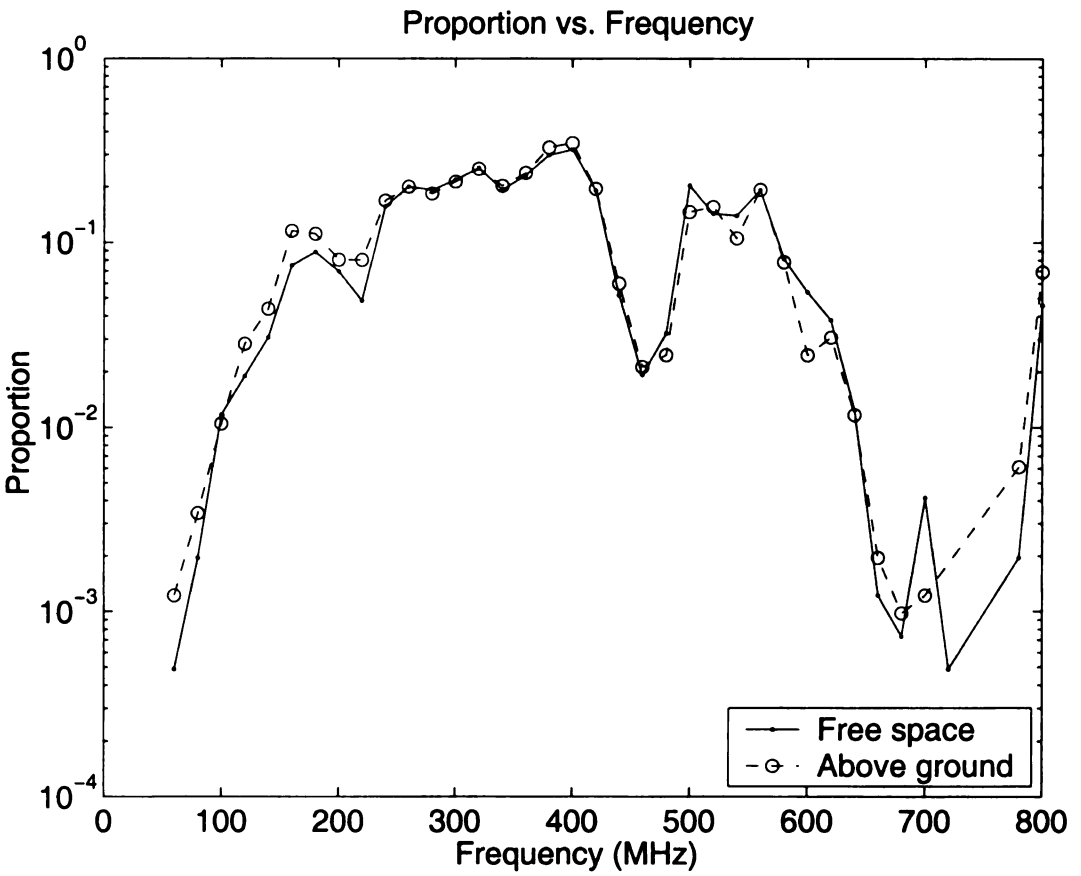


Figure 5.107. Proportion of configurations with SWRs less than 2.0 vs. frequency for the layer 2.5 Type II SSA template.

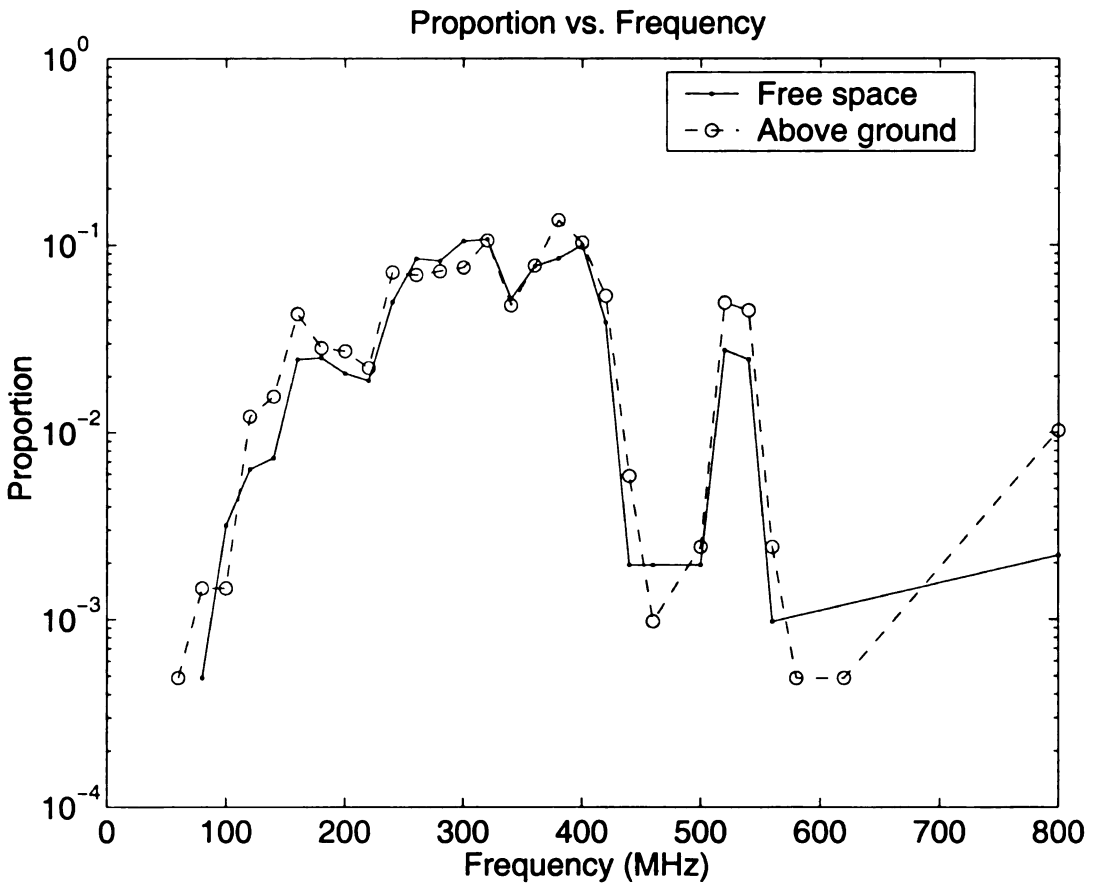


Figure 5.108. Proportion of configurations with SWRs less than 1.5 vs. frequency for the layer 2.5 Type II SSA template.

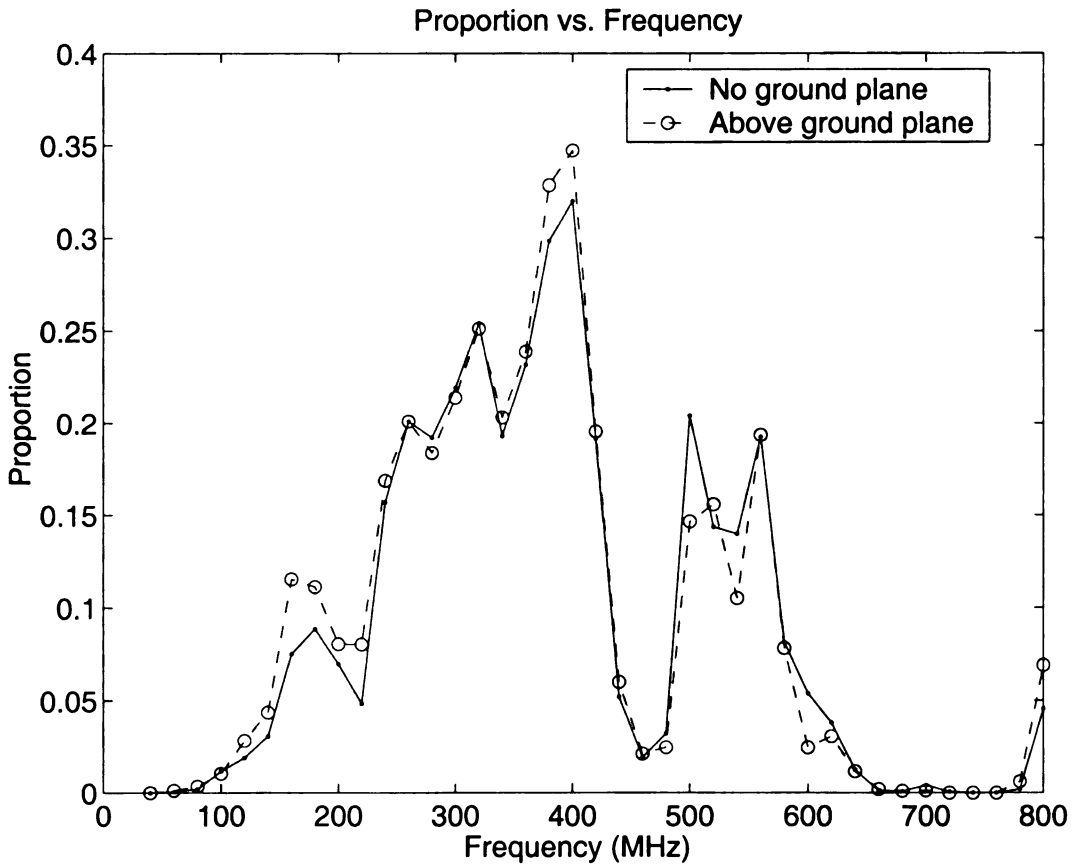


Figure 5.109. Proportion of configurations with SWRs less than 2.0 vs. frequency for the layer 2.5 Type II SSA template (linear scale).

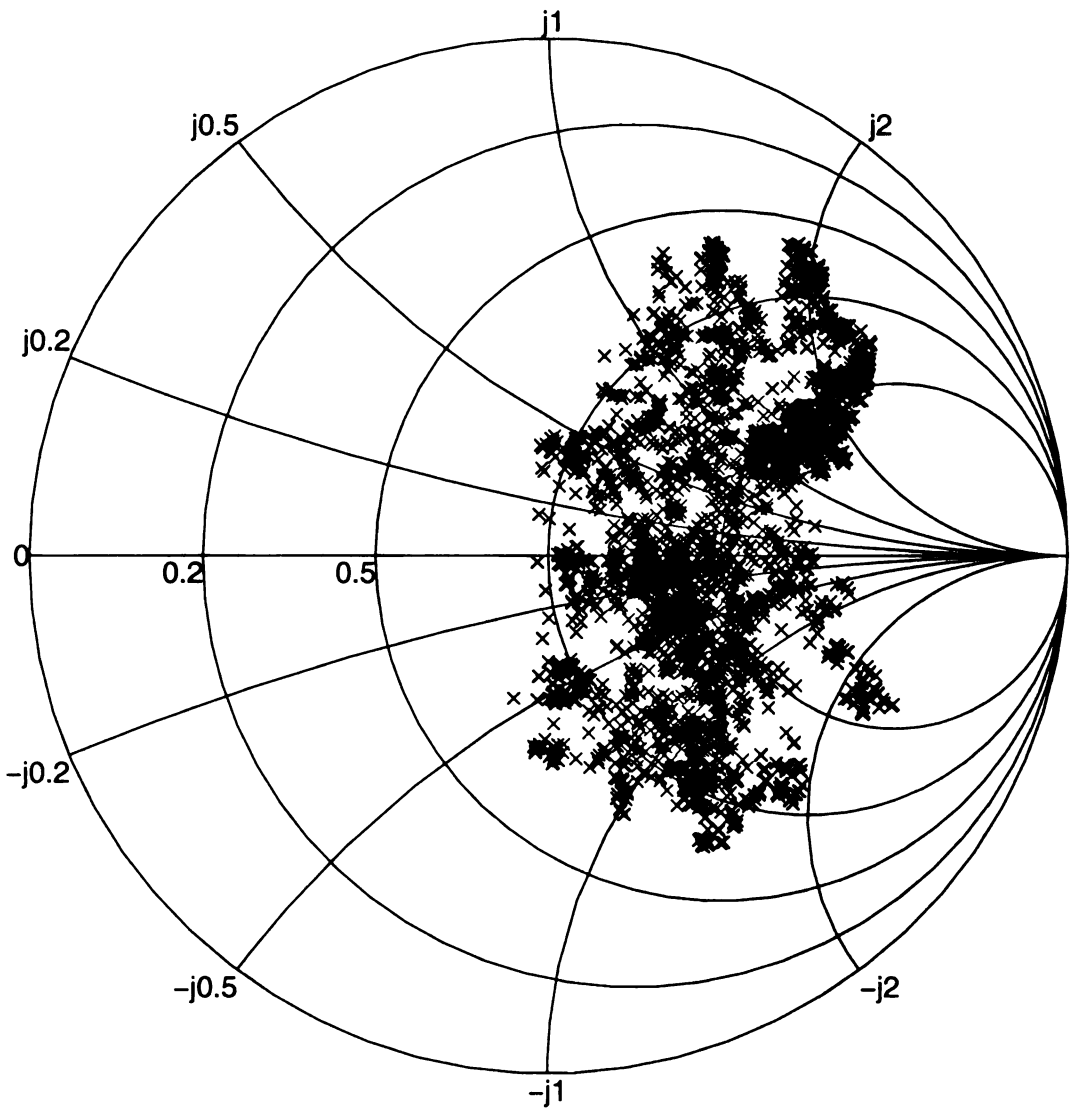


Figure 5.110. Smith chart for the layer 2.5 Type II SSA template in free space at 380 MHz.

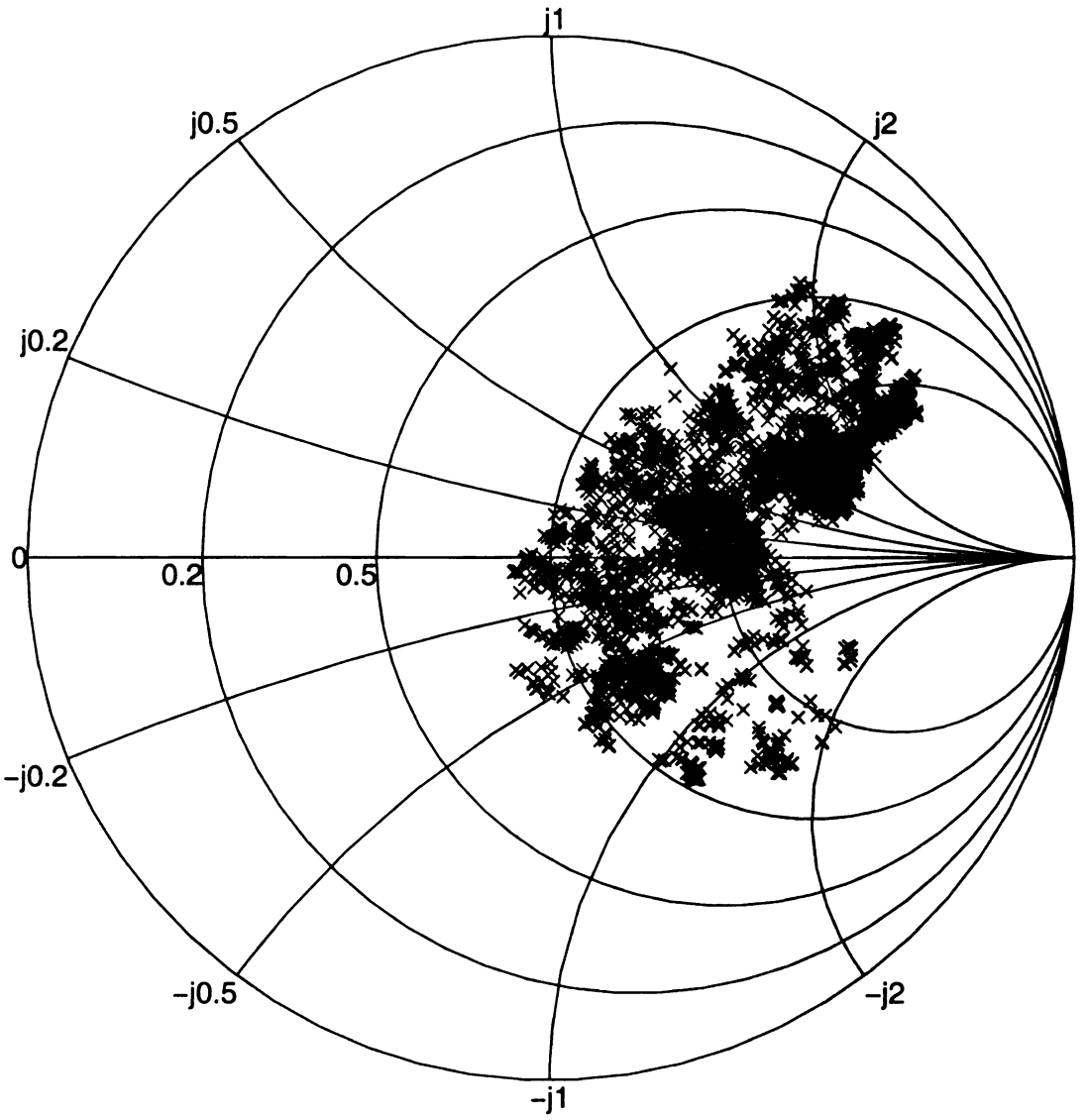


Figure 5.111. Smith chart for the layer 2.5 Type II SSA template in free space at 400 MHz.

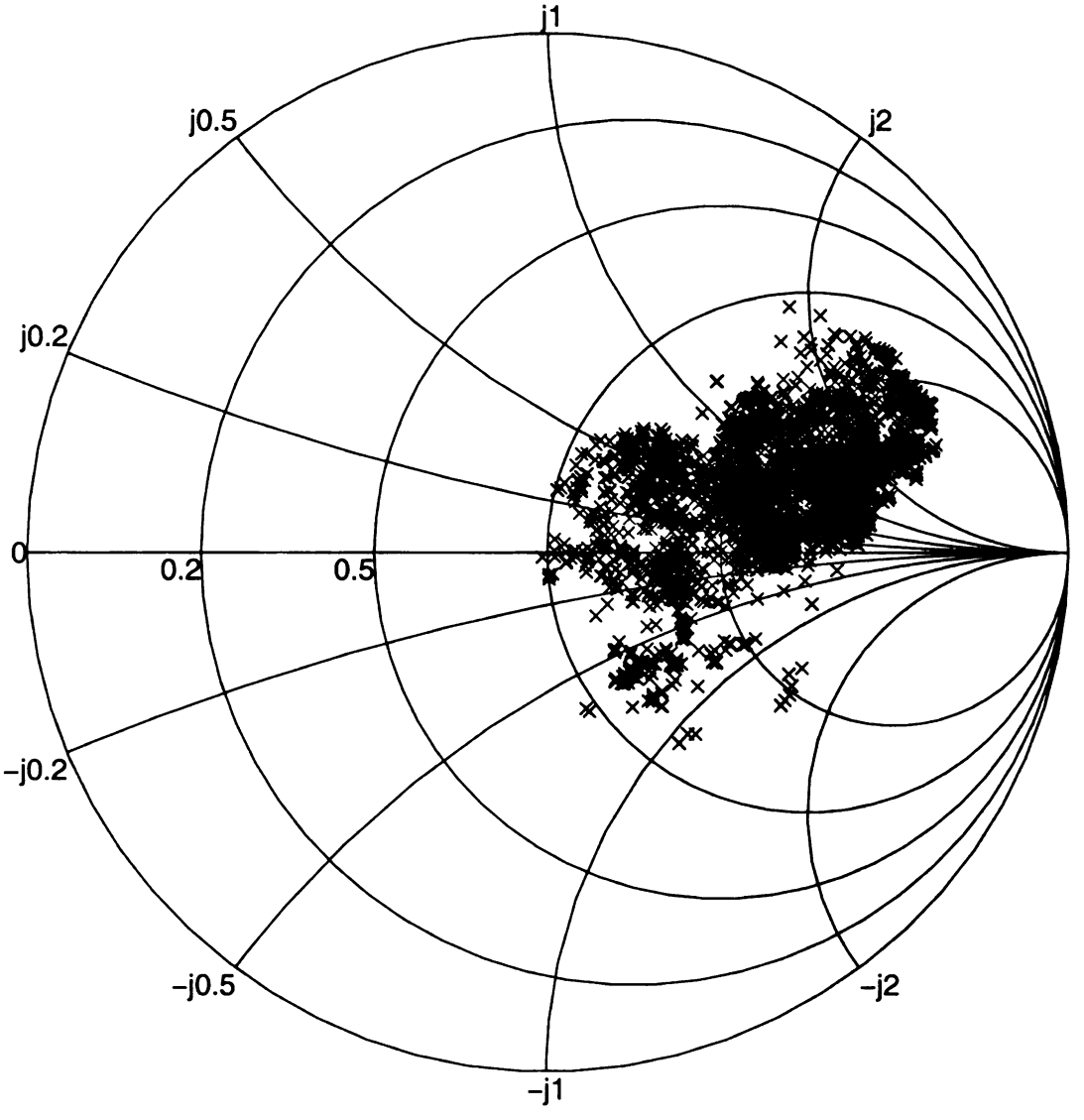


Figure 5.112. Smith chart for the layer 2.5 Type II SSA template in free space at 420 MHz.

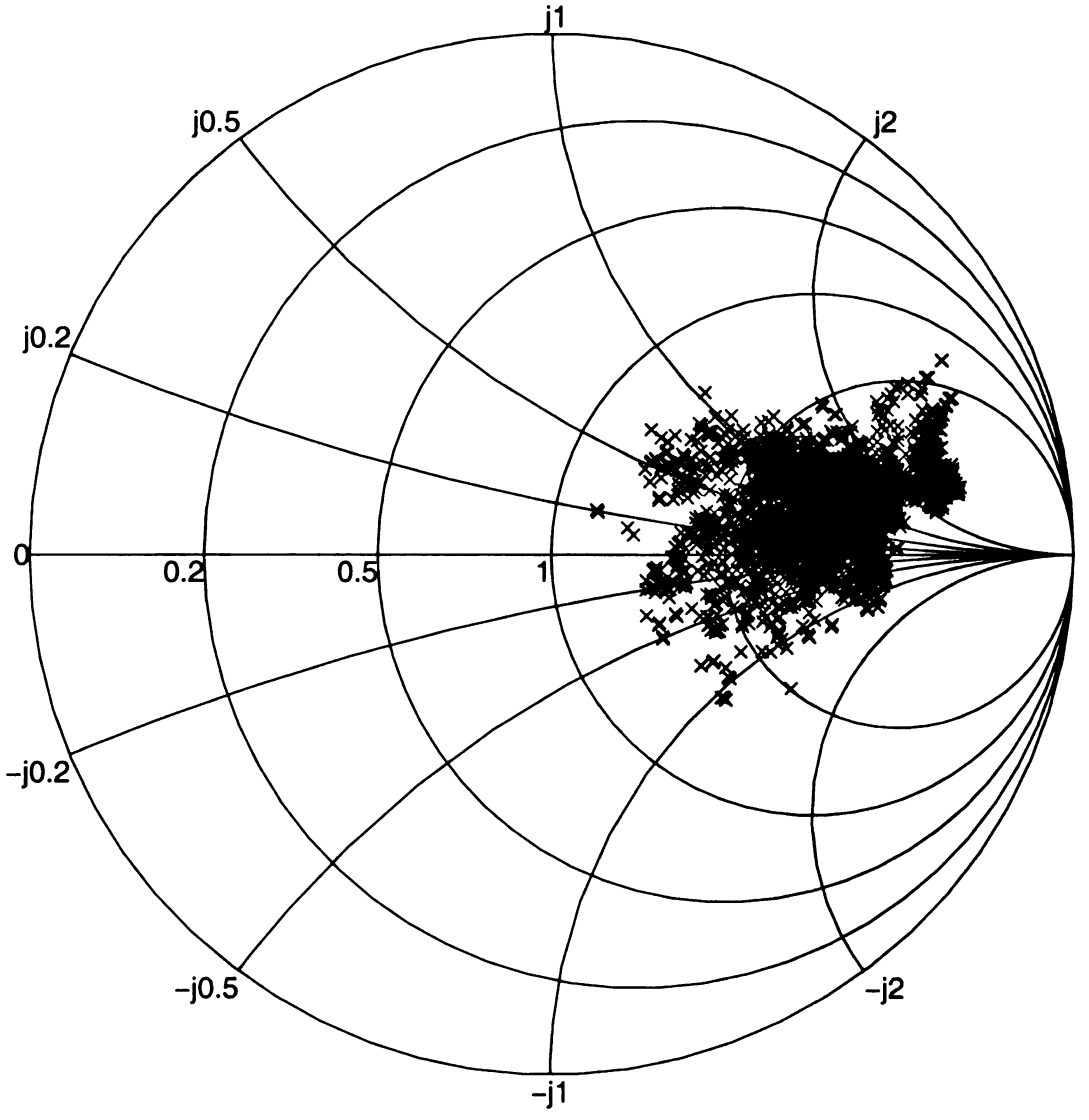


Figure 5.113. Smith chart for the layer 2.5 Type II SSA template in free space at 440 MHz.

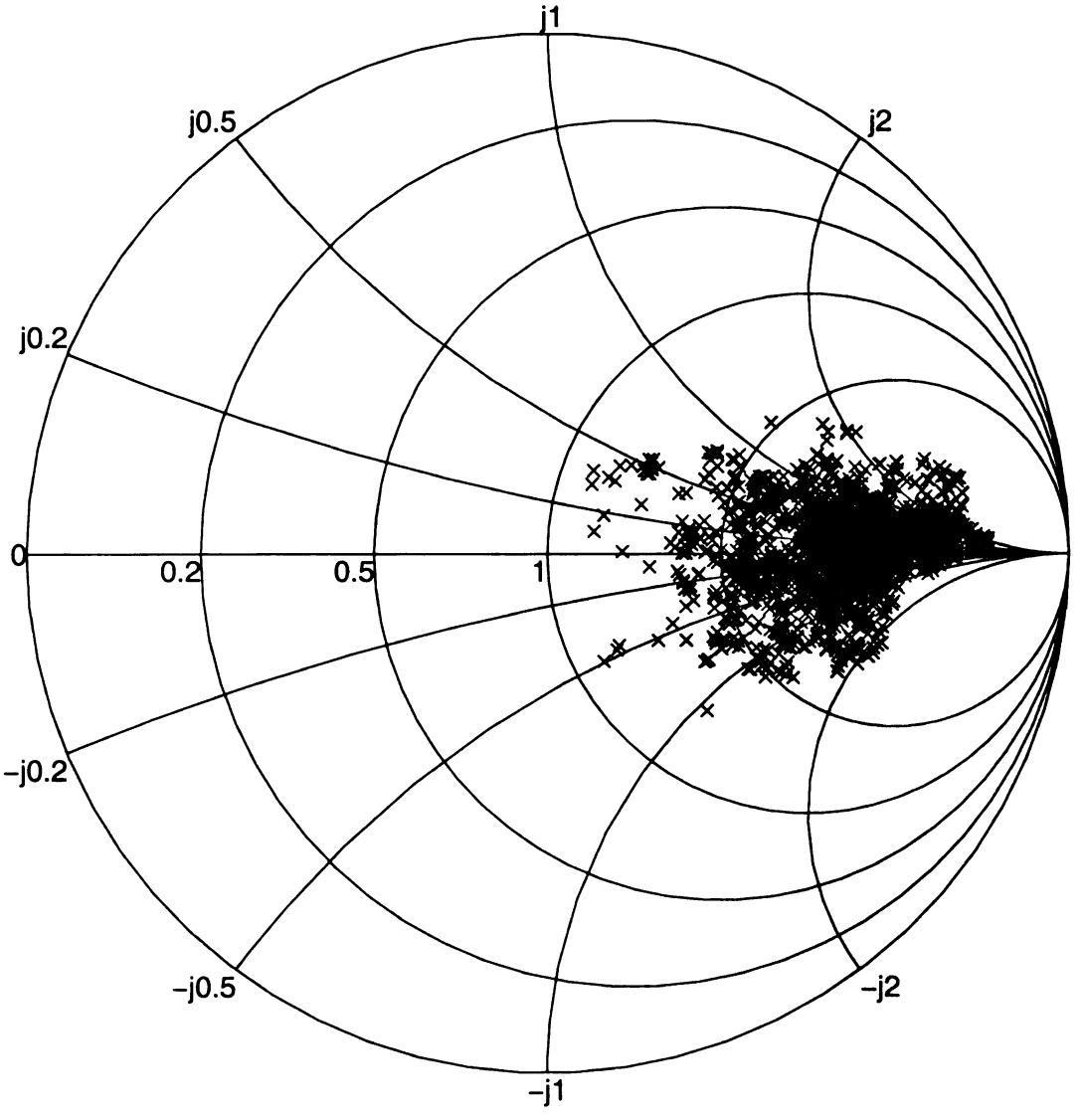


Figure 5.114. Smith chart for the layer 2.5 Type II SSA template in free space at 460 MHz.

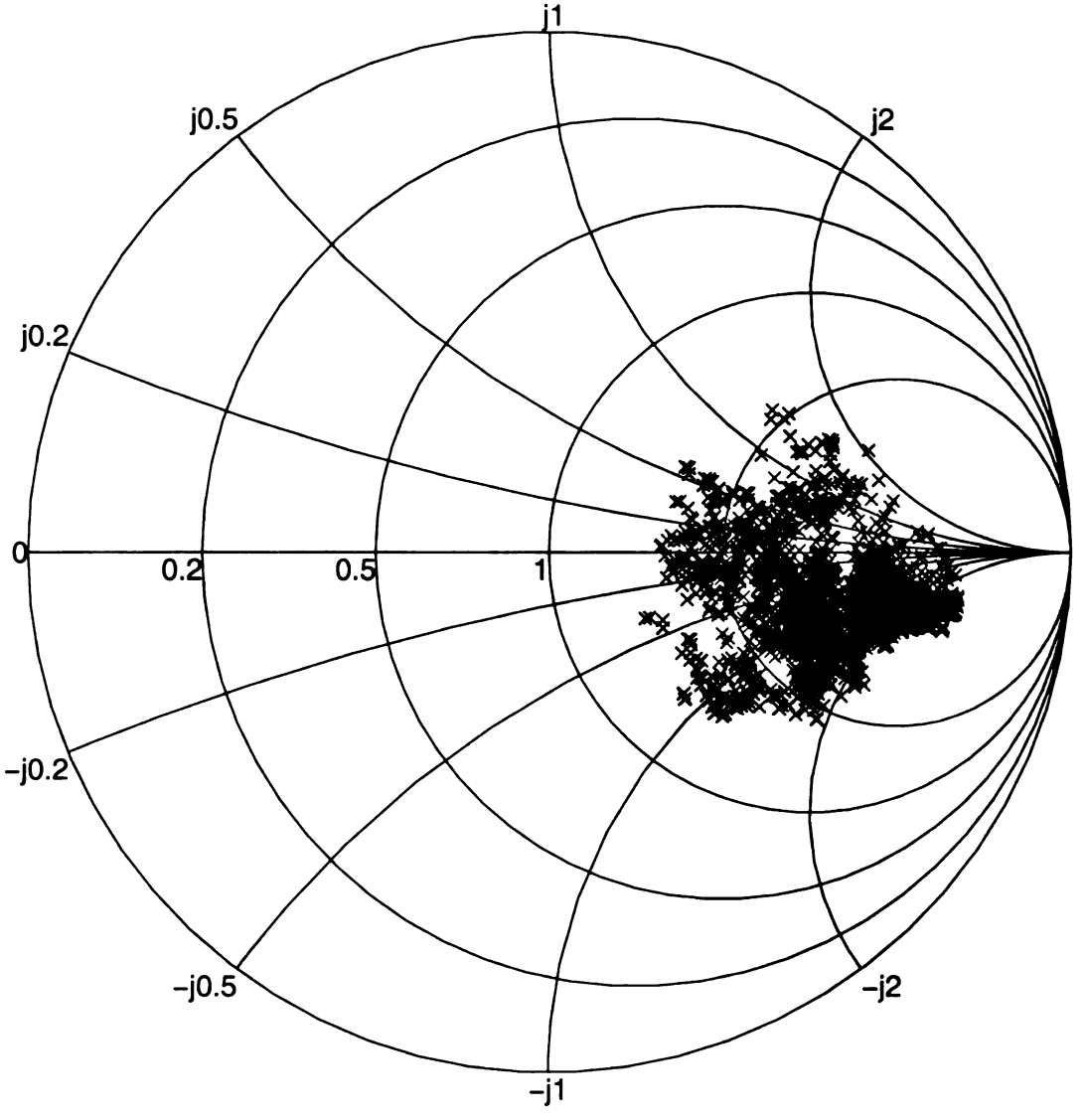


Figure 5.115. Smith chart for the layer 2.5 Type II SSA template in free space at 480 MHz.

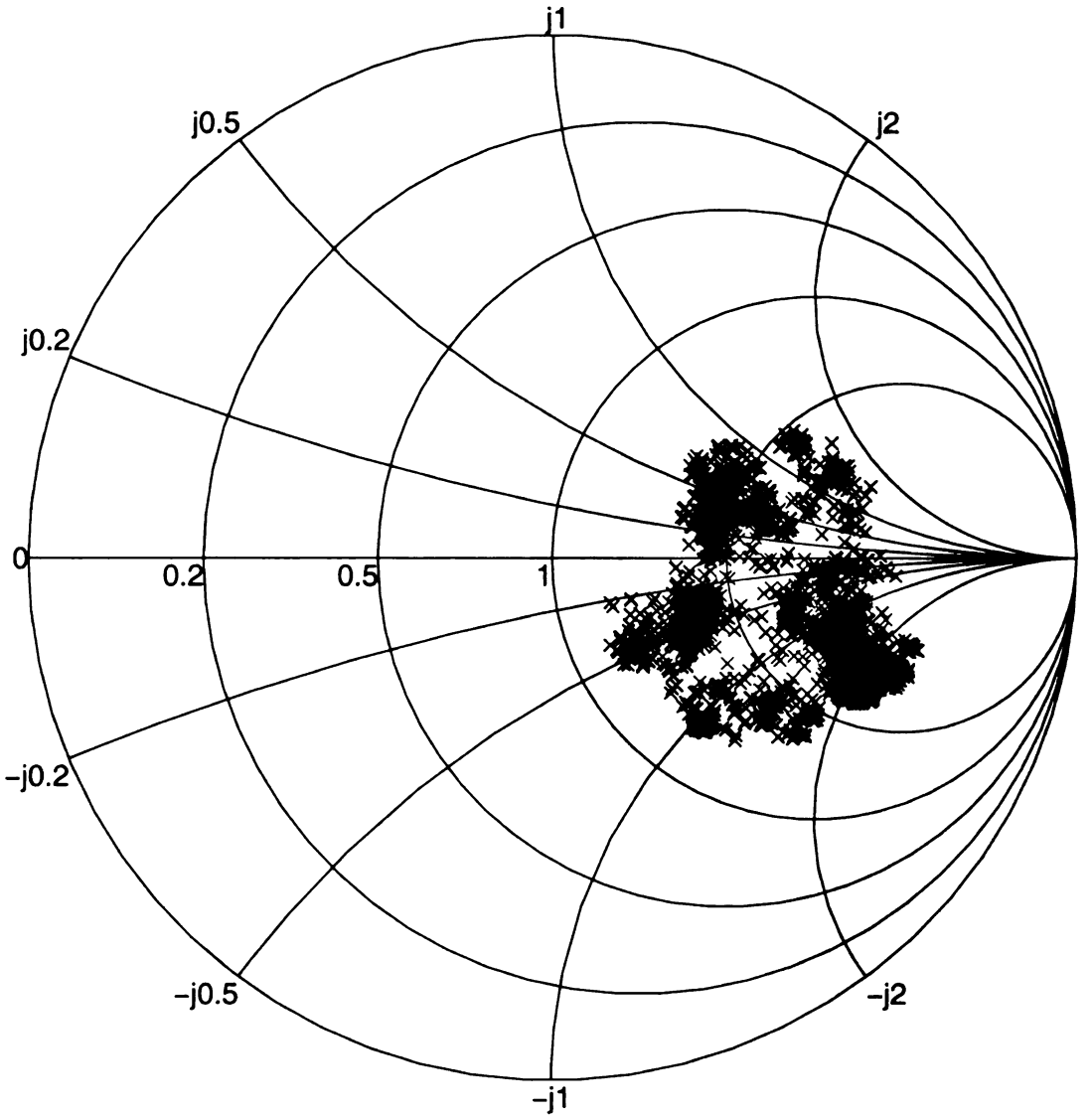


Figure 5.116. Smith chart for the layer 2.5 Type II SSA template in free space at 500 MHz.

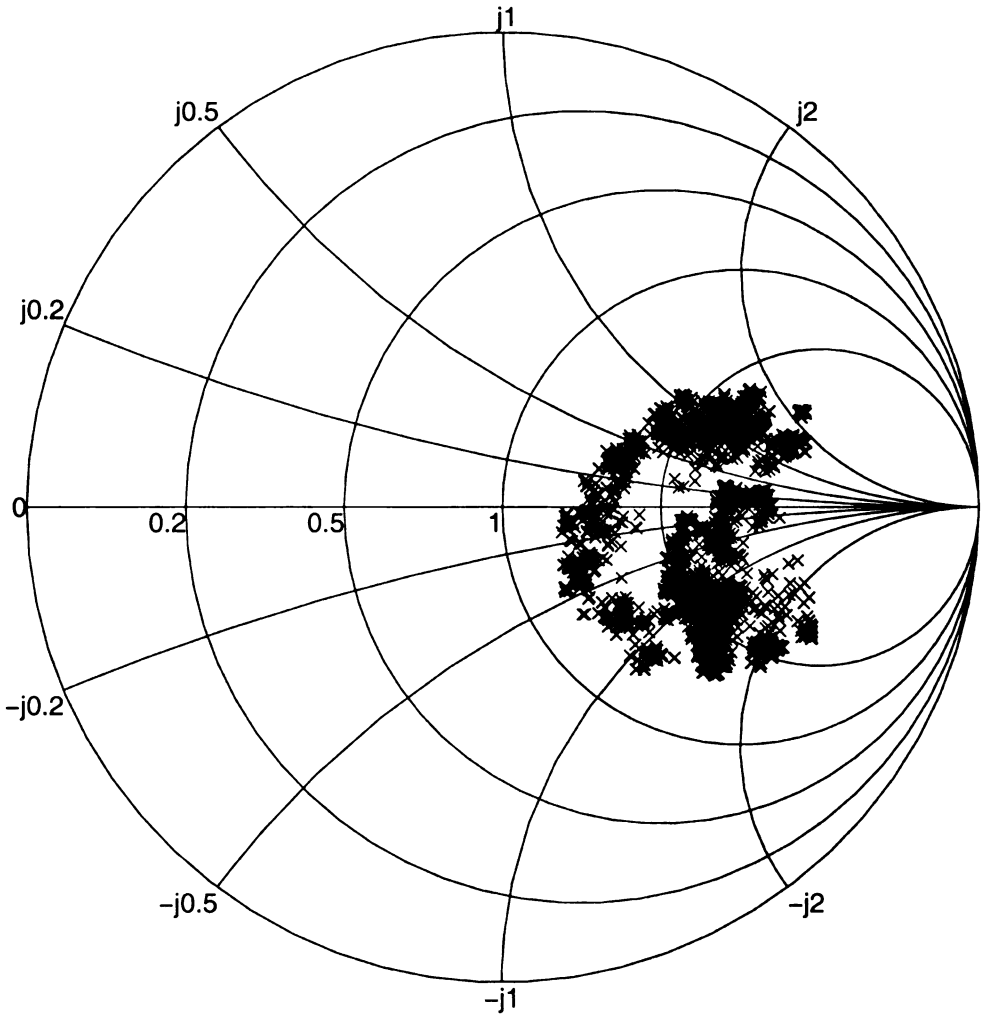


Figure 5.117. Smith chart for the layer 2.5 Type II SSA template in free space at 520 MHz.

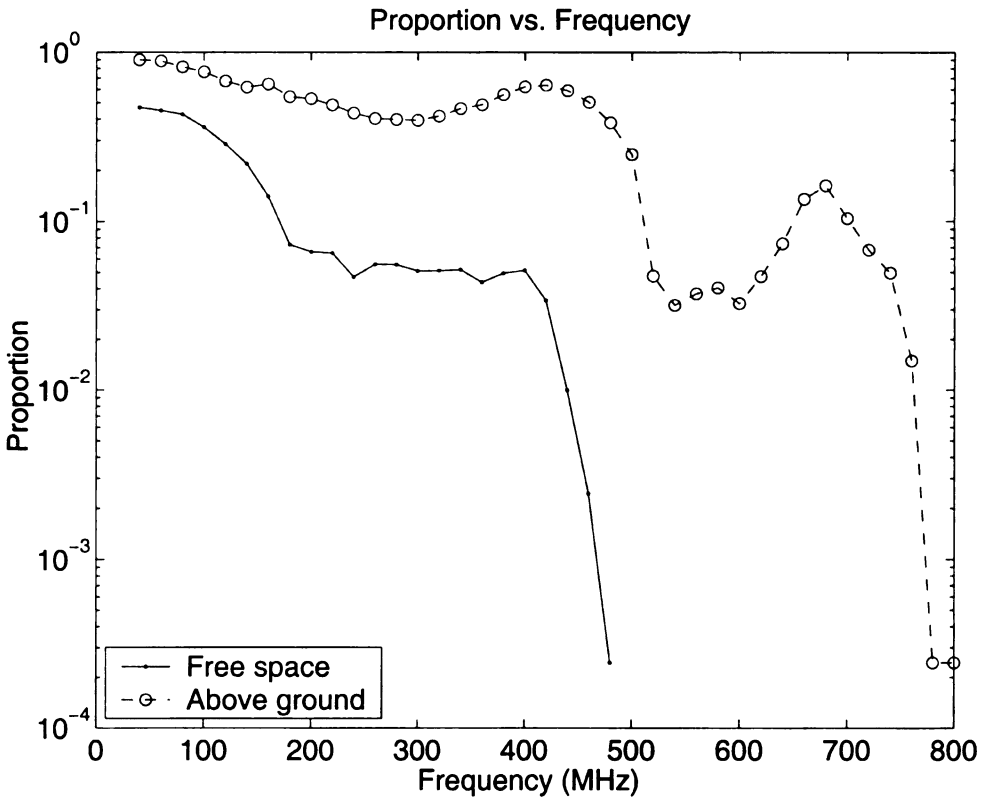


Figure 5.118. Proportion of configurations with minimum vertical gains in the horizontal plane above 0 dB vs. frequency for the layer 2.5 Type II SSA template.

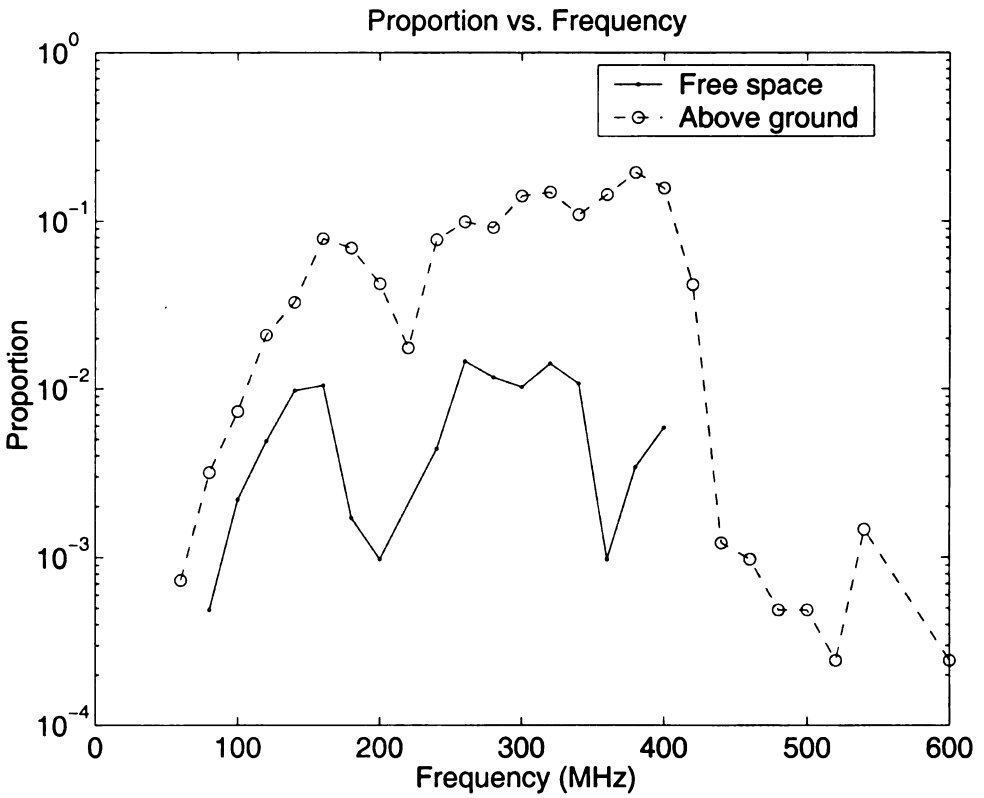


Figure 5.119. Proportion of configurations with SWRs less than 2.0 and minimum vertical gains in the horizontal plane above 0 dB vs. frequency for the layer 2.5 Type II SSA template.

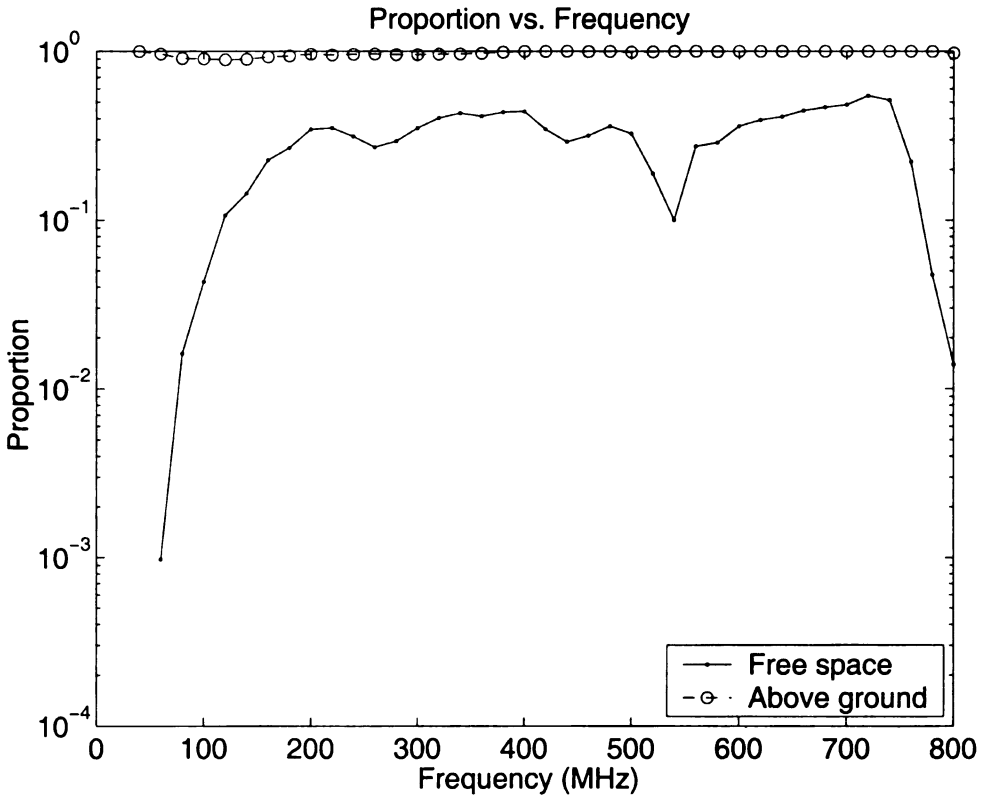


Figure 5.120. Proportion of configurations with maximum vertical gains in the horizontal plane above 3.0 dB vs. frequency for the layer 2.5 Type II SSA template.

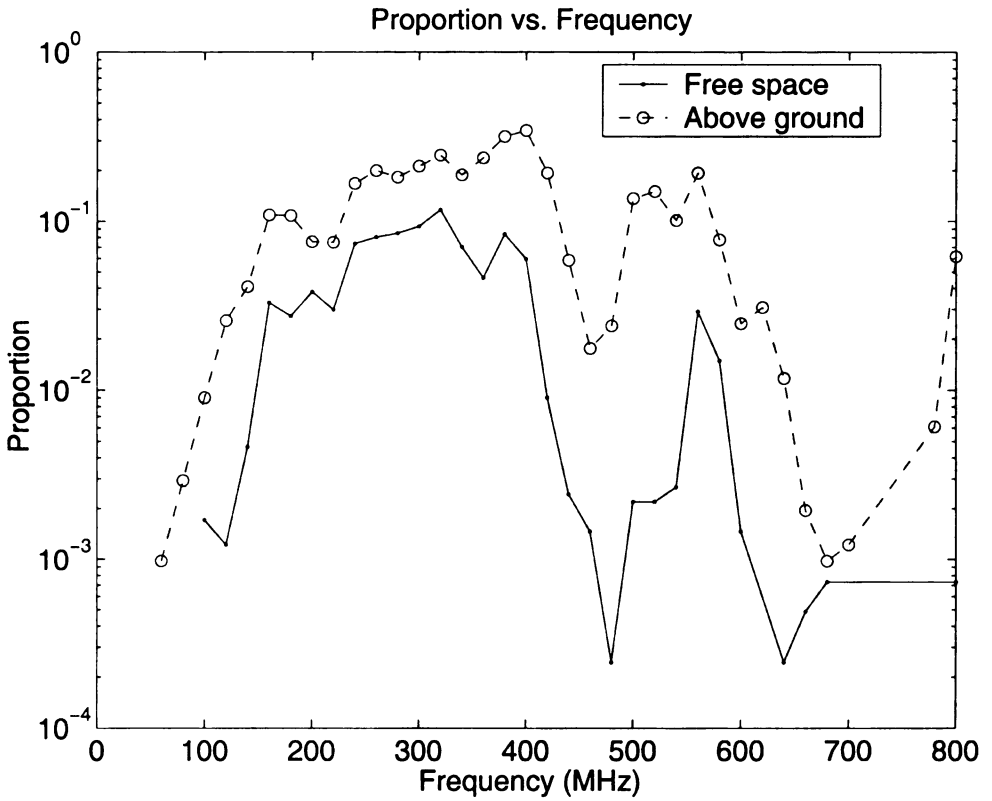


Figure 5.121. Proportion of configurations with SWRs less than 2.0 and maximum vertical gains in the horizontal plane above 3.0 dB vs. frequency for the layer 2.5 Type II SSA template.

5.3.5 Layer 3 SSA Template

The layer 3 SSA template, shown in Figure 5.122, uses fifteen switches for 32,768 possible SSA configurations. Exhaustive searches of these possible configurations are difficult because of the time required to perform the searches and because of programming difficulties. Thus, exhaustive searches are abandoned for layer 3 and higher templates. Random searches of these higher layer templates are performed.

For random searches, a sample of the possible configuration space is taken, and the electromagnetic characteristics of this sample are evaluated. The SSA templates

are analyzed by estimating parameters based on the sample. The parameters are estimates of the proportion of the population that meet given criteria. A sample trial will yield a success if the trial meets the criteria. For instance, a success can be defined as an SSA configuration with an SWR less than a threshold value or a gain above a threshold value.

Parameter and confidence interval estimation based on random samples is discussed in Chapter 4. The results presented in this chapter use 95% confidence intervals. For sampled data plots in this chapter, parameters are only displayed at frequencies at which enough data exist to estimate confidence intervals. The sample size for the layer 3–7 templates is 5000 for each template. This is much smaller than the sample size of 500,000 used for the population estimates presented for the SSA template studied in Chapter 4, but the templates studied in this chapter are evaluated over a much larger frequency band, and the computation time and programming issues require a much smaller sample size.

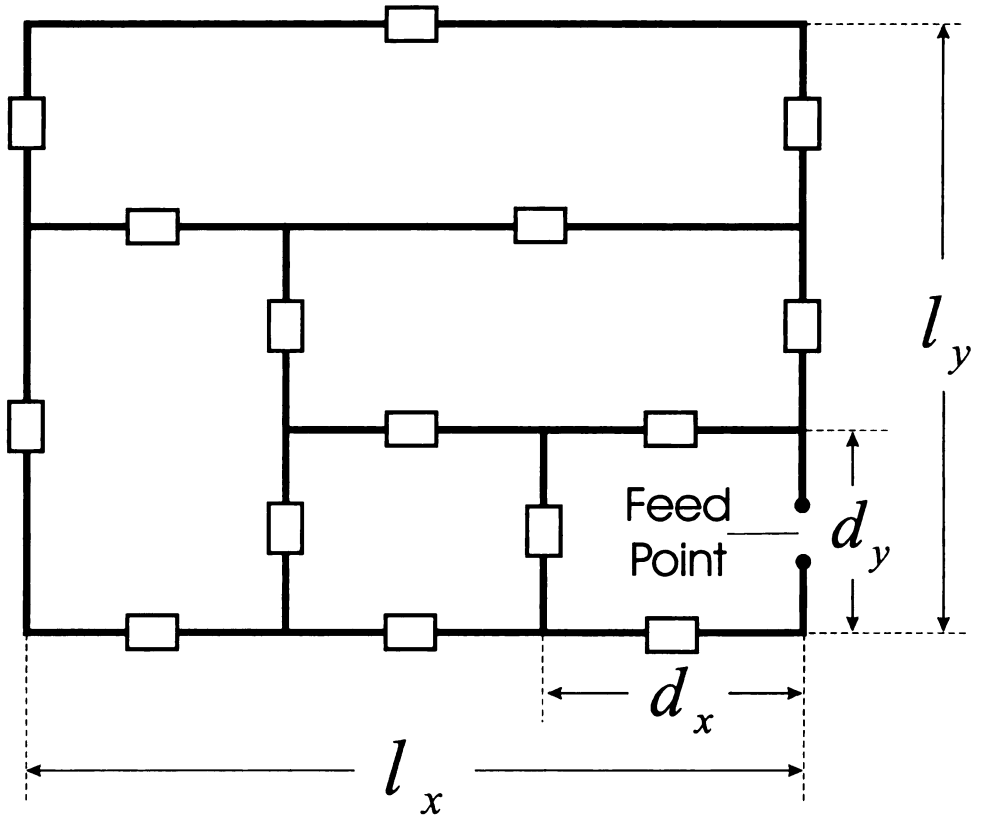


Figure 5.122. Diagram of the layer 3 SSA template.

The outer dimensions of the layer 3 Type I SSA template are shown in Table 5.11. Only results for the Type I template are presented, so Type I templates are implied for templates labeled 'layer 3' in this chapter.

The SWR values at each frequency for the 5000 random samples of the configurations are shown in Figure 5.123 and Figure 5.124 for the layer 3 templates in free space and above ground, respectively. As is the case for the layer 2.5 templates, nearly continuous possible SWR values exist at most frequencies. Above 200 MHz, SWR values close to 1.0 are found at most frequencies.

Figure 5.125 shows the minimum SWR value found at each frequency in the 5000

Table 5.11. Dimensions of the layer 3 Type I SSA template.

l_x	25.7 cm
d_x	8.57 cm
l_y	25.7 cm
d_y	8.57 cm
Outer electrical dimensions at 40 MHz	$0.0343\lambda \times 0.0343\lambda$
Outer electrical dimensions at 800 MHz	$0.686\lambda \times 0.686\lambda$

random samples of the configurations for the layer 3 templates in free space and above ground. SWRs of 1.3 or lower are found at 200 MHz and above for the templates in free space and above ground.

Figure 5.126 shows the proportion of configurations with SWRs less than 4.0 for the layer 3 template in free space. Since only a random sample of the data is available, confidence intervals are estimated for the proportions. Over 200 MHz, 95% confidence intervals span ranges within factors of 2 or less from the bottoms to the tops of the intervals. The template above ground exhibits similar behavior, as shown in the proportion of configurations with SWRs less than 4.0 found in Figure 5.127. This shows that a random sample of the population of configurations reveals important characteristics of the SSA templates without performing exhaustive searches.

The proportions for the layer 3 templates in free space and above ground are plotted separately so that distinct confidence intervals are seen without confusion. The proportion parameter estimates without the confidence intervals are combined and shown in Figure 5.128 for the templates in free space and above ground so that direct comparison is possible. Recall that only parameter estimates at frequencies where confidence intervals exist are displayed. The distributions of SWRs are similar for the templates in free space and above ground.

The proportion of configurations with SWRs less than 2.0 are shown in Figure 5.129 and Figure 5.130 for the layer 3 templates in free space and above ground,

respectively. Notice that the confidence intervals are growing at the lower frequencies due to fewer successful configurations in the sample. Also, there are not enough successful configurations at several frequencies in the lower part of the band to estimate confidence intervals. The combined proportion estimates for the templates in free space and above ground are shown in Figure 5.131.

Figure 5.132 and Figure 5.133 show the proportion of configurations with SWRs less than 1.5 for the layer 3 templates in free space and above ground, respectively. Confidence intervals are larger than those for the 2.0 SWR threshold due to fewer successful configurations. The combined proportion estimates are shown in Figure 5.134. Notice that many frequencies in the lower region of the band are missing estimates due to the low number of successes.

The proportions of configurations with minimum vertical gains in the horizontal plane above 0 dB are shown in Figure 5.135 and Figure 5.136 for the layer 3 templates in free space and above ground, respectively. The error bars are much larger for the template in free space at most frequencies because the number of successful configurations is less. This is shown in the combined proportion estimate plot found in Figure 5.137.

The proportions of configurations with minimum vertical gains in the horizontal plane above 0 dB and SWRs less than 2.0 are shown in Figure 5.138 and Figure 5.139 for the layer 3 templates in free space and above ground, respectively. The template in free space has fewer successful configurations than the template above ground, as also shown in the combined proportion estimate plot found in Figure 5.140.

The proportions of configurations with maximum vertical gains in the horizontal plane above 3.0 dB are shown in Figure 5.141 and Figure 5.142 for the layer 3 templates in free space and above ground, respectively. Again, the template above ground has far more configurations that meet this requirement than does the template in free space. This is also shown in the combined proportion estimate plot

found in Figure 5.143. An additional criterion requiring SWRs to be less than 2.0 further reduces the number of successful configurations, as shown in Figure 5.144 and Figure 5.145 for the templates in free space and above ground, respectively. The combined proportion estimate shown in Figure 5.146 again shows that the template above ground is more successful in providing configurations that meet the gain threshold criteria tested throughout this study.

The results for the SSA templates presented in this study for layers 3 and lower show that the ground plane helps the SSA template provide configurations with higher vertical gain values in the horizontal plane. Similar SWR distributions exist for the templates in free space and above ground. The results presented for the layer 4, 5, and 6 templates only include the template in free space for brevity.

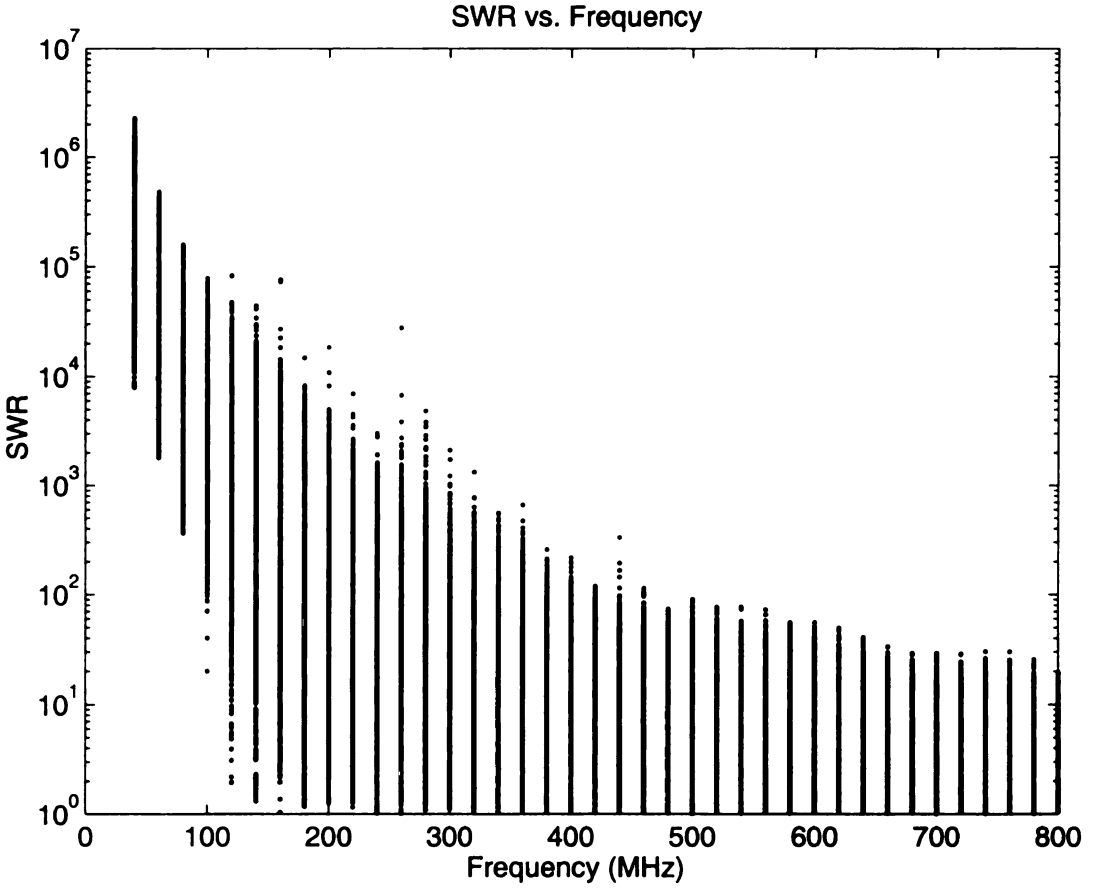


Figure 5.123. SWR vs. frequency for the layer 3 Type I SSA template in free space (5000 random samples).

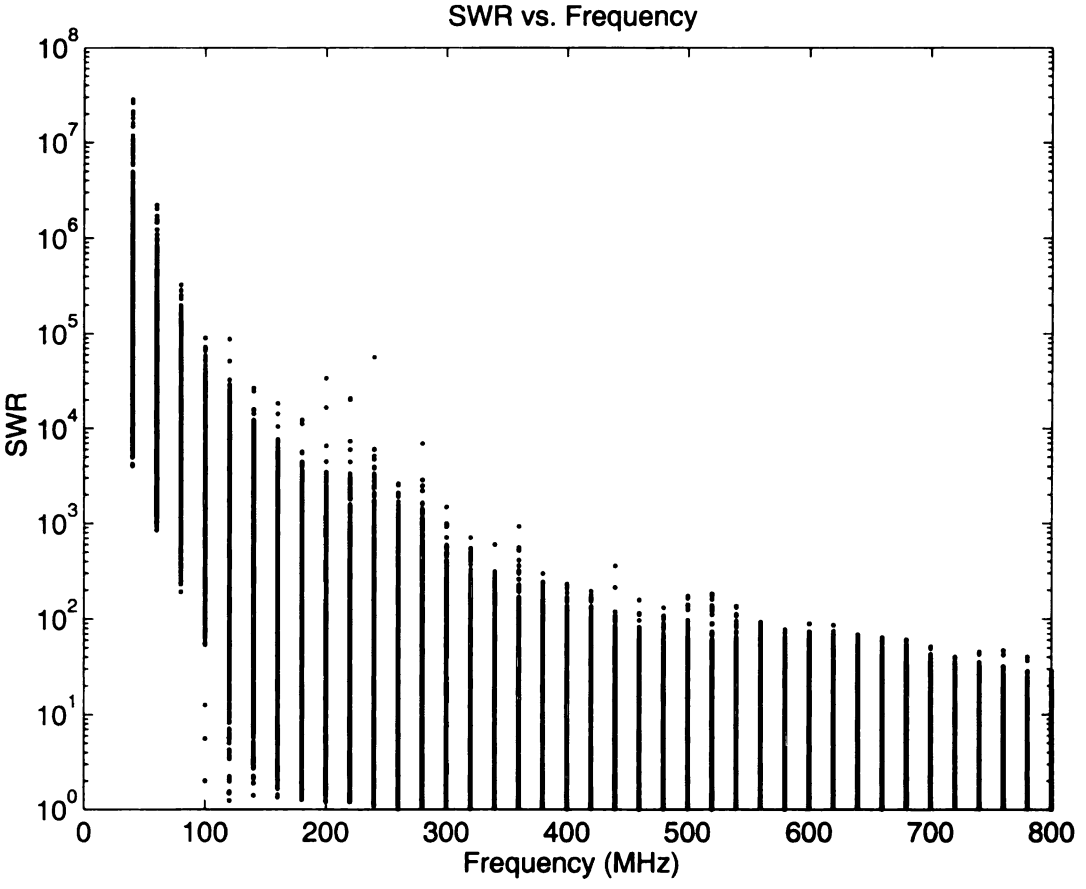


Figure 5.124. SWR vs. frequency for the layer 3 Type I SSA template above ground (5000 random samples).

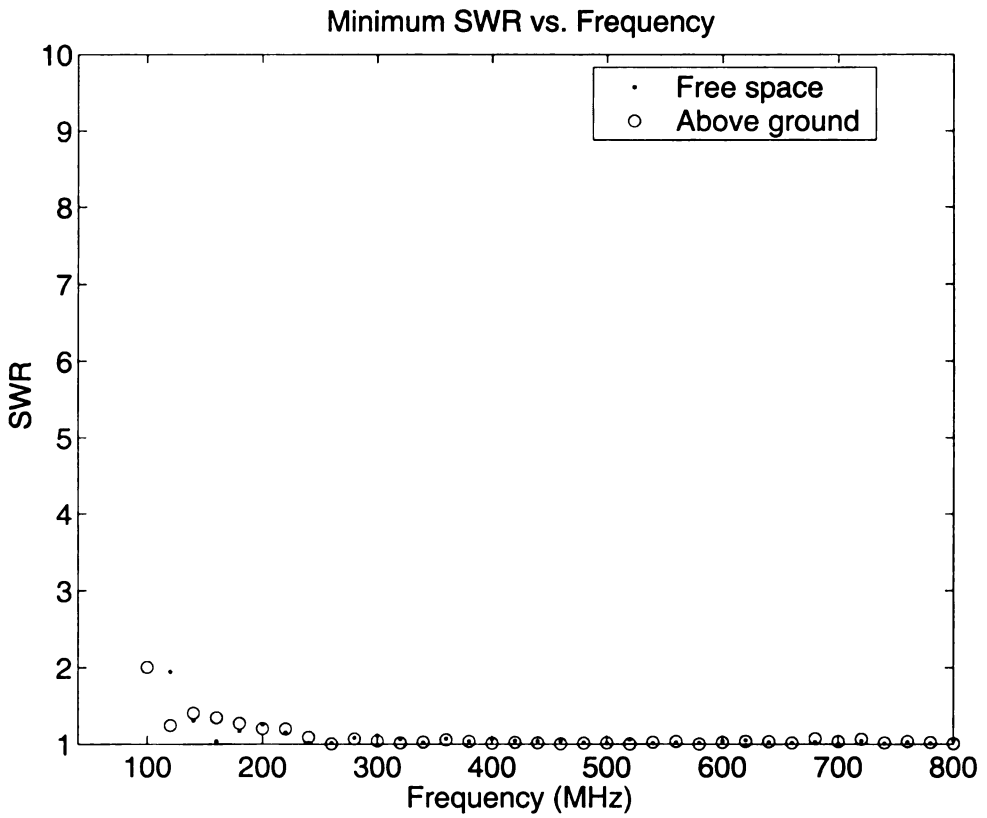


Figure 5.125. Minimum SWR vs. frequency for the layer 3 Type I SSA template (5000 random samples).

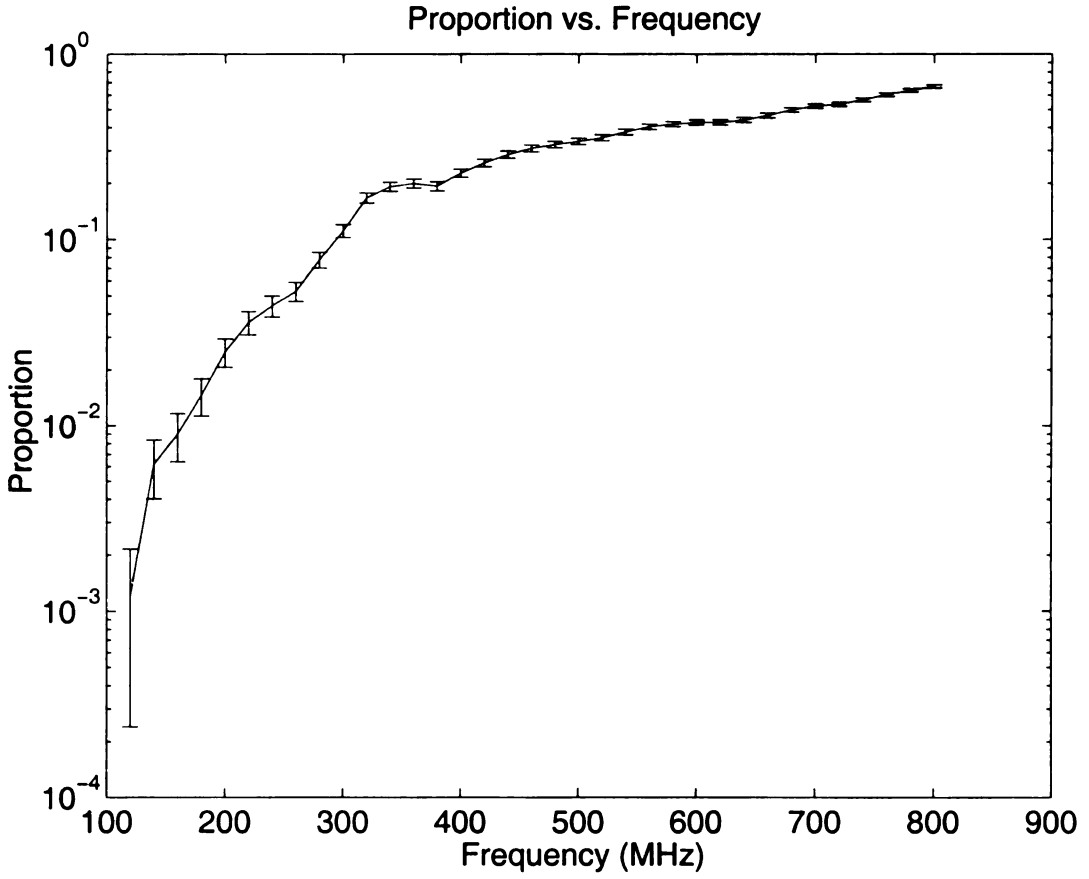


Figure 5.126. Proportion of configurations with SWRs less than 4.0 vs. frequency for the layer 3 Type I SSA template in free space (5000 random samples). Error bars show the 95% confidence intervals.

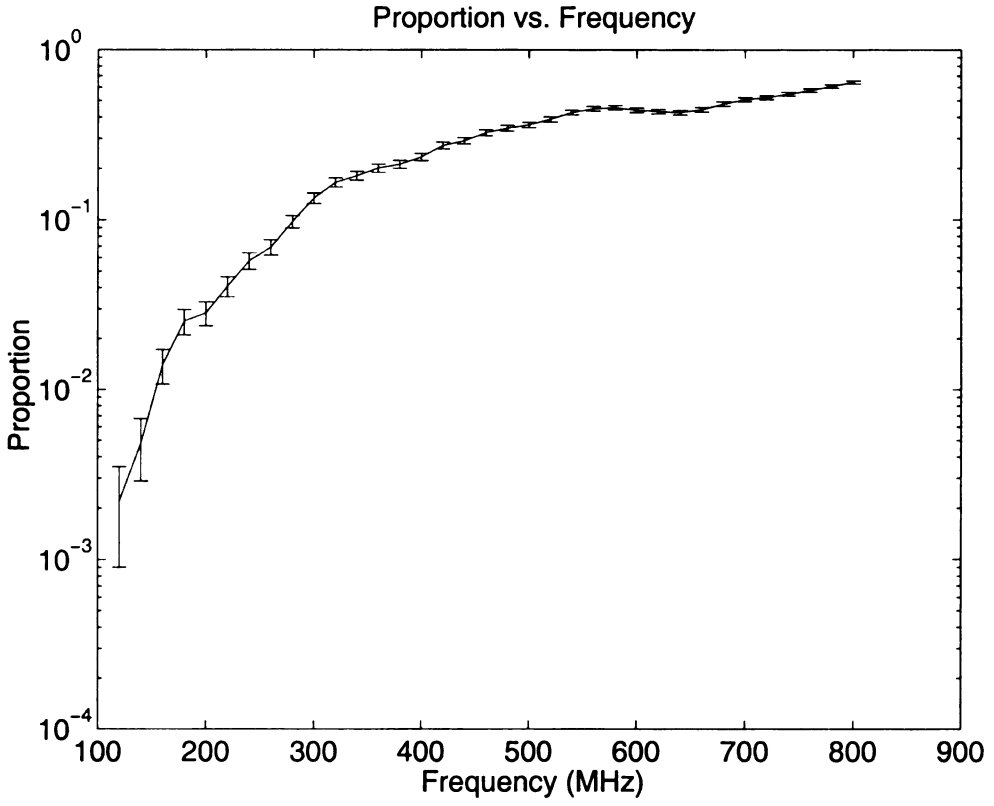


Figure 5.127. Proportion of configurations with SWRs less than 4.0 vs. frequency for the layer 3 Type I SSA template over ground (5000 random samples). Error bars show the 95% confidence intervals.

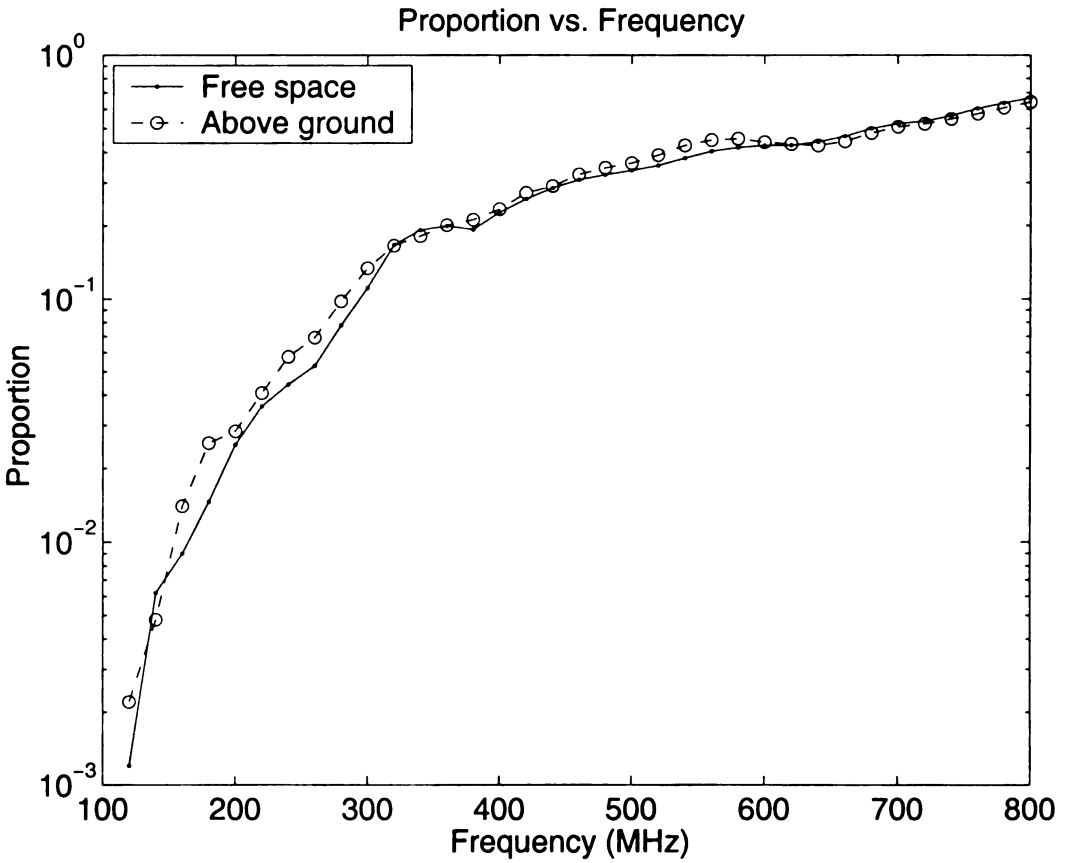


Figure 5.128. Proportion of configurations with SWRs less than 4.0 vs. frequency for the layer 3 Type I SSA template (5000 random samples).

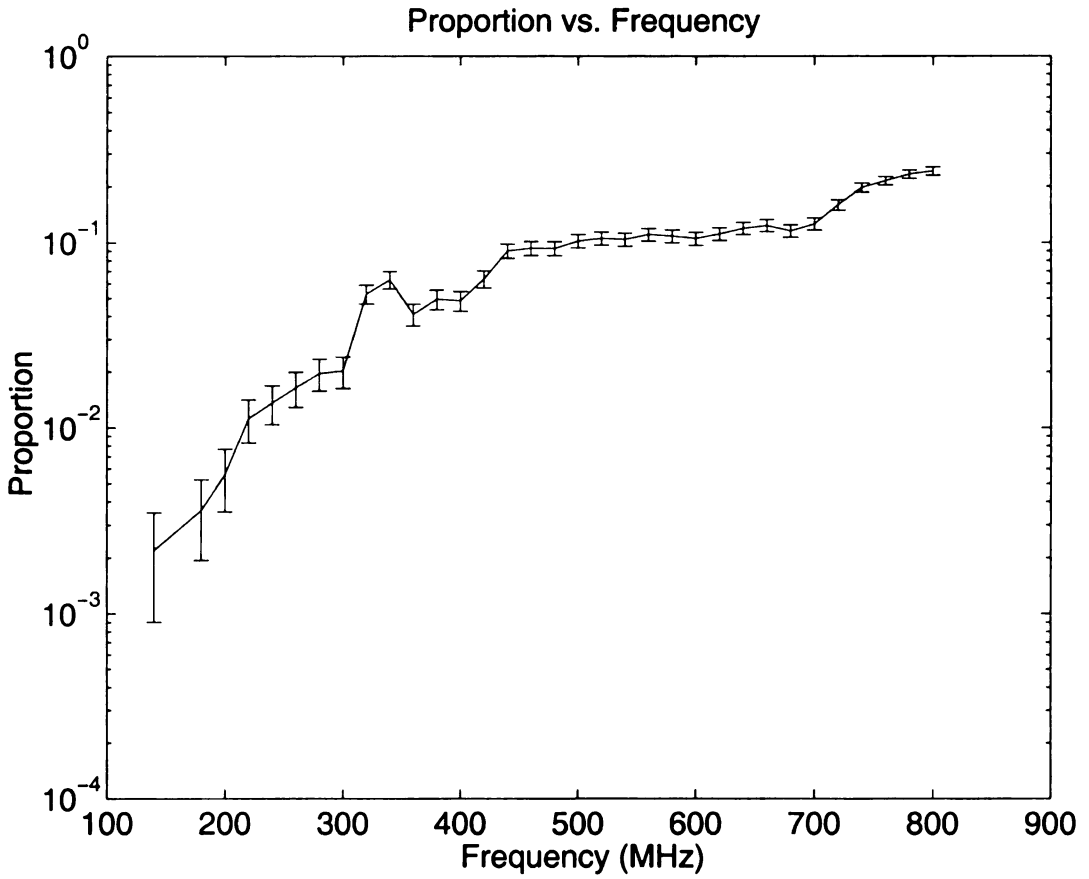


Figure 5.129. Proportion of configurations with SWRs less than 2.0 vs. frequency for the layer 3 Type I SSA template in free space (5000 random samples). Error bars show the 95% confidence intervals.

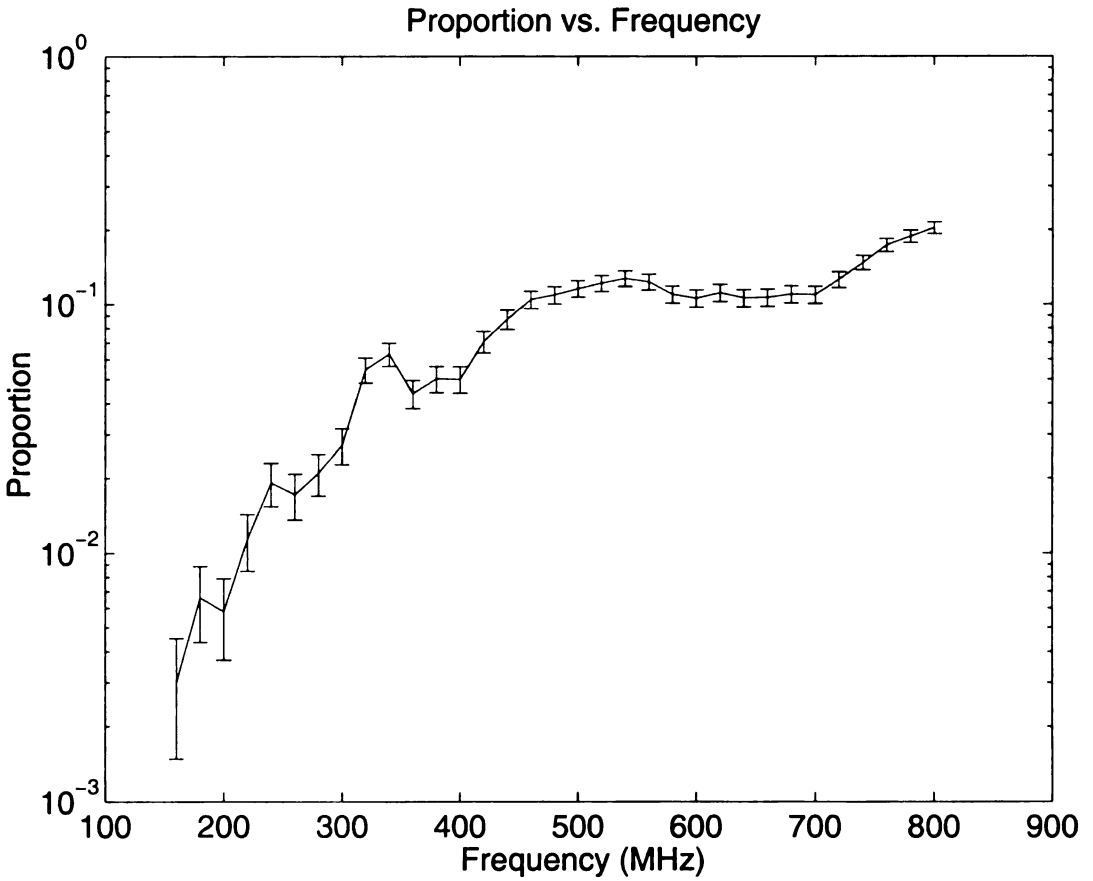


Figure 5.130. Proportion of configurations with SWRs less than 2.0 vs. frequency for the layer 3 Type I SSA template over ground (5000 random samples). Error bars show the 95% confidence intervals.

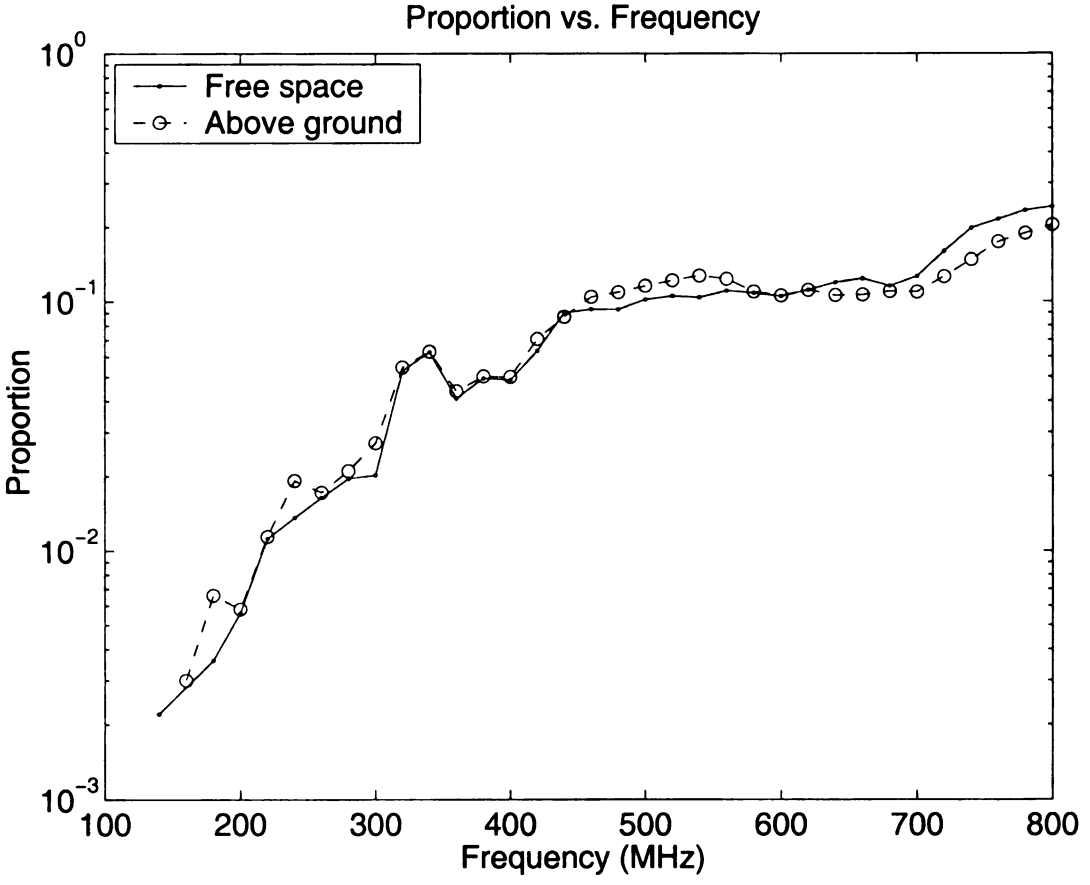


Figure 5.131. Proportion of configurations with SWRs less than 2.0 vs. frequency for the layer 3 Type I SSA template (5000 random samples).

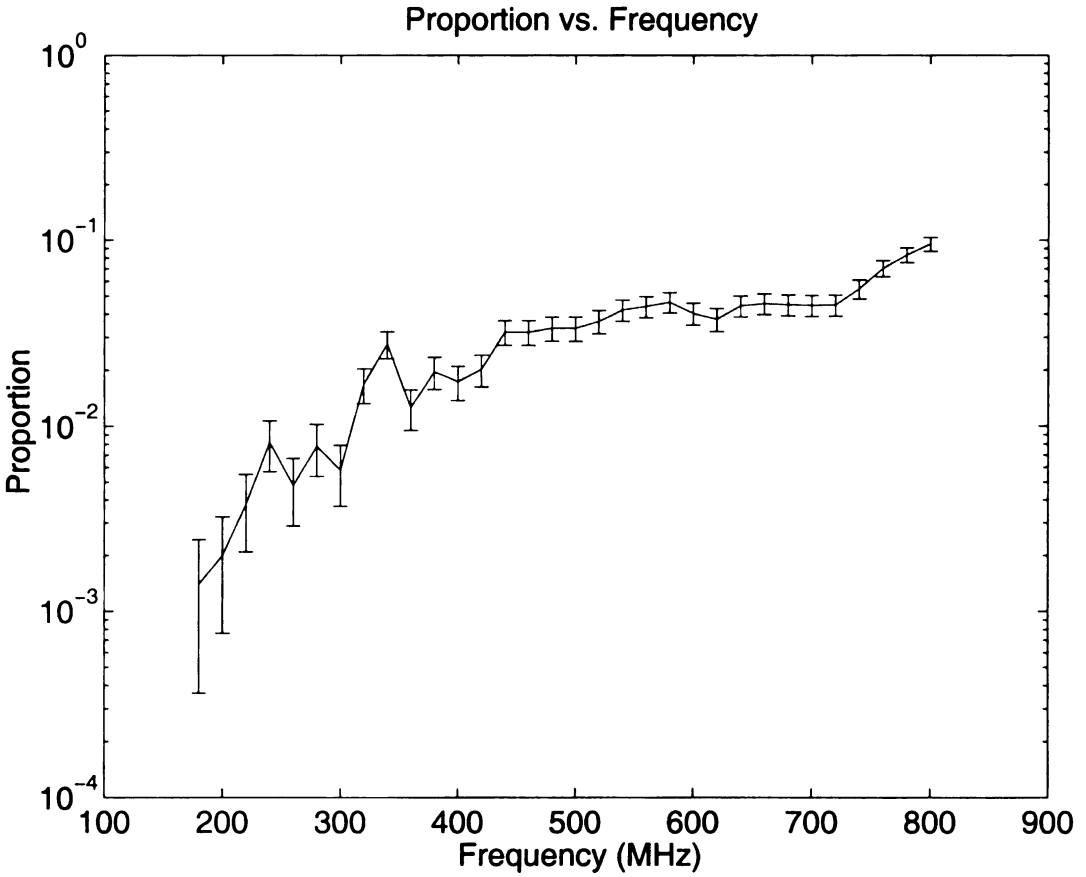


Figure 5.132. Proportion of configurations with SWRs less than 1.5 vs. frequency for the layer 3 Type I SSA template in free space (5000 random samples). Error bars show the 95% confidence intervals.

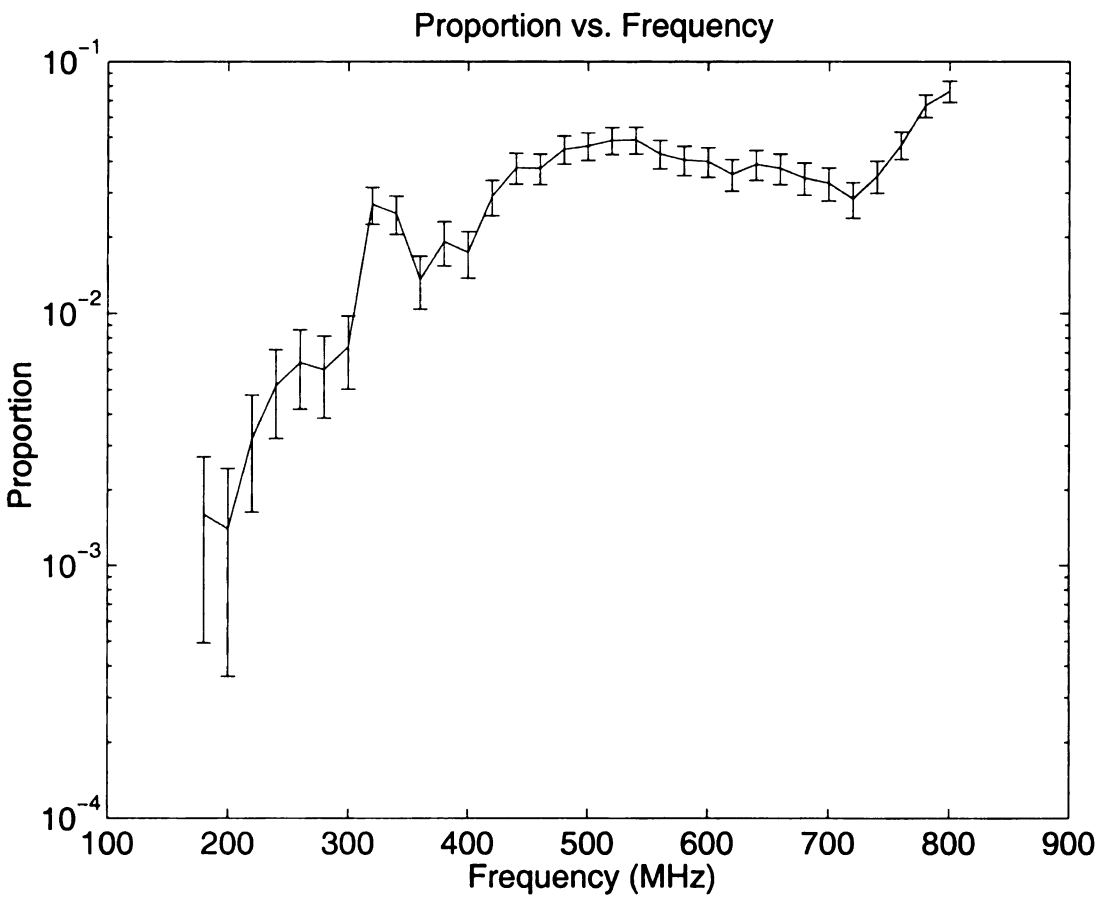


Figure 5.133. Proportion of configurations with SWRs less than 1.5 vs. frequency for the layer 3 Type I SSA template over ground (5000 random samples). Error bars show the 95% confidence intervals.

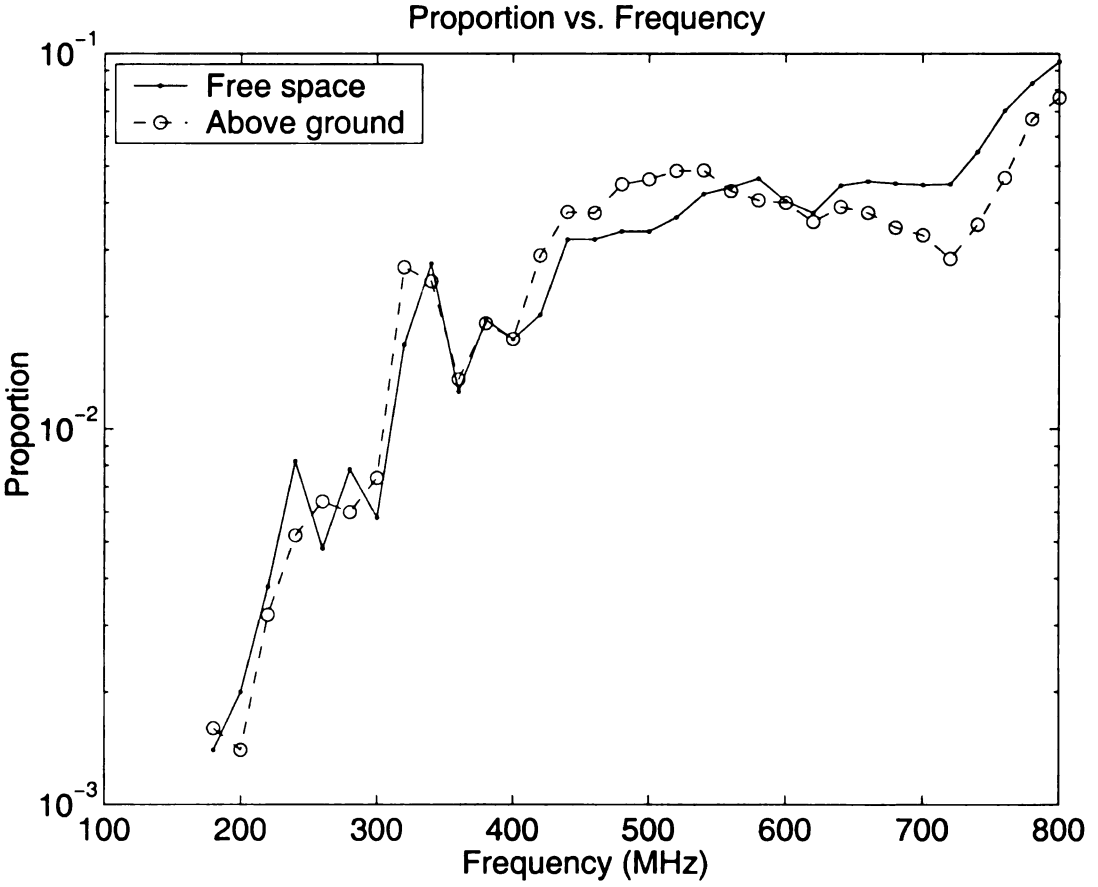


Figure 5.134. Proportion of configurations with SWRs less than 1.5 vs. frequency for the layer 3 Type I SSA template (5000 random samples).

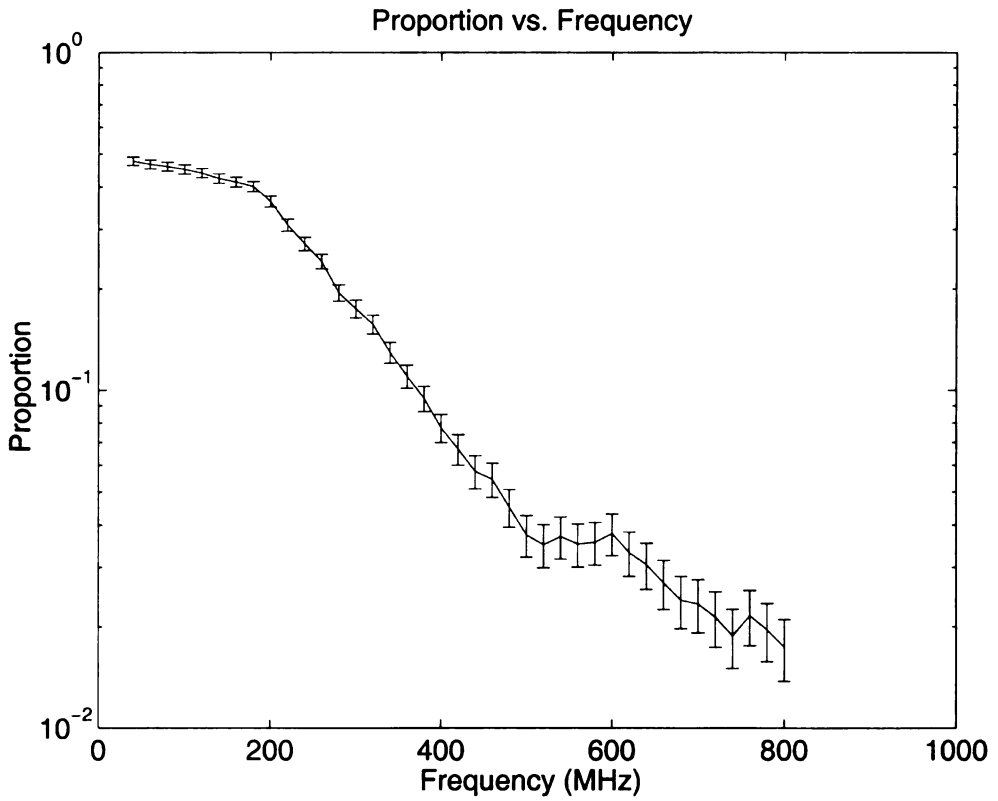


Figure 5.135. Proportion of configurations with minimum vertical gains in the horizontal plane above 0 dB vs. frequency for the layer 3 Type I SSA template in free space (5000 random samples). Error bars show the 95% confidence intervals.

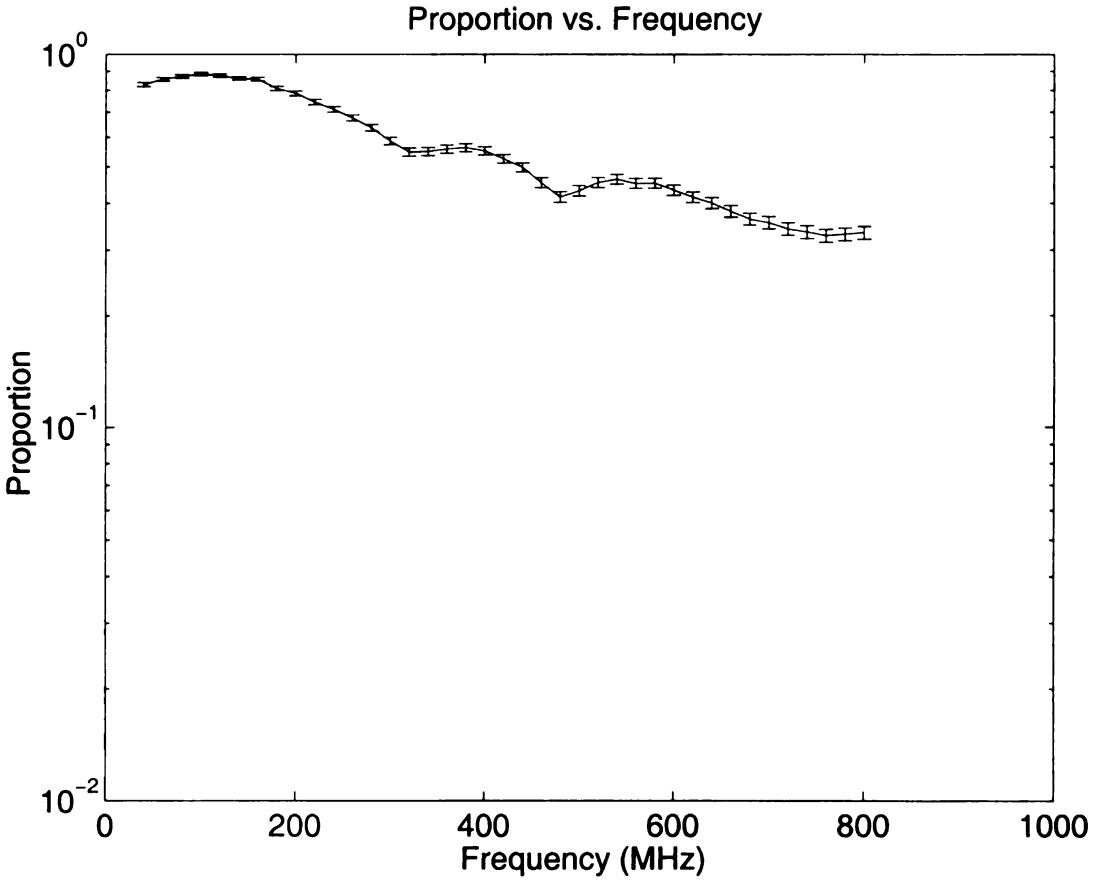


Figure 5.136. Proportion of configurations with minimum vertical gains in the horizontal plane above 0 dB vs. frequency for the layer 3 Type I SSA template above ground (5000 random samples). Error bars show the 95% confidence intervals.

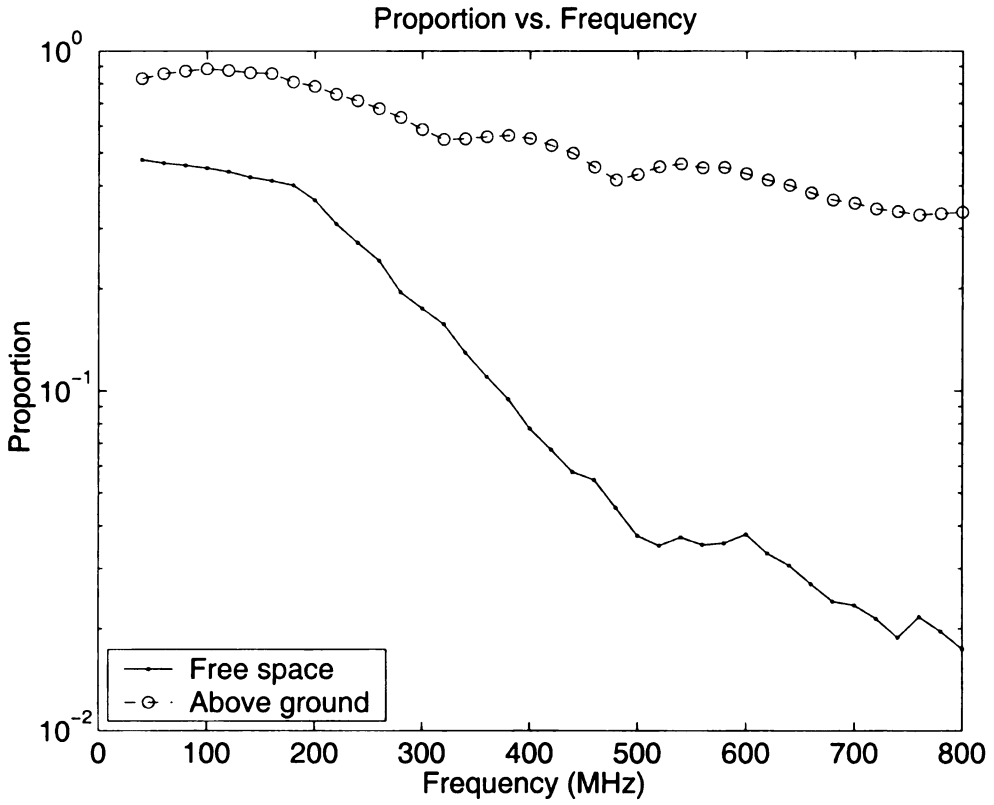


Figure 5.137. Proportion of configurations with minimum vertical gains in the horizontal plane above 0 dB vs. frequency for the layer 3 Type I SSA template (5000 random samples).

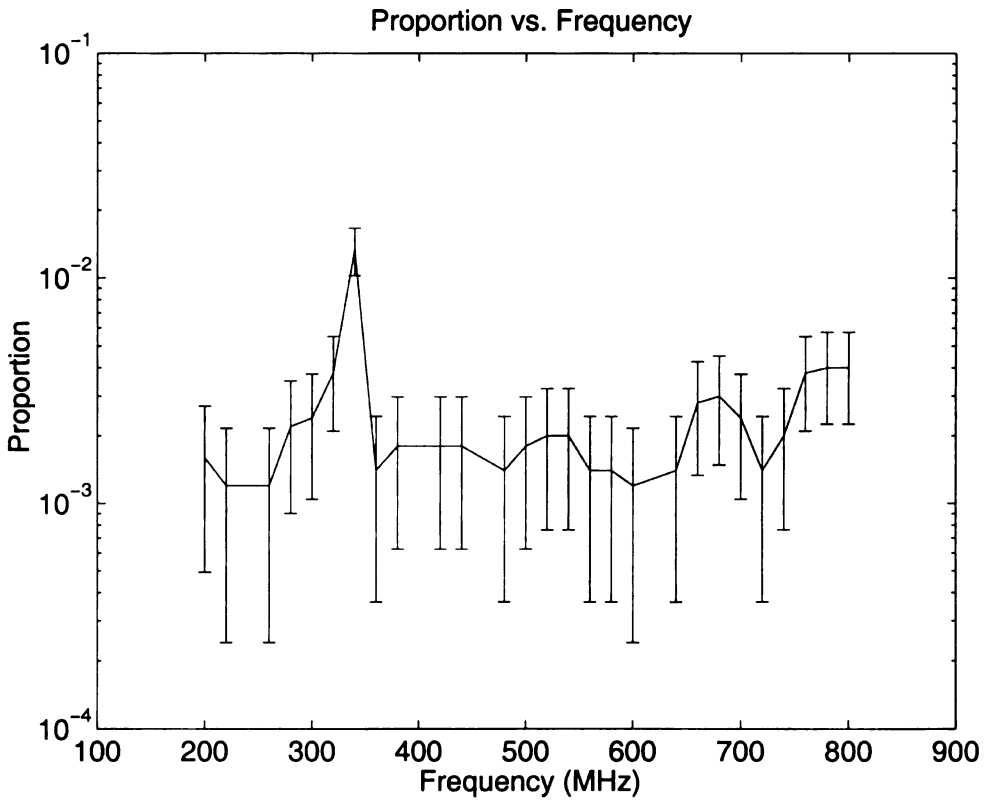


Figure 5.138. Proportion of configurations with SWRs less than 2.0 and minimum vertical gains in the horizontal plane above 0 dB vs. frequency for the layer 3 Type I SSA template in free space (5000 random samples). Error bars show the 95% confidence intervals.

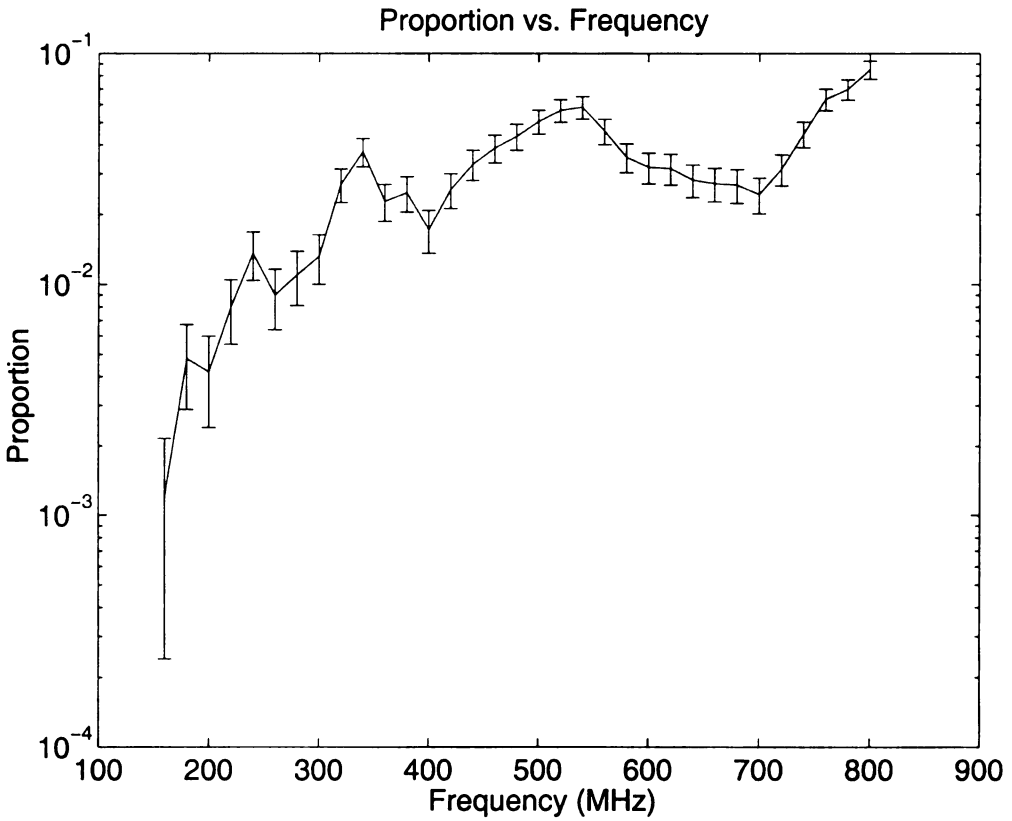


Figure 5.139. Proportion of configurations with SWRs less than 2.0 and minimum vertical gains in the horizontal plane above 0 dB vs. frequency for the layer 3 Type I SSA template above ground (5000 random samples). Error bars show the 95% confidence intervals.

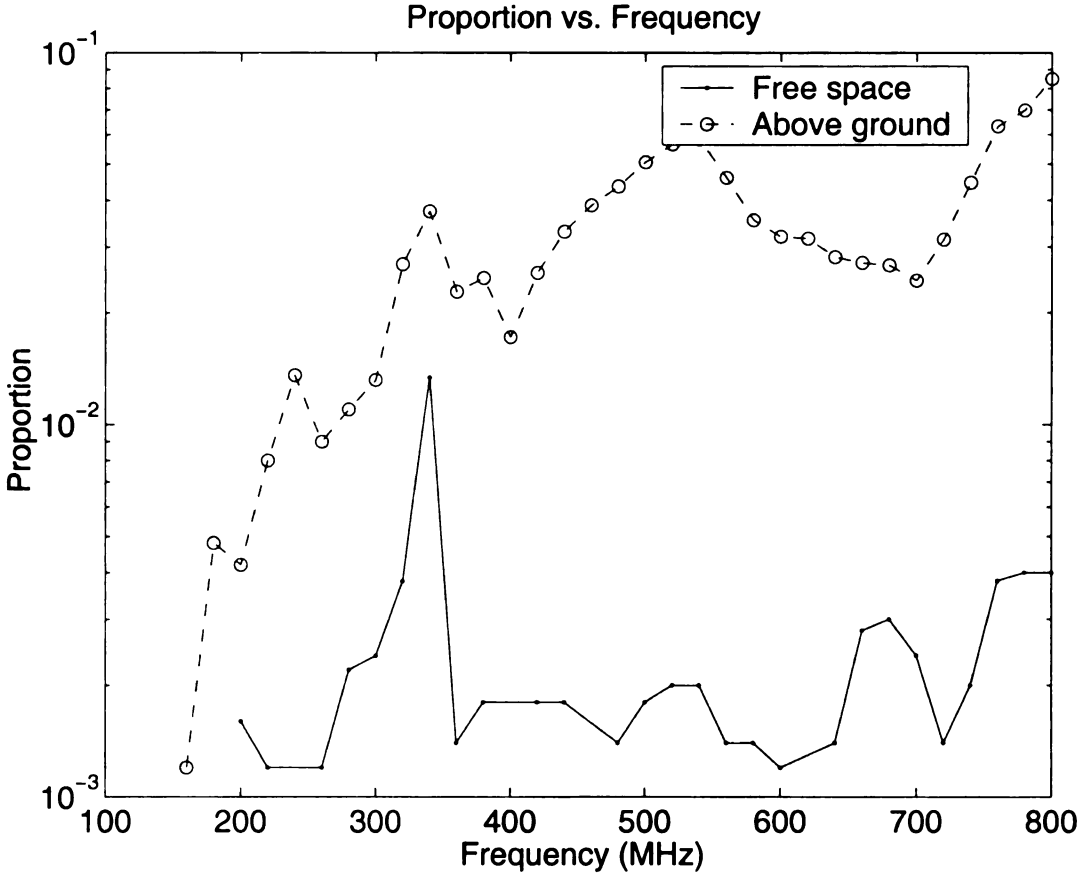


Figure 5.140. Proportion of configurations with SWRs less than 2.0 and minimum vertical gains in the horizontal plane above 0 dB vs. frequency for the layer 3 Type I SSA template (5000 random samples).

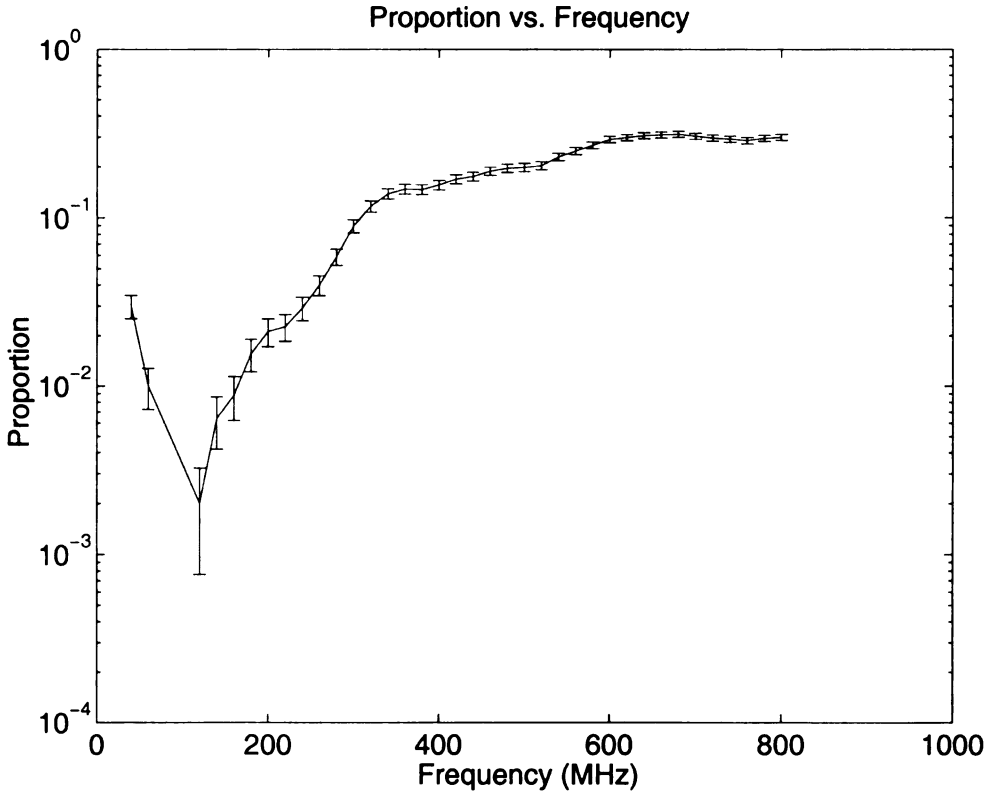


Figure 5.141. Proportion of configurations with maximum vertical gains in the horizontal plane above 3.0 dB vs. frequency for the layer 3 Type I SSA template in free space (5000 random samples). Error bars show the 95% confidence intervals.

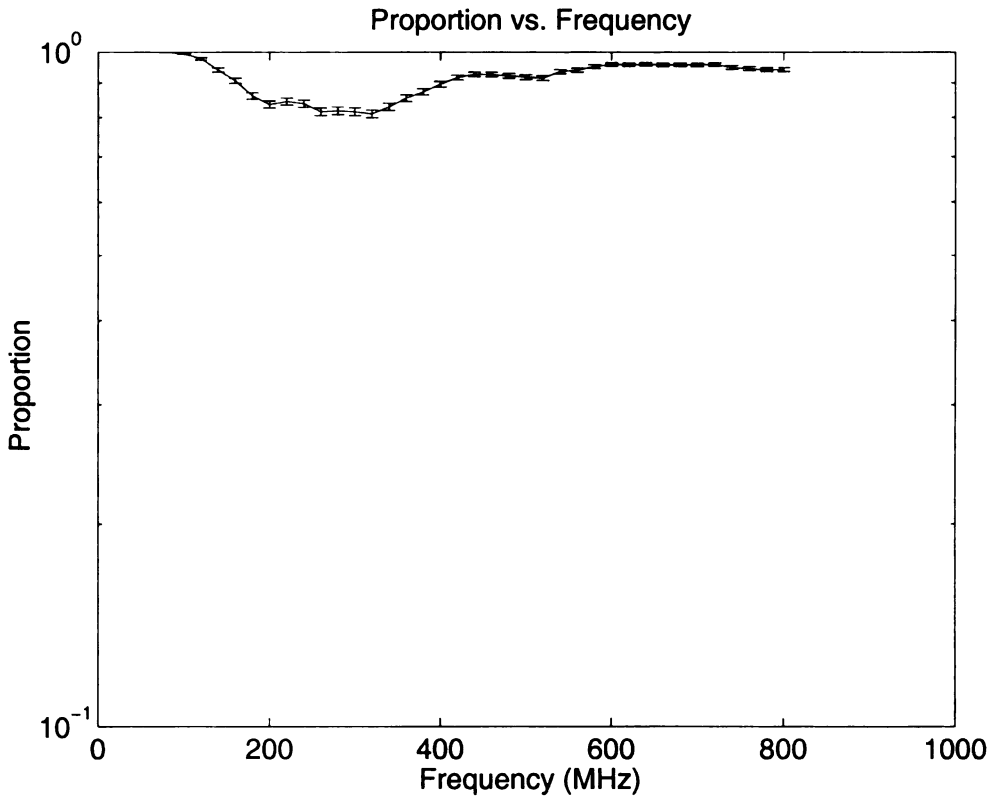


Figure 5.142. Proportion of configurations with maximum vertical gains in the horizontal plane above 3.0 dB vs. frequency for the layer 3 Type I SSA template above ground (5000 random samples). Error bars show the 95% confidence intervals.

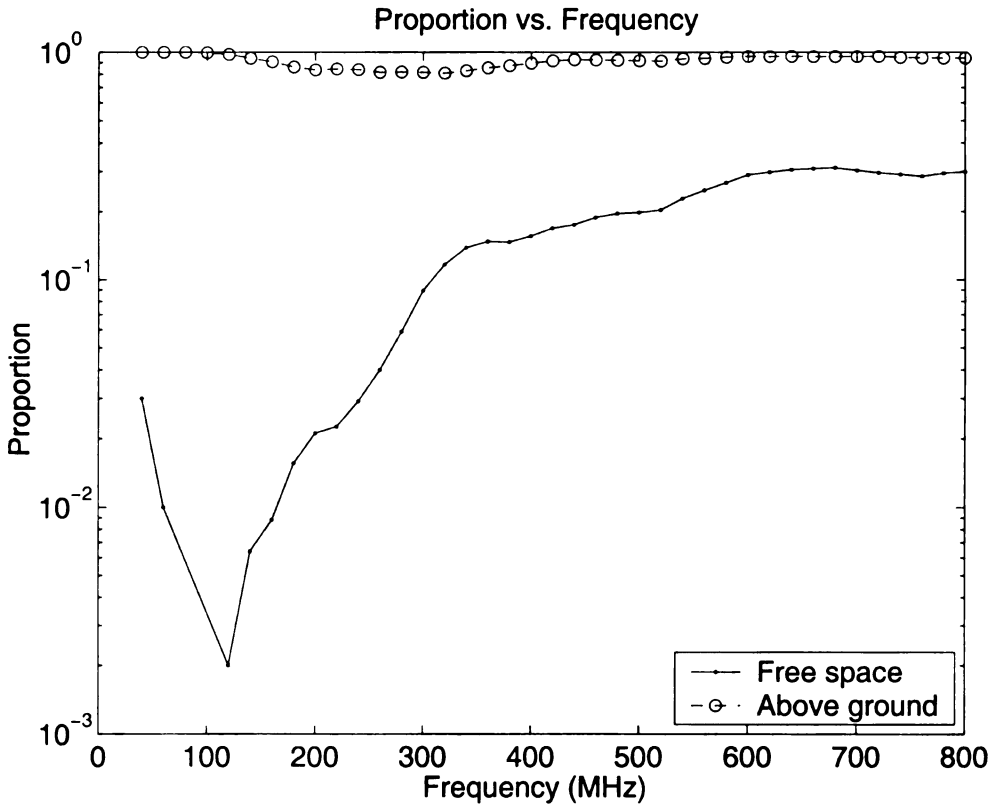


Figure 5.143. Proportion of configurations with maximum vertical gains in the horizontal plane above 3.0 dB vs. frequency for the layer 3 Type I SSA template (5000 random samples).

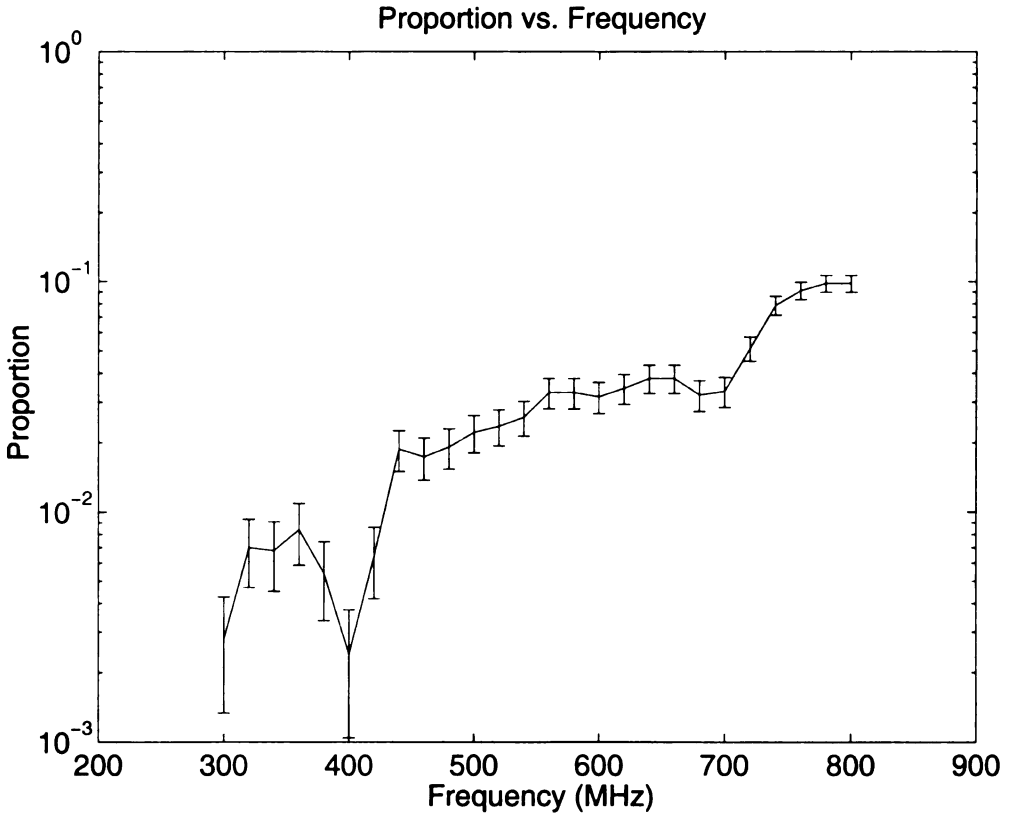


Figure 5.144. Proportion of configurations with SWRs less than 2.0 and maximum vertical gains in the horizontal plane above 3.0 dB vs. frequency for the layer 3 Type I SSA template in free space (5000 random samples). Error bars show the 95% confidence intervals.

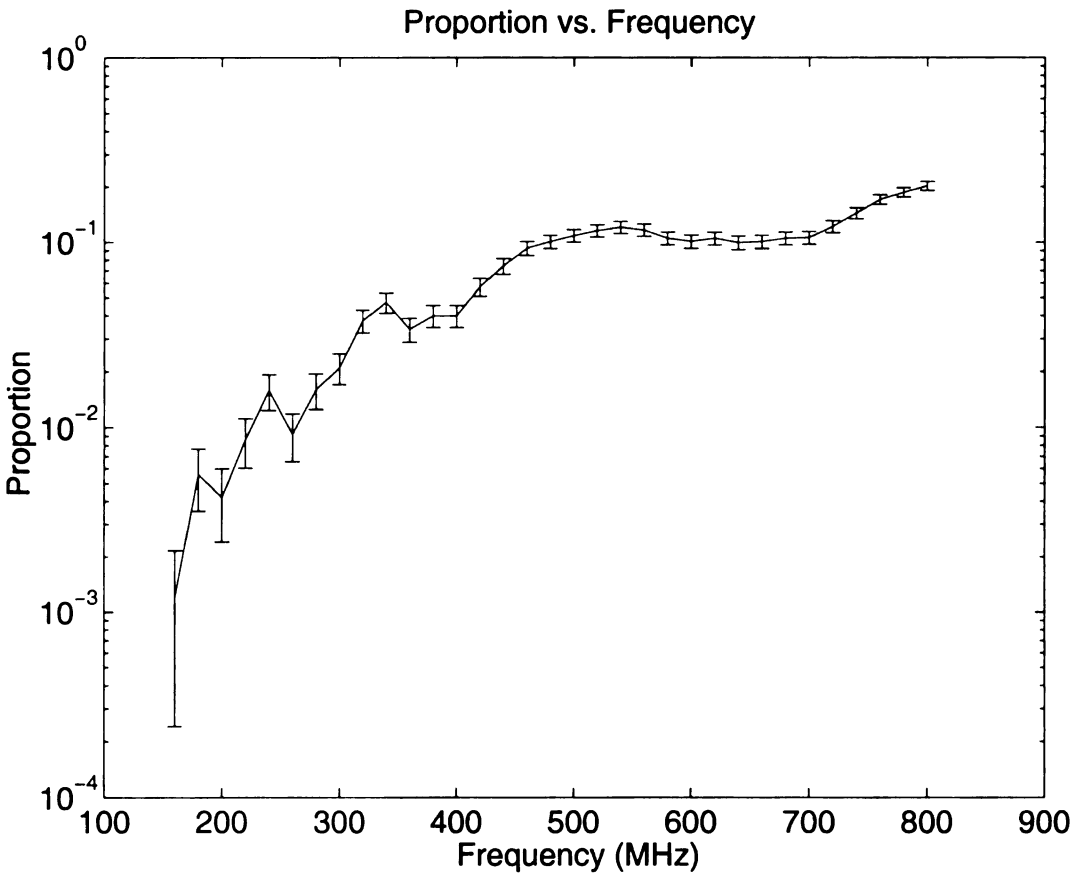


Figure 5.145. Proportion of configurations with SWRs less than 2.0 and maximum vertical gains in the horizontal plane above 3.0 dB vs. frequency for the layer 3 Type I SSA template above ground (5000 random samples). Error bars show the 95% confidence intervals.

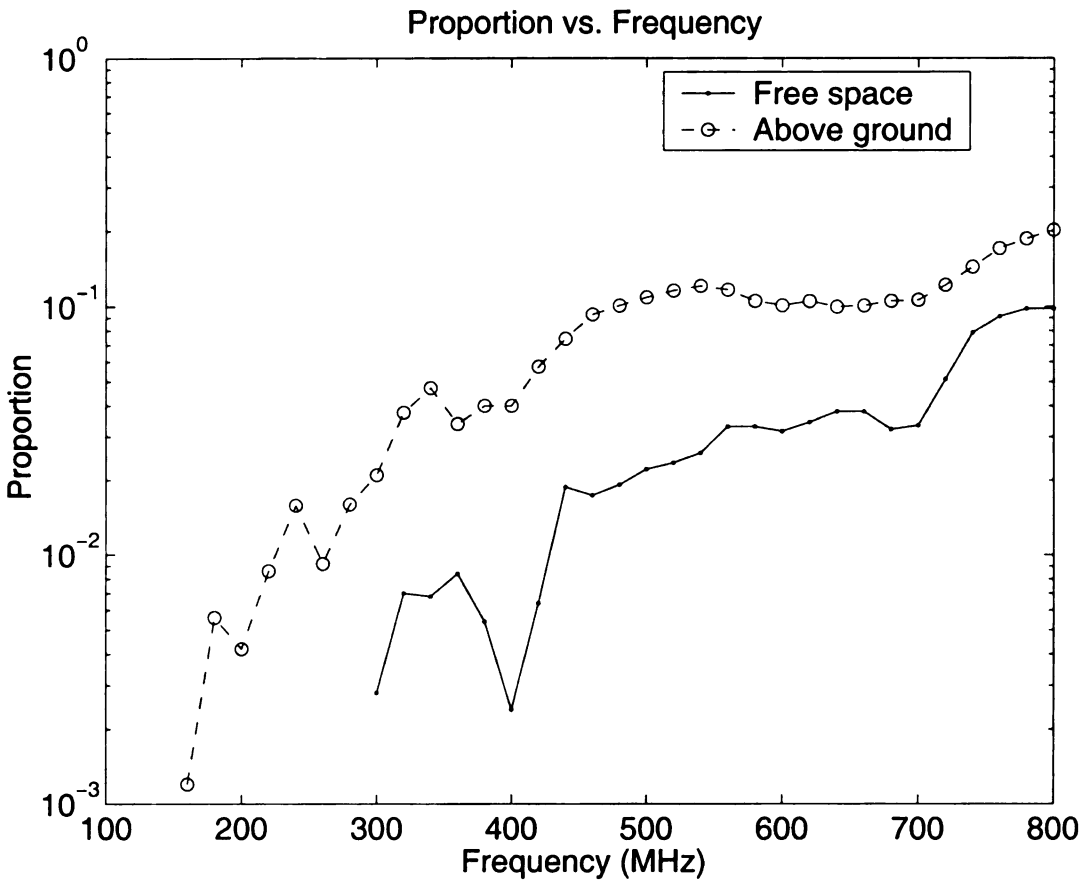


Figure 5.146. Proportion of configurations with SWRs less than 2.0 and maximum vertical gains in the horizontal plane above 3.0 dB vs. frequency for the layer 3 Type I SSA template (5000 random samples).

5.3.6 Layer 4 SSA Template

A diagram of the layer 4 template is shown in Figure 5.147. 21 switches are used for 2,097,152 possible SSA configurations. The outer dimensions of the layer 4 Type I SSA template are shown in Table 5.12.

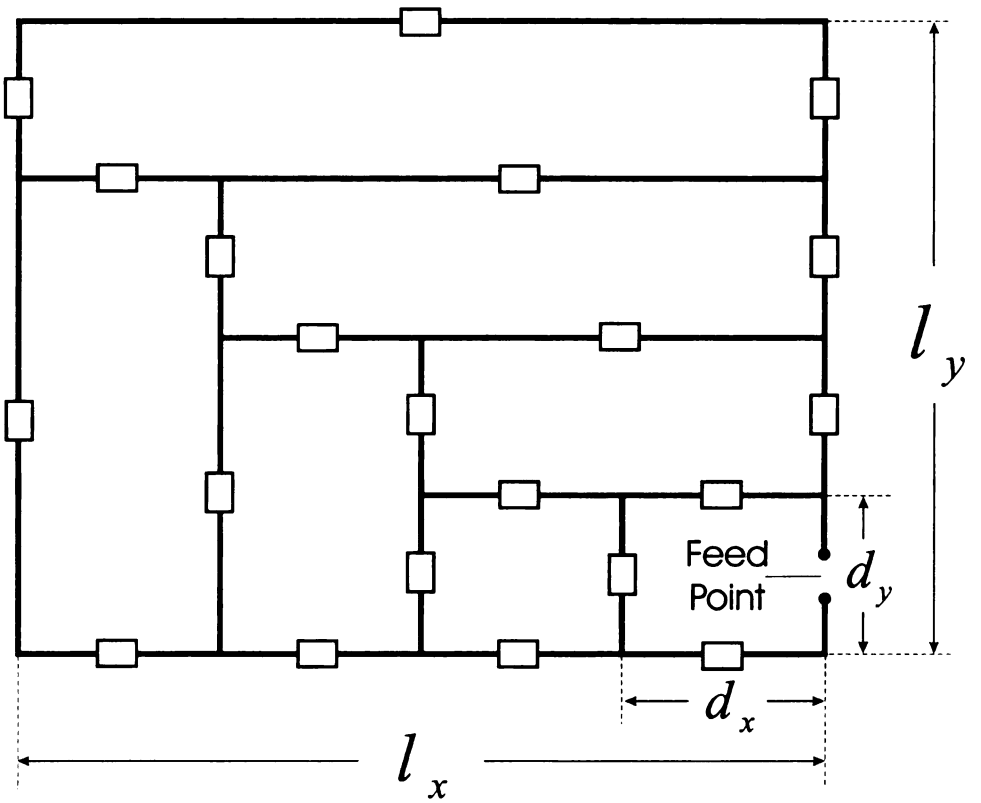


Figure 5.147. Diagram of the layer 4 SSA template.

As was performed for the layer 3 template, 5000 random samples of the SSA configurations were evaluated for the layer 4 Type I template. The results of this sample are presented here. Only the layer 4 Type I template in free space is presented, and is designated as the 'layer 4 template.'

The SWR of each random configuration at each frequency is plotted in Figure 5.148 for the layer 4 template. Nearly continuous possible SWRs exist at most frequencies. The minimum SWR found at each frequency is shown in Figure 5.149. The random sample of the layer 4 template has found configurations that exhibit SWRs below 2.0 at 100 MHz and above.

The estimate of the proportion $\hat{p}$ of SSA configurations for the layer 4 Type I

Table 5.12. Dimensions of the layer 4 Type I SSA template.

l_x	34.3 cm
d_x	8.57 cm
l_y	34.3 cm
d_y	8.57 cm
Outer electrical dimensions at 40 MHz	$0.0457\lambda \times 0.0457\lambda$
Outer electrical dimensions at 800 MHz	$0.914\lambda \times 0.914\lambda$

template with SWRs less than 4.0 is shown in Figure 5.150 across the studied frequency band. The error bars represent the 95% confidence interval for the estimate of $\hat{p}$. Notice that at the higher frequencies, the confidence intervals are much tighter around the population estimates because there are many samples that have SWRs less than 4.0. At the lower frequencies where the template is electrically smaller, the confidence intervals are much larger. For instance, the upper bound of the 95% confidence interval is nearly 50 times the size of the lower bound for the estimate at 60 MHz.

As Figure 5.150 shows, an SWR of 4.0 is not a very stringent threshold for this template at the higher frequencies. The proportions of configurations with SWRs less than 2.0, 1.5, 1.1, and 1.05 are shown in Figure 5.151 through Figure 5.154. As the threshold SWR is decreased, the number of configurations that meet the SWR criterion decrease. This is evident in Figure 5.153 and Figure 5.154, where the threshold SWR is 1.1 and 1.05, respectively. At many frequencies across the band, there are not enough successful trials to make valid confidence intervals on the parameter estimates. However, these figures show that some configurations do exist that meet the test criteria.

Figure 5.155 shows the estimate for the proportion of configurations with minimum vertical gains in the horizontal plane above 0 dB for the layer 4 template. These proportions are reduced if the criterion requiring SWRs to be less than 2.0 is added,

as shown in Figure 5.156.

Figure 5.157 shows the estimate for the proportion of configurations with maximum vertical gains in the horizontal plane above 3.0 dB for the layer 4 template. The proportion of configurations with SWRs less than 2.0 and maximum gains above 3.0 dB is shown in Figure 5.158. The additional SWR criterion has reduced the proportion across the frequency band.

The shape of the maximum and minimum gain and SWR proportions for the layer 4 template are similar to those of the layer 3 template in free space. Therefore, the results for the layer 5 and layer 6 templates do not present the same number proportion plots for the sake of brevity. The discussion of the layer 7 template, however, contains several gain and SWR proportion estimates.

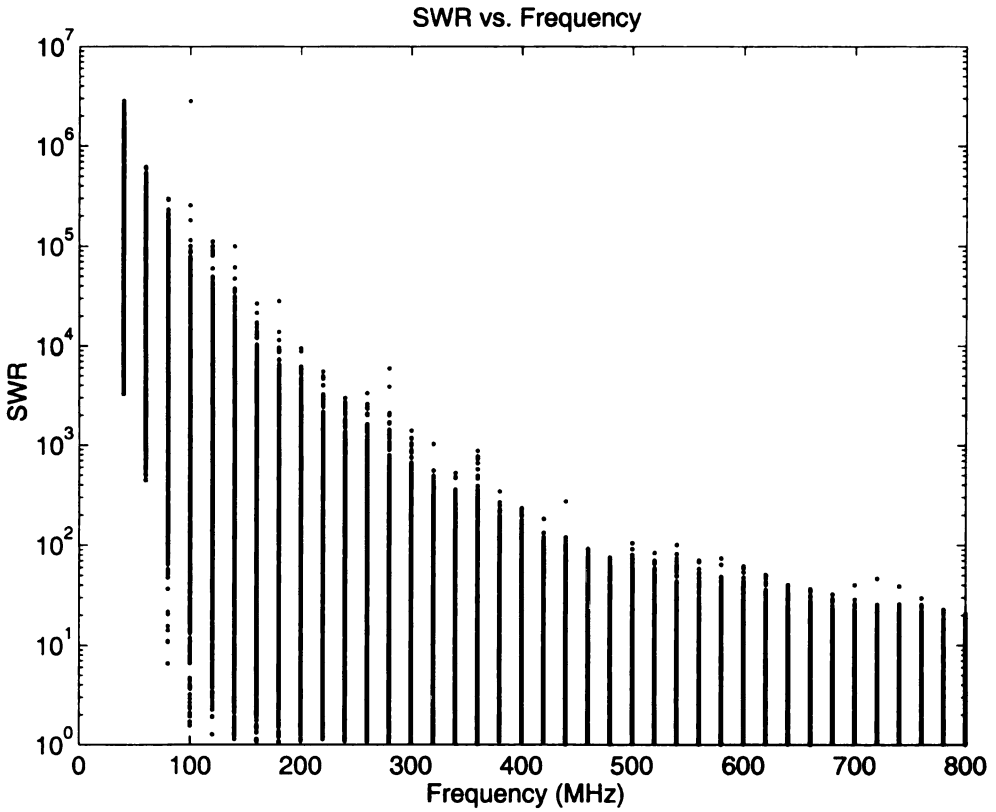


Figure 5.148. SWR vs. frequency for the layer 4 Type I SSA template (5000 random samples).

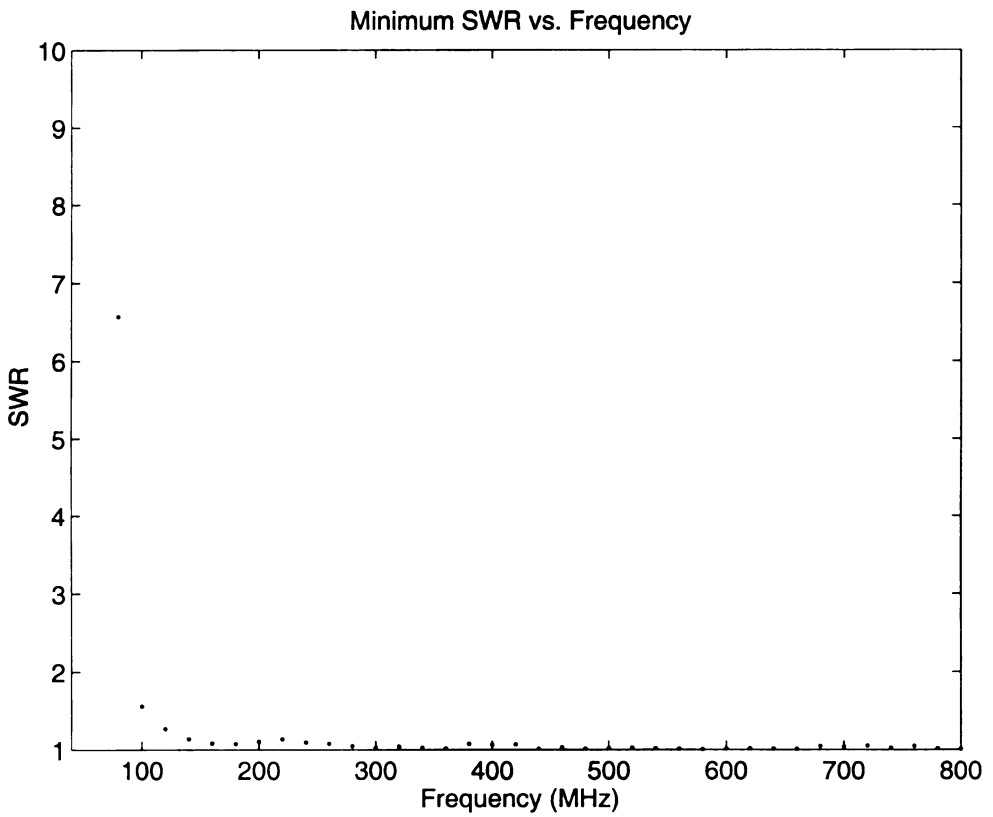


Figure 5.149. Minimum SWR vs. frequency for the layer 4 Type I SSA template (5000 random samples).

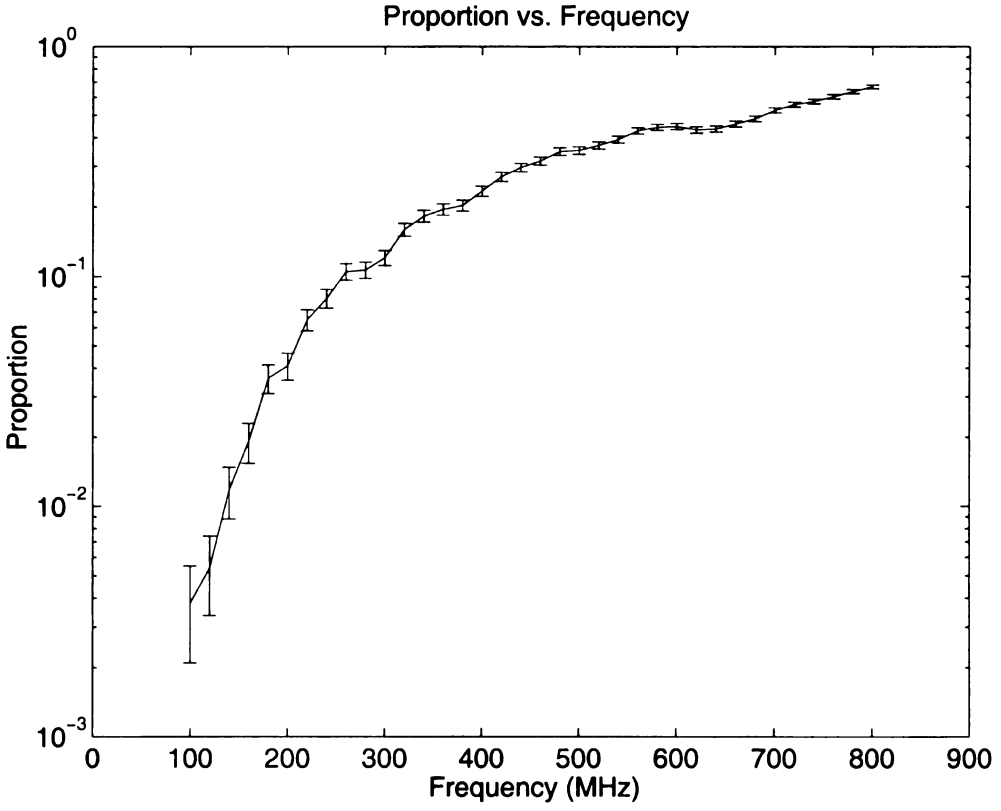


Figure 5.150. Proportion of configurations with SWRs less than 4.0 vs. frequency for the layer 4 Type I SSA template (5000 random samples). Error bars show the 95% confidence intervals.

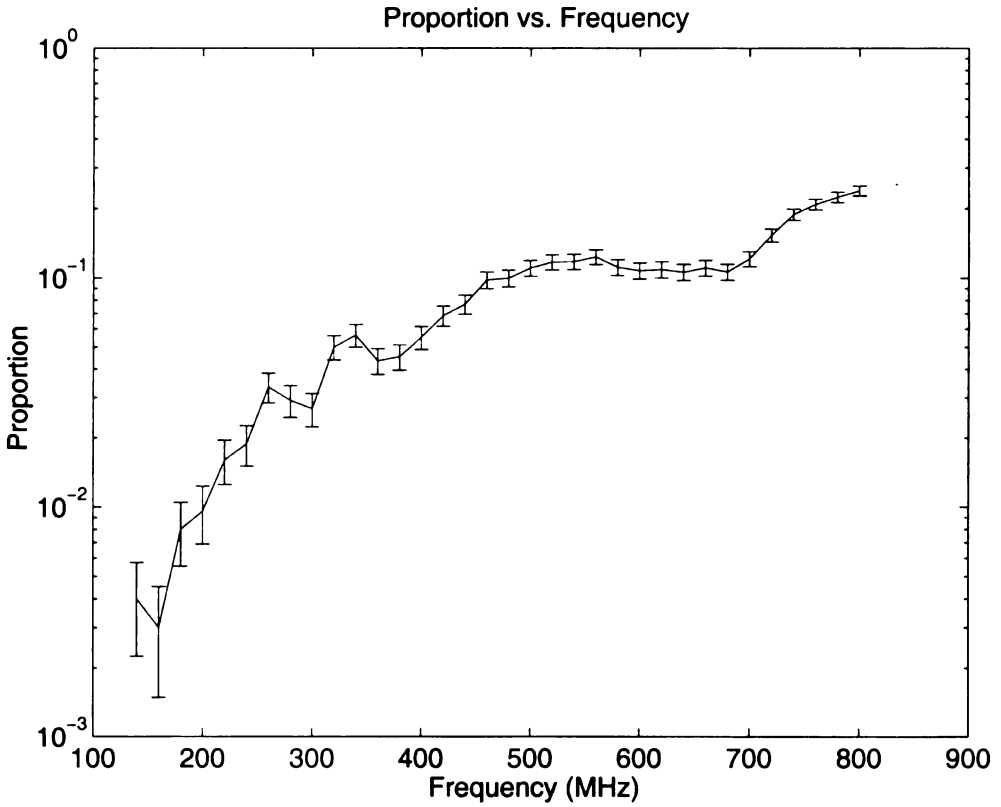


Figure 5.151. Proportion of configurations with SWRs less than 2.0 vs. frequency for the layer 4 Type I SSA template (5000 random samples). Error bars show the 95% confidence intervals.

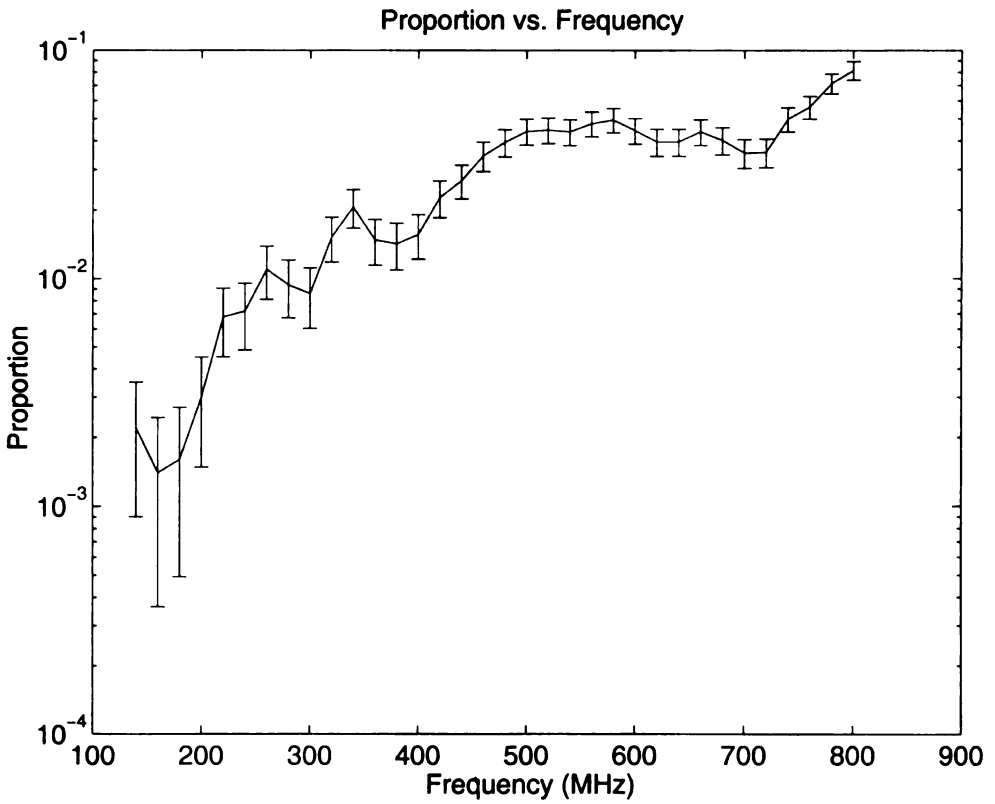


Figure 5.152. Proportion of configurations with SWRs less than 1.5 vs. frequency for the layer 4 Type I SSA template (5000 random samples). Error bars show the 95% confidence intervals.

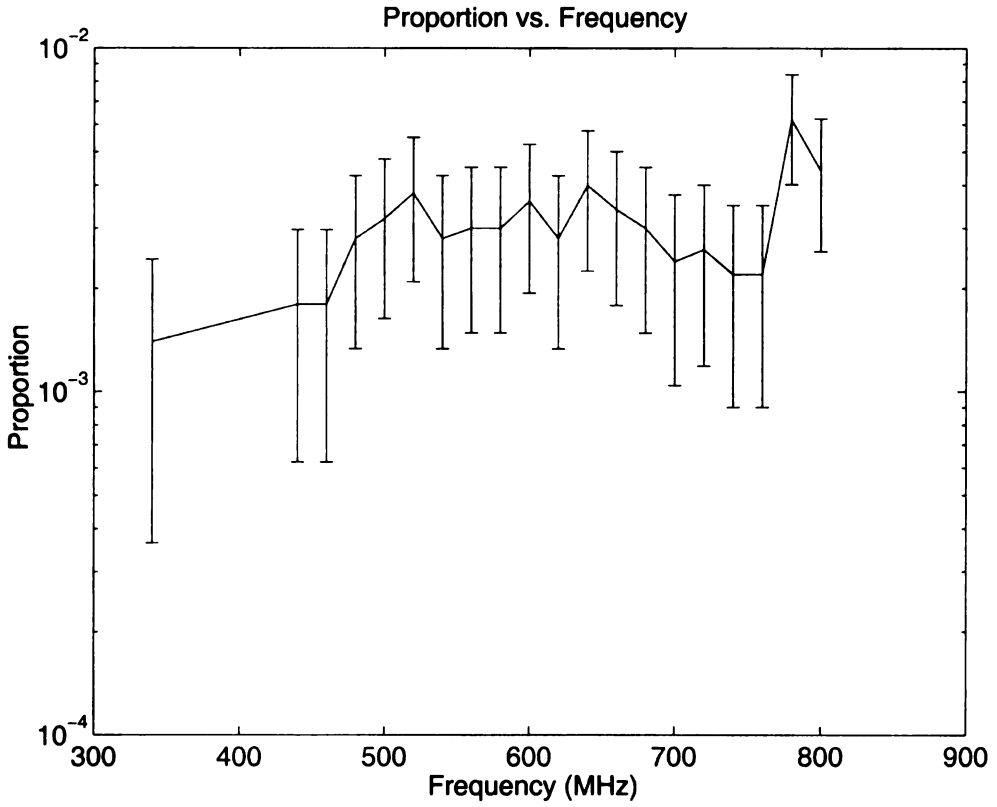


Figure 5.153. Proportion of configurations with SWRs less than 1.1 vs. frequency for the layer 4 Type I SSA template (5000 random samples). Error bars show the 95% confidence intervals.

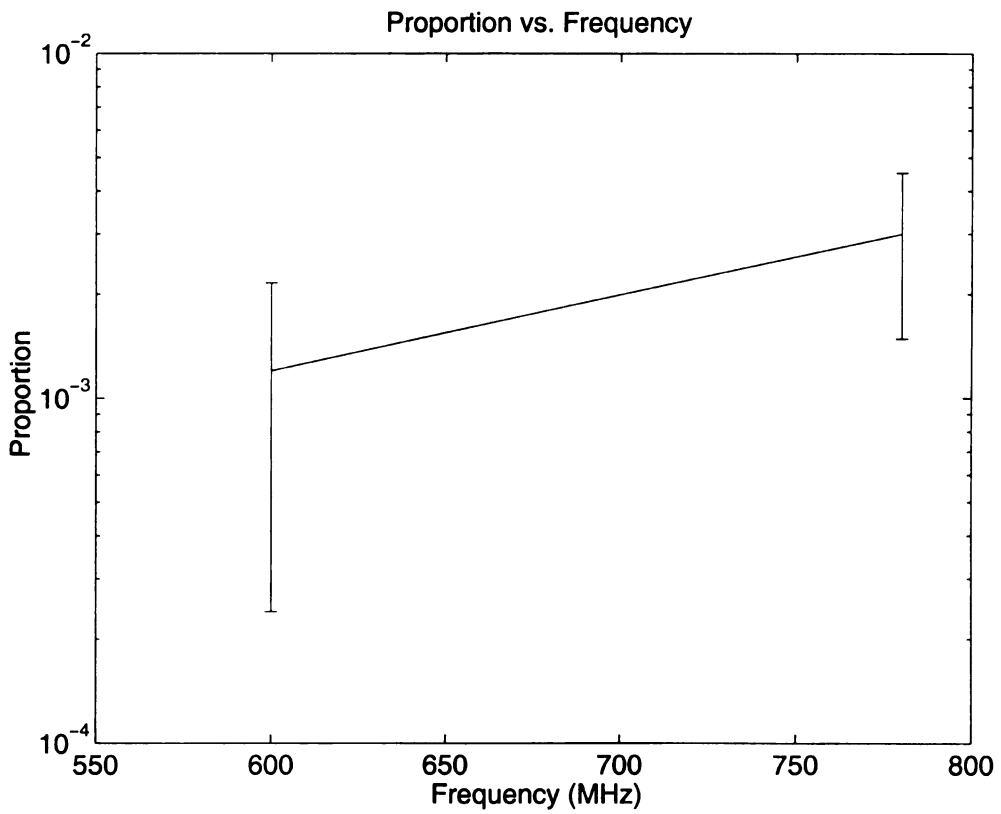


Figure 5.154. Proportion of configurations with SWRs less than 1.05 vs. frequency for the layer 4 Type I SSA template (5000 random samples). Error bars show the 95% confidence intervals.

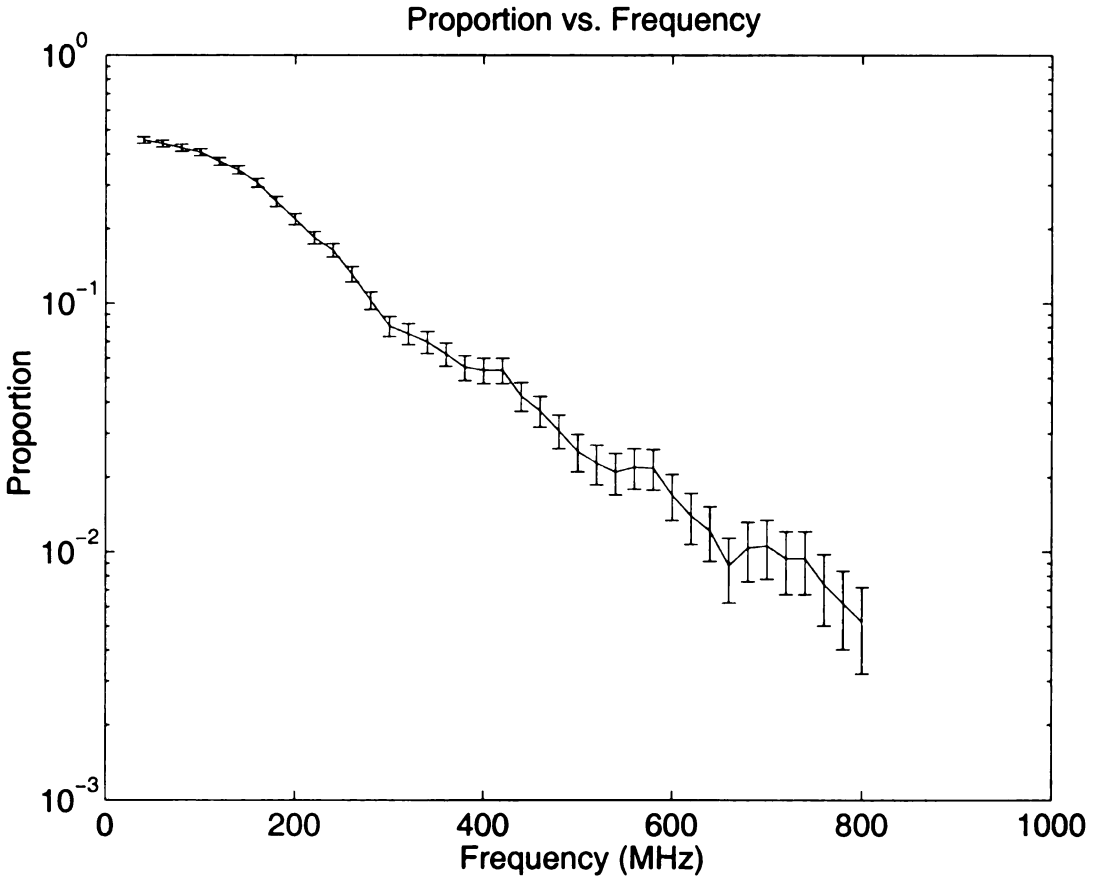


Figure 5.155. Proportion of configurations with minimum vertical gains in the horizontal plane above 0 dB vs. frequency for the layer 4 Type I SSA template (5000 random samples). Error bars show the 95% confidence intervals.

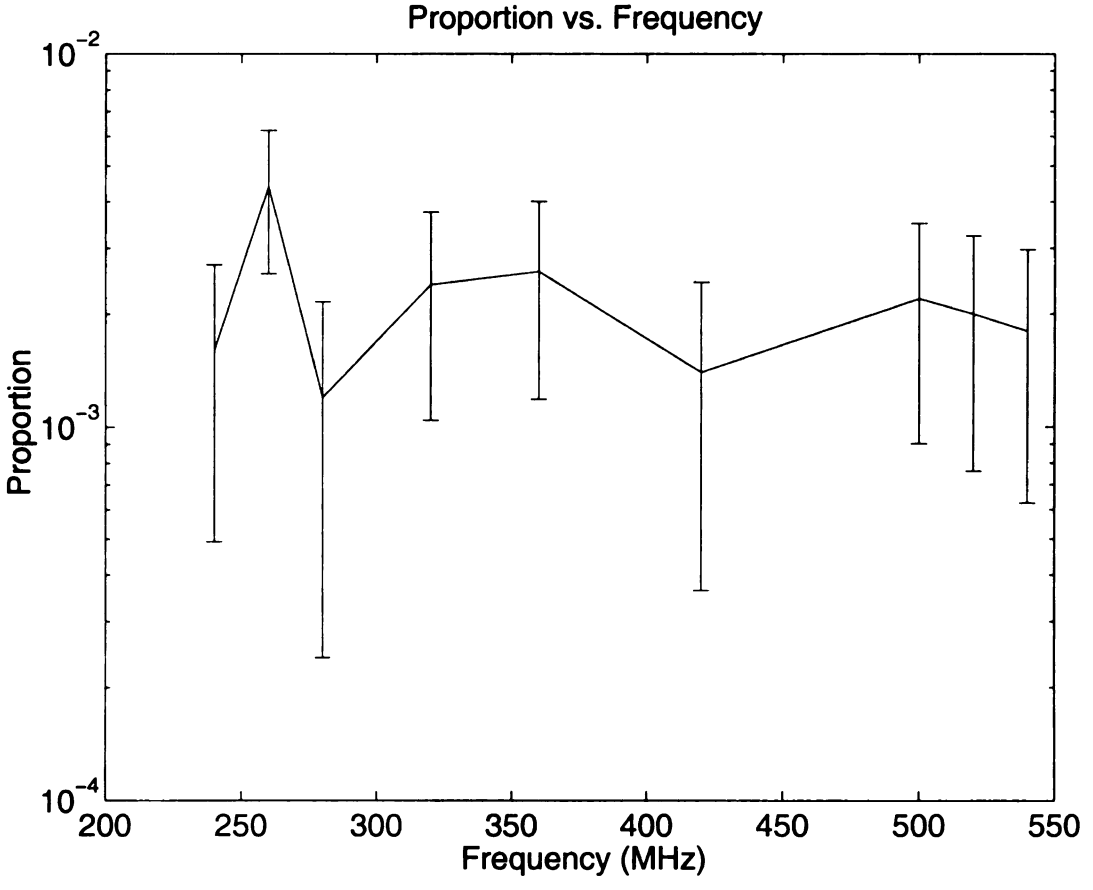


Figure 5.156. Proportion of configurations with SWRs less than 2.0 and minimum vertical gains in the horizontal plane above 0 dB vs. frequency for the layer 4 Type I SSA template (5000 random samples). Error bars show the 95% confidence intervals.

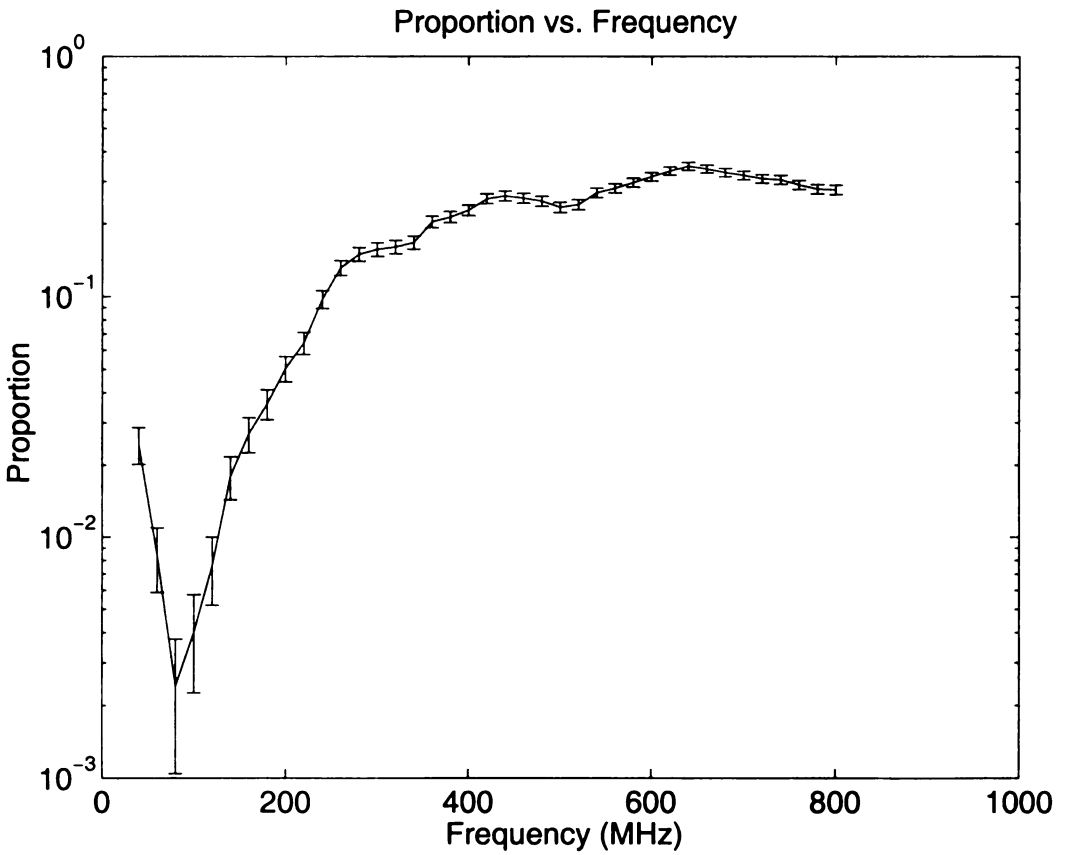


Figure 5.157. Proportion of configurations with maximum vertical gains in the horizontal plane above 3.0 dB vs. frequency for the layer 4 Type I SSA template (5000 random samples). Error bars show the 95% confidence intervals.

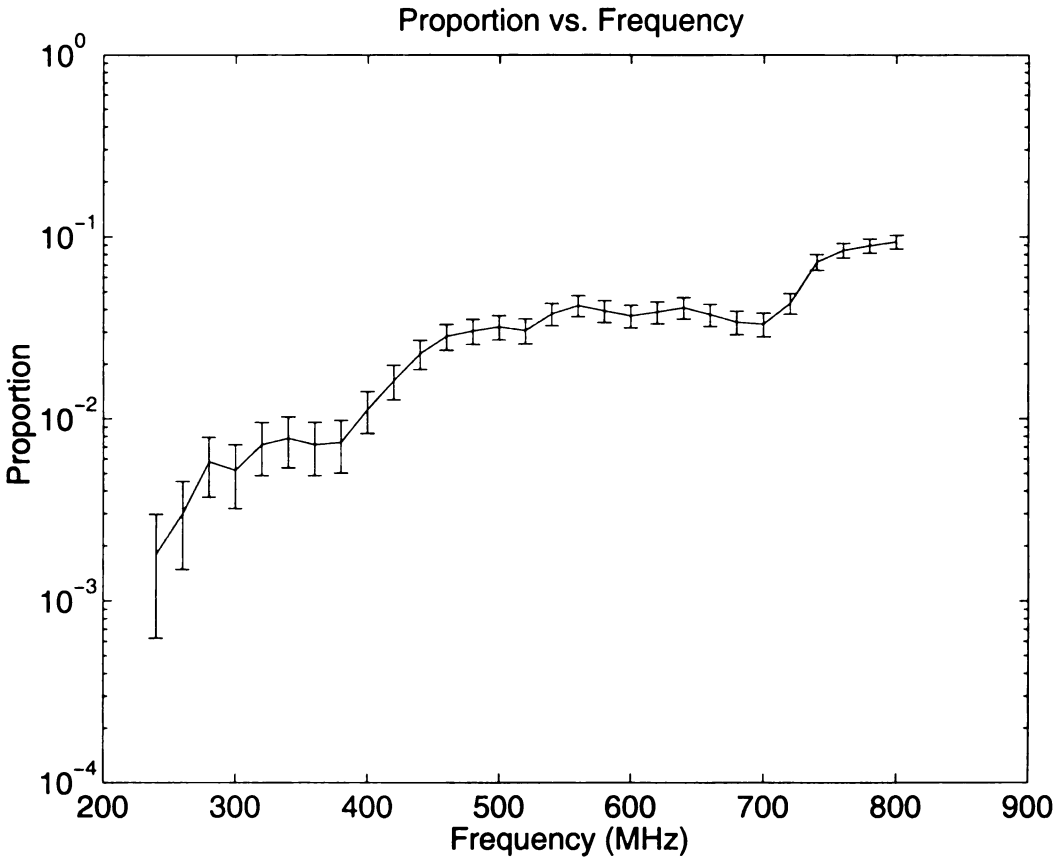


Figure 5.158. Proportion of configurations with SWRs less than 2.0 and maximum vertical gains in the horizontal plane above 3.0 dB vs. frequency for the layer 4 Type I SSA template (5000 random samples). Error bars show the 95% confidence intervals.

5.3.7 Layer 5 SSA Template

A diagram of the layer 5 template is shown in Figure 5.159. 27 switches are used for 134,217,728 possible SSA configurations. The outer dimensions of the layer 5 Type I SSA template are shown in Table 5.13.

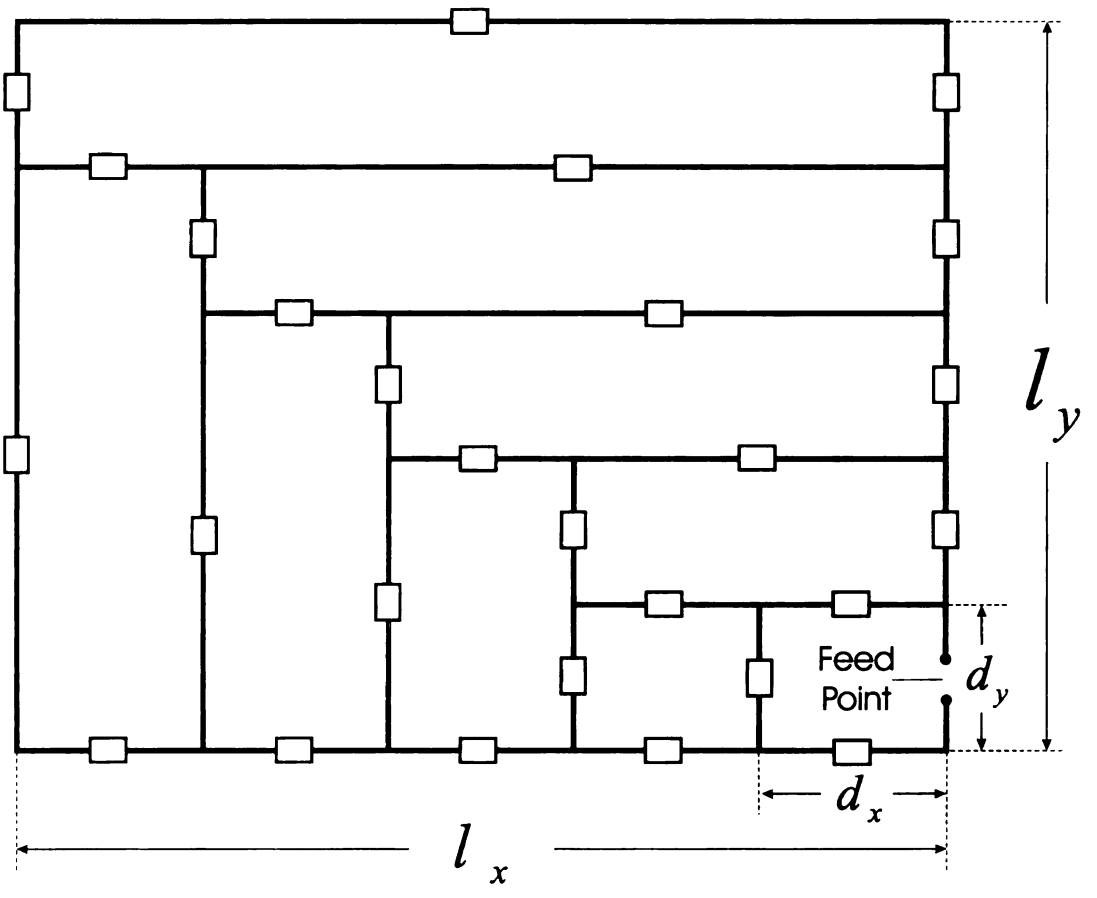


Figure 5.159. Diagram of the layer 5 SSA template.

As was performed for the layer 3 template described in Section 5.3.5, 5000 random samples of the SSA configurations were evaluated for the layer 5 Type I template. The results of this sample are presented here. Only the layer 5 Type I template in free space is presented, and is designated as the 'layer 5 template.'

The SWR of each random configuration at each frequency is plotted in Figure 5.160 for the layer 5 template. Nearly continuous possible SWRs exist at most frequencies. The minimum SWR found at each frequency is shown in Figure 5.161. These figures follow the trend of the layer 3 and layer 4 templates. Low SWR values extend lower in frequency for the layer 5 template.

The estimate of the proportion of configurations with SWRs less than 2.0 is shown

Table 5.13. Dimensions of the layer 5 Type I SSA template.

l_x	42.9 cm
d_x	8.57 cm
l_y	42.9 cm
d_y	8.57 cm
Outer electrical dimensions at 40 MHz	$0.0571\lambda \times 0.0571\lambda$
Outer electrical dimensions at 800 MHz	$1.14\lambda \times 1.14\lambda$

in Figure 5.162 for the layer 5 template. Figure 5.163 shows the proportion of configurations with SWRs less than 2.0 and maximum vertical gains in the horizontal plane above 3.0 dB. The estimate of the proportion of configurations with SWRs less than 2.0 and minimum vertical gains above 0 dB is shown in Figure 5.164. The proportion of configurations that meet these criteria is low across the band. Recall that the layer 5 template is in free space, and the templates above ground for the other layers exhibit higher vertical gains.

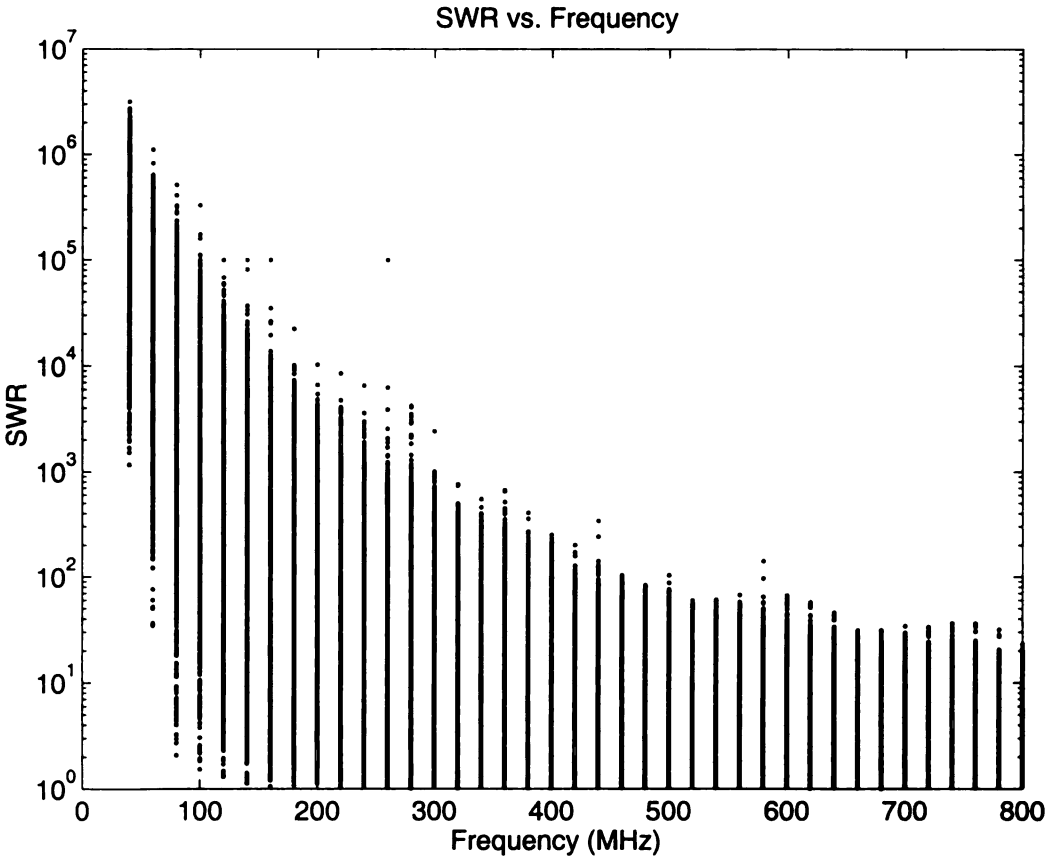


Figure 5.160. SWR vs. frequency for the layer 5 Type I SSA template (5000 random samples).

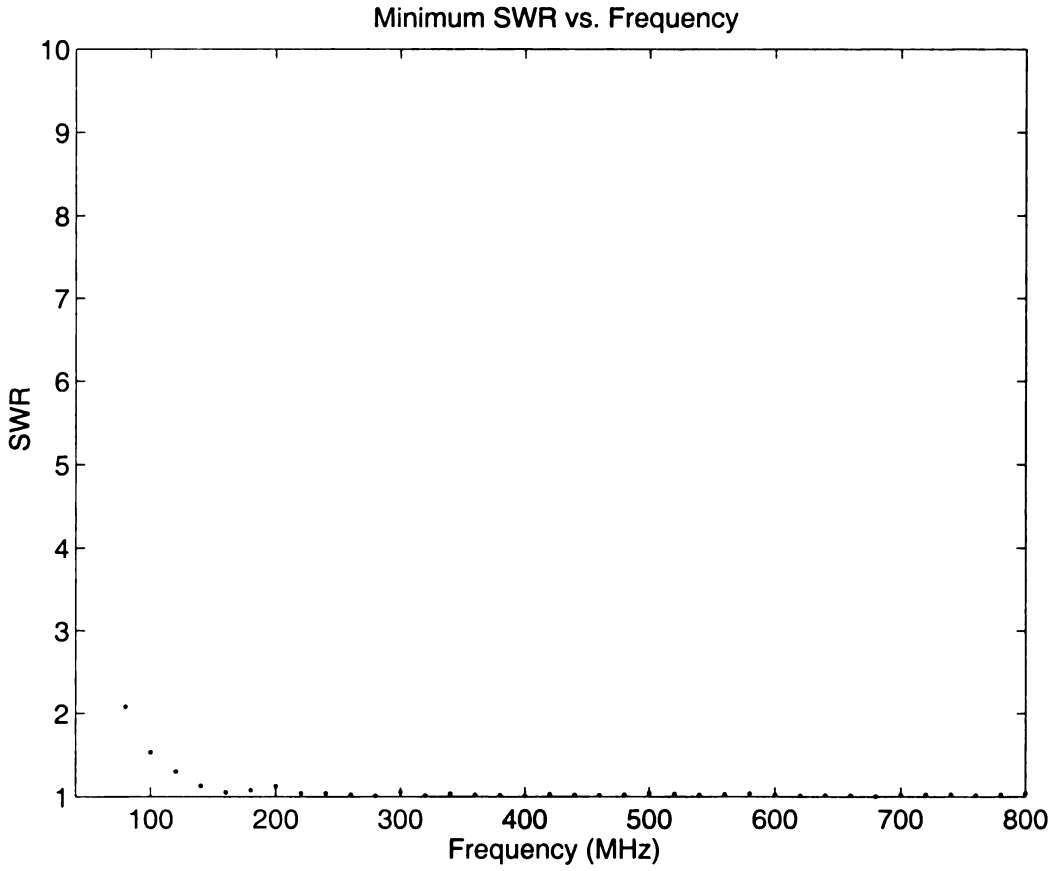


Figure 5.161. Minimum SWR vs. frequency for the layer 5 Type I SSA template (5000 random samples).

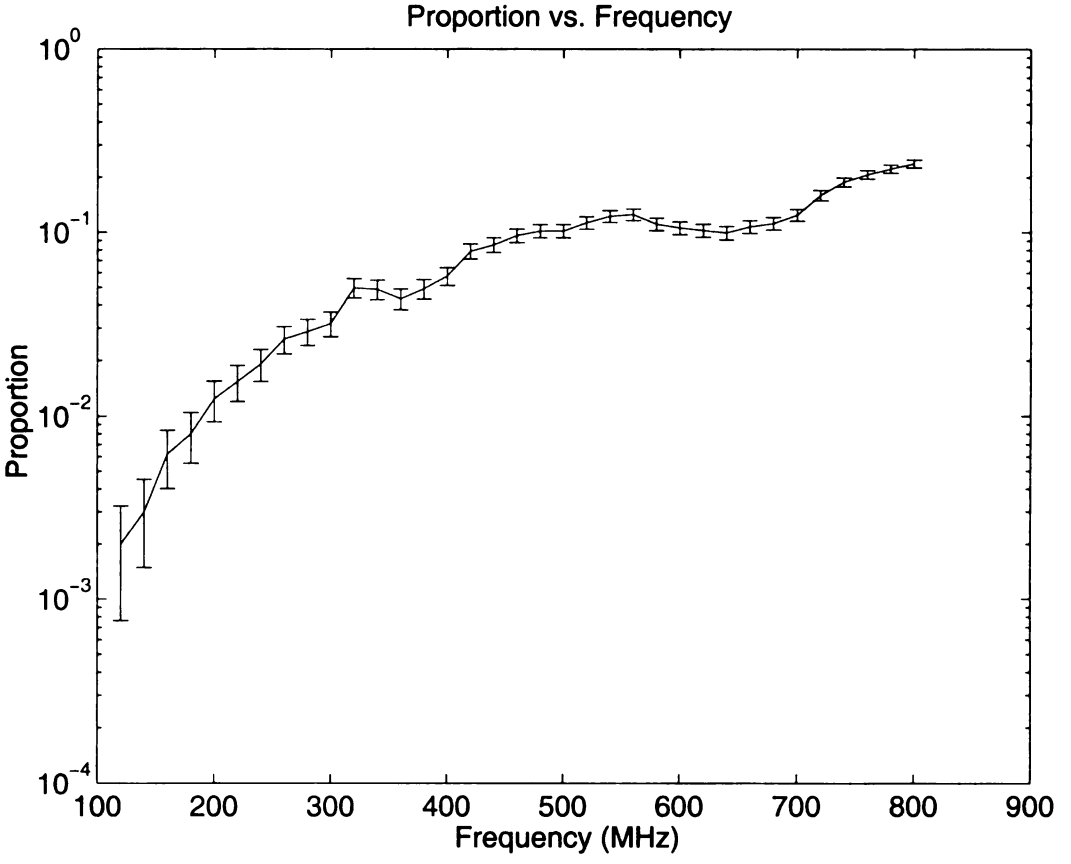


Figure 5.162. Proportion of configurations with SWRs less than 2.0 vs. frequency for the layer 5 Type I SSA template (5000 random samples). Error bars show the 95% confidence intervals.

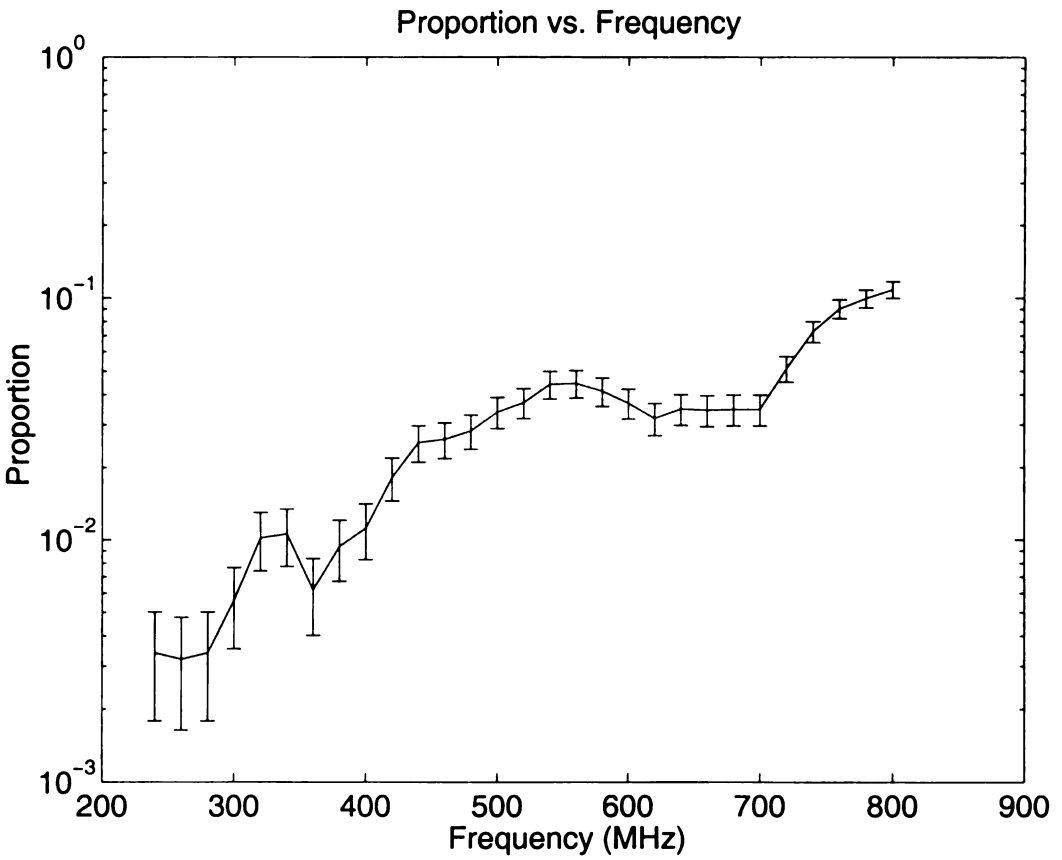


Figure 5.163. Proportion of configurations with SWRs less than 2.0 and maximum vertical gains in the horizontal plane above 3.0 dB vs. frequency for the layer 5 Type I SSA template (5000 random samples). Error bars show the 95% confidence intervals.

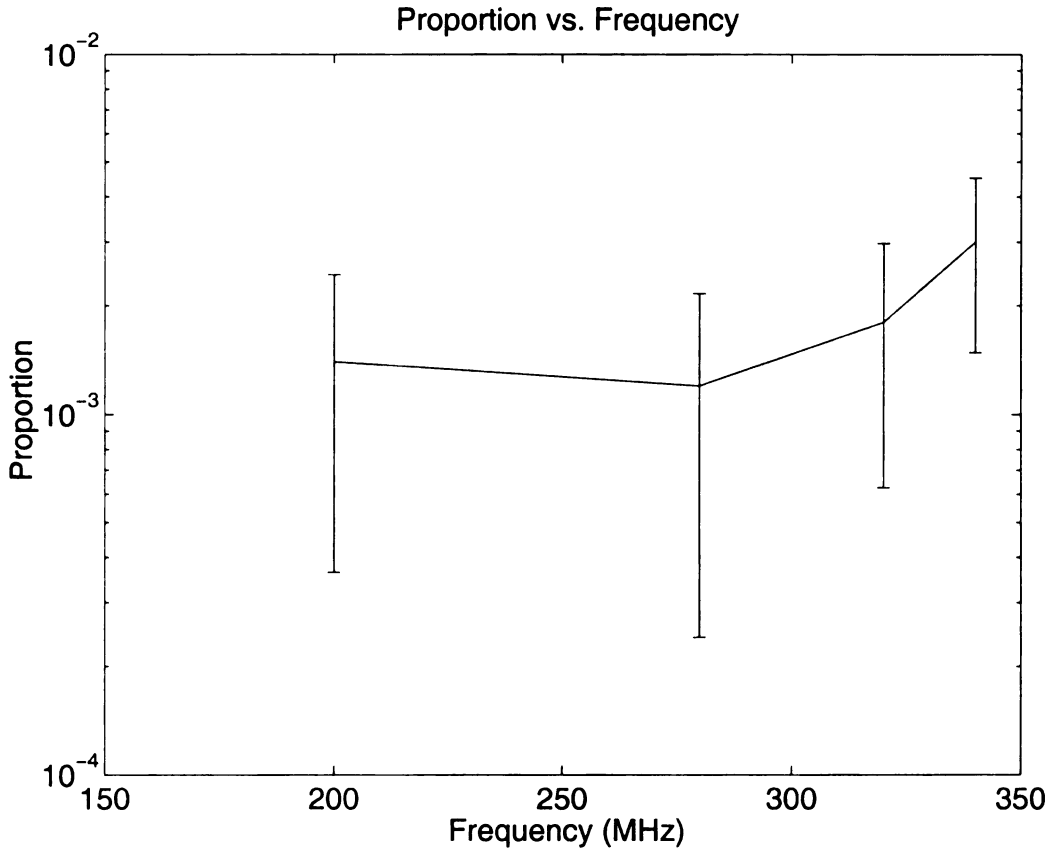


Figure 5.164. Proportion of configurations with SWRs less than 2.0 and minimum vertical gains in the horizontal plane above 0 dB vs. frequency for the layer 5 Type I SSA template (5000 random samples). Error bars show the 95% confidence intervals.

5.3.8 Layer 6 SSA Template

A diagram of the layer 6 template is shown in Figure 5.165. 33 switches are used for 8,589,934,592 possible SSA configurations. The outer dimensions of the layer 6 Type I SSA template are shown in Table 5.14.

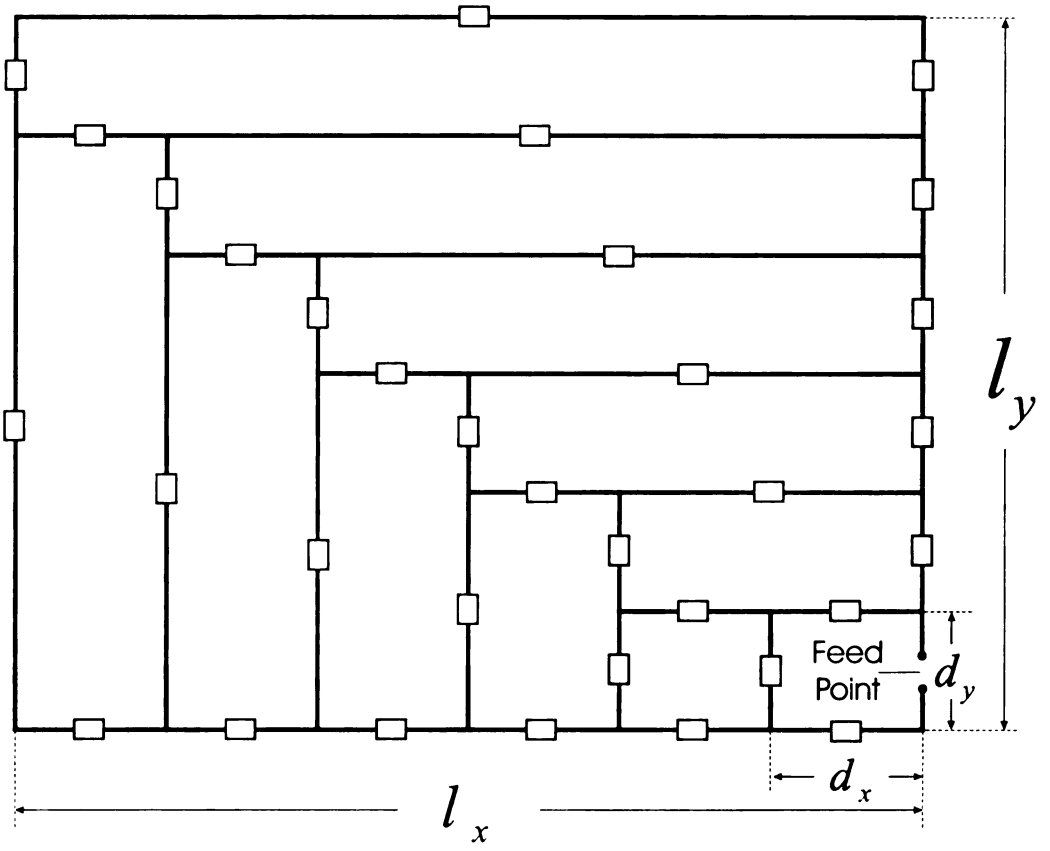


Figure 5.165. Diagram of the layer 6 SSA template.

As was performed for the layer 3 template described in Section 5.3.5, 5000 random samples of the SSA configurations were evaluated for the layer 6 Type I template. The results of this sample are presented here. Only the layer 6 Type I template in free space is presented, and is designated the 'layer 6 template.'

The SWR of each random configuration at each frequency is plotted in Figure 5.166 for the layer 6 template. Nearly continuous possible SWRs exist at most frequencies. The minimum SWR found at each frequency is shown in Figure 5.167. These figures follow the trend of the layer 3, layer 4, and layer 5 templates. Low SWR values extend lower in frequency for the layer 6 template.

The estimate of the proportion of configurations with SWRs less than 2.0 is shown

Table 5.14. Dimensions of the layer 6 Type I SSA template.

l_x	51.4 cm
d_x	8.57 cm
l_y	51.4 cm
d_y	8.57 cm
Outer electrical dimensions at 40 MHz	$0.0686\lambda \times 0.0686\lambda$
Outer electrical dimensions at 800 MHz	$1.37\lambda \times 1.37\lambda$

in Figure 5.168 for the layer 6 template. Figure 5.169 shows the proportion of configurations with SWRs less than 2.0 and maximum vertical gains in the horizontal plane above 3.0 dB. The estimate of the proportion of configurations with SWRs less than 2.0 and minimum vertical gains above -3.0 dB is shown in Figure 5.170. Recall that the layer 6 template is in free space, and the templates above ground for the other layers exhibit higher vertical gains.

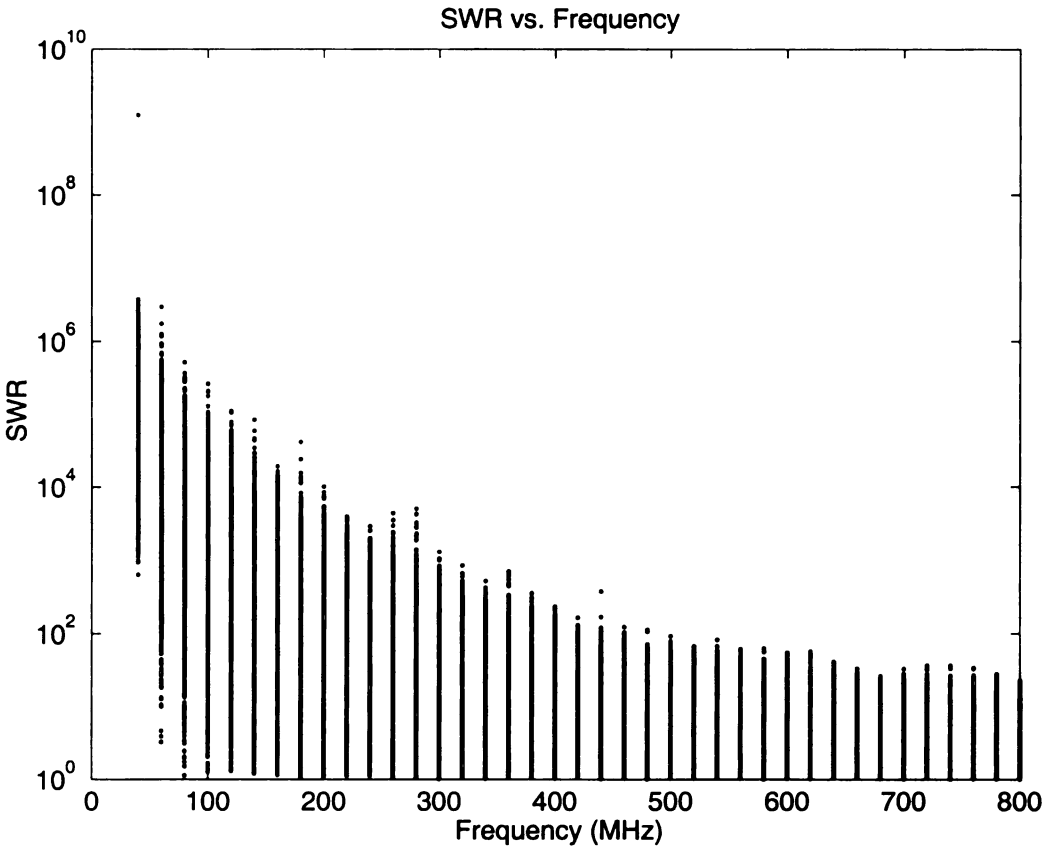


Figure 5.166. SWR vs. frequency for the layer 6 Type I SSA template (5000 random samples).

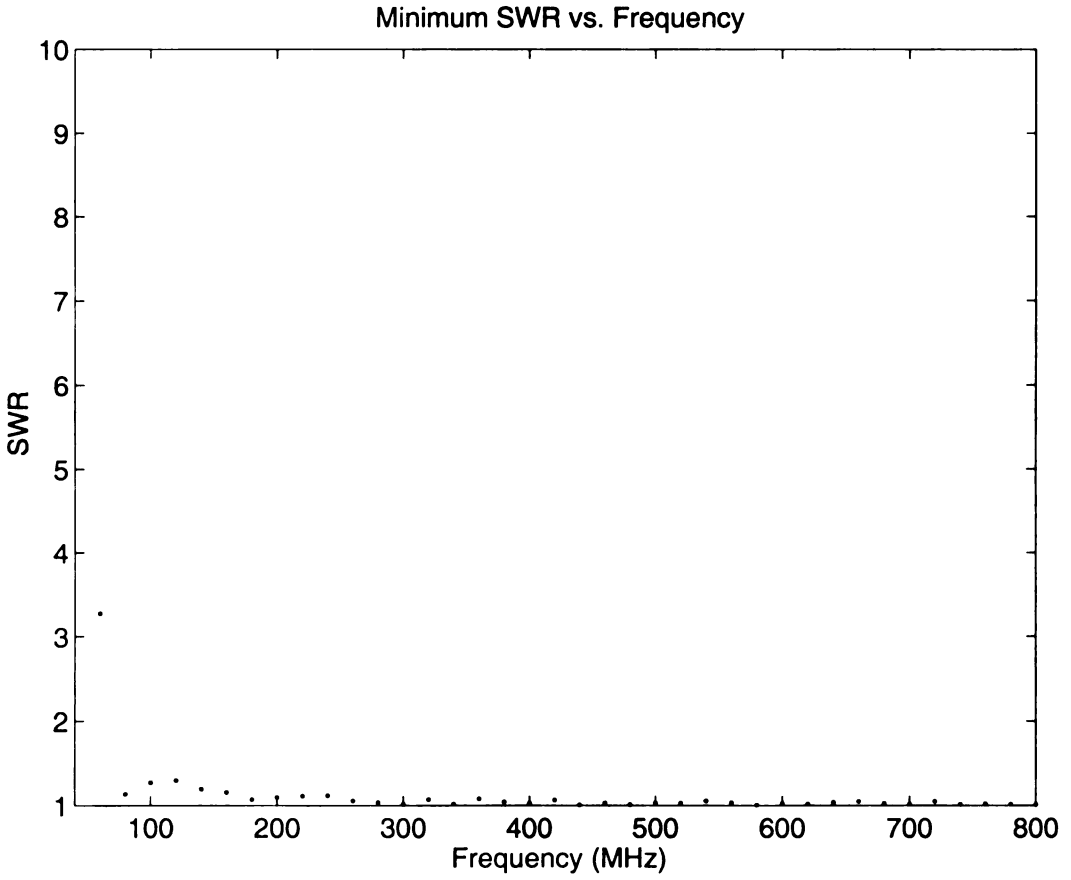


Figure 5.167. Minimum SWR vs. frequency for the layer 6 Type I SSA template (5000 random samples).

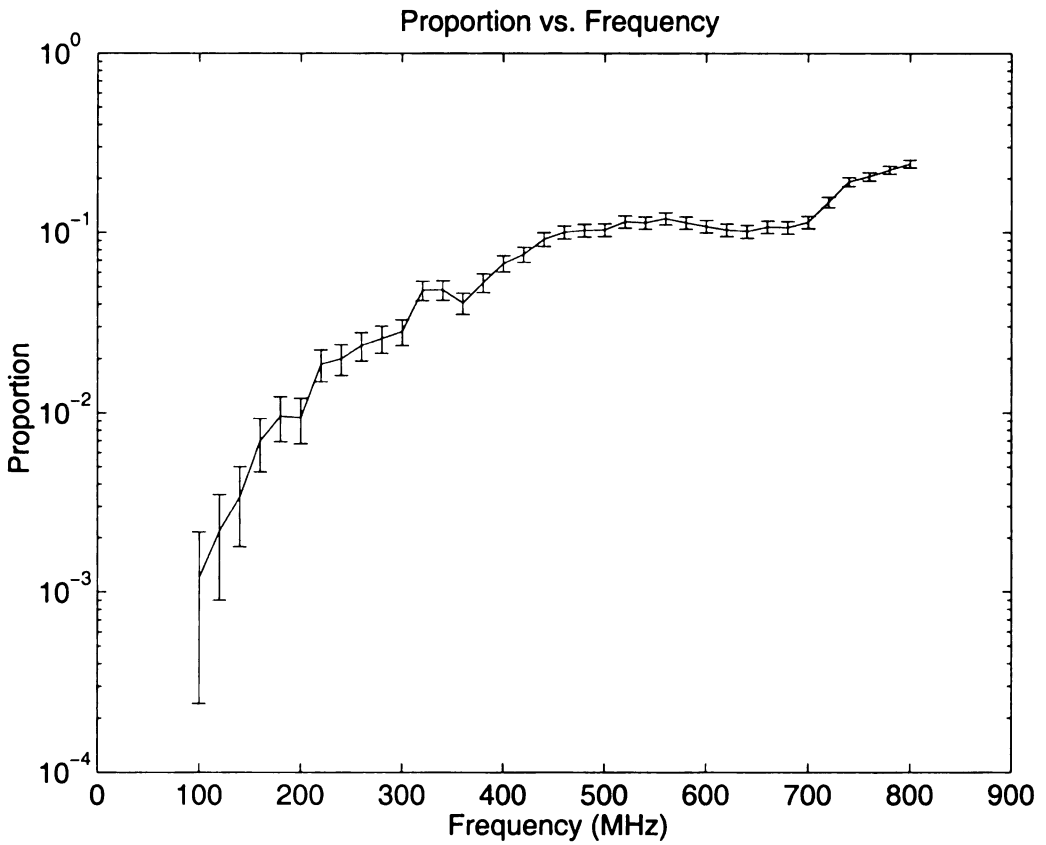


Figure 5.168. Proportion of configurations with SWRs less than 2.0 vs. frequency for the layer 6 Type I SSA template (5000 random samples). Error bars show the 95% confidence intervals.

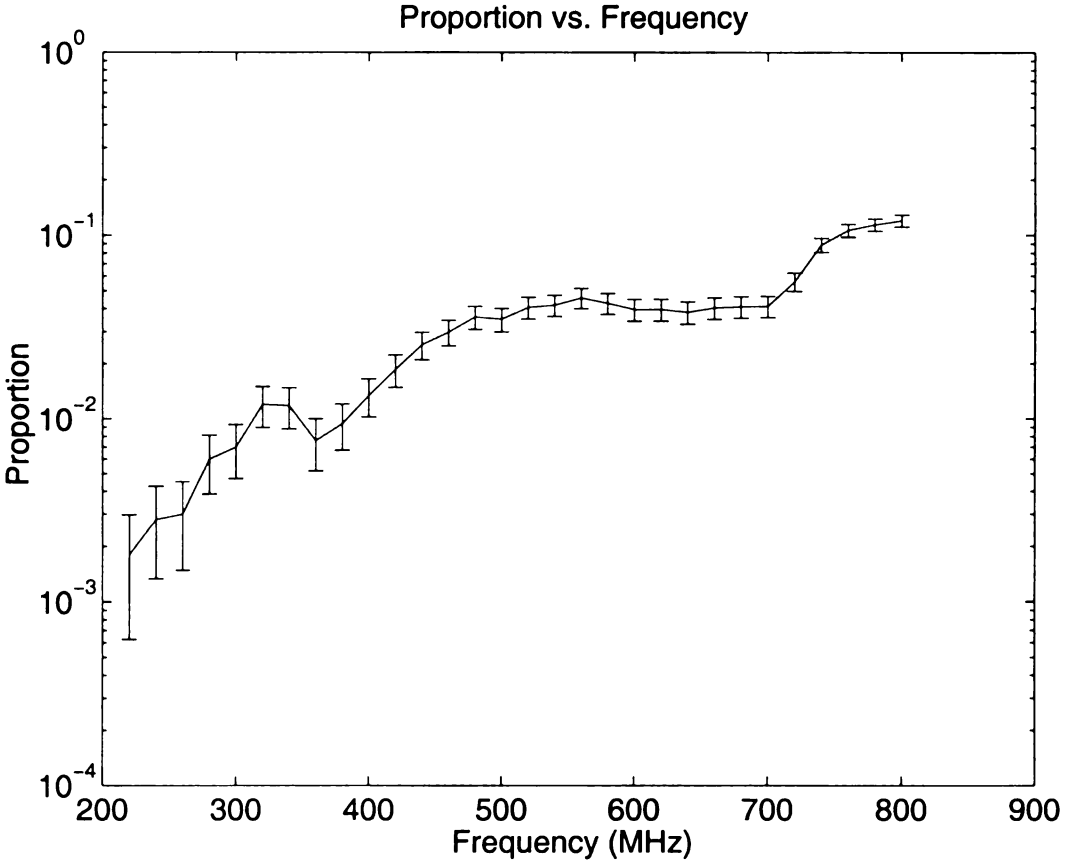


Figure 5.169. Proportion of configurations with SWRs less than 2.0 and maximum vertical gains in the horizontal plane above 3.0 dB vs. frequency for the layer 6 Type I SSA template (5000 random samples). Error bars show the 95% confidence intervals.

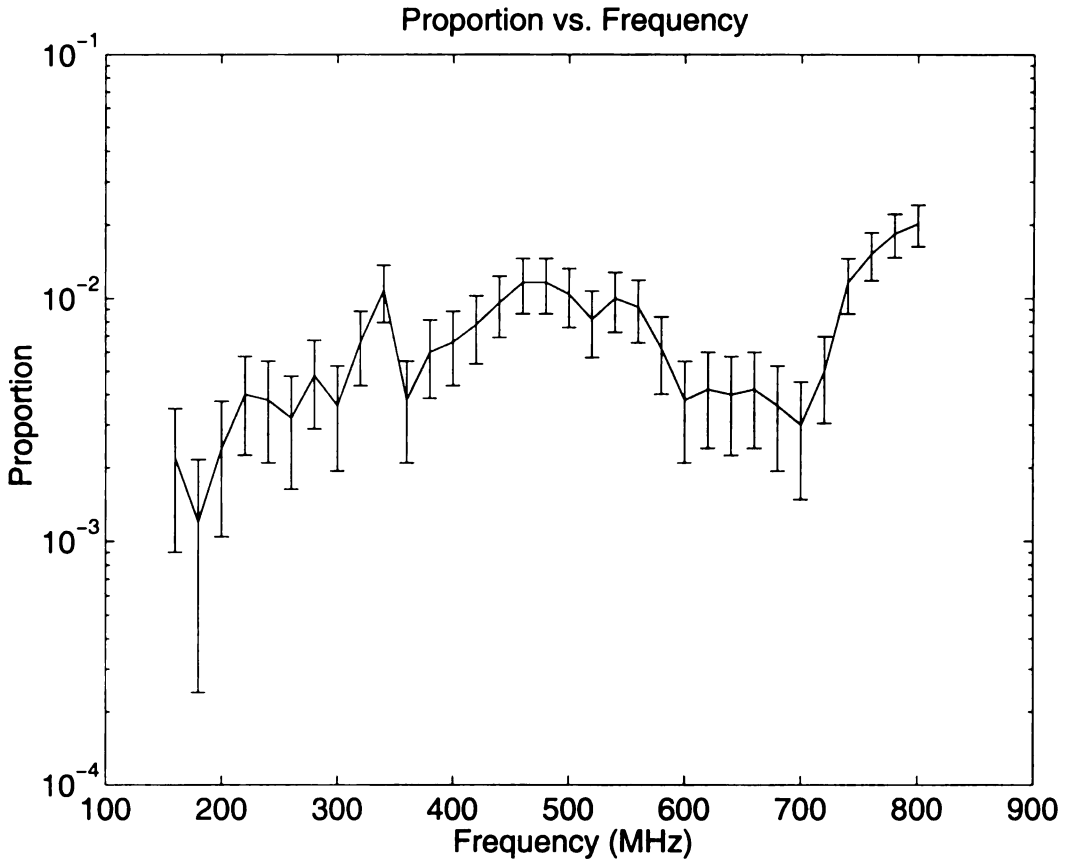


Figure 5.170. Proportion of configurations with SWRs less than 2.0 and minimum vertical gains in the horizontal plane above -3.0 dB vs. frequency for the layer 6 Type I SSA template (5000 random samples). Error bars show the 95% confidence intervals.

5.3.9 Layer 7 SSA Template

A diagram of the layer 7 template is shown in Figure 5.171. 39 switches are used for 549,755,813,888 possible SSA configurations. This is the highest SSA template layer presented in this study.

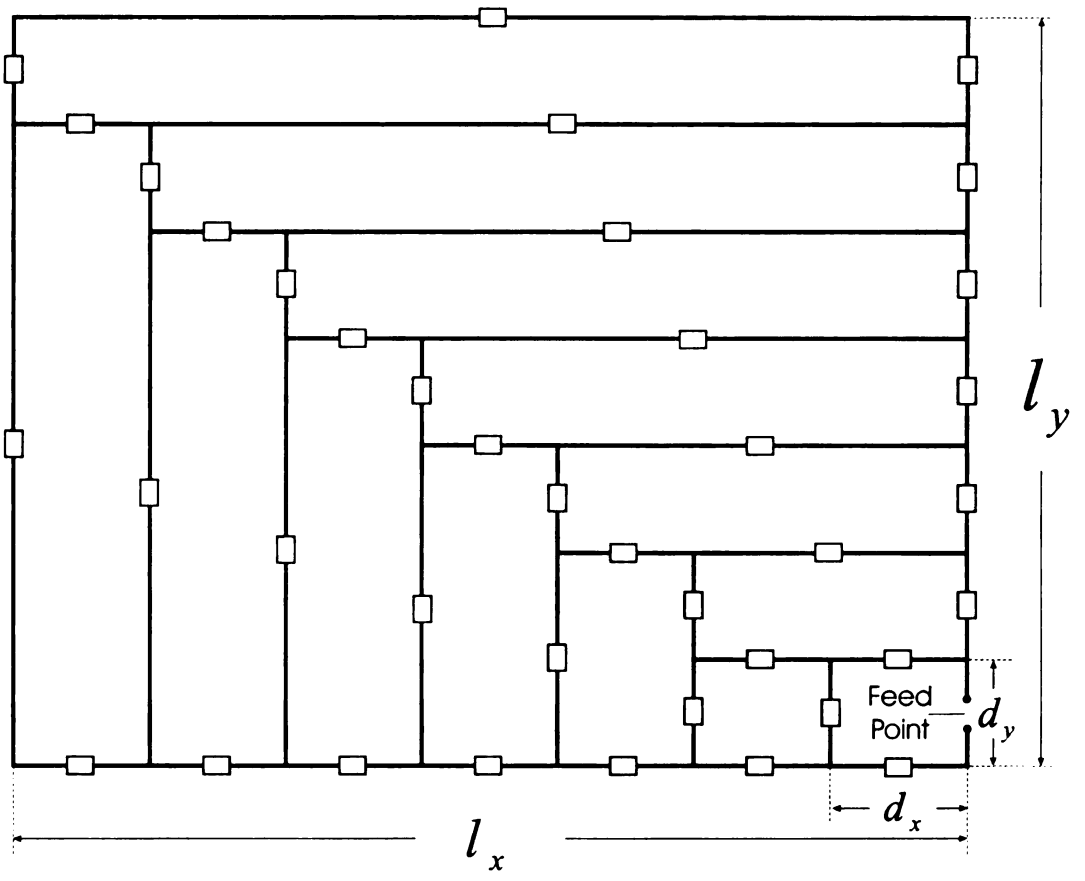


Figure 5.171. Diagram of the layer 7 SSA template.

As discussed in 5.2, the Type I and Type II layer 7 templates are identical. The dimensions of the layer 7 template are shown in Table 5.15.

The SWR of each random configuration at each frequency is plotted in Figure 5.172 and Figure 5.173 for the layer 7 templates in free space and above ground, respectively. Notice that the band of continuous possible SWRs stretches lower at the lower frequencies than do those for the smaller template layers. The minimum SWR found at each frequency is shown in Figure 5.174 for the templates in free space and above ground. SWR values below 2.0 are found at 60 MHz and above for the templates in free space and above ground. Compare this with the minimum SWR values for the layer 1 Type II template shown in Figure 5.18 on page 114. These tem-

Table 5.15. Dimensions of the layer 7 Type I and Type II SSA templates.

l_x	60.0 cm
d_x	8.57 cm
l_y	60.0 cm
d_y	8.57 cm
Outer electrical dimensions at 40 MHz	$0.0800\lambda \times 0.0800\lambda$
Outer electrical dimensions at 800 MHz	$1.60\lambda \times 1.60\lambda$

plates have the same outer electrical dimensions, but the added switches and wires to the inside of the layer 7 aperture have greatly increased its performance capabilities. There are frequencies where the layer 1 Type II template has minimum SWR values less than 2.0, but these are sporadic and do not exist below 120 MHz.

The estimates of the proportion of configurations with SWRs less than 4.0 are shown in Figure 5.175 and Figure 5.176 for the layer 7 templates in free space and above ground, respectively. More configurations meet the SWR threshold at higher frequencies, as is the general case for the lower template layers. The combined proportion estimates found in Figure 5.175 show similar trends for the layer 7 templates in free space and above ground.

Several more proportion estimates are presented here for other SWR thresholds. Figure 5.178, Figure 5.179, and Figure 5.180 show the estimates of the proportion of configurations with SWRs less than 2.0 for the layer 7 template in free space, the template above ground, and the combined templates, respectively. Figure 5.181, Figure 5.182, and Figure 5.183 show the estimates of the proportion of configurations with SWRs less than 1.5 for the template in free space, the template above ground, and the combined templates, respectively. Figure 5.184, Figure 5.185, and Figure 5.186 show the estimates of the proportion of configurations with SWRs less than 1.1 for the template in free space, the template above ground, and the combined templates, respectively. These proportion plots show the ability of the layer 7

template to randomly locate configurations with stringent SWR requirements.

Figure 5.187 and Figure 5.188 show the estimates of the proportion of configurations with minimum vertical gains in the horizontal plane above 0 dB for the layer 7 templates in free space and above ground, respectively. Again, the template above ground has higher minimum gains. This is also shown in the combined plot shown in Figure 5.189. The estimates of the proportion of configurations with SWRs less than 4.0 and minimum gains above 0 dB are shown in Figure 5.190 and Figure 5.191 for the templates in free space and above ground, respectively. The template in free space has few configurations that meet these criteria over the frequency band. This is also shown in the combined plot found in Figure 5.192.

The estimates of the proportion of configurations with maximum vertical gains in the horizontal plane above 3.0 dB are shown in Figure 5.193 and Figure 5.194 for the layer 7 templates in free space and above ground, respectively. Also shown in Figure 5.195, the proportion meeting the gain criterion is higher for the template above ground than for the template in free space. The estimates of the proportion of configurations with SWRs less than 2.0 and maximum gains above 3.0 dB are shown in Figure 5.196 and Figure 5.197 for the templates in free space and above ground, respectively. The template above ground has far more configurations that meet these criteria than does the template in free space. This is also shown in the combined plot found in Figure 5.198.

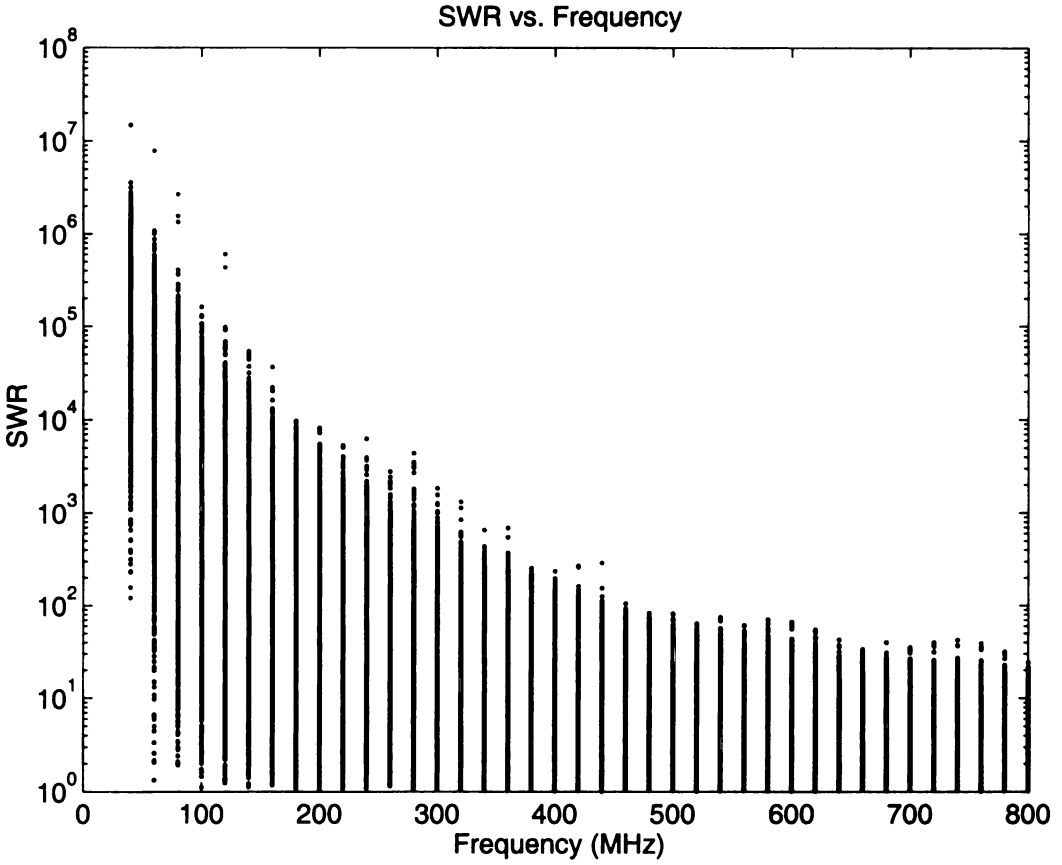


Figure 5.172. SWR vs. frequency for the layer 7 SSA template in free space (5000 random samples).

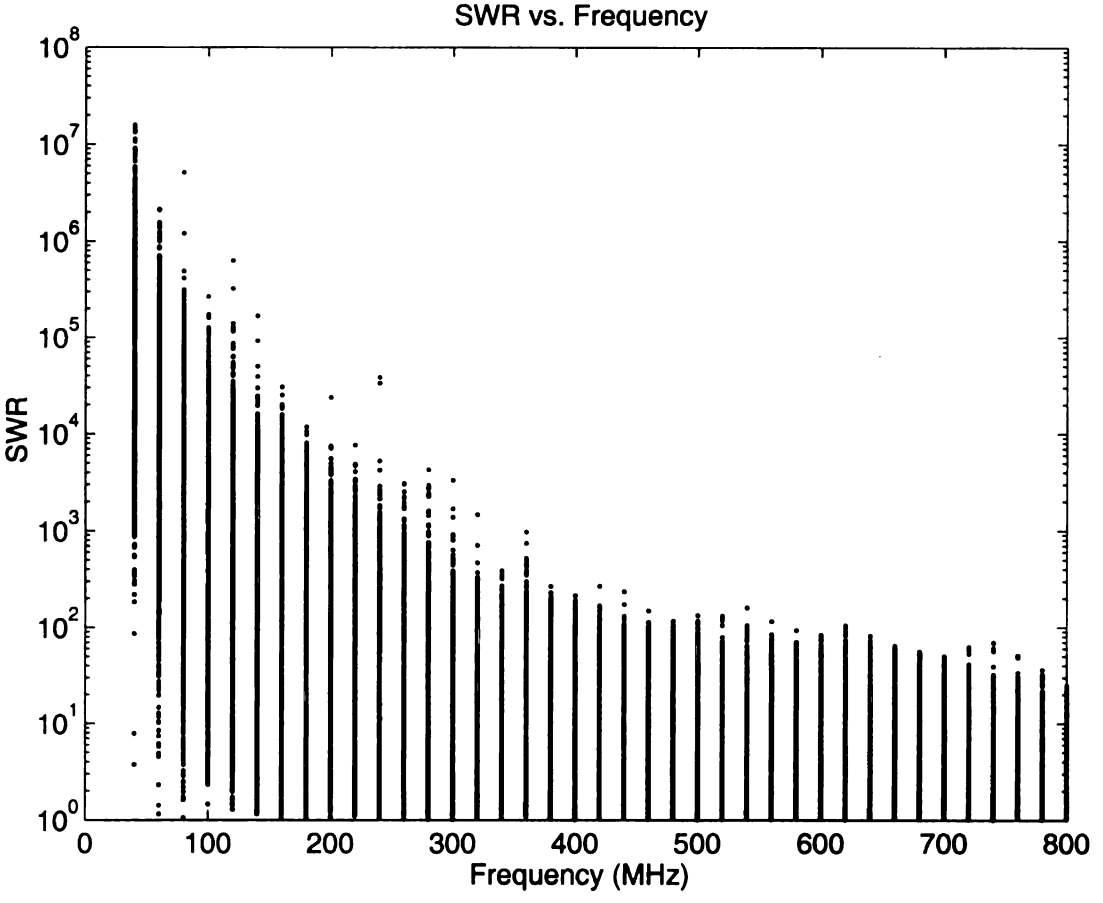


Figure 5.173. SWR vs. frequency for the layer 7 SSA template above ground (5000 random samples).

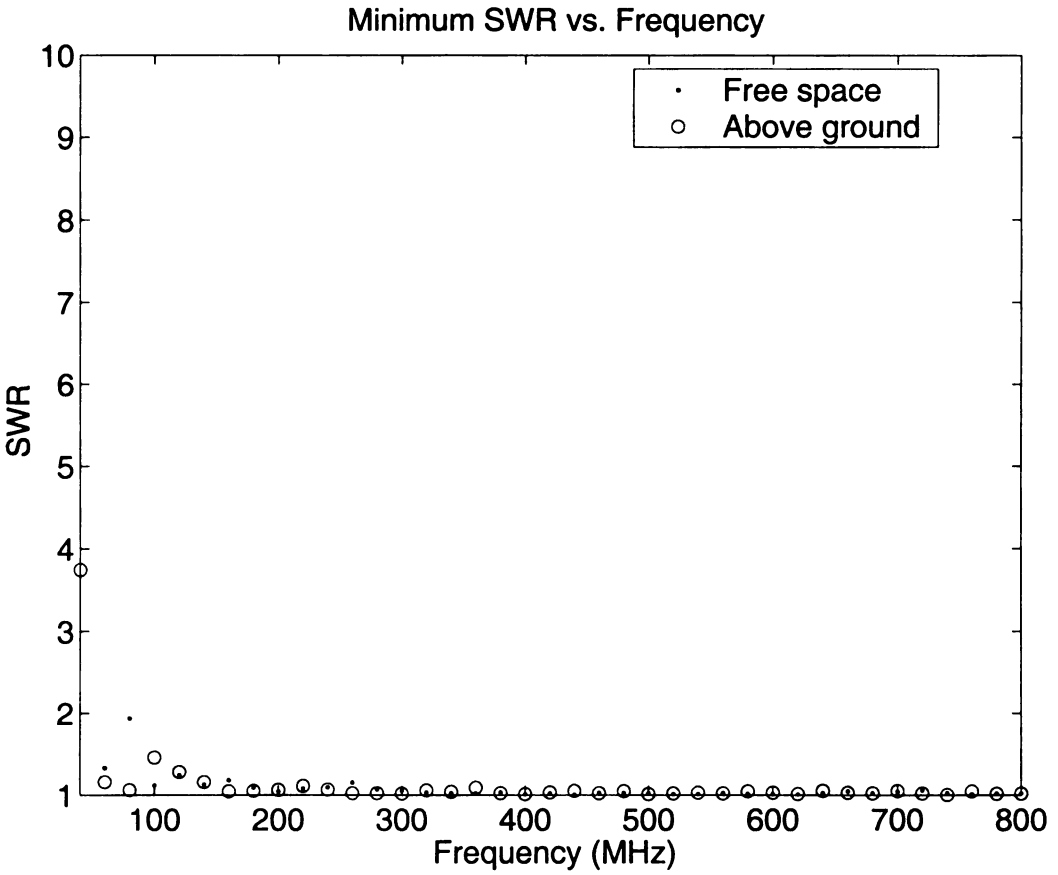


Figure 5.174. Minimum SWR vs. frequency for the layer 7 SSA template (5000 random samples).

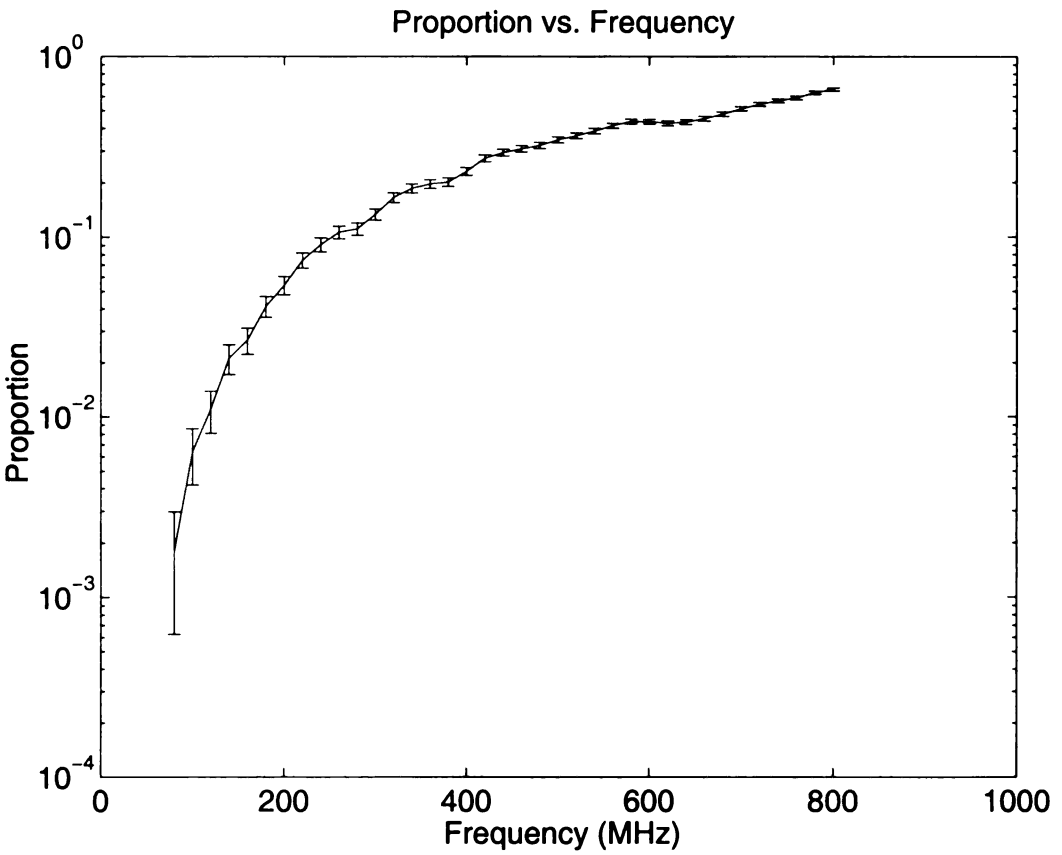


Figure 5.175. Proportion of configurations with SWRs less than 4.0 vs. frequency for the layer 7 SSA template in free space (5000 random samples). Error bars show the 95% confidence intervals.

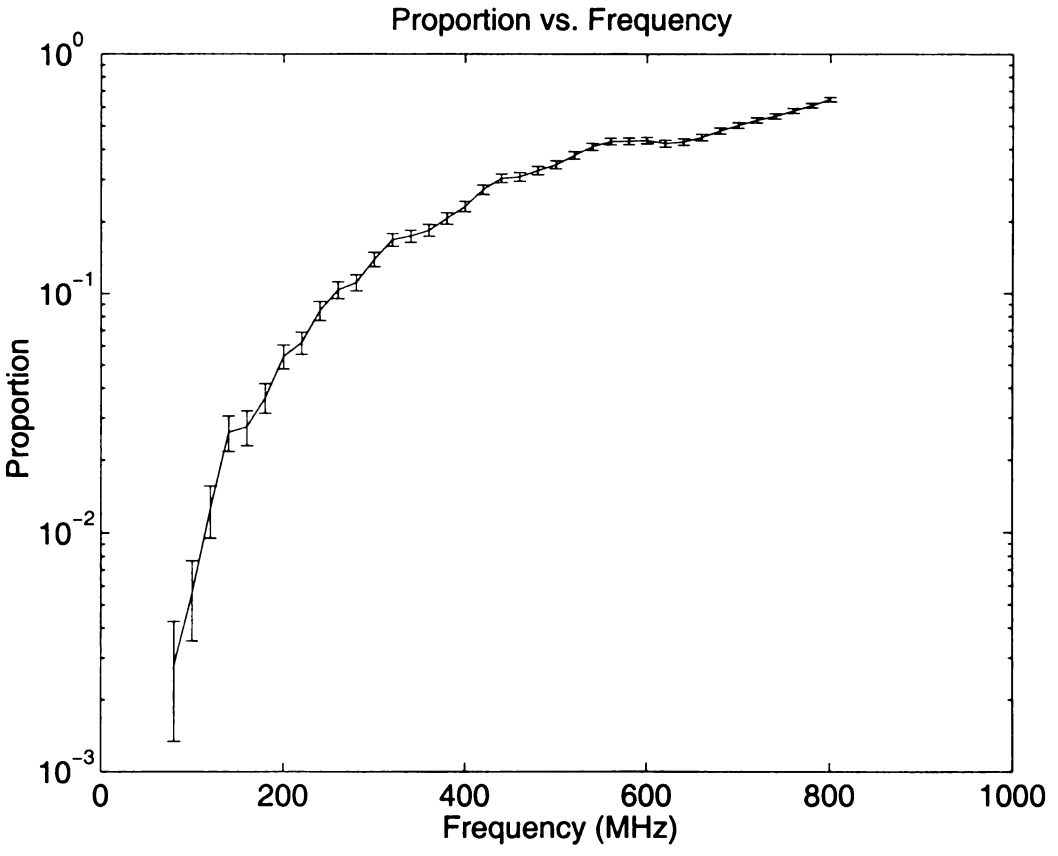


Figure 5.176. Proportion of configurations with SWRs less than 4.0 vs. frequency for the layer 7 SSA template over ground (5000 random samples). Error bars show the 95% confidence intervals.

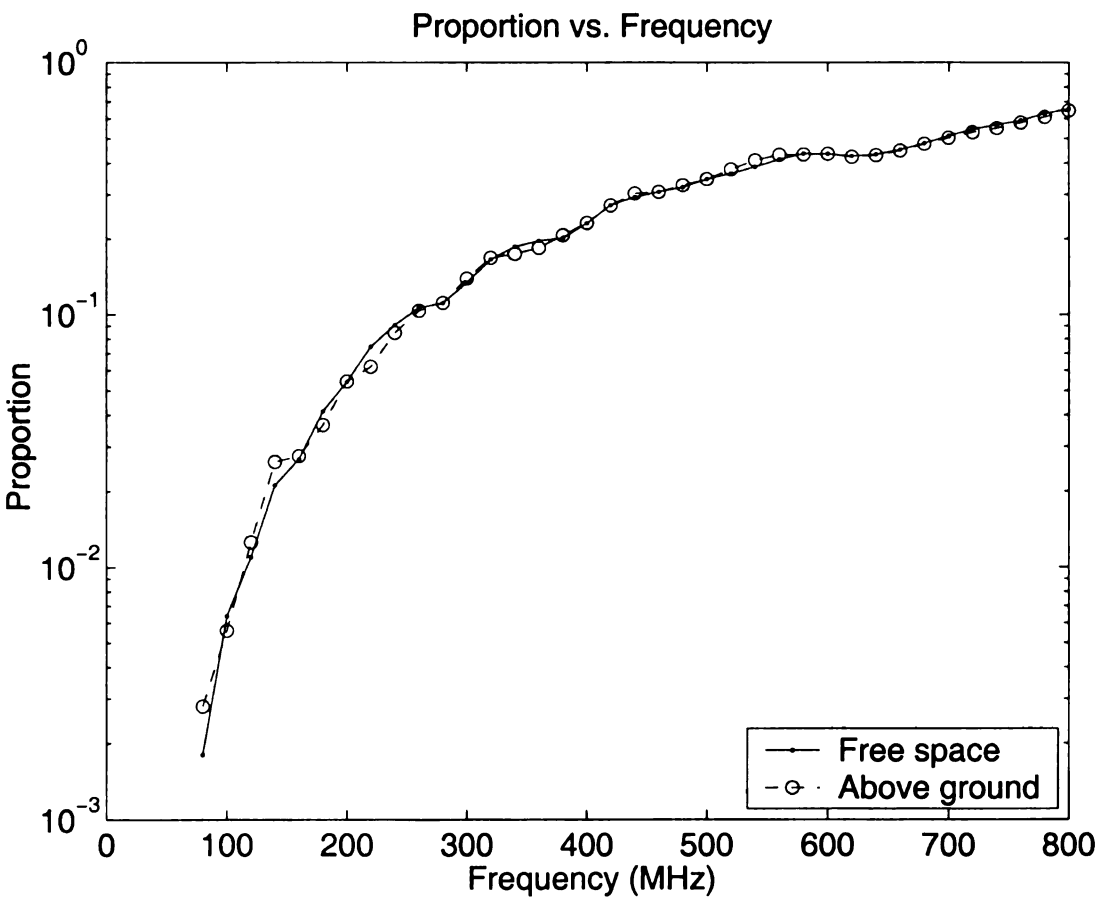


Figure 5.177. Proportion of configurations with SWRs less than 4.0 vs. frequency for the layer 7 SSA template (5000 random samples).

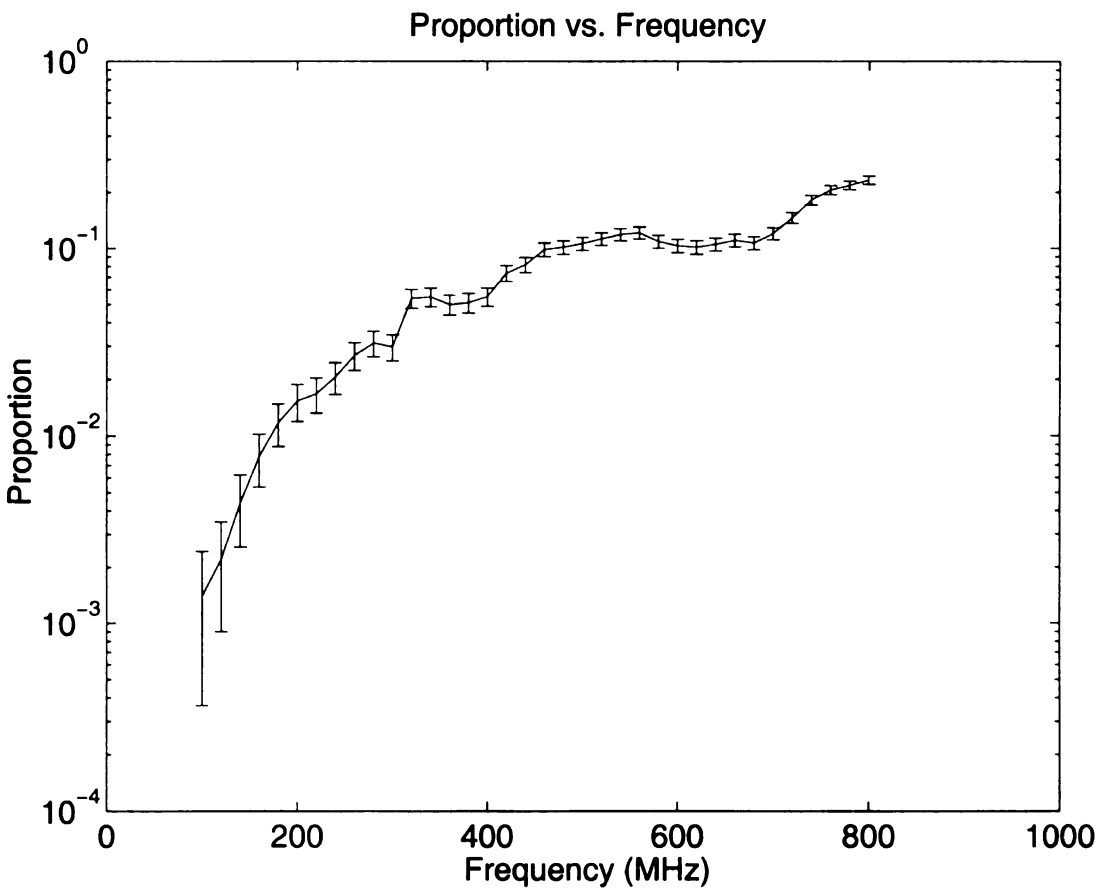


Figure 5.178. Proportion of configurations with SWRs less than 2.0 vs. frequency for the layer 7 SSA template in free space (5000 random samples). Error bars show the 95% confidence intervals.

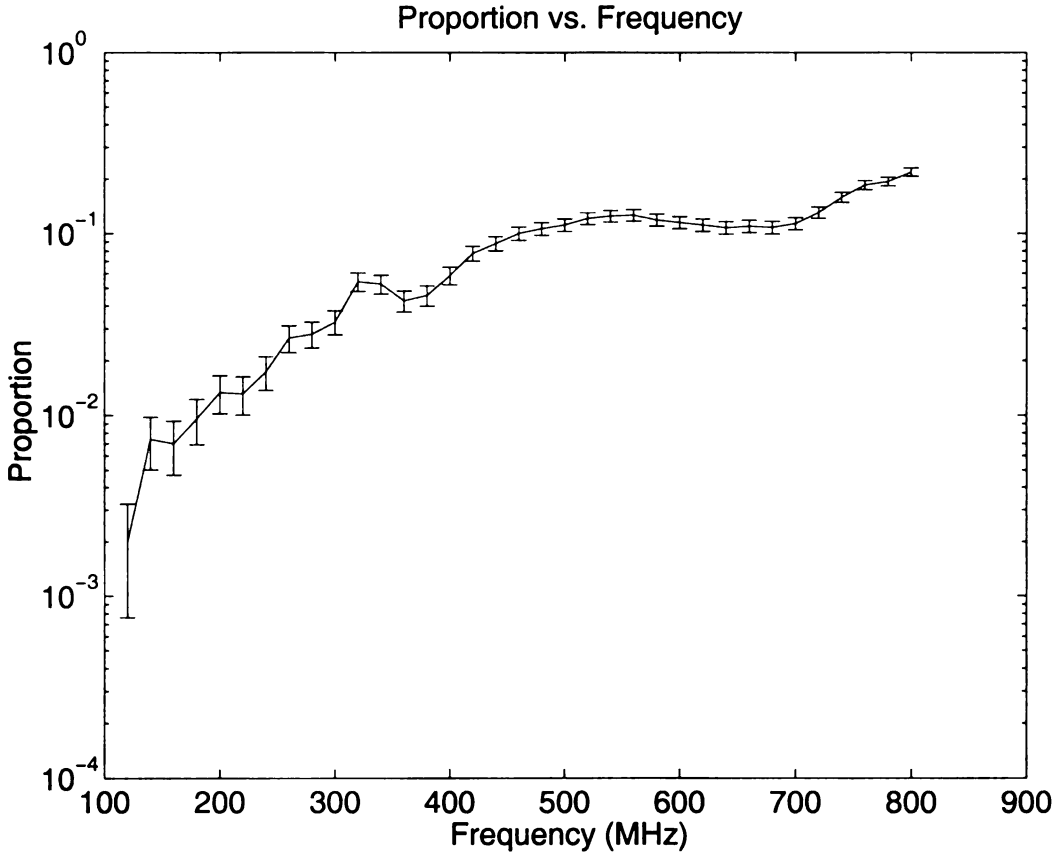


Figure 5.179. Proportion of configurations with SWRs less than 2.0 vs. frequency for the layer 7 SSA template over ground (5000 random samples). Error bars show the 95% confidence intervals.

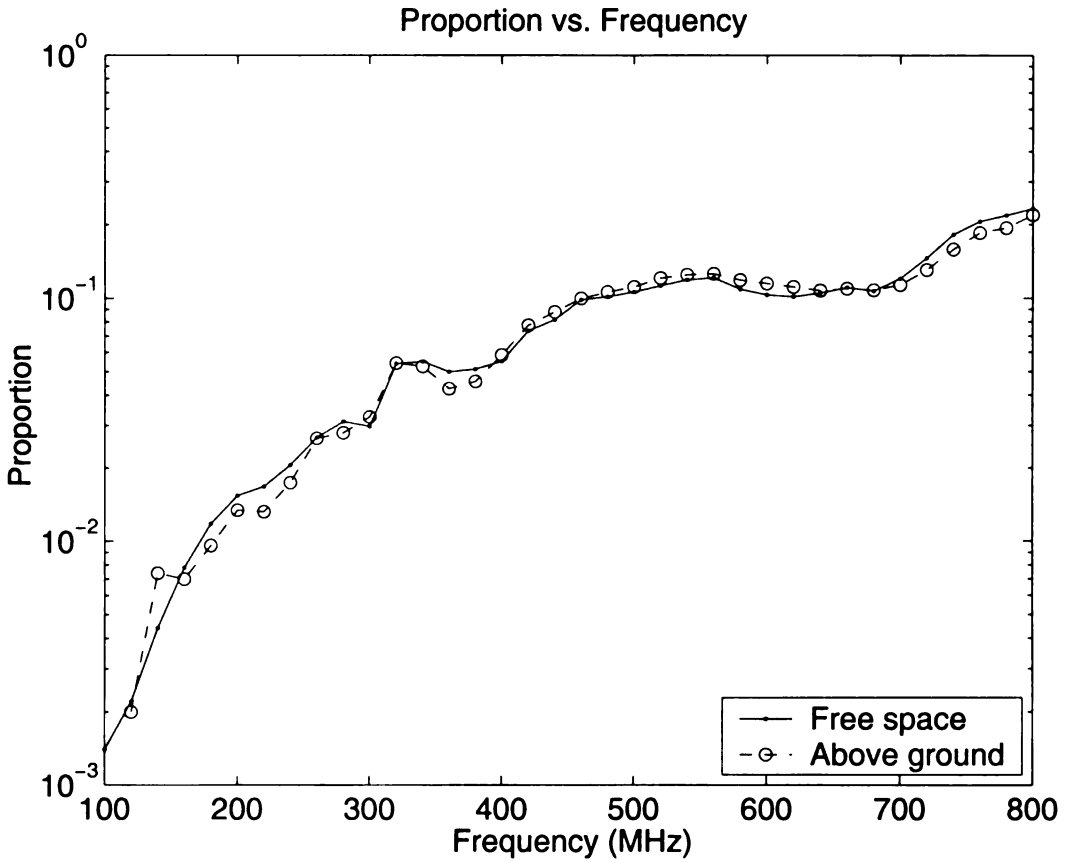


Figure 5.180. Proportion of configurations with SWRs less than 2.0 vs. frequency for the layer 7 SSA template (5000 random samples).

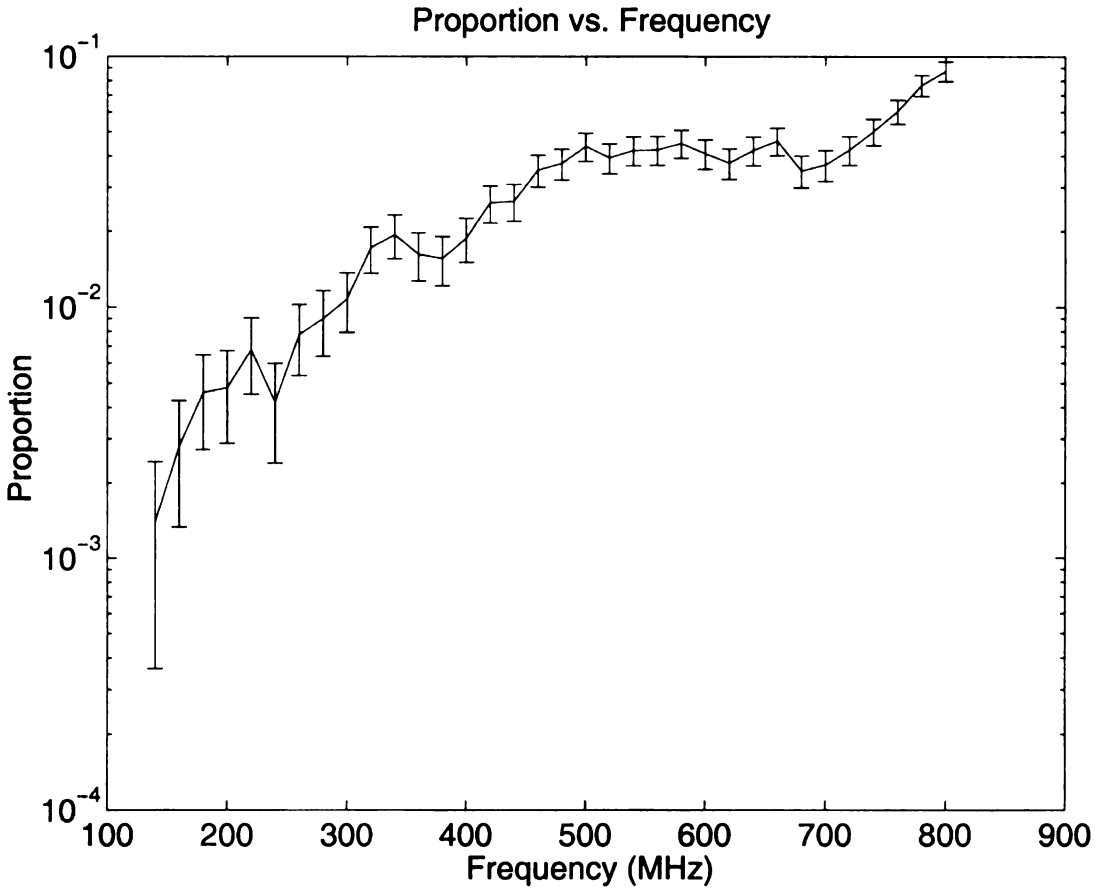


Figure 5.181. Proportion of configurations with SWRs less than 1.5 vs. frequency for the layer 7 SSA template in free space (5000 random samples). Error bars show the 95% confidence intervals.

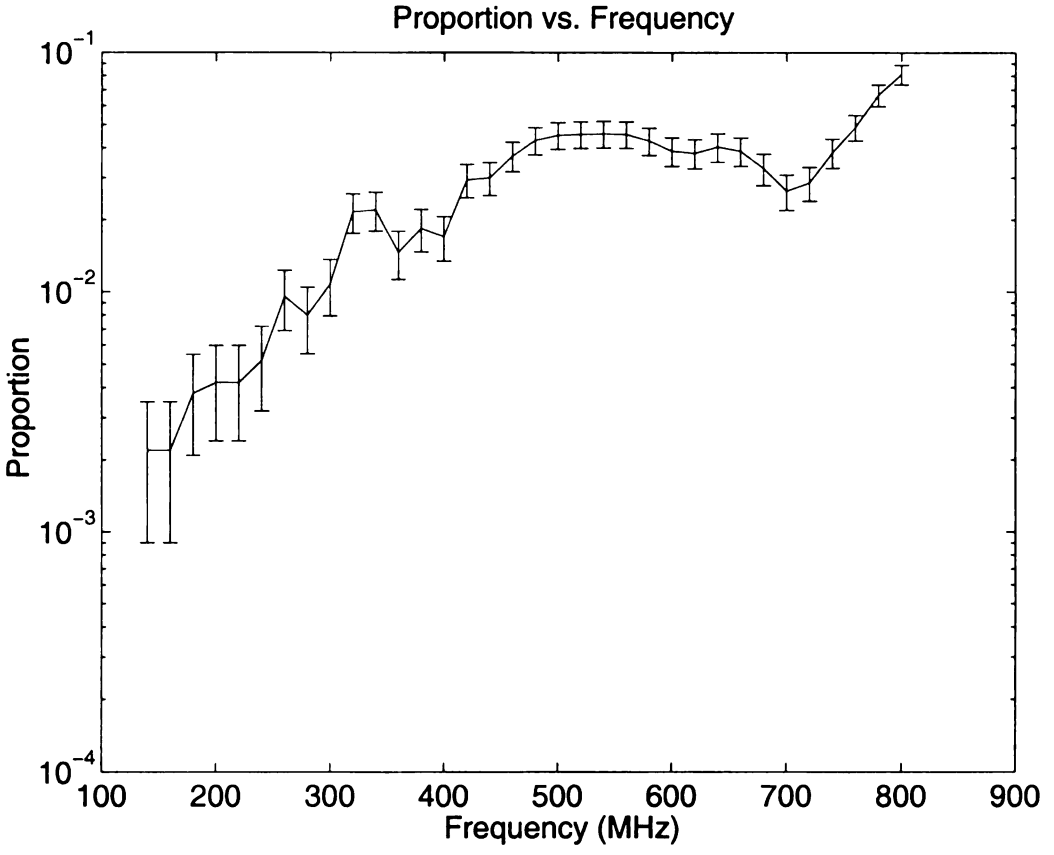


Figure 5.182. Proportion of configurations with SWRs less than 1.5 vs. frequency for the layer 7 SSA template over ground (5000 random samples). Error bars show the 95% confidence intervals.

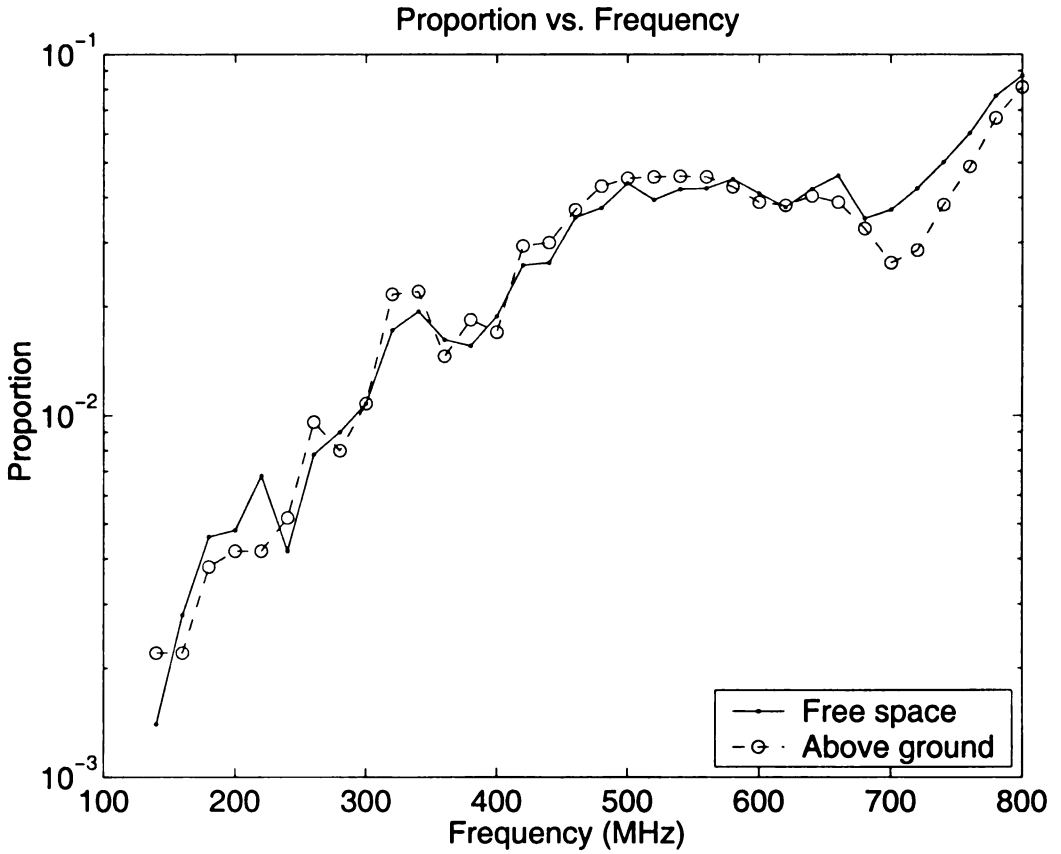


Figure 5.183. Proportion of configurations with SWRs less than 1.5 vs. frequency for the layer 7 SSA template (5000 random samples).

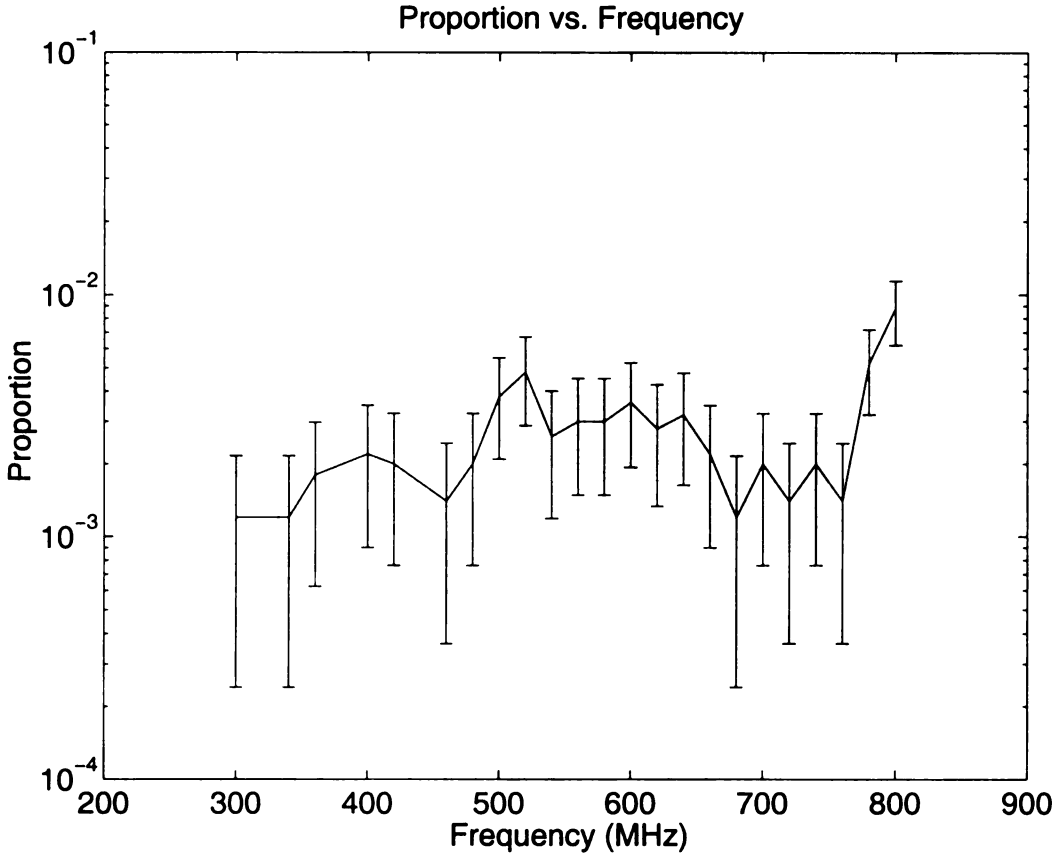


Figure 5.184. Proportion of configurations with SWRs less than 1.1 vs. frequency for the layer 7 SSA template in free space (5000 random samples). Error bars show the 95% confidence intervals.

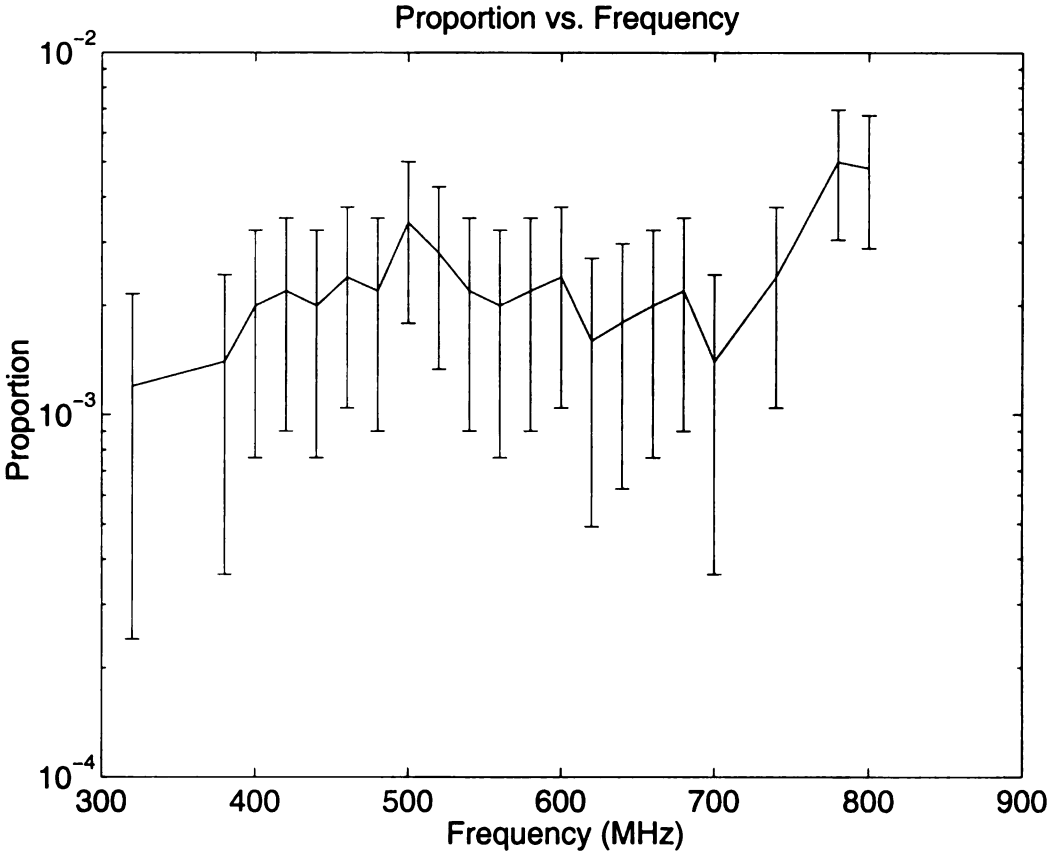


Figure 5.185. Proportion of configurations with SWRs less than 1.1 vs. frequency for the layer 7 SSA template over ground (5000 random samples). Error bars show the 95% confidence intervals.

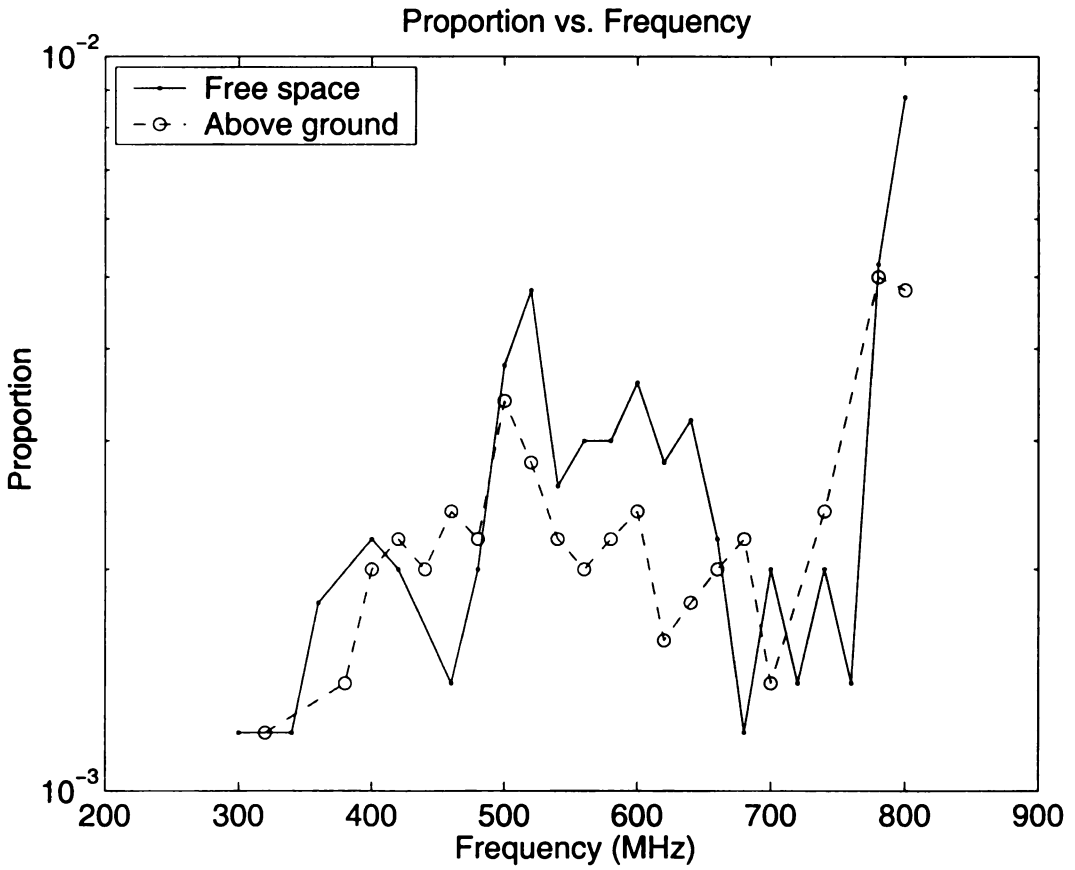


Figure 5.186. Proportion of configurations with SWRs less than 1.1 vs. frequency for the layer 7 SSA template (5000 random samples).

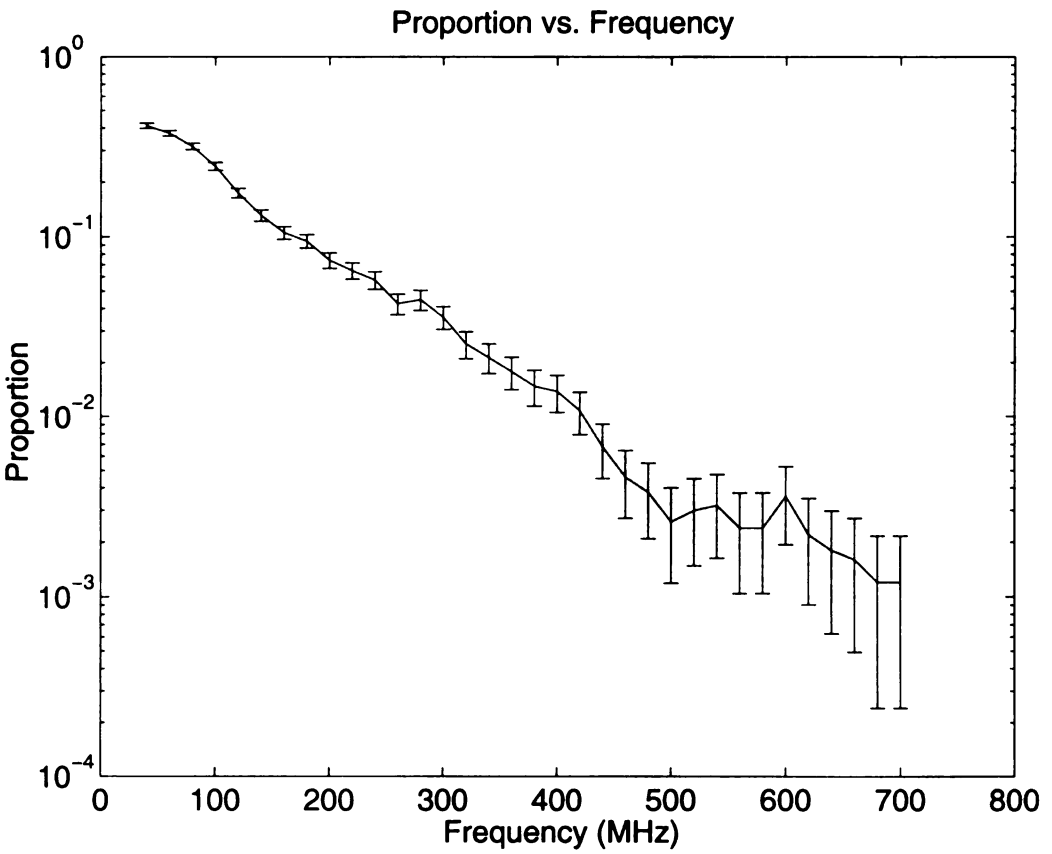


Figure 5.187. Proportion of configurations with minimum vertical gains in the horizontal plane above 0 dB vs. frequency for the layer 7 SSA template in free space (5000 random samples). Error bars show the 95% confidence intervals.

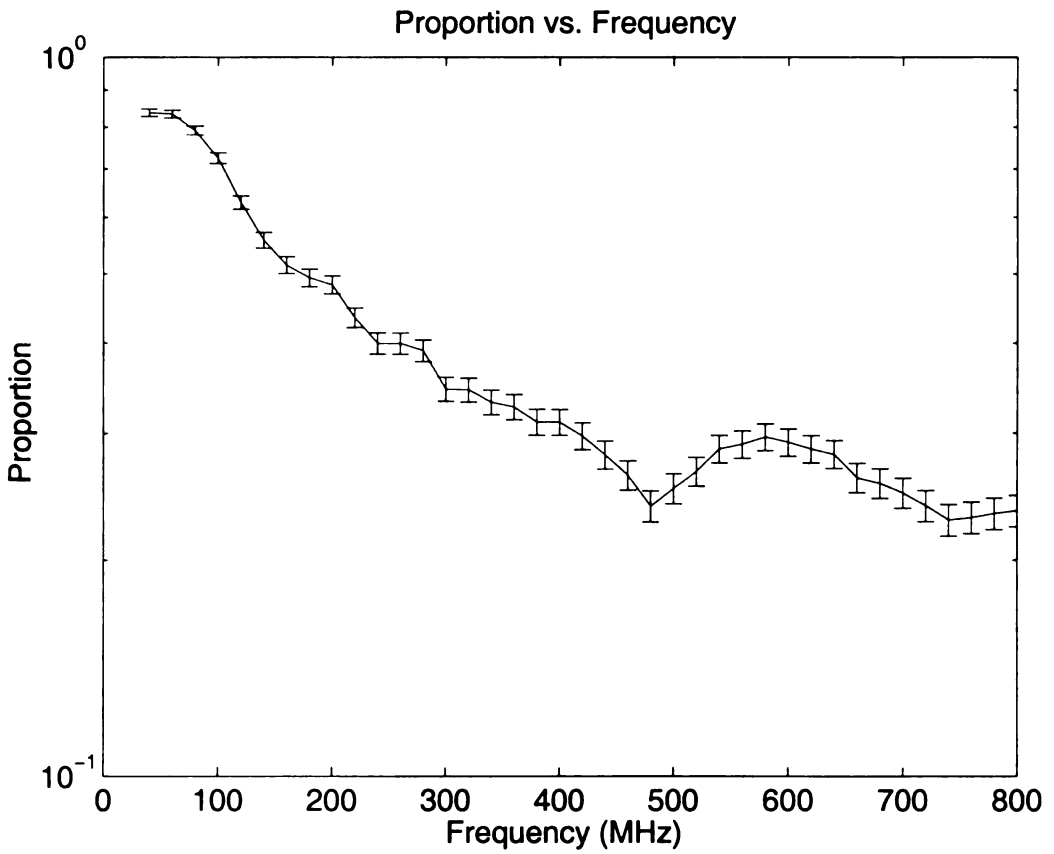


Figure 5.188. Proportion of configurations with minimum vertical gains in the horizontal plane above 0 dB vs. frequency for the layer 7 SSA template above ground (5000 random samples). Error bars show the 95% confidence intervals.

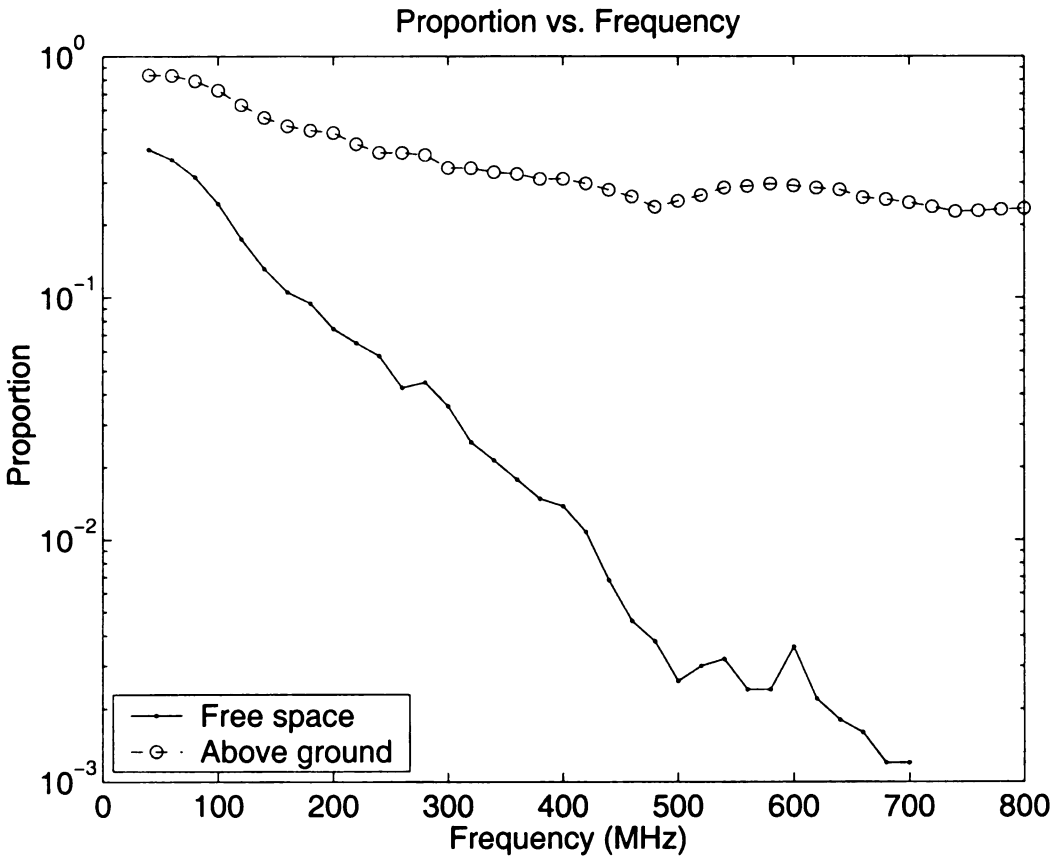


Figure 5.189. Proportion of configurations with minimum vertical gains in the horizontal plane above 0 dB vs. frequency for the layer 7 SSA template (5000 random samples).

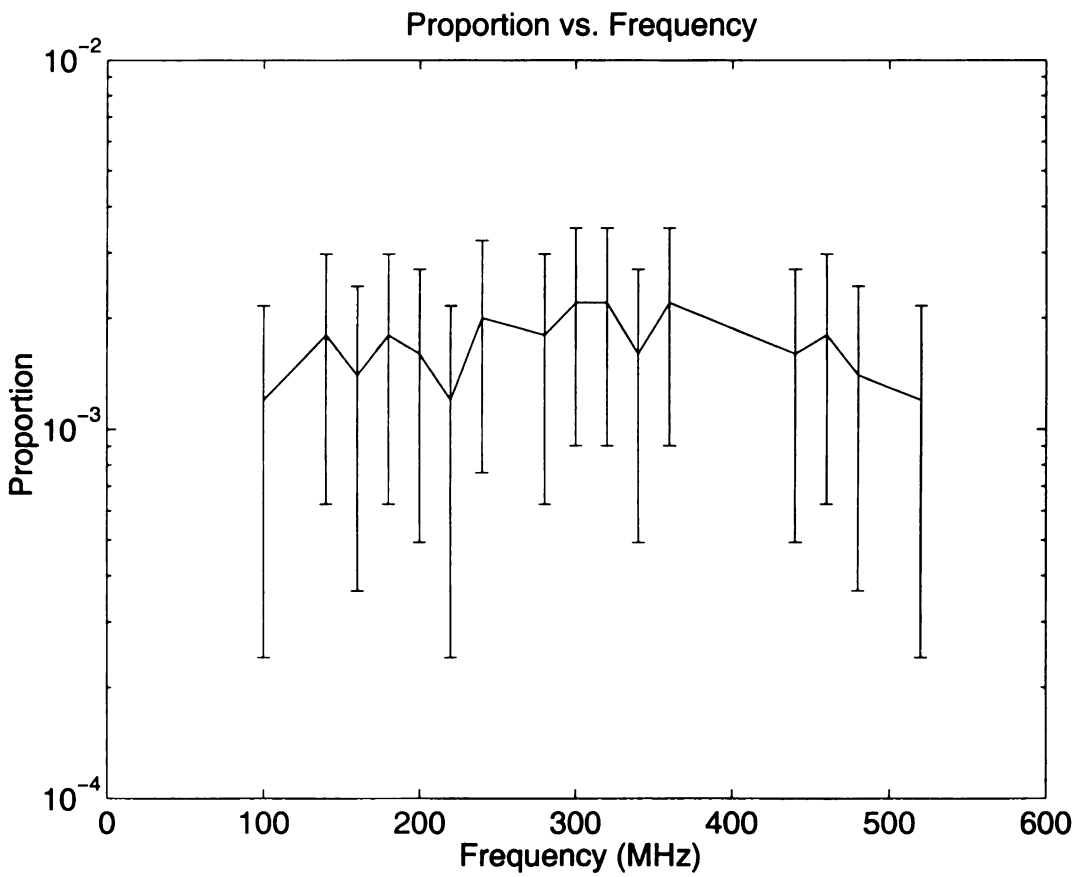


Figure 5.190. Proportion of configurations with SWRs less than 4.0 and minimum vertical gains in the horizontal plane above 0 dB vs. frequency for the layer 7 SSA template in free space (5000 random samples). Error bars show the 95% confidence intervals.

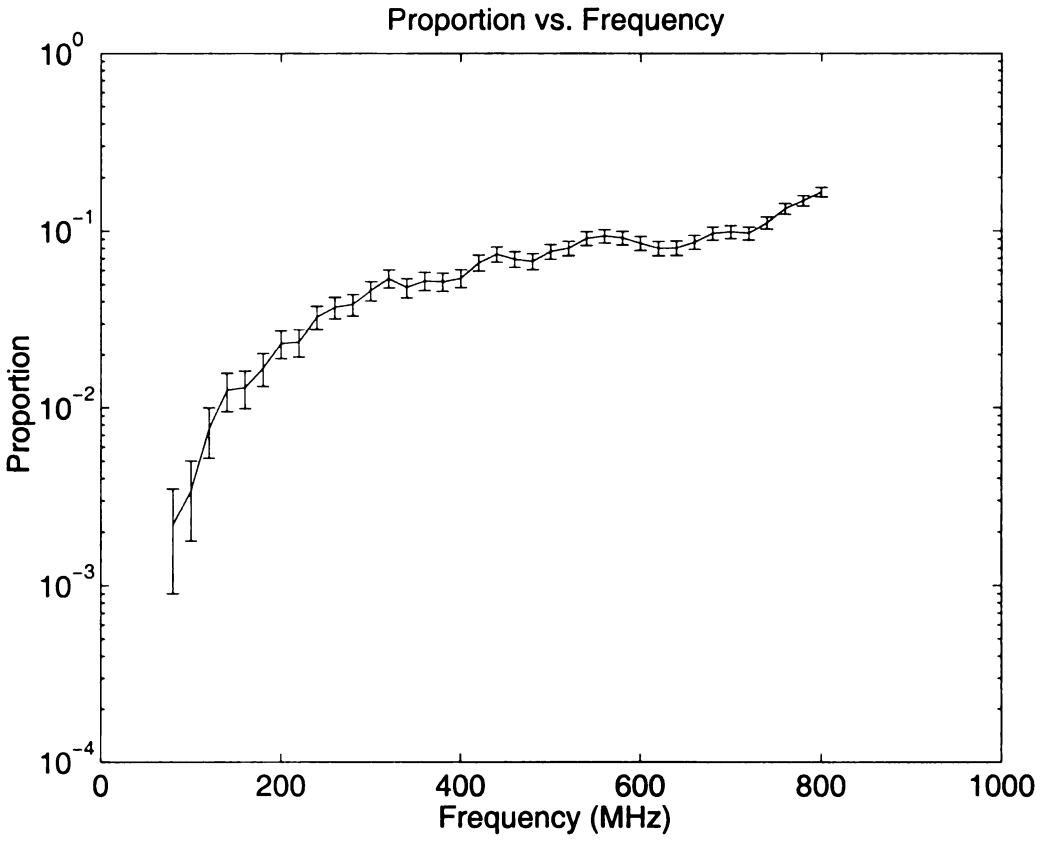


Figure 5.191. Proportion of configurations with SWRs less than 4.0 and minimum vertical gains in the horizontal plane above 0 dB vs. frequency for the layer 7 SSA template above ground (5000 random samples). Error bars show the 95% confidence intervals.

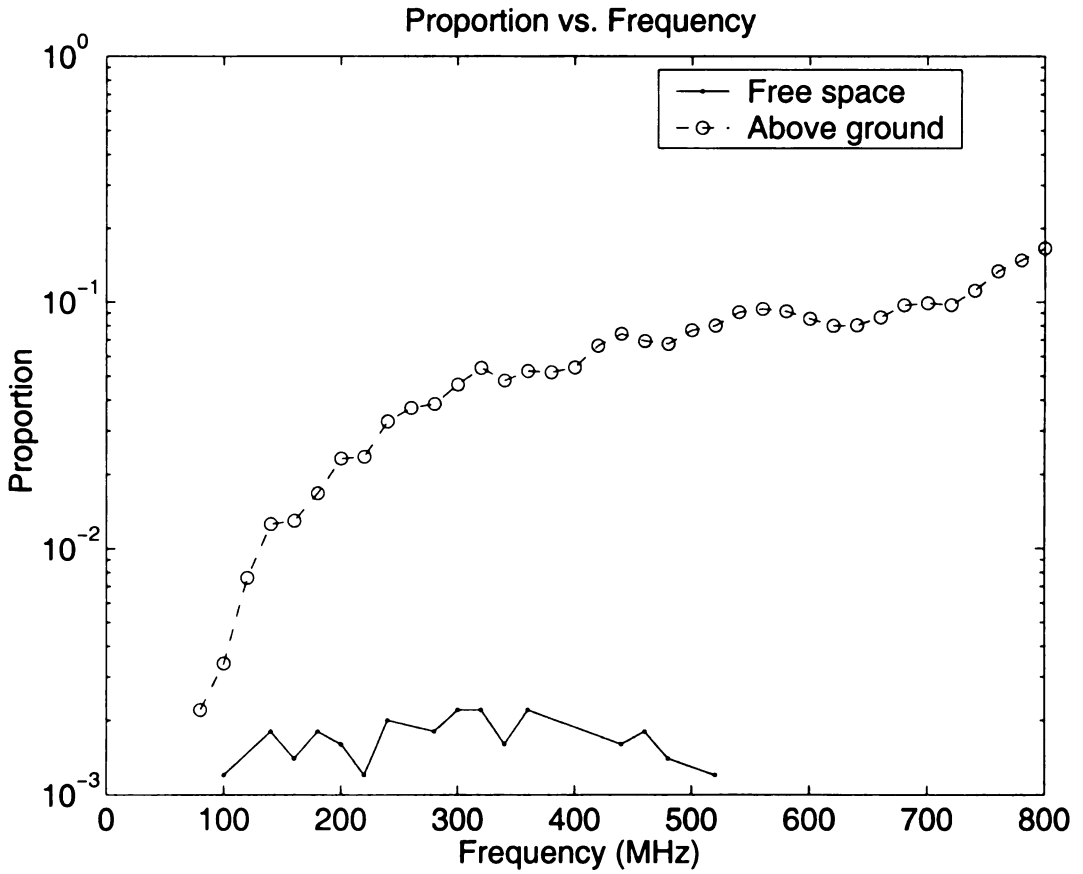


Figure 5.192. Proportion of configurations with SWRs less than 4.0 and minimum vertical gains in the horizontal plane above 0 dB vs. frequency for the layer 7 SSA template (5000 random samples).

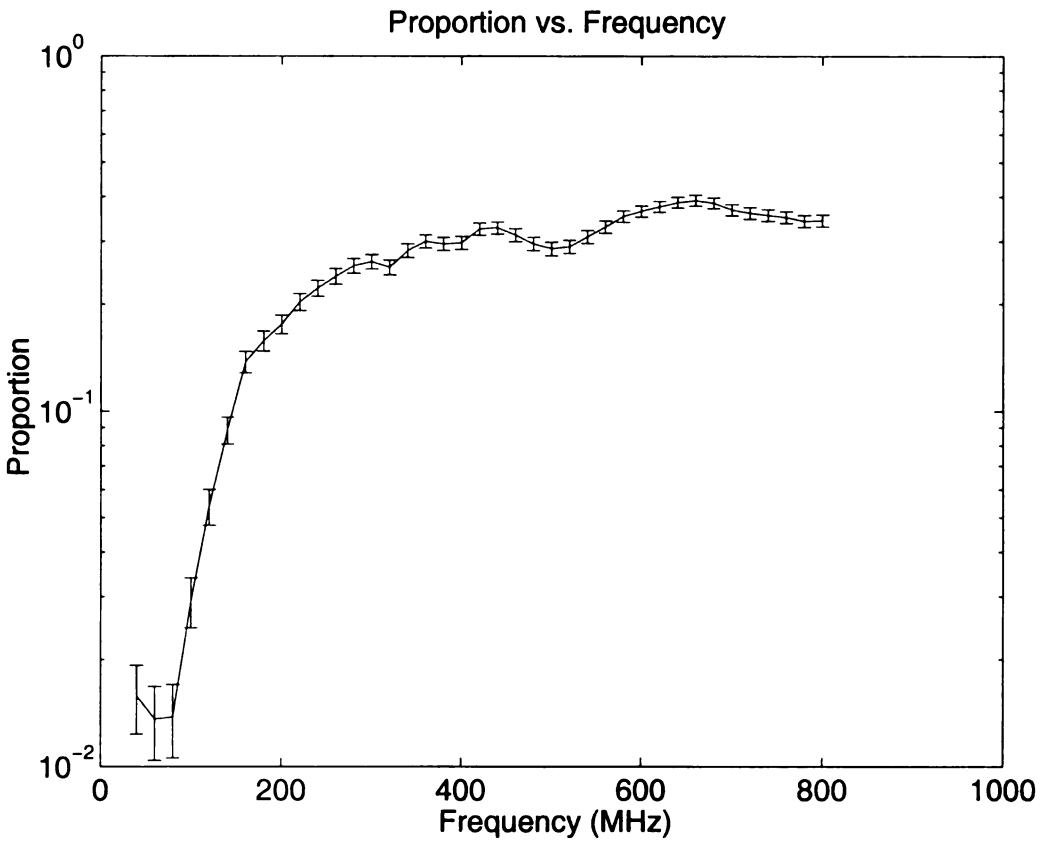


Figure 5.193. Proportion of configurations with maximum vertical gains in the horizontal plane above 3.0 dB vs. frequency for the layer 7 SSA template in free space (5000 random samples). Error bars show the 95% confidence intervals.

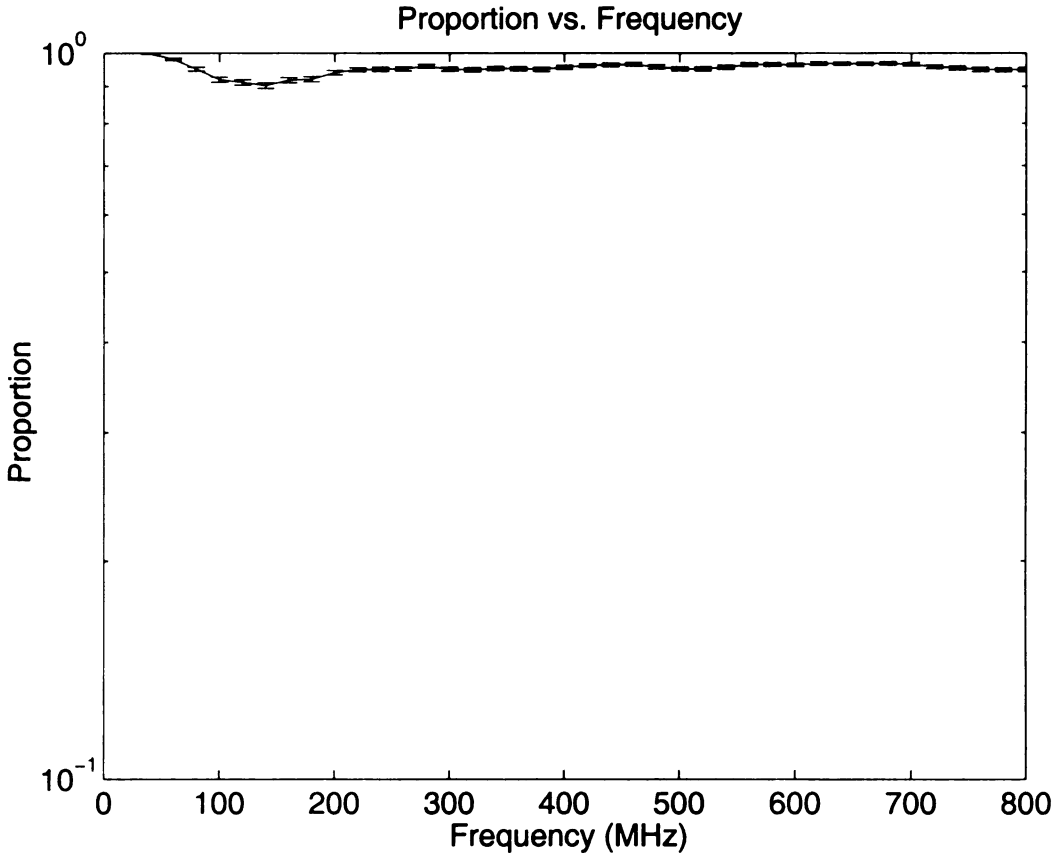


Figure 5.194. Proportion of configurations with maximum vertical gains in the horizontal plane above 3.0 dB vs. frequency for the layer 7 SSA template above ground (5000 random samples). Error bars show the 95% confidence intervals.

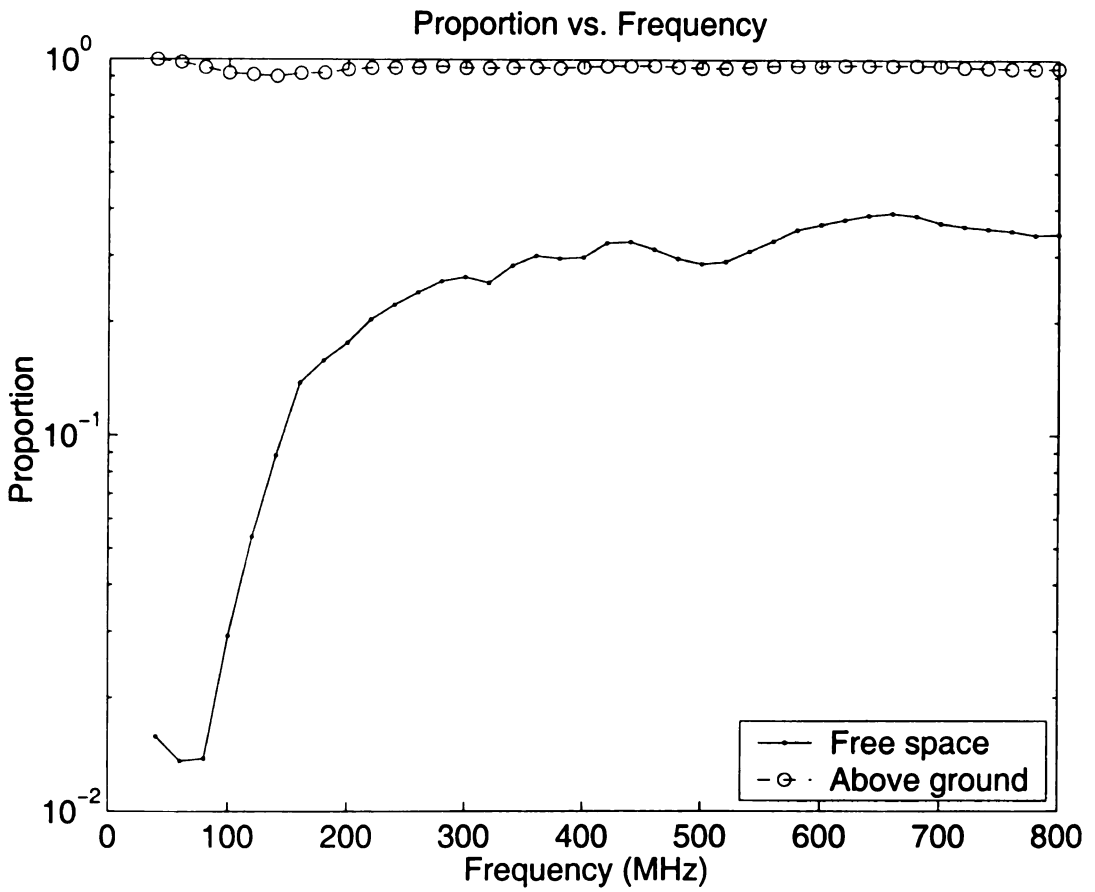


Figure 5.195. Proportion of configurations with maximum vertical gains in the horizontal plane above 3.0 dB vs. frequency for the layer 7 SSA template (5000 random samples).

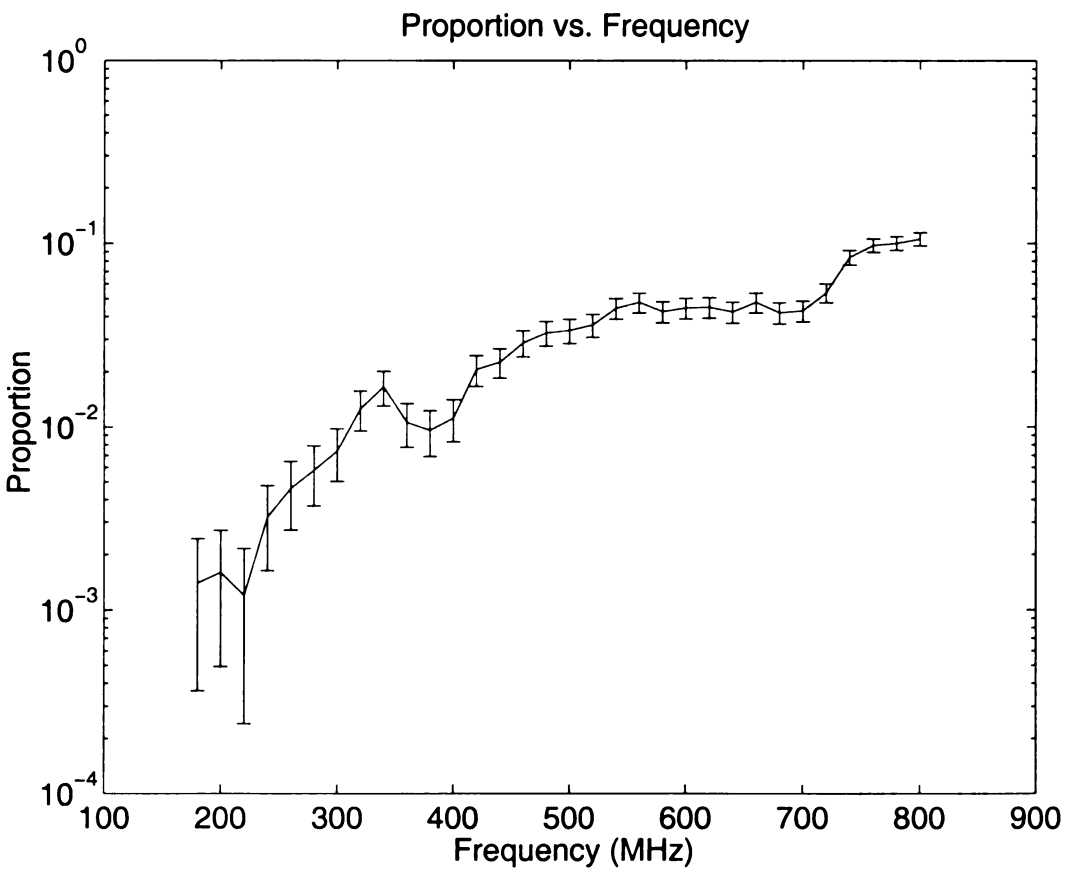


Figure 5.196. Proportion of configurations with SWRs less than 2.0 and maximum vertical gains in the horizontal plane above 3.0 dB vs. frequency for the layer 7 SSA template in free space (5000 random samples). Error bars show the 95% confidence intervals.

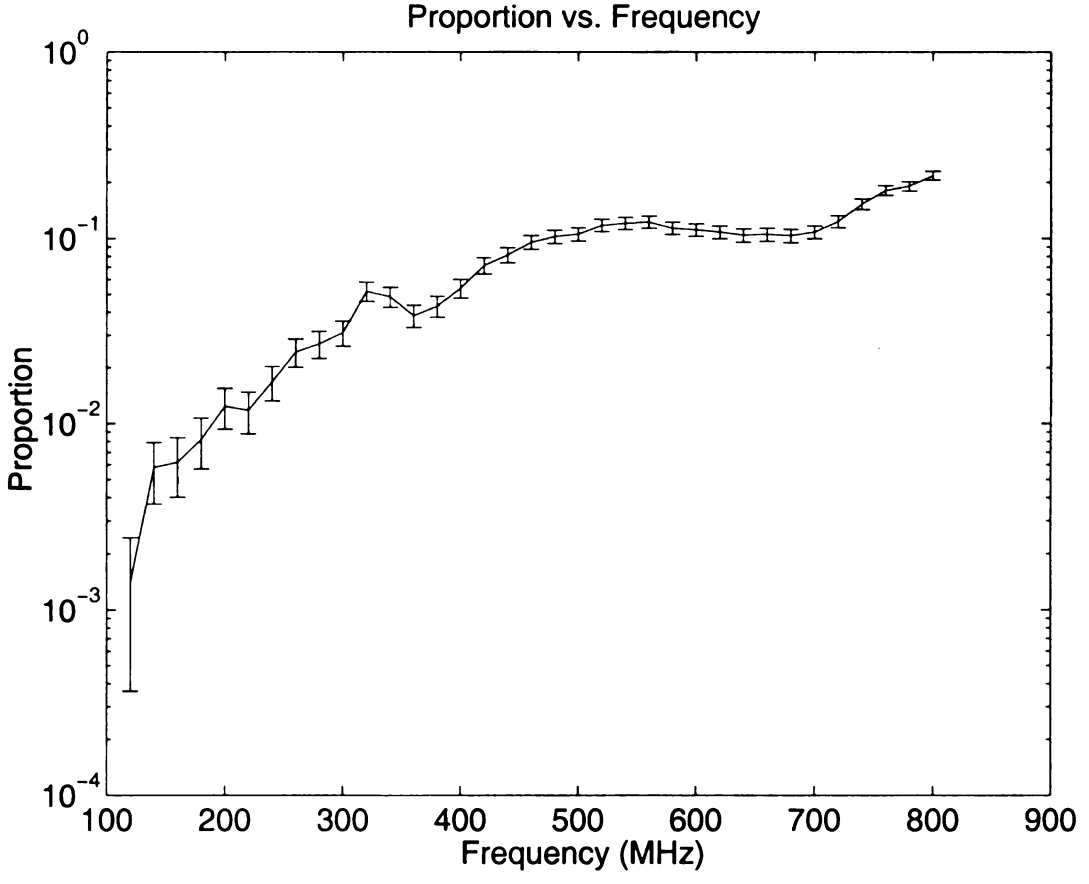


Figure 5.197. Proportion of configurations with SWRs less than 2.0 and maximum vertical gains in the horizontal plane above 3.0 dB vs. frequency for the layer 7 SSA template above ground (5000 random samples). Error bars show the 95% confidence intervals.

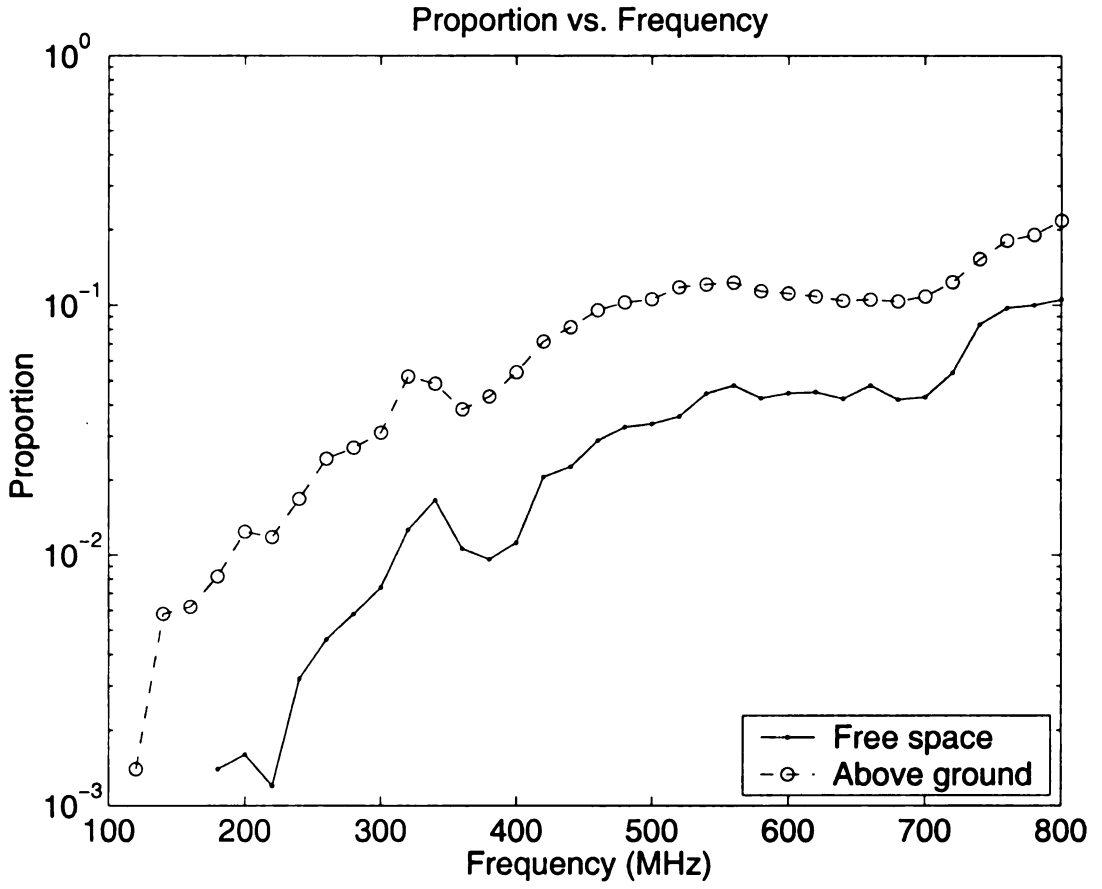


Figure 5.198. Proportion of configurations with SWRs less than 2.0 and maximum vertical gains in the horizontal plane above 3.0 dB vs. frequency for the layer 7 SSA template (5000 random samples).

5.4 Conclusion

This chapter presents a study of a series of simulated SSA templates. Exhaustive studies of simple templates with few switches and configurations are presented. Random searches of the possible configurations are presented for more complicated SSA templates with more switches. The simulated results are presented in Section 5.3.

As shown in Section 5.3.1, a layer 1 SSA template using only three switches for eight possible configurations may not perform adequately for most applications. The layer 1 Type I template is electrically small throughout the frequency band

studied, and the standing wave ratios of the possible configurations are very high across the band. The layer 1 Type II template is electrically larger, but as presented in Section 5.3.1.2, the eight possible switch configurations do not provide a wide range of possible impedance values. For applications where the electromagnetic environment is changing, the layer 1 Type II template may not be able to locate an acceptable configuration.

With only 64 possible configurations, the layer 1.5 templates discussed in Section 5.3.1 also do not have enough configurations that meet acceptable criteria. Although the Type II templates demonstrate acceptable impedance characteristics, a change in the characteristic impedance would be detrimental to the performance of the template.

The layer 2 and layer 2.5 SSA templates show nearly continuous standing wave ratio distributions. The Type I templates are able to represent SWR values between 1.0 and 10.0 over a large band of frequencies. The Type II templates demonstrate tight groupings of SWR values at some frequencies. Low SWR values are not possible for the Type II templates at these frequencies.

Random samples of the possible configurations are discussed for the layer 3 through layer 7 Type I templates. The results show that the proportion of acceptable configurations drops as the criteria become more stringent, as expected. The effect of a ground plane is studied for the layer 3 and layer 7 templates, and the results show that the distributions of impedance values are not greatly affected by the presence of a ground plane. The vertical gain performance in the horizontal plane is improved by the presence of the ground plane.

This study shows that very simple SSA templates with few switches may have trouble providing enough configurations that meet given performance criteria. Therefore, possible future research can be performed on more complicated templates with configuration spaces that are too large to be searched exhaustively. The study pre-

sented here used only 5000 random samples to estimate the characteristics of some of these more complicated templates. Future research can involve higher sample sizes, such as the 500,000 samples presented at single frequencies in Chapter 4, so that more accurate population estimates are found. High sample sizes were not possible for the study presented here due to computation time issues. Other future studies could involve using sophisticated search algorithms such as those presented in Chapter 4 to search for optimal configurations of all of the more complicated templates presented in this study. A study that investigates the angle at which maximum vertical gains exceed 3.0 dB could test the ability of template geometries to cover a usable range of angles from 0°–360° through reconfiguration.

CHAPTER 6

CONCLUSIONS AND FUTURE WORK

6.1 Conclusions

A new type of adaptive antenna, the self-structuring antenna (SSA), is presented in this dissertation. A description of SSAs is given in Chapter 2, as well as a review of the literature that summarizes how SSA research fits with existing antenna research. Experimental results of a prototype SSA presented in Chapter 3 demonstrate some of the properties and capabilities of an SSA.

Chapter 4 presents the application of modern binary search algorithms to SSAs. Ant Colony Optimization (ACO), simulated annealing (SA), and genetic algorithm (GA) searches are compared with random searches of simulated SSAs. Results show that ACO, SA, and GA search algorithms are useful in locating acceptable SSA configurations..

An investigation into the properties and capabilities of simple SSA templates is given in Chapter 5. Results show that templates with few switches have difficulties providing acceptable configurations. Random samples of the possible configurations of SSA templates with more switches are useful in describing their electromagnetic characteristics and capabilities.

The following topics presented in this dissertation are identified as original contributions to the research community:

1. Description and concept of self-structuring antennas: Several conference papers have been presented that describe the basic operation of SSAs with experimental and simulated results [2]–[5]. A refereed journal article that presents an overview of SSAs has been accepted to the IEEE Antennas and Propagation Magazine and is awaiting publication [6]. This article reviews the description of

SSAs presented in Chapter 2 and some of the measured results of the prototype antenna presented in Chapter 3.

2. Ant Colony Optimization (ACO) applied to self-structuring antennas: Applications of ACO to electromagnetic problems have not been published in the IEEE Transactions on Antennas and Propagation or the IEEE Antennas and Propagation Magazine. The work presented in this dissertation on ACO is an original contribution to the areas of evolutionary computation, SSAs, and electromagnetics.

3. Simplicity study of self-structuring antennas: The work presented in Chapter 5 of this dissertation is an addition to the body of knowledge available on SSAs. This work shows that SSA templates with few switches may be unacceptable for many applications, and that more complicated templates using additional switches may be necessary.

6.2 Potential Future Work

There is a large amount of potential research that remains for self-structuring antennas. This dissertation has only presented a brief overview of SSAs and has studied a small number of SSA topics. This final section provides a brief list of the possible new areas of research involving SSAs.

6.2.1 Fractal Template Geometries

Fractals belong to a relatively new area of mathematics that attempts to describe the behavior of natural systems [219]. Fractal mathematics has been applied to many topics, including geometry [212], [220], engineering [221]–[222], computer graphics [223], and finance [224].

In the past fifteen years, fractal mathematics has been applied to several areas of electromagnetics [225]–[228]. The scattering of electromagnetic energy from rough

or periodic surfaces has been a fruitful area of research for many years, and fractal mathematics have recently been applied to these problems [229]. The electromagnetic characteristics of structures with fractal geometries have been of considerable interest lately [226], [230]–[231], including fractal antenna geometries [139]–[146] and fractal-spaced arrays [232]–[233]. The self-similar nature of fractal geometries lends itself to frequency independent antenna characteristics. Many of the SSA template geometries that have been studied in this dissertation use a repeating pattern of wire sections. A new area of research is to extend this iterative-based method of creating template geometries into a more formal method of creating fractal-based wire geometries. Investigations of SSAs with these template geometries might be enlightening.

6.2.2 Search Algorithms

Although this dissertation has investigated the use of random, ACO, GA, and SA search algorithms for use with SSAs, more research can be performed in this area. Other agent-based or nature-based search algorithms might be useful in creating working real-time SSA systems. The application of complexity theory [213], [234], neural networks [100], [235]–[239], or combinations of algorithms are potential research topics.

6.2.3 Simulation of Self-Structuring Antennas

All of the electromagnetic simulations performed in this dissertation use the Numerical Electromagnetics Code (NEC) [214]–[215]. Other electromagnetic simulation or computational methods could be investigated for certain SSA applications. Possibilities include Diakoptic theory [240]–[242] and multilayered printed antenna analysis [243]–[244]

Modeling antennas conformal to automobile glass is a difficult electromagnetic problem [115]. The possibility of simulating SSAs in a more realistic automobile environment is a potential research topic.

6.2.4 Integrated Self-Structuring Antennas

Wireless communications and other technologies have created a need for antennas that are integrated with the electronics section of a device [245]. Since the traditional analysis of integrated environments is a difficult electromagnetics problem [246]–[247] [248], this is a promising potential application of SSAs due to their ability to adapt to unknown environments. It also may be possible to combine SSAs with novel impedance matching schemes in an integrated environment to enhance the capabilities of the system [249].

6.2.5 Prototype Self-Structuring Antenna Investigations

Chapter 3 presents studies of a single prototype SSA system. SWR and reception optimization studies are presented at single frequencies. Potential research that can be performed on prototype SSA systems includes the following:

- Improved prototype SSAs: Other prototype SSA templates, systems, and applications can be investigated. Investigations involving an SSA for television applications have been performed [5].

- Instantaneous bandwidth studies: Preliminary studies and simulations have indicated that SSA configurations with acceptable input impedances over large instantaneous frequency ranges are possible [3]. Investigations using prototype SSA systems are needed.

6.2.6 Applications of Self-Structuring Antennas

There are many possible applications for SSAs that have not been fully discussed or investigated in this dissertation. The following SSA applications are potential research topics:

- Wideband antennas: Antennas that exhibit good characteristics over a large frequency band or that have dual band capabilities are important to many

applications [250]. As shown in this dissertation, SSAs have the potential to operate over a wide band of frequencies, but more research is needed for specific applications.

- Wearable antennas: Wearable personal computers are becoming increasingly popular. SSA templates that are woven into the fabric of clothing may be used for network applications for these computers. The SSA's ability to adapt to a constantly changing environment makes it a promising antenna system for wearable computer and military communication applications.

- Partially-disabled antennas: Traditional antennas have difficulties adapting to situations where part of the antenna has been destroyed or disabled. An SSA has the ability to reconfigure to locate optimal configurations of a partially-disabled system. Preliminary research is being performed at Michigan State University to investigate switch failures on SSA templates. Other research may be performed to investigate the characteristics of SSA templates that have been physically damaged.

- Randomly deployed antennas: Military applications may need antenna systems that can be rapidly deployed without careful positioning. An SSA template can be woven into the fabric of a blanket that can be draped over a bush, tree, or stand for deployment. The SSA can then adapt to locate acceptable configurations.

- Electromagnetic Interference (EMI) mitigating antennas: Antennas that are able to reduce EMI are valuable but very difficult to design [251]. SSA technology may be of use to this area.

- Multiple-polarization antennas: Research has been performed on antennas that have dual- or multiple-polarization capabilities [145], [252]. SSAs have not been

fully investigated to determine the potential for their use in applications that require these capabilities.

6.2.7 Practical Self-Structuring Antenna Issues

There are several topics that need investigation related to the practical implementation of SSAs:

- Switch technology: The switches used on the prototype antennas are simple relays that require a large amount of current. The use of microelectromechanical systems (MEMS) [253] for SSA switches is a possible area for future research.

- Real-time operation: More research needs to be conducted to test the feasibility of real-time operation of SSAs. All measurements and simulations of SSAs in this dissertation have been performed in a research environment.

- Embedded processors: Little research has been performed to find suitable embedded microprocessors that are inexpensive but powerful enough to run sophisticated search algorithms and control the switches on the SSA template.

- Receiver or sensor technology: HP or Agilent network analyzers are too bulky and expensive to use as the SSA's receiver, especially for handheld mobile applications. More research needs to be performed to locate more suitable receivers for use in practical applications.

- Search algorithms: The search algorithms employed in a practical setting may need to be specialized. There are issues that may need to be addressed when dealing with practical search algorithms or adaptive algorithms [254].

This dissertation has presented several research contributions related to self-structuring antennas. As discussed in this conclusion, there are many SSA topics that remain to be investigated.

APPENDICES

APPENDIX A

SELF-STRUCTURING ANTENNA COMPUTER PROGRAMS

A.1 Overview

Several computer programs used to simulate self-structuring antennas were written to help complete the research for this dissertation. The source code for these programs is too large to include in this dissertation. However, an explanation of these programs is presented in this appendix.

The SSA simulation programs were written in C++. The C++ language was used because of its flexibility, its inherent object-oriented-programming capabilities, its support for dynamic memory allocation, and its ability to work with polymorphic data types [255].

Also included in this appendix is a brief explanation of the computer program used by the prototype antenna discussed in Chapter 3. This program is written in BASIC.

A.2 Self-Structuring Antenna Simulation Programs

The SSA programs used for this dissertation attempted to mimic the basic concept behind SSA operation described in Chapter 2. Several different programs were used to generate the data presented in this dissertation; all of these programs use common classes written in C++. The following subsections briefly describe these classes.

A.2.1 Self-Structuring Antenna Class

Objects of class **ssa** hold other class objects and have member functions that simulate the operation of SSAs. The member variables of an **ssa** class object model parts of an SSA as described in Chapter 2. There is an SSA template, a receiver, a search algorithm, and a microprocessor. There are therefore classes to model these

objects. Class `ssatemplate` and its derived classes model the SSA template, class `search_algorithm` and its derived classes model the search algorithm, and the class `nec_output_file` models the receiver. These classes are also described in this appendix. The SSA's microprocessor functions are handled by the computer that is used to perform the simulation.

A.2.2 EM Environment Class

The characteristics of an antenna system are greatly influenced by the its electromagnetic environment. The environment includes the frequency of operation, nearby conductors, the excitation of the antenna, the propagation characteristics of the surrounding medium, and other parameters. The `EM_environment` class holds data that describe similar parameters and uses functions to manipulate this data.

A.2.3 Fitness Class

When a microprocessor uses a search algorithm to locate optimal SSA configurations, it uses information from a receiver to evaluate the 'fitness' of the SSA configurations. The class `fitness` was written to use information from the NEC output file and the electromagnetic environment to calculate a fitness value that can be used by the search algorithms. Thus, the `fitness` class contains member variables of type `nec_output_file` and `EM_environment`.

A.2.4 Search Routine Classes

A basic component of SSAs is a search algorithm that is used to look for optimal SSA configurations. The class `search_routine` covers the basic framework of the search algorithms for simulated SSAs. The member variables for `search_routine` include objects of type `EM_environment`, `fitness`, `nec_input_file`, `nec_output_file`, `ssatemplate*`, and other objects.

The polymorphic capabilities of the C++ language were used to implement the search algorithm of the SSA. This was done by coding `search_routine` as a pure

virtual class, and then creating classes derived from `search_routine` that are specialized for the different search algorithm types. When the program uses a search algorithm, it operates on a `search_routine` pointer that has been set to the address of an object of a class derived from `search_routine`. The derived `search_routine` classes that are discussed in this appendix are `exhaustive_search`, `random_search`, `GA`, `SA`, and `ACO`.

The `search_routine` class operates on a binary string of length n that corresponds to the n switch states on an `ssatemplate`. The string is an object of type `valarray<bool>`. The `valarray` objects are used by including the `<valarray>` header.

The `ran2()` function described in Section A.2.7.7 is used to generate the random numbers needed for objects of type `search_routine`.

A.2.4.1 Exhaustive Search

The class `exhaustive_search` is derived from the pure virtual class `search_routine`. As the name implies, `exhaustive_search` implements an exhaustive search of the possible SSA configurations. Exhaustive searches are unfeasible for SSAs with many switches, but SSAs with small numbers of configurations can be searched exhaustively. This class was utilized for the simplicity study presented in Chapter 5.

A.2.4.2 Random Search

The class `random_search` is derived from the pure virtual class `search_routine`. This class implements a random search of the space of possible SSA configurations.

For each iteration of the algorithm, the `search_routine` member variable of type `valarray<bool>` that holds the switch state values is modified by randomly selecting a '0' or a '1' for each bit. The selection can be weighted more heavily to a '0' or a '1', but the results presented in this dissertation use a 50% weight for each value.

A.2.4.3 Genetic Algorithm

The class `GA` is derived from the pure virtual class `search_routine`. This class implements a genetic algorithm (GA) that is used to search for optimal SSA configurations. The application of GAs to SSAs is presented in Chapter 4.

A.2.4.4 Simulated Annealing

The class `SA` is derived from the pure virtual class `search_routine`. This class implements a simulated annealing (SA) algorithm that is used to search for optimal SSA configurations. The application of simulated annealing to SSAs is presented in Chapter 4.

A.2.4.5 Ant Colony Optimization

The class `ACO` is derived from the pure virtual class `search_routine`. This class implements an Ant Colony Optimization (ACO) algorithm that is used to search for optimal SSA configurations. The application of ACO to SSAs is presented in Chapter 4.

A.2.5 SSA Template Geometry Classes

The class `ssatemplate` serves as a base class for all of the SSA template classes. `ssatemplate` is a pure virtual class. The geometrical layout, wire coordinates, switch locations, and other properties of an SSA template are stored in the derived class objects of `ssatemplate`. Member functions calculate and manipulate these data to create the template geometries.

A.2.5.1 Simple Template

The class `simple_template` is derived from the base class `ssatemplate`. Objects of `simple_template` model the SSA templates discussed in the search algorithm study presented in Chapter 4 and the simplicity study presented in Chapter 5.

A.2.5.2 Irregular Template

The class `irregular_template` is derived from the base class `ssatemplate`. Objects of `irregular_template` model irregularly shaped SSA templates that are not presented in this dissertation.

A.2.5.3 Original Prototype Template

The class `original_prototype_template` is a derived from the base class `ssatemplate`. Objects of type `original_prototype_template` model SSA templates similar to the prototype template discussed in Chapter 3. Simulated results using SSA templates of type `original_prototype_template` are not presented in this dissertation.

A.2.5.4 Rectangles Template

The class `rectangles_template` is derived from the base class `ssatemplate`. Objects of `rectangles_template` model the SSA templates used in the two-level evolutionary algorithm study presented at the 2001 APS / URSI conference in Boston, Massachusetts [4]. The results presented at the conference are not included in this dissertation for the sake of brevity. An example template geometry created using `rectangles_template` is shown in Figure A.1.

A.2.6 NEC Manipulation Classes

The classes `nec_card`, `nec_input_file`, and `nec_output_file` were written to create an interface to the Numerical Electromagnetics Code (NEC). These classes are presented in the following subsections.

A.2.6.1 NEC Card Class

Objects of type `nec_card` model the NEC input cards used by a NEC input file. Geometry, control, and comment cards are built using `nec_card` objects.

An example of a NEC input card modeled by a `nec_card` object is the generate wire (`GW`) command. This command is written as follows:

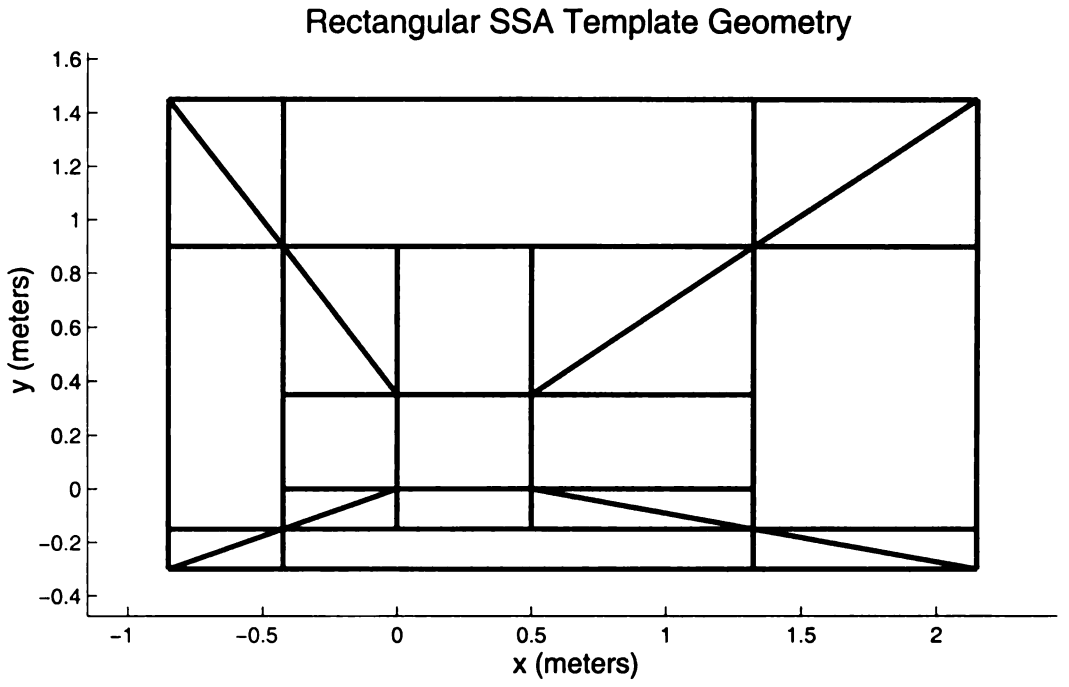


Figure A.1. Example SSA template generated using an object from the class `rectangles_template`.

```
GW   ITG  NS  XW1  YW1  ZW1  XW2  YW2  ZW2  RAD
```

where `GW` is the 'generate wire' command, `ITG` is the tag number for all the segments of the wire, `NS` is the number of segments on the wire, `XW1`, `YW1`, and `ZW1` are the x, y, and z coordinates of the first end of the wire, `XW2`, `YW2`, and `ZW2` are the x, y, and z coordinates of the second end of the wire, and `RAD` is the wire's radius [214]. All coordinates and radii are assumed to be in meters. The NEC input file modeled by objects of the class `nec_input_file` inserts this command as text into the NEC input file.

A.2.6.2 NEC Input File Class

The class `nec_input_file` holds objects of type `nec_card` and uses member functions to create input files used by NEC. A member variable of type `ofstream`, which requires the `fstream` header, is opened as the NEC input file.

A.2.6.3 NEC Output File Class

The class `nec_output_file` holds the data extracted from a NEC output file after NEC has finished execution. The member functions of `nec_output_file` strip the data from the file. The NEC output file is attached to a member variable of type `ifstream`. The `<fstream>` header is required for this member variable.

Files containing data calculated from the output file's information can also be created by `nec_output_file`. For the simplicity study presented in Chapter 5, a binary file was created for each evaluation of an SSA configuration. This file contains impedance and pattern information at each frequency studied.

A.2.7 Other Classes, Structures, and Functions

Several other classes were written for the SSA simulation programs. These are presented here. Structures and global functions were also used by the programs, and these are also described in the following subsections.

A.2.7.1 Wire Class

The class `wire` holds information about the conducting wires that are used to construct SSA templates. The endpoint coordinates, radii, and NEC tag and segment numbers are held by `wire` objects. Derived `ssatemplate` classes use `wire` objects to construct SSA templates.

A.2.7.2 XYZ Coordinate Classes

Objects of the class `xyzcoordinate` hold the geometrical information of a coordinate in three-dimensional space. Three member variables of type `double` hold the coordinate values. Member functions perform useful operations on the coordinate values, such as dot and cross products with other `xyzcoordinate` objects, vector normalization, coordinate rotations, and coordinate translations.

Objects of the class `xyzcoordinate_pair` have two member variables of type `xyzcoordinate` that hold the endpoint information for a line segment. Member func-

tions calculate the length of the segment and other perform other operations. Objects of type **xyzcoordinate** and **xyzcoordinate_pair** are used by derived **ssatemplate** classes and other classes.

A.2.7.3 General Switch Class

The class **general_switch** models the switches on an SSA template. The **TemplateSection** class uses **general_switch** objects. The enumerated type **SwitchModelType** was created to differentiate between the following switch models that are implemented by **general_switch**. **SwitchModelType** can take on the following values:

- **swLever**: A small distance is created laterally between two end wires to simulate an open circuit. The lever part of the wire is close to the size of a single NEC segment of the surrounding wire. The total length of the wires in an open circuit, however, is slightly longer than the total length of a short circuit.

- **swLeverWire**: A small distance is created laterally between two end wires to simulate an open circuit as in the **swLever** model. The length of the lever wire, however, is adjusted so that the the total length of the wires in an open circuit is the same as the total length of a short circuit. A diagram of the **swLever** and **swLeverWire** switch models are shown in Figure A.2. Notice that the short circuit is the same for both switch models.

- **swGap**: A small gap in the wire is introduced at the switch location for an open circuit. A short is made by adding a segment to the gap, resulting in an extra segment that is modeled in NEC.

- **swGapConstSegs**: A small gap wire is introduced for an open as in the **swGap** model, but the wires are reconnected for a short circuit using the same number

of segments in NEC that are used for an open circuit. The segment coordinates along the wire near the switch are different for a short or open circuit.

- **swSeg**: A segment at the switch location is moved using the `GM` command. This model was used for the SSA simulations presented at Salt Lake City [3].

- **swImpedance**: The NEC `LD` command is used to load an impedance at the switch location.

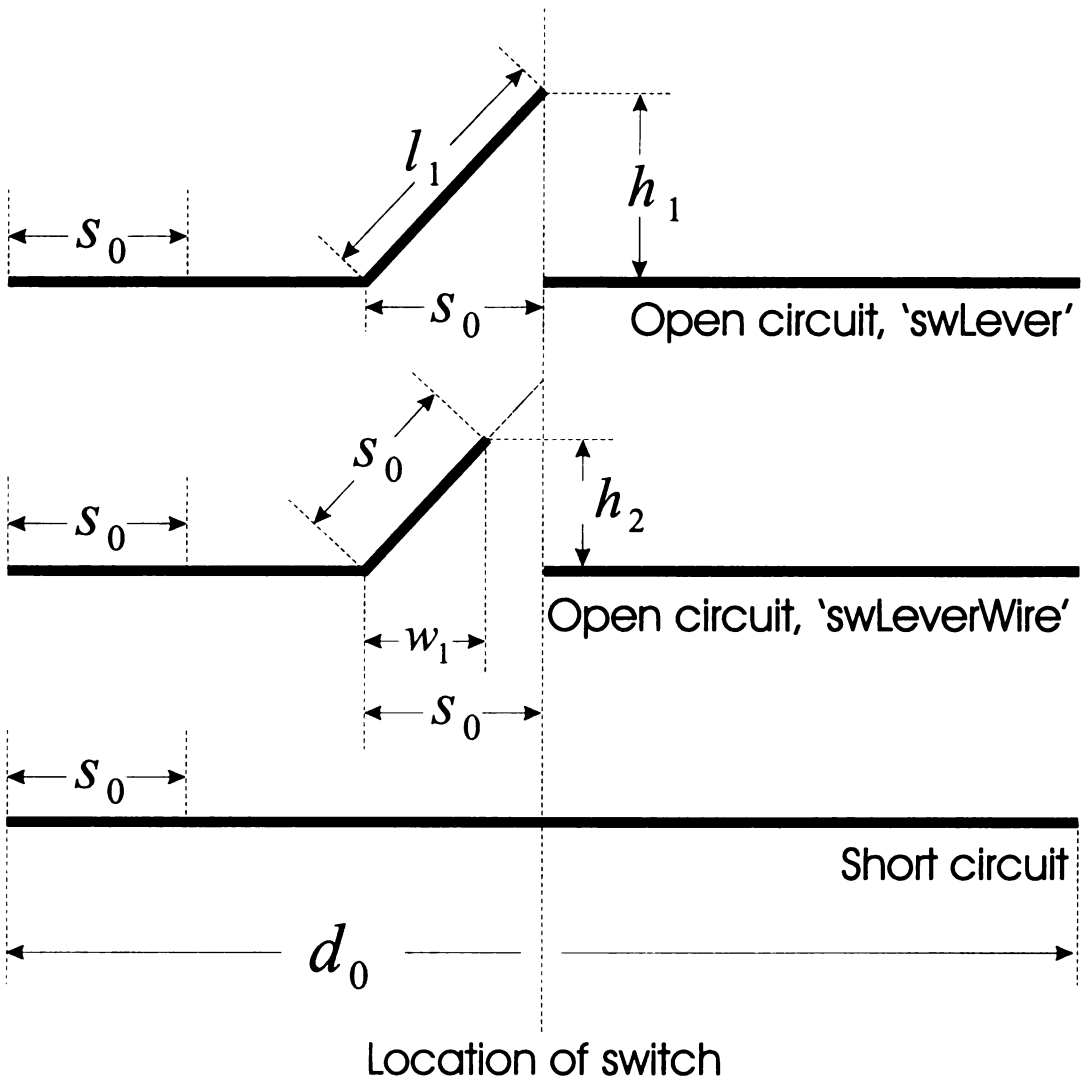


Figure A.2. Diagram of the switch model **swLeverWire**.

A.2.7.4 Template Section Class

The class **TemplateSection** is used by derived **ssatemplate** objects to hold information about straight wire sections of SSA templates. Wire information is held by member arrays of **wire** objects and switch models are held by **general_switch** member variables. Feed structure models are also held in **TemplateSection** objects.

A.2.7.5 File String Structure

The SSA simulation programs use many input and output files during operation. These files include NEC input and output files and output data files. Some SSA simulation executions generate hundreds or thousands of independent output files and generate many temporary input and output files. To keep track of the names needed for these files, the structure `file_strings` was created. Member variables of type `string`, which require the `<string>` header, are used to hold the file names.

A.2.7.6 Radiation Pattern Parameter Structure

The structure `radiation_pattern_parameters` holds several variables that specify the desired radiation pattern that NEC will calculate. The `nec_input_file`, `nec_output_file`, and `fitness` classes use this structure.

An `RP` command with data taken from the `radiation_pattern_parameters` object is created by the `nec_card` class and then inserted into the NEC input file by the `nec_input_file` class. Member variables of the structure `radiation_pattern_parameters` include `int` data types that hold the number of θ and ϕ angles to request in a radiation pattern, `double` data types that hold the initial θ and ϕ values and the θ and ϕ increments, and other variables that hold information about the type of pattern requested.

A.2.7.7 Random Number Generating Function

Because the search algorithms used for SSAs are directed random searches, a random number generator is needed for the SSA programs. Therefore, a function is used to return a random number of type `float` (single precision). This function was adapted from the `ran2` function found in Numerical Recipes in 'C' [209]. The prototype for the function is:

```
float ran2( void );
```

The seed for the random number generator is type **static long**. This is altered from the original function so that the seed is set only once during program execution. Thus, the random number generator function keeps track of the seed, and the other parts of the program do not have to pass a seed to the function.

A.2.7.8 String Locating Functions

Functions were written to search a text file for a given string. Type **string** variables using the **<string>** header are passed to the functions, as well as references to the **ifstream** objects that correspond to the text files being searched. One version of the function also operates on file position indicators of type **streampos**. This variable will hold the position in the file where the string was found. Both **ifstream** and **streampos** require the **<fstream>** header.

The two function prototypes for the string locating functions are:

```
int f_LocateString(string & NextString, ifstream & File,
        streampos & FilePos);
int f_LocateString(string & NextString, ifstream & File);
```

A.3 Prototype SSA Computer Programs

Computer programs were written in BASIC to control the SSA prototype antenna presented in Chapter 3. These programs use the Hewlett Packard Interface Bus (HPIB) and Arrick MD2 stepper motor libraries and were compiled in Microsoft Professional Basic for MS-DOS. The source code for these programs is too lengthy to present in this dissertation.

These programs search for optimal SSA configurations using simulated annealing and genetic algorithm subroutines. The stepper motor is used to rotate the prototype's template for reception optimization measurements.

A.3.1 Basic Stamp II Programs

A Basic Stamp II was used to control the states of fifteen switches on the prototype SSA described in Chapter 3. Computer code written in the Basic Stamp II language is downloaded through a serial cable to the Basic Stamp II using a terminal program on a PC [208]. This program is summarized in the following block of code written by Dr. Edward Rothwell:

```
x0      var     word
x1      var     word
i       var     word
loop:
        serin 15, 16780, [wait("ok"),dec x1, x0]
        for i=0 to 14
                low i
                if x1.bit0=0 then skipthis
                high i
                skipthis:
                x1=x1>>1
        next
goto loop
```

A.3.1.1 LTC-1298 AD Converter Basic Stamp II Code

As described in Chapter 3, a second Basic Stamp II is used for the prototype SSA during reception optimization investigations. The secondary Basic Stamp II is used to control the LTC-1298 A/D converter in the data acquisition circuit illustrated in Figure 3.6 on page 24. The computer code used by the second Basic Stamp II is not included in this dissertation for the sake of brevity. The code used is very similar to the demonstration code available with the LTC-1298 module.

BIBLIOGRAPHY

BIBLIOGRAPHY

[1] S. Ramo, J. R. Whinnery, and T. Van Duzer, *Fields and Waves in Communication Electronics.* New York: John Wiley and Sons, Second ed., 1984.

[2] C. M. Coleman, E. J. Rothwell, and J. E. Ross, "Self-structuring antennas," in *2000 IEEE AP-S International Symposium*, (Salt Lake City, Utah), July 16–21 2000.

[3] J. E. Ross, E. J. Rothwell, C. M. Coleman, and L. L. Nagy, "Numerical simulation of self-structuring antennas based on a genetic algorithm optimization scheme," in *2000 USNC / URSI National Radio Science Meeting*, (Salt Lake City, Utah), July 16–21 2000.

[4] C. M. Coleman, E. J. Rothwell, and J. E. Ross, "Application of two-level evolutionary algorithms to self-structuring antennas," in *2001 USNC / URSI National Radio Science Meeting*, (Boston, Massachusetts), July 9–13 2001.

[5] B. T. Perry, C. M. Coleman, B. F. Basch, E. J. Rothwell, and J. E. Ross, "Self-structuring antenna for television reception," in *2001 IEEE AP-S International Symposium*, (Boston, Massachusetts), July 9–13 2001.

[6] C. M. Coleman, E. J. Rothwell, J. E. Ross, and L. L. Nagy, "Self-structuring antennas," *IEEE Antennas and Propagation Magazine*, to appear.

[7] A. F. Gangi, "The active adaptive antenna array system," *IEEE Transactions on Antennas and Propagation*, vol. AP-11, pp. 405–414, July 1963.

[8] R. T. Adams, "Beam tagging for control of adaptive transmitting arrays," *IEEE Transactions on Antennas and Propagation*, vol. AP-12, pp. 224–227, March 1964.

[9] S. N. Andre and D. J. Leonard, "An active retrodirective array for satellite communications," *IEEE Transactions on Antennas and Propagation*, vol. AP-12, pp. 181–186, March 1964.

[10] C. A. Belfi, C. Rothenberg, L. Schwartzman, R. E. Tilley, and A. Wills, "A satellite data transmission antenna," *IEEE Transactions on Antennas and Propagation*, vol. AP-12, pp. 200–206, March 1964.

[11] N. Burtnyk, C. W. McLeish, and J. L. Wolfe, "A wide aperture sampling linear array for direction finding," *IEEE Transactions on Antennas and Propagation*, vol. AP-12, pp. 248–256, May 1964.

[12] J. R. Copeland, W. J. Robertson, and R. G. Verstraete, "Antennafier arrays," *IEEE Transactions on Antennas and Propagation*, vol. AP-12, pp. 227–233, March 1964.

[13] J. W. Eberle, "An adaptively phased, four-element array of thirty-foot parabolic reflectors for passive ((echo),"

[14] R. N. Ghose, "Electronically adaptive antenna systems," *IEEE Transactions on Antennas and Propagation*, vol. AP-12, pp. 161–169, March 1964.

[15] E. L. Gruenberg and C. M. Johnson, "Satellite communications relay system using a retrodirective space antenna," *IEEE Transactions on Antennas and Propagation*, vol. AP-12, pp. 215–223, March 1964.

[16] E. I. Muehldorf, "Self-steered retrodirective arrays with amplification," *IEEE Transactions on Antennas and Propagation*, vol. AP-17, pp. 42–49, January 1969.

[17] C. Y. Pon, "Retrodirective array using the heterodyne technique," *IEEE Transactions on Antennas and Propagation*, vol. AP-12, pp. 176–180, March 1964.

[18] E. J. Putzer and R. N. Ghose, "Redirective and retrodirective antenna arrays," *IEEE Transactions on Antennas and Propagation*, vol. AP-17, pp. 276–279, May 1969.

[19] E. M. Rutz-Philipp, "Spherical retrodirective array," *IEEE Transactions on Antennas and Propagation*, vol. AP-12, pp. 187–194, March 1964.

[20] J. H. Schrader, "A phase-lock receiver for the arraying of independently directed antennas," *IEEE Transactions on Antennas and Propagation*, vol. AP-12, pp. 155–161, March 1964.

[21] B. A. Sichelstiel, W. M. Waters, and T. A. Wild, "Self-focusing array research model," *IEEE Transactions on Antennas and Propagation*, vol. AP-12, pp. 150–154, March 1964.

[22] M. I. Skolnik and D. D. King, "Self-phasing array antennas," *IEEE Transactions on Antennas and Propagation*, vol. AP-12, pp. 142–149, March 1964.

[23] D. E. Svoboda, "A phase-locked receiving array for high-frequency communications use," *IEEE Transactions on Antennas and Propagation*, vol. AP-12, pp. 207–215, March 1964.

[24] W. M. Waters and J. O. Wedel, "Adaptive receiving arrays for wide-band lunar relay communications," *IEEE Transactions on Antennas and Propagation*, vol. AP-12, pp. 195–199, March 1964.

[25] A. F. Gangi, "Doppler tracking loops for the active adaptive antenna array system," *IEEE Transactions on Antennas and Propagation*, vol. AP-14, pp. 502–504, July 1966.

[26] A. F. Kay, "Comments on "self-phasing array antennas" and "electronically adaptive antenna systems"," *IEEE Transactions on Antennas and Propagation*, vol. AP-12, pp. 792–793, November 1964.

[27] A. P. Anderson, W. S. Davies, M. M. Dawoud, and D. E. Galanakis, "Note on transistor-fed active-array antennas," *IEEE Transactions on Antennas and Propagation*, vol. AP-19, pp. 537–539, July 1971.

[28] A. P. Anderson and M. M. Dawoud, "The performance of transistor fed monopoles in active antennas," *IEEE Transactions on Antennas and Propagation*, vol. AP-21, pp. 371–374, May 1973.

[29] S. P. Applebaum, "Adaptive arrays," *IEEE Transactions on Antennas and Propagation*, vol. AP-24, pp. 585–598, September 1976.

[30] S. P. Applebaum and D. J. Chapman, "Adaptive arrays with main beam constraints," *IEEE Transactions on Antennas and Propagation*, vol. AP-24, pp. 650–662, September 1976.

[31] C. A. Baird and G. G. Rossweiler, "Adaptive sidelobe nulling using digitally controlled phase-shifters," *IEEE Transactions on Antennas and Propagation*, vol. AP-24, pp. 638–649, September 1976.

[32] L. E. Brennen, J. D. Mallett, and I. S. Reed, "Adaptive arrays in airborne MTI radar," *IEEE Transactions on Antennas and Propagation*, vol. AP-24, pp. 607–615, September 1976.

[33] L. E. Brennan, "Efficient simulation of external noise incident on arrays," *IEEE Transactions on Antennas and Propagation*, vol. AP-24, pp. 740–741, September 1976.

[34] D. J. Chapman, "Partial adaptivity for the large array," *IEEE Transactions on Antennas and Propagation*, vol. AP-24, pp. 685–697, September 1976.

[35] R. T. Compton, Jr., R. J. Huff, W. G. Swarner, and A. A. Ksienski, "Adaptive arrays for communication systems: An overview of research at The Ohio State University," *IEEE Transactions on Antennas and Propagation*, vol. AP-24, pp. 599–607, September 1976.

[36] R. T. Compton, Jr., "An experimental four-element adaptive array," *IEEE Transactions on Antennas and Propagation*, vol. AP-24, pp. 697–706, September 1976.

[37] J. Gobert, "Adaptive beam weighting," *IEEE Transactions on Antennas and Propagation*, vol. AP-24, pp. 744–749, September 1976.

[38] L. J. Griffiths, "Time-domain adaptive beamforming of HF backscatter radar signals," *IEEE Transactions on Antennas and Propagation*, vol. AP-24, pp. 707–720, September 1976.

[39] P. W. Howells, "Explorations in fixed and adaptive resolution at GE and SURC," *IEEE Transactions on Antennas and Propagation*, vol. AP-24, pp. 575–584, September 1976.

[40] M. K. Leavitt, "A phase adaptation algorithm," *IEEE Transactions on Antennas and Propagation*, vol. AP-24, pp. 754–756, September 1976.

[41] G. G. Rassweiler, M. R. Williams, L. M. Payne, and G. P. Martin, "A miniaturized lightweight wideband null steerer," *IEEE Transactions on Antennas and Propagation*, vol. AP-24, pp. 749–754, September 1976.

[42] S. Sensiper, "Suggested signal generator-simulator for adaptive antenna test," *IEEE Transactions on Antennas and Propagation*, vol. AP-24, pp. 760–764, September 1976.

[43] S. H. Taheri and B. D. Steinberg, "Tolerances in self-cohering antenna arrays of arbitrary geometry," *IEEE Transactions on Antennas and Propagation*, vol. AP-24, pp. 733–739, September 1976.

[44] K. Takao, M. Fujita, and T. Nishi, "An adaptive antenna array under directional constraints," *IEEE Transactions on Antennas and Propagation*, vol. AP-24, pp. 662–669, September 1976.

[45] P. A. Thompson, "Adaptation by direct phase-shift adjustment in narrow-band adaptive antenna systems," *IEEE Transactions on Antennas and Propagation*, vol. AP-24, pp. 756–760, September 1976.

[46] T. W. Washburn and L. E. Sweeney, Jr., "An on-line adaptive beamforming capability for HF backscatter radar," *IEEE Transactions on Antennas and Propagation*, vol. AP-24, pp. 721–732, September 1976.

[47] W. D. White, "Cascade preprocessors for adaptive antennas," *IEEE Transactions on Antennas and Propagation*, vol. AP-24, pp. 670–684, September 1976.

[48] B. Widrow and J. M. McCool, "A comparison of adaptive algorithms based on the methods of steepest descent and random search," *IEEE Transactions on Antennas and Propagation*, vol. AP-24, pp. 615–637, September 1976.

[49] W. D. Wirth, "Suboptimal suppression of directional noise by a sensor array before beam forming," *IEEE Transactions on Antennas and Propagation*, vol. AP-24, pp. 741–744, September 1976.

[50] N. G. Alexopoulos, P. L. E. Uslenghi, and G. A. Tadler, "Antenna beam scanning by active impedance loading," *IEEE Transactions on Antennas and Propagation*, vol. AP-22, pp. 722–723, September 1974.

[51] C. Nelson Dorny, "A self-survey technique for self-cohering of antenna systems," *IEEE Transactions on Antennas and Propagation*, vol. AP-26, pp. 877–881, November 1978.

[52] J. J. Gustincic, "The determination of active array impedance with multielement waveguide simulators," *IEEE Transactions on Antennas and Propagation*, vol. AP-20, pp. 589–595, September 1972.

[53] L. R. Lewis and A. Hessel, "A novel small array technique for active phased array impedance measurement," *IEEE Transactions on Antennas and Propagation*, vol. AP-20, pp. 107–110, January 1972.

[54] E. D. Banta, "The root-trajectory method–a tool for analyzing linear adaptive arrays," *IEEE Transactions on Antennas and Propagation*, vol. AP-26, pp. 881–883, November 1978.

[55] R. N. Ghose, "Correlating antenna array," *IEEE Transactions on Antennas and Propagation*, vol. AP-19, pp. 447–450, May 1971.

[56] D. R. Morgan, "Partially adaptive array techniques," *IEEE Transactions on Antennas and Propagation*, vol. AP-26, pp. 823–833, November 1978.

[57] S. Prasad, "Linear antenna arrays with broad nulls with applications to adaptive arrays," *IEEE Transactions on Antennas and Propagation*, vol. AP-27, pp. 185–190, March 1979.

[58] K. Bakhru and D. J. Torrieri, "The maximin algorithm for adaptive arrays and frequency-hopping communications," *IEEE Transactions on Antennas and Propagation*, vol. AP-32, pp. 919–928, September 1984.

[59] R. T. Compton, Jr., "Power optimization in adaptive arrays: A technique for interference protection," *IEEE Transactions on Antennas and Propagation*, vol. AP-28, pp. 79–85, January 1980.

[60] R. T. Compton, Jr., "The tripole antenna: An adaptive array with full polaization flexibility," *IEEE Transactions on Antennas and Propagation*, vol. AP-29, pp. 944–952, November 1981.

[61] R. T. Compton, Jr., "The bandwidth performance of a two-element adaptive array with tapped delay-line processing," *IEEE Transactions on Antennas and Propagation*, vol. 36, pp. 5–14, January 1988.

[62] R. T. Compton, Jr., "The relationship between tapped delay-line and FFT processing in adaptive arrays," *IEEE Transactions on Antennas and Propagation*, vol. 36, pp. 15–26, January 1988.

[63] E. C. Dufort, "Pattern synthesis based on adaptive array theory," *IEEE Transactions on Antennas and Propagation*, vol. 37, pp. 1011–1018, August 1989.

[64] I. J. Gupta and A. A. Ksienski, "Dependence of adaptive array performance on conventional array design," *IEEE Transactions on Antennas and Propagation*, vol. AP-30, pp. 549–553, July 1982.

[65] I. J. Gupta and A. A. Ksienski, "Effect of mutual coupling on the performance of adaptive arrays," *IEEE Transactions on Antennas and Propagation*, vol. AP-31, pp. 785–791, September 1983.

[66] I. J. Gupta, "SMI adaptive antenna arrays for weak interfering signals," *IEEE Transactions on Antennas and Propagation*, vol. AP-34, pp. 1237–1242, October 1986.

[67] R. C. Hansen, "Gain limitations of large antennas," *IRE Transactions on Antennas and Propagation*, vol. AP-8, pp. 490–495, September 1960.

[68] R. L. Haupt, "Adaptive nulling in monopulse antennas," *IEEE Transactions on Antennas and Propagation*, vol. 36, pp. 202–208, February 1988.

[69] K. Hirasawa, "The application of a biquadratic programming method to phase-only optimization of antenna arrays," *IEEE Transactions on Antennas and Propagation*, vol. 36, pp. 1545–1550, November 1988.

[70] Y. J. Hong, D. R. Ucci, and C.-C. Yeh, "The performance of an adaptive array combining reference signal and steering vector," *IEEE Transactions on Antennas and Propagation*, vol. AP-35, pp. 763–770, July 1987.

[71] H.-C. Lin, "Spatial correlations in adaptive arrays," *IEEE Transactions on Antennas and Propagation*, vol. AP-30, pp. 212–223, March 1982.

[72] M. Ohmiya, Y. Ogawa, and K. Itoh, "Howells-applebaum adaptive superresolution array for accelerated scanning," *IEEE Transactions on Antennas and Propagation*, vol. 36, pp. 1700–1706, December 1988.

[73] B. D. Steinberg and E. Yadin, "Effect of multipath and scattering on array gain of a large adaptive beam forming phased array," *IEEE Transactions on Antennas and Propagation*, vol. AP-33, pp. 481–487, May 1985.

[74] K. M. Buckley and L. J. Griffiths, "An adaptive generalized sidelobe canceller with derivative constraints," *IEEE Transactions on Antennas and Propagation*, vol. AP-34, pp. 311–319, March 1986.

[75] R. M. Davis, D. C. Farden, and P. J.-S. Sher, "A coherent perturbation algorithm," *IEEE Transactions on Antennas and Propagation*, vol. AP-34, pp. 380–388, March 1986.

[76] R. J. Dinger, "A planar version of a 4.0 GHz reactively steered adaptive array," *IEEE Transactions on Antennas and Propagation*, vol. AP-34, pp. 427–431, March 1986.

[77] M. H. Er and A. Cantoni, "A new set of linear constraints for broad-band time domain element space processors," *IEEE Transactions on Antennas and Propagation*, vol. AP-34, pp. 320–329, March 1986.

[78] W. F. Gabriel, "Introduction: Special issue on adaptive processing antenna systems," *IEEE Transactions on Antennas and Propagation*, vol. AP-34, pp. 273–275, March 1986.

[79] W. F. Gabriel, "Using spectral estimation techniques in adaptive processing antenna systems," *IEEE Transactions on Antennas and Propagation*, vol. AP-34, pp. 291–300, March 1986.

[80] K. Gerlach and R. H. Lang, "Exact solution for control loop adaptive antenna weights in band-limited noise," *IEEE Transactions on Antennas and Propagation*, vol. AP-34, pp. 395–403, March 1986.

[81] K. Gerlach, "Fast orthogonalization networks," *IEEE Transactions on Antennas and Propagation*, vol. AP-34, pp. 458–462, March 1986.

[82] L. C. Godara and A. Cantoni, "Analysis of constrained LMS algorithm with application to adaptive beamforming using perturbation sequences," *IEEE Transactions on Antennas and Propagation*, vol. AP-34, pp. 368–379, March 1986.

[83] R. P. Gooch and J. J. Shynk, "Wide-band adaptive array processing using pole-zero digital filters," *IEEE Transactions on Antennas and Propagation*, vol. AP-34, pp. 355–368, March 1986.

[84] I. J. Gupta and A. A. Ksienski, "Adaptive antenna arrays for weak interfering signals," *IEEE Transactions on Antennas and Propagation*, vol. AP-34, pp. 420–426, March 1986.

[85] F. Haber and M. Zoltowski, "Spatial spectrum estimation in a coherent signal environment using an array in motion," *IEEE Transactions on Antennas and Propagation*, vol. AP-34, pp. 301–310, March 1986.

[86] R. C. Hanumara, "An alternate derivation of the distribution of the conditioned signal-to-noise ratio," *IEEE Transactions on Antennas and Propagation*, vol. AP-34, pp. 463–464, March 1986.

[87] W. S. Hodgkiss, Jr. and D. Alexandrou, "An adaptive algorithm for array processing," *IEEE Transactions on Antennas and Propagation*, vol. AP-34, pp. 454–457, March 1986.

[88] N. K. Jablon, "Steady state analysis of the generalized sidelobe canceller by adaptive noise cancelling techniques," *IEEE Transactions on Antennas and Propagation*, vol. AP-34, pp. 330–337, March 1986.

[89] M. Klemes, "A practical method of obtaining constant convergence rates in LMS adaptive arrays," *IEEE Transactions on Antennas and Propagation*, vol. AP-34, pp. 440–446, March 1986.

[90] J. T. Mayhan, "Area coverage adaptive nulling from geosynchronous satellites: Phased arrays versus multiple-beam antenna," *IEEE Transactions on Antennas and Propagation*, vol. AP-34, pp. 410–419, March 1986.

[91] M. Ohmiya, Y. Ogawa, and K. Itoh, "Considerations on a scanned adaptive superresolution array," *IEEE Transactions on Antennas and Propagation*, vol. AP-34, pp. 447–454, March 1986.

[92] R. H. Ott and R. B. Dybdal, "The effects of reflector antenna diffraction on the interference cancellation performance of coherent sidelobe cancellers," *IEEE Transactions on Antennas and Propagation*, vol. AP-34, pp. 432–439, March 1986.

[93] R. O. Schmidt, "Multiple emitter location and signal parameter estimation," *IEEE Transactions on Antennas and Propagation*, vol. AP-34, pp. 276–280, March 1986.

[94] R. O. Schmidt and R. F. Franks, "Multiple source DF signal processing: An experimental system," *IEEE Transactions on Antennas and Propagation*, vol. AP-34, pp. 281–290, March 1986.

[95] H. Steyskal, R. A. Shore, and R. L. Haupt, "Methods for null control and their effects on the radiation pattern," *IEEE Transactions on Antennas and Propagation*, vol. AP-34, pp. 404–409, March 1986.

[96] Y. L. Su, T. J. Shan, and B. Widrow, "Parallel spatial processing: A cure for signal cancellation in adaptive arrays," *IEEE Transactions on Antennas and Propagation*, vol. AP-34, pp. 347–354, March 1986.

[97] K. Takao and N. Kikuma, "Tamed adaptive antenna array," *IEEE Transactions on Antennas and Propagation*, vol. AP-34, pp. 388–394, March 1986.

[98] C. R. Ward, P. J. Hargrave, and J. G. McWhirter, "A novel algorithm and architecture for adaptive digital beamforming," *IEEE Transactions on Antennas and Propagation*, vol. AP-34, pp. 338–347, March 1986.

[99] Éric Charpentier and Jean-Jacques Laurin, "Sectorial direction finding antenna array with a MLP beamformer," in *1997 IEEE AP-S International Symposium*, (Montreal, Canada), July 13–18 1997.

[100] A. H. El Zooghby, C. G. Christodoulou and M. Georgiopoulos, "Antenna array signal processing with neural networks for direction of arrival estimation," in *1997 IEEE AP-S International Symposium*, (Montreal, Canada), July 13–18 1997.

[101] Y. Rahmat-Samii and W. L. Stutzman, "Guest editorial: Special issue on wireless communications," *IEEE Transactions on Antennas and Propagation*, vol. 46, pp. 745–748, June 1998.

[102] B. Lindmark, S. Lundgren, J. Sanford, and C. Beckman, "Dual-polarized array for signal-processing applications in wireless communications," *IEEE Transactions on Antennas and Propagation*, vol. 46, pp. 758–763, June 1998.

[103] P. L. Perini and C. L. Holloway, "Angle and space diversity comparisons in different mobile radio environments," *IEEE Transactions on Antennas and Propagation*, vol. 46, pp. 764–775, June 1998.

[104] K. Cho, T. Hori, and K. Kagoshima, "Effectiveness of four-branch height and polarization diversity configuration for street microcell," *IEEE Transactions on Antennas and Propagation*, vol. 46, pp. 776–781, June 1998.

[105] F. Demmerle and W. Wiesbeck, "A biconical multibeam antenna for space-division multiple access," *IEEE Transactions on Antennas and Propagation*, vol. 46, pp. 782–787, June 1998.

[106] H. Nakano, N. Ikeda, Y.-Y. Wu, R. Suzuki, H. Mimaki, and J. Yamauchi, "Realization of dual-frequency and wide-band VSWR performances using normal-mode helical and inverted-F antennas," *IEEE Transactions on Antennas and Propagation*, vol. 46, pp. 788–793, June 1998.

[107] A. Ando, Y. Honma, and K. Kagoshima, "A novel electromagnetically coupled microstrip antenna with a rotatable patch for personal handy-phone system units," *IEEE Transactions on Antennas and Propagation*, vol. 46, pp. 794–797, June 1998.

[108] R. Y.-S. Tay, Q. Balzano, and N. Kuster, "Dipole configurations with strongly improved radiation efficiency for hand-held transceivers," *IEEE Transactions on Antennas and Propagation*, vol. 46, pp. 798–806, June 1998.

[109] N. Herscovici, "New considerations in the design of microstrip antennas," *IEEE Transactions on Antennas and Propagation*, vol. 46, pp. 807–812, June 1998.

[110] J. S. Colburn and Y. Rahmat-Samii, "Human proximity effects on circular polarized handset antennas in personal satellite communications," *IEEE Transactions on Antennas and Propagation*, vol. 46, pp. 813–820, June 1998.

[111] W.-T. Chen and H.-R. Chuang, "Numerical computation of human interaction with arbitrarily oriented superquadric loop antennas in personal communications," *IEEE Transactions on Antennas and Propagation*, vol. 46, pp. 821–828, June 1998.

[112] A. D. Tinniswood, C. M. Furse, and O. P. Gandhi, "Computations of SAR distributions for two anatomically based models of the human head using CAD files of commercial telephones and the parallelized FDTD code," *IEEE Transactions on Antennas and Propagation*, vol. 46, pp. 829–833, June 1998.

[113] O. Nørklit and J. Bach Andersen, "Diffuse channel model and experimental results for array antennas in mobile environments," *IEEE Transactions on Antennas and Propagation*, vol. 46, pp. 834–840, June 1998.

[114] S. L. Preston, D. V. Thiel, T. A. Smith, S. G. O'Keefe, and J. W. Lu, "Base-station tracking in mobile communications using a switched parasitic antenna array," *IEEE Transactions on Antennas and Propagation*, vol. 46, pp. 841–844, June 1998.

[115] R. Abou-Jauude and E. K. Walton, "Numerical modeling of on-glass conformal automobile antennas," *IEEE Transactions on Antennas and Propagation*, vol. 46, pp. 845–852, June 1998.

[116] G. Liang and H. L. Bertoni, "A new approach to 3-D ray tracing for propagation prediction in cities," *IEEE Transactions on Antennas and Propagation*, vol. 46, pp. 853–864, June 1998.

[117] R. Mazar, A. Bronshtein, and I.-T. Lu, "Theoretical analysis of UHF propagation in a city street modeled as a random multislit waveguide," *IEEE Transactions on Antennas and Propagation*, vol. 46, pp. 864–871, June 1998.

[118] S. A. Torrico, H. L. Bertoni, and R. H. Lang, "Modeling tree effects on path loss in a residential environment," *IEEE Transactions on Antennas and Propagation*, vol. 46, pp. 872–880, June 1998.

[119] C. Brennan and P. J. Cullen, "Application of the fast far-field approximation to the computation of UHF pathloss over irregular terrain," *IEEE Transactions on Antennas and Propagation*, vol. 46, pp. 881–890, June 1998.

[120] C. H. Bianchi and K. Sivaprasad, "A channel model for multipath interference on terrestrial line-of-sight digital radio," *IEEE Transactions on Antennas and Propagation*, vol. 46, pp. 891–901, June 1998.

[121] N. Kuga, H. Arai, and N. Goto, "A notch-wire composite antenna for polarization diversity reception," *IEEE Transactions on Antennas and Propagation*, vol. 46, pp. 902–906, June 1998.

[122] C.-F. Yang, B.-C. Wu, and C.-J. Ko, "A ray-tracing method for modeling indoor wave propagation and penetration," *IEEE Transactions on Antennas and Propagation*, vol. 46, pp. 907–920, June 1998.

[123] S. Obayashi and J. Zander, "A body-shadowing model for indoor radio communication environments," *IEEE Transactions on Antennas and Propagation*, vol. 46, pp. 920–927, June 1998.

[124] P. Marinier, G. Y. Delisle, and C. L. Despins, "Temporal variations of the indoor wireless millimeter-wave channel," *IEEE Transactions on Antennas and Propagation*, vol. 46, pp. 928–934, June 1998.

[125] F. J. Dietrich, P. Metzen, and P. Monte, "The Globalstar cellular satellite system," *IEEE Transactions on Antennas and Propagation*, vol. 46, pp. 935–942, June 1998.

[126] G. Lazzi, S. S. Pattnaik, C. M. Furse, and O. P. Gandhi, "Comparison of FDTD computed and measured radiation patterns of commercial mobile telephones in presence of the human head," *IEEE Transactions on Antennas and Propagation*, vol. 46, pp. 943–944, June 1998.

[127] C. M. Montiel, L. Fan, and K. Chang, "Active-notch antennas stabilized with a slotline-ring resonator for wireless applications," *IEEE Transactions on Antennas and Propagation*, vol. 46, pp. 945–946, June 1998.

[128] T. Su, H. Ling, and W. J. Vogel, "Markov modeling of slow fading in wireless mobile channels at 1.9 GHz," *IEEE Transactions on Antennas and Propagation*, vol. 46, pp. 947–948, June 1998.

[129] K. W. Kim and Y. Rahmat-Samii, "Handset antennas and humans at *Ka*-band: The importance of directional antennas," *IEEE Transactions on Antennas and Propagation*, vol. 46, pp. 949–950, June 1998.

[130] K.-F. Tsang, W.-S. Chan, D. Jing, K. Kang, S.-Y. Yuen, and W.-X. Zhang, "Radiosity method: A new propagation model for microcellular communication," in *1998 IEEE AP-S International Symposium*, (Atlanta, Georgia), June 21–26 1998.

[131] Sami Tabbane, *Handbook of Mobile Radio Networks.* Boston: Artech House Publishers, 2000.

[132] S.-S. Jeng, G. T. Okamoto, G. Xu, H.-P. Lin, and W. J. Vogel, "Experimental evaluation of smart antenna system performance for wireless communications," *IEEE Transactions on Antennas and Propagation*, vol. 46, pp. 749–757, June 1998.

[133] S.-S. Jeng, G. Xu, H.-P. Lin, and W. J. Vogel, "Experimental studies of spatial signature variation at 900 MHz for smart antenna systems," *IEEE Transactions on Antennas and Propagation*, vol. 46, pp. 953–962, July 1998.

[134] F. P. S. Chin and M. Y. W. Chin, "Smart antenna array for high data rate mobile communications," in *1997 IEEE AP-S International Symposium*, (Montreal, Canada), July 13–18 1997.

[135] J. K. Tillery, G. T. Thompson, and J. J. H. Wang, "Low-power low-profile multifunction helmet-mounted smart array antenna," in *1999 IEEE AP-S International Symposium*, (Orlando, Florida), July 11–16 1999.

[136] G. Xu and W. J. Vogel, "Smart antenna systems for wireless communications," in *1998 IEEE AP-S International Symposium*, (Atlanta, Georgia), June 21–26 1998.

[137] L. J. Chu, "Physical limitations of omni-directional antennas," *Journal of Applied Physics*, vol. 19, pp. 1163–1175, December 1948.

[138] J. S. McLean, "A re-examination of the fundamental limits on the radiation Q of electrically small antennas," *IEEE Transactions on Antennas and Propagation*, vol. 44, pp. 672–676, May 1996.

[139] N. L. Cohen and R. G. Hohlfeld, "Fractal loops and the small loop approximation," *Communications Quarterly*, pp. 77–81, December 1996.

[140] R. G. Hohlfeld and N. Cohen, "The electrically small limit of fractal element antennas," in *2001 IEEE AP-S International Symposium*, (Boston, Massachusetts), pp. 624–627, July 9–13 2001.

[141] C. Puente-Baliarda, J. Romeau, R. Pous, and A. Cardama, "On the behavior of the Sierpinski multiband fractal antenna," *IEEE Transactions on Antennas and Propagation*, vol. 46, pp. 517–524, April 1998.

[142] C. Puente-Baliarda, J. Romeu, and A. Cardama, "The Koch monopole: A small fractal antenna," *IEEE Transactions on Antennas and Propagation*, vol. 48, pp. 1773–1781, November 2000.

[143] C. Puente Baliarda, C. Borja Borau, M. Navarro Rodero, and J. Romeu Robert, "An iterative model for fractal antennas: Application to the Sierpinski gasket antenna," *IEEE Transactions on Antennas and Propagation*, vol. 48, pp. 713–719, May 2000.

[144] J. Romeu and J. Soler, "Generalized Sierpiński fractal multiband antenna," *IEEE Transactions on Antennas and Propagation*, vol. 49, pp. 1237–1239, August 2001.

[145] D. H. Werner and P. L. Werner, "Genetically engineered dual-band fractal antennas," in *2001 IEEE AP-S International Symposium*, (Boston, Massachusetts), pp. 628–631, July 9–13 2001.

[146] S. D. Eason, R. Libonati, D. H. Werner, P. L. Werner, and S. Mummareddy, "UHF fractal antennas," in *2001 IEEE AP-S International Symposium*, (Boston, Massachusetts), pp. 636–639, July 9–13 2001.

[147] Z. D. Liu, P. S. Hall, and D. Wake, "Dual-frequency planar inverted-F antenna," *IEEE Transactions on Antennas and Propagation*, vol. 45, pp. 1451–1458, October 1997.

[148] C. R. Rowell and R. D. Murch, "A capacitively loaded PIFA for compact mobile telephone handsets," *IEEE Transactions on Antennas and Propagation*, vol. 45, pp. 837–842, May 1997.

[149] C. R. Rowell and R. D. Murch, "A compact PIFA suitable for dual-frequency 900/1800-MHz operation," *IEEE Transactions on Antennas and Propagation*, vol. 46, pp. 596–598, April 1998.

[150] K. L. Virga and Y. Rahmat-Samii, "Low-profile enhanced-bandwidth PIFA antennas for wireless communications packaging," *IEEE Transactions on Microwave Theory and Techniques*, vol. 46, pp. 1879–1888, October 1997.

[151] F. Auzanneau and R. W. Ziolkowski, "Artificial composite materials consisting of nonlinearly loaded electrically small antennas: Operational-amplifier-based circuits with applications to smart skins," *IEEE Transactions on Antennas and Propagation*, vol. 47, pp. 1330–1339, August 1999.

[152] H. Lindenmeier, J. Hopf, L. Reiter, R. Kronberger, "Optimization of the antenna-diversity-effectiveness of complex FM-car-antenna systems," in *1999 IEEE AP-S International Symposium*, (Orlando, Florida), July 11–16 1999.

[153] E. R. Brown, "On the gain of a reconfigurable-aperture antenna," *IEEE Transactions on Antennas and Propagation*, vol. 49, pp. 1357–1362, October 2001.

[154] L. Huang, J.-C. Chiao, and M. P. De Lisio, "An electronically switchable leaky wave antenna," *IEEE Transactions on Antennas and Propagation*, vol. 48, pp. 1769–1772, November 2000.

[155] S. Preston and D. V. Thiel, "Direction finding using a switched parasitic antenna array," in *1997 IEEE AP-S International Symposium*, (Montreal, Canada), July 13–18 1997.

[156] H. Y. D. Yang, "Characteristics of switchable ferrite microstrip antennas," *IEEE Transactions on Antennas and Propagation*, vol. 44, pp. 1127–1132, August 1996.

[157] N. Kuga and H. Arai, "A flat four-beam switched array antenna," *IEEE Transactions on Antennas and Propagation*, vol. 44, pp. 1227–1230, September 1996.

[158] R. G. Vaughan, J. Bach Andersen, and M. H. Langhorn, "Circular array of outward sloping monopoles for vehicular diversity antennas," *IEEE Transactions on Antennas and Propagation*, vol. 36, pp. 1365–1374, October 1988.

[159] C. B. Dietrich, Jr., K. Dietze, J. R. Nealy, and W. L. Stutzman, "Spatial, polarization, and pattern diversity for wireless handheld terminals," *IEEE Transactions on Antennas and Propagation*, vol. 49, pp. 1271–1281, September 2001.

[160] K. Ogawa and T. Uwano, "A diversity antenna for very small 800-MHz band portable telephones," *IEEE Transactions on Antennas and Propagation*, vol. 42, pp. 1342–1345, September 1994.

[161] C. Braun, G. Engblom and C. Beckman, "Antenna diversity for mobile telephones," in *1998 IEEE AP-S International Symposium*, (Atlanta, Georgia), June 21–26 1998.

[162] J. H. Holland, *Adaptation in Natural and Artificial Systems.* Ann Arbor: The University of Michigan Press, 1975.

[163] D. E. Goldberg, *Genetic Algorithms in Search, Optimization, and Machine Learning.* Reading, Massachusetts: Addison-Wesley, 1989.

[164] Lawrence Davis, *Handbook of Genetic Algorithms.* New York: Van Nostrand Reinhold, 1991.

[165] M. Mitchell, *An Introduction to Genetic Algorithms.* Cambridge, Massachusetts: The MIT Press, 1996.

[166] K. A. De Jong and W. M. Spears, "Using genetic algorithms to solve NP-complete problems," in *International Conference on Genetic Algorithms*, pp. 124–132, 1989.

[167] Y. Rahmat-Samii and E. Michielssen, eds., *Electromagnetic Optimization by Genetic Algorithms.* New York: John Wiley and Sons, 1999.

[168] R. Haupt, "An introduction to genetic algorithms for electromagnetics," *IEEE Antennas and Propagation Magazine*, vol. 17, pp. 7–15, April 1995.

[169] D. S. Weile and E. Michielssen, "Genetic algorithm optimization applied to electromagnetics: A review," *IEEE Transactions on Antennas and Propagation*, vol. 45, pp. 343–353, March 1997.

[170] J. M. Johnson and Y. Rahmat-Samii, "Genetic algorithms in engineering electromagnetics," *IEEE Antennas and Propagation Magazine*, vol. 39, pp. 7–25, August 1997.

[171] P. Ilavarasan, E. J. Rothwell, K. M. Chen, and D. P. Nyquist, "Natural resonance extraction from multiple data sets using a genetic algorithm," *IEEE Transactions on Antennas and Propagation*, vol. 43, pp. 900–904, August 1995.

[172] Q. Li, E. J. Rothwell, K. M. Chen, and D. P. Nyquist, "Scattering center analysis of radar targets using fitting scheme and genetic algorithm," *IEEE Transactions on Antennas and Propagation*, vol. 44, pp. 798–207, February 1996.

[173] S. Caorsi, A. Costa, and M. Pastorino, "Microwave imaging within the second-order born approximation: Stochastic optimization by a genetic algorithm," *IEEE Transactions on Antennas and Propagation*, vol. 49, pp. 22–31, January 2001.

[174] S. Caorsi and M. Pastorino, "Two-dimensional microwave imaging approach based on a genetic algorithm," *IEEE Transactions on Antennas and Propagation*, vol. 48, pp. 370–373, March 2000.

[175] H. Mosallaei and Y. Rahmat-Samii, "Nonuniform luneburg and two-shell lens antennas: Radiation characteristics and design optimization," *IEEE Transactions on Antennas and Propagation*, vol. 49, pp. 60–69, January 2001.

[176] H. Mosallaei and Y. Rahmat-Samii, "RCS reduction of canonical targets using genetic algorithm synthesized RAM," *IEEE Transactions on Antennas and Propagation*, vol. 48, pp. 1594–1606, October 2000.

[177] T. Su and H. Ling, "Determining the equivalent impedance boundary condition for corrugated coatings based on the genetic algorithm," *IEEE Transactions on Antennas and Propagation*, vol. 48, pp. 374–382, March 2000.

[178] E. E. Altshuler and D. S. Linden, "Wire antenna designs using genetic algorithms," *IEEE Antennas and Propagation Magazine*, vol. 39, pp. 33–43, April 1997.

[179] E. E. Altshuler, "Design of a vehicular antenna for GPS/IRIDIUM using a genetic algorithm," *IEEE Transactions on Antennas and Propagation*, vol. 48, pp. 968–972, June 2000.

[180] E. E. Altshuler and D. S. Linden, "Design of a loaded monopole having hemispherical coverage using a genetic algorithm," *IEEE Transactions on Antennas and Propagation*, vol. 45, pp. 1–4, January 1997.

[181] Z. Altman, R. Mittra, and Alona Boag, "New designs of ultra wide-band communication antennas using a genetic algorithm," *IEEE Transactions on Antennas and Propagation*, vol. 45, pp. 1494–1501, October 1997.

[182] R. L. Haupt, "Thinned arrays using genetic algorithms," *IEEE Transactions on Antennas and Propagation*, vol. 42, pp. 993–999, July 1994.

[183] E. A. Jones and W. T. Joines, "Design of Yagi-Uda antennas using genetic algorithms," *IEEE Transactions on Antennas and Propagation*, vol. 45, pp. 1386–1391, September 1997.

[184] J. M. Johnson and Y. Rahmat-Samii, "Genetic algorithms and method of moments (GA/MOM) for the design of integrated antennas," *IEEE Transactions on Antennas and Propagation*, vol. 47, pp. 1606–1614, October 1999.

[185] D. Marcano and F. Durán, "Synthesis of antenna arrays using genetic algorithms," *IEEE Antennas and Propagation Magazine*, vol. 42, pp. 12–20, June 2000.

[186] Alona Boag, Amir Boag, E. Michielssen, and R. Mittra, "Design of electrically loaded wire antennas using genetic algorithms," *IEEE Transactions on Antennas and Propagation*, vol. 44, pp. 687–695, May 1996.

[187] K.-K. Yan and Y. Lu, "Sidelobe reduction in array-pattern synthesis using genetic algorithm," *IEEE Transactions on Antennas and Propagation*, vol. 45, pp. 1117–1122, July 1997.

[188] F. J. Ares-Pena, J. A. Rodriguez-Gonzalez, E. Villanueva-Lopez, and S. R. Rengarajan, "Genetic algorithms in the design and optimization of antenna array patterns," *IEEE Transactions on Antennas and Propagation*, vol. 47, pp. 506–510, March 1999.

[189] B.-K. Yeo and Y. Lu, "Array failure correction with a genetic algorithm," *IEEE Transactions on Antennas and Propagation*, vol. 47, pp. 823–828, May 1999.

[190] T. Isernia, P. Di Iorio, and F. Soldovieri, "An effective approach for the optimal focusing of array fields subject to arbitrary upper bounds," *IEEE Transactions on Antennas and Propagation*, vol. 48, pp. 1837–1847, December 2000.

[191] D. S. Weile and E. Michielssen, "The control of adaptive antenna arrays with genetic algorithms using dominance and diploidy," *IEEE Transactions on Antennas and Propagation*, vol. 49, pp. 1424–1433, October 2001.

[192] R. L. Haupt, "Phase-only adaptive nulling with a genetic algorithm," *IEEE Transactions on Antennas and Propagation*, vol. 45, pp. 1009–1015, June 1997.

[193] W. H. Press, B. P. Flannery, S. A. Teukolsky, and W. T. Vetterling, *Numerical Recipes, The Art of Scientific Computing.* New York: Cambridge University Press, 2nd ed., 1989.

[194] I. Ziskind and M. Wax, "Maximum likelihood localization of diversely polarized sources by simulated annealing," *IEEE Transactions on Antennas and Propagation*, vol. 38, pp. 1111–1114, July 1990.

[195] C. S. Ruf, "Numerical annealing of low-redundancy linear arrays," *IEEE Transactions on Antennas and Propagation*, vol. 41, pp. 85–90, January 1993.

[196] F. Hsu, P.-R. Chang, and K.-K. Chan, "Optimization of two-dimensional radome boresight error performance using simulated annealing technique," *IEEE Transactions on Antennas and Propagation*, vol. 41, pp. 1195–1203, September 1993.

[197] A. Colorni, M. Dorigo, and V. Maniezzo, "Distributed optimization by ant colonies," in *Proceedings of the First European Conference on Artificial Life* (F. Varela and P. Bourgine, ed.), (Paris, France), pp. 134–142, Elsevier Publishing, 1992.

[198] A. Colorni, M. Dorigo, and V. Maniezzo, "An investigation of some properties of an 'ant algorithm'," in *Proceedings of the Parallel Problem Solving from Nature Conference* (R. Männer and B. Manderick, ed.), (Brussels, Belgium), pp. 509–520, Elsevier Publishing, 1992.

[199] M. Dorigo and L. M. Gambardella, "A study of some properties of ant-Q," in *Proceedings of PPSN IV-Fourth International Conference on Parallel Problem Solving From Nature*, (Berlin, Germany), pp. 656–665, Springer-Verlag, September 1996.

[200] A. Colorni, M. Dorigo, F. Maffioli, V. Maniezzo, G. Righini, and M. Trubian, "Heuristics from nature for hard combinatorial optimization problems," *International Transactions in Operational Research*, vol. 3, no. 1, pp. 1–21, 1996.

[201] M. Dorigo and A. Colorni, "The ant system: Optimization by a colony of cooperating agents," *IEEE Transactions on Systems, Man and Cybernetics-Part B*, vol. 26, no. 1, pp. 1–13, 1996.

[202] M. Dorigo and L. M. Gambardella, "Ant colony system: A cooperative learning approach to the traveling salesman problem," *IEEE Transactions on Evolutionary Computation*, vol. 1, no. 1, pp. 53–66, 1997.

[203] M. Dorigo and L. M. Gambardella, "Ant colonies for the traveling salesman problem," *BioSystems*, vol. 43, pp. 73–81, 1997.

[204] T. Stützle and M. Dorigo, *Evolutionary Algorithms in Engineering and Computer Science*, ch. ACO Algorithms for the Traveling Salesman Problem. John Wiley and Sons, 1999.

[205] M. Dorigo and Gianni Di Caro, "Ant algorithms for discrete optimization," *Artificial Life*, vol. 5, no. 3, pp. 137–172, 1999.

[206] E. Bonabeau, M. Dorigo, and G. Théraulaz, *Swarm Intelligence: From Natural to Artificial Systems.* New York: Oxford University Press, 1999.

[207] E. Bonabeau and Guy Théraulaz, "Swarm smarts," *Scientific American*, pp. 72–79, March 2000.

[208] Parallax, Inc., *Basic Stamp Programming Manual 1.9*, 1998.

[209] W. H. Press, B. P. Flannery, S. A. Teukolsky, and W. T. Vetterling, *Numerical Recipes in C, The Art of Scientific Computing.* New York: Cambridge University Press, 2nd ed., 1992.

[210] H. Cohn and M. Fielding, "Simulated annealing: Searching for an optimal temperature schedule," *Society for Industrial and Applied Mathematics Journal on Optimization*, vol. 9, no. 3, pp. 779–802, 1999.

[211] W. M. Spears, *Cliques, Coloring, and Satisfiability: Second DIMACS Implementation Challenge*, vol. 26 of *DIMACS Series in Mathematics and Theoretical Computer Science*, ch. Simulated Annealing for Hard Satisfiability Problems, pp. 533–558. American Mathematical Society, 1996.

[212] H. Peitgen, H. Jürgens, D. Saupe, *Chaos and Fractals: New Frontiers of Science.* New York: Springer-Verlag, 1992.

[213] M. Mitchell Waldrop, *Complexity: The Emerging Science at the Edge of Order and Chaos.* New York: Simon and Schuster, 1992.

[214] Gerald J. Burke, *Numerical Electromagnetics Code - NEC - 4 Method of Moments Part I: User's Manual.* Lawrence Livermore National Laboratory, January 1992.

[215] Gerald J. Burke, *Numerical Electromagnetics Code - NEC - 4 Method of Moments Part II: Program Description.* Lawrence Livermore National Laboratory, January 1992.

[216] W. Mendenhall, *Introduction to Probability and Statistics.* North Scltuate, Massachusetts: Duxbury Press, fourth ed., 1975.

[217] P. H. Smith, "Transmission-line calculator," *Electronics*, vol. 12, p. 29, January 1939.

[218] P. H. Smith, "An improved transmission-line calculator," *Electronics*, vol. 17, p. 130, January 1944.

[219] B. B. Mandelbrot, *The Fractal Geometry of Nature.* New York: Freeman, 1983. Updated and Augmented.

[220] N. Lesmoir-Gordon, W. Rood and R. Edney, *Introducing Fractal Geometry.* Lanham, Maryland: Totem Books, 2000.

[221] J. Lévy Véhel, E. Lutton, and C. Tricot, eds., *Fractals in Engineering: From Theory to Industrial Applications.* London: Springer-Verlag, 1997.

[222] W.-H. Steeb, *The Nonlinear Workbook.* New Jersey: World Scientific, 1999.

[223] D. Oliver, *FractalVision: Put Fractals to Work for You.* Carmel, Indiana: Sams Publishing, 1992.

[224] B. B. Mandelbrot, *Fractals and Scaling in Finance.* New York: Springer, 1997.

[225] A. Lakhtakia, N. S. Holter, V. K. Varadan, and V. V. Varadan, "Self-similarity in diffraction by a self-similar fractal screen," *IEEE Transactions on Antennas and Propagation*, vol. 35, pp. 236–239, February 1987.

[226] D. L. Jaggard and X. Sun, "Scattering from bandlimited fractal fibers," *IEEE Transactions on Antennas and Propagation*, vol. 37, pp. 1591–1597, December 1989.

[227] N. Engheta, "On the role of fractional calculus in electromagnetic theory," *IEEE Antennas and Propagation Magazine*, vol. 39, pp. 35–46, August 1997.

[228] N. Engheta, "On fractional calculus and fractional multipoles in electromagnetism," *IEEE Transactions on Antennas and Propagation*, vol. 44, pp. 554–556, April 1996.

[229] F. Berizzi and E. Dalle-Mese, "Fractal analysis of the signal scattered from the sea surface," *IEEE Transactions on Antennas and Propagation*, vol. 47, pp. 324–338, February 1999.

[230] E. Troncet, G. Ablart, and L. Allam, "Microwave characterization and modeling of the surface impedance of fractal structure copper films," *IEEE Transactions on Antennas and Propagation*, vol. 46, pp. 434–441, March 1998.

[231] J. Romeu and Y. Rahmat-Samii, "Fractal FSS: A novel dual-band frequency selective surface," *IEEE Transactions on Antennas and Propagation*, vol. 48, pp. 1097–1105, July 2000.

[232] C. Puente-Baliarda and R. Pous, "Fractal design of multiband and low side-lobe arrays," *IEEE Transactions on Antennas and Propagation*, vol. 44, pp. 731–739, May 1996.

[233] D. H. Werner, R. L. Haupt, and P. L. Werner, "Fractal antenna engineering: The theory and design of fractal antenna arrays," *IEEE Antennas and Propagation Magazine*, vol. 41, pp. 37–59, October 1999.

[234] S. Kauffman, *At Home in the Universe.* New York: Oxford University Press, 1995.

[235] P.-R. Chang, W.-H. Yang, and K.-K. Chan, "A neural network approach to MVDR beamforming problem," *IEEE Transactions on Antennas and Propagation*, vol. 40, pp. 313–321, March 1992.

[236] H. L. Southall, J. A. Simmers, and T. H. O'Donnell, "Direction finding in phased arrays with a neural network beamformer," *IEEE Transactions on Antennas and Propagation*, vol. 43, pp. 1369–1374, December 1995.

[237] É. Charpentier and J.-J. Laurin, "An implementation of a direction-finding antenna for mobile communications using a neural network," *IEEE Transactions on Antennas and Propagation*, vol. 47, pp. 1152–1159, July 1999.

[238] K.-T. Kim, I.-S. Choi, and H.-T. Kim, "Efficient radar target classification using adaptive joint time-frequency processing," *IEEE Transactions on Antennas and Propagation*, vol. 48, pp. 1789–1801, December 2000.

[239] G. Washington, "Aperture antenna shape prediction by feedforward neural networks," *IEEE Transactions on Antennas and Propagation*, vol. 45, pp. 683–688, April 1997.

[240] G. Goubau, N. Nath Puri, and F. K. Schwering, "Diakoptic theory for multielement antennas," *IEEE Transactions on Antennas and Propagation*, vol. AP-30, pp. 15–26, January 1982.

[241] F. Schwering, N. N. Puri, and C. M. Butler, "Modified diakoptic theory of antennas," *IEEE Transactions on Antennas and Propagation*, vol. AP-34, pp. 1273–1281, November 1986.

[242] E. Niver, H. H. Smith, and G. M. Whitman, "Frequency characterization of a thin linear antenna using a diakoptic antenna theory," *IEEE Transactions on Antennas and Propagation*, vol. 40, pp. 245–250, March 1992.

[243] N. K. Das and D. M. Pozar, "Multiport scattering analysis of general multilayered printed antennas fed by multiple feed ports: Part I–theory," *IEEE Transactions on Antennas and Propagation*, vol. 40, pp. 469–481, May 1992.

[244] N. K. Das and D. M. Pozar, "Multiport scattering analysis of general multilayered printed antennas fed by multiple feed ports: Part II–applications," *IEEE Transactions on Antennas and Propagation*, vol. 40, pp. 482–491, May 1992.

[245] P. I. Irazoqui-Pastor, E. Swanson, C. Short, and J. T. Bernhard, "An analysis and design tool for evaluation of integrated antenna diversity systems in portable wireless devices," in *1999 IEEE AP-S International Symposium*, (Orlando, Florida), July 11–16 1999.

[246] D. P. Nyquist, "Advanced topics in electromagnetics: Planar waveguides and circuits." EE 929A Course Notes, Michigan State University Department of Electrical Engineering, 1994.

[247] G. W. Hanson, *The Singularity Expansion Method for Integrated Electronics.* PhD thesis, Michigan State University, 1991.

[248] M. J. Havrilla, *Analytical and Experimental Techniques for the Electromagnetic Characterization of Materials.* PhD thesis, Michigan State University, 2001.

[249] A. Ali-Khan, W. F. Richards, and S. A. Long, "Impedance control of microstrip antennas using reactive loading," *IEEE Transactions on Antennas and Propagation*, vol. 37, pp. 247–251, February 1989.

[250] D. Liu, "A multi-branch monopole antenna for dual-band cellular applications," in *1999 IEEE AP-S International Symposium*, (Orlando, Florida), July 11–16 1999.

[251] C. R. Paul, *Introduction to Electromagnetic Compatibility.* New York: John Wiley and Sons, 1992.

[252] M. Nilsson and B. Lindmark, "Correlation between the output signals from a dual polarized antenna," in *1998 IEEE AP-S International Symposium*, (Atlanta, Georgia), June 21–26 1998.

[253] E. R. Brown, "RF-MEMS switches for reconfigurable integrated circuits," *IEEE Transactions on Microwave Theory and Techniques*, vol. 46, pp. 1868–1880, November 1998.

[254] R. S. Adve and T. K. Sarkar, "Compensation for the effects of mutual coupling on direct data domain adaptive algorithms," *IEEE Transactions on Antennas and Propagation*, vol. 48, pp. 86–94, January 2000.

[255] H. Schildt, *C++: The Complete Reference*. Berkeley: Osborne McGraw-Hill, third ed., 1998.

MICHIGAN STATE UNIVERSITY LIBRARIES
3 1293 02334 0908